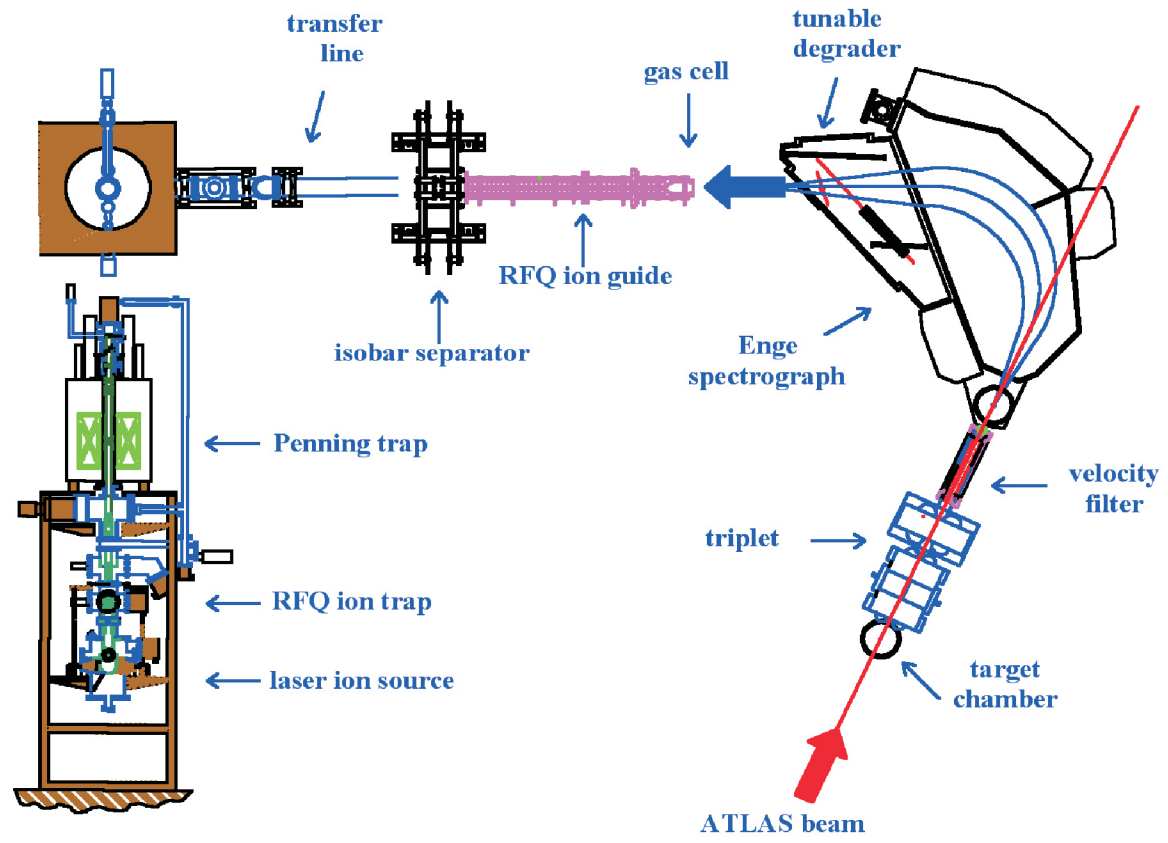# Physics Division Annual Report
2002

Physics Division
Physics Division
Physics Division
Physics Division
Physics Division
Physics Division
Physics Division
Physics Division
Physics Division

Physics Division
Physics Division
Physics Division
Physics Division
Physics Division
Physics Division

Physics Division
Physics Division
Physics Division
Physics Division
Physics Division
Physics Division
Physics Division
Physics Division

Physics Division
Physics Division
Physics Division
Physics Division
Physics Division
Physics Division
Physics Division
Physics Division

Physics Division
Physics Division
Physics Division
Physics Division
Physics Division

Physics Division
Physics Division
Physics Division
Physics Division
Physics Division
Physics Division

transfer line

tunable degrader

gas cell

RFQ ion guide

isobar separator

Enge spectrograph

Penning trap

velocity filter

triplet

RFQ ion trap

target chamber

laser ion source

ATLAS beam

Argonne National Laboratory

operated by The University of Chicago
for the United States Department of Energy
under Contract W-31-109-Eng-38

Physics Division
Physics Division

Argonne National Laboratory, with facilities in the states of Illinois and Idaho, is owned by the United States Government and operated by The University of Chicago under the provisions of a contract with the Department of Energy.

DISCLAIMER

ABOUT THE COVER:

An overview of the Canadian Penning Trap apparatus. This instrument is used at ATLAS to make precise measurements of the masses of the short-lived nuclei involved in the processes that create the chemical elements in the cosmos. The ion-stopping technology for this trap was a pioneering development that helped lead to the concept for the Rare Isotope Accelerator. The lower left section of the figure is a side view of the ion trap.

ANL-03/23

ARGONNE NATIONAL LABORATORY
9700 S. Cass Avenue
Argonne, Illinois 60439-4801

PHYSICS DIVISION ANNUAL REPORT
2002

Donald F. Geesaman
Director

September 2003

Edited by Karen J. Thayer

FOREWORD

This report highlights the research performed in 2002 in the Physics Division of Argonne National Laboratory. The Division's programs include operation of ATLAS as a national user facility, nuclear structure and reaction research, nuclear theory, medium energy nuclear research and accelerator research and development. The great progress that was made in meeting the exciting intellectual challenges of modern nuclear physics reflects the talents and dedication of the Physics Division staff and the visitors, guests and students who bring so much to the research.

The focus of research in the Division is on understanding the structure of strongly interacting matter, hadrons and nuclei, and the role nuclear processes take in the cosmos in the energy generation in stars and the formation of the very elements of which we are made. A great strength of these efforts is the critical interplay of theory and experiment. Major strides have been made both in understanding the basis of the strong interaction from quantum chromodynamics, and in realizing how the resulting interactions between protons and neutrons lead directly to the properties of the world around us. These theoretical advances provide a firm foundation to move forward in the science agenda expressed in the Nuclear Science Advisory Committee's 2002 Long Range Plan for Nuclear Science.

Notable results in research at ATLAS include precise measurements of nuclear masses with the Canadian Penning Trap, significant insights into the structure of the heaviest nuclei and the role of new modes of nuclear pairing. The year ended amidst a concerted effort to complete the move of Gammasphere back to ATLAS and everyone is eagerly looking forward to the prospect of the next epoch of exciting results with this, the world's most powerful instrument for nuclear structure research, in 2003. Under constrained budgets, ATLAS operated for 4416 hours of research in FY2002 while achieving 95% efficiency of beam delivery for experiments. Numerous improvements resulted in increased capabilities for the users, especially in higher beam intensities and reliability. In Medium Energy Physics new measurements of the proton's elastic form factors will resolve a major puzzle in understanding the distribution of charge and magnetization of the proton and an exciting initiative to search for the violation of time-reversal invariance using trapped Ra atoms has begun.

The DOE/NSF Nuclear Science Advisory Committee has recommended that the Rare Isotope Accelerator is the highest priority of our field for major new construction. Argonne continues to lead in the development and exploitation of the new technical concepts that will truly make RIA, in the words of NSAC, "the world-leading facility for research in nuclear structure and nuclear astrophysics." New classes of superconducting cavities are being fabricated. High power liquid-lithium targets have been prototyped. A full RIA scale gas-catcher system was constructed and has achieved the extraction efficiency projected for the RIA facility. Our science and our technology continue to point the way to this major advance. It is a tremendously exciting time in science for RIA holds the keys to unlocking important secrets of nature. The work described here shows how far we have come and makes it clear we know the path to meet these intellectual challenges.

Donald F. Geesaman, Director, Physics Division

TABLE OF CONTENTS

C.   NUCLEAR STRUCTURE AND HEAVY-ION REACTIONS

D.   ATOMIC THEORY AND FUNDAMENTAL QUANTUM MECHANICS

E.   OTHER ACTIVITIES

I.   HEAVY-ION NUCLEAR PHYSICS RESEARCH

OVERVIEW

This research involves investigating the structure, stability, reactions and decays of nuclei. This information is crucial for understanding the evolution of the universe, the workings of stars and the abundances of the elements that form the world around us. The forefront area of research is investigating the properties of nuclei which lie very far from stability, and which are critical in understanding nucleosynthesis. Most of our research is based at the Argonne Tandem-Linac Accelerator (ATLAS), a national heavy-ion user facility. Programs are also mounted at the Relativistic Heavy Ion Collider (RHIC), at the 88" cyclotron at Berkeley and at other forefront facilities. The major thrusts of the program are: a) deepening and generalizing our understanding of nuclear structure to allow a reliable description of all bound nuclear systems, b) studying the reactions which are important in the cataclysmic events in the cosmos which lead to the synthesis of the chemical elements, c) testing the limits of the Standard Model, the fundamental theory that currently best represents our understanding of the laws and fundamental symmetries of nature.

The specific research topics we are pursuing include the studies of transfermium nuclei (Z > 100) with a goal of studying the very heaviest nuclei, the study of the shapes and stability of nuclei along the proton dripline, the effects of deformation on proton radioactivity, the production and acceleration of short-lived nuclei and their use in measurements of reactions which are important in astrophysics, and the high-precision measurement of nuclear masses. In addition, there are complimentary efforts in the use of Accelerator Mass Spectrometry (AMS) for environmental research; in the investigation of nuclear matter at relativistic energies; and in the dynamics of cooled ions confined in storage rings or traps. The ATLAS-based research exploits the unique capabilities of the accelerator, both in the stable beam program, and in production of accelerated beams of short-lived isotopes.   The experiments employ state-of-the-art research equipment, including the Fragment Mass Analyzer (FMA), a large solid angle silicon array, "Ludwig", and the Canadian Penning Trap, (CPT) which is operating at ATLAS. Several new detector initiatives are being pursued including the return of Gammasphere to ATLAS, upgrading the FMA and its focal plane counters, refining the "In-Flight" radioactive beam facility and its detector systems, and constructing the Advanced Penning Trap (APT). Considerable effort continues in developing the next generation gamma ray detectors with "tracking" capability. Intensive participation in the PHOBOS experiment at Brookhaven has continued.

Some of the specific goals of the program can be summarized as follows:

- Develop and utilize beams of short-lived nuclei, ^{8}Li, ^{8}B, ^{14}O, ^{17,18}F, ^{20,21}Na, ^{25}Al, ^{37}K, ^{44}Ti, ^{56}Ni, and others, to improve the understanding of reactions of astrophysical importance. Emphasis has focused on "in-flight" production of short-lived ion-species using kinematically inverse reactions on light gaseous targets. Considerable scope still remains for further improving the intensity and quality of these beams in the future.

- Study the structure, stability, and modes of excitation and decay of the heaviest elements and study of the reaction mechanisms through which they can be synthesized. This research has many facets, including exploring the opportunities for producing the very heaviest nuclei (Z > 106), studies of isomeric decays, studies of "fine-structure" in the alpha decay of heavy elements, and "inbeam" spectroscopy and calorimetry.

- Study the shapes, stability and decay modes of nuclei along the proton dripline in order to improve understanding of partially bound nuclei. Study proton tunneling through deformed barriers, in order to increase the spectroscopic information obtained through proton radioactive decay rates. Study the influence of vibrations and coupling to other nucleons in odd-odd systems to generalize the understanding of proton radioactivity.

- Make high-precision measurements of nuclear masses with the CPT, particularly the masses of N = Z nuclei which are of astrophysical interest and are important for testing CVC theory, and measuring the masses of neutron fission fragments which lie close to the anticipated r-process path. Improve the efficiency for production, separation, cooling, transportation, and trap loading of ions to increase sensitivity.

- Develop position sensitive germanium detectors, for "tracking" gamma rays in order to allow the imaging of the source of radiation. The ANL focus is on developing planar germanium wafer technologies, in parallel with involvement in national plans to construct a 4-π germanium shell, following the GRETA concept.

- Investigate the collisions and deconfinement of nucleons in nuclear matter at very high temperatures and densities that are achieved in relativistic heavy-ion collisions of gold nuclei at 200 GeV/u. Our participation is using the PHOBOS detector at the RHIC accelerator at Brookhaven National Laboratory.

- Perform detailed R&D studies for the Rare Isotope Accelerator (RIA) and participate in all efforts to refine the designs for the accelerators, target stations, post accelerator, and experimental equipment. Intense effort is being directed to development of the "gas catcher" technology for cooling primary beams.

A. REACTIONS OF ASTROPHYSICAL IMPORTANCE USING STABLE AND RADIOACTIVE BEAMS

The "in-flight" technique for producing radioactive beams using reactions in inverse kinematics continues to evolve and be refined. Studying reactions involving these exotic beams helped clarify and quantify some reaction processes like the "breakout" from the hot CNO cycle and the beginning of the more explosive rp-process. Recent beams that were developed and used for physics projects now include: ^{8}Li ($t_{1/2}$ = 842 ms), ^{8}B ($t_{1/2}$ = 770 ms), ^{14}O ($t_{1/2}$ = 70.6 s), ^{17}F ($t_{1/2}$ = 65 s), ^{20}Na ($t_{1/2}$ = 446 ms), ^{21}Na ($t_{1/2}$ = 22.5 s), ^{25}Al ($t_{1/2}$ = 7.2 s), and ^{37}K ($t_{1/2}$ = 1.22 s). The reconfigured radioactive ion production beam line, which now includes a large-bore solenoid, was tested and successfully used in experiments. In addition to the ATLAS projects with accelerated radioactive beams, several more conventional heavy-ion reaction studies produced data on nuclei critical to the rp-nucleosynthesis path. A significant opportunity lies in studying compound nuclear states near the (p,γ) reaction threshold, populated with near-barrier fusion of heavy ions, and spectroscopically investigated using Gammasphere. This technique seems to have many possibilities, as it is excellent for precisely determining the excitation energy of levels and their angular momentum properties.

a.1.   Determination of the ^{8}B Neutrino Spectrum (J. P. Schiffer, K. E. Rehm, I. Ahmad, J. Greene, A. Heinz, D. Henderson, R. V. F. Janssens, C. L. Jiang, E. F. Moore, G. Mukherjee, R. C. Pardo, T. Pennington, G. Savard, D. Seweryniak, G. Zinkann, W. T. Winter,* S. J. Freedman,* and M. Paul†)

The solar neutrino "problem" originated in 1968 when the Homestake ^{37}Cl capture experiment placed a limit on the solar neutrino flux that was less than half of solar model predictions. Additional solar neutrino data have since been collected by the Gallex, SAGE, and GNO ^{71}Ga capture experiments and the Kamiokande, Super-Kamiokande, and Sudbury Neutrino Observatory (SNO) water Cherenkov experiments.

Neutrinos from the β-decay of ^{8}B, produced in the solar core, account for 80% of the ^{37}Cl capture events, and Super-Kamiokande and SNO are sensitive to the differential ^{8}B neutrino spectrum. A determination of the physics of leptonic flavor mixing from the solar neutrino data requires an understanding of the α-decay of ^{8}B into ^{8}Be, which depends strongly on the energy profile of the unstable ^{8}Be, which must be determined experimentally.

Previous measurements of the α-spectrum involved the production of ^{8}B ($t_{1/2}$ = 778 ms) which was stopped in a catcher foil and positioned adjacent to a Si detector. Energy deposition in the detector was measured and corrections were made for energy losses in the catcher foil and detector dead layer. The first experiments, by Farmer and Class,[1] De Braeckeleer and Wright,[2] and Wilkinson and Alburger,[3] observed the singles α-spectrum. Data from these measurements differ from each other by energy offsets of order 100 keV, an effect attributed to systematic problems with detector calibration and energy loss in the dead layer.

Additional information on the ^{8}B β-decay is provided by the β-spectrum which, like the neutrino spectrum, is altered by the broad ^{8}Be resonance. A precise measurement of the β-spectrum above 9 MeV was performed using a 180° magnetic spectrograph.[4] The singles α-spectrum data and β-spectrum data were used to predict a neutrino spectrum, based on varying assumptions with the most comprehensive analysis performed by Bahcall *et al.*[5]

Recently, the coincidence α-spectrum was measured using two detectors resulting in a spectrum quite different from the earlier measurements.[6] Both the Super-Kamiokande and SNO collaborations interpreted their data using the ^{8}B neutrino spectrum from the most recent coincidence measurement.

We developed an experiment that was designed to minimize systematic effects which may have affected the previous α measurements. A beam of ^{8}B ions was implanted into the center of a planar Si detector, which eliminated energy loss corrections due to catcher foils and detector dead layers and allowed the energy deposited by both α-particles to be observed with a single detector.   Beta-particle energy deposition is unavoidable with this technique, but was minimized by the use of a thin (91 μm) Si detector, sufficient to stop the most energetic α-particles, and by the requirement of a β coincidence. For calibration ^{20}Na ions were implanted into the same detector immediately before the ^{8}B measurement. The β-decay of ^{20}Na proceeds 20% of the time to α-unstable levels in ^{20}Ne and provides calibration lines in the region of the ^{8}B α-spectrum peak.

The experiment was performed using the ATLAS superconducting linear accelerator at the Argonne National Laboratory. A ^{8}B beam was produced with the "In-Flight Technique" using the ^{3}He(^{6}Li,^{8}B)n reaction. A 36.4 MeV ^{6}Li beam was incident on a 3.5 cm long gas cell filled with 700 mbar of ^{3}He and cooled to 82 K. The pressure and temperature in the cell were held constant to ±1%. The ^{8}B reaction products were separated from the primary ^{6}Li beam with a 22° bending magnet and transported into the focal plane of the Enge Split Pole spectrograph where they were identified with respect to mass, charge, and energy in the gas-filled focal plane detector. The magnetic field in the spectrograph was then adjusted to implant 27.3 MeV ^{8}B ions (range ≈45 μm) into a 91 μm thick Si detector located adjacent to the gas-filled detector in the focal plane. An 11-mm diameter Ta collimator in front of the Si detector ensured that the ^{8}B ions were implanted only into the central region of the detector.
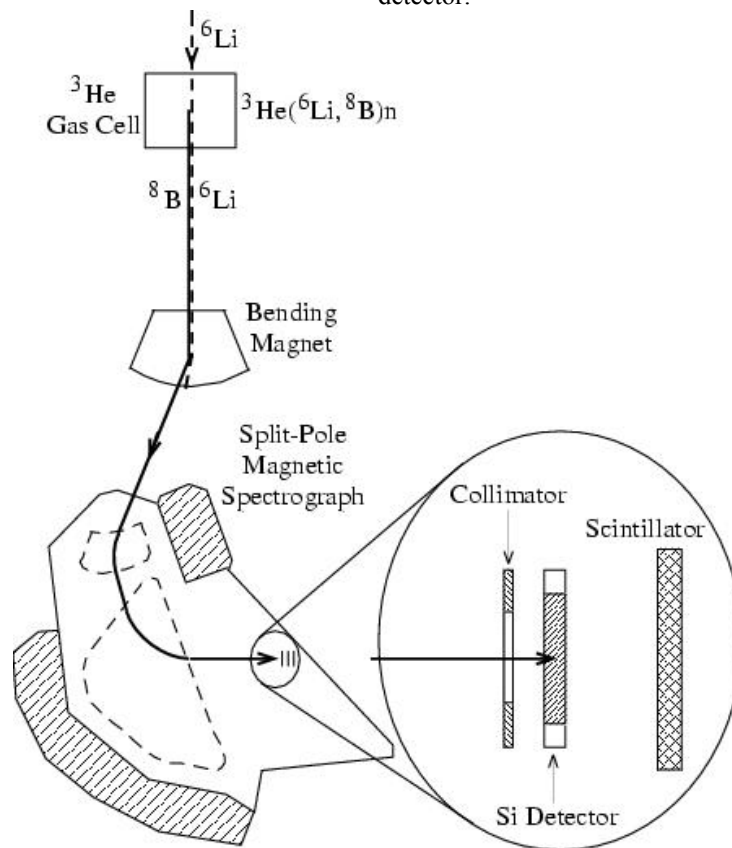
Fig. I-1. Schematic sketch of the experimental apparatus used in the measurement

A 25-mm diameter × 2-mm thick plastic scintillator coupled by a light guide to a Hamamatsu R647 photo-multiplier tube was positioned 12 mm behind the Si detector. The plastic scintillator, operated in coincidence, selected events where the β trajectory was within ≈40° to normal. This provided a sample of events with minimum β energy deposition. The Si/scintillator detector system was cooled to -5° C. A schematic representation of the apparatus is shown in Fig. I-1.

The ^{6}Li beam was cycled (1.5 sec on/1.5 sec off) and data taken only during the beam-off cycle. With an average ^{6}Li current of 60 pnA about 3 ^{8}B ions/sec were implanted. Energy signals and the relative timing between the Si and β detectors were recorded, as well as the timing of the Si signal with respect to the beam-off cycle. Over three days, 4.5×10^5 ^{8}B events were observed, 16% of which were in coincidence with a β event in the scintillator.

The system was calibrated using a ^{20}Na ($t_{1/2}$ = 448 ms) beam immediately before the ^{8}B run. The ^{20}Na beam was produced using the same in-flight technique with a 199-MeV ^{19}F beam via the ^{3}He(^{19}F,^{20}Na)2n reaction. The spectrograph selected ^{20}Na ions of 170 MeV, and a Mylar foil in front of the Si detector slowed the ^{20}Na ions to 85 MeV (range in the Si detector ≈45 μm). Data acquisition was identical to the ^{8}B runs, but the on-off cycle time was reduced to 1 sec on/1 sec off. With a 0.5 pnA ^{19}F beam, about 8 ^{20}Na decays/min were detected in the Si detector, resulting in 1.0×10^4 ^{20}Na events over a one day run. Spectra from the implanted ^{8}B and ^{20}Na are shown in Fig. I-2.
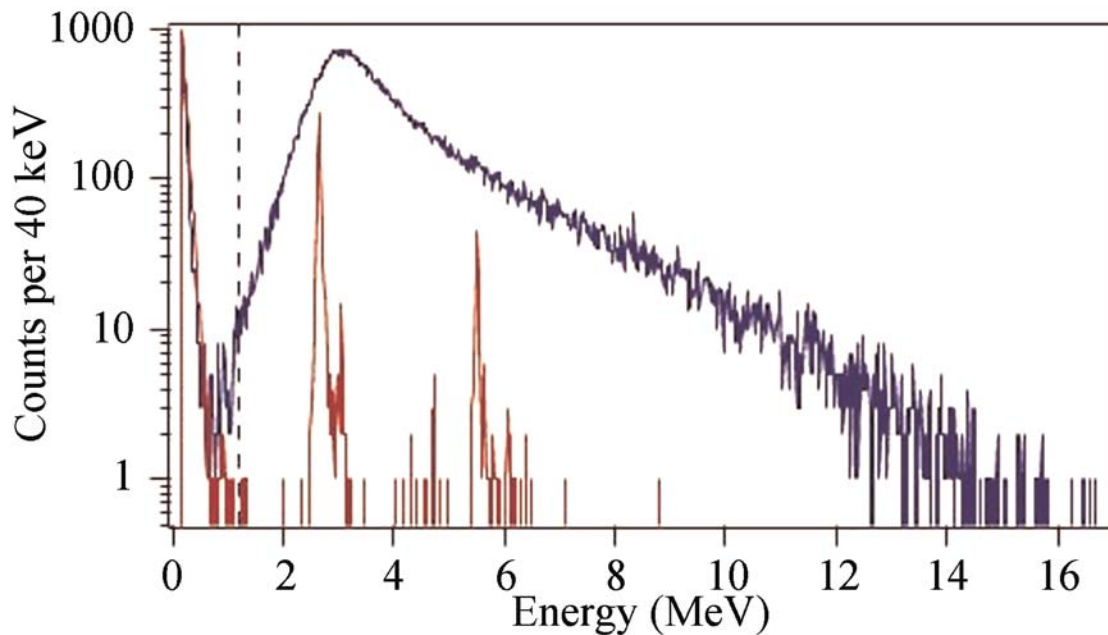
Fig. I-2. The measured alpha-particle spectrum from the decay of ^{8}B imbedded in the Si detector is shown in blue, together with the calibration spectrum of alpha particles following the decay of ^{20}Na, similarly imbedded, in red. The data shown here were in coincidence with the scintillation beta detector to better define the energy deposition from betas in the Si detector

The three largest branches in ^{20}Na decay provide a good calibration, covering a large fraction of the ^{8}B decay spectrum. The pulse-height defect associated with the recoil ^{16}O nucleus, which carries one fifth of the energy of the alpha disintegration in ^{20}Na decay, has been measured for ^{16}O nuclei in the energy range of interest. The correction is 40-50 keV for the various ^{20}Na alpha lines.

The detector resolution consists of a noise component and a β energy-loss component. The noise was estimated from the ^{20}Na peaks and was removed from the ^{8}B spectrum. The effect of β energy loss was modeled in a Monte Carlo simulation. The high-energy tail of the β energy deposition spectrum is suppressed by the coincidence requirement. Correction for β energy loss lowered the peak of the coincidence data by 24 keV, as compared to 55 keV for the total data. After the correction, the peaks of the coincidence and total spectra agree within 2 keV.

The recoil energy of the ^{8}Be nucleus following the Gamow-Teller β-decay contributes an energy shift of

5 keV at the peak of the alpha spectrum. At the highest alpha energies, contributions from electron capture and a Fermi β-decay branch are significant; however, the recoil effect is ≤0.5 keV there, which is negligible compared to uncertainties in the energy scale, so these effects can be safely neglected.

The α spectrum from this measurement is given in Fig. I-3 (blue lines) in comparison with the coincidence measurement from Ref. 6 (red lines). The present result is peaked 53 keV higher in energy than the spectrum by Ortiz et al.
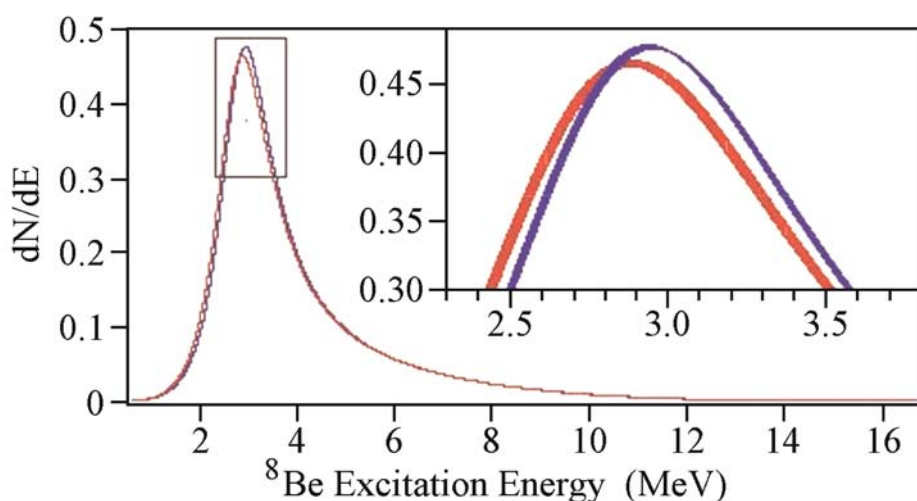
Fig. I-3. Comparison of the measured alpha spectrum from the present measurement, shown in blue, with that of Ortiz et al. in Ref. 6 shown in red. The widths of the lines indicate the estimated systematic uncertainties.

The ^{8}B β-spectrum was deduced from the measured α-spectrum. Recoil order effects and radiative corrections contribute to the spectrum at the 5% level. The deduced β-spectrum was compared to the experimental spectrum,[4] and gave an agreement of $\chi^2/\text{dof} = 32.9/31$, where only statistical uncertainties were included in the minimization function. The calibration uncertainty in the measured β-spectrum is reported in Ref. 5 as 25 keV, and the spectrum deduced here was allowed to float by an energy offset

to mimic the effect of a possible calibration error. Best agreement ($\chi^2/\text{dof} = 32.5/31$) occurs at an offset of -13 ± 20 keV. The β-spectrum predicted by Ortiz requires a -75 ± 20 keV offset to produce the best agreement with the data.

A comparison of the ^{8}B neutrino spectra recommended by Bahcall et al. and Ortiz et al. to the spectrum determined here are shown in Fig. I-4.
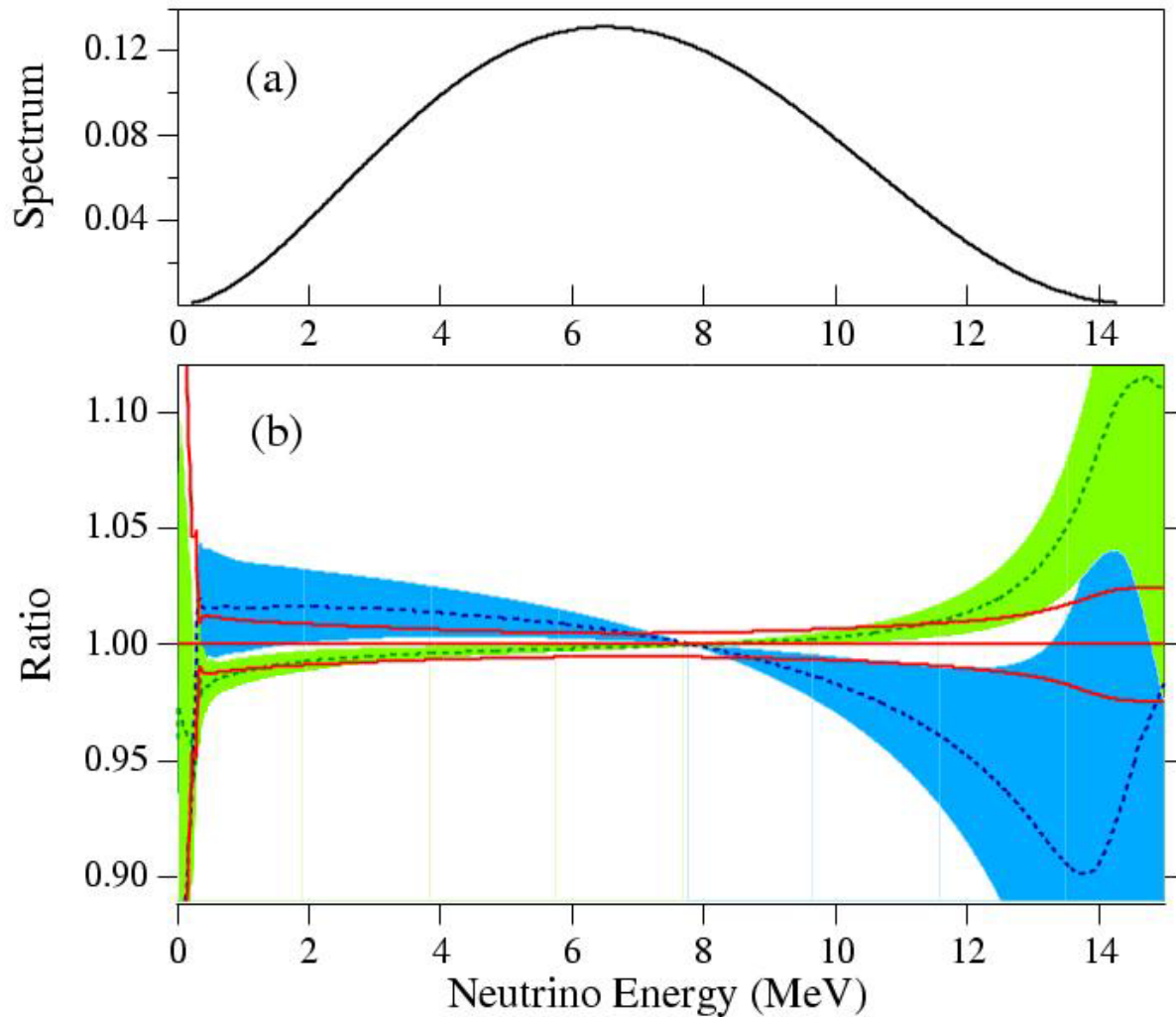
Fig. I-4. The neutrino spectrum deduced from the present measurement is shown in (a). On the bottom the ratio of the neutrino spectrum obtained in Ref. 6 (Ortiz et al.) to the present one is shown in green, while that of the spectrum recommended in Ref. 5 from measurements before the work of Ref. 5 (by Bahcall et al.) is in blue. The bands indicate 1-sigma errors.

The deviations between the predicted [8]B neutrino spectra, shown in Fig. I-4, are comparable to the precision with which Super-Kamiokande measured the differential energy spectrum of solar neutrinos.

Interpretation of solar neutrino data will become increasingly dependent on the uncertainties in the neutrino spectrum as the quality of solar neutrino data increases.

---

*Lawrence Berkeley National Laboratory and the University of California-Berkeley, †Hebrew University, Jerusalem, Israel.
[1]B. Farmer and C. Class, Nucl. Phys. **15**, 626 (1960).
[2]L. De Braeckeleer *et al*., Phys. Rev. C **51**, 2778 (1995).
[3]D. Wilkinson and D. Alburger, Phys. Rev. Lett. **16**, 1127 (1971).
[4]J. Napolitano, S. J. Freedman, and J. Camp, Phys. Rev. C **36**, 298 (1987).
[5]J. Bahcall *et al*., Phys. Rev. C **54**, 411 (1996).
[6]C. Ortiz *et al*. Phys. Rev. Lett. **85,** 2909 (2000).

a.2.   Production of a ^{8}Li Beam with the In-Flight Technique (A. H. Wuosmaa, R. C. Pardo, J. P. Greene, A. Heinz, C. L. Jiang, E. F. Moore, K. E. Rehm, and S. Sinha)

For a planned ^{8}Li(d,p)^{9}Li experiment we developed ^{8}Li (T$_{1/2}$ = 0.84 s) beams with energies between 50 and 75 MeV using the in-flight technique. The ^{8}Li beam was produced via the d(^{7}Li,^{8}Li)p reaction with a ^{7}Li beam from the ATLAS accelerator. The specific rate on target (^{8}Li per sec and per pnA of incident ^{7}Li beam) was between 2000 - 2500, independent of the bombarding energy. The contamination from the primary ^{7}Li beam was less than 1%. At present the total ^{7}Li beam intensity that

can be put on the production target is less than 13 pnA, limited by the radiation monitors of the ATLAS Radiation Interlock System (ARIS). The new Safety Assessment Document which was recently approved, will allow this value to increase by a factor of about 30, which should result in ^{8}Li beam intensities of ~10^6 ^{8}Li/sec on target. With beams of ~10^6 ^{8}Li/sec the study of the ^{8}Li(d,p)^{9}Li reaction should be well within the experimental sensitivity.

a.3.   The Branching Ratio $\Gamma_\alpha/\Gamma_\gamma$ of the 4.033 MeV State in ^{19}Ne (K. E. Rehm, A. H. Wuosmaa, C. L. Jiang, J. P. Greene, A. Heinz, D. Henderson, R. V. F. Janssens, E. F. Moore, G. Mukherjee, R. C. Pardo, T. Pennington, J. P. Schiffer, R. H. Siemssen, L. Jisonna,* M. Paul,† and R. E. Segel*)

In novae, on accreting neutron stars or in super-massive stars where explosive hydrogen burning occurs, the energy production proceeds via the so-called hot CNO (HCNO) cycle which is a reaction cycle consisting of a sequence of (p,γ), (p,α) reactions and β^+ decays: ^{12}C(p,γ)^{13}N(p,γ)^{14}O(e$^+\nu_e$)^{14}N(p,γ)^{15}O(e$^+\nu_e$)^{15}N(p,α)^{12}C In this network, the rate of energy production is limited by the slow β decays of ^{14,15}O (T$_{1/2}$ = 70.6 s and 123 s, respectively). At higher temperatures (T $\geq$ 3.5 × 10^8 K), however, α induced reactions on ^{14,15}O can bypass these waiting points. This results in a strong increase of the energy production as well as in a breakout from the HCNO into the rapid proton capture (rp) process where, through a sequence of (p,γ) reactions and β decays, nuclei above mass 20 are produced.

There are three pathways for this breakout mechanism: ^{18}F(p,γ)^{19}Ne, ^{15}O(α,γ)^{19}Ne and ^{18}Ne(α,p)^{21}Na. The large cross section measured for the ^{18}F(p,α)^{15}O reaction leads to a very small branching ratio $\Gamma_\gamma/\Gamma_\alpha$ and, thus, to a negligible breakout probability through the ^{18}F(p,γ) route. The ^{18}Ne(α,p) path has the highest Coulomb barrier of the three breakout reactions and it, thus, contributes only at higher temperatures and densities. It is presently assumed that the ^{15}O(α,γ) reaction is the most likely path for a breakout into the rp process.[1]

The astrophysical reaction rate for the ^{15}O(α,γ)^{19}Ne reaction is dominated by the contribution from the 3/2$^+$ state in ^{19}Ne at E$_x$ = 4.033 MeV, the first level

above the (α,γ) threshold at 3.529 MeV. We studied the inverse ^{3}He(^{20}Ne,α)^{19}Ne reaction to populate the 3/2$^+$ state in ^{19}Ne with a 105 MeV ^{20}Ne beam from the ATLAS accelerator at Argonne National Laboratory. The ^{3}He target consisted of a 1.5-mm long gas cell filled with 700 mbar of ^{3}He with two 1.5-mg/cm^2 titanium windows. It was cooled to LN$_2$ temperatures, resulting in an areal density of about 50 μg/cm^2.

The α particles from the (^{3}He,α) reaction were detected in a Si detector telescope consisting of a 500-μm thick 32 × 32-mm^2 double-sided silicon-strip ΔE detector and a 300-μm 50 × 50-mm^2 E$_{res}$ detector. The ΔE detector was segmented into 32 horizontal and 32 vertical, 1-mm wide, strips.

The coincident ^{19}Ne particles emitted at an angle θ_{lab} = 3.7 ± 1.4° were separated from the incident ^{20}Ne beam with the Enge Split Pole magnetic spectrograph and identified with respect to mass and nuclear charge in the focal plane using a hybrid position-sensitive parallel-plate-avalanche-counter (PPAC) ionization chamber (IC) detector system. Through a measurement of magnetic rigidity, energy, time-of-flight, range and height of the Bragg peak, mass and charge could be determined by two independent methods, resulting in excellent background suppression. The whole system was tested by studying elastic and inelastic scattering of ^{20}Ne on ^{4}He populating high-lying states in ^{20}Ne which also decay by α emission. The Q-value resolution of this setup was about 250-keV FWHM mainly determined by the geometry of the detector-target system.

Q-value spectra for α particles measured in the position sensitive Si detector telescope, in coincidence with either ^{19}Ne (left) or ^{15}O (right), are shown in Fig. I-5. The ^{15}O spectrum is free of background especially in the critical region around E_x

= 4 MeV. The solid lines in Fig. I-5 represent Gaussians for which the location in excitation energy was kept fixed to the values obtained in a high resolution ^{20}Ne(^{3}He,α)^{19}Ne experiment measured at the same c.m. energy.[2]
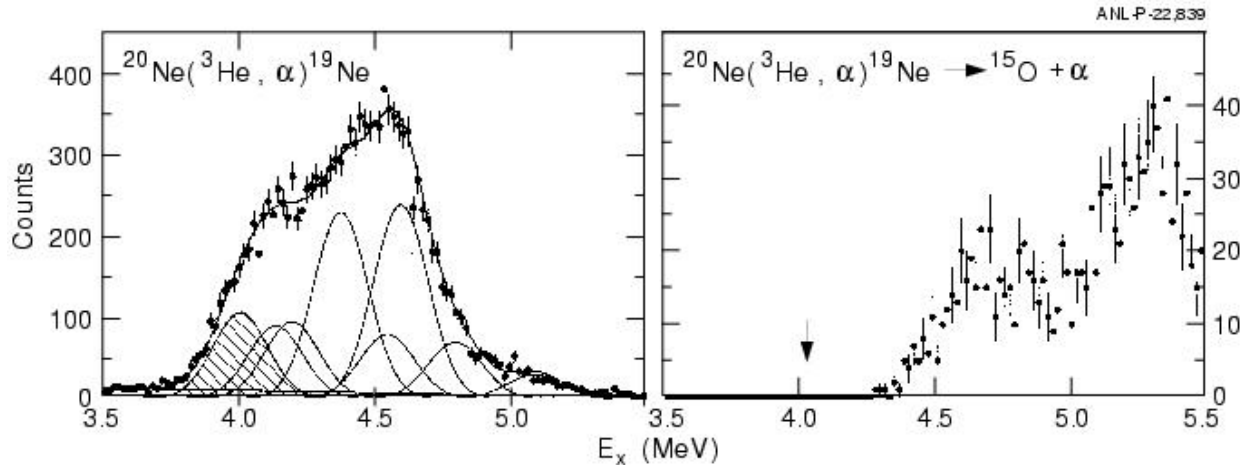
Fig. I-5. Q-value spectra for α particles in coincidence with ^{19}Ne (left) or ^{15}O (right). In both cases the location of the 4.033 MeV state is indicated.

From the two spectra shown in Fig. I-5 upper limits for the branching ratios $\Gamma_\alpha/\Gamma_\gamma$ for the two astrophysically important states at 4.033 MeV ($3/2^+$) and 4.379 MeV ($7/2^+$) can be deduced. The contribution from the neighboring states at 4.140 ($9/2^-$) and 4.197 ($7/2^-$) MeV is, due to the larger angular momentum transfer, much smaller. Taking into account the detection efficiencies for ^{15}O and ^{19}Ne particles transported to the focal plane of the magnetic spectrograph, which was determined from a Monte Carlo calculation, limits of $\Gamma_\alpha/\Gamma_\gamma \le 6 \times 10^{-4}$ (4.033 MeV) and $\le 1.5 \times 10^{-3}$ (4.379 MeV) were obtained.

From these branching ratios B and the radiative widths Γ_γ (typically tens to hundreds of meV) the resonance

strengths $\omega\gamma = \omega\dfrac{\Gamma\alpha\Gamma\gamma}{\Gamma_{total}} = \omega\dfrac{B}{1+B}\Gamma\gamma$ can be calculated.

For the two important resonances in ^{19}Ne, good measurements of Γ_γ are not yet available. Assuming for Γ_γ (4.033 MeV) the limits from Ref. 3 and a theoretical value of $\Gamma_\gamma = 460 \pm 90$ meV for the 4.379 MeV state,[4] the astrophysical reaction rate for the ^{15}O (α,γ) reaction can be calculated. The results (also including the contributions from higher-lying states) are shown in Fig. I-6.
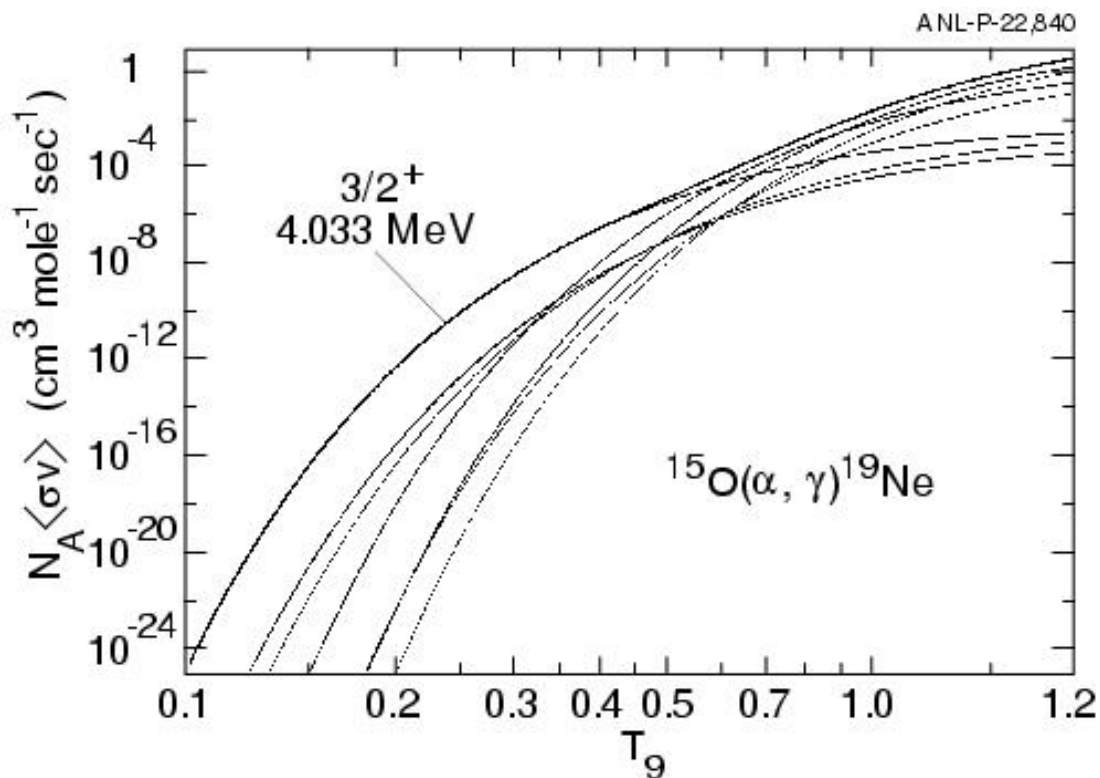
Fig. I-6. Astrophysical reaction rate for the $^{15}O(\alpha,\gamma)^{19}Ne$ reaction.

At low temperatures typical for novae ($T_9 \sim 0.2$ - 0.4), the contribution from the $3/2^+$ state dominates the reaction rate. Converting the reaction rate into an interaction time, one finds at temperature-density conditions typical of novae $\rho \sim 10^2$-10^4 g/cm^3, $T_9 \sim 0.2$ - 0.4) values in the regime of 10^7-10^8 s, i.e. much longer than the β lifetime of ^{15}O (τ = 177s). Thus, no appreciable breakout occurs via the $^{15}O(\alpha,\gamma)^{19}Ne$ reaction in novae. On the surface of acreeting neutron stars, i.e. at temperature-densities of $T_9 \sim 1.5$ and $\rho \sim 10^4$ - 10^7, the interaction time is $\sim 10^{-5}$ s, leading to a considerable breakout under these conditions.

_____

*Northwestern University, †Hebrew University, Jerusalem, Israel.
[1]A. E. Champagne and M. Wiescher, Annu. Rev. Nucl. Part. Sci. **42**, 39 (1992).
[2]J. D. Garrett, R. Middleton, and H. T. Fortune, Phys. Rev. C **2**, 1243 (1970).
[3]G. Hackman *et al.*, Phys. Rev. C **61**, 052801 (2001).
[4]B. A. Brown, private communication.

a.4. The Astrophysical Rate of the $^{15}O(\alpha,\gamma)^{19}Ne$ Reaction Studied via the $^{21}Ne(p,t)^{19}Ne$ Reaction (K. E. Rehm, A. H. Wuosmaa, B. Davids,* A. M. van den Berg,* P. Dendooven,* F. Fleurot,* M. Hunyadi,* M. A. de Huu,* R. H. Siemssen,* H. W. Wilschut,* and H. J. Woertche*)

The $^{15}O(\alpha,\gamma)^{19}Ne$ reaction represents one of the possible breakout paths from the hot CNO cycle into the rp-process. A direct measurement of this reaction, which has an estimated cross section of $\sim$100 pb, is currently not feasible because it requires very intense ^{15}O beams which are not yet available. For this reason, only indirect measurements have been performed so far. In these experiments states in ^{19}Ne above the (α,γ) threshold are populated by various transfer reactions (e.g. $^{20}Ne(^3He,\alpha)^{19}Ne$) and their branching ratios $\Gamma_\gamma/\Gamma_\alpha$

measured by identifying the corresponding decay products. The best transfer reaction for populating the first $3/2^+$ state at 4.033 MeV in ^{19}Ne which has the strongest influence on the astrophysical reaction rate is the ^{21}Ne(p,t)^{19}Ne reaction, which, however, requires high energetic particle beams ($\geq$ 20 MeV/u).

We studied this reaction in inverse kinematics via the reaction $p(^{21}Ne,t)^{19}Ne$ with a 43 MeV/u ^{21}Ne beam from the Kernfysisch Versneller Institut in Groningen bombarding a 1 mg/cm^2 (CH$_2$)$_n$ target. Both triton ejectiles and ^{19}Ne recoils entered the Big-Bite Spectrometer which was positioned at 0º. The ^{19}Ne recoils and ^{15}O decay products were identified in two phoswich detectors, which provided energy loss, total energy and timing information. The tritons were identified in a similar array of phoswich detectors after passing through the vertical drift chambers located in the focal plane of the spectrometer. Due to the excellent energy resolution in the spectrometer the branching ratio Γ_α/Γ of 6 states above the alpha threshold in ^{19}Ne could be determined. These values and the resulting α widths Γ_α (obtained from measured and calculated radiative widths) are summarized in Table I-1. Because of the small value of the α width the ^{15}O(α,γ)^{19}Ne reaction does not play a significant role in the breakout from the hot CNO cycle into the rp process in nova explosions.

_____

*Kernfysisch Versneller Instituut, Groningen, The Netherlands.

Table I-1. Branching ratios $B_\alpha \equiv \Gamma_\alpha/\Gamma$ and decay widths.

E_x (MeV)	J^π	B_α	Γ_γ (meV)	Γ_α (meV)
4.033	$3/2^+$	$< 4.3 \times 10^{-4}$	45^{+200}_{-33}	<0.13
4.379	$7/2^+$	$< 3.9 \times 10^{-3}$	458 ± 92	<2.3
4.549	$(3/2)^-$	0.16 ± 0.04	39^{+34}_{-15}	$4.4^{+4.0}_{-2.0}$
4.600	$(5/2^+)$	0.32 ± 0.04	101 ± 55	43 ± 24
4.712	$(5/2^-)$	0.85 ± 0.04	43 ± 8	230 ± 80
5.092	$5/2^+$	0.90 ± 0.06	107 ± 17	960 ± 530

a.5.   On the γ Decay of the 2643-keV State in the rp Breakout Nucleus ^{20}Na

(D. Seweryniak, A. Heinz, R. V. F. Janssens, T. L. Khoo, E. Rehm, P. J. Woods,*
H. Mahmud,* F. Sarazin,* J. Goerres,† A. Aprahamian,† M. Shawcross,† J. Shergur,‡
M. Wiescher,† and A. Woehr‡)

The reaction sequence ^{15}O(α,γ)^{19}Ne(p,γ)^{20}Na is thought to be the dominating nucleosynthetic mechanism responsible for breakout from the hot CNO cycles into the rp process. However, neither of these reaction rates has been determined. One of the key uncertainties in the ^{19}Ne(p,γ)^{20}Na reaction is the structure of the resonance state in ^{20}Na at an excitation energy of about 2.643 MeV, which is thought to dominate the astrophysical reaction rate. Contradictory 3^+ and 1^+ assignments were proposed for this state in the literature.

An in-beam γ-ray experiment was performed using the Argonne Fragment Mass Analyzer to study γ-decaying states in ^{20}Na. The ^{10}B(^{12}C, 2n) reaction was used to populate excited states in ^{20}Na. Gamma rays were detected using 2 Ge clover detectors and a 4π array of BGO scintillators placed around the target. Recoiling reaction products were separated from the beam and dispersed according to their mass over charge state ratio in the FMA. Mass-20 residues, selected by the slits at the focal plane of the FMA, were stopped in an ionization chamber and their atomic number was deduced based on the energy loss and energy measurement.

Figure I-7 shows the γ-ray spectrum tagged by ^{20}Na recoils. The transitions present in this spectrum were placed in the preliminary level scheme shown in Fig. I-8. Figure I-8 shows only the states observed in this work. The energies of the observed γ rays are in agreement with level energies obtained from previous transfer reaction studies. The state depopulated by the 1029 keV γ ray was seen for the first time. Based on the comparison with the mirror ^{20}F spin 5^+ was assigned to this state. A 1237-keV transition is proposed to deexcite a new 2^+ state. A γ-ray line can be seen at the energy of about 1851 keV in the inset of Fig. I-7. The energy of this line agrees within experimental errors with the energy difference between the 2643 keV state and the 798 keV state. The BGO spectrum gated by the three bottom transition contains excess of counts around 1800-1900 keV, although the statistics are low (see Fig. I-9). This could imply that the 3^+ assignment for the 2643 keV state is more likely than 1^+. However, the 1851-keV transition might deexcite the known 2^- state at 1837(7) keV. To resolve this ambiguity another experiment using Gammasphere was proposed and will be carried out this year.
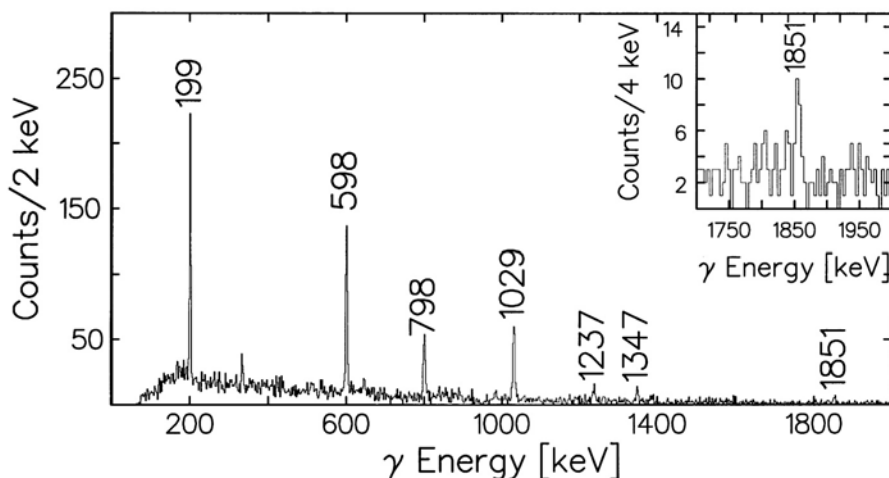
Fig. I-7. Ge γ-ray spectrum measured in coincidence with ^{20}Na residues.
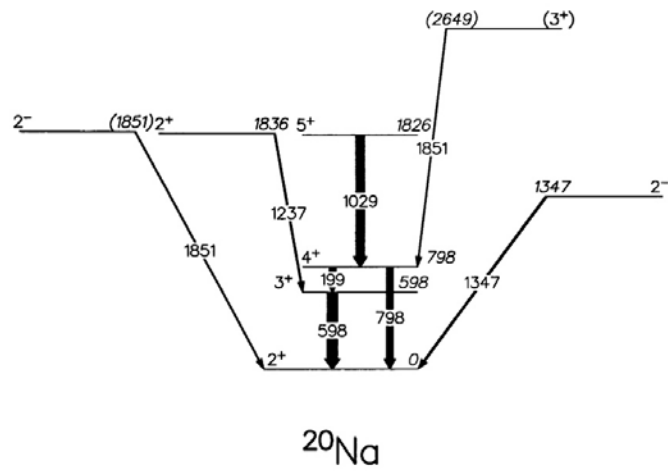
Fig. I-8. Preliminary ^{20}Na level scheme.
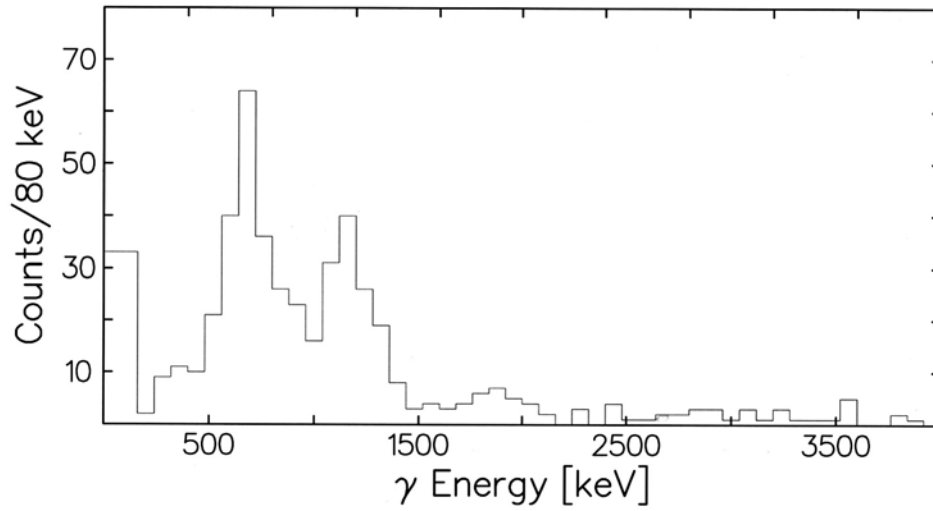
Fig. I-9 BGO γ-ray spectrum gated by the 199 keV, 598 keV and 798 keV Ge gates.

a.6. Study of the Breakout Reaction ^{18}Ne(α,p)^{21}Na (S. Sinha, J. P. Greene, D. Henderson, R. V. F. Janssens, C. L. Jiang, E. F. Moore, G. Mukherjee, R. C. Pardo, T. Pennington, K. E. Rehm, J. P. Schiffer, S. Artemov,* A. Chen,† L. Jisonna,‡ R. E. Segel,‡ and A. H. Wuosmaa§)

The breakout from the hot CNO cycle into the rp-process is controlled by three reactions: ^{18}F(p,α)^{15}O, ^{15}O(α,γ)^{19}Ne, and ^{18}Ne(α,p)^{21}Na.[1] The first of these reactions has to compete with the ^{18}F(p,γ)^{15}O cross section, which is stronger by a factor of about 2×10^3.[2] The second reaction was found to be negligible at nova temperatures, due to the small alpha width of the first excited state above the threshold in ^{19}Ne. The third reaction has the highest Coulomb barrier among the three possible candidates, but has so far been studied only in the excitation energy region E_x (^{22}Mg) ≥ 10.12 MeV.[3] We performed an experiment with the goal to extend these measurements down to E_x = 9.3 MeV. To avoid the use of a ^{4}He gas target we studied the (α, p) reaction through its time-inverse p(^{21}Na, α)^{18}Ne reaction using a ^{21}Na beam produced with the in-flight technique. A gas cell target filled with deuterium was bombarded with a ^{20}Ne beam from ATLAS and the ^{21}Na^{11+} ions produced via the d(^{20}Ne,^{21}Na)n reaction were transported into a scattering chamber located in front the Split–pole spectrograph. Beam intensities of 2×10^5 Na/s on target were obtained, limited by the amount of ^{20}Ne beam that could be put on the gas cell foils. The hydrogen target consisted of a 360-μg/cm^2 thick CH$_2$ foil, equivalent to a range of 150 KeV in excitation energy. The outgoing particles (^{18}Ne and α) were detected in coincidence in a PPAC-ionization chamber—position sensitive Si detector array consisting of two annular strip detectors, providing energy and angle information. This setup also allows us to obtain information about elastic and inelastic scattering of protons on a ^{21}Na which is needed to obtain the transition strengths to excited states in ^{21}Na populated via the ^{18}Ne(α,p)^{21}Na reaction. With this setup, an excitation function in the energy range E_x = 9.3-10.5 MeV was measured. The data are presently being analyzed.

---

*Institute of Nuclear Physics, Tashkent, Uzbekistan, †McMaster University, Hamilton, Ontario, ‡Northwestern University, §Western Michigan University.

[1]A. E. Champagne and M. Wiescher, Annu. Rev. Nucl. Part. Sci. **42**, 39 (1992).
[2]K. E. Rehm *et al.,* Phys. Rev. C **55**, R566 (1997).
[3]D. Groombridge *et al.,* Phys. Rev. C **66**, 055802 (2002).

a.7. Ne, Na and Al Burning in Astrophysically Important (p,γ) Reactions (C. J. Lister, M. P. Carpenter, T. L. Khoo, R. V. F. Janssens, E. F. Moore, G. Mukherjee, K. E. Rehm, A. H. Wuosmaa, D. G. Jenkins,* B. R. Fulton,† M. Freer,† B. J. Truett,‡ and J. Jose§)

The exact excitation energies, spins, parities and widths of near-threshold states in astrophysically important (p,γ) burning reactions have a very strong impact on the reaction rates which produce and destroy elements. For some time we have been investigating the possibility of using heavy ion reactions to populate these states, and then exploiting the power of Gammasphere to investigate the radiative decays. This approach seems generally very useful in precisely placing the excitation energy of states with "germanium-quality" resolution, (i.e. to a few kilo-electron volts), in resolving close doublets, in constraining spins through angular distribution and branching determinations, and in measuring short lifetimes through the Differential Doppler Shift technique.

Our first project, investigating the ^{22}Na(p,γ)^{23}Mg reaction through use of the ^{12}C(^{12}C,n)^{23}Mg population mechanism, made most progress. We were helped by collaboration with an astrophysicist, Professor J. Jose from the University of Vilanova in Spain, who is interested in production and destruction of intermediate mass isotopes and helped with interpretation of the significance of our new reaction rate determination, and its implication for space-based gamma-ray astronomy. A Physical Review Letter[1] was submitted on this subject.

We also collected some data relevant to the ^{26}Al(p,γ)^{27}Si reaction, through investigation of the ^{16}O(^{12}C,n)^{27}Si production mechanism. This destruction reaction is important, as gamma-rays associated with

[26]Al beta-decay were seen in space-based observatories, so production and destruction rates are crucial for investigating the amount of [26]Al produced in explosive cosmic events. It is clear that a new dedicated experiment will be needed to produce the data set required for a useful investigation.

_____

a.8. Production of a Radioactive [37]K Beam with the In-Flight Technique (K. E. Rehm, R. C. Pardo, J. P. Greene, A. Heinz, D. Henderson, R. V. F. Janssens, C. L. Jiang, L. Jisonna, E. F. Moore, G. Mukherjee, T. Pennington, J. P. Schiffer, R. E. Segel, and S. Sinha)

In some explosive astrophysical environments the reaction flow proceeds through a series of (α,p) reactions or proton-rich nuclei. One of these is the [34]Ar(α,p)[37]K reaction which plays an important role for the light curve of x-ray bursts.[1] Earlier plans to measure this reaction directly with a [34]Ar beam and a [4]He target were unsuccessful due to difficulties with separating the heavy reaction products ([37]K, [34]Ar) from the [32]S primary beam which is used to produce the [34]Ar beam. It was, therefore, decided to study the time-inverse [37]K(p,α)[34]Ar reaction, and to obtain the necessary information through the principle of detailed balance. The [37]K beam is produced via the inverse d([36]Ar,[37]K)n reaction with a 300 MeV [36]Ar beam from the ATLAS accelerator bombarding a gas cell target filled with deuterium and cooled to liquid nitrogen temperatures. The [37]K[19+] ions (E = 260 MeV) were collected with a superconducting solenoid located directly behind the production target and separated from the primary [36]Ar beam with the 22° bending magnet. The beam intensity and purity were monitored with the position-sensitive ionization chamber located in the focal plane of the magnetic spectrograph. The specific production rate measured at this energy was 1200 [37]K/sec/(pnA of [36]Ar beam). Although the ATLAS accelerator could provide sufficient [36]Ar intensity to produce secondary beam intensities of 5 × 10^{5} [37]K/s on target, the HAVAR entrance and exit foils of the gas target could only withstand a primary beam intensity of 50 pnA. In order to increase this value we plan to replace the foils with a higher melting point material in a future run.

_____

[1]M. Wiescher et al., J. Phys. G 25, R133 (1999).

a.9. Measurement of [44]Ti Half-Life (I. Ahmad, J. P. Greene, E. F. Moore, W. Kutschera,* and M. Paul†)

The half-life measurement of [44]Ti, which was started in March 1992, is being continued at Argonne and Jerusalem with the aim of reducing systematic uncertainties. The half-life determined from 5 years decay was published[1] in 1998. Now we have data for more than 10 years decay. The half-life is being measured by recording spectra of a mixed source of [44]Ti and ^{60}Co with a 25% Ge detector at regular intervals. At Argonne, the spectra of the mixed source are being measured at two source-to-detector distances of 5.2 cm and 10.2 cm. Also, spectra of pure [44]Ti and pure ^{60}Co are measured separately at 5.2 and 10.2 cm. The half-life values were obtained by analyzing the 1157/1173 and 1157/1333 ratios of the [44]Ti and ^{60}Co gamma rays. The preliminary analysis shows that the half-life of 59.2 ± 0.6 yr reported in our 1998 article is still correct within the quoted uncertainty. The decay of the 1157/1173 ratio measured for a source-to-detector distance of 5.2 cm is displayed in Fig. I-10 The spectra are being analyzed and the results will be published by the end of the year.

_____
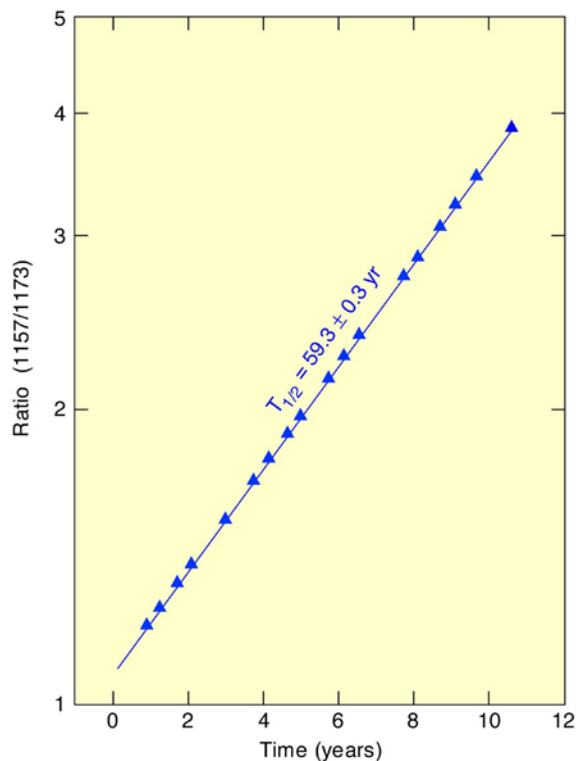
Fig. I-10. A semilograthmic plot of the ratio of counts in 1157.0-keV peak of ^{44}Ti and 1173.2-keV peak of ^{60}Co against decay time. The measurements were performed at ANL using a mixed source of ^{44}Ti and ^{60}Co.

a.10. Mass Measurements Along the rp-Process Using the Canadian Penning Trap Mass Spectrometer (G. Savard, B. Blank, A. Heinz, A. F. Levand, D. Seweryniak, W. Trimble, Z. Zhou, J. A. Clark,* J. Vaz,* J. C. Wang,* R. C. Barber,† K. S. Sharma,† C. Boudreau,‡ F. Buchinger,§ J. E. Crawford,§ S. Gulick,§ J. K. P. Lee,§ and G. D. Sprouse¶)

A large variety of elements are known to exist in the universe, but the processes that created many of them are not well understood. A possible scenario for their production is a rapid proton-capture process (rp-process[1]), which is thought to occur in such explosive astrophysical events as novae and X-ray bursts. The masses of the nuclides involved are essential in determining the exact path of the rp-process. Particularly important are the masses of "waiting-point" nuclides along the rp-process path where the process stalls until the subsequent β-decay of these nuclides. The masses of two significant waiting-point nuclides, namely ^{68}Se and ^{64}Ge, are critical in determining the final abundance of the elements and the light-curve profiles and energy generation of X-ray bursts. For

temperatures of 10^9 K which occur on the surface of these stellar environments, a mass precision of at least $kT/c^2 \sim 100\ keV/c^2$ is required. Such a precision is obtained easily with the Canadian Penning Trap (CPT) mass spectrometer.

The nuclides investigated are produced in fusion-evaporation reactions between targets mounted on a rotating wheel and heavy-ion beams from the ATLAS facility (see Fig. I-11). Once created, the reaction products are separated from the primary beam using a velocity filter and enter an Enge magnetic spectrograph where they are mass separated and focussed into a gas catcher system. There, the initially high-energy recoil products are thermalized in 200 mbar of helium.

The ions are extracted from the gas cell via a combination of gas flow and electric fields and are guided towards the isobar separator as the helium is pumped away.

It is necessary to limit the number of impurity ions injected into the precision Penning trap. Any contaminants may overwhelm the weakly-produced isotopes of interest and affect the measured cyclotron frequency. The reduction of these contaminant ions is accomplished by the newly installed isobar separator (see report g.10.). The desired ions are then periodically ejected and guided to a radio-frequency quadrupole (RFQ) ion trap where they are accumulated before being transferred to the precision Penning trap.

During the past year, mass measurements of ^{64}Ge and ^{68}Se were completed. The production of ^{68}Se was provided by the reaction between a 220 MeV beam of ^{58}Ni upon a carbon target. The masses of other nuclides created in this reaction, notably ^{68}Ge and ^{68}As, were also measured and improved. Recently, an experiment was conducted to measure the mass of ^{64}Ge, the resulting TOF spectrum is shown in Fig. I-12. In this case, a 185 MeV ^{54}Fe beam was incident upon the carbon target. The analysis of ^{68}Se is almost complete (m = 67941798 ± 35 μu) and a preliminary value for the mass of ^{64}Ge is 63941653 ± 34 μu. The influence of these new masses on the duration and intensity of the light curve will now be studied.
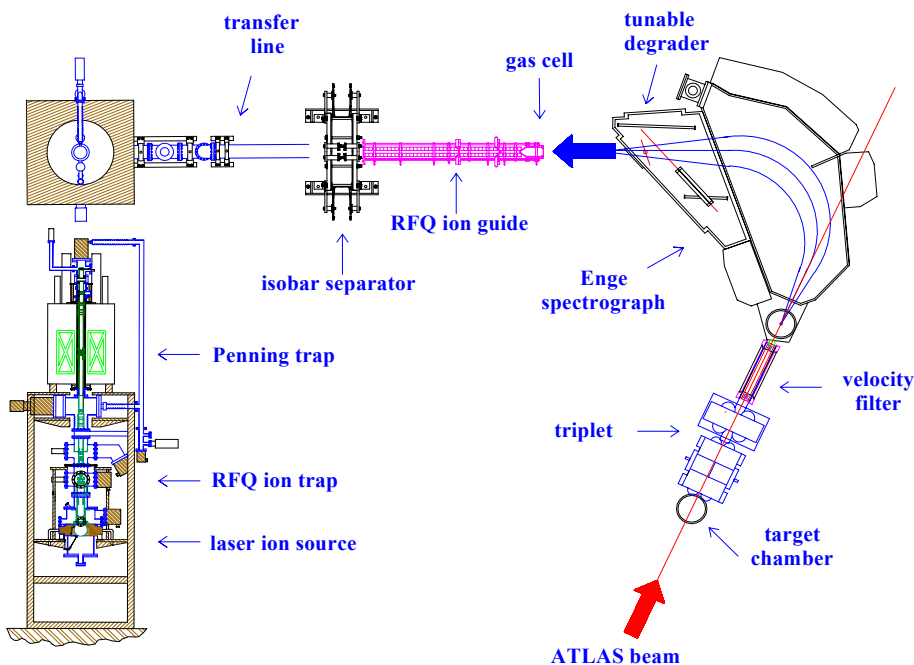
Fig. I-11. An overview of the CPT apparatus, including the recent addition of the isobar separator. The lower left section of the figure is a side view of the CPT.

Attention will now move to the end-point of the rp-process which has been calculated to reach the Sb-Te region and occurs during the cooling phase of the X-ray burst. Mass information is critical as inputs to these calculations. We are therefore setting up for a measurement of the masses of neutron-deficient Sb and Sn isotopes which dictate the behavior of the alpha-cycling expected to be responsible for the rp-process termination.

_____

*Argonne National Laboratory and University of Manitoba, Winnipeg, Manitoba, †University of Manitoba, Winnipeg, Manitoba, ‡Argonne National Laboratory and McGill University, Montreal, Quebec, §McGill University, Montreal, Quebec, ¶State University of New York at Stony Brook.
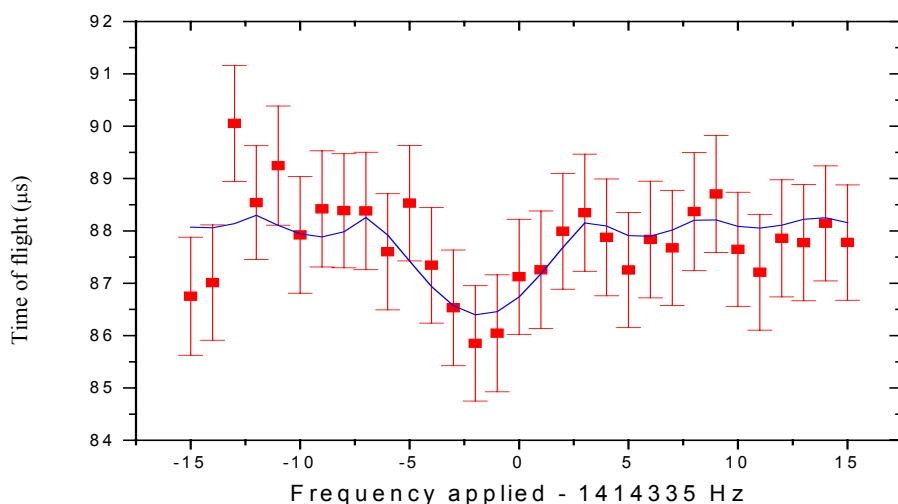
Fig. I-12. Time-of-flight spectrum for ^{64}Ge ions. The ions excited at resonance gain energy and hence exhibit a slightly shorter flight time in transit to the detector.

a.11. Direct Q_β Measurement of the N = Z rp-Process Waiting-Point Nucleus ^{68}Se and Its Astrophysical Implications (A. Wöhr,* C. N. Davids, A. M. Heinz, R. F. V Janssens, D. Seweryniak, S. M. Fischer,† A. Aprahamian,‡ P. Boutachkov,‡ D. S. Brenner,§ J. L. Galache,‡ J. Görres,‡ A. Teyrurazyan,‡ M. Shawcross,‡ and M. C. Wiescher‡)

The motivation of this experiment is the behavior of the rp-process at the ^{68}Se-waiting point (see Fig. I-13). The question is, whether the waiting point is overcome by β-decay into ^{68}As or by the reaction ^{68}Se(2p,γ)^{70}Kr. One tile in this jigsaw puzzle is the mass of ^{68}Se, which is deduced via β-endpoint measurement. This endpoint was measured at the Fragment Mass Analyzer at Argonne National Laboratory using a moving tape collector system. The reaction which was used was ^{12}C (^{58}Ni,2n)^{68}Se. Since ^{68}Se was produced three orders of magnitude less in yield than its isobar ^{68}As, the analysis proved to be difficult.

The analysis is close to being finished and a publication is in preparation. A preliminary Q_β value could be determined (see Fig. I-14). This value is in agreement with the prediction of Audi and Wapsta. Theoretical calculations performed during the analysis process indicate that there might be an isomer in ^{68}Se. In previous experiments including this one the predicted the isomer could not be observed. Presently an experiment to search for the isomer in ^{68}Se using the inverse reaction is in preparation at the Notre Dame Nuclear Structure Laboratory.

Furthermore, network calculations to study the influence of different nuclear masses on the rp-process are under way.

_____

*Argonne National Laboratory, University of Notre Dame and University of Maryland, †Argonne National Laboratory and DePaul University, ‡University of Notre Dame, §Clark University.
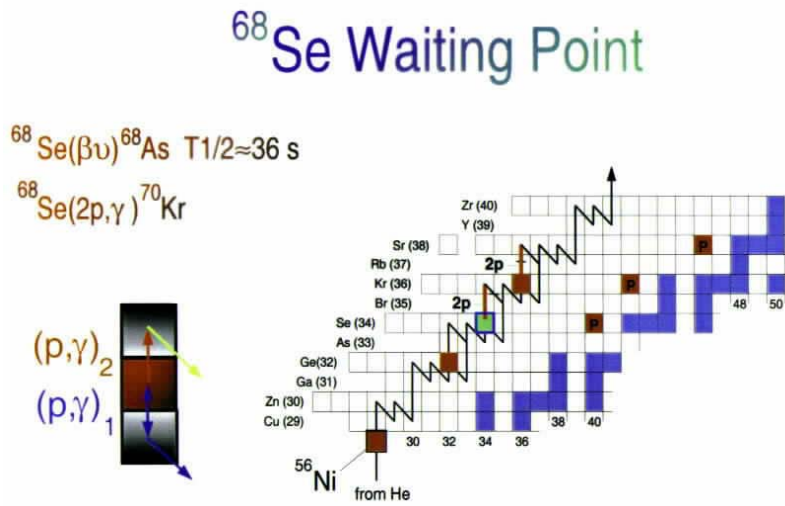
Fig. I-13. The N = Z rp-process ^{68}Se waiting point is shown. Possible nucleosynthesis reactions are indicated. The "waiting point" nuclei are very important for setting the timescale for x-ray bursts.
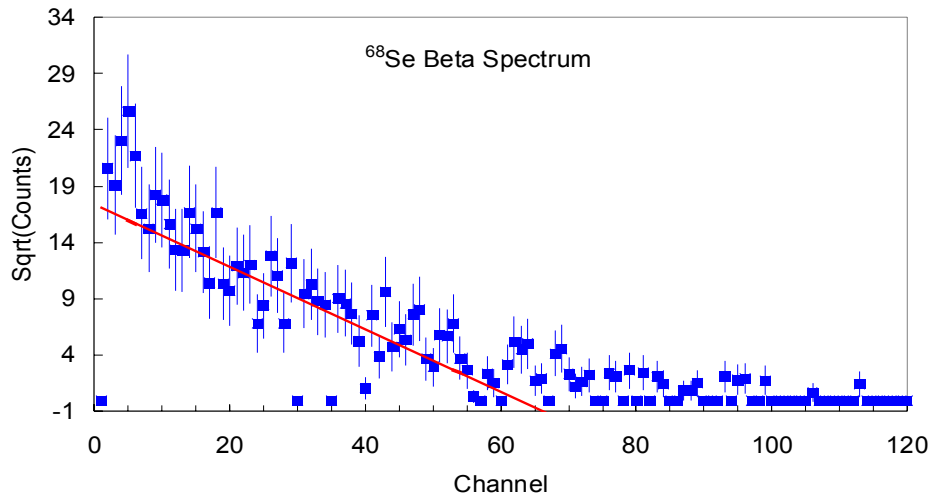
Fig. I-14. Fermi-Kuri plot of the ^{68}Se β-spectrum. Shown here is the sum of all gates feeding the 426 keV level in ^{68}As.

B. STRUCTURE OF NUCLEI VERY FAR FROM THE VALLEY OF STABILITY

The program to explore the structure and stability of nuclei along the proton dripline continues to be a forefront theme in our nuclear structure research. It has many interesting facets, both for astrophysical processes (especially the rp-process) and for developing our understanding of the structure and stability of poorly-bound nuclei. It provides a natural bridge that connects contemporary research with future projects which exploit radioactive beams. Modifications that will allow a higher level of sensitivity for Gammasphere experiments at the dripline are being executed and will be in place for operation in 2003. The techniques of proton decay spectroscopy also continue to be refined, allowing studies of shorter lived, and more weakly produced species further from stability. In both cases, upgrades to the FMA have significantly increased the sensitivity of future experiments.

The possibility of studying the structure of very neutron-rich nuclei in the future seems very good, including some nuclei close to the predicted r-process nucleosynthesis trajectory. In this domain conventional heavy-ion fusion-evaporation is not useful, due to the curvature of the valley of stability, but by investigating the prompt gamma-ray spectroscopy of fission fragments, and by studying gamma rays following multi-nucleon transfer reactions, very considerable progress is possible. Many of these studies provide a natural compliment to the data recently obtained from fast-fragmentation facilities. The fast fragmentation allows the identification of low-lying states in these nuclei, which can be developed in many cases with detailed spectroscopy using Gammasphere. The precise determination of the masses of dozens of very neutron-rich fission fragments has started, using a fission source, the gas-cooler and the CPT. Many of these masses have not been measured before, and of the nuclides that have been measured, most are being improved in precision from hundreds of kilo-electron volts to tens of kilo-electron volts.

B.1.   Proton-Rich Nuclear Spectroscopy

b.1.1. The ^{56}Ni(^{3}He,p) Reaction and the Question of T = 0, T = 1 Pairing in N = Z Nuclei
(K. E. Rehm, C. N. Davids, J. P. Greene, A. Heinz, R. V. F. Janssens, C. L. Jiang, E. F. Moore, G. Mukherjee, R. Pardo, D. Seweryniak, J. P. Schiffer, A. O. Macchiavelli,* A. Görgen,* P. Fallon,* M. Cromaz,* J. Cizewski,† J. Thomas,† and M. Paul‡)

A wealth of experimental evidence has accumulated over the years in support of the existence of *nn* and *pp* pairs, but there is little or no evidence for *np* pairing mainly because of the experimental difficulties in studying intermediate mass N = Z nuclei. Nevertheless, following recent advances in the experimental techniques and considering the new possibilities that are becoming available with radioactive beams, there has been a revival of nuclear structure studies along the N = Z line. Our analysis of experimental binding energies of nuclei along the N = Z line indicates that the odd-odd T = 1 states are as bound as the ground-state in their even-even neighbors, and this can be interpreted as a consequence of full isovector pairing.[1] The odd-odd T = 0 states were found to be less bound than the even-even neighbors by an energy $2\Delta \sim 2(12/A^{1/2})$ MeV which amounts to the blocking of the T = 1 correlations. This result not only suggests that the T = 0 states behave like any other odd-odd nucleus ground state in the nuclear chart, but also leaves no room to support the existence of an isoscalar pair condensate. Near closed shells, the strength of the pairing force relative to the single-particle level-spacing is expected to be less than the critical value needed to obtain a superconducting solution, and the pairing field then gives rise to a collective phonon.[2] It then seems natural to ask whether T = 0 collective effects may show as a vibrational phonon.

Based on a re-analysis of the pairing vibrational spectra near ^{56}Ni[3] one can infer a rather collective behavior in the T = 1 particle-particle channel and a single-particle character for the T = 0, consistent with the results from the binding energy differences. We know however, that a more sensitive probe of pairing correlations is provided by two nucleon transfer reactions and submitted a proposal to study the reaction ^{56}Ni(^{3}He,p) to confirm the conclusions implied by the analysis above. We argued that the (^{3}He,p) reactions in even-even N = Z nuclei will give a unique fingerprint of *np* pairing correlations.

The work proceeded in two steps. First, we carried out a series of runs to study the (^{3}He,p) reaction in inverse kinematics, using the stable beams of ^{28}Si, ^{32}S, ^{36}Ar, and ^{40}Ca. The setup, similar to that previously used in Refs. 4 and 5, consisted of an annular Si strip detector (16 rings × 16 sectors) covering the angular range from 167° to 154°, a ^{3}He gas target cell (50 μg/cm^2) and the FMA. Although the (^{3}He,p) reaction is extremely clean in the backward angles, the singles spectrum is dominated by charged particles emitted by compound reactions in the Ti windows of the gas cell. Therefore, coincidences with the FMA are very important, even for the stable beam reactions, to sufficiently clean up the spectrum.

We note that the angular range covered by the Si detector in the CM system is 8° - 16°, where the $\Delta l = 0$ transfer cross sections are favored. A summary of the energy matched proton spectra for the systems studied is shown in Fig. I-15. The different number of counts reflects the different running times. In each case, the beam current was kept at a level of about 200 epA. The 0^+ and 1^+ states of interest are indicated. A strong proton group with energy ~3 MeV is observed in all cases, and requires further analysis.
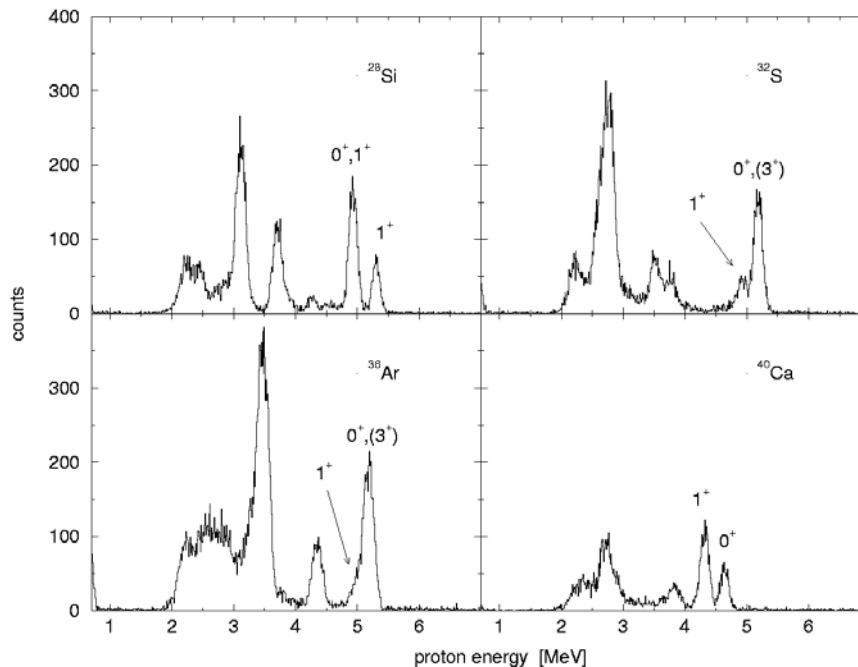
Fig. I-15. Summary of the proton spectra in coincidence with the FMA, obtained for several (d,p) reactions using stable beams. The protons are measured at backward angles in the laboratory and the beam-like reaction products are detected near 0° in the FMA.

*Lawrence Berkeley National Laboratory, †Rutgers University, ‡Hebrew University, Jerusalem, Israel.
[1]A. O. Macchiavelli *et al.*, Phys. Rev. **61**, 041303R (2000).
[2]D. R. Bes and R. A. Broglia, Nucl. Phys. **80**, 289 (1966).
[3]A. O. Macchiavelli *et al.*, Phys. Lett. **B480**, 1 (2000).
[4]K. E. Rehm *et al.*, Phys. Rev. Lett. **80**, 259 (1996).

[5]C. L. Jiang *et al.*, to be published.

After the successful completion of this part, we proceeded with the ^{56}Ni experiment. In September 2002, a ^{56}Ni cone was produced at the IPNS that was then transferred to the ATLAS tandem source. Unfortunately, the beam intensity on target turned out to be at least a factor of 10 less than our original estimate of 3×10^5 /s, which was insufficient to accumulate enough statistics for the (^{3}He,p) reaction. Possible improvements in the Tandem injection and transmission are presently being considered for a second attempt.

b.1.2. Unravelling the Backbends in ^{68}Se and ^{72}Kr: The Quest for np-Pairing (C. J. Lister, S. M. Fischer,* and D. P. Balamuth†)

It has been widely speculated that short range neutron-proton correlations, either with *T = 0* or *T = 1* would influence the high-spin behavior of nuclei, particularly in modifying the rotational frequencies at which correlated pairs break apart. It was suggested that evidence for an effect of this kind would be found in studying the cascades of gamma rays following heavy-ion reactions, as the pair breaking is associated with changes in moment of inertia. The effect is widely expected to be most clear-cut in *N = Z* nuclei, as those nuclei have the biggest overlap of neutrons and protons near the Fermi surface, so are most susceptible to np-pairing correlations. Thus, comparison of *N = Z* and *N = Z + 2* nuclei in middle mass (A ~ 70) nuclei, seems to offer the optimum situation for studying these correlations. Of particular interest is the *T = 0, J ≠ 0* deuteron-like isoscalar mode that could lead to a recondensation of particles at the Fermi Surface.

We conducted several investigations of the key *N = Z* nuclei ^{68}Se and ^{72}Kr. It is clear that these nuclei behave unusually. However, our new data, when combined with other recent studies of *N = Z + 2* ^{70}Se and ^{74}Kr, reveal a complicated situation of shape-coexistence, and the naïve expectations that np-pairing strengths can be extracted seem very optimistic. All the nuclei show evidence for two shapes, both triaxial, one with lower collectivity (triaxiality parameter, γ, positive) and one of high collectivity (γ negative). Each shape has its own alignment scheme. One also can observe that the bands in each minima have very different quadrupole moments, and irregularities in the moments of inertia arise when bands of very different structure cross. Figure I-16 shows the experimental routhians (the relative energy of states in the rotating frame). Even spin, positive parity bands are shown. Clearly, several common features can be seen, with one set of states which evolve smoothly with rotational frequency, and a further set that shows very strong irregularities.

In all, when like bands are compared, there seems very little room for "alignment delay" the fingerprint expected for enhanced pairing. It must be said, however, that it is very difficult to reproduce the very high crossing frequencies in the more collective sequences in krypton isotopes without invoking some new physics.

A paper has been accepted for publication in Physical Review C.[1]

_____

[1]S. M. Fischer, C. J. Lister, and D. P. Balamuth, Phys. Rev. C**67**, 064318/1-13 (2003).
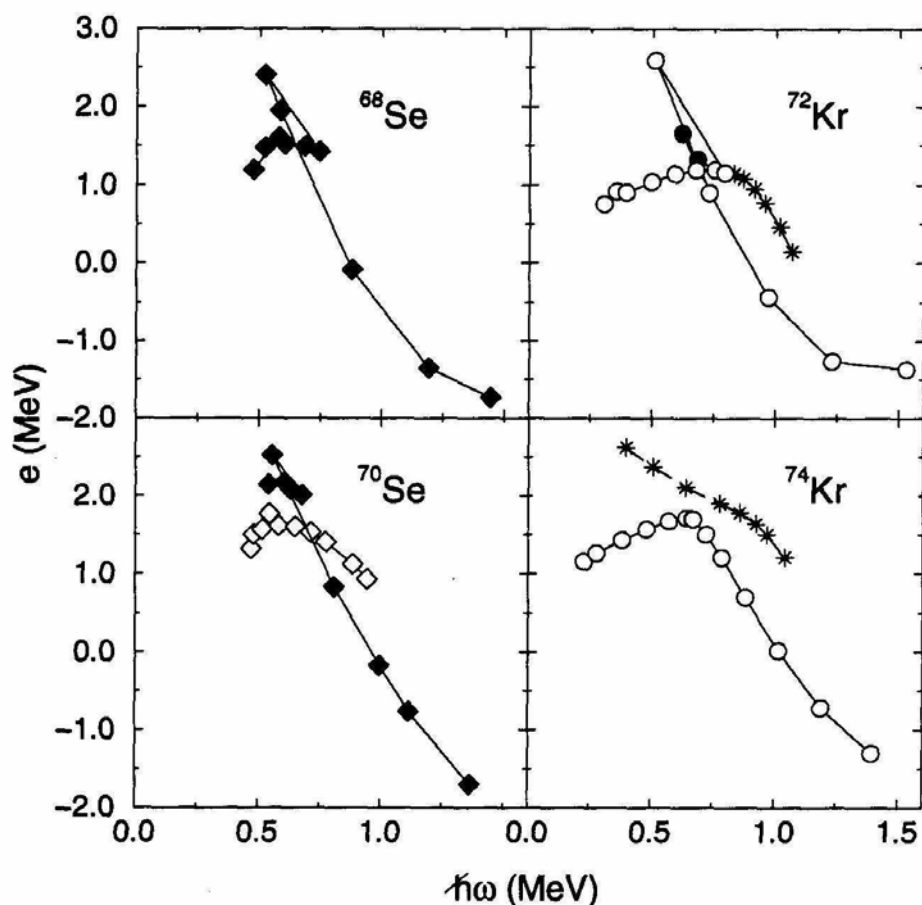
Fig. I-16. The experimental routhians for even spin, positive parity bands in ^{68,70}Se and ^{72,74}Kr, revealing evidence for shape coexistence in all spin ranges, but little evidence for "alignment delay" that might be associated explicitly with np-pairing correlations.

b.1.3. Structure and Significance of Isomers in Intermediate Mass N = Z Even-Even Nuclei (C. J. Lister, N. Hammond, S. Sinha, G. Mukherjee, S. M. Fischer,* D. Balamuth,† B. Blank,‡ A. Aprahamian,§ and A. Woehr§)

Isomers in intermediate mass N = Z nuclei are interesting for structural and astrophysical reasons. In structure, the interest in the isomers arises from investigating and understanding their shape co-existence. In ^{72}Kr, a low-lying shape-isomeric first excited state was found[1] which can only decay through conversion electrons, so that it will have a very long lifetime in hot, highly ionized nucleosynthesis sites. In astrophysics, these isomers can have a strong influence on "waiting points" in the rp-process; suitable isomers can drastically enhance the destruction rates of the parent nuclei through (p,γ) reactions.

A key waiting point nucleus of interest is ^{68}Se. It was shown[2] to exhibit extremely clear-cut shape co-existence, with an oblate groundstate and prolate excited states. The low-lying prolate bandhead was expected to be isomeric in analogy with the recent ^{72}Kr discovery. However, both isomer searches following fragmentation[3] at GANIL and prompt spectroscopy with Gammasphere[2] failed to find the prolate bandhead. These studies constrain the possible location of this state rather tightly. A recoil-shadow experiment to find this shortlived (~10 ns) bandhead and understand its decay properties is being designed and will be constructed at the University of Notre Dame.

A further experiment was approved to run at ATLAS using Gammasphere and the FMA. The goal is to seek "linking" transitions between oblate and prolate shapes in ^{72}Kr. The intensity of these γ-decays will provide information about mixing of wavefunctions in the two minima.

*DePaul University, †University of Pennsylvania, ‡Sabbatical visitor from the University of Bordeaux, France, §University of Notre Dame.
[1]E. Bouchez *et al*., Phys. Rev. Lett. **90**, 082502 (2003).[2]S. M. Fischer *et al*., Phys. Rev. Lett. **84**, 4064 (2000).
[3]A. Goergen, University of Saclay, private communication (2003).

b.1.4. Gamma Vibration and Quasiparticle Excitations in ^{80}Sr (C. J. Lister, T. Sienko, and R. A. Kaye*)

^{80}Sr lies towards the middle of the deformed A ~ 80 region. It was studied extensively and detailed papers[1-4] were published on its properties, which now include several superdeformed bands. Surprisingly, despite its large production cross section and the numerous investigations, there remains considerable disagreement about spin assignments and band structure, even at the lowest spins.

In this study, ^{80}Sr was copiously produced following the ^{24}Mg(^{58}Ni,2p)^{80}Sr reaction at 200 MeV. The investigation of the prompt decay γ-rays used Gammasphere, triggered by both Mass and Charge selection. Mass identification was achieved using the Fragment Mass Analyzer (FMA) selecting only A/q = 80/25 ions, and charge selection was obtained using an ion chamber. After suitable data manipulation, a γ–γ coincidence matrix was produced which consisted of >95% ^{80}Sr correlations. A coincidence window on the 386 keV first excited state had >10^6 correlated counts.

Many new excited states were found. The unusually clean data set allowed identification of weakly populated non-yrast structures. Several features were clarified. The even- and odd- spin members of the gamma vibrational band were found and extended to high spin. The band starts at low excitation, well below other quasi-particle excitation, as might be expected for a collective excitation. The odd- even-energy staggering of spins was found to be intermediate between the "rigid" and "gamma-soft" limits. The new assignments now fit well with systematic trends of gamma-vibrational structures in the region (see Fig. I-17). The J = 7 states identified by Davie *et al*.[1] are now assigned to have negative parity, again in better agreement with neighboring nuclei. Finally, at the highest spins, the yrastline stops being a smooth rotational sequence, and considerable "forking" is found as quasi-particle excitations with larger moments of inertia approach and then cross the rotational ground state band. The highest spins may well correspond to the low-collectivity, near-oblate motion predicted by Nazarewicz *et al*.[5] many years ago.[6]

A paper was written and accepted for publication in Physical Review C.

*Purdue University-Calumet.
[1]R. F. Davie *et al*., Nucl. Phys. **A463**, 683 (1987).
[2]D. Winchell *et al*., Phys. Rev. C **61**, 044322 (2000).
[3]J. Döring *et al*., Phys. Rev. C **59**, 59 (1999).
[4]M. Devlin, F. Lerma, D. Sarantites, *et al.*, Phys. Lett. **B415**, 328 (1997); Phys. Rev. Lett. **83**, 5447 (1999).
[5]W. Nazarewicz, J. Dudek, R. Bengtsson, T. Bengtsson, and I. Ragnarsson, Nucl. Phys. **A435**, 397 (1985).
[6]T. Sienko, C. J. Lister, and R. A. Kaye, Phys. Rev. C**67**, 964311/1-8 (2003).
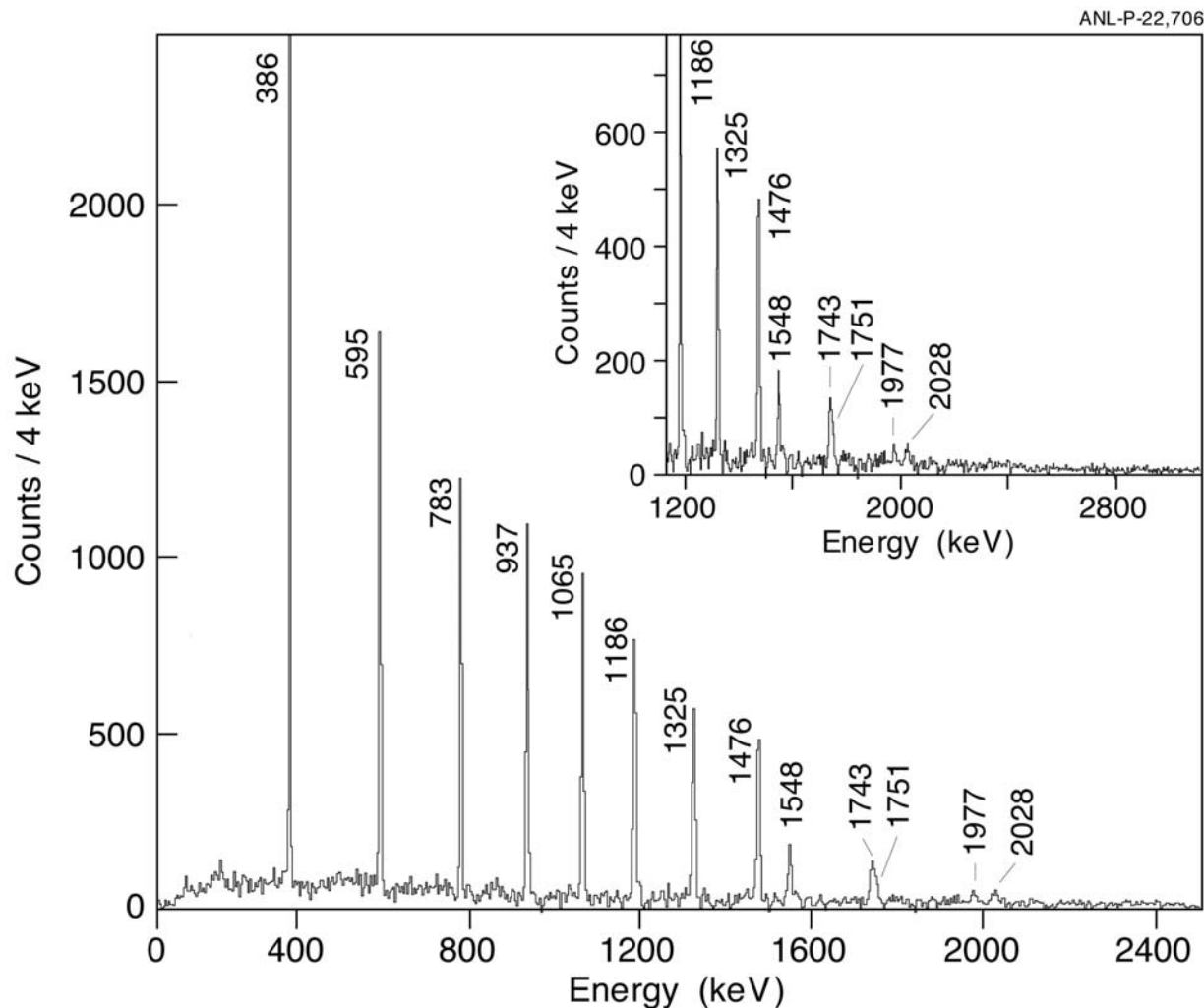
Fig. I-17. A sample of the high quality γ–γ data from this experiment, showing a single gate set on the 1579 keV J = 18 →16 decay in the yrast line. Above this point "forking" of the band occurs; the yrast sequence has a backbend which has been predicted to correspond to a change from a collective near-prolate to non-collective near-oblate shape.

b.1.5. The Spectroscopy of T = 0 and T = 1 Low-Lying States in Odd-Odd N = Z Nuclei
(C. J. Lister, G Mukherjee, N. Hammond, S. Sinha, S. M. Fischer,* D. P. Balamuth,† and S. Freeman‡)

The study of N = Z odd-odd nuclei beyond [58]Cu is topical for many reasons. The nuclei are structurally interesting as the low-lying multiplets contain information about both long- and short-range neutron-proton correlations and coupling with both isospin T = 0 and T = 1. They lie along the rp-nucleosynthesis path, so low lying isomers can influence rp-reaction rates. Finally, the ground states have superallowed Fermi decays, so understanding the wavefunctions of low-lying states help improve the calculation of small

structure-dependent corrections needed to test the Standard Model.

We completed a study of [70]Br.[1] In it we investigated methods to optimize the population of the important low spin, non-yrast states. This was difficult; the nuclei lie far from stability, so reactions to populate the isotopes of interest are limited and fusion of very heavy ions appears to be essential for detailed spectroscopy. The states of greatest interest have
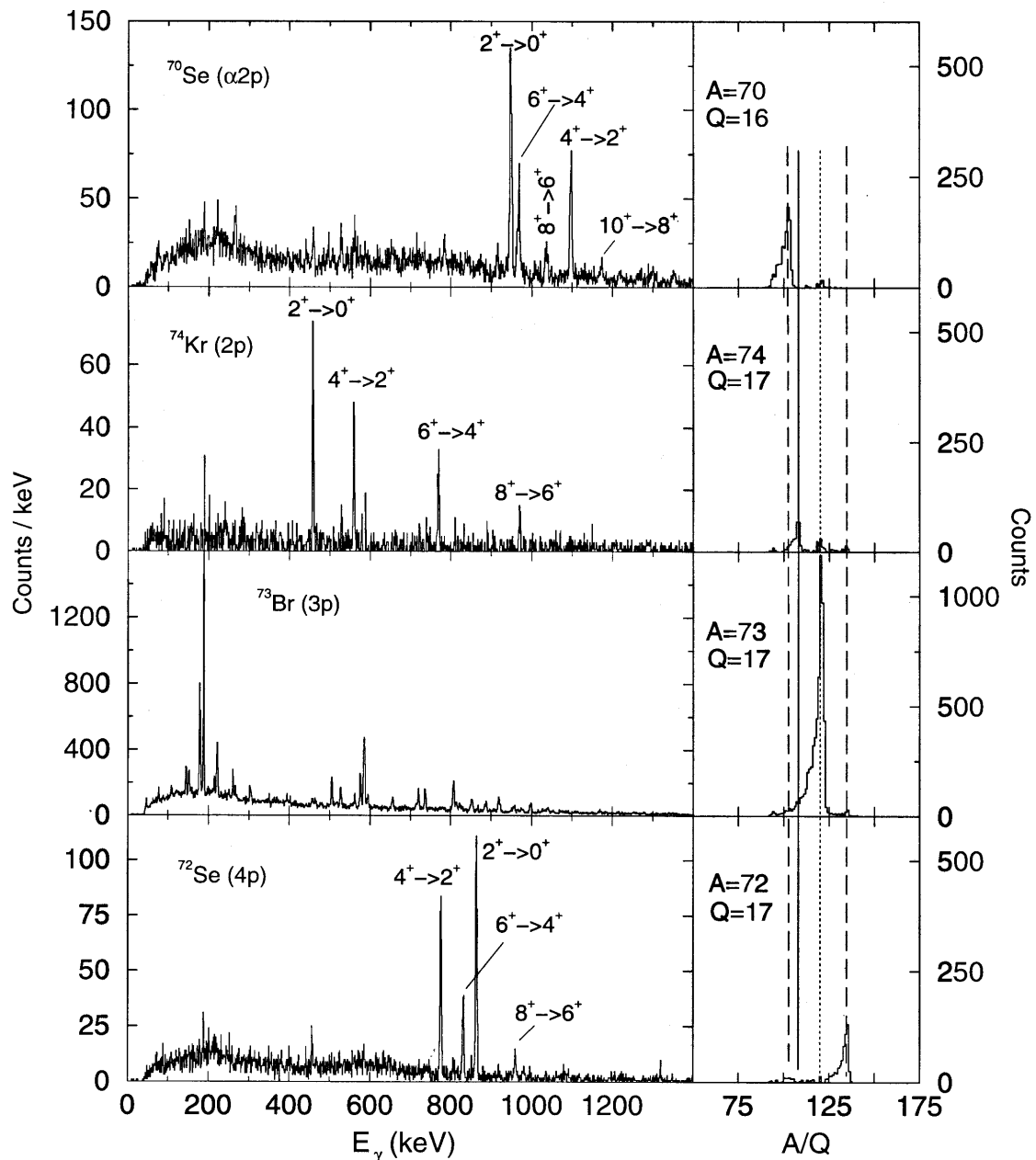
Fig. I-18. The panels on the left show recoil and mass gated γ-ray spectra from a single, unsuppressed 70% HPGe detector from the reaction $^{36}Ar + {}^{40}Ca$ at 104 MeV. The panels on the right show the PGAC "X" spectra with a recoil requirement and a gate on a strong γ-ray transition in the corresponding nucleus of interest. The mass peaks are identified by mass number and charge state. These data were collected over a period of ~14.5 hours.

low spin, and so are not normally well populated in heavy ion reactions. They are best reached by cold, near-barrier (even sub-barrier) fusion.   These cold reactions at very low energy have small production-cross sections, typically ~100's μb.   Consequently,

even with the largest current detector arrays, this type of study is difficult and lies at the edge of feasibility.

With the anticipation of a new Gammasphere campaign at ANL we performed a test experiment to find the optimum conditions for studying ^{74}Rb and ^{78}Y

identified using the FMA. These odd-odd N = Z nuclei lie near the center of the A ~ 80 region. They are expected to have quite stable deformation, so provide the best base for investigating neutron-proton correlations. We are interested in the energy dependence of populating the important states in these nuclei through the ^{40}Ca(^{36}Ar,pn)^{74}Rb and ^{40}Ca(^{40}Ca,pn)^{78}Y reactions. In practice, these channels are too weak for a test experiment using a single germanium detector, but the stronger (~50 mb) surrogate ^{40}Ca(^{36}Ar,2p)^{74}Kr and ^{40}Ca(^{40}Ca,2p)^{78}Sr reactions allow the partial wave distributions to be extracted by measuring the yields of known states. We studied Fragment Mass Analyzer (FMA) gated gamma

spectra, and neutron-gated spectra in order to optimize settings for clean, high beam current investigations. Figure I-18 shows some mass-gated spectrum which clearly reveals the excellent channel selection. We measured excitation functions for both systems, and studied the spin distributions in the residues. At the peak of the yield, the mean entry spin appears to be ~8 h, ideal for low spin, non-yrast studies.

The cross sections appear to be similar to the ^{70}Br project, and clearly FMA gating is ideal for these weak channels. With Gammasphere and the neutron shell, mass and neutron gated gamma-spectra should be very clean and ideal for the investigations planned in 2003.

*DePaul University, †University of Pennsylvania, ‡Sabbatical Visitor from University of Manchester, United Kingdom.
[1]D. G. Jenkins *et al*., Phys. Rev. C **65**, 064302 (2002).

b.1.6. Single Particle States in ^{111,113,115}Sb Populated via β-Decay (D. Seweryniak, C. N. Davids, G. Mukherjee, S. Sinha, J. Shergur,* W. B. Walters,* A. Woehr,* P. Boutachkov,† I. Dillmann,‡ A. Teymurazyan,† and I. Zartova†)

The structure of the odd-A Sb nuclides attracted interest over the years mainly because their low-energy, low-spin states involve the coupling of the single Sb proton with the adjacent Sn core.[1] Specifically, the neutron deficient odd-A Sb isotopes provide an important testing ground for shell model calculations based on the heaviest self-conjugate double magic nucleus, ^{100}Sn. Difficulties with the shell model arise as A increases because the higher density of states and more complex configurations. One complication arises from the monopole shift that lowers the $g_{7/2}$ single-proton level to ~800 keV in the light Sb nuclei. As a result, the lowered $g_{7/2}$ core coupled states mix with the core-coupled states associated with the $d_{5/2}$ proton ground state. In addition, more states are added because of the presence of a $9/2^+$ intruder orbital that also mixes with the other configurations to form complicated level structures. Some of these collective states in the A ≥ 115 region have been described well by particle-phonon coupling using the Interacting Boson-Fermion Model (IBFM).[2,3] The nuclei in the region of A ~ 110-115 then provide an ideal place to map the model spaces of both approaches and to compare their predictive power.

The low-energy states in ^{109}Sb were identified by J. J. Ressler *et al*. in a study of the β$^+$/EC decay of ^{109}Te. At the time of these measurements, the significantly lowered positions of the $1/2^+$ and $3/2^+$ states were a surprise, as the $1/2^+$ level is well below the minimum for ^{121}Sb. However, the positions of the lowest $1/2^+$ and

$3/2^+$ states were well reproduced in two recent shell-model calculations.[5,6] It was noted that with present day capabilities, this is as far from ^{100}Sn as the shell model could be properly used. Given the success of the calculations on ^{115,117}Sb with the IBFM, an attempt was made by J. J. Ressler at Yale, in collaboration with V. Zamfir to extend such IBFM calculations to fit the levels observed for ^{109}Sb. The results were not encouraging and, with only poor or no data for the low-spin levels in the intervening nuclides, there was little guidance as to how to evolve the IBFM parameters away from the N = 64 partial shell closure. The goal of the calculations is more ambitious than just a few low-energy levels, but also to account for the rather extensive level structure which arises from the mixing of the two sets of core-coupled states up to the pairing energy that is rather well fit for ^{117}Sb as reported by Lobach and Bucurescu.[2] Thus, the goal of these experiments was the determination of the energy levels in ^{111,113}Sb with low spins (≤ $9/2^+$) up to the 2 MeV pairing energy that can be populated in the β-decay of the respective ^{111,113}Te parents. These new data would be used to bridge the gap between the shell-model region for nuclides with A ≤ 109 and the mid-shell nuclides with N = 64 and 66 to determine how the IBFM and the shell model overlap in this region.

Our experiment was performed at the Argonne Tandem Linear Accelerator System (ATLAS). The parent ^{111,113,115}Te nuclides were produced using a fusion-

evaporation reaction of a beam of 225 MeV ^{56}Fe ions on targets of ^{60,62,64}Ni. All of the Te recoils were produced through the 2pn reaction channel. Reaction products were separated on the basis of their mass to charge ratio M/Q at charge state 24. Following mass separation, the recoils were implanted in the tape of a moving tape collector (MTC). The tape was moved periodically to a Pb-shielded counting station. Count and collect times were varied from ~1 half life for the nuclide of interest to maximize coincidence events, to as long as 3 half-lives in order to permit identification of parent and daughter gamma rays on the basis of half-life. We used two large HPGe detectors (45% and 65%) and two small Ge detectors (~25%) to detect the γ-rays coming from the deposited radioactive source on the tape. In addition to the Ge detectors, two β-scintillators were used to veto zero-degree β–γ coincidences in the same detector, and gate 180º β–γ coincidences. We collected γ-singles, γ–γ coincidences, and γ-t data to isolate transitions in the corresponding ^{111,113,115}Sb daughters. Towards the end of the experiment, the collection and counting periods were shortened to permit observation of the decay of the short-lived ^{111,113,115}I nuclides into their corresponding Te daughters.

Analysis of γ–γ matrices and γ-t spectra confirmed the previously reported low-spin structure for ^{115}Sb. Similar analysis resulted in the identification of at least 20 new gamma transitions and eight new levels in ^{113}Sb. Six of the new levels are above 2 MeV, and are probably 3-quasi-particle levels formed from the coupling of a $d_{5/2}$ proton, the odd $g_{7/2}$ neutron, and a $d_{3/2}$ neutron formed from the spin-flip Gamow-Teller decay of the formerly paired $d_{5/2}$ proton. Recent results also suggest that the previously reported 1018-keV level has a spin of $5/2^+$. Previous experiments had suggested either $3/2^+$ or $5/2^+$, but feeding from the $9/2^+$ 1550 keV level, and feeding to the $7/2^+$ 815-keV level lends support for our $5/2^+$ assignment. As for ^{111}Sb, at least 6 coincidences are seen with the previously observed 851-keV transition, most which come from levels ~2 MeV (Fig. I-19). Once level structures in ^{111,113}Sb are identified, calculations will be performed to test the applicability of various models to this light Sb region.

_____

*University of Maryland, †University of Notre Dame, ‡University of Mainz, Germany.
[1]G. Van den Berghe and K. Heyde, Nucl. Phys. **A163**, 478 (1971).
[2]Yu N. Lobach and D. Bucurescu, Phys. Rev. C **58**, 1515 (1998).
[3]Yu N. Lobach and D. Bucurescu, Phys. Rev. C **57**, 2880 (1998).
[4]J. J. Ressler *et al.*, Phys. Rev. C **66**, 024308 (2002).
[5]D. Dean, Oak Ridge National Laboratory, private communication (2002).
[6]E. Dikman *et al.*, Phys. Rev. C **64**, 067305 (2001).
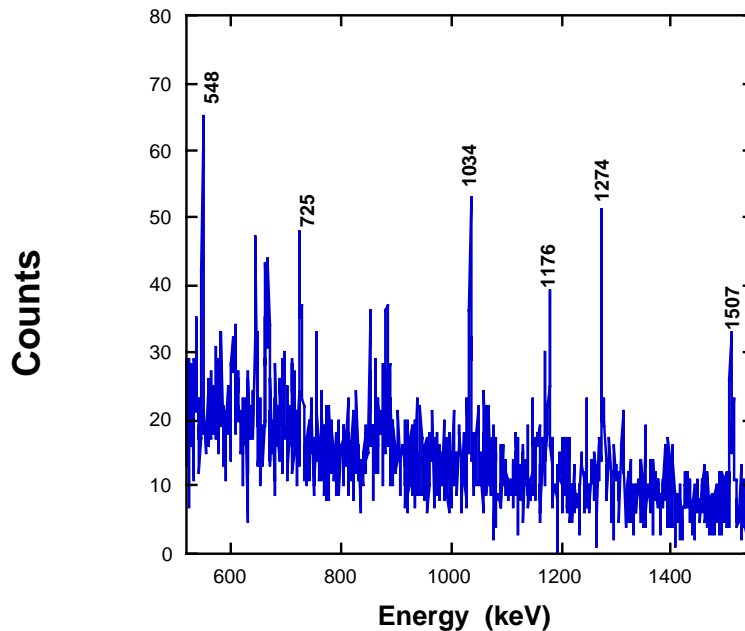
Fig. I-19. γ–γ coincidences with the 851-keV transition in ^{111}Sb. Transitions associated with ^{111}Te decay are labeled.

b.1.7. Identification of Excited States in ^{140}Dy (M. P. Carpenter, C. N. Davids, R. V. F. Janssens, C. J. Lister, D. Seweryniak, I. Ahmad, A. Heinz, T. L. Khoo, E. F. Moore, D. M. Cullen,* A. M. Fletcher,* S. J. Freeman,* L. K. Pattison,* J. F. Smith,* F. G. Kondev,† A. M. Bruce,‡ K. Abu Saleem,§ G. Mukherjee,¶ C. Wheldon,‖ and A. Woehr**)

Recently, a new region of deformed proton emitters was established ranging from La to Tm. The first cases found were in ^{131}Eu and ^{141}Ho.[1] Initially, the deformation and single-particle parentage of the proton-emitting states were deduced from calculations employing the multiparticle theory of Bugarov and Kadmensky.[2] In the case of ^{141}Ho, the deformation of the proton emitting states were confirmed by in-beam γ-ray spectroscopy utilizing the Recoil Decay Tagging (RDT) technique which established rotational bands on top of the these states.[3] While the deformation of the ^{141}Ho rotational bands deduced from the in-beam work is consistent with those inferred from the proton decay measurements, critical information about the ^{140}Dy daughter nucleus is still missing. In fact, one of the important assumptions in the calculations of the decay rates from deformed proton emitters is that the parent and daughter have the same deformation. Proton emission to the 2^+ level in ^{140}Dy was not observed, however, an upper limit for the branching ratio between the 2^+ and 0^+ feedings into ^{140}Dy was placed at 1% for decays from the assigned 7/2$^-$ ^{141}Ho, ground state.[3] Due to the fact that ^{140}Dy decays by β emission, in-beam γ spectroscopy using the RDT technique is not possible.

Recently, Cullen et al.[4] suggested that the yrast band of ^{140}Dy could be identified at least up to the 8^+ level by measuring γ rays emitted following the decay of a predicted K = 8$^-$ isomer. Studies to identify this isomer in ^{140}Dy and its subsequent γ decay were performed recently at the ATLAS facility by looking for delayed γ rays after implantation of mass selected recoils at the focal plane of the Fragment Mass Analyzer. From an analysis of the data, the 8$^-$ isomer in ^{140}Dy was established at 2.16 MeV, and its subsequent decay by γ emission was followed to the ground state. The half-life of the isomer was measured to be 7.3(15) μs, and the excitation energy of the 2^+ state is 202 keV. Figure I-20 shows both the time spectrum associated with the decay of the isomer and the proposed level structure deduced from the isomer's decay. Using the Grodzins formula, the deformation of the ground state in ^{140}Dy is deduced to be $\beta_2 = 0.24(3)$ which agrees well with the value of 0.25(3) deduced for the rotational bands in ^{141}Ho. The new information obtained here supports the role of deformation in proton emission and the previous assignments of single-particle configurations to the two proton emitting states in ^{141}Ho. In addition, the reduced hindrance factor measured for the isomer is consistent with the trend observed for 8$^-$ isomers observed in the lighter even-even N = 74 isotones.

A paper reporting the results of this work was recently been published in Physics Letters B.[5] A similar study at Oak Ridge National Laboratory[6] has also been published.

_____

∗University of Manchester, United Kingdom, †Technology Division, Argonne National Laboratory, ‡University of Brighton, United Kingdom, §Illinois Institute of Technology, ¶University of Massachusetts-Lowell, ‖University of Surrey, Guildford, United Kingdom, **University of Maryland.
[1]C. N. Davids *et al*., Phys. Rev. Lett. **80**, 1849 (1998).
[2]V. P. Bugrov and S. G. Kadmensky, Sov. J. Nucl. Phys. **49**, 967 (1989).
[3]D. Seweryniak *et al*., Phys. Rev. Lett. **86**, 1458 (2001).
[4]D. M. Cullen *et al*., Nucl. Phys. **A682**, 264c (2001).
[5]D. M. Cullen *et al*., Phys. Lett. **B529**, 45 (2002).
[6]W. Krolas et al., Phys. Rev. C**65**, 031303 (2002).
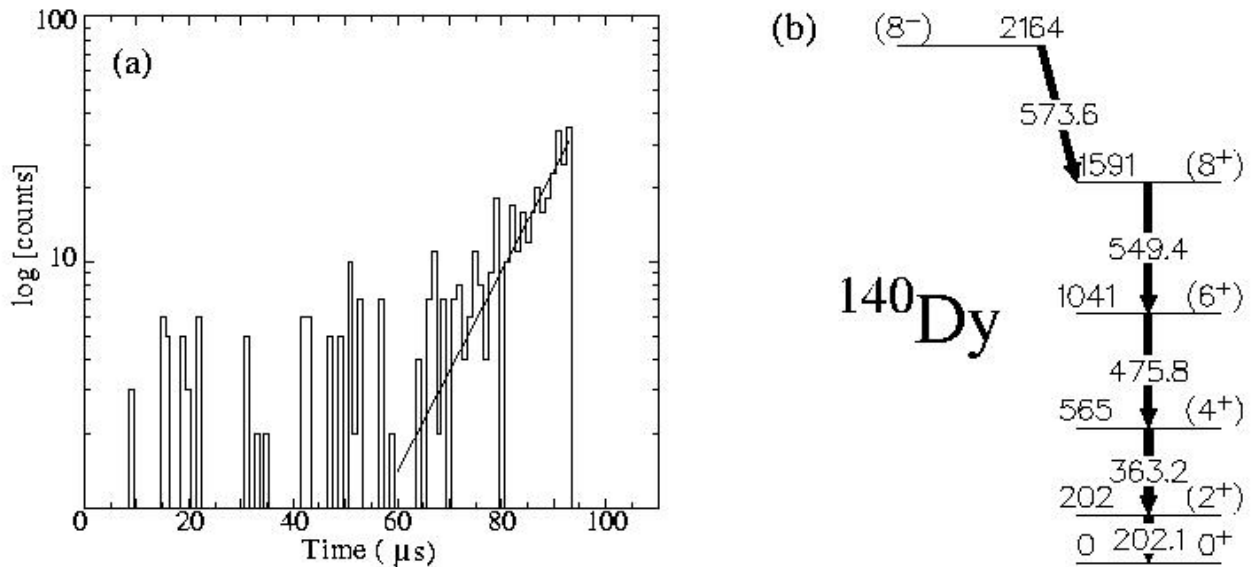
Fig. I-20. (a) Time delay between the implant of a residue and the detection in prompt coincidence of any two of the five γ transitions associated with the decay of the isomer. The solid line represents a fit to the data which yields a half-life of 7.3 μsec. (b) Proposed level sequence following the decay of the 8⁻ isomer in ¹⁴⁰Dy.

b.1.8. In-Beam Spectroscopy of the Proton Unbound Nucleus ¹⁴³Ho (D. Seweryniak, M. P. Carpenter, C. N. Davids, N. Hammond, R. V. F. Janssens, T. L. Khoo, F. G. Kondev, T. Lauritsen, C. J. Lister, G. Mukherjee, P. J. Woods,* S. J. Freeman,† D. Cullen,† C. J. Chiara,‡ W. Reviol,‡ D. G. Sarantites,‡ R. Clark,§ P. Fallon,§ A. Gorgen,§ A. O. Macchiavelli,§ and D. Ward§)

The proton-rich nuclei ¹⁴⁵,¹⁴⁶,¹⁴⁷Tm and ¹⁴¹Ho are known proton emitters.[1-4] They are situated in the transitional region where the nuclear shape changes from spherical, close to the N = 82 shell, to oblate, and than rapidly to prolate. Properties of the ground-state rotational band in ¹⁴¹Ho indicate possible triaxiality. The ¹⁴⁵Tm proton decay rate and the branching to the 2⁺ state was reproduced using the particle-vibrator picture. The ¹⁴³Ho nucleus is the nearest isotone of ¹⁴⁵Tm and has only two neutrons more than ¹⁴¹Ho. Information on its excited states will allow connections to be made with the more complete information on more neutron-rich nuclei.

A ⁵⁴Fe beam from the 88-inch Cyclotron at LBNL impinging on a thin ⁹²Mo target was used to populate nuclei around ¹⁴¹Ho. Prompt γ rays were detected in Gammasphere. To select reaction channels evaporated protons and α particles were detected using MICROBALL, and evaporated neutrons were measured in the Neutron Wall. The ¹⁴³Ho nuclei were produced as the p2n evaporation channel with the calculated cross section of about 50 μb. Figure I-21 shows γ-ray spectra measured in coincidence with different numbers of detected protons, α particles and neutrons. Three γ-ray lines can be seen in Fig. I-21d corresponding to the p2n channel. These transitions are coincident and form a band. Based on the γ-ray energies this band is most likely the decoupled $h_{11/2}$ proton band. Further data analysis is in progress.

[1]M. Karny et al., Phys. Rev. Lett. **90**, 012502 (2003).
[2]P. J. Woods et al., Nucl. Phys. **A553**, 485c (1993).
[3]O. Klepper et al., Z. Phys. **A305**, 125 (1982).
[4]C. N. Davids et al., Phys. Rev. Lett. **80**, 1849 (1998).

Figure I-22 shows the energies of the $15/2^- \rightarrow 11/2^-$ transitions in the decoupled proton $h_{11/2}$ bands and the energies of 2^+ states in the even-even nuclei around ^{141}Ho. The energy of the first transition in ^{143}Ho agrees very well with the 2^+ energy in the daughter nucleus ^{142}Dy. The $15/2^- \rightarrow 11/2^-$ energies observed in the lighter N = 76 isotones are similar to ^{143}Ho which indicates that deformation does not change when more protons are added to the core. It is consistent with the calculated deformations. Thus the structure of the proton emitter ^{145}Tm could indeed be similar to ^{143}Ho.
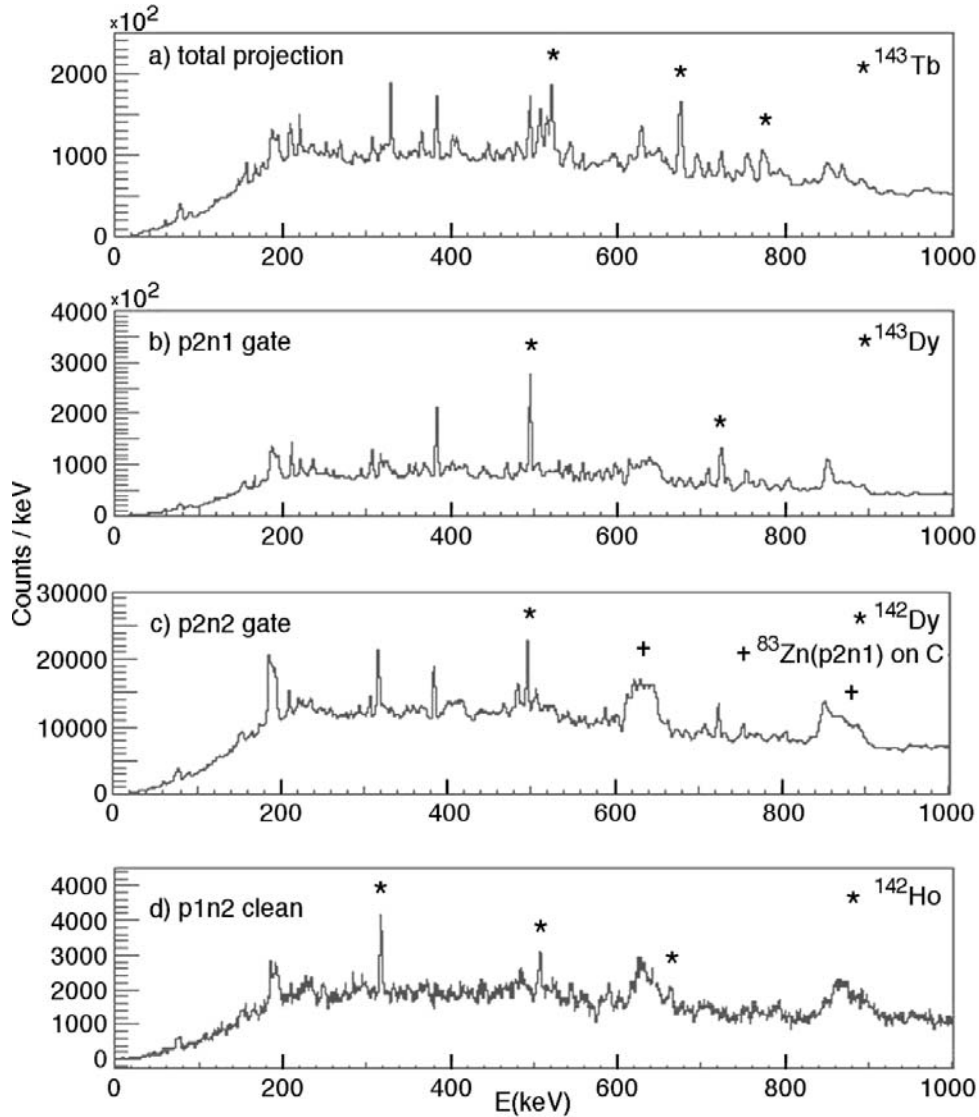
Fig. I-21. Gamma-ray spectra measured in coincidence with different number of detected evaporated particles: a) total γ-ray spectrum, b) 2 protons and 1 neutron, c) 2 protons and 2 neutrons, d) 1 proton and 2 neutrons. In spectrum d) contribution from higher proton multiplicity and 1 neutron channels were subtracted out.

Fig. I-22. Systematics of the E(15/2⁻)-E(11/2⁻) energies in odd-Z nuclei and the E(2⁺) energies in even-even nuclei around ¹⁴¹Ho.

b.1.9. New Results in Proton Radioactivity (C. N. Davids, D. Seweryniak, A. Heinz, G. Mukherjee, P. J. Woods,* J. Shergur,† P. Munro,* A. Robinson,* T. Davinson,* A. A. Sonzogni,‡ and W. B. Walters†)

Analysis of data on the new proton emitter ^{135}Tb was completed. It was produced with an estimated cross-section of 1 nb via the ^{92}Mo(^{50}Cr,p6n) reaction. This proton emitter is expected to be highly deformed, with a predicted β_2 value of 0.32. We observed a single proton peak at 1.18(15) MeV, with a half-life of 1.00(28) ms. No fine structure was observed. The predicted branching ratio to a 2^+ state at an excitation energy of 127 keV is about 8%, which is just below our sensitivity. The candidate proton single-particle states for this nucleus are $3/2^+$, $5/2^+$, and $7/2^-$. Figure I-23 shows a comparison between experimental and calculated half-lives for decay from these three states, using a spectroscopic factor S_j of 0.5. It is clear that only a spin-parity of $7/2^-$ agrees with the observed half-life for this nuclide.

A search for the predicted deformed proton emitter ^{125}Pm (Z = 61) proved to be unsuccessful. We used the ^{92}Mo(^{40}Ca,p6n) fusion-evaporation channel, but were unable to see any proton events after several days of running with about 20 pnA of beam.

_____

*University of Edinburgh, United Kingdom, †University of Maryland, ‡Brookhaven National Laboratory.

Half-life for ^{135}Tb, S_j=0.5
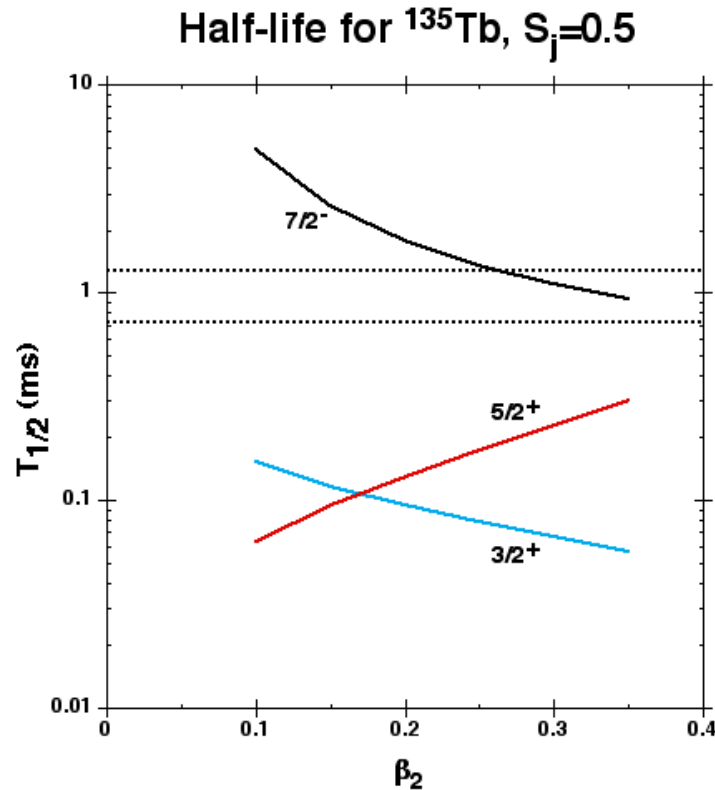
Fig. I-23. Calculated half-lives vs. quadrupole deformation parameter β_2 for ^{135}Tb. The dashed lines indicate the experimental results.

b.1.10. Proton Decay of Non Axially-Symmetric Deformed Nuclei (C. N. Davids and H. Esbensen)

Current calculations of decay rates and fine structure branching ratios for deformed proton emitters assume that both the parent emitter and daughter nucleus are axially symmetric. We calculated, in the adiabatic limit, the decay rate of a deformed nucleus where this symmetry requirement is relaxed. One obtains a set of coupled equations for the radial wave functions of the system consisting of an unbound proton coupled to a deformed even-even core. In the adiabatic limit these equations are diagonal in K, which is the projection of the total angular momentum on the long or 3-axis. However, the wave functions also contain components with different Ω, which is the projection of the proton angular momentum j on the 3-axis. Only Ω-values differing from K by ± 2, ± 4, etc. are allowed, subject to the restriction $|\Omega| \leq j$.

This formalism was applied to the ground state decay of the proton emitter ^{141}Ho, with K = 7/2⁻. The wave function is expanded in spherical components with j = 7/2⁻, 9/2⁻, 11/2⁻, 13/2⁻, and 15/2⁻, resulting in a total of 30 coupled equations. This is to be compared with the axially-symmetric case, where there are only 5 equations. Figure I-24 shows the calculated total decay rate and 2⁺ branching ratio, as a function of $a_{22} = 0.707 \beta_2 \sin\gamma$. For $a_{22} = 0$, the calculated total width has a value that agrees with experiment, with a spectroscopic factor of 0.73,[1] and the calculated branching ratio for decay to the 2⁺ state of 0.007 also agrees with the experimental value of 0.0070(15).[2] As a_{22} is increased the total decay rate decreases slowly and the 2⁺ branching ratio increases rapidly.

[1]C. N. Davids *et al*., Phys. Rev. Lett. **80**, 1849 (1998).
[2]K. Rykaczewski *et al*., Proceedings of the International Conference on Nuclear Structure "Mapping the Triangle", Grand Teton National Park, WY, May 22-25, 2002, AIP Proceedings **638**, 149 (2002).
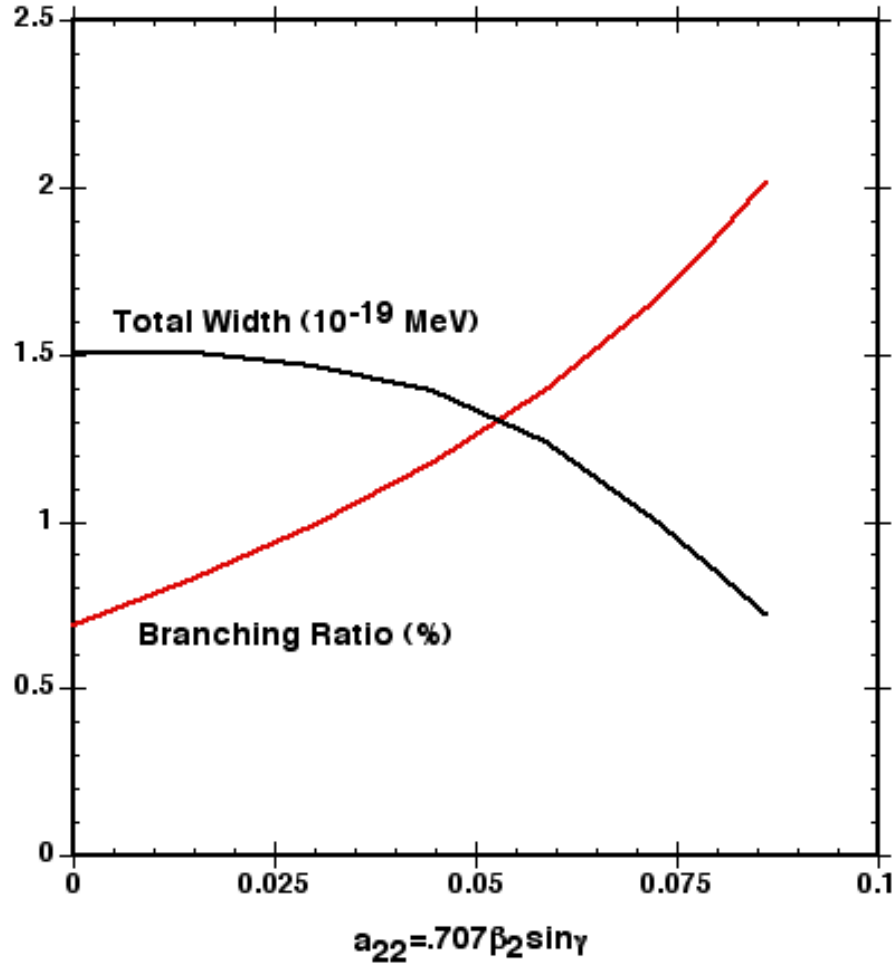
Fig. I-24. Calculated total decay width and 2^+ branching ratio for ^{141}Ho, plotted as a function of a_{22}.

b.1.11. Limits of the Energy-Spin Phase Space Beyond the Proton Drip Line: Entry Distributions of Pt and Au Isobars (M. P. Carpenter, F. G. Kondev, T. L. Khoo, T. Lauritsen, R. V. F. Janssens, K. Abu Saleem, I. Ahmad, C. N. Davids, A. Heinz, C. J. Lister, G. L. Poli, J. J. Ressler, D. Seweryniak, I. Wiedenhöver, M. B. Smith,* J. A. Cizewski,* H. Amro,† M. Danchev,‡ D. J. Hartley,‡ W. C. Ma,† W. Reviol,§ and L. L. Riedinger‡)

Nuclei lying beyond the proton drip line provide an ideal laboratory for the study of the amount of energy and angular momentum which a weakly-bound system can sustain.   These limits of existence can be determined by measuring the entry distribution[1] populated in a fusion-evaporation reaction. The entry distribution is the initial population as a function of excitation energy E and spin I, after particle evaporation from the compound system, from which γ emission to the ground state originates.   It was suggested[2] that the entry distribution should be limited

beyond the drip line, since only a small region of the energy-spin phase space, just above the yrast line, does not decay by proton emission.

Entry distributions were measured for $^{173-177}$Au nuclei, all of which lie beyond the drip line, and compared with those of the more stable Pt isobars. These systems were populated following the bombardment of ^{92,94,96}Mo targets by beams of ^{84}Sr, provided by the ATLAS accelerator. Fusion-evaporation products were selected using the Argonne Fragment Mass Analyzer, and the

recoil-decay tagging method was used to select the α-decaying states of interest. Prompt γ rays were detected using the 106-module Gammasphere array as a calorimeter. Total modular energy H and multiplicity K were measured. The response functions of the array enable the conversion of modular (H, K) to energy and multiplicity, which can be related to spin by realistic assumptions[1] of the angular momenta carried by the components of the γ-ray cascade. Comparisons were made between the entry distributions associated with odd-A Au and Pt isobars.   In [173]Au the entry distribution is colder than that at [173]Pt, which provides the first evidence for the limits of excitation energy and angular momentum which a nucleus beyond the proton drip line can sustain. The observed results cannot be explained by simple calculations based on Q-values or by statistical model calculations, both of which predict similar distributions for isobars.

A paper reporting these results was recently published in Physics Letters B.[3]

*Rutgers University, †Mississippi State University, ‡University of Tennessee, §Washington University.
[1]P. Reiter *et al.*, Phys. Rev. Lett. **84**, 3542 (2000).
[2]T. L. Khoo, in Tunneling in Complex Systems, Proceedings from the Institute for Nuclear Theory, ed. Steven Tomsovic (World Scientific 1998) v. 5, p. 229.
[3]M. B. Smith *et al.*, Phys. Lett. **B551**, 262 (2003).

b.1.12. In-Beam γ-Ray Spectroscopy of [172]Pt (M. P. Carpenter, R. V. F. Janssens, K. Abu Saleem, I. Ahmad, C. N. Davids, A. Heinz, T. L. Khoo, T. Lauritsen, C. J. Lister, G. L. Poli, J. Ressler, D. Seweryniak, I. Wiedenhöver, M. Danchev,* D. J. Hartley,* F. G. Kondev,† L. L. Riedinger,* H. Amro,‡ D. L. Balabanski,* J. A. Cizewski,§ W. C. Ma,‡ W. Reviol,¶ and M. B. Smith§)

Collective structures in [172]Pt were investigated by measuring in-beam γ rays with mass selection and the recoil-decay tagging technique. The experiment was performed with the ATLAS superconducting linear accelerator at the Argonne National Laboratory. The main emphasis of this experiment was to study high-spin states in the proton unbound systems [173,175,177]Au, and a paper reporting the results on these nuclei was published recently.[1] High-spin states in [172]Pt were weakly populated in the 2p2n channel of the [84]Sr + [92]Mo reaction. Two energies, 390 and 395 MeV, were used to bombard the self-supporting, isotopically enriched, [92]Mo target. Prompt γ rays were detected with 101 Ge detectors in the Gammasphere array. Mass and alpha decay information was obtained at the focal plane of the Fragment Mass Analyzer using the PGAC and DSSD setups. The discrepancy in the ground-state band from previous studies was resolved, and a new collective structure that is likely based on an octupole vibration was identified. The level scheme for [172]Pt deduced from this work is shown in Fig. I-25. A paper reporting the results of this work was recently published in Phys. Rev. C.[2]

*University of Tennessee-Knoxville, †Technology Division, Argonne National Laboratory, ‡Mississippi State University, §Rutgers University, ¶Washington University.
[1]F. G. Kondev *et al.*, Phys. Lett. **B512**, 268 (2001).
[2]M. Danchev *et al.*, Phys. Rev. C **67**, 014312 (2003).
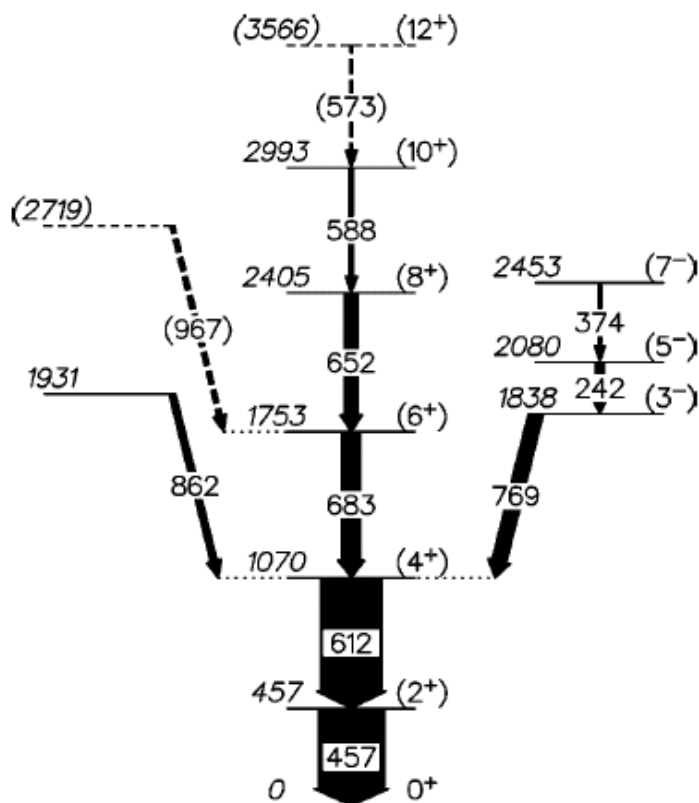
Fig. I-25. Level scheme for ^{172}Pt deduced from this work.

b.1.13. Triple Shape-Coexistence in ^{179}Hg (M. P. Carpenter, F. G. Kondev, D. Jenkins,*
R. V. F. Janssens, I. Ahmad, J. Caggiano, C. N. Davids, A. Heinz, T. L. Khoo,
T. Lauritsen, C. J. Lister, D. Seweryniak, A. A. Sonzogni, I. Wiedenhöver,
K. Abu Saleem,† H. Amro,‡ A. N. Andreyev,* T. Enqvist,§ P. T. Greenlees,§
B. Herskind,¶ P. M. Jones,§ D. T. Joss,|| R. Julin,§ S. Juutinen,§ H. Kettunen,§
P. Kuusiniemi,§ M. Leino,§ A.-P. Leppännen,§ W. C. Ma,‡ P. Nieminen,§ R. D. Page,*
J. Pakarinen,§ C. D. O'Leary,** P. Raddon,§ P. Rahkila,§ J. Ressler,†† W. Reviol,‡‡
L. L. Riedinger,¶¶ D. G. Sarantites,‡‡ S. Siem,§§ A. Simons,** J. Uusitalo,§
P. G. Varmette,‡ and R. Wadsworth**)

Neutron-deficient, even-even Hg (Z = 80) isotopes between N = 96 and 110 exhibit a coexistence at low spin between two shapes: a weakly deformed oblate ground state and a more deformed, excited, prolate band. The energy difference between the two minima exhibits a parabolic trend as a function of neutron number and minimizes around mid-shell (N ~ 102) where the prolate 0^+ state lies ~260 keV above the 0^+ ground state. In contrast, the ground states of the odd-mass, ^{181,183,185}Hg (N = 101,103,105) isotopes are associated with a prolate shape. In addition, a weakly-deformed, oblate high-spin ($J^\pi = 13/2^+$) isomer was identified in each of the three odd-mass Hg isotopes, albeit the excitation energies were not established. The

mechanism responsible for this preferred prolate shape at low spin in the odd-mass isotopes is still not understood

Based on the experimental results available at present, it is hard to predict which type of structures will be observed in the neutron-deficient odd-A Hg isotopes (N < 100). In particular, it is of interest to map out the evolution of the single-particle states for both the prolate and oblate shapes in the lightest odd-A isotopes and to compare these with trends observed in the even-even Hg neighbors. We started such investigations by performing several measurements on
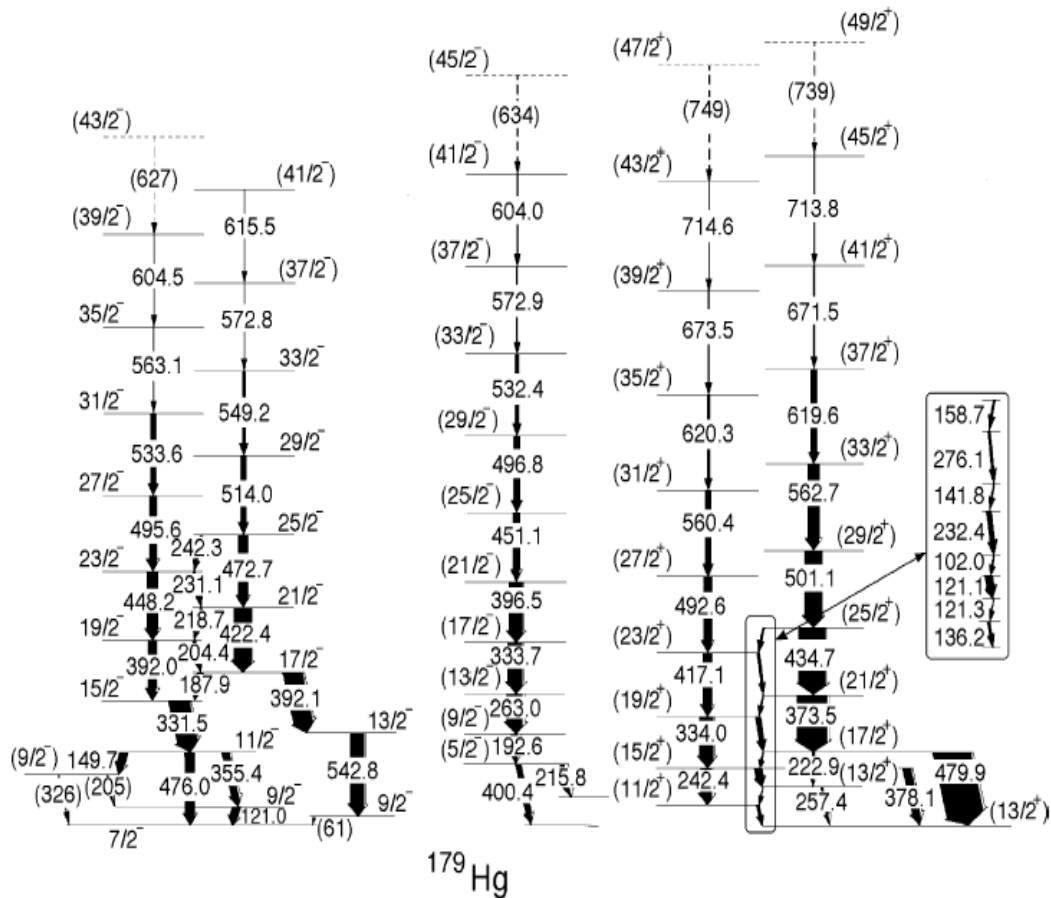
Fig. I-26. Level scheme for ^{179}Hg deduced from γ-ray coincidence data measured with Gammasphere. High-spin states in ^{179}Hg were populated in the reaction ^{90}Zr(^{90}Zr,n) reaction. The beam was supplied by the ATLAS accelerator at Argonne National Laboratory.

^{179}Hg (N = 99). The first was an in-beam experiment using Gammasphere coupled to the FMA. The second measurement was performed at RITU and studied in detail the α decay of ^{183}Pb into ^{179}Hg.

For the in-beam study, excited states in ^{179}Hg were populated with the ^{90}Zr(^{90}Zr,n) reaction using beams delivered by ATLAS. Gamma rays associated with ^{179}Hg were identified by the RDT technique using Gammasphere coupled to the FMA. The level structure deduced from this work is shown in Fig. I-26. In the heavier odd-A Hg isotopes, the ground state spin/parity is ½⁻ and associated with a deformed configuration. For ^{179}Hg, the ground state is established to be 7/2⁻ and

is associated with a near-spherical shape. Three rotational bands are evident in the level scheme and have a deduced prolate deformation of $\beta_2 \sim 0.2$. The oblate shape is associated with the 13/2⁺ isomer into which rotational band 3 decays into.

For the decay experiment, a 200-MeV ^{42}Ca beam from the cyclotron at the University of Jyväskylä was incident on a target consisting of two stacked 500-μg/cm^2 self supporting ^{144}Sm foils, producing ^{183}Pb via the ^{144}Sm(^{42}Ca,3n) reaction. Gamma rays at the target position were detected by the JUROSPHERE II. Fusion-evaporation residues were separated from scattered beam and fission products using the RITU

gas-filled separator. Five 25-35% HPGe surrounded the focal plane detector affording a total efficiency of about 1% at 1.3 MeV.

Before the current study was performed, four distinct α–decay lines were identified in the decay of ^{183}Pb. While a detailed level scheme had not been established, it was assumed that the four α decays represent branches from a single state in the parent.[1] Our data confirms the existence of these four previously known α decays, however, the lifetimes associated with the four α lines allows them to be divided into two pairs of decays from two different states (see Fig. I-27); one with a half-life of 415(20) ms and one with a half-life of 535(30) ms. By observing coincidences with γ rays at the focal plane, we find that the 6698(5) keV and 6570(10) keV α decays feed excited states in ^{179}Hg which decay by γ emission. The 6698 keV α decay is correlated with two γ rays with energies of 110.8 and 60.6 keV which are in prompt coincidence with each other, but in delayed coincidence with the emission of the α particle. The half-life of the isomeric state at 172 keV from which these transitions decay is determined to be 6.4(9) μs. The 60.6 keV transition was also observed in the in-beam work and corresponds to a decay of a $9/2^-$ state into the $7/2^-$ ground state. Based on intensity balances and the half life, we deduce that the 110.8 keV transition has M2 multiploarity and thus comes from a $13/2^+$ state. The deduced hindrance factor of 1.3 for the 6698 keV α decay is essentially unhindered and establishes a $13/2^+$ isomer in ^{183}Pb. This $13/2^+$ to $13/2^+$ decay is also observed in both ^{185}Pb and ^{187}Pb and is interpreted as the decay from a spherical single-particle state in the parent to a weakly deformed oblate state in the daughter. This is also our interpretation as well, allowing us to assign excitation energies to all levels measured above the isomer in the in-beam work. The $13/2^+$ isomer in ^{183}Pb also decays to the ground state via a 6860(11) keV decay with a deduced hindrance factor of 67(18). This large hindrance factor for the α decay is not inconsistent with the structural change associated with a decay connecting a spherical state in ^{183}Pb with the ground state of ^{179}Hg which has been suggested to arise from the coupling of a $h_{9/2}$ or $f_{7/2}$ neutron to a weakly-deformed prolate core. In fact, the decay work fully confirms the conclusions we deduced on the shape of the ground and $13/2^+$ isomeric state from our in-beam work, and thus confirming the three-shape scenario.

A paper reporting the results from the in-beam work was recently been published in Physics Letters B.[2] A paper reporting the results from the decay work was recently published in Physical Review C.[3]

_____

*University of Liverpool, United Kingdom, †Argonne National Laboratory and Illinois Institute of Technology, ‡Mississippi State University, §University of Jyväskylä, Finland, ¶Niels Bohr Institute, Copenhagen, Denmark, ‖University of Keele, United Kingdom, **University of York, United Kingdom, ††Argonne National Laboratory and University of Maryland, ‡‡Washington University, §§Argonne National Laboratory and University of Oslo, Norway, ¶¶University of Tennessee-Knoxville.
[1]K. S. Toth *et al*., Phys. Rev. C **39,** 1150 (1989).
[2]F. G. Kondev *et al*., Phys. Lett. **B528**, 221 (1989).
[3]D. J. Jenkins *et al*., Phys. Rev. C **66**, 011301(R) (2002).
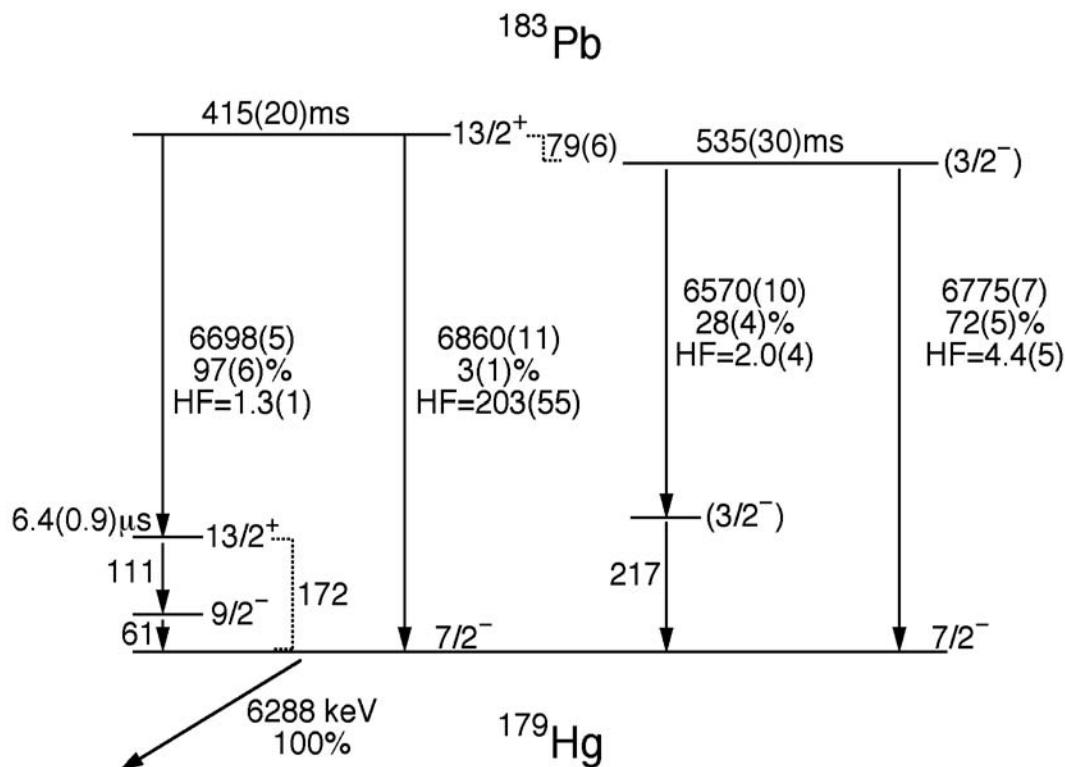
Fig. I-27. Decay scheme showing the α decay of two isomers in ^{183}Pb to low-lying states in ^{179}Hg.

b.1.14. Alpha Decay of ^{181}Pb *(M. P. Carpenter, F. G. Kondev, S. Sinha, R. V. F. Janssens, I. Ahmad, C. N. Davids, S. Freeman, N. Hammond, T. L. Khoo, T. Lauritsen, C. J. Lister, G. Mukherjee, D. Seweryniak, A. Woehr,* and D. J. Jenkins†)*

This past fall, we measured with the FMA and DSSD setup, the α decay of recoils produced in the ^{90}Zr + ^{92}Mo reaction. For one of these products, ^{181}Pb, we observe two α lines at 7035 and 7090 keV with nearly equal intensity. Both of these decays are correlated with the 6580-keV α decay of ^{177}Hg. This is in contrast to the previously reported α line at 7065 keV.[1] It is likely that this singly reported α decay is in fact the two that we observe. In the heavier odd-A Pb isotopes, two α-decaying states were identified and associated with a high-spin (13/2^{+}) and a low-spin (3/2^{-}) isomer. Presumably, the two α-decaying states that we observe correspond to similar states in ^{181}Pb. With respect to

^{181}Tl, our preliminary analysis confirms the 6180-keV α line reported in Ref. 1, and no other α decays associated with ^{181}Tl were identified. We do, however, observe a significant β-decay branch inferred from the observation of the 6005-keV α line of ^{181}Hg, a nuclide we cannot make via the 1-particle evaporation channel from the compound ^{182}Pb. Whether the β-decay competes directly with the state emitting the 6180-keV α line or comes from another state whose α decay is highly hindered cannot be determined from the present data. A complete analysis of this data set is currently underway.

_____

* University of Maryland, †University of York, United Kingdom.
[1]K. S. Toth *et al.*, Phys. Rev. C **53**, 2513 (1996).

B.2.   Neutron-Rich Nuclear Spectroscopy

b.2.1.   Structure of ^{52,54}Ti and Shell Closures in Neutron-Rich Nuclei Above ^{48}Ca

(R. V. F. Janssens, M. P. Carpenter, F. G. Kondev, T. Lauritsen, D. Seweryniak,
B. Fornal,* P. F. Mantica,† B. A. Brown,† R. Broda,* P. Bhattacharyya,‡
M. Cinausero,§ P. J. Daly,‡ A. D. Davies,† T. Glasmacher,† Z. W. Grabowski,‡
D. E. Groh,† M. Honma,¶ W. Krolas,* S. N. Liddick,†, S. Lunardi,‖ N. Marginean,§
T. Mizusaki,** D. J. Morrissey,† A. C. Morton,† W. F. Mueller,† T. Otsuka,††
T. Pawlat,* H. Schatz,† A. Stolz,† S. L. Tabor,‡‡ C. A. Ur,‖ G. Viesti,‖
I. Wiedenhover,‡‡ and J. Wrzesinski*)

The structure of neutron-rich nuclei recently became the focus of much theoretical and experimental effort. Central to the on-going investigations is the expectation that substantial modifications can occur to the intrinsic shell structure of nuclei with a sizable neutron excess. Alterations to the energy spacings of the orbitals and/or to their ordering can have a considerable impact on global nuclear properties such as the nuclear shape or the type of excitations characterizing the low-energy level spectra. The so-called "island of inversion" phenomenon discovered in neutron-rich exotic nuclei near N = 20 ^{30}Ne, ^{31}Na, $^{32-34}$Mg is perhaps one of the best examples so far of an unanticipated structural change.

Interactions between protons and neutrons were invoked to account for the presence of a subshell gap at N = 32 in neutron-rich nuclei located in the vicinity of the doubly-magic nucleus ^{48}Ca.[1] Specifically, it was proposed that a weakening of the $\pi 1f_{7/2}$ $\nu f_{5/2}$ proton-neutron monopole interaction as protons are removed from the $1f_{7/2}$ single-particle orbital (filled at Z = 28), combined with a significant $2p_{1/2}$-$2p_{3/2}$ spin-orbit splitting results in the emergence of the N = 32 subshell in nuclei such as ^{52}Ca and ^{56}Cr. This subshell manifests itself by the large excitation energy of the first 2^+ state. More recently, shell-model calculations introducing a new effective interaction for pf-shell nuclei were carried out.[2] They are able to account for the observations of Ref. 1. In particular, the energy of the first 2^+ states in Ca, Ti, Cr, Fe and Ni isotopes are well reproduced. Interestingly, these calculations also suggest the presence of an additional N = 34 shell gap in the Ca and Ti isotopic chains.

The purpose of the present work was two-fold. First, the observation that the N = 32 subshell gap survives in the presence of $f_{7/2}$ protons, which so far relies mostly on the Cr systematics of Ref. 1, was reinforced by presenting first data on the ^{54}Ti nucleus. Second, new tests of the effective interaction for pf-shell nuclei[2] were carried out by confronting the level structures of ^{52}Ti and ^{54}Ti up to medium spin with the results of

shell-model calculations. These new data were obtained by combining two experimental techniques seldom used together to investigate exotic nuclei: beta-decay studies of products from a fragmentation reaction and in-beam gamma-ray spectroscopy following deep-inelastic reactions. This approach was necessary because the two Ti isotopes of interest are neutron-rich and cannot be readily investigated at high spin with the more commonly used (HI,xn) fusion-evaporation reactions.

Prior to the present studies, nothing was known about the excited states of ^{54}Ti. Information about low lying levels was obtained from an investigation of the beta decay of the parent, ^{54}Sc, produced via fragmentation of a 140 MeV/nucleon ^{86}Kr beam at the National Superconducting Cyclotron Laboratory (NSCL) at Michigan State University. The MSU study identified the first two gamma-ray transitions in ^{54}Ti. Based on the MSU data, the high spin structure in this nucleus up to a spin $J^\pi = 10^+$ was then delineated from a Gammasphere experiment at ATLAS, where a 305 MeV ^{48}Ca beam was sent on a thick ^{208}Pb target. Data were obtained as well for the $^{50-52}$Ti isotopes. It should be pointed out that the identification of ^{54}Ti using a cross coincidence technique with transitions in reaction partners from the Gammasphere data was impossible. Thus, the beta-decay measurement described above was of crucial importance to validate the ^{54}Ti assignment. We believe that this approach of combining beta decay studies following fragmentation with prompt spectroscopy measurements following deep inelastic reactions represents a new, powerful tool to study nuclei on the neutron-rich side of the valley of stability. The new level schemes obtained for the neutron-rich even Ti isotopes are given in Fig. I-28. The first important result from the present measurements can be readily inferred from a close inspection of the figure: the E(2^+) energy dips from 1554 to 1050 keV between ^{50}Ti and ^{52}Ti, before increasing significantly to 1495 keV in ^{54}Ti$_{32}$. This behavior mirrors the one found in Ref. 1, and is consistent with the suggestion of a subshell closure at N = 32.

Another distinct feature of the level structures in Fig. I-28 is the presence of higher-energy transitions ($E_\gamma > 2$ MeV) at moderate spins. Large jumps in transitions energies of this type are often regarded as signatures for excitations involving the breaking of the core, e.g., the valence space was exhausted and higher angular momentum levels require excitations across a (sub)shell gap. In order to explore both of these observations further, a number of shell-model calculations were carried out with the Hamiltonian described in Ref. 2. The results of the calculations are compared with the data in Fig. I-28, where it can be seen that the data a reproduced satisfactorily. From this comparison, it is clear that the ^{54}Ti data strongly support the calculations with a high $f_{5/2}$ effective single-particle energy at $N = 34$ and are, thus, pointing towards a shell closure at $N = 34$.

These results were recently published.[3] Follow-up experiments to delineate the level structure of ^{56}Ti and to measure the degree of collectivity of the 2^+ state in the even Ti isotopes are being planned.

_____

[1]J. I. Prisciandaro et al., Phys. Lett. B510, 17 (2001).
[2]M. Honma et al., Phys. Rev. C 65, 061301 (2002).
[3]R. V. F. Janssens et al., Phys. Lett. B546, 55 (2002).

Fig. I-28. Comparisons between shell-model calculations and data for the even-even $^{50-54}$Ti isotopes.

b.2.2. First Observation of the ν9/2[404] Orbital in A ~ 100 Mass Region (I. Ahmad, W. Urban,* J. A. Pinston,† T. Rzaca-Urban,* A. Zlomaniec,* G. Simpson,‡ J. L. Durell,§ W. R. Phillips,§ A. G. Smith,§ B. J. Varley,§ and N. Schulz¶)

A new band was identified in ^{99}Zr from our investigation of ^{248}Cm fission fragment prompt gamma ray spectroscopy. The prompt γ-γ coincidence measurement was performed with the Eurogam2 array of Compton-suppressed Ge spectrometers using a ^{248}Cm fission source. The level scheme built on the basis of the coincidence relationships between gamma rays in ^{99}Zr and its complementary fragments is shown in Fig. I-29. Angular correlations establish spin-parity of 9/2$^+$ to the 1038.8 keV level. The half-life of this level was measured to be 54(10) ns. We give a 9/2$^+$[404] assignment to this level because this is the only 9/2$^+$ Nilsson state available in this mass region. This is the first observation of the 9/2$^+$[404] orbital in the mass 100 region. The results of this work were published.[1]
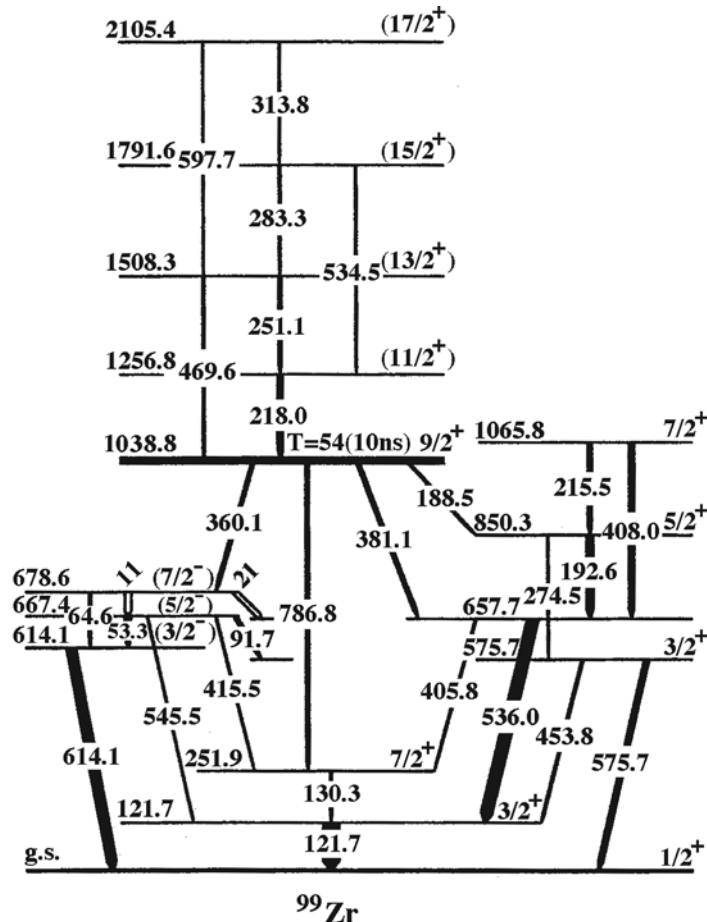
Fig. I-29. A partial level scheme of ^{99}Zr showing the new band at 1038.8 keV.

b.2.3.   Precise Mass Measurement of Neutron-Rich Nuclei from Fission Fragments of ^{252}Cf

(G. Savard, J. P. Greene, A. Heinz, Z. Zhou, J. C. Wang,* J. Clark,* F. Buchinger,†
J. E. Crawford,† S. Gulick,† J. K. P. Lee,† K. S. Sharma,‡ and J. Vaz‡)

Precise mass measurements for neutron-rich isotopes $^{141-145,147}$Ba, $^{143-149}$La, $^{145,147-149,151}$Ce, and ^{149,151}Pr were made at the Canadian Penning Trap (CPT) mass spectrometer. In these measurements, a ^{252}Cf fission source is mounted in front of the Havar window of the CPT gas catcher (see Fig. I-11 in section a.10.) filled with about 150 torr of helium gas. Fission fragments entering the gas catcher are thermalized in the helium gas and guided by electric fields to the nozzle of the gas catcher.   The high-purity of the system allows a significant fraction of the ions to remain in the 2^+ charge state in the helium gas. The ions are extracted out of the gas catcher by the gas flow and injected into a RFQ cooler in which the ions are captured, cooled by buffer gas collisions and ejected as ion bunches. The ion bunches are then transported, mass selected through

a deflector pulse and transferred to a linear RF trap where they are captured, further cooled by helium buffer gas and accumulated. The ions ejected from the linear RF trap are finally delivered into a precision Penning trap where their cyclotron frequency ν_c = $qB/(2\pi m)$ is measured. The mass of a nuclei can then be obtained by comparing its ν_c and $\nu_c{}'$ of a reference ion whose mass is well known. In the Penning trap, a dipole radio frequency field is used to clean out contaminant ions or excite the wanted ions to a certain magnetron motion orbit before a quadrupole radio frequency field is applied to convert the magnetron motion into cyclotron motion with the same radius of orbit.   The cyclotron frequency is determined by employing a time-of-flight technique.
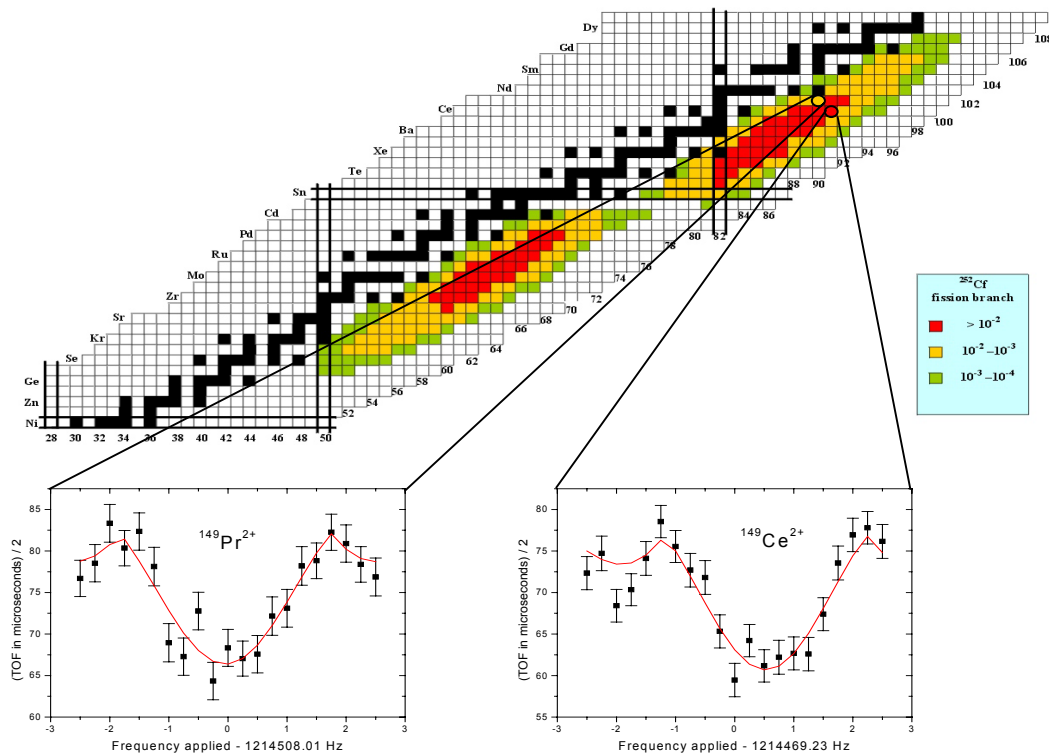
Fig. I-30. Distribution of fission fragments from ^{252}Cf and resonance curves for ^{149}Pr^{2+} and ^{149}Ce^{2+} obtained during the May 2002 run.

During March 2002, ν_c of $^{145}Ba^{2+}$, $^{145,147}La^{2+}$, $^{147,149}Ce^{2+}$, and $^{149}Pr^{2+}$ were measured with a quadrupole field excitation time of 200 ms. During each measurement, a molecule, C_5H_9, was used as a reference to calibrate the magnetic field. The masses of the C_xH_y (or $C_xH_yO_z$) molecules are known to better than 10^{-9} accuracy and this uncertainty is negligible for these measurements. ν_c of $^{145}Ba^{2+}$ was also measured with 500 ms excitation time. This longer excitation time yields a resolution of 600000 and a typical accuracy of about 5×10^{-8} (or about 7 keV) for the statistics accumulated in these measurements. In the May 2002 run, a 500 ms excitation time for the quadrupole field was employed for all of the measurements of $^{145}Ba^{2+}$, $^{145,147}La^{2+}$, $^{147,149}Ce^{2+}$, and $^{149}Pr^{2+}$. Four other isotopes ^{147}Ba, $^{145,151}Ce$ and ^{151}Pr were measured with 200 ms excitation time. In the June and July 2002 run, $^{141-144}Ba^{2+}$, $^{143,144,146,148}La^{2+}$ and $^{148}Ce^{2+}$ were measured with either 500 ms excitation or 200 ms excitation. Before and after each measurement, molecules C_5H_{11}, C_4H_9O and $C_3H_6O_2$ were used to calibrate the magnetic field. The masses of ^{145}Ba, $^{145,147}La$, $^{147,149}Ce$, and ^{149}Pr obtained from the above first two runs are consistent within the uncertainty. ν_c of C_5H_9, C_5H_{11}, C_4H_9O and $C_3H_6O_2$ during the whole measurement period are consistent to a few part 10^{-8}. A later test showed the frequency shift caused by contaminant ions to be less than a part 10^{-8} per ion if only a few ions are stored in the Penning trap. Since in all of the above

measurements only a few ions were stored in the Penning trap for each cycle, frequency shifts caused by contaminant ions are not a problem. Fig. I-30 shows the distribution of fission fragments from ^{252}Cf and the resonances of $^{149}Pr^{2+}$ and $^{149}Ce^{2+}$ obtained during the May 2002 run.

The masses measured at the CPT are compared with the Audi & Wapstra tabulated/extrapolated mass tables in Fig. I-31. For $^{141-144}Ba$, $^{143-145}La$, $^{145,148}Ce$ and ^{149}Pr, the measured masses are in excellent agreement with tabulated values. The masses of four of these isotopes (the less exotic barium isotopes $^{141-144}Ba$) were measured to high precision with the ISOLTRAP system at CERN and we agree with these measurements. For the other isotopes, we find larger deviations with the largest deviations occurring at ^{145}Ba and ^{147}La where the differences between our measured masses and the tabulated values are more than 500 keV. These masses were previously obtained by beta-endpoint measurements which are more prone to systematic errors than the present technique. We performed a series of systematic checks which confirm that no unexpected systematic shifts are present at this level in our measurements and must conclude that previous measurements in this region were in error. The effects these new measurements will have on masses in the region are being investigated.
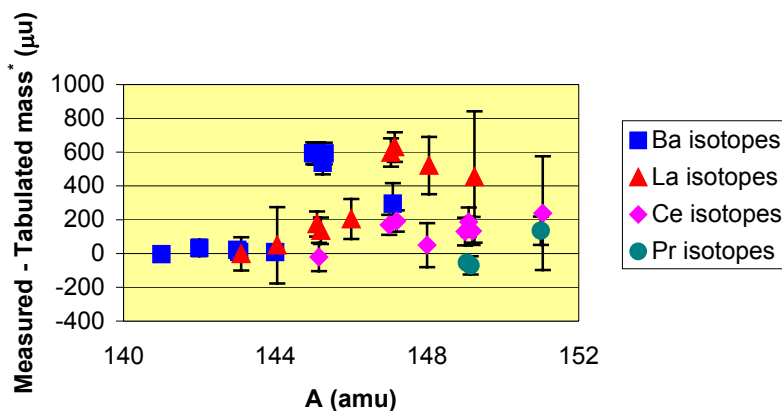
Fig. I-31. Comparison between masses measured at the CPT and tabulated values.

_____
*Argonne National Laboratory and University of Manitoba, Winnipeg, Manitoba, †McGill University, Montreal, Quebec, ‡University of Manitoba, Winnipeg, Manitoba.

b.2.4. Beta-Decay Studies of r-Process Nuclides in the ^{132}Sn Region (A. Wöhr,*
D. Seweryniak, B. Truett, W. B. Walters†, K.-L. Kratz,‡ O. Arndt,‡ B. A. Brown,§
I. Dillman,‡ D. Fedorov,¶ V. Fedoseyev,‖ L. Fraile,‖ P. Hoff,** U. Köster,‖
A. N. Ostrowski,‡ B. Pfeiffer,‡ H. L. Ravn,‖ M. D. Selliverstov,†† J. Shergur,* and the
ISOLDE Collaboration)

Very neutron rich Ag, Cd, In and Sn isotopes lying in or near the r-process path were studied at CERN/ISOLDE using the highest achievable isotopic selectivity. These methods include the use of a resonance-ionization-laser-ion-source (RILIS) and a two step neutron-converter target in combination with a high-resolution mass separator.

Recently, it was possible to use the Cd-RILIS to study the β and γ-decay of ^{130}Cd to levels of ^{130}In.[1-3] This particular nuclide is of considerable importance to r-process nucleosynthesis as its half-life of 162 ms provides the ultimate barrier to the matter flow in the A ≅ 130 region. Moreover, a full understanding of the structure and decay of ^{130}Cd is essential to the calculation of the lower-Z N = 82 nuclides that also play a role in the buildup of the rising wing of the solar r-abundance A ≅ 130 peak. In order to observe γ-rays from ^{130}Cd decay in a region where large backgrounds of surface-ionized Cs and In isobars are present, many improvements have been incorporated. Hence, the ^{130}Cd was produced via neutron induced fission, but not by spallation. The use of the neutron converter target thus resulted in a considerable lowering of the ^{130}In

contaminant and an almost complete suppression of spallation produced ^{130}Cs. For ^{130}Cd, it was possible to determine the 2120 keV energy for the 1^+ level to which the Gamow-Teller β-decay goes. Using βγ-coincidences, we measured the end-point for β-population of this level which allowed us to determine the Q_β value for ^{130}Cd decay. That Q value appears to be considerably higher than predicted by the mass formulae of Möller et al.,[4] Aboussir et al.[5] or Duo and Zuker,[6] but rather lies in the high-energy range of recent *"quenched"* mass models (HFB/SKP, HFB-2)[7,8] and the value listed in the Atomic Mass Evaluation of Audi and Wapstra.[9] The 8 major gamma rays found to follow the β-decay of ^{130}Cd include a γ–ray at 388 keV, reported by Hellström et al.,[10] to stem from a microsecond isomer. Since it seems that this level is populated in the decay of the 1^+ level at 2120 keV by the 1732 keV -ray, we can assume that it is likely to have spin and parity of 3^+. The relatively (and unanticipatedly) high energy of the 2120 keV 1^+ level is a consequence of two unexpectedly large position shifts in going from ^{128}In via ^{130}In. These levels are shown in Fig. I-32 where the evolution of the positions
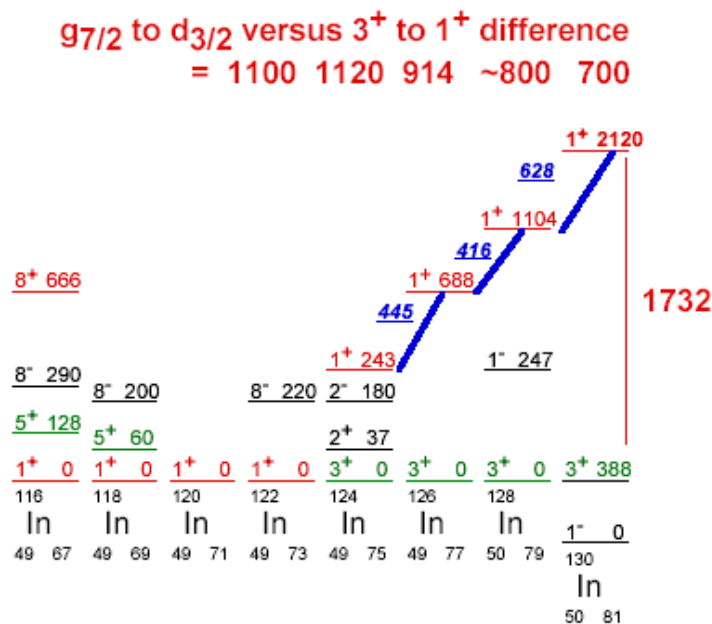
Fig. I-32. Evolution of nuclear structure upon approaching the N = 82 closed shell for the odd-mass Sn nuclides and the odd-odd In nuclides. The structure of ^{130}In is shown graphically relative to the 3^+ levels in the adjacent lighter In nuclides which are the ground states.

of the 1^+ levels in the odd-odd In nuclides are shown as N increases toward the closed shell at N = 82. The position of the 1^+ level is seen to increase by 445 and 416 keV in going from ^{124}In via ^{126}In to ^{128}In, but then jumps by 628 keV to ^{130}In. Added to that larger than expected shift is the dramatic inversion of the 3^+ and 1^- levels which lifts the 1^+ level to a position 2120 keV above the ground state. Earlier shell-model calculations showed a position for the 1^+ level at about 1500 keV and near degeneracy for the 1^- and 3^+ levels.

As a consequence of the renormalization of the $\nu\pi$ monopole interaction for ^{130}Cd decay, the half-lives of the so far unknown N = 82 "waiting-point" nuclei ^{128}Pd to ^{122}Zr will become longer than those predicted by recent shell models (see, e.g. Ref. 11). This leads to a better insight into the buildup of the solar r-process abundance peak at A $\cong$ 130.

Presently, we are approaching or have already reached the technical limits of studying very neutron-rich nuclei around N = 82 with the currently available ISOL techniques. However, there are still improvements that can be sought. In the near future the remaining r-process "waiting points" may be easier reached with fragmentation processes and their cocktail beams at fragment separators such as the A1900 at MSU. For further improvements and the accessibility of the N = 126 waiting-point nuclei, devices like the rare isotope accelerator RIA are needed.

*Argonne National Laboratory and University of Maryland, †University of Maryland, ‡Universität Mainz, Germany, §Michigan State University, ¶CERN, Geneva, Switzerland, ‖Petersburg Nuclear Physics Institute, Gatchina, Russia, **University of Oslo, Norway, ††Russian Academy of Science, Troitzk, Russia.
[1]I. Dillmann *et al.*, Proceedings of the International Conference on Capture Gamma Rays and Related Topics CGS11, Pruhonice, (World Scientific Press 2003) in print.
[2]A. Wöhr, *et al.*, Proceedings of the 11th Workshop on "Nuclear Astrophysics" MPA/**P13** (2002).
[3]I. Dillmann, Diploma Thesis, University of Mainz, unpublished (2002).
[4]P. Möller *et al.*, Atomic Data and Nuclear Data Tables **59**, 1983 (1995).
[5]Y. Aboussir *et al.*, Atomic Data and Nuclear Data Tables **61**, 127 (1995).
[6]J. Duflo and A. P. Zuker, Phys. Rev. C **52**, R23 (1995).
[7]J. Dobaczewski *et al.*, Phys. Rev. Lett. **72**, 981 (1994).
[8]M. Samyn *et al.*, Nucl. Phys. **A700**, 142 (2001).
[9]G. Audi and A. H. Wapstra, Nucl. Phys. **A624**, 1 (1997).
[10]M. Hellström *et al.*, Proceedings of the International Workshop XXXI on Gross Properties of Nuclei and Nuclear Excitations, Hirschegg (2003), in print.
[11]G. Martinez-Pinedo and K. Langanke, Phys. Rev. Lett. **83**, 4502 (1999).

b.2.5. The Strength of Octupole Correlations in Neutron-Rich Xe Isotopes (I. Ahmad, W. Urban,* T. Rzaca-Urban,* J. L. Durell,† W. R. Phillips,† A. G. Smith,† B. J. Varley,† and N. Schulz‡)

Excited states in ^{140}Xe and ^{142}Xe were studied using prompt gamma coincidences measured with the Eurogam2 array of Compton-suppressed Ge spectrometers and a ^{248}Cm fission source. Level schemes of the two nuclei were constructed on the basis of coincidence relationships between gamma rays in ^{140}Xe and ^{142}Xe, and their respective complementary fission fragments. Angular correlations and linear polarization measurements were used to deduce spins and parities of levels. On the basis of these results we report the first observation of an octupole band in ^{142}Xe which is shown in Fig. I-33. The octupole band in ^{140}Xe was extended to higher spins. Properties of octupole bands in Xe isotopes indicate that octupole correlations in these nuclei are weaker than the values in the corresponding Ba nuclei, contrary to theoretical predictions. This may be due to the role of the N = 88 neutron number. The results of this study were published.[1]

*Warsaw University, Krakow, Poland, †University of Manchester, United Kingdom, ‡Institut de Recherches Subatomiques, Strasbourg, France.
[1]Eur. Phys. J. A **16**, 303 (2003).
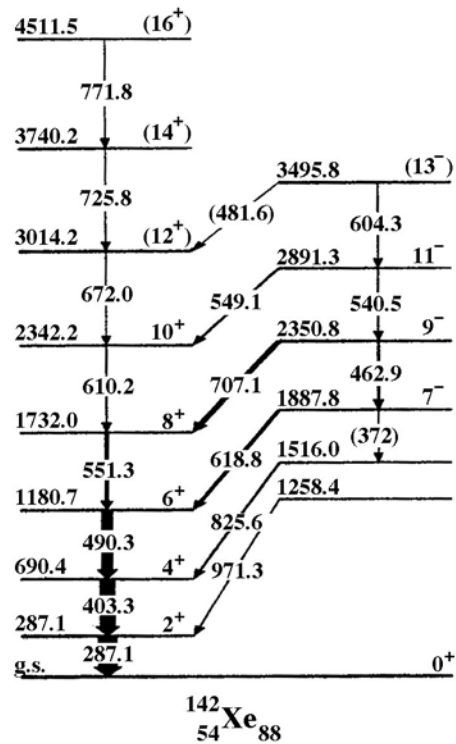
Fig. I-33. A partial level scheme of ^{142}Xe showing the octupole band identified in the present work.

b.2.6. New Low-Spin States in ^{134}Sb Observed in the Decay of ^{134}Sn and Estimate of the Energy of the 7⁻ Isomer (I. Ahmad, L. R. Morss,* A. Korgul,† H. Mach,‡ B. Fogelberg,‡ W. Urban,† W. Kurcewicz,† T. Rzaca-Urban,† P. Hoff,§ H. Gausemel,§ J. Galy,‡ J. L. Durell,¶ W. R. Phillips,¶ A. G. Smith,¶ B. J. Varley,¶ N. Schulz,‖ M. Gorska,** V. I. Isakov,†† K. I. Erokhina,‡‡ J. Blomquist,§§ F. Andreozzi,¶¶ F. Coraggio,¶¶ A. Covello,¶¶ and A. Gargano¶¶)

Excited states in ^{134}Sb ($t_{1/2}$ = 0.75 s), populated in the β⁻ decay of ^{134}Sn ($t_{1/2}$ = 1.2 s), were studied at the mass separator OSIRIS. Mass separated ^{134}Sn atoms were provided by the OSIRIS facility at Studvik where ^{134}Sn decay was first studied using thermal neutron fission of ^{235}U. In the present work, the ^{134}Sn activity was produced by the fast neutron fission of ^{238}U to improve the experimental sensitivity. The mass separated ^{134}Sn atoms were deposited on aluminized mylar tape. Gamma singles and γ-γ coincidence spectra were measured with a LEPS and a Ge spectrometers, in coincidence with β⁻ particles detected with a thin plastic scintillator. From these studies a level scheme, shown in Fig. I-34, was constructed. One of the important results of this investigation is the identification of a 13-keV level, which led to a revision of the ^{134}Sb level scheme. The new results are compared with different theoretical calculations and with the known data for the analogous neutron and proton two-particle nucleus ^{210}Bi. On the basis of this comparison, the energy of the ($\pi g_{7/2} \nu f_{7/2}$)7⁻ isomer is estimated to be about 250 keV, ~100 keV lower than previously reported. The results of this work were published.[1]

[1]Eur. Phys. J. A **15**, 181 (2002).
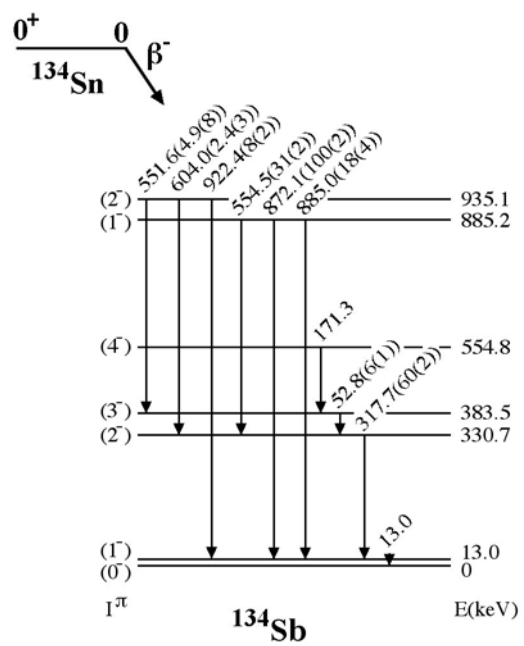
Fig. I-34. A partial level scheme of ^{134}Sb deduced from the results of the present investigation.

C. SPECTROSCOPY OF TRANS-LEAD NUCLEI

The structure and stability of the very heaviest elements continues as a forefront area of our research, both theoretically and experimentally, as it provides one of the ultimate tests of our understanding of nuclear binding. Progress in understanding the shapes of nuclei and the sequence of quantum states near the Fermi surface of the very heaviest nuclei continued. This progress will lead to an improved vision of the location and stability of possible "superheavy" elements. In addition, investigations of the spin and excitation dependence of the fission barrier in these very heavy systems may help guide future synthesis experiments.

c.1. Structure of ^{208}Bi from Deep Inelastic Heavy Ion Reactions (M. P. Carpenter, R. V. F. Janssens, F. G. Kondev, T. Lauritsen, D. Seweryniak, I. Wiedenhöver, B. Fornal,* R. Broda,* W. Krolas,* T. Pawlat,* J. Wresinski,* K. H. Maier,† P. J. Daly,‡ P. Bhattacharyya,‡ Z. W. Grabowski,‡ S. Lunardi,§ C. A. Ur,§ G. Viesti,§ M. Cinausero,¶ N. Marginean,¶ and M. Rejmund‖‖)

High-spin states in ^{208}Bi were studied at Gammasphere using deep inelastic reactions induced by a 305-MeV ^{48}Ca beam on a thick ^{208}Pb target. Much new information was obtained, in particular about states located above the known 10⁻ isomer in this nucleus. Specifically, yrast and near-yrast levels up to 5.6 MeV were delineated. The new findings include high spin members of πv^{-1} multiplets (considering ^{208}Pb as the core) and states arising from two-particle two-hole couplings. Considerable overlap between these new data and earlier charged-particle spectroscopy studies turned out to be important for the interpretation of the results. Comparisons with shell-model calculations were carried out as well. Embedded among the 2p-2h states were three levels explained as octupole excitations built on specific 1p-1h states. Their energies were shown to be consistent with empirical predictions. A paper reporting these results qas recently submitted for publication.[1]

[1]B. Fornal et al., submitted to Phys. Rev. C.

c.2. First Identification of a μs Isomer in N = 127 ^{217}Th (G. Mukherjee,* T. L. Khoo, D. Seweryniak, I. Ahmad, M. P. Carpenter, C. N. Davids, A. Heinz, F. G. Kondev, T. Lauritsen, C. J. Lister, R. V. F. Janssens, A. Woehr,† A. Aprahamian,§ P. Boutachakov,§ P. A. Butler,¶ P. Chowdhury,‡ J. A. Cizewski, R. Herzberg,¶ G. Jones,¶ R. Julin,** M. Leino,** E. Ngijoi-yogo, P. Reiter,†† M. Shawcross,§ M. B. Smith,‖ A. Teymurazyan,§ and J. Uusitalo**)

Superheavy nuclei are stabilized only due to the shell effects. Thus the predictions of the stable superheavies depend on the knowledge of the single particle energies. In the Pb region, the presence of $\Delta\ell = 3$ and $\Delta j = 3$ $f_{7/2}$ and $i_{13/2}$ proton orbitals give rise to ocutpole correlations which are, generally, not treated in the standard mean field calculations. In thorium isotopes, extra octupole correlation comes from the neutron $g_{9/2}$ and $j_{15/2}$ orbitals. The comparison of calculated single-particle energies to the experimental ones can be masked by the existence of this correlation. For example, calculations by K. Rutz et al.[1] recently predicted a substantial shell gap for Z = 92 between $\pi h_{9/2}$ and $\pi f_{7/2}$ orbitals and for N = 126. However, K. Hauschild et al. argued, from their experimental data, that the single particle orbitals near Z = 90 and N = 126 get modified due to a strong L = 3 correlation, as in ^{216}Th,[2] which contradicts the prediction.

Neighboring odd-A nuclei are the best laboratory to study the single-particle orbitals. A strong octupole core vibration in ^{217}Th is indicated from the systematics of low energy 15/2⁻ states in odd-A N = 127 nuclei. The level scheme of ^{217}Th is not known except for one excited state at 673 keV[3] which was assumed to be the 15/2⁻ state.

It is difficult to study these neutron deficient nuclei by prompt coincidence method because of the very low (~ few μb) production cross section and also since the fission channel cominates in this region. We studied the spectroscopy of ^{217}Th at the focal plane of the FMA at Argonne. The excited states in ^{217}Th were populated by the reaction ^{172}Yb(^{48}Ca,3n) with a 219 MeV of beam energy from the ATLAS at Argonne. The recoils were identified by (M/Q) in the FMA and by gating on a ΔE-TOF 2D matrix. ΔE is the energy loss in the focal plane PPAC and TOF the time-of-flight between the PPAC and a micro channel plate detector. After traversing these detectors, residues were implanted onto a catcher foil in front of a Si IN diode box. The γ rays were detected in two clover Ge detectors and two

LEP's, surrounding the catcher foil. The flight time of the recoils through the FMA were ~1.4 μs, so we could only detect the γ rays decayed from a long-lived (more than a μs half life) isomer.

The mass gated γ-ray spectra are quite clean. Spectra gated by mass 216 and 217 are shown in Fig. I-35. The raw spectrum is shown in the upper panel for comparison. The x-rays are seen in both the gated spectra. The γ rays below the 128 μs isomer in ^{216}Th are observed in the spectrum gated by mass 216. In the spectrum gated by mass 217, two γ rays, 673 keV and 1270 keV, are seen clearly along with the Th x rays. Thus we assigned these γ rays to ^{217}Th.
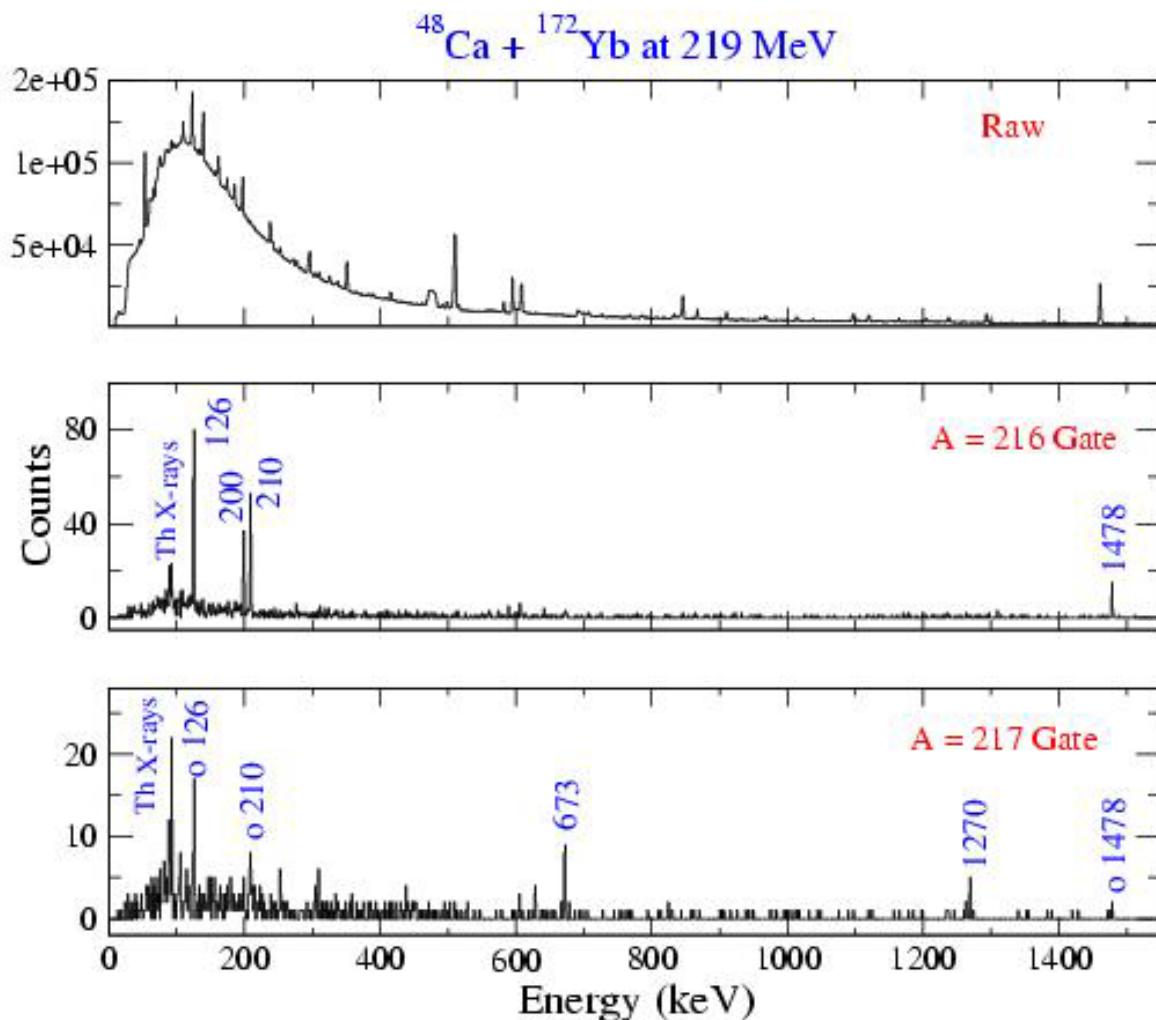
Fig. I-35. The γ-rays spectra from the present measurement. The raw spectrum (no mass gate) and the mass gated spectrum (gate on A = 216 and A = 217) are shown. The γ-rays accompanied by ``o'' in the third panel correspond to the contamination from A = 216.

The half life corresponding to these two transitions are measured to be 20 ± 5 μs and is shown in Fig. I-36. Thus we could identify a long-lived isomer for the first time in this nucleus. The $25/2^+$ states in N = 127 isotones are isomeric with half lives of the order of a few μs. So, from the systematics of N = 127 we have assigned a spin-parity of $25/2^+$ to the isomer. In the γ-γ matrix gated by mass 217, we could identify a few

other transitions and correlations among them. The statistics were low and have only a few founts in the peaks in the gated spectra due to the mass gating, but the spectra were very clean with almost zero background and the thorium x rays were observed in all the gated spectra. The proposed level scheme, based on the γ-γ correlation and the systematics, is shown in Fig. I-36.
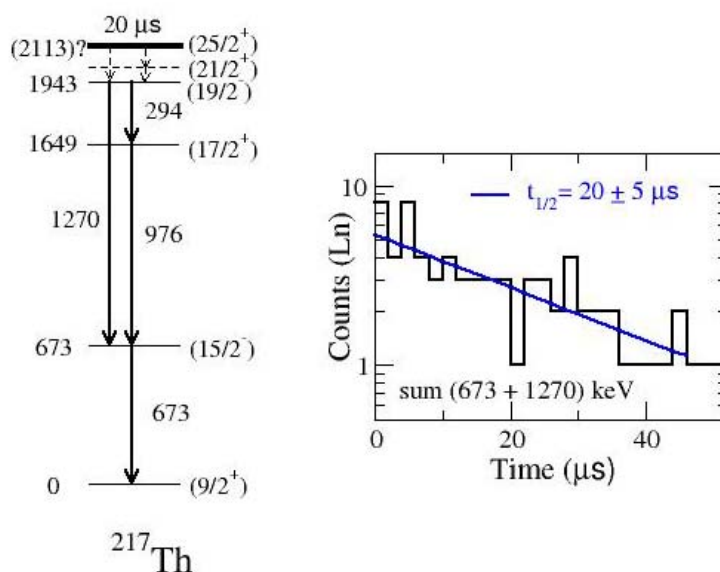
Fig. I-36.   Tentative level scheme of ^{217}Th based on present measurement and systematics.   These states are from the decay of a ~20 μs isomer.   The half life fit of the isomer is also shown.

It can be seen from Fig. I-36 that the x-ray intensities in ^{217}Th are quite high ($K_{\alpha 1}$ = 74% of the 673 keV γ-ray intensity).   The observed transitions in ^{217}T cannot account for this high yield of x rays, thereby indicating that there should be highly converted M2 and E3 transitions.   A simple computation indicates the presence of at least 2 highly converted ($\alpha_\kappa \geq 10$) transitions.   In the neighboring N = 127 isotones, the $25/2^+$ isomers decay by a low energy E2 transition (e.g. 57 keV in ^{215}Ra) to the $21/2^+$ state.   The K electron binding energy in thorium is 109 keV, so the converted transitions should have energies more than 109 keV. A 115-keV E2 transition has a K electron conversion coefficient of aonly 0.24 which cannot account for the high yield of K x rays.   Also, such an E2 transition fails to account for the half life of the isomer.   The other possibility is that the isomer decays by a mixed E3/M2 transition to a $19/2^-$ state generated by the coupling of $j_{15/2}$ orbital with the 2^+ state in even-even ^{216}Th.   Such a state was observed in the isotone ^{213}Rn,[4] about 400 keV above the $21/2^+$ state.   The half life of the isomer and

the yield of K x rays can be accounted for with a 170-KeV E3 transition between these two states.   The $25/2^+$ state is generated by the coupling of the $g_{9/2}$ orbital with the octupole coupled 8^+ state observed in the neighboring even-even nucleus and so an enhanced E3 transition from this isomeric state can complete with an E2 transition (to the $21/2^+$ state).   Thus the $19/2^+$ and $21/2^+$ states seem to lie close to each other in ^{217}Th. Though the $19/2^+$ state has been shown below $21/2^+$ state in Fig. I-36 but the ordering can be reversed as well and the 1270 keV γ ray to the $15/2^-$ state can either be an E12 or an E3 transition.   The excitation of the isomer, shown in Fig. I-36, is, however, tentative since we do not know the energies of the missing converted transitions.

In conclusion, we observed a 20 ± 5μs isomer in ^{217}Th and proposed, for the first time, a level scheme beyond the first excited state from its decay.   The spin-parity assignments are from the systematics and are tentative. The level scheme around the long lived isomeric state

at 25/2$^+$ seems different than its isotone ^{215}Ra. There appears to be a 19/2$^-$ state similar to that in ^{213}Rn. But unlike in ^{213}Rn, this state lies close in energy to the 21/2$^+$ state. This is apparently due to the low energy of the 15/2$^-$ state in ^{217}Th because of the larger octupole correlation. Though the present data indicate a larger ocupole correlation in this nucleus but more data are required to extend the level scheme above this isomer. This is important to look for the second 25/2$^+$ state and for the measurement of the E3 transition strength of the 21/2$^-$ to 25/2$^+$ decay which would shed light on the possibility of the vanishing of Z = 92 shell gap.

---

*Argonne National Laboratory and University of Massachusetts-Lowell, †Argonne National Laboratory and University of Maryland, ‡University of Massachusetts-Lowell, §University of Notre Dame, ¶University of Liverpool, United Kingdom, ‖Rutgers University, **University of Jyvaskyla, Finland, ††Ludwig-Maximillians-Universitat, Garching, Germany, ‡‡University of Maryland.
[1]K. Rutz et al.,. Nucl, Phys. **A634**, 67 (1998).
[2]K. Hauschild et al., Phys. Rev. Lett **87**, 072501 (2001).
[3]G. D. Dracoulis et al., Nucl. Phys. **A493**, 145 (1989).
[4]A.E. Stuchbery et al., Nucl. Phys. **A482**, 692 (1988).
[5]A. E. Stuchbery et al., Nucl. Phys. **A641**, 401 (1998).
[6]A. E. Stuchbery et al., Nucl. Phys. **A555**, 355 (1993).

c.3.   Coulomb Excitation and Few Nucleon Transfer Reactions in ^{209}Bi + ^{232}Th at 1400 MeV and ^{209}Bi + ^{248}Cm at 1450 MeV (K. Abu Saleem,* R. V. F. Janssens, M. P. Carpenter, F. G. Kondev, I. Ahmad, J. Caggiano, J. P. Greene, A. Heinz, T. L. Khoo, T. Lauritsen, C. J. Lister, D. Seweryniak, I. Wiedenhöver, G. Hackman,† P. Chowdhury,‡ D. Cline,§ M. Devlin,¶ N. Fotiades,¶ A. O. Macchiavelli,‖ E. H. Seabury,¶ and C. Wu§)

For the last few years, the actinide nuclei were extensively investigated at ATLAS. The so-called "Unsafe" Coulex technique was used with ^{232}Th, ^{237}Np, ^{241}Am, and ^{248}Cm targets and ^{209}Bi beams from ATLAS with energies ~15% above the respective Coulomb barriers. The data of interest were collected with the Gammasphere array. Partial results on some of the nuclei were presented in earlier annual reports.

Here, some of the new results on the even-even ^{232}Th and ^{248}Cm nuclei are presented. These nuclei offer the possibility to investigate in detail alignment phenomena as a function of angular momentum up to fairly high spin. In addition, low-lying rotational bands built on beta, gamma and octupole vibrations are also present in the level structures of these nuclei. Thus, there are ample possibilities to confront the data with theoretical calculations.

The level scheme of ^{248}Cm is given in Fig. I-37. The yrast band was traced to the 32$^+$ state. The observed alignment was attributed to a pair of $i_{13/2}$ protons, as is the case in other even-even nuclei in the region. These results can be understood in the framework of the cranked shell model, although the latter also predicts a $j_{15/2}$ neutron alignment that was not seen experimentally. In addition, three excited bands based on octupole (band 2), beta (band 3) and gamma (band 4) vibrations were delineated. The latter offer an opportunity to test the applicability of recent RPA calculations by Nakatsukasa *et al*.[1] Satisfactory agreement between calculated and observed alignments was observed. Similar conclusions were reached in the case of ^{232}Th, where a total of eleven band structures were found.
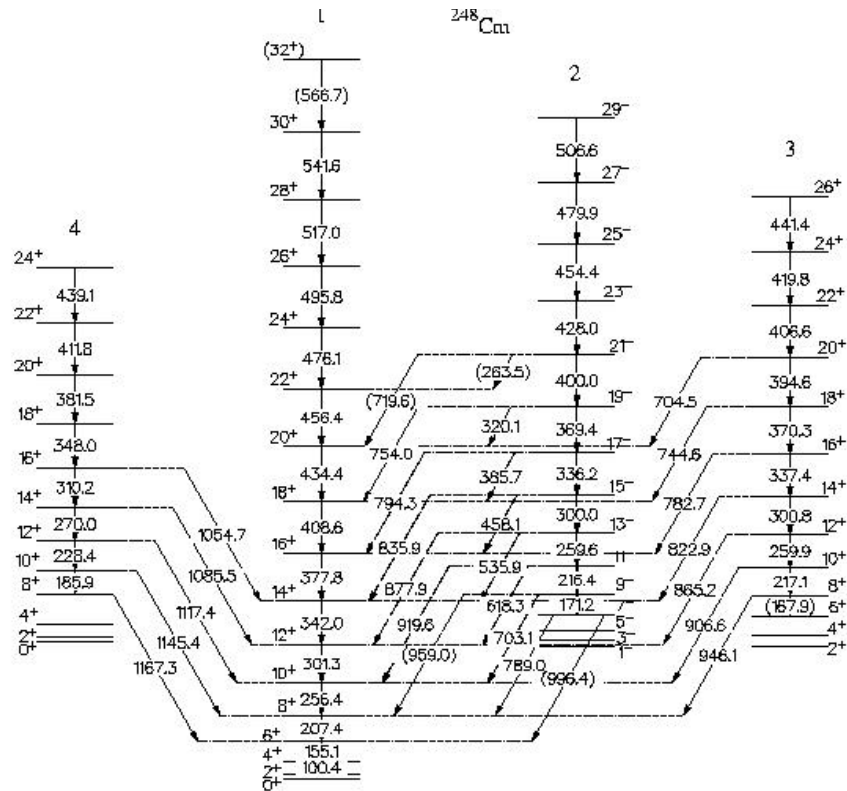
Fig. I-37. Level scheme obtained for ^{248}Cm in the present work.

The RPA calculations can be tested further by taking advantage of the so-called generalized intensity relations such as:

$$\sqrt{B(E\lambda; i \rightarrow f)} = Q_T < J_i, K_i, \lambda, (K_f - K_i) \mid J_f, K_f > (1 + q(E\lambda)[J_f (J_f + 1) - J_i (J_i +1)])$$

As illustrated in Fig. I-38 for the case of an octupole band in ^{232}Th, the Coriolis mixing parameter q(E1) can be extracted from the measured relative γ-ray intensities between various decay pathways out of the levels of a vibrational band. In the same way the Q_T moment can be obtained. These two quantities then offer additional tests of the RPA predictions. Table I-2 compares theory and experiment for all even-even actinide nuclei

where data are currently available, including the two cases studied in the present work.

The agreement between theory and experiment is rather satisfactory. In particular, theoretical general trends of q(E1) and Q_T with K and A are well reproduced.

These data are part of the thesis of K. Abu Saleem, which was submitted recently.[2]

*Argonne National Laboratory and Illinois Institute of Technology, †University of Kansas, ‡University of Massachusetts-Lowell, §University of Rochester, ¶Los Alamos National Laboratory, ‖Lawrence Berkeley National Laboratory.
[1]T. Nakatsukasa *et al*., J. Phys. G **25**, 795 (1999) and references therein.
[2]K. Abu Saleem, PhD Thesis, Illinois Institute of Technology, December 2002.

Table I-2. Measured and calculated q(E1) (in units of $\hbar^{-1}$) Coriolis mixing parameter and Q_T moments (in units of e.fm) for the even-even actinide nuclei where data are presently available.

^{232}Th		$K = 0^-$	$K = 1^-$	$K = 1^-$
q(E1)	calc.	0.22	-0.11	-0.11
	exp.	0.0513(3)	-0.03(2)	-0.01(10)
Q_T	calc.	0.16	0.066	0.066
	exp.	0.0097(4)	0.0031(5)	0.0031(5)
^{238}U		$K = 0^-$	$K = 1^-$	$K = 1^-$
q(E1)	calc.	-0.017	0.12	0.12
	exp.	-0.002	0.044	-
Q_T	calc.	0.12	0.067	0.067
	exp.	0.016	0.0058	-
^{240}Pu		$K = 0^-$	$K = 1^-$	$K = 1^-$
q(E1)	calc.	0.006	-	-
	exp.	0.001(6)	-	-
^{248}Cm		$K = 0^-$	$K = 1^-$	$K = 1^-$
q(E1)	calc.	-	0.019	-
	exp.	-	0.0513(5)	-
Q_T	calc.	-	0.08	-
	exp.	-	0.0099(18)	-
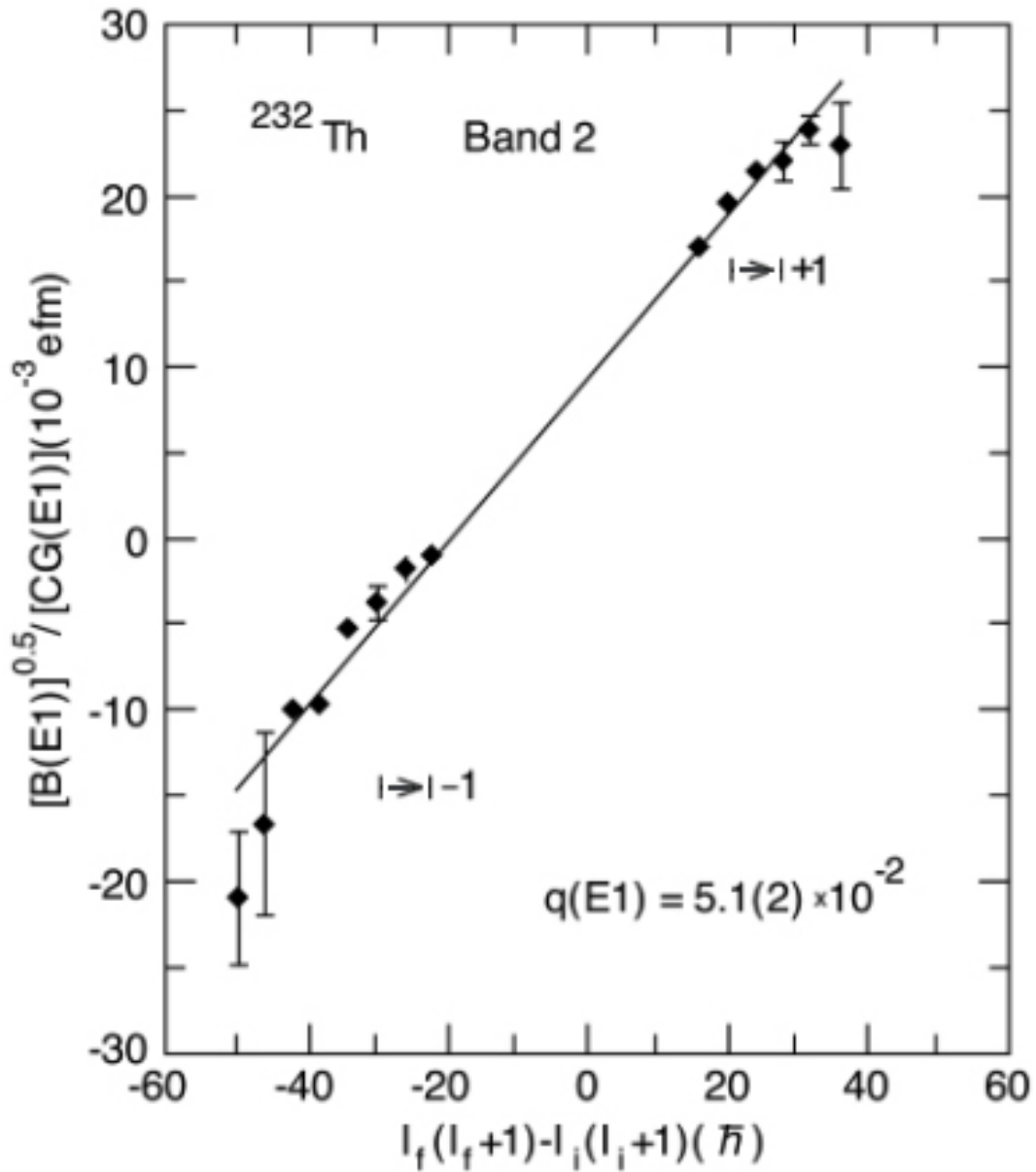
Fig. I-38. *Reduced transition probabilities B(E1) as a function of the final and initial spins for the E1 transitions in the main octupole band in ^{232}Th. The line represents a fit with the generalized intensity relation given in the text.*

c.4.   Quantitative Determination of ^{252}Cf Source Strength from Fission γ-Rays
(I. Ahmad, E. F. Moore, J. P. Greene, C. E. Porter,* and L. K. Felker*)

The nuclide ^{252}Cf ($t_{1/2}$ = 2.645 yr) is routinely used in industry and research as a neutron source and also as a source of neutron-rich fission fragments. The main mode of decay is by α-particle emission (alpha branch 96.91%). More than 99% of the decay occurs to the ground state and the 43.4-keV, 2$^+$ state of ^{248}Cm. Thus there is no γ ray with sufficient intensity which can be used for ^{252}Cf assay. However, in the fission of ^{252}Cf (3.09%), many fragments are produced which decay by emission of high energy γ rays. We measured the absolute intensities of two γ rays which can be used for qualitative and quantitative analysis of ^{252}Cf samples.

We prepared thin sources of ^{252}Cf by molecular plating. Alpha pulse height analysis was used to determine the fraction of α particles from the ^{252}Cf decay. The source strength was obtained by measuring the alpha spectrum with a Si detector of known geometry. The gamma singles spectrum of ^{252}Cf source of known alpha decay rate was measured with a 25% Ge spectrometer whose absolute efficiency was determined with a calibrated source. We found two γ rays with large peak areas and determined their intensities. A high-energy portion of the γ-ray spectrum showing the γ rays of interest is displayed in Fig. I-39. The intensities of the 1435.8 and 1596.5 keV γ rays were determined to be (0.134 ± 0.006)% per ^{252}Cf decay and (0.19 ± 0.01)% per ^{252}Cf decay, respectively. The 1435.8 keV γ ray is produced in the decay of the fission fragment ^{138}Cs ($t_{1/2}$ = 32.2 min) and 1596.5 keV γ ray is associated with the decay of ^{140}Ba-La ($t_{1/2}$ = 12.746 d). The results of this investigation were submitted for publication.[1]

_____
*Oak Ridge National Laboratory.
[1]Nucl. Instrum. Methods, in press.
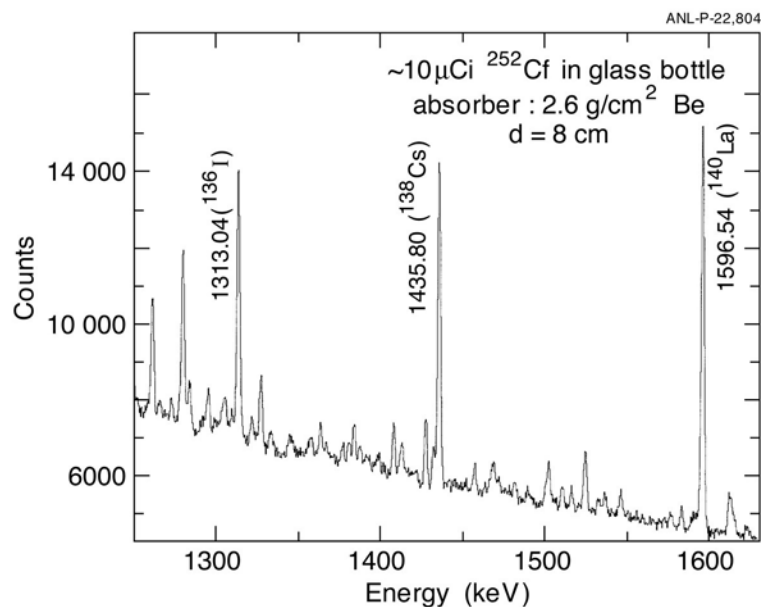
Fig. I-39. A portion of the γ-ray spectrum showing the γ rays of interest. The spectrum was measured with a 25% Ge spectrometer. The source was 10 μCi ^{252}Cf in a glass bottle.

c.5.   Structure of [253]No (T. L. Khoo, A. Heinz, T. Lauritsen, C. J. Lister, D. Seweryniak, I. Ahmad, M. P. Carpenter, C. N. Davids, W. F. Henning, F. Kondev, R. V. F. Janssens, A. A. Sonzogni, S. Siem, I. Wiedenhöver, P. Reiter,[*] N. Amzal,[†] P. A. Butler,[†] A. J. Chewter,[†] J. A. Cizewski,[‡] P. T. Greenlees,[¶] K. Helariuta,[¶] R. D. Herzberg,[†] G. Jones,[†] R. Julin,[¶] H. Kankaanpää,[¶] H. Kettunen,[¶] W. Korten,[§] P. Kuusiniemi,[¶] M. Leino,[¶] J. Uusitalo,[¶] and K. Vetter[||])

The heaviest nuclei are stabilized by a shell-correction energy, which lowers the ground-state, thereby creating a barrier against fission. The shell-correction energy originates from the clustering of single-particle orbitals. Hence, the single-particle eigenstates form the basis of the shell stabilization. The most direct data on the orbital energies come from odd-A nuclei, providing our motivation to investigate the odd-N nucleus [253]No. The single-particle energies also provide a direct test of nuclear models that predict the properties of superheavy nuclei. Thus, by testing model predictions[1] against data on the heaviest nuclei that are accessible for spectroscopy, one may judge their reliability for predicting the properties of superheavy elements, e.g. the next spherical shell closures beyond [208]Pb.

The production cross section of ^{207}Pb(^{48}Ca,2n)^{253}No reaction was measured as ~0.5 μb at Jyväskylä. In a subsequent experiment at Argonne, the γ rays were detected with Gammasphere, in coincidence with [253]No residues detected in the FMA. The γ-ray spectrum for [253]No has many weak lines, but is dominated by the K x-rays. Heavy odd-A nuclei, such as [253]No, represent the limits of in-beam γ spectroscopy due to overwhelming conversion electron competition in M1 transitions. Of the expected low-lying configurations in [253]No, only the 7/2+[624] orbital is expected to have sufficiently small M1 branching ratios to permit detection of intraband E2 γ rays. However, due to the low γ-ray cross sections of 25-50 nb, it was necessary to develop new methods based on (a) quantitative comparisons of results from experiment and from

model predictions and (b) enhancement of transitions with high γ multiplicity. Similar methods will be required for in-beam γ spectroscopy of nuclei far from stability, which have diminishing cross sections.

The kinematic and dynamic moments of inertia, $J^{(1)}$ and $J^{(2)}$, of the 7/2+[624] band are shown in Fig. I-40, where they are compared with values from those of the neighboring nuclei ^{252,254}No. In the lower panel, the moments of inertia predicted[1,2] by Skyrme Hartree-Fock Bogolyubov theory (SHFB, with the Sly4 force) are given. The general trends are reproduced by theory, but details are not.

A bandhead energy of 355 keV is deduced from the data for the 7/2+[624] configuration. This energy compares with theoretical predictions of 222, 400 and 1200 keV, which are given by, respectively, a Nilsson model based on the Wood-Saxon potential and by self-consistent mean-field theories using the cranked relativistic Hartree Bogoliubov methods.[1,2] Of course, a systematic test of theory should encompass a set of quasiparticle states, and was recently performed for self-consistent mean-field theories.[1,2] For example, Ref. 3 points out that the relativistic mean-field method is able to describe many single-particle energies, but that several (including the 7/2+[624] orbital) that originate from specific spherical orbitals deviate by more than 1 MeV from experimental energies.

A Letter on the results is being prepared.

_____
[*]University of Munich, Germany, [†]University of Liverpool, United Kingdom, [‡]Rutgers University, [§]DAPNIA/SPhN CEA-Saclay, France, [¶]University of Jyväskylä, Finland, [||]Lawrence Berkeley National Laboratory
[1]T. Bender et al., Nucl. Phys. A (2003), in press.
[2]Th. Duguet et al., Nucl. Phys. **A679**, 427 (2001).
[3]A. Afanasjev et al., Phys. Rev. C **67**, 024309 (2003); see report in theory section.
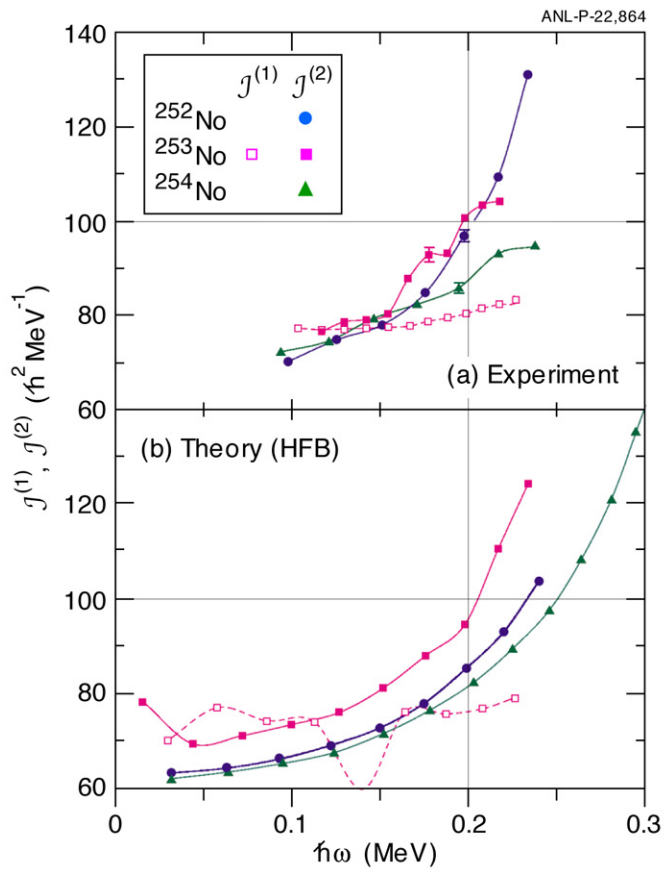
Fig. I-40. The moments of inertia $J^{(1)}$, for $J^{(2)}$ for the 7/2+[624] band in ^{253}No and $J^{(2)}$ for ^{252,254}No, given as a function of rotational frequency. (a) Experimental data; (b) results from SHFB theory, from Refs. 1 and 2. Typical error bars for $J^{(2)}$ are shown.

D. OTHER TESTS OF NUCLEAR STRUCTURE UNDER EXTREME CONDITIONS

Investigation of hot nuclei was made using the FMA and a large array of barium fluoride detectors. The analysis of these data is nearing completion, as is analysis of the "ridge" structure in the gamma-continuum of superdeformed nuclei. In discrete line spectroscopy, a collective octupole vibrational band has been found in the classic superdeformed rotor ^{152}Dy, and other studies on nuclear structure of "superdeformed" structures continue.

d.1. Hot Giant Dipole Resonance γ Rays in Sn Nuclei (B. B. Back, M. P. Carpenter, T. L. Khoo, T. Pennington, P. Heckman,* J. P. Seitz,* E. Tryggestad,* T. Baumann,* M. Thoennessen,* R. L. Varner,† D. J. Hofman,‡ and V. Nanal§)

The GDR in Sn was studied by employing two fusion-evaporation reactions, namely ^{18}O + ^{100}Mo and ^{17}O + ^{100}Mo. The beams of ^{18}O and ^{17}O were accelerated to energies of 95 and 78.8 MeV, respectively.[1]

The final γ-ray spectra extracted in this experiment are shown in Fig. I-41a,b. The parameters of the GDR are the sum rule strength (S), energy (E_D), and Width (Γ). The γ-ray spectra were fit with CASCADE[2,3] by varying the GDR parameters to minimize χ^2. It was also necessary to include a non-statistical bremsstrahlung component in the fits. The curved-bremsstrahlung parameterization was used to account for this non-statistical component, just as in Ref. 4. Since the same reaction was used in Ref. 4, this form should be valid here. The CASCADE and bremsstrahlung calculations were folded to account for the detector response, as simulated with GEANT,[5] before comparisons were made with data.

The result of the fits are shown as the solid curves in Fig. I-41a,b. The quality of the fits to the data is very good. The reduced χ^2 for the reactions ^{17}O + ^{100}Mo (^{117}Sn) and ^{18}O + ^{100}Mo (^{118}Sn) was found to be 1.5 and 1.1, respectively. To further demonstrate this point,

divided plots of F(E_γ) were created by dividing both the experimental and calculated spectra by a statistical spectrum assuming a constant E1 strength of 0.2 W.u. The divided plots are shown in Fig. I-41c,d. In the case of ^{117}Sn, the GDR parameters were found to be S = 0.87, E_D = 15.08 MeV, and Γ = 6.9 MeV at a temperature (T) of 1.74 MeV. For ^{118}Sn, S = 0.63, E_D = 15.16 MeV, and Γ = 8.17 MeV at T = 1.84 MeV.

The extracted GDR widths allow for comparisons to be made between this data and previous measurements. The results of this analysis are shown in Fig. I-42, along with previous experimental results. The widths found in this work are very similar to other measurements performed.

The γ-ray spectra measured in this work can be further used to test the validity of thermal shape fluctuation model calculations. In a recent work,[6] it was shown that the thermal shape fluctuation model fails to predict the behavior of the GDR width at low T. Using this data, it may be able to verify this finding. Also, since the reactions used in this work populate high spin states, it may also be possible to test if the spin dependence of the GDR width is well understood.

_____

*Michigan State University, †Oak Ridge National Laboratory, ‡University of Illinois at Chicago, §Tata Institute of Fundamental Research, Mumbai, India.
[1]Argonne Annual Report, "Hot GDR in ^{118}Sn", (2001).
[2]F. Pühlhofer, Nucl. Phys. **A280**, 267 (1977).
[3]R. Butsch et al., Phys. Rev. C **41**, 1530 (1990).
[4]M. P. Kelly et al., Phys. Rev. Lett. **82**, 3404 (1999).
[5]Detector Description and Simulation Tool GEANT, Version 3.21, CERN Program Library, Geneva.
[6]P. Heckman et al., Phys. Lett. **B555**, 43 (2003).
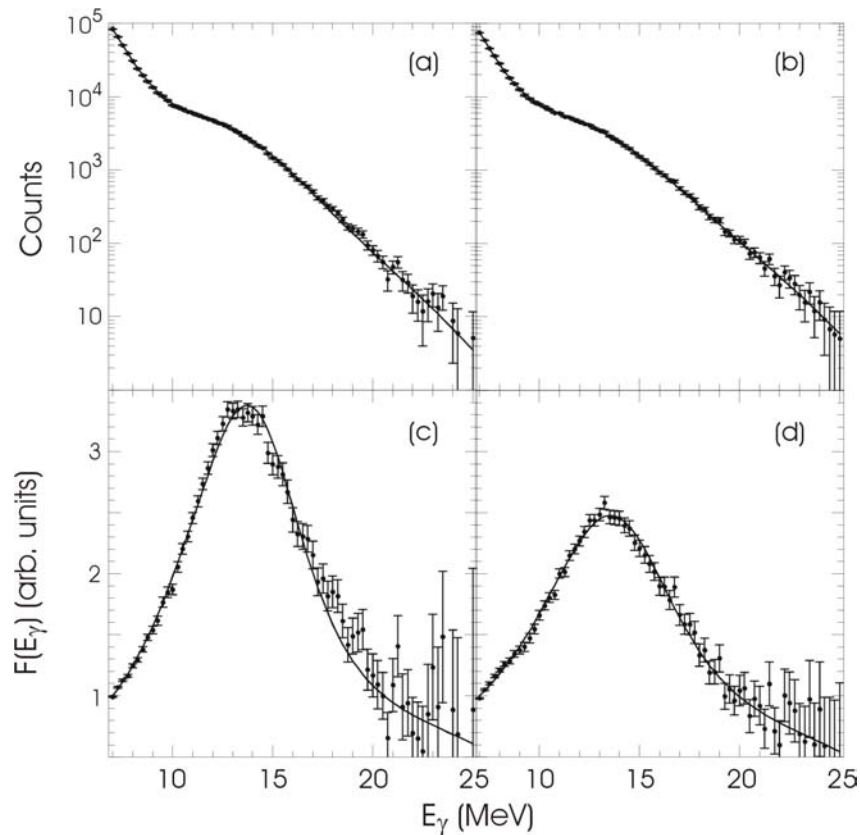
Fig. I-41. Panels (a) and (b) show the γ-ray spectra, while panels (c) and (d) show divided plots of the γ-ray spectra from experiment 889. The plots in panels (a) and (c) show the result from ^{117}Sn formed in the reaction ^{17}O + ^{100}Mo. The plots in panels (b) and (d) show the result from ^{118}Sn formed in the reaction ^{18}O + ^{100}Mo. In all panels, the data is shown as the solid points, and the calculations are shown by solid curves.
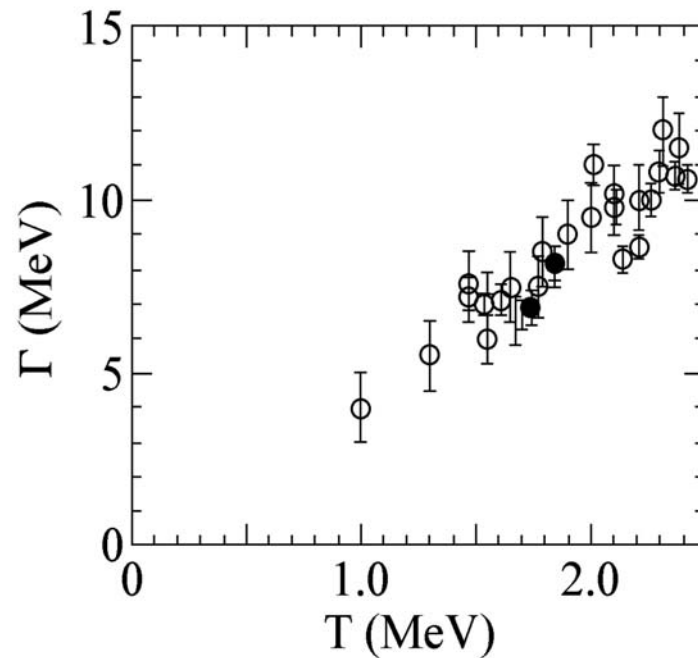
Fig. I-42. The experimental data for the GDR width as a function of temperature is shown. The solid circles are from this work and the open circles are from previous experiments.

d.2.   Highly Selective Studies of GDR in ^{164}Er (V. Nanal,* T. L. Khoo, B. B. Back,
M. P. Carpenter, A. M. Heinz, D. Henderson, D. Jenkins, M. P. Kelly, F. G. Kondev,
T. Lauritsen, C. J. Lister, B. McClintock, S. Mitsuoka, T. Pennington, R. H. Siemssen,
R. J. van Swol, P. Wilt, D. J. Hofman,† I. Dioszegi,‡ K. Eisenman,§ M. L. Halbert,¶
P. Heckman,§ J. Seitz,§ M. Thoennessen,§ R. L. Varner,¶ and Y. Alhassid‖)

We initiated a program to study the properties of the giant dipole resonance (GDR) in hot nuclei with at a well-defined spin and excitation energy. These properties are revealed through the GDR spectra emitted by hot compound nuclei, which eventually decay into uniquely identified evaporation residue channels. For this purpose, the ORNL/MSU/TAMU BaF$_2$ array of 148 detectors was integrated with the 50 element BGO spin/sum-energy spectrometer and the fragment mass analyzer (FMA) at the ATLAS facility (ANL). We also introduced a new but simple method for specifying the spin and internal excitation energy above the yrast line, from which GDR gamma emission occurs. For a given decay channel at different bombarding energies, it is possible to map out a wide range of angular momentum region while keeping the excitation energy above yrast line similar. These efforts constitute the most comprehensive systematic investigation of the GDR spectra from hot nuclei in

exclusive measurements (see Fig. I-43). The high-energy gamma rays from ^{164}Er are measured in coincidence with the 4n evaporation channel. The ^{164}Er is a well-deformed nucleus. With increasing temperature, shape fluctuations will appear but the spread will be less than that for transitional nucleus. There are theoretical predictions indicating a rapid increase in width at high spin.[1]

The experiment was carried out at ATLAS (at ANL) using 163 and 187 MeV ^{40}Ar beams on a ^{124}Sn target. The average angular momenta for the 4n decay channel are 26 $\hbar$ and 45 $\hbar$, respectively. The high-energy gamma ray spectra for BGO fold K $\geq$ 2, gated by mass A = 160 residues, are shown in the figure after dividing by the constant exponential (with arbitrary normalization). There is an implication that the increase in width at higher incident energy is related to the angular momentum effect as predicted in Ref. 1.

_____

*Argonne National Laboratory and Tata Institute of Fundamental Research, Mumbai, India, †University at Illinois at Chicago, ‡State University of New York at Stony Brook, §Michigan State University, ¶Oak Ridge National Laboratory, ‖Yale University.
[1]Y. Alhassid, Nucl. Phys. **A649**, 107c (1999).
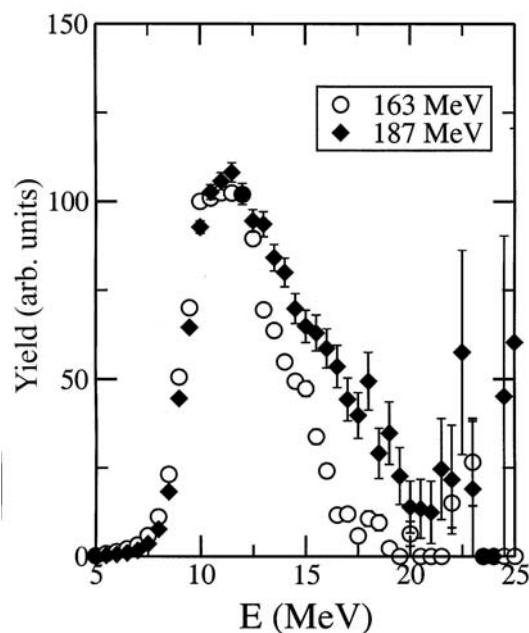
Fig. I-43. The GDR in ^{164}Er extracted following an analysis similar to that described in section d.1. The high energy gamma-rays were detected in coincidence with A = 164 residues.

d.3.   Observation of the GDR in Highly Excited ^{224}Th (B. B. Back, M. P. Carpenter, M. P. Kelly, T. L. Khoo, B. McClintock, T. Pennington, R. van Swol, R. H. Siemssen, S. Mitsuoka,* V. Nanal,† J. Seitz,‡ T. Baumann,‡ K. Eisenman,‡ P. Heckman,‡ M. Thoennessen,‡ R. L. Varner,§ D. J. Hofman,¶ and I. DiÓszegi‖)

The observation of the GDR in heavy fissile nuclei has so far been measured in coincidence with fission fragments. The pre-fission GDR has to be extracted from a large background of γ rays from the highly excited fission fragments. We performed a first measurement to observe the GDR γ rays in coincidence with evaporation residues in a system which is dominated by fission and where only a small fraction of the cross section leads to evaporation residues. The

reaction ^{48}Ca + ^{176}Yb at 256 MeV formed the compound nucleus ^{224}Th at an excitation energy of 83 MeV. The evaporation residues were measured with the FMA at ANL, and the high-energy γ rays were detected with the ORNL-MSU-TAMU BaF$_2$ array. The γ-ray spectrum shows evidence for the GDR at a resonance energy of ~12 MeV, consistent with the predicted value for the GDR of the ground state for this mass region.

_____

*Argonne National Laboratory and Japan Atomic Energy Research Institute, Ibaraki-ken, Japan, †Argonne National Laboratory and Tata Institute for Fundamental Research, Mumbai, India, ‡Michigan State University, §Oak Ridge National Laboratory, ¶University of Illinois at Chicago, ‖State University of New York at Stony Brook.

d.4.   Octupole Vibration in Superdeformed ^{152}Dy (T. Lauritsen, R. V. F. Janssens, M. P. Carpenter, D. G. Jenkins, T. L. Khoo, F. G. Kondev, K. Abu Saleem, I. Ahmad, A. M. Heinz, C. J. Lister, D. Seweryniak, P. Fallon,* B. Herskind,† A. Lopez-Martens,‡ A. O. Macchiavelli,* D. Ward,* R. M. Clark,* M. Cromaz,* T. Dossing,† A. Korichi,‡ and G. Lane*)

Nine transitions of dipole character were identified linking an excited superdeformed (SD) band in ^{152}Dy to the yrast SD band. As a result, the excitation energy of the lowest level in the excited SD band was measured to be 14238 keV. This corresponds to a 1.3 MeV excitation above the SD ground state. The levels in this band were tentatively determined to be of negative parity and odd spin. The measured properties are consistent with an interpretation in terms of a rotational band built on a collective octupole vibration.

The large data set used to link the ^{152}Dy yrast SD band to the normal deformed levels[1] was also exploited to obtain the best possible spectrum of the very weakly populated SD band 6 (~5% of the yrast SD band[2]). ^{152}Dy was produced with the ^{108}Pd(^{48}Ca,4n) reaction using a 191 MeV (at mid-target) ^{48}Ca beam delivered by the 88-inch cyclotron facility at the Lawrence Berkeley National Laboratory. The target consisted of a stack of two 0.4-mg/cm self-supporting ^{108}Pd foils. The Gammasphere array, with 100 Compton suppressed germanium detectors, measured the gamma rays of interest. As described in Ref. 1, events associated with ^{152}Dy were selected by detecting with high efficiency the decay of a 86 ns, 17+ yrast isomer (isomer tag). The result of summing triple coincidence spectra gated on clean SD lines in band 6 is shown in Fig. I-44: the members of the yrast SD band (from 601 keV to ~1113 keV) are clearly in coincidence with SD

band 6, as was suggested in Ref. 2. As a matter of fact, 53(8)% of the decay of band 6 proceeds through band 1.

Due to small differences in the moments of inertia of SD bands 1 and 6, any set of linking transitions between them will be characterized by specific energy spacings that depend on which levels are actually linked. Fig. I-45A presents the high energy part of the coincidence spectrum of Fig. I-45A. Nine weak transitions can be seen from 1645 to 1795 keV separated by one of the possible energy spacings (~20 keV). Coincidence gates were placed on the 1696 keV transition together with relevant lines in SD band 6, while also requiring the isomer tag: the resulting spectrum is given in Fig. I-45. It clearly shows only transitions in SD band 6 with energies Eγ ± 850 keV, i.e. the 805 keV and 762 keV gamma rays of the sequence are clearly missing. Under the same coincidence conditions, only transitions of the yrast SD band with Eγ ± 784 keV are observed. This unambiguously establishes the ordering proposed in the level scheme of Fig. I-47. Additional supporting evidence is given in Fig. I-45. In panel B, the gamma cascades are required to pass through SD band 6 and include the 830 keV band 1 transition: the decay-out transitions below 1715 keV are clearly absent. Conversely, in panel C, the gamma cascades are required to pass through the lower part
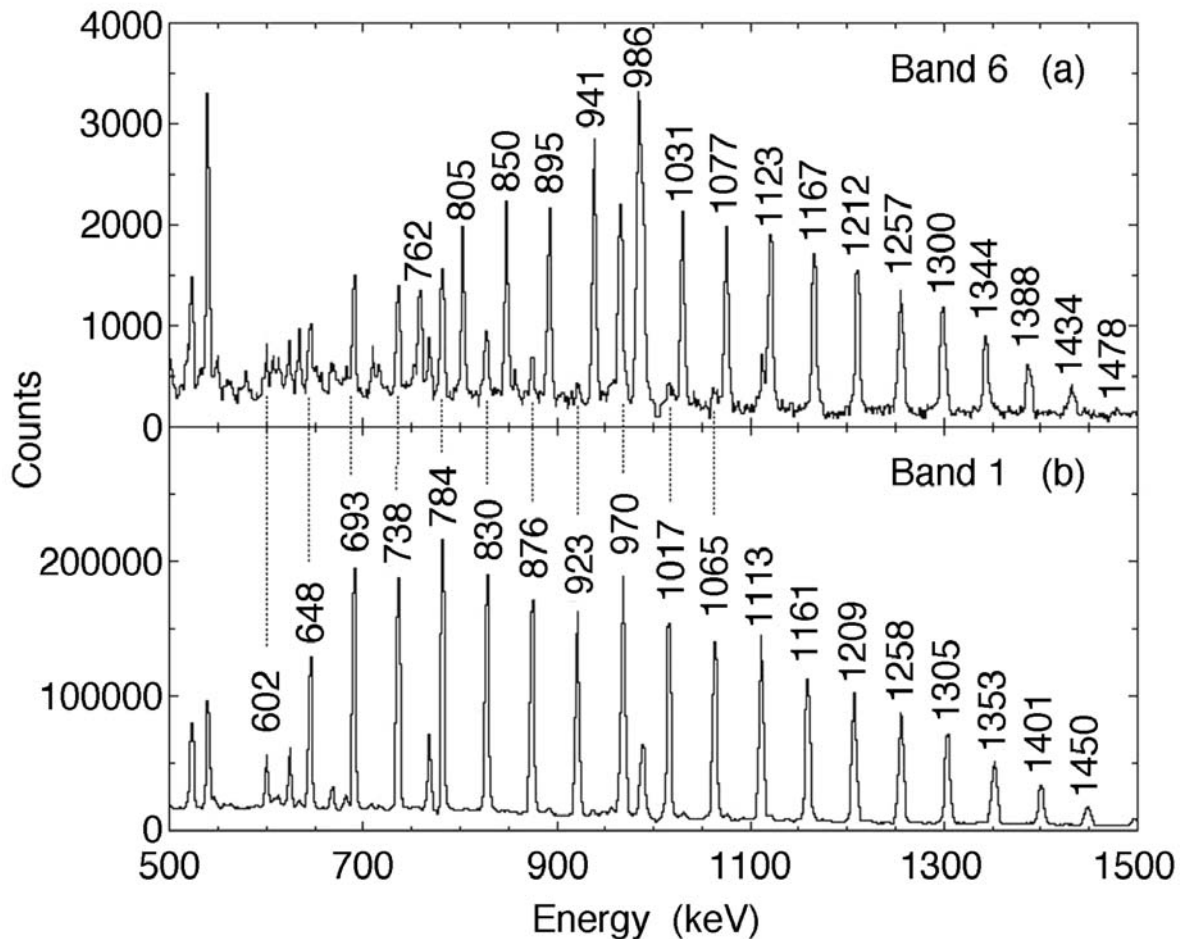
Fig. I-44. [A] Spectrum from triple coincidence gates on lines in SD band 6 of ^{152}Dy. Clean combinations of the following SD transitions were used in the analysis: 762, 805, 850, 895, 941, 1031, 1077, 1123, 1167, 1212, 1257, 1300, 1344 and 1388 keV. [B] Spectrum obtained from setting pairwise gates on clean SD lines in band 1 of ^{152}Dy.

of band 1 and include the 895 keV band 6 transition. Now the lower decay-out transitions are present, but the upper ones, from 1734 keV on, are missing. Thus, an excited SD band in the mass 150 region has for the first time been linked to an yrast SD band, which in turn is firmly connected to the normal states it decays into.[1]

An angular distribution analysis of the three linking transitions at 1676, 1696 and 1715 keV finds negative

A2 coefficients in every case (-0.9(4), -0.3(3) and -0.3(3), respectively). If the yields of these three lines are added up and analyzed together, the combined A2 coefficient is determined to be -0.5(2), see Fig. I-45D. This value is consistent with those expected for stretched or anti-stretched E1 or M1 transitions (-0.24 – -0.21), but inconsistent   with transitions of E2
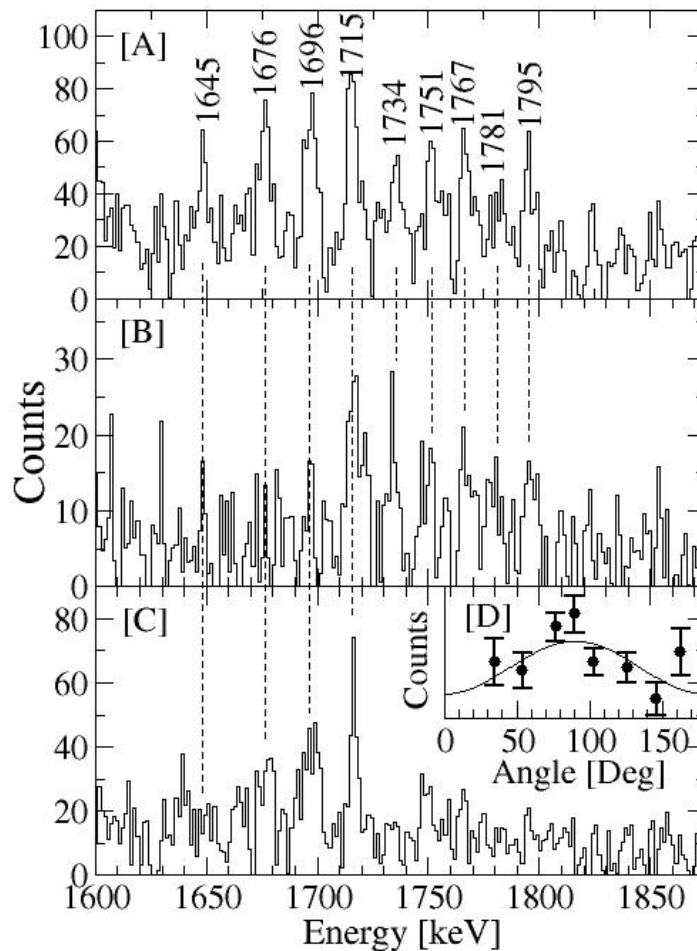
Fig. I-45. [A] Summed coincidence spectrum obtained by placing gates on clean SD band 6 high energy transitions and SD band 1 low energy transitions. The nine transitions linking SD band 6 to band 1 are marked with their energies. [B] As A, but requiring the 830 keV transition in band 1. [C] As A, but requiring the 895 keV transition in band 6 and any SD band 1 transitions below 876 keV. [D] Angular distribution of the sum of the intensities in the 1676, 1696 and 1715 keV linking transitions vs. the polar angle of the Gammasphere detectors.

character or with E1 transitions without spin change (where large positive A2 values of +0.34 and +0.45 are expected).

Assuming that SD band 6 has the same transition quadrupole moment of 17.5 eb as the yrast SD band,[3] it is possible to extract the partial half-lives of the interband transitions. Some of these are given in Table I-3, along with the transition strengths in Weisskopf units (W.u.) under the assumptions of E1 and M1 multipolarity. It is unlikely that M1 transitions between different quasiparticle configurations would occur with

such short partial half-lives; the B(M1) values in Table I-3 are roughly one order of magnitude larger than those typically observed in deformed nuclei for interband gamma rays.[4] On the other hand, while the B(E1) values of Table I-3 are stronger than typical E1 transitions in heavy nuclei,[4] they are similar to those observed among actinide nuclei exhibiting strong octupole collectivity in the normally deformed well.[5] These B(E1) values are also comparable to those reported recently for transitions in the SD wells of the A ~ 190 nuclei[6,7,8,9] that have been interpreted in terms of an octupole vibration. These considerations lead us

to propose a negative parity for the levels of SD band 6. Based on the measured angular distribution, two possible spin values could be assigned to these levels, making the nine interband gamma rays either J + 1 → J or J - 1 → J transitions. While the former transitions could a priori be expected to dominate (because the larger energy is favored), it is sometimes the case for octupole vibrations that J - 1 → J deexcitations gather more of the strength.[10,11]
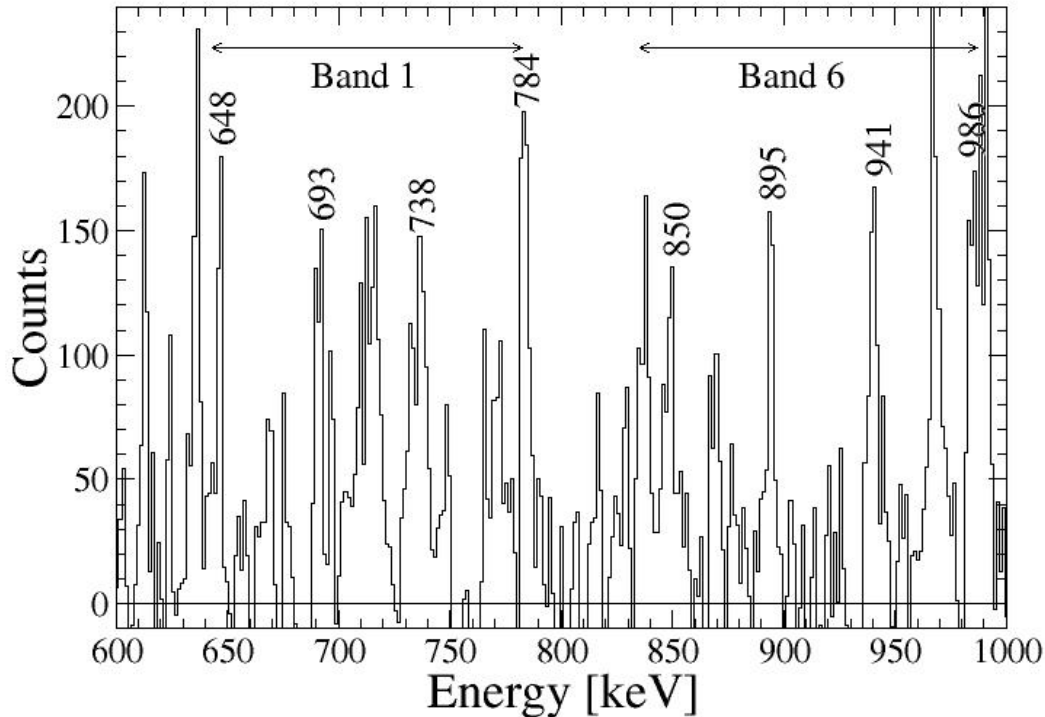
Fig. I-46. Summed coincidence spectrum obtained by placing gates on the 1696 keV linking transition and clean lines in SD band 6.

An RPA calculations by Nakatsukasa *et al.*[12] interpret SD band 6 as an octupole excitation with signature α = 1. At zero frequency, the band is characterized by K = 0, but K-mixing is significant at the frequencies of interest because of the Coriolis force. Experiment and calculations are compared in Fig. I-48, where the Routhian of band 6 with respect to the yrast SD band is given as a function of the rotational frequency. The figure presents the lowest octupole excitation (dashed

_____

*Lawrence Berkeley National Laboratory, †Niels Bohr Institute, Copenhagen, Denmark, ‡CSNSM, IN2P3-CNRS, Orsay, France.
[1]T. Lauritsen *et al.*, Phys. Rev. Lett. **88**, 042501 (2002).
[2]P. J. Dagnall *et al.*, Phys. Lett. **B335**, 313 (1994).
[3]D. Nisius *et al.*, Phys. Lett. **B392**, 18 (1997).
[4]K. E. G. Loebner. Phys. Lett. **B26**, 369 (1968).
[5]I. Ahmad and P. A. Butler. Annu. Rev. Nucl. Part. Sci. **43**, 71 (1993).
[6]H. Amro *et al.*, Phys. Lett. **B413**, 15 (1997).
[7]A. Korichi *et al.*, Phys. Rev. Lett. **86**, 2746 (2001).
[8]G. Hackman *et al.*, Phys. Rev. Lett. **79**, 4100 (1997).
[9]D. Rosbach *et al.*, Phys. Lett. **B513**, 9 (2001).
[10]G. D. Dracoulis, C. Fahlander, and M. P. Fewell, Nucl. Phys. **A383**, 119 (1982).
[11]F. G. Kondev *et al.*, Phys. Rev. C **61**, 044323 (2000).
[12]T. Nakatsukasa, K. Matsuyanagi, S. Mizutori, and W. Nazarewicz, Phys. Lett. **B343**, 19 (1995).

line), and the first 1p-1h configuration (solid line). From Fig. I-48, it is clear that the excitation energy and the evolution of the Routhian with frequency are well reproduced when the interband transitions are considered to be of the J + 1 → J type. This agreement argues for the spin assignment given in Fig. I-47. These results were published in Phys. Rev. Lett. **89**, 282501 (2002).

Table I-3. Branching ratios, partial half-lives and Weisskopf estimates for some of the strongest linking transitions.

Eγ (keV)	Branching Ratio	Part Half-Life (fs)	B(E1) W.u. 10^{-4}	B(E2) W.u. 10^{-2}
1751	0.08(3)	130	4.9	4.6
1734	0.08(3)	169	3.9	3.7
1715	0.11(3)	152	4.5	4.2
1696	0.12(4)	185	3.8	3.6
1676	0.22(10)	331	2.2	2.1
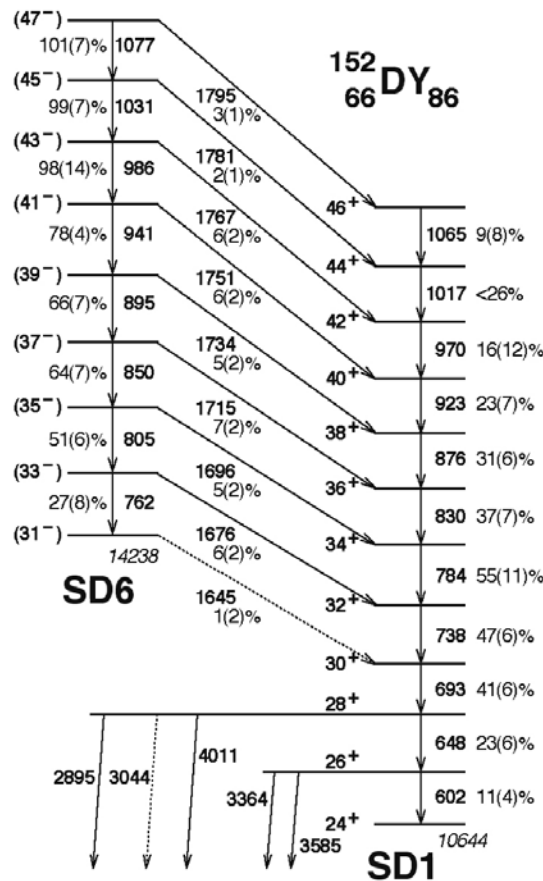
Fig. I-47. Partial level scheme of ^{152}Dy showing the lowest part of SD band 6, the lowest part of the yrast SD band 1 and the transitions that link the yrast SD band 1 to the normal states.[1] The transition intensities, given in %, reflect the requirement of the isomer tag and are with respect to the strongest lines in SD band 6 (the 1031 and 1077 keV lines). The intensities shown for band 1 are from the feeding by band 6 only.
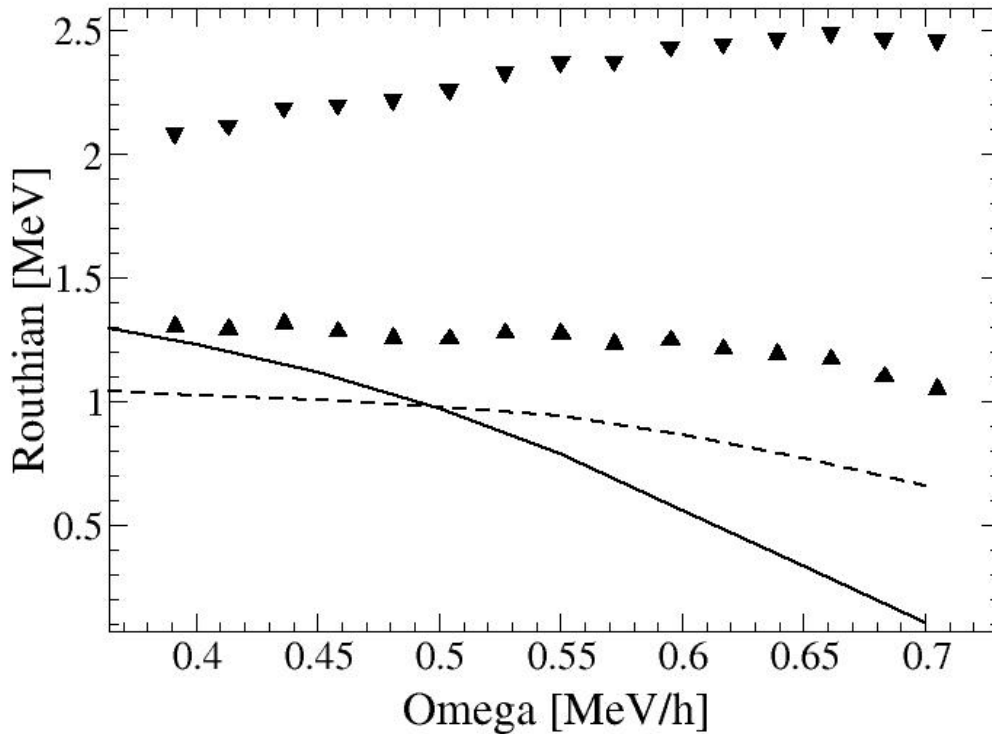
Fig. I-48. Routhians of band 6 with respect to band 1 as a function of rotational frequency. The up (down)-triangles are the data with the high (low) spin assignments to band 6. The lines are the result of the RPA calculations protect[12] for negative-parity states with signature $\alpha = 1$. The dashed line characterizes the lowest SD excitation associated with an octupole vibration. The solid line likewise shows the lowest 1p-1h excitation which, according to,[12] corresponds to SD band 2.

d.5.   Narrow Spreading Widths of Excited Bands in a Superdeformed Well (T. L. Khoo,
T. Lauritsen, D. Ackermann, I. Ahmad, H. Amro, D. J. Blumenthal, I. Calderin,
S. M. Fischer, G. Hackman, R. V. F. Janssens, D. Nisius, M. P. Carpenter,
A. Lopez-Martens,* T. Døssing,† B. Herskind,† M. Matsuo,‡ K. Yoshida,§
S. Asztalos,¶ R. M. Clark,¶ M. A. Deleplanque,¶ R. M. Diamond,¶ P. Fallon,¶
F. Hannachi,* A. Korichi,* R. Krücken,¶ I. Y. Lee,¶ A. O. Macchiavelli,¶
R. W. MacLeod,¶ G. J. Schmid,¶ F. S. Stephens,¶ and K. Vetter¶)

Excited states within a superdeformed (SD) well provide opportunities to investigate: (i) the excited states of a false vacuum; (ii) a transition from ordered motion along the yrast line to chaotic motion above, where quantum numbers and symmetries break down, perhaps through an ergodic regime; (iii) the robustness of collectivity with increasing excitation energy; (iv) the evolution with energy and spin of moments of inertia, collective spreading widths, in-band probabilities, quadrupole moments; and (v) the largely-unexplored feeding mechanism of SD bands.

Data for the present work came from a Gammasphere experiment conducted at LBNL with the ^{150}Nd(^{48}Ca,4n)^{194}Hg reaction. E_γ - E_γ matrices were constructed from pair wise gates on (a) SD and (b) normal-deformed (ND) transitions in ^{194}Hg; (a) selects only transitions feeding SD band 1, while (b) includes other SD transitions, which do not necessarily feed into the SD yrast line, but continue to lower spin. In the SD-gated matrix, 3 ridges (parallel to the diagonal) with $E_\gamma > 450$ keV can be seen (see Fig. I-49) and, in the ND-gated matrix, 5 - 6 ridges, which persist
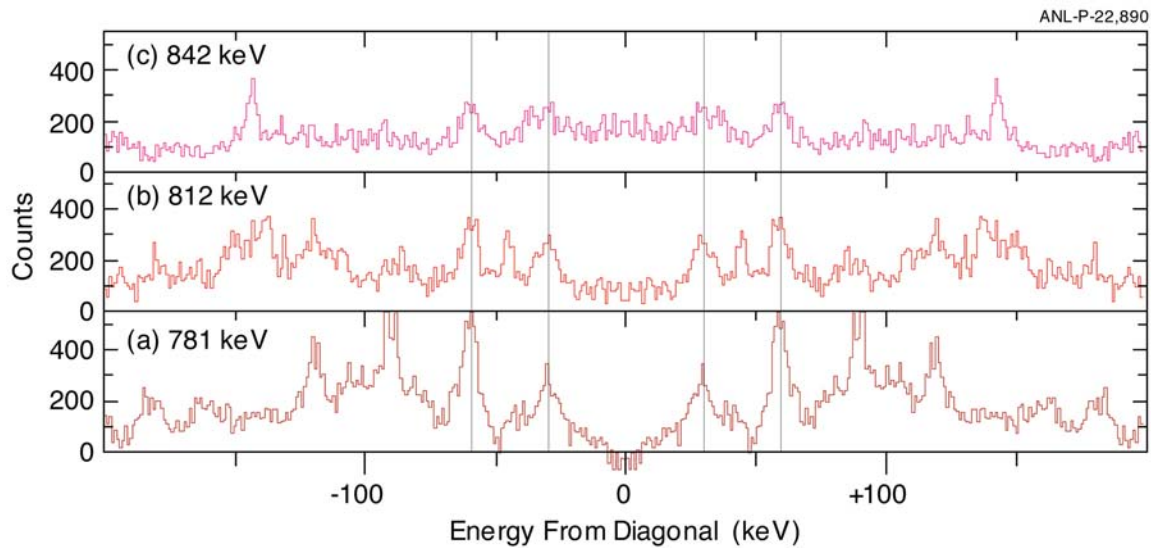
Fig. I-49. Projections perpendicular to the diagonal of an E_γ - E_γ matrix, obtained with pair wise gates on lines of the yrast superdeformed (SD) band I in ^{194}Hg. The diagonal is at channel 0. The projections, which are centered at 781, 812 and 842 keV, cover 24 keV of the ~30 keV interval between the SD lines and show peaks (marked by vertical lines) separated by about 30 keV from the diagonal. The innermost peak from the diagonal contains counts from only the quasicontinuum ridge, while the next one contains an additional contribution from a SD peak.

down to ~340 keV. The former matrix represents the first instance where ridges are detected with gates on SD transitions. The persistence of ridges to lower energy in the ND-gated matrix occurs because the γ cascades are not forced into the SD yrast line and implies small tunneling to ND states – even ~2 MeV above the SD minimum. The ridges reveal the following properties: (1) narrow spreading widths (~ 5 - 10 keV), which increase with spin; (2) ridge spacings and, hence, $J^{(2)}$ identical to that of SD band 1; (3) N_{path} ~ 100 - 150, from fluctuation properties; (4) in-band probability ~1, for $E_\gamma > 790$ keV; and (5) ratio of ridge intensity/total E2 strength ~1 for $E_\gamma < 770$ keV. The large number of unresolved bands suggests that they are excited, probably from an interval 1.5 - 2 MeV above the SD yrast line. Yet, unexpectedly, the moments of inertia are nearly identical to that of the yrast SD band.

The two most prominent features of the ridges are the narrow spreading widths and the $J^{(2)}$ moments of inertia, which are identical to the those of the yrast SD band. The narrow ridges imply that that E2 flow connects bands that must be parallel. For this to occur,

the multitude of excited bands (100 - 150) must have the same $J^{(2)}$ moments of inertia. Furthermore, the different components in the wavefunctions cannot change much with spin increments of 2 ℏ. The similarity of the $J^{(2)}$ values is intimately connected with the observation that the $J^{(2)}$ values of many SD in the A = 190 nuclei are almost identical at high frequency. Hence, the SD bands in this mass region have the remarkable property of being nearly perfect rotors, with the appearance of moments of inertia governed ostensibly by only the SD shape. A second interesting observation is that the collective flow is constrained within bands, even though the wavefunction for each band is complicated, with many components; i.e. they are almost chaotic. In other words, they probably have level spacings given by the Wigner distribution and interband decay strengths that are governed by Porter-Thomas fluctuations (although these properties have not yet been established by experiment). Yet the collective E2 flow is very ordered. Bands with these unusual properties have been predicted[1] and have been labelled ergodic bands.

_____
*CSNSM, IN2P3-CRNS, Orsay, France, †Niels Bohr Institute, Copenhagen, Denmark, ‡Niigata University, Japan, §Nara University, Japan, ¶Lawrence Berkeley National Laboratory.
[1]B. R. Mottelson, Nucl. Phys. **A557**, 717c (1993).
[2]K. Yoshida and M. Matsuo, Nucl. Phys. **A636**, 169 (1998).

Detailed analyses of the band properties were conducted within the cranked shell model,[2] which predicts the narrow ridges. They indicate that there are 2 - 8 components in the wave functions of the excited SD states. They further suggest that the excited SD bands are precursors to ergodic bands, which meet a

condition $T < D_2$, but not the condition $T < D$ required for ergodic bands. T is defined as the width of the ridges, D the average separation between SD states (of the same spin) and D_2 the separation between SD states that are connected by the two-body residual interaction.

d.6. Excitation Energies, Spins and Pairing in the Yrast Superdeformed Band in ^{191}Hg

(S. Siem,* P. Reiter, T. L. Khoo, T. Lauritsen, M. P. Carpenter, I. Ahmad, I. Calderin, S. M. Fischer, D. Gassmann, G. Hackman, R. V. F. Janssens, D. Nisius, P.-H. Heenen,† H. Amro,‡ T. Døssing,¶ U. Garg,‖ F. Hannachi,** B. Kharraja,‖ A. Korichi,** I-Y. Lee,†† A. Lopez-Martens,** A. O. Macchiavelli,†† E. F. Moore,§ and C. Schück**)

Although about 250 superdeformed (SD) bands were found in the A = 150 and 190 regions, the energies and quantum numbers weren determined for only a handful of SD bands. The excitation energies and spins of the yrast superdeformed band in ^{191}Hg were found from two single-step γ transitions and the quasi-continuum

spectrum connecting the superdeformed and normal-deformed states. This is this the first case where the energies and spins of a SD band were determined in an odd-A nucleus. The results are compared with those from theoretical mean field-calculations with different interactions.
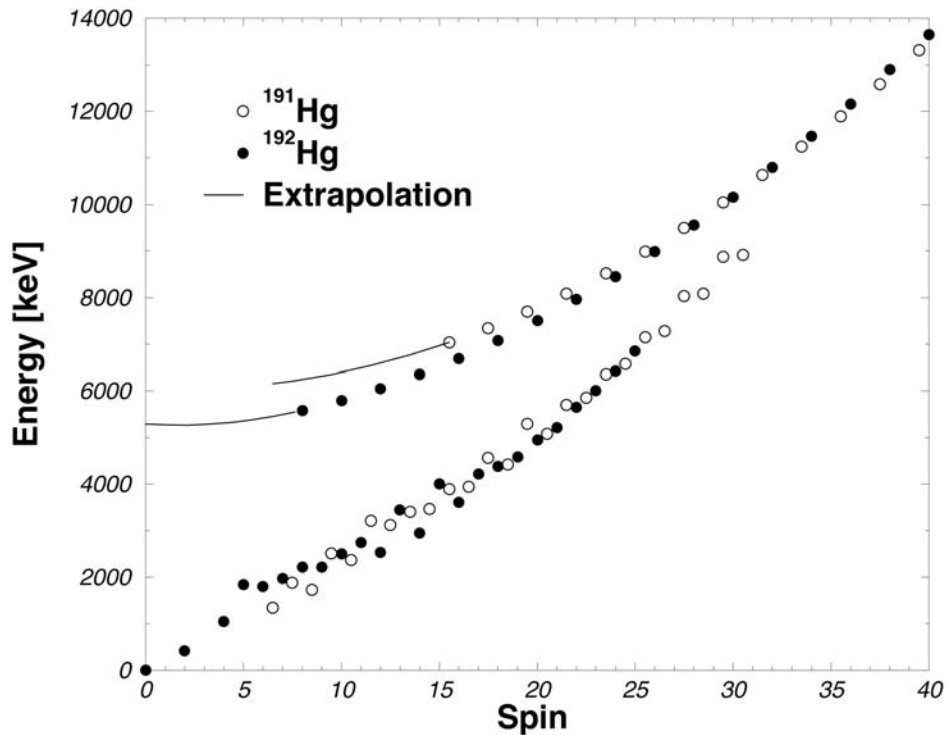
Fig. I-50. The spins and excitation energies of the SD and ND yrast bands for ^{192}Hg (filled circles) and ^{191}Hg (open circles), plotted after correcting for the difference in mass excess, i.e. $E(^{191}Hg) = E_x(^{191}Hg)$ - mass excess(^{192}Hg) + mass excess(^{191}Hg). The ground state of ^{192}Hg is set at zero. The solid lines are extrapolations of the ^{191,192}Hg SD bands to the respective "ground-state" spins.

By comparing the energies of SD bands in adjacent even-even and odd-A nuclei, we can extract information of the pair correlations in the SD well. Figure I-50 shows both normal- and super-deformed bands in ^{191,192}Hg, plotted on an absolute mass scale, i.e. after correcting for the mass excess. The energy of the ground state of ^{192}Hg is lower than that of ^{191}Hg by 1.4 MeV, reflecting the extra binding from the pair correlation energy. For the SD states at the "ground-

state" spins, the mass difference is 0.9 Mev. This provides a quantitative measure that the pair correlation energy is smaller in the SD well. However, it is interesting to note that the energy difference in the two nuclei persists to higher spin in the SD well, suggesting that pairing for SD states is less affected by angular momentum than for normal states.

A paper is being prepared for publication.

_____

*Argonne National Laboratory and University of Oslo, Norway, †Service de Physique Nucleaire Theorique, Brussels and Oak Ridge National Laboratory, ‡Argonne National Laboratory and North Carolina State University, §North Carolina State University, ¶Niels Bohr Institute, Copenhagen, Denmark, ||University of Notre Dame, **CSNSM, Orsay, France, ††Lawrence Berkeley National Laboratory.

d.7.   Composite Chiral Pair of Rotational Bands in the Odd-A Nucleus ^{135}Nd

(R. V. F. Janssens, S. Zhu,* U. Garg,* B. K. Nayak,* S. S. Ghugre,† N. S. Pattabiraman,† D. B. Fossan,‡ T. Koike,‡ K. Starosta,‡ C. Vaman,‡ R. S. Chakrawarthy,§ M. Whitehead,§ A. O. Macchiavelli,¶ and S. Frauendorf*)

The rotational motion of triaxial nuclei attains a chiral character if the angular momentum has substantial projections on all three principal axes of the triaxial density distribution. Up to now, the phenomenon was observed only in odd-odd nuclei.

High-spin states in ^{135}Nd were populated with the ^{110}Pd(^{30}Si,5n)^{135}Nd reaction at a bombarding energy of 133 MeV. Two $\Delta I = 1$ bands with close excitation energies and the same parity were observed. These bands are directly linked by $\Delta I = 1$ and $\Delta I = 2$ gamma-ray transitions. The chiral nature of these two bands

was confirmed by comparison with three-dimensional tilted axis cranking calculations. These results represent an important confirmation of the geometrical interpretation in terms of broken chiral symmetry, which claims that pairs of nearly degenerate $\Delta I = 1$ bands with the same parity appear whenever there is a chiral geometry of the angular momentum components, irrespective of how they are composed. ^{135}Nd represents the first case where three quasiparticle excitations (rather than two quasiparticle) are involved in chirality. A paper describing the results was submitted for publication.[1]

_____

*University of Notre Dame, †IUCDAEF-Calcutta Center, Calcutta, India, ‡State University of New York at Stony Brook, §University of Manchester, United Kingdom, ¶Lawrence Berkeley National Laboratory.
[1]S. Zhu et al., to be published.

E. RELATIVISTIC HEAVY ION COLLISIONS

The PHOBOS experiment at Brookhaven's Heavy-Ion Collider, RHIC, continues to be very productive. New data were collected for Au + Au collisions, supplemented by p + p and d + Au interactions all at maximum colliding beam energies of 200 GeV/u.

In addition, the PHOBOS collaboration continues their leadership role in publishing new results, with several new Letters appearing.

e.1.   Mean Transverse Momentum at Large Pseudo-Rapidity, η (B. B. Back)

The almost hermetic coverage of the PHOBOS multiplicity detector allows for measurement of the total number and the pseudo-rapidity distribution of charged particles emitted in central Au + Au collisions (Fig. I-51, bottom panel). In fact, only about 1% of the charged particles are emitted in the high-η region, where there is no detector coverage. The present work exploits this large coverage to derive information on the mean transverse momentum, $\langle p_T \rangle$, by requiring energy conservation from the initial to the final stage of the collisions.
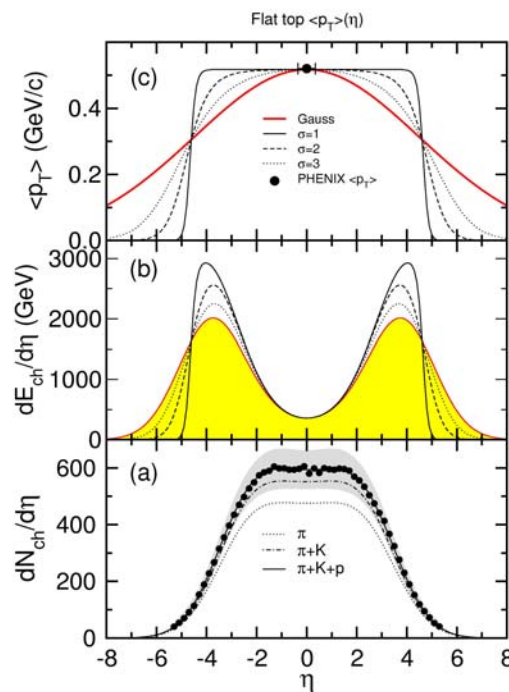
Fig. I-51. (a) The charged particle pseudo-rapidity distribution for 0-3% central Au + Au collisions at 130 GeV (PHOBOS Collab.) is shown as solid points. The grey band represents systematical and statistical errors. An analytical fit to the data using three Gaussians is shown as a solid curve with contributions from pions (dotted curve) and pion+kaons (dotted-dashed curve) shown separately. (b) The pseudo-rapidity distribution of charged particle energy is shown for four different assumptions of the shape of the <p_T> on pseudo-rapidity, as illustrated in panel (c). The solid data point in panel (c) represents a measurement by the PHENIX collaboration.

First, accounting for the energy carried by neutral particles that are not observed in the PHOBOS detector is based on isospin symmetry assumptions, such that $\pi^0 = 0.5(\pi^+ + \pi^-)$, $K_S^0 + K_L^0 = K^+ + K^-$, and $n = p$. From measurements by the PHENIX collaboration of identified charged particles we thus find that the charged particle fraction is $f_{ch} = 0.633$. Second, one should only expect to observe the energy (and particles) associated with the participating nucleons, N_{part}, of the incoming Au + Au ions. For the 0-3% centrality bin of 130 GeV Au + Au collisions $N_{part} = 355$ and we should thus expect to find a total energy of

$$E_{ch} = 0.633 \times 0.5 N_{part} \sqrt{s_{NN}} = 14,606 \text{ (GeV)}$$

is carried by the emitted charged particles. Since the total energy carried by a single particle is

$$E = \sqrt{m^2 + p_T^2 \cosh^2(\eta)}$$

one can therefore obtain the total energy in the exit channel as

$$E_{ch}^{out} = \sum_{i=1}^{3} \int_{-\infty}^{\infty} d\eta \int_{0}^{\infty} dp_T \frac{d^2 N}{d\eta dp_T} \sqrt{m_i^2 + p_T^2 \cosh^2(\eta)} \,,$$

where i denotes the three particle species, pions, kaons and nucleons and an integration over the η and p_T is carried out to account for all charged particles.

At mid-rapidity, $\eta \approx 0$, the total hadronic charged particle spectra are known to have a power-law p_T dependence and that the mean transverse momentum, $<p_T>$, increases linearly with particle mass to yield an overall value of $\langle p_T \rangle_{ch}^{\eta=0} = 508$-520 MeV/c. Under simplifying, but weak, assumptions about the fixed abundances of particle species and spectral shapes for particles emitted at non-zero pseudo-rapidities, one can thus evaluate E_{ch}^{out} and compare to the value of 23,075 GeV required by energy conservation. The first observation is that assuming the p_T are independent of pseudo-rapidity leads to a gross over-estimation of the energy of outgoing charged particles, namely $E_{ch}^{out} =$ 21,788 GeV, about 50% higher than the available energy. This leads to the conclusion that the mean p_T must fall off away from mid-rapidity. In Fig. I-51b,c is shown the results of a Gaussian η–dependence of $<p_T>$ (thick solid curves), which fulfills the energy conservation requirement. However, other dependences approaching a flat-top distributions given by the relation $<p_T> \alpha$ 1/{1 + exp [(η - a)/ σ^2 + (η + a)/σ^2]}, where the parameter a is adjusted to yield the required total energy value for three different choices, σ = 1, 2, and 3, of the fall-off parameter are also possible. It is interesting to note that all four $\langle p_T \rangle$ dependences that satisfy the energy conservation requirement coincide at a value of $<p_T>$ = 0.305 at $|\eta|$ = 4.6. We may therefore consider this analysis a measurement of the mean transverse momentum of charged particles, since it is based on a simple requirement of energy conservation and rather weak assumptions for the shapes of particle spectra. However, further analysis is required to establish a systematical error on this value.

e.2. The PHOBOS Experiment at RHIC (B. B. Back, A. H. Wuosmaa and the PHOBOS Collaboration*)

The PHOBOS experiment has made significant progress over the past year. Most of the effort was devoted to the analysis and interpretation of data obtained during RHIC runs 1 and 2, the latter of which concluded at the end of January 2002. This run included Au + Au collisions at $\sqrt{s_{NN}}$ = 200 GeV for which ~10 M minimum bias events were acquired followed by a period of $\sqrt{s_{NN}}$ = 200 GeV $p + p$ collisions yielding ~4 M min bias events. A major milestone in 2002 was the Quark Matter 2002 conference that was held in Nantes, France, July 18-24 at which the PHOBOS collaboration presented several new and unique results from the $\sqrt{s_{NN}}$ = 200 GeV Au + Au running. The third RHIC run which started on November 1, 2002 was devoted to d + Au collisions at $\sqrt{s_{NN}}$ = 200 GeV. During this run ~130 M events minimum bias events and ~20 M spectrometer triggered

events were collected. The justification for studying this asymmetric system was to acquire reference spectra to compare to the ones obtained for Au + Au collisions, which showed strong suppression of high p_T particles traversing the hot and dense volume created in these collisions. Several detector upgrade and maintenance projects were carried out in preparation of the RHIC run-3 in order to improve the data taking capability of the experiment. These projects included: 1) moving the time-of-flight walls to larger distances to improve their capabilities, 2) upgrading the data-acquisition system to be able to handle an event rate of 250 Hz (up from 30 Hz), 3) installation of an array of plastic scintillators outside of the PHOBOS spectrometer in order to enhance the spectrometer event sample, and 4) installation of calorimeters around the beam-pipe in order to improve the triggering on low multiplicity

events from d + Au and p + p collisions. In addition, several Si ring modules were replaced.

ELLIPTICAL FLOW

The elliptical flow signal, v_2, is defined as the amplitude of the second Fourier component of the azimuthal distribution of particles, *i.e.*

$$dN/d(\varphi - \psi) \propto 1 + 2v_2 \cosh(\varphi - \psi)$$

where ψ is the azimuthal angle of the event-plane estimated for each event. The collective flow of particles from the collision zone provides an important indication for the underlying reaction mechanism as it

signals the build-up of pressure gradients in the overlap-zone of the colliding ions. The PHOBOS detector is particularly well suited to measure the elliptical flow because of the near azimuthal symmetry of the multiplicity detectors (the octagon and ring detectors) and because it can obtain these measurements over a wide range of pseudo-rapidity, a feature that is unique to the PHOBOS experiment. The study and analysis of the elliptical flow signal for the 130 GeV Au + Au collisions was completed in 2002 and was published in Phys. Rev. Lett.[1] The analysis of the 200 GeV Au + Au data is in progress and nearing completion. The main results of the 130 GeV analysis are shown in Figs. I-52 and I-53.
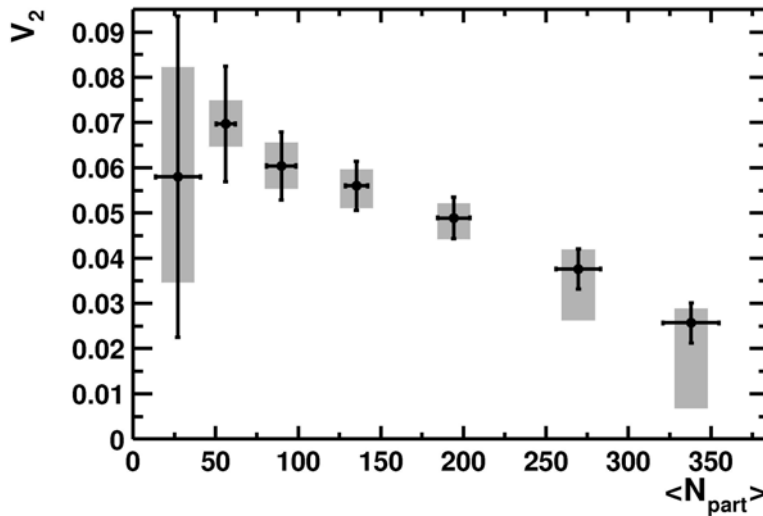
Fig. I-52. Fully corrected measurement of elliptic flow, v_2, as a function of the number of participants for $|\eta| < 1.0$. The black error bars represent the 1σ statistical errors and the gray bands give a measure of the systematic error for each point ~90% confidence level.

The amplitude of the flow signal, v_2, is shown in Fig. I-52 as a function of $\langle N_{part} \rangle$, which is a measure of the collision centrality, reaching a value of ~7% for peripheral collisions and decreasing to ~2.5% for the most central bin. Note that symmetry considerations demand that the flow signal vanish for truly central collisions. The large flow signals observed at RHIC

energies, first observed by the STAR collaboration,[2] are surprisingly large and approach the hydrodynamic limit indicating that the interaction zone is characterized by a high density of strongly interacting particles, possibly of partonic nature, allowing for the build-up of pressure gradients that manifest themselves in the observed azimuthally asymmetrical emission patterns.
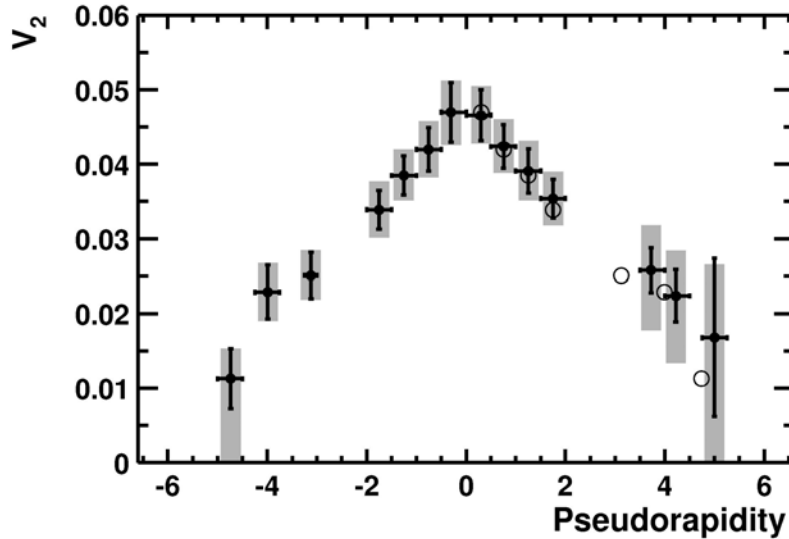
Fig. I-53. Elliptic flow, averaged over centrality, as a function of pseudo-rapidity, η. The graphical representation of the errors is similar to that shown in Fig. I-52. The points on the negative side are reflected about η = 0 and shown on the positive side as open circles.

The elliptical flow amplitude, v_2, is shown as a function of pseudo-rapidity, η, in Fig. I-53 for centrality averaged events. The ability to measure the flow signal over a wide range of pseudo-rapidity (angle) is unique to PHOBOS. The value of v_2 is seen to decrease away from the mid-rapidity region, an effect that has yet to find a theoretical explanation.

CHARGED PARTICLE MULTIPLICITY
The PHOBOS collaboration has carried out complete measurements[3-7] of the charged particle multiplicity in Au + Au collisions at three different energies $\sqrt{s_{NN}}$ = 19.6, 130, and 200 GeV in addition to a rudimentary measurement at $\sqrt{s_{NN}}$ = 56 GeV, which was obtained during the initial commissioning period of RHIC in 1999. A recent analysis[8] of the pseudo-rapidity distributions of the charged particle multiplicities, $dN/d\eta$, shows that the charged-particle multiplicity distribution exhibit "limited fragmentation" scaling behavior when displayed as a function of the parameter $\eta' = \eta - y_{beam}$, where y_{beam} is the beam rapidity. This scaling behavior has been seen previously in $p + p$ collisions over a wide energy range, but is even more pronounced for the high quality heavy-ion data obtained by PHOBOS. The full set of multiplicity distributions measured by PHOBOS is presented in Fig. I-54.
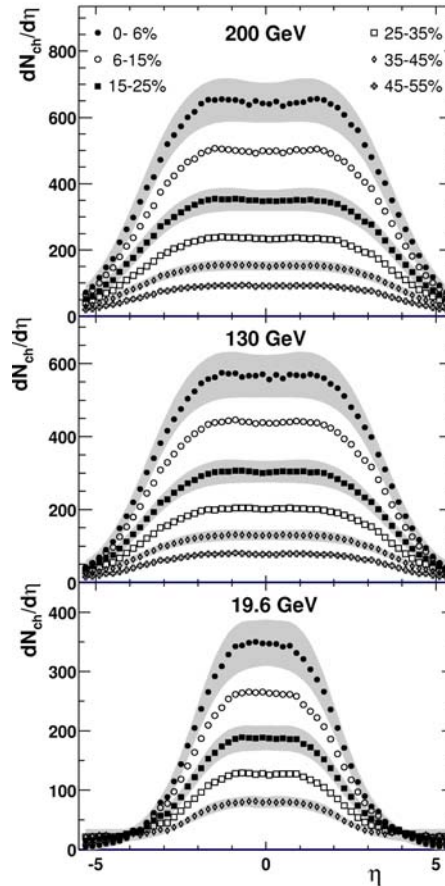
Fig. I-54. The charged particle pseudorapidity distribution, $dN_{ch}/d\eta$, measured for Au + Au at $\sqrt{s_{NN}}$ = 200, 130, and 19.6 GeV for the specified centrality bins. These bins range from 0-6% central to 45-55% in the case of the higher energy data and 0-6% to 35-45% for 19,6 GeV data. The statistical errors are negligible. The typical systematic errors (90% C.L.) are shown as bands for selected centrality bins.

The data show a typical plateau at mid-rapidity indicative of boost-invariance in this region. The width and height of the boost invariant region increases with collision energy followed by a gentle fall-off to larger pseudo-rapidities. Because of the large coverage of the PHOBOS Multiplicity Detector it is possible to estimate with good accuracy the total number of charged particles produced in the collisions. For the bin covering the 6% most central collisions the total number of charged particles are $N_{tot} = 1680 \pm 100$, 4170 ± 210, and 5060 ± 250 for the 19.6, 130, and 200 GeV collision energy, respectively.

TRANSVERSE MOMENTUM SPECTRA

Using the PHOBOS spectrometer inclusive hadron p_T-spectra have been measured for Au + Au collisions at

200 GeV. The quality of the spectra is displayed in Fig. I-55. By comparison to proton-antiproton spectra measured at the same energy we observe a pronounced deficit for central collisions when accounting for the number of elementary two-body collisions ($N_{coll} = 1050$) expected in central (0-6%) Au + Au collisions. This suppression of the high-p_T part of the spectrum has also been observed by the STAR and PHENIX collaborations. It is conjectured to be caused by large energy losses of partons from hard scatterings in the hot and dense (and presumably partonic) medium formed in the collision. Further information on this topic may be expected from this year's d + Au data, where hard scattered partons traverse only the cold and less dense (Au) nuclear medium.
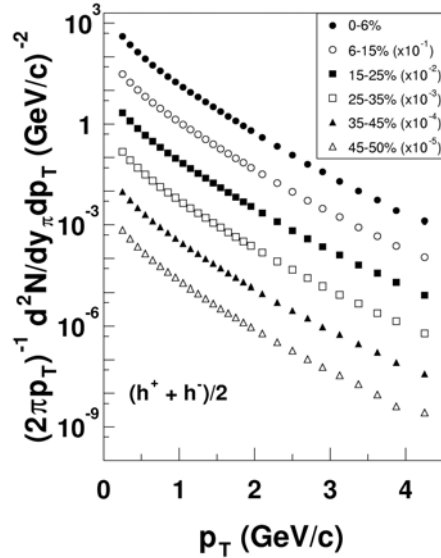
Fig. I-55. Invariant yields for charged hadrons as a function of p_T for six centrality bins. For clarity, consecutive bins are scaled by factors of 10. Statistical and systematic uncertainties are smaller than the symbol size.
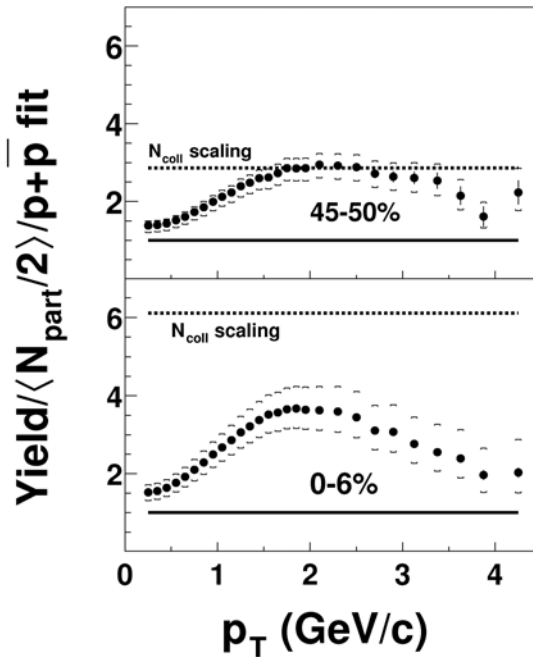
Fig. I-56. Ratio of the yield of charged hadrons as a function of p_T for the most peripheral bin ($<N_{part}>$ = 65 ± 4, upper panel) and the most central bin ($<N_{part}>$ 344 ± 11, lower panel) to a fit of proton-antiproton data scaled by $<N_{part}/2>$. The dashed (solid) line shows the expectation for N (N_{part}) scaling relative to p + p collisions. The brackets show the systematic uncertainty of the Au + Au data.

The PHOBOS collaboration has observed that the high-p_T part of the spectra appears to scale instead rather well with the number of participants N_{part} in collisions (N_{part} = 344 ± 11 for 0-6% centrality), which is largely consistent with a picture in which only hard-scattered partons from the surface are observable because those from the interior of the overlap zone suffer large energy losses and are shifted down to the soft part of the spectrum, see Fig. I-56. A manuscript presenting these data was submitted to Phys. Rev. Lett.[9]

ANTI-PARTICLE TO PARTICLE RATIOS

The anti-particle to particle ratio for pions, kaons and protons has been measured for 200 GeV Au + Au collisions using the PHOBOS spectrometer. The following results were found[10]: $\langle \pi^+ \rangle / \langle \pi^- \rangle = 1.025 \pm 0.006(\text{stat}) \pm 0.018(\text{syst})$, $\langle K^+ \rangle / \langle K^- \rangle = 0.95 \pm 0.03(\text{stat}) \pm 0.03(\text{syst})$, and $\langle \bar{p} \rangle / \langle p \rangle = 0.73 \pm 0.02(\text{stat}) \pm 0.03(\text{syst})$. When analyzed within a statistical model of particle production assuming thermal equilibrium between various particle species,[11] one obtains a value of the ratio of the baryo-chemical potential, μ_B, to the temperature, T, of $\mu_B/T = 0.17 \pm 0.01(\text{stat.})$, see Fig. I-57. For a typical chemical freeze-out temperature of $T = 165$ MeV, one obtains a value of $\mu_B = 27 \pm 2(\text{stat.})$ MeV, which is about half of the value of $\mu_B = 45 \pm 5(\text{stat.})$ MeV found at 130 GeV. These results therefore show that an almost baryon-free region is generated in Au + Au collisions at the highest RHIC energy.
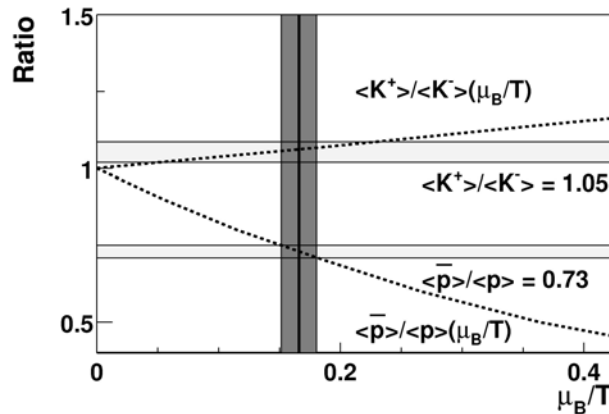
Fig. I-57. Statistical model calculation (dotted curves) of $\langle K^+ \rangle / \langle K^- \rangle$ and $\langle \bar{p} \rangle / \langle p \rangle$ as a function of μ_B/T from Becattini et al.[9] The horizontal bands show the ratios observed in the data (statistical errors only). The vertical shaded area indicates the allowed region in μ_B/T.

_____
*Brookhaven National Laboratory, Institute of Nuclear Physics, Krakow, Poland, Massachusetts Institute of Technology, National Central University, Taoyuan, Taiwan, University of Rochester, University of Illinois at Chicago, University of Maryland.
[1]B. B. Back et al., (PHOBOS Collaboration), Phys. Rev. Lett. **89**, 222301 (2002).
[2]K. H. Ackermann et al., (STAR Collaboration), Phys. Rev. Lett. **86**, 402 (2001).
[3]B. B. Back et al., (PHOBOS Collaboration), Phys. Rev. Lett. **85**, 3100 (2000).
[4]B. B. Back et al., (PHOBOS Collaboration), Phys. Rev. Lett. **87,** 102303 (2001).
[5]B. B. Back et al., (PHOBOS Collaboration), Phys. Rev. C **65**, 31901R (2002).
[6]B. B. Back et al., (PHOBOS Collaboration), Phys. Rev. Lett. **88**, 22302 (2002).
[7]B. B. Back et al., (PHOBOS Collaboration), Phys. Rev. C **65**, 061901R (2002).
[8]B. B. Back et al., (PHOBOS Collaboration), Phys. Rev. Lett., in press.
[9]B. B. Back et al., (PHOBOS Collaboration), Phys. Rev. Lett., submitted.
[10]B. B. Back et al., Phys. Rev. C **67**, 021901 (2003).
[11]F. Becattini et al., Phys. Rev. C **64**, 024901 (2001).

F. HIGH PRECISION AND HIGH SENSITIVITY
MEASUREMENTS AND INVESTIGATIONS

The nucleus continues to be one of nature's classic laboratories for investigating both the strong and weak interactions. The equipment and techniques developed for investigating nuclei can be used to tackle many problems in nature. A range of ultra-sensitive investigations was pursued. One area of investigation concerns to fusion mechanism of heavy-ions, especially at very low energies. Beyond these projects, synchrotron radiation from the Argonne Advanced Photon Source (APS) was used to determine the probability in enhancing the decay rate of the 31-year nuclear isomer in ^{178}Hf and refuting earlier claims of substantial enhancements. Investigations into the dynamics of confined plasmas also continued, focusing on the melting of confined cold plasmas. We continue to be interested in finding new avenues where our knowledge and equipment allow us to make significant contributions to important fundamental projects.

f.1.   Measuring the ^{3}He Content of Ultra-Pure ^{4}He: A Step Toward Determining the Neutron's Half-Life to High Precision (R. C. Pardo, K. E. Rehm, R. V. F. Janssens, C. L. Jiang, J. P. Schiffer, R. H. Scott, S. Sinha, R. Vondrasek, D. P. Moehs,* C. Bavlsik,† P. Huffman,‡ J. Doyle,§ S. Dzhosyuk,§ D. McKinsey,§ and L. Yang§)

An experiment to determine the fractional concentration of ^{3}He remaining in isotopically purified ^{4}He was initiated at ATLAS using the technique of Accelerator Mass Spectroscopy(AMS). This measurement is in support of a program to improve the accuracy of the neutron beta-decay lifetime to 1 part in 10^5.

The major difficulty in making this measurement is reducing the helium background coming from materials used in the ion source and achieving stable, high-pressure operation of the source. Last year we reported progress on this project including the design and testing of a new, small quartz MINIECR ion source which significantly reduced the helium background compared to the normal ATLAS ECR ion sources. This year that source design was improved by redesigning the quartz cylinder to remove one uncooled o-ring which limited RF power and made it impossible to run the source with nitrogen or oxygen support gas. This new source design was successfully used in the most recent runs.

In January, 2003 a run with this new source design allowed us to clearly measure the ^{3}He content in highly purified samples used in the neutron lifetime experiment. A variety of source operating modes were compared – helium only, helium + nitrogen feed, and helium + oxygen feed. This combination of source operating conditions made it possible to cleanly measure the residual helium background and clearly demonstrate measurement of the ^{3}He/^{4}He ratio. The data obtained during that run is summarized in Figure I-58.

The value of the ^{3}He/^{4}He ratio measured in this run is $2.6 \times 10^{-13} \pm 1.1 \times 10^{-13}$. Continued work to improve the repeatability of the results is planned. We have some concern as to whether aluminum in our MINIECR is the optimum material for this application and improved measurement of the absolute transmission of ^{3}He in the system is necessary to improve our precision.

_____

*Fermi National Laboratory, †University of Chicago, ‡National Institute of Standards and Technology, §Harvard University.

Background Corrected 3He/4He Ratio
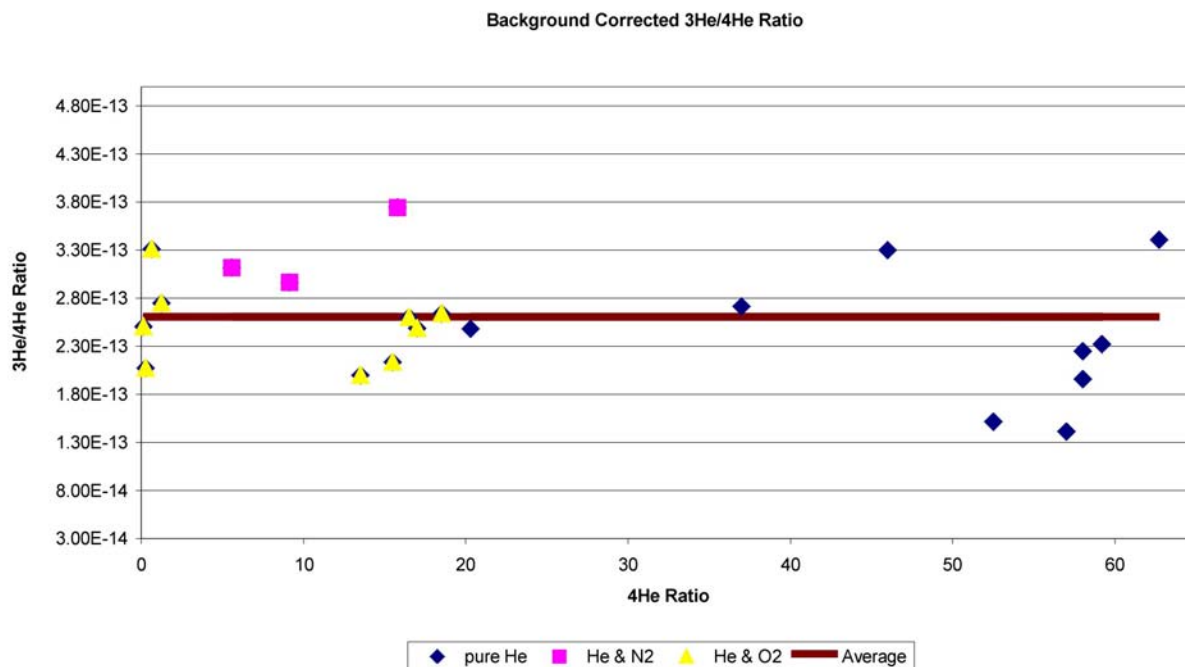
Fig. I-58. Background corrected ^{3}He/^{4}He ratio as a function of ^{4}He current. A power law curve is shown in green and a linear fit is shown in red. The raw average of all data is ^{3}He/^{4}He = 2.6 × 10^{-13}.

f.2. Accelerator Mass Spectrometry of the Heaviest Long-Lived Radionuclides
(I. Ahmad, C. Vockenhuber,* R. Golser,* W. Kutschera,* V. Liechtenstein,†
A. Priller,* P. Steier,* and S. Winkler*)

One of the best ways to determine very low concentrations of long-lived radionuclides is by Accelerator Mass Spectrometry (AMS). The Vienna Environmental Research Accelerator (VERA), based on a 3-MV Pelletron tandem accelerator, was used to measure long-lived radioisotopes at natural abundances across the nuclear chart from ^{10}Be to ^{244}Pu. The facility was recently upgraded to measure heavy ions, which enabled us to measure isotopes of ^{182}Hf, ^{236}U and ^{244}Pu. The nuclides ^{182}Hf (t$_{1/2}$ ~ 9 Ma) and ^{244}Pu (t$_{1/2}$ = 81 Ma) are of interest because they are produced in supernovae and may be detectable in deep-sea sediments, which would indicate the occurrence of recent supernovae in relatively close neighborhood to our earth. The results of this methodological AMS study were published.[1]

_____
*University of Vienna, Austria, †Kurchatov Institute, Moscow, Russia.
[1]Int. J. Mass Spectrom. **223-224**, 713 (2003).

f.3. Precision Measurement of the ^{62}Ga Beta-Decay (G. Savard, D. J. Henderson,
B. Blank,* A. Blazhev,‡ G. Canchel,† M. Chartier,§ J. Döring,‡ Z. Janas,¶
R. Kirchner,‡ I. Muhka,‡ E. Roeckl,‡ and K. Schmidt‡)

As part of the program to extend the set of high-precision superallowed Fermi emitters to heavier systems, we performed a remeasurement of the half-life of ^{62}Ga and a precise branching ratio measurement in this decay. Both measurements were performed at the isotope separator at GSI under experiment number U192 (spokesperson G. Savard). These measurements will then be completed by the Q-value measurement required to determine the ft-value and together with calculated corrections provide the heaviest point for which a full high-precision data set is available to improve the CVC and CKM unitarity tests.

The data taking for the half-life measurement took place in December 2001. An accuracy of about 0.05% is required for this lifetime. About 20 million β's from the decay of ^{62}Ga were observed with a dedicated 4π gas counter. Over 150000 accumulation and decay cycles were collected with the decay in each cycle observed for about 14 half-lives to properly identify background and contaminant activities. The data were recorded simultaneously with two independent electronics chains of fixed deadtime of 3 and 5 μs respectively. The two data sets can be analysed independently to check for rate dependent systematic errors. Proper software to analyse such data with the required accuracy was developed at Chalk River for a CDC parallel computer. The code corrects for deadtime, removes spectra with detector noise, provides proper statistical weighing of the data point and performs the maximum likelihood fit while also generating simulated spectra to verify that the analysis is performed properly. The code however utilized a number of statistical subroutines proper to the CDC parallel architecture that are not supported by machines now available. It was therefore updated and ported to the SUN cluster where the analysis is being performed. The graphics program GD from GSI was also installed on the SUN cluster and used to provide an easier interface to the output of the analysis program.

Analysis of the data is progressing together with a careful search for possible sources of systematic errors. The analysis for both deadtime settings is in excellent agreement. The data were separated in 39 runs taken with different settings for the detector bias and electronics thresholds. The preliminary results for the individual runs are shown in Fig. I-59. No statistically significant indication of shifts related to these different settings was observed. The data taking also included a γ-ray detector located behind one of the halves of the gas counter and used to look for possible contamination of the mass separated samples. Beta-delayed gammas from the long-lived isotope ^{62}Zn, daughter of the ^{62}Ga decay, are observed but no other contaminant seems to be present. These bounds will be used to determine possible effect of long-lived activity on the measured lifetime. A preliminary value of 116.18(3) ms (statistical error only) is obtained from the analysis at this point. The half-life value seems quite sturdy but the final error bar might change as the analysis progresses.

As a continuation of this work, a measurement of the branching ratio in the decay of ^{62}Ga was also performed this year to help complete the required data set. The measurement was performed in September 2002 with separated samples collected at the GSI on-line isotope separator. Five large γ-detectors, a cluster detector (7 crystals), 2 GSI clovers (each with 4 crystals) and two single crystal detectors, with a total of 17 Ge crystals were used for this experiment. Four silicon detectors were also installed around the collection point to detect the βs. A tape transport system was used to remove long-lived activity. This detector combination will yield β-γ, γ-γ and β-γ-γ data of sufficient quality to determine allowed branches to low lying 1^+ states and non-analog branches to low-lying 0^+ states of sufficient intensity.

The branching ratio data set contains 225 runs for a total of roughly 45 GB of unpacked data. A program to unpack the data in a format acceptable by the DAPHNE analysis program is being modified. The final measurement required, that of the Q-value, is in preparation at the CPT spectrometer.

_____

*Argonne National Laboratory and Centre d'études Nucléaires de Bordeaux-Gradignan, France, †Centre d'études Nucléaires de Bordeaux-Gradignan, France, ‡Gesellschaft für Schwerionenforschung mbH, Darmstadt, Germany, §University of Liverpool, United Kingdom, ¶Warsaw University, Krakow, Poland.
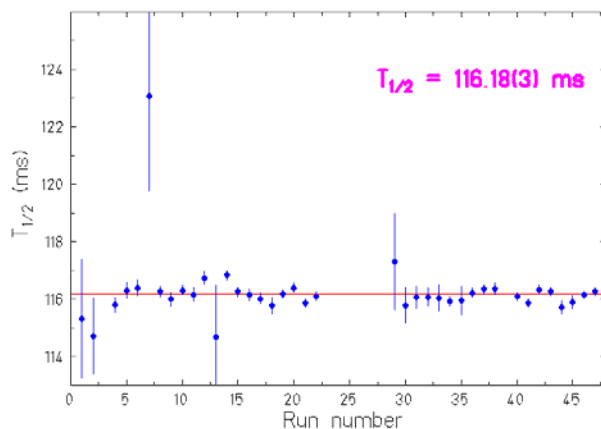
Fig. I-59. Preliminary ^{62}Ga half-life result and variation amongst the 39 runs performed.

f.4. Search for X-Ray Induced Decay of the 31-yr Isomer of ^{178}Hf at Low X-Ray Energies (I. Ahmad, D. S. Gemmell, E. F. Moore, J. P. Schiffer, J. Banar,* J. A. Becker,† T. A. Bredeweg,* J. R. Cooper,† A. Mashayekhi,‡ D. McNabb,† P. Palmer,* S. Rundberg,* S. D. Shastri,‡ T. F. Wang,† and J. B. Wilhelmy*)

The 31-yr isomer of ^{178}Hf, which has J^π, K = 16^+,16 and an excitation energy of 2.446 MeV, was the object of several studies for possible mechanisms that might trigger its decay. The potential to control nuclear energies (MeV) with atomic energies (keV) is the driving interest. This isomer is the favorite for this purpose because it is long-lived, available in microgram quantities, has a well known decay scheme, has high excitation energy, and targets can be readily fabricated. The accelerated emission of gamma rays from the ^{178}Hf isomer when irradiated with photons from a dental x-ray machine was first reported by Collins *et al.*[1] The triggering x-ray energy was reported to be in the 20-60 keV range. Using the synchrotron radiation at the Advanced Photon Source (APS) we had published[2] limits on such accelerated emission some 5 orders of magnitude lower than those in Ref. 1. Very recently, a new measurement using monochromatic x rays from the SPring-8 synchrotron was reported by Collins *et al.*[3] They report enhancement in the decay of this Hf isomer for x-ray energies of 9-13 keV. In order to check this observation, we modified our original experiment to extend our sensitivity to lower energy x-rays.

We used a Hf isomeric target that was much thinner than in the previous experiment. It was electroplated onto a Be disk, and the activity was covered by another similar Be disk. This target was then irradiated by the white beam from a tapered undulator at the SRI-CAT 1-ID beam line of the APS. The photon beam was collimated to 1.4×2 mm^2, and the target was placed at 45° with respect to the incident beam. The gamma spectrum from the decay of the isomer was measured with a Ge detector placed at 90° through a set of Pb, Ta, Cd, Cu absorbers. On the other side of the chamber a Si(Li) detector was placed at 90° and at a distance of about 50 cm, with a collimator of $.05 \times .05$-mm^2 in order to reduce the counting rate to a manageable level. This latter detector measured the Hf fluorescent K x-rays during the irradiation to determine the beam luminosity. The beam was cycled as previously: 11 s on-target followed by two 11-s counting periods with the beam-off target. We analyzed the data in all these periods in a way similar to Ref. 2. No significant enhancement was found. Using the upper limit in the difference of gamma-ray peak areas, we calculated the energy-integrated cross sections. These are shown in Fig. I-60 and are several orders of magnitude below the reported values. The results of this investigation were accepted for publication.[4]

_____
*Los Alamos National Laboratory, †Lawrence Livermore National Laboratory, ‡Advance Photon Source, Argonne National Laboratory.
[1]Phys. Rev. Lett. **82**, 695 (1999).
[2]Phys. Rev. Lett. **87**, 072503 (2001).
[3]Europys. Lett. **57**, 677 (2002).
[4]I. Ahmad et al., Phys. Rev. C**67**, 041305(R)/1-4 (2003).
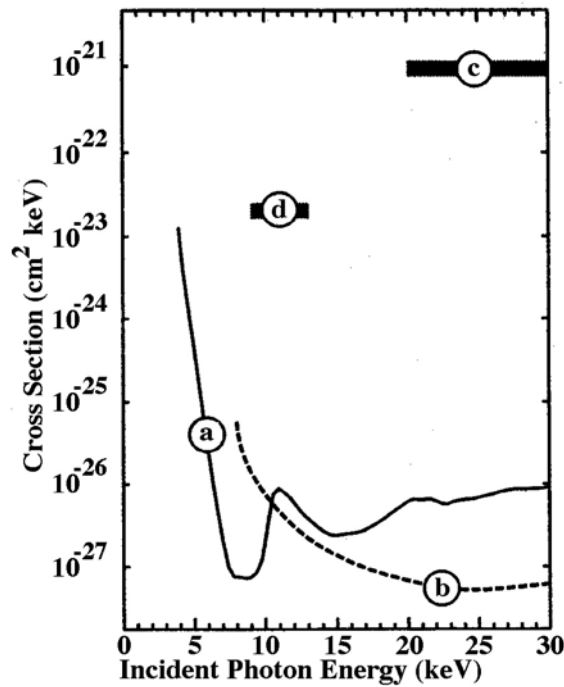
Fig. I-60. The upper limit of the integrated cross section for the photon induced de-excitation of the 31-y ^{178}Hf isomer for incident photon energies between 4 and 30 keV from the present measurement is shown as solid line (a). The previous limit from Ref. 2 is shown as dashed line (b). The cross sections from Refs. 1 and 3 are shown as cross-hatched bars (c) and (d).

f.5.   The Fusion Excitation Function for the System ^{64}Ni + ^{64}Ni at Extremely Sub-Barrier Energies (C. L. Jiang, K. E. Rehm, H. Esbensen, R. V. F. Janssens, B. B. Back, C. N. Davids, J. P. Greene, A. M. Heinz, D. J. Henderson, G. Mukherjee, T. Pennington, R. C. Pardo, D. Seweryniak, S. Sinha, M. Paul,* and P. Collon†)

In the simplest picture, fusion reactions between two heavy ions at low energies are governed by the penetration through the interaction barrier (formed by the repulsive Coulomb and the attractive nuclear potentials) followed by absorption inside the barrier. With the discovery of sub-barrier fusion enhancement, it was found that coupling between fusion and other degrees of freedom creates a multi-dimensional potential barrier resulting in increased fusion probabilities. The study of the interplay between the interaction barrier, the tunneling process and the absorption has been restricted mostly to the region in the vicinity of the barrier, for heavy-ion reactions because of difficulties with measuring fusion cross sections below ~100 μb. Naively, one expects that coupled-channels effects should saturate at low bombarding energies and the product σE should therefore exhibit a simple exponential fall-off with decreasing energy.[1]

Measurements of fusion reactions between heavy-ions at extreme sub-barrier energies is of interesting for reaction mechanism studies as well as for their astrophysical consequences. It was pointed out recently[2] that, at these energies, the fusion cross sections exhibit a behavior that is different from the predictions of coupled-channels calculations, with a much steeper falloff observed at energies far below the Coulomb barrier for the systems ^{58}Ni + ^{58}Ni,[3] ^{90}Zr + ^{90}Zr, ^{92}Zr and ^{89}Y,[4] and ^{60}Ni + ^{89}Y.[2] This feature is emphasized in the so-called logarithmic derivative, $L(E) = d(ln(\sigma E))/dE$, which continues to increase with decreasing energies.

Recently, we measured fusion-evaporation cross sections in the system ^{64}Ni + ^{64}Ni. This system was selected because 1) it was studied previously by two groups (Beckerman *et al.*[5] and Ackermann *et al.*[6]), and it was compared with coupled-channels

calculations; 2) to avoid complications arising from reactions on small amounts of heavier isotopic contaminants in the target, or lower-Z isobaric contaminants in the beam which can dominate the low-energy yields, the ^{64}Ni + ^{64}Ni system is free of these complications.

The experiment was performed at ATLAS with the Fragment Mass Analyzer (FMA). The target used was isotopic ^{64}Ni metal, evaporated on a thin carbon foil (100 μg/cm^2) with a thickness of 82 μg/cm^2. The detection technique for the residues used in the experiment and the data analysis are rather similar to our previous experiment.[2] Due to the installation of a split anode in the first electric dipole of the FMA, the background from scattered beam particles was greatly reduced.

The fusion-evaporation cross sections were measured down to the 100 nb region. The results are shown in Fig. I-61, together with the cross sections obtained in Refs. 5 and 6, respectively. At the lowest energy, no events have been observed. The upper limit in Fig. I-61 represents the cross section for one count. Our measurements are in good agreement with the results from Ref. 5, but are shifted by about 2 MeV (in the laboratory system) towards lower energies, compared to the results from Ref. 6. Such a shift was observed similarly earlier for the system ^{64}Ni + ^{92}Zr measured at ANL[7] and at Legnaro.[8] The systematic energy differences are not important for the discussions of the derivatives. However, we are planning to recalibrate the energy of the ^{64}Ni beam at ATLAS in the near future. Compared to the previous experiment, our results extend the fusion cross sections measurement by about three order of magnitudes.

The logarithmic derivatives $L(E)$ are shown as function of E in Fig. I-62 including results obtained from earlier experiments. For the system ^{64}Ni + ^{64}Ni, the values $L(E)$ extracted from data again show an increase with decreasing energy. The coupled-channels calculation (shown by the dashed curve) is found to increase only modestly at low energies. A similar result is observed for a one-dimensional barrier penetration calculation (see dotted curve). The solid curve, $L_0(E)$ represents an s-wave transmission for a pure Coulomb potential, which is discussed in the subsequent contribution.[9] At the lowest energies, the three curves are nearly parallel but all are unable to describe the general behavior of the experimental results, indicating that a yet to be identified physical contribution is missing in the description of the reaction.

_____

*Hebrew University, Jerusalem, Israel, †Columbia University.
[1]R. Vandenbosch, Annu. Rev. Nuc. Part. Sci. **42**, 447 (1992).
[2]C. L. Jiang *et al*., Phys. Rev. Lett. **89**, 052701 (2002).
[3]M. Beckerman *et al*., Phy. Rev. C **23**, 1581 (1982).
[4]J. G. Keller *et al*., Nucl. Phys. **A452**, 173 (1986).
[5]M. Beckerman *et al*., Phys. Rev. C **25**, 837 (1992).
[6]D. Ackermann *et al*., Nucl. Phys. **A609**, 91 (1996).
[7]W. Henning *et al*., private communications (1993).
[8]A. M. Stefanini *et al*., Phys. Lett. **B252**, 43 (1990).
[9]C. L. Jiang *et al*., see annual report f.6.
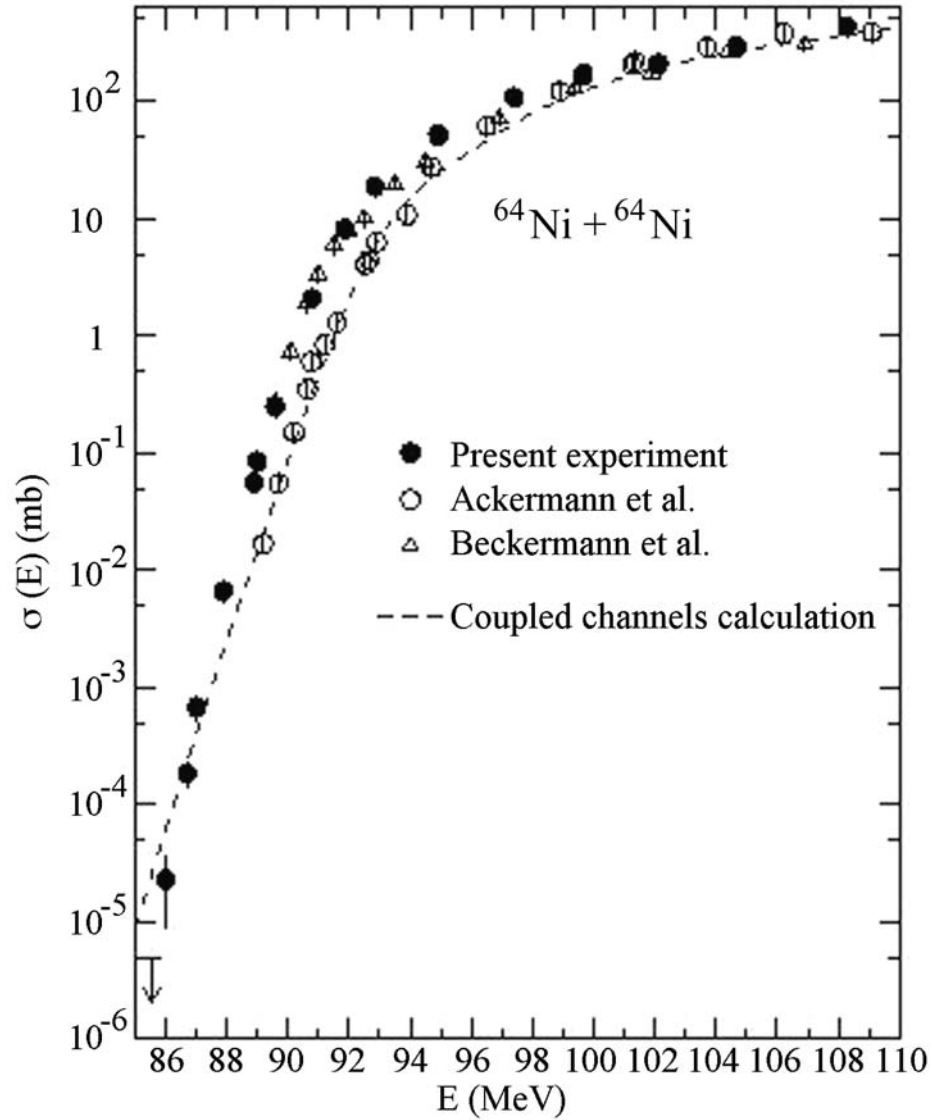
Fig. I-61. Experimental evaporation residue cross sections σ(E) plotted as function of the center-of-mass energy E for the system ^{64}Ni + ^{64}Ni. The incident energies have been corrected for the finite target thickness (including the effect of sharp changes in the excitation function with energy). The uncertainties in the cross sections for many points are smaller than the size of the symbol. The dashed curve shows the coupled-channels calculations fitted to the results of Ref. 6.
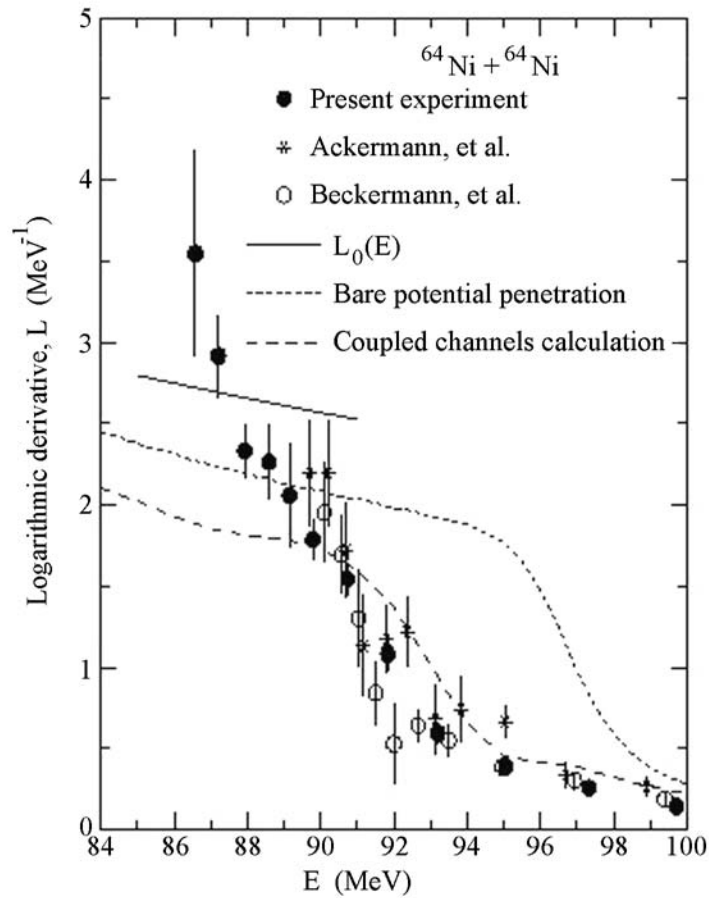
Fig. I-62. Logarithmic derivative L(E) = d(ln(σE))/dE, plotted as function of center-of-mass energy E for the systems ^{64}Ni + ^{64}Ni, obtained from least-squares fits to three neighboring cross sections points. Dashed line and dotted lines are the results of theoretical calculations using the coupled-channels formalism or a one-dimensional barrier penetration without coupling, respectively. The solid line is obtained from an s-wave transmission as discussed in the subsequent contribution.

f.6.   The Behavior of Heavy-Ion Fusion Reactions at Extreme Sub-Barrier Energies
(C. L. Jiang, H. Esbensen, K. E. Rehm, B. B. Back, and R. V. F. Janssens)

The asymptotic behavior of reaction cross sections at extremely low energies is very important for calculating reaction rates in nuclear astrophysics. To compensate for the rapid energy dependence at very low energies, the so-called S-factor has been introduced, which is defined by the equation:

$$\sigma E = S(E)e^{-2\pi\eta}. \qquad (1)$$

Here, E is the center-of-mass energy and η is the Sommerfeld parameter. This parameterization is based on the pure s-wave scattering in a Coulomb potential between point like nuclei. In light-ion reactions (e.g. (p,γ)), the data usually exhibit a constant S-factor[1] if extrapolated towards very low energies. This parameterization has also been used for light-heavy-ion reactions, (e.g. $^{12}C + ^{16}O^{2}$ and $^{16}O + ^{16}O$ etc.[3-5]),

although the fusion reactions for these systems are not restricted to s-wave scattering even at rather low energies. For these cases the S-factor is found to be flat or only weakly dependent on the energy as well, in the vicinity of the lowest energies.

When using the parameterization of Eq. (1) for fusion reactions induced by medium-mass nuclei, an interesting and unexpected result is observed. In Fig. I-63, the S-factor is plotted for five medium-mass systems, which were studied to low enough energies ($^{58}Ni + ^{58}Ni,^{6}$ $^{90}Zr + ^{92}Zr$ and $^{89}Y,^{7}$ $^{60}Ni + ^{89}Y^{8}$ and $^{64}Ni + ^{64}Ni^{9-11}$). In all these systems one observes a maximum in $S(E)$ followed by a steep decrease at the lowest energies. Extending these studies towards even lower energies is very difficult, since the cross sections mostly are already in the sub-μb region.
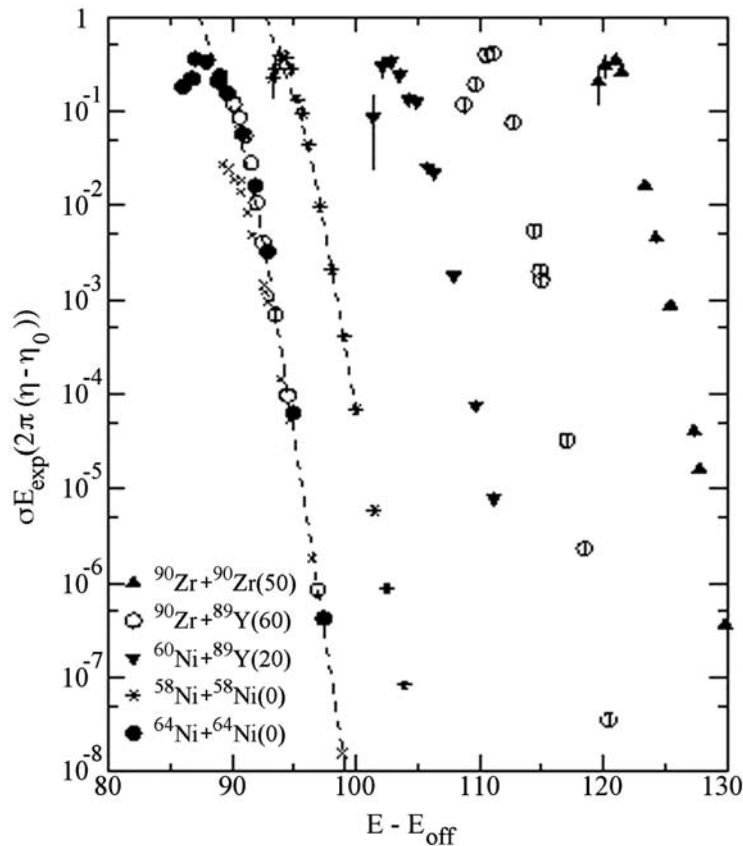
Fig. I-63. Plots S(E) vs. E - E_{off} for the systems $^{64}Ni + ^{64}Ni$, $^{58}Ni + ^{58}Ni$, $^{60}Ni + ^{89}Y$, $^{90}Zr + ^{89}Y$ and $^{90}Zr + ^{92}Zr$. The E_{off} values are 0, 0, 20, 60 and 50 MeV, respectively. Dashed curves are the results of coupled-channels calculations.

The phenomenon observed here is closely related with the observation,[8,11] that the fusion cross sections exhibit a behavior which is different from the predictions of coupled-channels calculations, with a much steeper falloff at energies far below the Coulomb barrier. To discuss this effect, the logarithmic derivative, $L(E) = d(ln(\sigma E))/dE$, has been introduced.

In order to understand these two phenomena and the difference in the behavior for light and medium (and heavy) mass systems, we consider the fusion cross section formula

$$\sigma_{fusion}(E) = \frac{\pi}{k^2} \sum_{l=0}^{\infty} (2l+1)P_l(E)A_l. \qquad (2)$$

In Eq. (2) k is the wave vector, $P_l(E)$ is the transmission coefficient for the partial wave l, and A_l is the absorption coefficient. In most cases it is assumed that $A_l = 1$, since the excitation energy and the level density in the compound nucleus are high. This still holds for fusion reactions at $E = 0$, as long as the reaction Q-value is sufficiently positive. Under these conditions, one obtains a finite (although extremely small) cross section at very low energies. Using Eq. (1), one finds that at $E = 0$, both the product σE as well as the factor $exp(-2\pi\eta)$ approach zero, but not $S(E)$, which can remain at a finite value. All light-ion induced reactions studied so far, which are of astrophysical interest, have positive Q-values and, thus, finite S-factors are observed.

The situation changes for fusion reactions induced by medium or heavy mass nuclei. In these cases the Q-values are mostly negative (for the five systems in Fig. I-63, Q-values range from -48.783 to -157.35 MeV). For a negative Q-value, the fusion cross section must be zero below $E = -Q$, because of energy conservation. Since no compound nucleus formation is possible under these conditions, fusion cross section must be zero. Since at $E = -Q$, the factor $exp(-2\pi\eta)$ is finite, one needs to have $S(E) = 0$ at $E = -Q$ in order to fulfill Eq. (1). Thus, one expects, that the $S(E)$ factor should exhibit a maximum for all systems with negative Q-values as shown in Fig. I-63.

For medium and heavy-mass system, at energies where $E \ll E_c$ (Ec is the Coulomb barrier), or equivalently, when the classical turning point is much larger than the nuclear radius, the transmission for an s-wave (point charge approximation) is:[12]

$$P_0 = 2\pi\eta \frac{1}{exp(2\pi\eta)-1} \approx 2\pi\eta exp(-2\pi\eta), \qquad (3)$$

and the corresponding logarithmic derivative is

$$L_0(E) = \frac{dln((\sigma E)_0)}{dE} \approx \frac{\pi\eta}{E}, \qquad (4)$$

where the Sommerfeld parameter is typically larger than 50.

_____
[1]C. E. Rolf and W. S. Rodney, Cauldrons in the Cosmos, The University of Chicago press (1988).
[2]B. Cujec et al., Nucl. Phys. **A266**, 461 (1976).
[3]R. G. Stokstad et al., Phys. Rev. Lett. **37**, 888 (1976).
[4]H. Reeves, Ap. J. **135**, 779 (1962).
[5]S. Schramm and S. E. Koonin et al., Ap. J. **127**, 296 (1990).
[6]M. Beckerman et al., Phy. Rev. C **23**, 1581 (1982).
[7]J. G. Keller et al., Nucl. Phys. **A452**, 173 (1986).
[8]C. L. Jiang et al., Phys. Rev. Lett. **89**, 052701 (2002).
[9]M. Backerman et al., Phys. Rev. C **25**, 837 (1992).
[10]D. Ackermann et al., Nucl. Phys. **A609**, 91 (1996).
[11]C. L. Jiang et al., see annual report f.5.
[12]M. Abramowitz, in *Handbook of Mathematical Functions*, eds. M. Abramowitz and I. Stegun, Dover Publications, Inc., New York, 1964.

Calculated results of the function $L_0(E)$ are given in Fig. I-64 by the solid lines for four of the six systems mentioned above. In the figure, coupled-channels calculations are available for ^{58}Ni + ^{58}Ni and ^{64}Ni + ^{64}Ni, which are shown as dashed curves. $L_0(E)$ may represent an extreme value of $L(E)$, because it implies a s-wave penetration of the Coulomb potential all the way to r = 0 (under the assumption of $A_0 = 1$). The slope $L(E)$ extracted from the data exceeds the value of $L_0(E)$. This could be a common behavior of all heavy-ion fusion reactions with negative Q-values, as discussed in Ref. 8.

The curves $L(E)$ extracted from the data cross the function $L_0(E)$ at E_s. From Eq. (1-3) it can be shown easily that this occurs exactly at the energy where the $S(E)$ curve shown in Fig. I-63 has a maximum.

It is surprising that these phenomena occur at such high excitation energies of the compound nuclei (17 - 44 MeV for these six systems). This indicates that some approximation made for calculating the transmission or the absorption coefficients may not be correct.
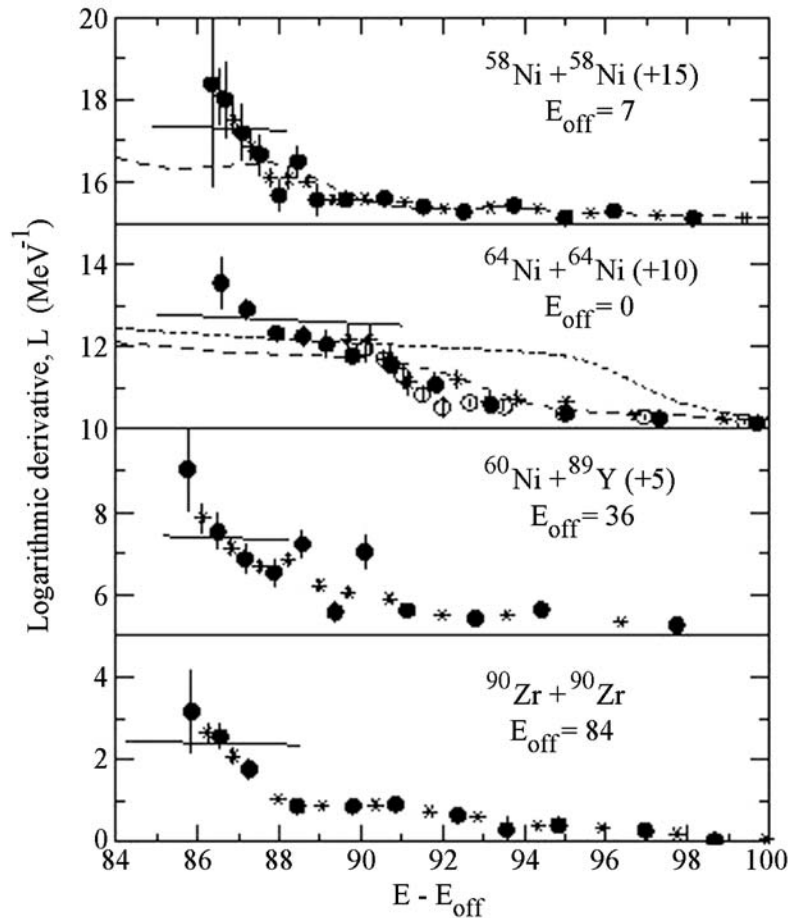
Fig. I-64. Logarithmic derivative L(E) plotted as function of E-E$_{off}$ for systems ^{58}Ni + ^{58}Ni, ^{64}Ni + ^{64}Ni, ^{60}Ni + ^{89}Y and ^{90}Zr + ^{92}Zr. The E$_{off}$ values are 7, 0, 36, 84 MeV, respectively. For ^{64}Ni + ^{64}Ni, the L(E) values are obtained from least-squares fits to three neighboring cross section points. Solid circles, stars and open circles are results from present,[11] Refs. 10 and 9 measurements, respectively. For the other three systems, solid circles and stars correspond to determinations of the logarithmic derivative from consecutive data points and from least-squares fits to three points. Dashed curves are the results of coupled-channels calculations, the dotted curve is an one-dimensional barrier penetration calculation and the solid curve, L$_0$(E) represents an s-wave transmission for a pure Coulomb potential.

f.7.   Progress in Measuring the Radiative Capture Cross Sections in ^{12}C + ^{12}C
(C. J. Lister, M. P. Carpenter, S. Freeman, N. Hammond, R. V. F. Janssens, T. L. Khoo,
T. Lauritsen, A. H. Wuosmaa, D. G. Jenkins,* B. R. Fulton,* J. Pearson,* P. Fallon,†
A. Gorgen,† A. O. Macchiavelli,† M. McMahan,† M. Freer,‡ and F. Haas§)

Radiative capture of heavy ions, their complete fusion without particle evaporation, is an unusual and interesting reaction channel. It may be important in understanding the connection between the numerous resonances in the ^{12}C + ^{12}C fusion and reaction cross sections, and the underlying states in the fused ^{24}Mg compound nucleus. These connections have been sought for many years. The seminal work of Sandorfi and Nathan[1] showed that studying the very high energy gamma-rays from the capture states to levels near the ^{24}Mg groundstate could yield considerable insight into this issue. However, the "1 step" capture decays are only a small part of the radiative capture process. Gamma ray spectroscopy involving the intermediate "doorway" states following radiative capture can provide insight both into the fusion mechanism and into the structure of exotic, highly deformed states in ^{24}Mg.

Earlier experiments using Gammasphere as a calorimeter,[2] picking out radiative capture through its high, positive Q-value, were successful in demonstrating that multi-step gamma decays are very important and that rather few "doorway" states are involved. However, the response of Gammasphere for very high energy gamma rays is not well categorized, so only an estimate of the multi-step radiative capture cross section could be achieved.

To measure the absolute radiative capture cross section for ^{12}C + ^{12}C, we performed a direct measurement of the ^{24}Mg residues using the Argonne Fragment Mass Analyzer (FMA) and an ion chamber. Measuring the fused residue yield directly has different systematic uncertainties than the gamma ray measurements, so serve to confirm the results obtained previously. In addition, selecting the optimum conditions for running the FMA provided a precursor to the final goal of performing a combined Gammasphere-FMA study in the future. The experiment was very successful. ^{24}Mg could be clearly detected in the ion chamber, as evidenced by detecting the 1368-keV first excited state decay at the target position. Considerable attention was paid to producing ^{24}Mg through the competing ^{13}C(^{12}C,n)^{24}Mg and ^{16}O(^{12}C,α)^{24}Mg background contaminant reactions. Several cross-checks were possible to measure the contributions from these undesirable ^{24}Mg ions, and eliminate them from the estimate of radiative cross section. Most importantly, the ^{24}Mg ions associated with fusion have a well defined energy, close to half the beam energy, so can be separated from the ^{24}Mg produced in other reactions by directly measuring their energy in the ion chamber, and through measuring their time of flight. Evaporation and Q-value effects shift the ^{24}Mg ions from the background reactions away from this region. We performed measurements with targets of several thicknesses to look for resonances in yield and seek consistency of measurement. We are performing final analysis of the data to establish a reliable total cross section for radiative capture, but it is clearly ~3 μb, more than a factor of five bigger than the "1-step" decays studied by Sandorfi and Nathan.

We are preparing a manuscript for publication in Physical Review Letters in 2003.

_____

*University of York, United Kingdom, †Lawrence Berkeley National Laboratory, ‡University of Birmingham, United Kingdom, §Centre National de la Recherche Scientifique, Strasbourg, France.
[1]A. M. Sandorfi, "Treatise on Heavy Ion Science", Vol. 2, ed. D. A. Bromley (Plenum 1984) p. 53 and references therein.
[2]D. G. Jenkins. *et al*., "Frontiers of Nuclear Structure", eds. P. Fallon and R. Clark (American Institute of Physics 2003) p. 329.

f.8.   Elastic Scattering of ^{17}F from ^{208}Pb Near the Coulomb Barrier (K. E. Rehm,
J. P. Greene, A. Heinz, D. J. Henderson, C. L. Jiang, E. F. Moore, R. C. Pardo,
A. H. Wuosmaa, J. F. Liang,** M. Romoli,* M. Mazzocco,† E. Vardaci,* M. Di Pietro,*
R. Bonetti,‖ A. De Francesco,* A. De Rosa,* T. Glodariu,†‡ A. Guglielmetti,‖
G. Inglima,* M. La Commara,* B. Martin,* D. Pierroutsakou,* M. Sandoli,*
C. Signorini,† F. Soramel,§ and L. Stroe¶)

Elastic scattering of ^{17}F nuclei from ^{208}Pb was measured at 90.4 MeV incident energy in the angular range θ_{lab} = 98° - 154°. The ^{17}F beam was produced with the In-Flight technique via the inverse p(^{17}O,^{17}F)n reaction. The ^{17}F beam intensity on target was about 10^6 pps. The scattered particles were detected using large-area (50 × 50 mm^2) solid-state detector telescopes with thicknesses of 60 μm (ΔE) and 500 μm (ER), segmented into 100 strips on the front. For a measurement of the angular distribution, the strips of the ΔE detectors were oriented perpendicular to the beam direction. The strips of the ER detectors were oriented orthogonal to those, allowing a determination of the position of particles passing through the ΔE detector with an accuracy of 0.5 mm. The readout of the position information was obtained using ASIC chips. The data stream from the chip contains, for each

hit, the strip identification number, the TOT (Time Over Threshold) and the Jitter Time (the time distance between the event trigger and the strip signal). The energy of the ions is obtained with standard electronics using the backside of the detectors which is not segmented.

In the event analysis, the elastically scattered ^{17}F ions were selected from the contaminant ^{17}O beam on the basis of their energy distributions, as shown in Fig. I-65. Both ^{17}F and ^{17}O ions were stopped in the ΔE detectors. Due to the experimental energy resolution, it was not possible to separate the contribution from the first excited state in ^{17}F at 495.3 keV. From DWBA calculations its contribution is estimated to be less than 2%.
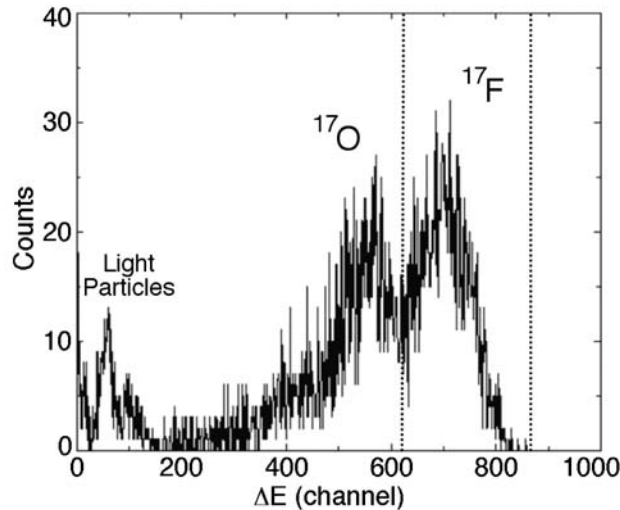
Fig. I-65. Energy spectrum of particles detected by the ΔE layer of the telescope.

Preliminary results from the experiment are shown in Fig. I-66. The solid points represent the experimental data, corrected for the efficiency of the detection apparatus and normalized to the Rutherford cross section. Optical model calculations were performed with the code FRESCO [I. J. Thompson, Comp. Phys. Rep. **7**, 167 (1998)] using a χ^2 minimizing procedure to find the optimum values of the potential. Woods-Saxon shapes for the real and imaginary parts of the potential and different families of the parameters were used (r_0 =

r_W = 1.20, 1.24 fm and a_0 = a_W = 0.43 - 0.73 fm) following the procedure used previously for the ^{19}F + ^{208}Pb system at 91 MeV [C. J. Lin *et al.*, Phys. Rev. C **63**, 064606 (2001)]. From the least-squares fits it is possible to obtain the strong absorption radius (r_{saV} = 11.97 ± 0.14 fm and r_{saW} = 13.50 ± 0.19 fm) and to extract the related potentials: V_{sa} = 3.84 ± 0.51 MeV and W_{sa} = 0.020 ± 0.002 MeV. These values are different from those obtained for the stable system ^{19}F + ^{208}Pb, where the two radii (r_{saV}, r_{saW}) are very similar

(~12.2 fm), while for ^{17}F + ^{208}Pb a difference of about 1 fm is observed. Using the same parameter set ($r_0 = r_W = 1.24$ fm and $a_0 = a_W = 0.53$ fm) for both the systems, the real part of the potential is found to be 30% less deep in the present case, while the imaginary one is

deeper by about 60%. These results give an indication of the sensitivity of elastic scattering measurements to the role played by weakly bound nucleons for a determination of optical model parameters.   The breakup cross sections are presently being analyzed.

_____

*University and INFN of Napoli, Italy, †University and INFN of Padova, Italy, ‡NIPNE, Bucharest, Romania, Italy, §University and INFN of Udine, Italy, ¶INFN of LNL, Legnaro, Italy, ||University and INFN of Milano, **Oak Ridge National Laboratory.
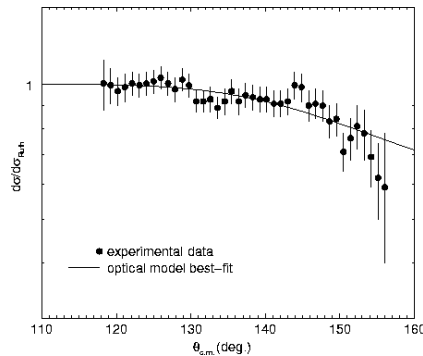
Fig. I-66. Ratio between the elastic scattering cross sections and the Rutherford values in the system $^{17}F + {}^{208}Pb$. The experimental data (circles) are compared to an optical potential model calculation. The parameters used are $r_0 = r_W = 1.24$ fm, $a_0 = a_W = 0.53$ fm, $V = 60.55$ MeV and $W = 5.71$ MeV.

f.9.   Deviations from Constant Density in Confined Plasmas (J. P. Schiffer)

The behavior of a cold plasma cloud that is confined in an external field (such as an ion trap or an accelerator storage ring), was previously studied. Such systems settle into arrays with concentric layers, whose shapes are determined by that of the external confining field. Within each layer the ions arrange themselves in a triangular lattice with equilateral triangles.   The macroscopic density of the cloud is constant, with a sharp outer surface determined by the boundary conditions of the confinement. The interior layers (or shells) are equally spaced and each has the same areal density of ions.

This **constant density** depends on three conditions that have to be fulfilled:

- The ion cloud must be **three-dimensional**.

- The confining field has to be **harmonic** (the restoring force proportional to the displacement from the origin, though the constant of

proportionality can be different in different dimensions).

- The force between the particles has to be a **Coulomb force** (a repulsive force varying as *1/r²*).

The consequences of deviations from these conditions were investigated by Molecular Dynamics simulations.

Ions Confined To Fewer Than Three Dimensions. Such confinement can occur in the 1-dimensional case, whenever the focusing forces in 2 dimensions are much stronger than the weak *harmonic* force along one axis, for instance in a so-called linear trap pushed to its limits or in a beam bunch in a storage ring.   An example of such a *one-dimensional* configuration is shown in Fig. I-67 along with the spacings between the ions.   It is evident that the density of ions is not uniform: the ions are more densely packed in the interior than near the ends.
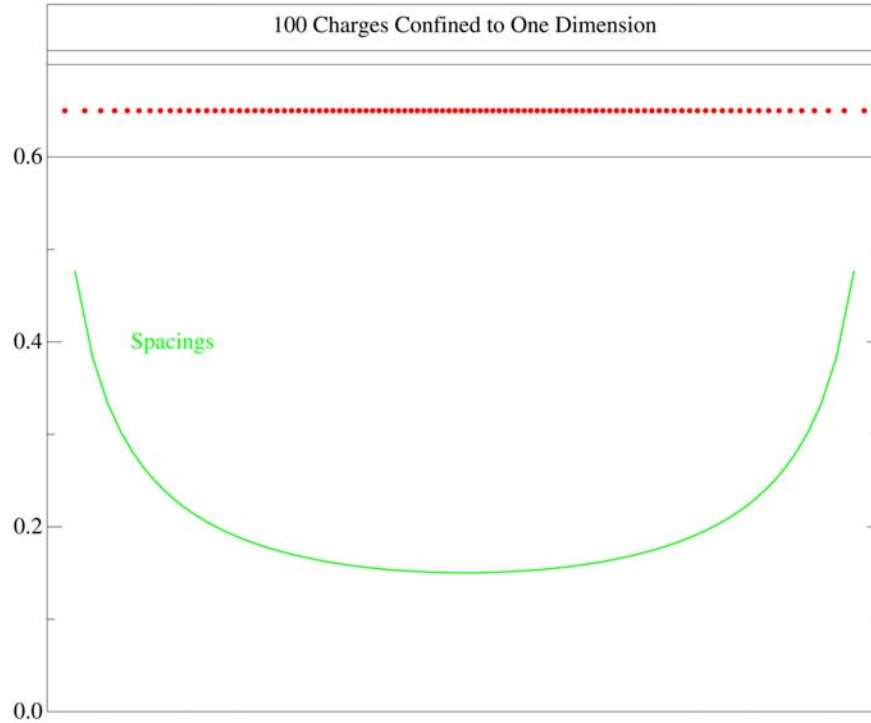
Fig. I-67 One hundred ions on a line confined by a harmonic force.

Similarly, a system of charges on a surface, and then confined within the surface by a harmonic force, is also shown in the lower part of Fig. I-68. Here also it is evident that the density of ions along the periphery of the disk is lower than in the central region.
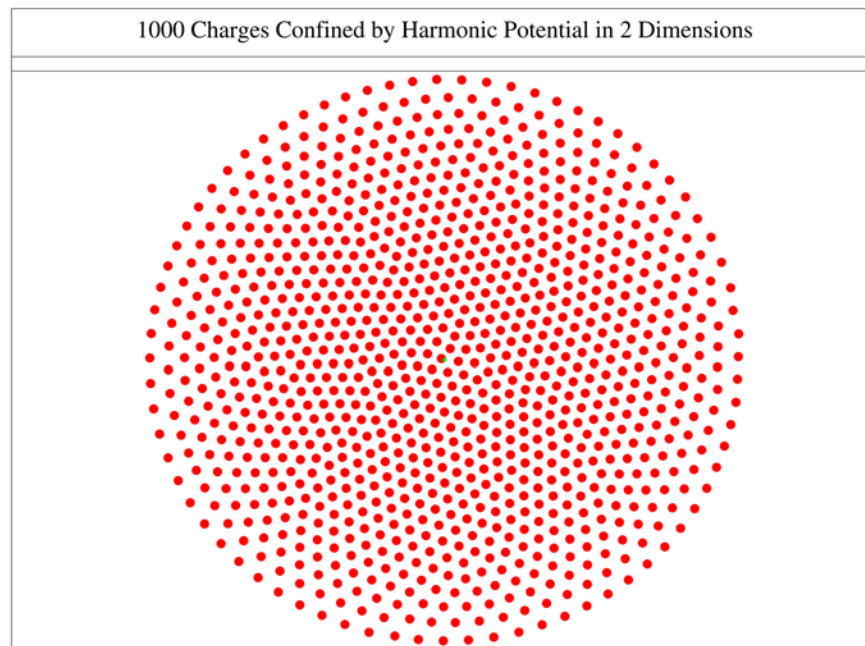
Fig. I-68. One thousand ions confined on a surface by an isotropic harmonic force.

Ions Confined By Non-Harmonic Forces.   Such confinement may be produced in a variety of ways. For instance, rf quadrupole fields (Paul traps) produce an effective potential that corresponds to a harmonic force. But rf traps with more electrodes will produce potentials that will change with a correspondingly higher power of the radius. Another example is in the "linear traps" which have an rf quadrupole field to confine a cloud perpendicular to the long axis, but confinement in the third dimension is usually provided by a biasing electrode with a force that is localized at the ends of the trapping region.   Several cases are considered below, not all of which correspond to specific existing traps.

- _Square-well in three dimensions_ implies a force that is infinitely strong at a given radius. The consequence of this is the same as for charges in a conducting sphere. By Gauss's theorem, since there is no force in the interior, all charges will be on the surface defined by the radius of the square well.

- _Radial dependence **faster** than r^2_ can take many forms other than the limiting case of a square well. It can be an exponential potential or one that is a simple higher power of the radius. In Fig. I-69 the case is shown for a potential that is proportional to r^{12}.   It is evident that the (cold) ions are concentrated with increasing density toward the outside and there is a hollow space in the interior with the radius 0.69 times that of the outer sphere. The surface density in the shells increases with radius, approximately as r^9 and the spacing between the shells decreases roughly as $1/r^3$.
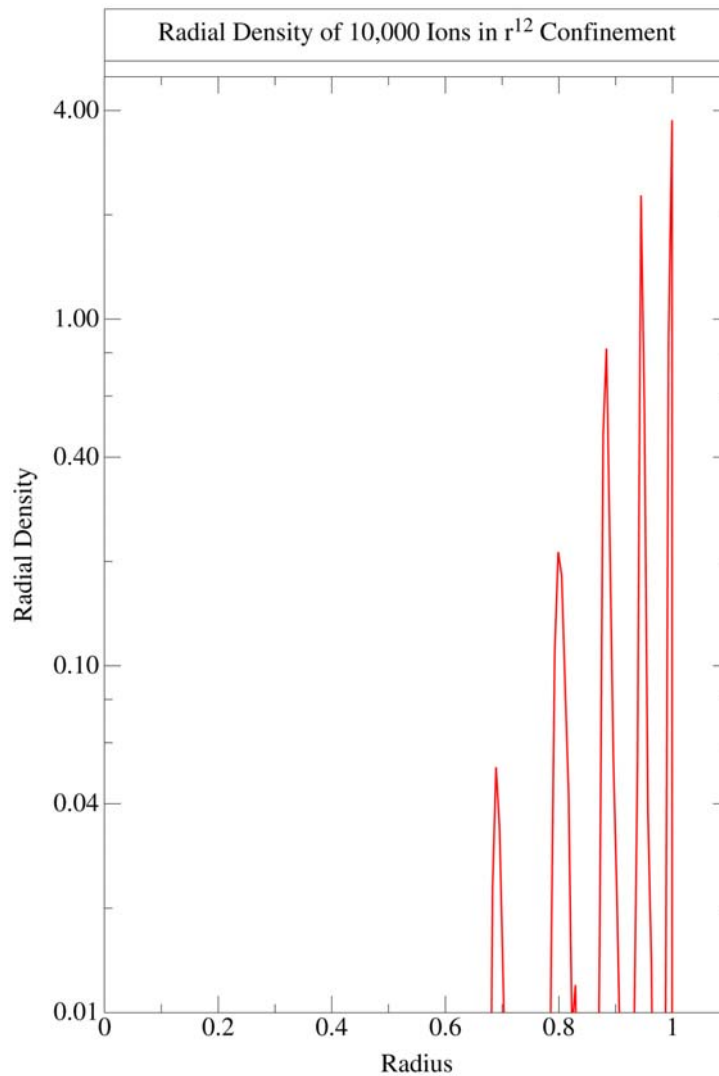
Fig. I-69. _Radial density in a potential that varies as r^{12}._

- *Radial dependence **slower** than $1/r^2$.* There are many possible functional forms, for the force, from a screened harmonic force: $-K r e^{-kr}$ to a force that is constant and pointing toward the origin. All of these have in common a density that is increasing toward the center of the cloud, with corresponding changes in the shell structure.

- *Square well in one dimension, harmonic well in others.* This arrangement is an approximation to the confining field in a linear trap. The resulting

configuration is shown in Fig. I-70 where it is seen that the sharp cutoff in density gives rise to a disk of charge, an endplate to the ion cloud. The density of ions on this surface is much higher than the other surfaces. The rest of the ions arrange themselves along roughly cylindrical surfaces in the space in between, with the radius of the endplates larger than that of the cylinders. There is also a tendency for disks parallel to the endplate to appear near the ends.

-

'Linear Trap' with sharp ends
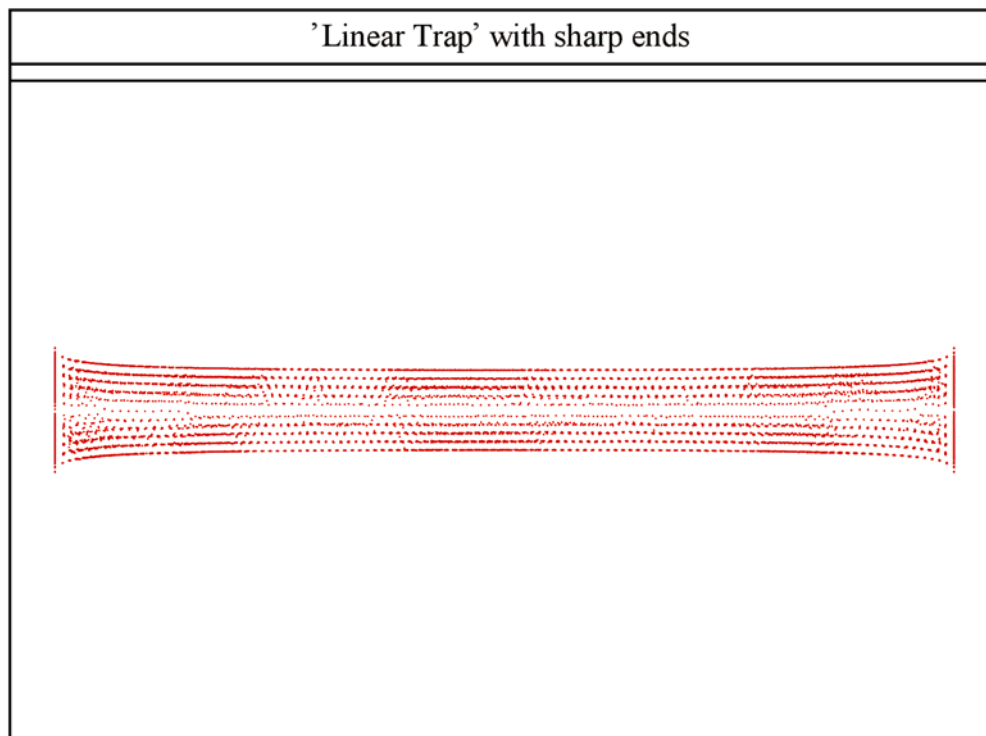
Fig. I-70. 10,000 ions confined by a harmonic force in two dimensions and a square well in the third. The projection corresponds to a 180 degree rotation of a plane about the long axis showing the radius vs the z-coordinate of the ions.

- *Square well in two dimensions, harmonic in the third.* This potential would result in a cylinder with high charge density and interior cylinders of lower density.

Interparticle Forces That Are Not Coulombic. Simulations were tried where the interparticle forces are changing *faster* than $1/r^2$, such as a Yukawa-like screened Coulomb force: e^{-kr}/r^2, and this results in densities that are higher in the interior than near the

surface. With forces that are changing more slowly with distance than the Coulomb force the density in the interior is lower than near the surface.

Some values for spherically symmetric confinement are shown in the Table I-4 for the fraction of ions that are in the surface layer and the ratio of ions in the outer third of the volume to those in the inner third.

Table I-4. Effects of various confining potentials and interparticle forces with 10,000 ions.

Radial Confinement	Interparticle Force	Fraction of Ions in Outer Shell	Ratio of Ions in Outer/Inner Thirds of Volume
$-Kr$	$1/r_{ij}^2$	19%	1.000
Square well	$1/r_{ij}^2$	100%	∞
$-Kr^{11}$	$1/r_{ij}^2$	46%	112
$-K$	$1/r_{ij}^2$	15%	0.54
$-Kre^{-kr}$	$1/r_{ij}^2$	15%	0.61
$-Kr$	$1/r_{ij}$	37%	2.9
$-Kr$	$e^{-kr_{ij}}/r_{ij}$	11.9%	0.55

G. EQUIPMENT DEVELOPMENT

A strength of the heavy-ion group program is continuing excellence in developing new equipment. During the last year, considerable progress was made in many areas. A new data-acquisition system was developed and was deployed in experiments.   The FMA is being upgraded and its focal plane detectors enhanced.   The production, separation, capture and transport of ions to the CPT was greatly improved and numerous measurements are now underway.   Our development of large area planar detectors for gamma-ray tracking reached sufficient maturity to start a full program of measurements. Involvement in the national gamma ray tracking project GRETA has increased.

g.1.   Development of the SCARLET/PICA Data Acquisition System (K. Teh, B. G. Nardi, and A. H. Wuosmaa)

Development on the core SCARLET data-acquisition system is completed. The core system is designed with few assumptions. This makes it easy to adapt the system to different acquisition hardware. However, it also excludes components needed to make it transparently usable. Effort is now being directed to interfacing the system to the ROOT data-analysis software in a user-friendly manner and developing a working setup for ATLAS-based experiments.

At present, the SCARLET software supports the Wiener CC32 CAMAC controller. The PICA CAMAC controller, which is being developed in-house, is nearing completion and support for it will be added to SCARLET system.   Other plans are to add VME readout support to SCARLET.

The SCARLET system was used successfully for two on-line experiments. The first on-line experiment at Berkeley revealed various problems that were subsequently corrected for the second experiment at ATLAS where it ran flawlessly. A second SCARLET system is now being assembled for a group in the Chemistry Division for experiments at the APS.

g.2.   A Gammasphere Sorting Engine for Use with ROOT (Torben Lauritsen)

To monitor data on-line during experiments with Gammasphere, two principal systems were used so far: DAPHNE and UPAK. The former system only works under the VMS operating system, which is no longer supported and is being phased out. The latter system only works on an old implementation of SunOS, which is out of date and hard to maintain. Thus, there is a need for a new on-line sorting and data display facility for use with Gammasphere.

The 'GSSort' sorting engine and 'GSUtil' utility package for ROOT were created to provide a new on-line sorting environment using the powerful ROOT display/data-analysis package from CERN as the graphical interface to the user. GSSort is able to take input from tape and disk as well as receive UDP data sent to it over the network from the Gammasphere VME data sender. The sorter can sort data into regular root files and shared memory so that the user can dynamically see the data as it is being sorted.

The sorter will completely parse the Gammasphere data as well as external FERA data. Thus, there is no need for the user to know the details of the formats of the Gammasphere data stream. A number of 'standard' Gammasphere spectra are generated in GSSort and the user can control the binning and gating of FERA and Gammasphere data through 1D and 2D conditions via simple sorting commands in a 'chat' script. In this script the user will assign names to the FERA data (by specifying VSN numbers and channels) and manipulate the FERA data. New, so-called, pseudo event vector entries can be generated from the original FERA data named entries via simple arithmetic operations. 1D and 2D plots of the data are also specified in the chatscript and 1D and 2D (banana) conditions can be specified and applied to any of the pseudo event vector entries

with simple, often English-like, commands in the sorting chat script.

Most on-line monitoring tasks, that are not too specialized, can be accomplished through sort instructions in this chat script *without any recompilation of the sorting code*. Thus, the user need not know about C++ or FORTRAN programming and compiling in order to look at their data on-line. This should make this new sorting utility significantly more user friendly than DAPHNE and UPAK for the average user.

The GSSort engine is normally controlled from inside root where the sorted spectra are displayed. In addition

to utilities for displaying data, setting gates on matrices, fitting peaks, etc. the GSUtil control package also contains utilities for starting and stopping the sorting engine and a utility to look at the interpreted Gammasphere data stream.

GSSort and GSUtil runs on both Solaris (where it is developed and maintained) and Linux machines and can be used for off-line sorting as well. GSSort is well suited to run unattended from script files sorting data from 8 mm tapes in a stacker. See http://www.phy.anl.gov/gs/doc/GSSort for the latest information about the new ROOT based Gammasphere sorting utility.

g.3.   Nuclear Target Development (J. P. Greene and G. E. Thomas)

The Physics Division operates a target development laboratory that produces targets and foils of various thicknesses and substrates, depending on the requirements, for experiments performed at the ATLAS and Dynamitron accelerators. The targets are prepared from both naturally occurring materials and stable isotopes that are supplied either in pure, elemental form or as stable compounds. In addition to ATLAS experiments, targets and foils are provided for all staff members whether working within the Physics Division or undertaking experiments at other facilities, for instance, the Advance Photon Source (APS). Also, wherever possible, support is provided to other ANL Divisions, and in particular to requests from researchers at the University of Chicago. Numerous collaborations have grown out of efforts between the Physics Division and target laboratory staff with outside groups in order to provide targets. Many of these, unfortunately, cannot be accepted due to the limited resources of, and time constraints placed on the target laboratory staff.

In the past year, numerous targets were fabricated either as self-supporting foils, on various substrates or as "sandwich" targets. Targets produced included ^{107}Ag, Al, Au, ^{136}Ba, Be, ^{13}C, C$_{60}$, ^{40}Ca, CaO, Cd, Cu, ^{170}Er, ^{54}Fe, Havar, HfO$_2$, In, ^{7}LiF, ^{24}Mg, ^{24,26}MgO ^{92}Mo, mylar, ^{142}Nd, ^{58,60,62,64}Ni, ^{nat}Ni^{16}O, ^{208}Pb, phosphor, polypropylene, Pt, ^{96}Ru, ^{28}Si, ^{144}Sm, ^{112,116}Sn, ^{130}Te, Th, U, UC$_2$, V, ^{182,184}WO$_3$, Y, and ZrO$_2$. Many of these target foils were fabricated via mechanical rolling using our small rolling mill. During 2002, approximately 685 targets were prepared for various experiments.

We look forward to the return of Gammasphere to

ATLAS and the increase in demands for various targets prepared by the target laboratory. For the past calendar year, 55 targets were prepared for experiments at Gammasphere while at LBNL.

For experiments undertaken to explore and increase the production of the heaviest elements a new, devoted target chamber and larger diameter rotating target wheel were constructed. Intense beams, by necessity, must be employed, requiring new demands upon target performance. Target wheels of isotopic lead on carbon backings were prepared for these initial experimental runs using this chamber coupled to the FMA. The goal of this present work was the production of Rf, element 104 and the study of detection limits and beam rejection employing the split-anode installed as an upgrade to the FMA. Beam intensities up to 250 pnA were put on target. An online target monitoring system was developed to detect target degradation. Calculations were performed in an effort to model the target behavior. This new target chamber system will also allow for gas cooling of the target. A larger wheel of similar design is already in use within a new target chamber at the front end of the CPT experiment using the SPS in Area II. By employing a target wheel station, increased beam currents will be available for the production of low cross section reaction products for precision mass measurements. Sixteen sector, large area target wheels of carbon and nickel were prepared for use in these studies.

Outside of target development, support is being provided for the production of thin plastic films and foils for use in various detector systems developed for

experiments at ATLAS as well as energy degraders needed for the CPT and for astrophysics research using radioactive beams at SPS III and the FMA. Several variations of metallized plastic foils were prepared for use in the gas counter detector used at the FMA focal plane.

As part of ATLAS support, the target lab routinely produces carbon stripper foils of 2 μg/cm^2 for use in the Tandem as well as other thickness for additional stripping throughout the accelerator. Over 285 carbon stripper and gold foils of various types were prepared for ATLAS during this past year. There continues to be an increase in the preparation of various dilutions of isotopic source material into a form and shape suitable for introduction into the ion sources for the production of enriched beams at ATLAS. These included ^{6,7}Li, ^{64}Ni, ^{33,34}S, and ^{50}Ti. The continuing procurement of stable and enriched material for ATLAS consumption and maintenance of isotope inventories for enriched beam production is being provided by the target laboratory staff.

The target development laboratory includes state-of-the-art equipment used for thin-film fabrication. The available techniques consist of multiple resistive heating, focused ion beam sputtering, glow-discharge plasma deposition, electron beam and electron bombardment evaporation, electrodeposition and mechanical rolling. The evaporators are maintained under high vacuum and each vessel contains a quartz-crystal film-thickness monitor with deposition rate indicators. Also included are movable shutters, quartz-lamp substrate heaters and thermocouple temperature sensors, allowing for complete process monitoring during target deposition.

Other auxiliary equipment used for target development includes electrodeposition apparatus, a small rolling mill, an alpha particle counting chamber, inert atmosphere glove box, laminar flow clean bench, pellet press, a reduction furnace, and a variety of precision balances. A turbo-pumped target storage facility is in operation for maintaining, under high vacuum, those targets that readily oxidize in air. This system utilizes computer-controlled circuitry to prevent targets from exposure to atmosphere during power interruptions. A second storage system employing a bank of vacuum desiccators and connected to a mechanically pumped manifold is available for use by individual experimenters. An additional set-up, consisting of two large glass desiccators evacuated using a small turbo-pump system, is in operation for long-term material storage. This allows a separation of material storage from target storage, hence eliminating repeated exposure when transferring and retrieving targets.

A low-level radioactive source and target preparation laboratory exists at a separate location within the Division that is dedicated to the production of these sources and targets. Available preparation techniques include multiple resistive heating, employing a diffusion-pumped vacuum evaporator. A second, smaller evaporator system was constructed for close proximity evaporations of higher activity materials, to be used as targets as well as radioactive sources. The small size of this system allows for installation within a hood. Preparation and handling of fission targets (mainly ^{252}Cf) by electrodeposition has been done in this lab for experimental studies at ATLAS as well as routine rolling of natural U and Th foils.

Another area of increased research effort was toward development of radioactive beams for the RIA proposal and involves neutron producing targets which in turn induce fission in uranium or a uranium compound production target. Toward this end, direct measurements of the thermal conductivity of uranium carbide were made using the method of electron beam heating provided by a 10 kV mortar source in vacuum with the temperature measured as a function of beam current using a two-color pyrometer. This work is still in progress.

The 21st World Conference of the International Nuclear Target Development Society (INTDS) was held in the Physics Division at Argonne National Laboratory on November 4-8, 2002. The conference was attended by 60 participants from 14 countries. Thirty-three contributions were presented in 8 sessions coverings a wide variety of target topics. Each session was preceded by an invited talk with the speakers covering general overview of projects, problems, and experimental aspects related to the session topic. Highlights included high power targets and stripper foil applications for the development of the next generation RIB facilities.

g.4.   "Relocating" Gammasphere at ATLAS (M. P. Carpenter, C. J. Lister,
R.V. F. Janssens, N. Hammond, T. L. Khoo, T. Lauritsen, E. F. Moore, D. Seweryniak,
F. G. Kondev,* G. Mukherjee,† S. J. Freeman,‡ and S. F. Zhou§)

During 2002, the Physics Division submitted a proposal to DOE to site Gammasphere back at ATLAS. While this proposal emphasized the use of Gammasphere with the FMA, it also discussed the possibility of utilizing the second beam-line position in Area IV as a standalone position for Gammasphere. This would allow Gammasphere to operate with its full complement of Ge detectors (108) and allow unencumbered operations with several of ancillary devices, namely CHICO, and Hercules. The proposal to move Gammasphere back to ANL was accepted by DOE, and it was agreed that operations at LBNL would cease on October 15, 2002. A group of LBNL and ANL scientists and technicians dismantled Gammasphere in roughly one month and shipped the components to ANL for reassembly.

During the fall of 2002, a scheme for moving Gammasphere between the two beam lines in area IV was devised. Three industrial rollers, each having a 40,000 lb. capacity, were procured. These rollers are routinely used in industrial settings to move heavy equipment. The support structure that the Gammasphere frame rests on when at ANL, was set up at the secondary beam line. Two 10,000 lb. shielding blocks were placed on top of the support structure in order to approximate the weight of Gammasphere. After lifting the support structure with jacks, the rollers were placed underneath. By slowly lowering the jacks, the support structure was positioned on top of the rollers. A team of six was then able to move the 20,000 lb structure over to the FMA and back without incident. After this test, it was concluded that Gammasphere

could be moved safely between beam lines in the same manner without removing the detectors.

During the period 12/02 – 1/03, the Ge detectors were annealed and Gammasphere was reassembled in area IV. Initially, Gammasphere will operate in front of the FMA, and we anticipate moving it to the second beam line sometime in 2003. Approximately 10% of the Ge detectors did not operate properly after annealing. At present, we have been able to fix ~½ of these detectors in-house. We anticipate having to send 2 - 5 detectors back to ORTEC for repair. In addition, we discovered that nearly all the BGO detectors had at least one sector not functioning properly. All BGO detectors were repaired. Most of these repairs were to the bias chain of the bases. We anticipate such failures to continue and are considering replacing the bases on all BGO detectors.

Upgrades to the Ge-BGO VXI boards were also made during the shutdown period. All boards were configured to support both single- and split-crystal detectors. The time a Ge detector was available for readout after detecting a γ ray was also extended from 1 to 2 μsecs in order to allow for a better triggering scheme when operating Gammasphere with the FMA.

In February 2003, a beam of ^{58}Ni was tuned into the Gammasphere target chamber. A test experiment using a ^{40}Ar beam on various targets took place 3/11/03 – 3/14/03 with 93 Ge detectors operating in the array. The first PAC approved experiment was performed with Gammasphere during the period 3/17/03 - 3/22/03. Gammasphere is fully operational and the experimental program is in full gear.

_____
*Technology Division, Argonne National Laboratory, †University of Massachusetts-Lowell, ‡University of Manchester, United Kingdom, §University of Notre Dame.

g.5.   Electron-Capture Branch of ^{100}Tc and the Efficiency of a Proposed Mo Neutrino Detector (I. Ahmad, F. Naab,* A. Garcia,* S. Triambak,* I. Leikola,† H. Penttilä,† A. Jokinen,† J. Huikari,† S. Rinta-Antila,† J. Aystö,† J. Szerypo,† and P. Dendooven†)

Recently Ejiri *et al.*[1] proposed to use ^{100}Mo as a neutrino detector.   Neutrinos would undergo the reaction $\nu + {}^{100}$Mo $\rightarrow e^- + {}^{100}$Tc and ^{100}Tc would decay with a half-life of 15.8 s emitting another e^-. The signature for a neutrino absorption would be two electrons, providing a way to obtain clean signals. We performed a first run on an experiment to measure the matrix element for the E.C. decay of ^{100}Tc, which determines the neutrino absorption cross section on ^{100}Mo. A previous experiment[2] measured the ^{100}Tc EC branch to be $(1.8 \pm 0.9) \times 10^{-5}$ from which one obtains B(GT; ^{100}Mo $\rightarrow {}^{100}$Tc) $= 0.66 \pm 0.33$, consistent with

zero at 95% c.l.   The present experiment was undertaken to produce a more significant result by using a separated beam of ^{100}Tc. This would reduce backgrounds that hindered a more accurate measurement in the previous experiment. The present experiment was performed using the IGISOL facility at the University of Jyväskylä.[3]   The production of separated ^{100}Tc was very successful. Figure I-71 shows our x-ray spectrum. The Mo x rays are the signature for the EC capture. We are presently analyzing the data and waiting to get more time at Jyväskylä to finish the data taking.

_____

*University of Notre Dame and University of Washington, †University of Jyväskylä, Finland.
[1] Phys. Rev. Lett. **85**, 2917 (2000).
[2] Phys. Rev. C **51**, 439 (1995).
[3] Nucl. Phys. **A693**, 477 (2001).
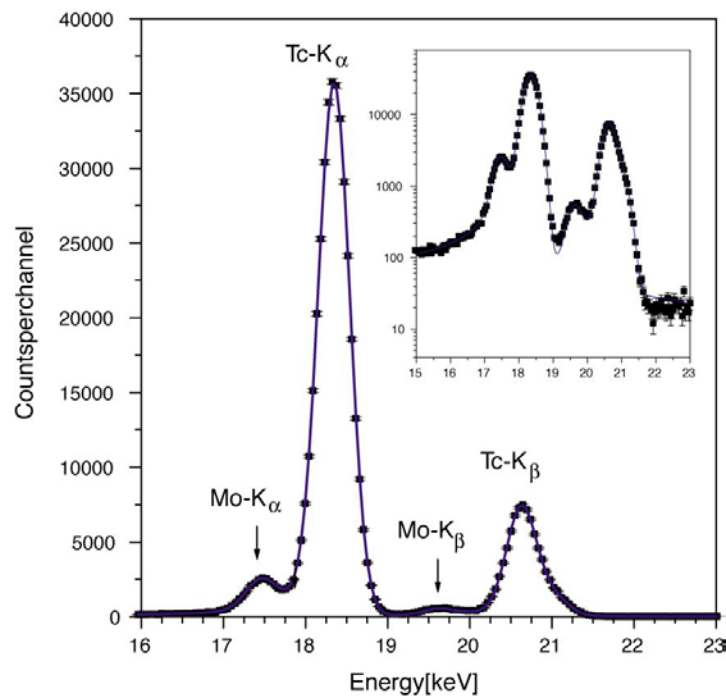
Fig. I-71. X-ray spectrum from ^{96}Tc and ^{96}Tc^m. These data were used to get the relative efficiency between Mo-Kα and 590 keV transitions. The inset is the same, but it is in logarithmic scale for the number of counts per channel.

g.6.   Split Anode for the First FMA Electric Dipole (C. N. Davids)

The split anode for the first electric dipole of the FMA was installed and tested using the ^{58}Ni + ^{92}Mo reaction. The unused primary beam passes into the anode structure through a 1-cm slit and stops on a tantalum plate inside the anode. It is thus electrically identical to the original anode. In the test the flux of scattered beam detected at the focal plane was reduced by a factor of 8 for the new anode.   In experiments conducted with the new anode, lower background rates at the focal plane were reported.

g.7.   Delay-Line Shaping Amplifiers for a Double-Sided Silicon Strip Detector
(C. N. Davids, P. Wilt, and D. Seweryniak)

A delay-line shaping amplifier system for a double-sided silicon strip detector (DSSD) was constructed, with a total of 200 channels being built. The system was tested using the 80×80 DSSD, observing the fast proton emitter ^{113}Cs($T_{1/2}$ = 17 µs) produced via the ^{58}Ni(^{58}Ni,p2n)^{113}Cs reaction. The results are shown in Fig. I-72, which shows that decay proton events can be seen down to about 1 µs after the implantation event. The energy resolution of these amplifiers is nearly as good the Gaussian shaping amplifiers that were used up to now with the DSSDs. Normal usage will be to employ both sets of amplifiers in parallel in order to study both long and short half-lives without changing amplifiers.
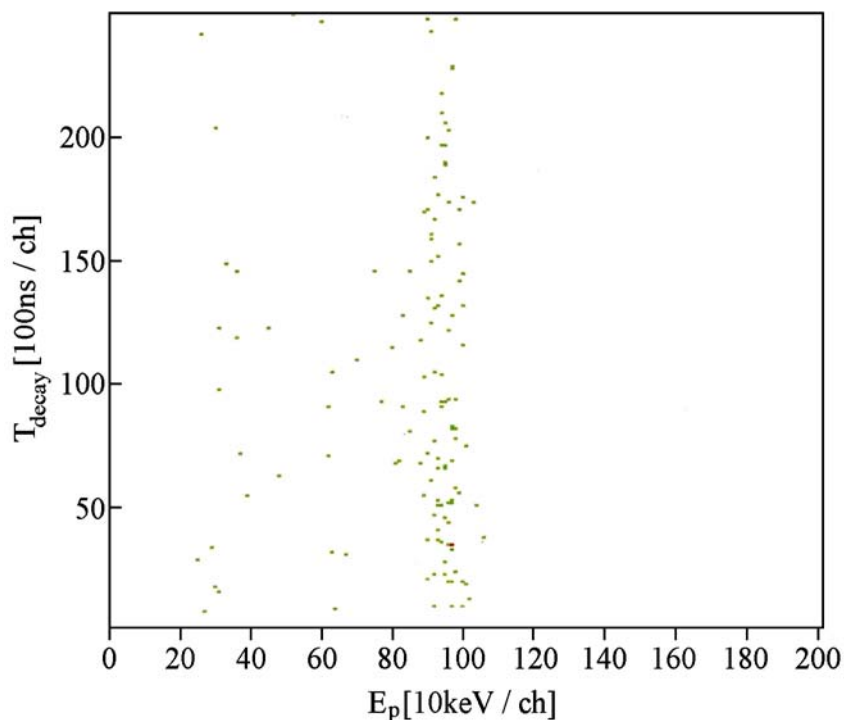
Fig. I-72. Decay time (vertical) vs. energy (horizontal) for protons from ^{113}Cs. The minimum decay time interval is ~1 µs.

g.8.   A Bragg Scattering Method to Search for the Neutron Electric Dipole Moment

(M. Peshkin, G. R. Ringo, T. W. Dombeck,* H. Kaiser,† D. Koetke,‡ S. Shirvel,‡
R. K. Smither,§ and S. A. Werner¶)

Polarized neutrons will undergo several thousand Bragg reflections in a slot cut in a perfect silicon crystal and the rotation of their polarization by the crystalline electric fields will be measured to determine the neutron electric dipole moment (EDM). We hope to achieve a sensitivity several times better than that of the best previous measurement (around 1×10^{-25} e-cm, limited by systematic errors) and equally importantly to have very different systematic errors. We developed a suitable slotted crystal. Our experimentally demonstrated reflectivity of 0.99998 was published (Physical Review A **64**, 53607 (2001).

A preliminary experiment to measure the neutron's known magnetic dipole moment (MDM) in the same way, using the interaction of the effective EDM, equal to v/c times the MDM, with the crystalline electric field, should test the principles of the EDM experiment in an easier case. That experiment was approved for running at the Missouri University Research Reactor. The needed solenoid was fabricated and tested, and a beam line is under construction at the reactor.

Issues involving the penetration of the neutrons into the silicon, which may impact aspects of the design of the experiment.   Those issues are currently under investigation in theoretical models.   They are also expected to be clarified in the MDM experiment.

_____
*Fermi National Accelerator Laboratory, †University of Missouri, ‡Valparaiso University, §APS User Program Division, Argonne National Laboratory, ¶National Institute of Standards and Technology.

g.9.   Transmission Ion Chamber (T. Pennington, D. J. Henderson, D. Seweryniak, K. E. Rehm, C. L. Jiang, C. N. Davids, C. J. Lister, B. J. Zabransky, and B. Blank*)

A Transmission Ionization Chamber (TIC) was constructed for the use at the focal plane of the Fragment Mass Analyzer (FMA). The motivation for the construction of the TIC was twofold. First, an astrophysics experiment studying ^{69}Br via the β decay of ^{69}Kr[1] would benefit greatly by adding a TIC to the existing implantation station. Second, in the study of extreme sub-barrier heavy-ion fusion evaporation reaction, the background due to the scattering of the beam particles can be reduced by developing a hybrid detector system such as PPAC-TIC-PPAC-TIC-PPAC.

The TIC is basically a copy of the normal ion chamber used with the FMA, based on a Daresbury design with some construction improvements. The transmission chamber has an active length of 8.82 inches (~22.4 cm). It is equipped with a segmented anode ΔE_1 located 2.00 inches (~5 cm) from the front face of the detector, followed by ΔE_2 2.00 inches further back (~5 cm), and ΔE_3 is located 4.88 inches (~12.4 cm) behind $\Delta E2$. All three of the ΔE signals can be combined internally by the use of jumpers between each of the ΔE areas. One design improvement of the TIC is the removal of all polymers containing materials (except for the anode and Frisch grid which were constructed on PC Board material) and their replacement with ceramic. This improvement will allow easier pump down and shorter outgassing of the detector. A new detector mounting system allows for the modular use of the vacuum chamber for other types of detectors, e.g. the Microchannel Plate (MCP) detector. Also, during the design discussions for the TIC it was decided that the focal plane PPAC exit window would be reinforced to take reverse pressure up to 50 torr using a 302 stainless steel mesh that was photo-etched by FOTOFAB. The mesh is 0.003 inches (76.2 μ) thick with 0.003 inch wide approximately square cross section wires to support the window. In Fig. I-73 a photograph of the window support mesh is shown. The exit window of the TIC has a modified version of the 302 stainless steel window support structure, shown in Fig. I-74.
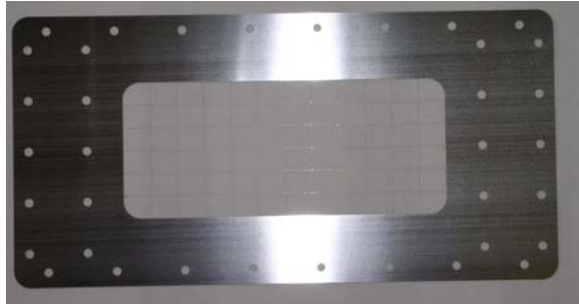
Figure I-73

Figure I-74

The TIC exit window consists of 120 µg/cm^2 Mylar film mounted on a Lexan support, shown in Fig. I-75.
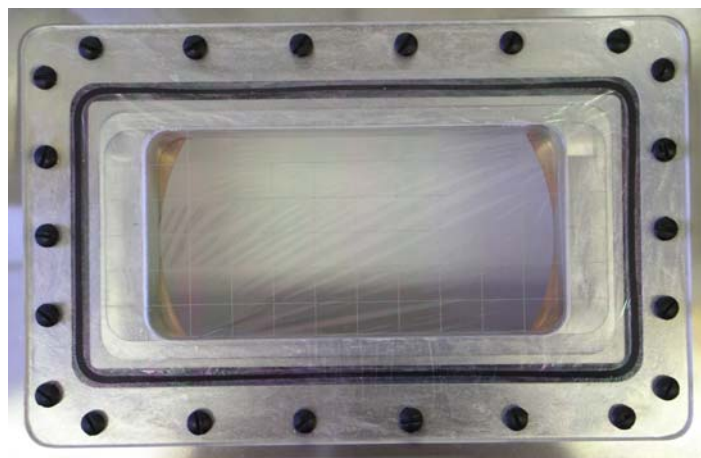
Figure I-75

A calculation shows that the shielding efficiency of the Frisch grid is 99.17 percent,[4] which is approximately the same for the DIC. In Figs. I-76, I-77, and I-78, pictures of the completed TIC are shown in the detector support structure with the vacuum chamber removed.
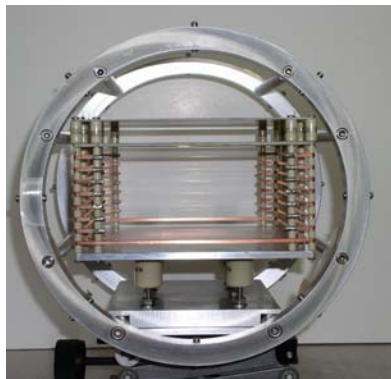
Figure I-76

Figure I-77

Figure I-78

Currently the Frisch grid is grounded but this can be easily changed with a small modification of the detector wiring to allow a potential to be applied.

On April 25-27, 2003, the TIC was used in an experiment with good results.

_____

*Argonne National Laboratory and Centre d'études Nucléaires de Bordeaux-Gradignan, France.
[1]B. Blank et al., ATLAS PAC Proposal Experiment Number 994, Submitted Feb. 07, 2003.
[2]C. L. Jiang, K. E. Rehm, and T. Pennington, private communication.
[3]T. Pennington and B. J. Zabransky, private communication.
[4]O. Buneman, T. E. Cranshaw and J. A. Harvey, Canadian Journal of Research **27A**, 191-206 (1949).

g.10.   Isobar Separator for the Canadian Penning Trap (G. Savard, A. R. Levand, W. Trimble, Z. Zhou, J. Clark,* J. Vaz,* J. C. Wang,* and K. S. Sharma†)

During this year, a one Tesla Penning trap was designed, built and operated as an isobar separator for the Canadian Penning Trap (CPT) mass spectrometer system.   Both stable and unstable isotopes can be precisely measured in the CPT mass spectrometer. In practice, the Penning trap requires ion beam at low kinetic energy (~ few eV) and accepts only few ions in one injection to obtain precise mass measurement.[1]

However, radioactive ions produced either on-line (the nuclear reactions between the heavy-ion beams from ATLAS and the targets) or off-line (fission fragments of ^{252}Cf source) are of high kinetic energy (~100 MeV) and cover a large mass range. This means the ions have to be de-accelerated and the contaminants removed before sending them to the Penning trap (Fig. I-79).
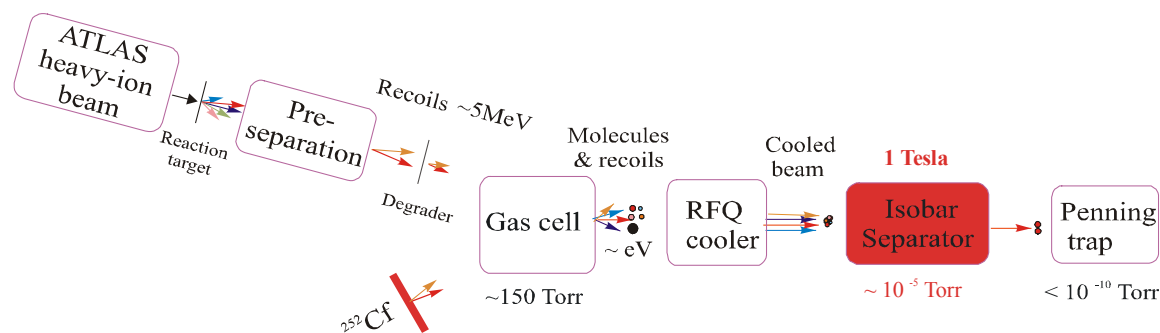
Fig. I-79. Schematic view of the Canadian Penning Trap system with isobar separator.

For the first issue, the gas cell is an ideal solution.[2] High-energy beams can be stopped in ~150 Torr helium and extracted by the combination of a DC axial field, gas flow, and RF voltage at the cone. However, while ions are thermalized in the gas cell, all the components of the gas can be ionized, including helium and hydrocarbons.   Essentially, the hydrocarbon ions become the main contaminant ions in the Penning trap. For the cleaning of the contaminants, we need an isobar separator.   For example, Table I-5 shows the main contaminants during a measurement of the ^{68}Se, which is an important waiting-point along the rp-process. The resolving powers required to remove the various contaminants are listed as well.

The isobar separator is a Penning trap, operated with 10^{-5} Torr helium pressure.[3] Ions in a constant magnetic field B and an axial quadrupolar electric field (Fig. I-

80a) have three eigen frequencies of motions: magnetron ω_-, modified cyclotron ω_+, and axial ω_z (Fig. I-80b). If buffer gas is present in the trap, the kinetic energy of the ions will be lost due to collisions, resulting in the increase of the orbital radius of the unstable ω_- motion for all ions, called ω_- cooling (Fig. I-80c). If an RF excitation voltage at frequency ω_c is applied on the ring electrode of the trap (Fig. I-80d), only the ions with $m/q = B/\omega_c$ will receive and lose kinetic energy periodically from $m(\omega_- r)^2/2$ to $m(\omega_+ r)^2/2$ (Fig. I-80e). The ions will be led to the center of the trap due to energy loss of ω_+ motion (reverse Fig. I-80c, called ω_+ cooling) and since the ω_+ cooling is faster than the ω_- cooling, the selected ions (red in Fig. I-80f) will be separated from the other ions. Typical parameters of this isobar separator for $m/q = 71$ are shown in Table I-6.

(a)   (b)   (c)

(d)   (e)   (f)
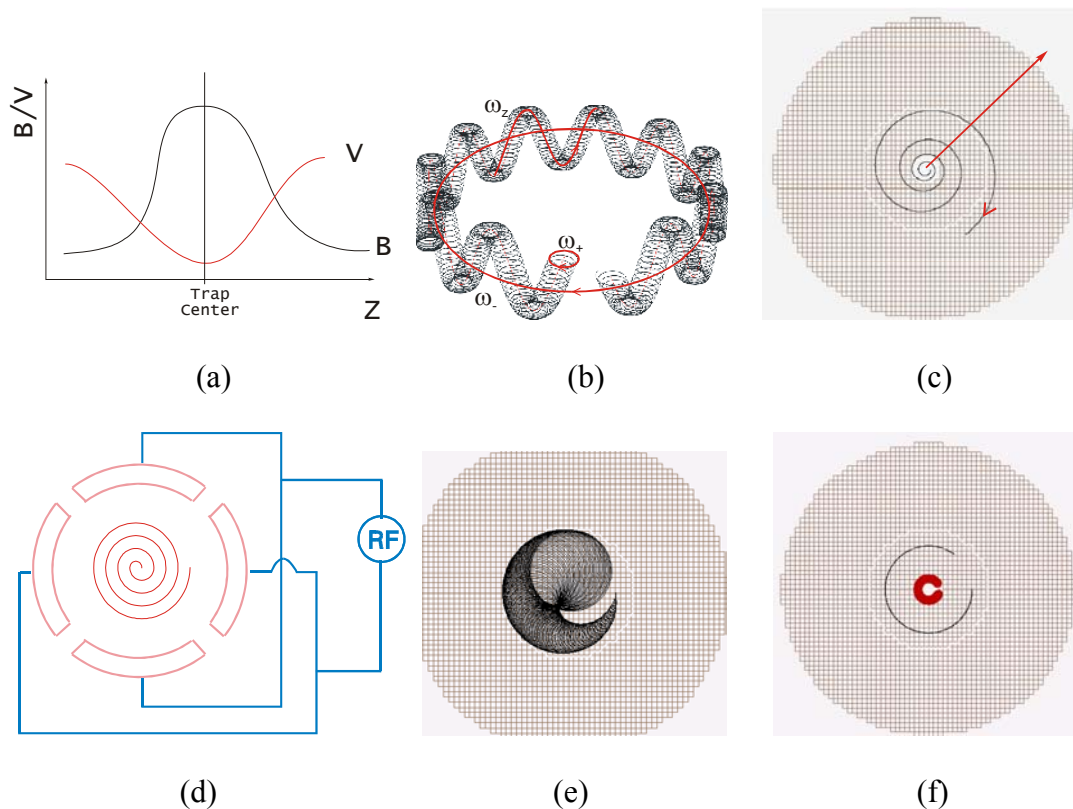
Fig. I-80. Principle of the isobar separator.

Table I-5. Main contaminants associated with ^{68}Se.

isotope	mass	abundance	R (resolution)
^{68}Se	67.9419	1	
^{68}Ge	67.9281	98	5000
^{68}As	67.9368	54	13000
C_5H_8	68.0626	400	600
C_4H_4O	68.0262	100	800

Table I-6. Working parameters of the isobar separator for m/q = 100.

parameter	symbol	value
magnetic field	B	1 Tesla
cyclotron frequency	ω_c	211.40 kHz
RF voltage	V_{RF}	10 mV
cooling time	t	200 ~ 430 ms
He pressure	P	<0.1 mTorr

At present, the mass resolving power of the isobar separator is about 1000. At this resolving power, with the suppression of 95% of the molecular contaminants, many isotopes, like ^{64}Ge, ^{64}Ga, ^{65}Ge, ^{68}Se, ^{68}As, ^{107}Sb,

^{107}Sn, ^{108}Sb, ^{108}Sn, which were previously very difficult to deal with, can now be measured. Efforts to further improve the resolving power are being undertaken.

_____

*Argonne National Laboratory and University of Manitoba, Winnipeg, Manitoba, †University of Manitoba, Winnipeg, Manitoba.
[1]G. Bollen, S. Becker, H.-J. Kluge, M. König, R. B. Moore, T. Otto, H. Raimbault-Hartmann, G. Savard, L. Schweikhard, H. Stolzenberg (the ISOLDE Collaboration), Nucl. Instrum. Methods **A368**, 675, (1996).
[2]G. Savard, J. Clark, C. Boudreau, F. Buchinger, J. E. Crawford, H. Geissel, J. P. Greene, S. Gulick, A. Heinz, J. K. P. Lee, A. Levand, M. Maier, G. Münzenberg, C. Scheidenberger, D. Seweryniak, K. S. Sharma, G. Sprouse, J. Vaz, J. C. Wang, B. J. Zabransky, Z. Zhou and the S258 collaboration, Nucl. Instum. Methods B, in press.
[3]G. Savard, St. Becker, G. Bollen, H.-J. Kluge, R. B. Moore, T. Otto, L. Schweikhard, H. Stolzenberg, U. Wiess, Phys. Lett. **A158**, 247, (1991).

g.11.   A Compact High-Homogeneity Solenoid Magnet for the CPT Isobar Separator
(G. Savard, A. Levand, J. Clark, J. Nolen, J. Wang, W. Trimble, and Z. Zhou)

A Penning-trap-based isobar separator was constructed for the CPT mass spectrometer system. The space available for the device was limited which put severe constraints on the size of the magnet for the isobar separator. A very compact design for the high-field solenoidal magnet that provides the uniform axial field for the isobar separator was required. The resolution and thus the usefulness of the trap depend on the strength and quality of the field. The strength of the field for this type of magnet is limited by resistive heating from the amount of current passing though the windings. The requirements are a resistive solenoid magnet with a 2-inch clear bore, a one Tesla field uniform to on part in 10,000 in a cylindrical volume of 1 cm radius by 2 cm long. To design the magnet, the Poisson electromagnetic simulation program from Los

Alamos was used to analyze and optimize possible configurations. A long solenoid is usually needed to achieve field uniformity. A shorter solenoid can be used but to compensate for the fringing effects we must remove some of the center windings. This can allow one to meet the field requirements but the magnet power is then too high at about 25 kW. Tailoring the flux return steel near the bore produces a flatter field from a shorter solenoid, but the dimensions are critical, mainly due to nonlinear effects of saturation. A steel ring was found to effectively flatten the field in the shorter solenoid and also provide a tunable element. In the end, two concentric rings were used, the smaller inner ring being easily accessed through the bore to tweak the field. The magnet power is 10 kW and meets the field requirements (see Fig. I-81).
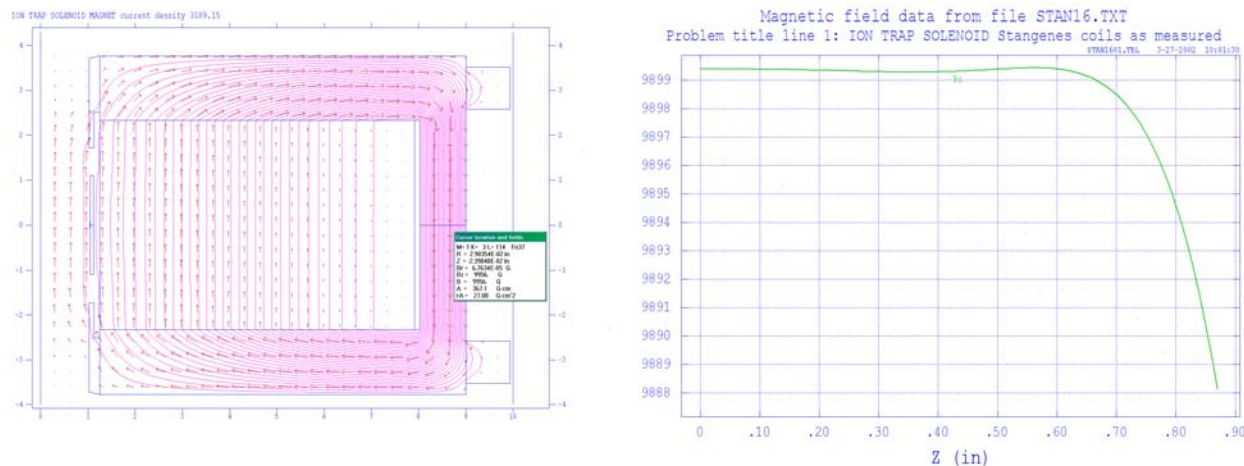
Fig. I-81. Magnetic field predictions.

The physical construction of the magnet is designed for easy assembly without introducing asymmetries in the field (see Fig. I-82). The magnet consists of steel circular end plates, a tubular outer shell, eight pancake windings (Fig. I-83), an inner brass tube to support the windings and packing gland nuts to locate and center the brass tube to the end plates. The whole assembly (Fig. I-84) is clamped together with tie rods around the periphery. Pancake coil windings are simpler to assemble and to connect to power and cooling water. The coils are staggered so the connections exit through the split outer tube at four quadrants. Standard 18 inch by 1.15-inch steel pipe was used for the outer tube. Some magnetic flux is leaving the outer tube, since the magnetic properties of the pipe are not as good as assumed and a thicker wall would have been better but the field properties still meet specifications.

For field mapping, a GMW teslameter with a Hall effect probe was used with the analog output to a high-resolution voltmeter. The trap vacuum chamber material is slightly magnetic, due to cold working of the 304 stainless steel bar. This causes a slight axial asymmetry of the field, but it is still within specifications (Fig. I-85). A slight off-axis field component cannot be excluded by these measurements but is calculated to have a negligible effect on the trap precision.

Various aspects of the magnet stability were investigated. Current ripples are damped heavily by the inductance of the magnet and are at a level where they are of no concern. Heating of the power supply shunt causes a long term drift. Additional circuitry to correct this using a current transformer sensor was installed but later found to produce a fluctuation with a period of approximately one second. It was removed. An existing more stable power supply was found that will eliminate the current stability issues. It was also found that the bore of the magnet reached temperatures in excess of 40 C after many hours of operation. At a field of 1 Tesla, the magnet is operated at 40 volts and 250 amps for a total of 10 kW for a magnet bore of less than 20 cm length. This causes outgassing of the vacuum chamber hosting the Penning trap which then limits the lifetime of the ions in the trap. Reversing water flow through the magnet put cool inlet water next to the end plates, reducing trap temperatures somewhat. A booster pump to increase water flow will be installed to lower temperature further and totally eliminate this problem.
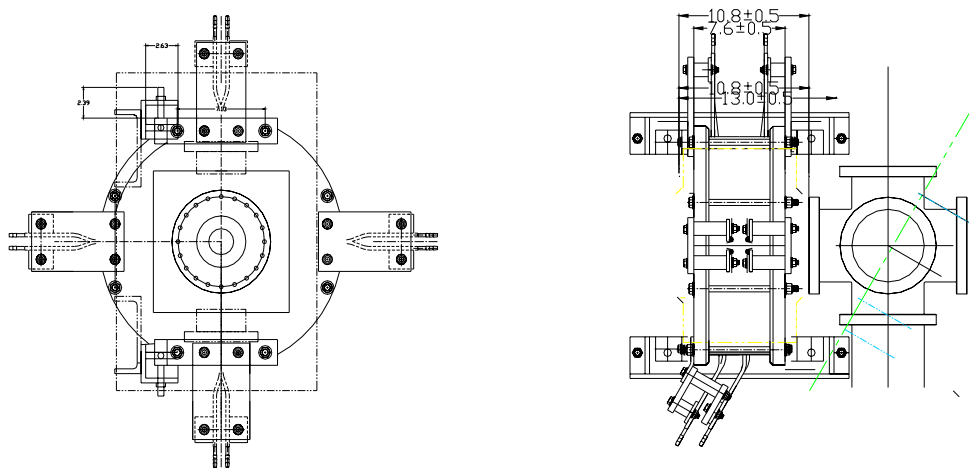
Fig. I-82. Magnet assembly drawing.

Fig. I-83. The Stangenes pancake coil winding.
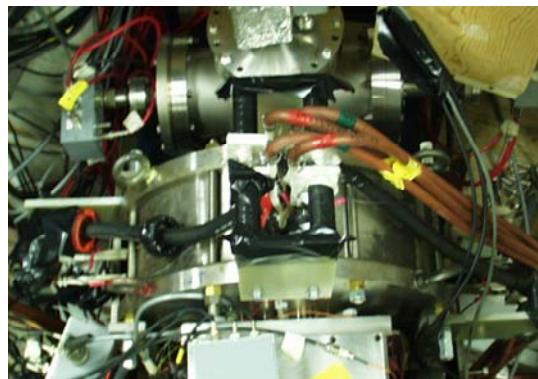
Fig. I-84. The installed magnet in Area 2.
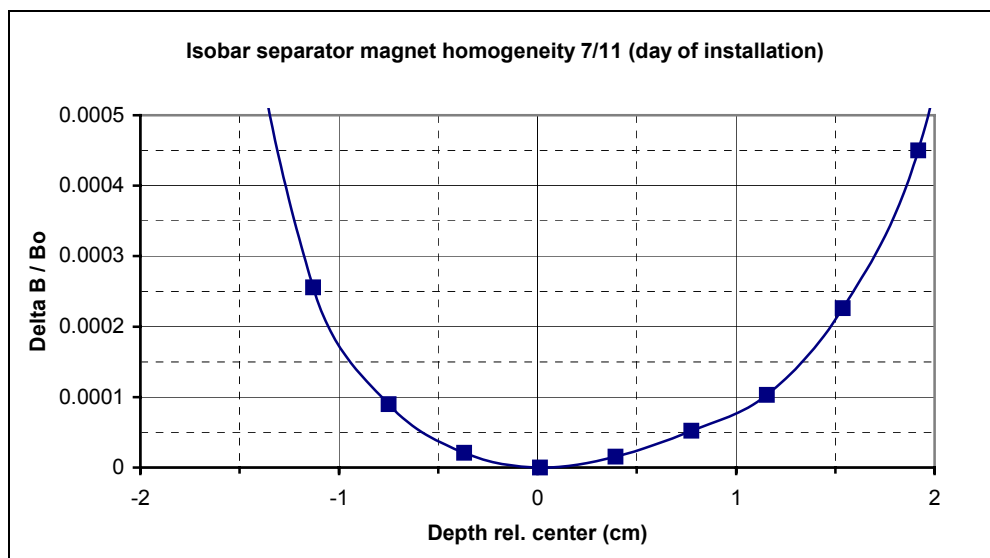
Fig. I-85. An early magnet axial field measurement.

g.12.   Technical Progress in Hyper Pure Germanium Double-Sided Strip Detector Development (S. J. Freeman,* C. J. Lister, S. Fischer, N. Hammond, and K. Teh)

Tests were made of a hyper pure germanium doubled-sided strip detector. This detector is the third in a series of models which form part of a development program in collaboration with Pat Sangsingkoew, AMETEK Industries. The germanium wafer is approximately 92 × 92 mm and 2-cm thick. The nominal front face has a sixteen vertical strip electrodes of 5-mm width formed by ion implantation of boron to a depth of <1 μm. The bias voltage of 1300 V is applied to this face and the strips are AC-coupled to warm preamplifiers.   The nominal back face has sixteen horizontal strips with 5-mm wide electrodes formed by lithium diffusion to a depth of approximately 600 μm. In order to prevent the subsequent migration of lithium in the crystal destroying the strip integrity, 1-mm deep saw cuts of width 0.5 mm are made between the horizontal strips. The back electrodes are also DC-coupled to warm preamplifiers.   In order to mount the crystal in the cryostat, the germanium is sandwiched between two 1-mm thick sheets of boron nitride and the edges surrounded by an aluminum ring. Condensed sixteen-channel electronics were used to amplify and digitize signals from the front and back of the detector and events involving the coincidence between at least one pair of strips on the front and back were recorded. Data was taken with a variety of sources spanning γ-ray energies from 88 to 1836 keV.

The lithium and boron strips show distinct differences in the variation of resolution with energy as shown in Fig. I-86. The variation on the boron strips is similar to that expected for a regular unsegmented planar detector. The absolute magnitude of the resolution is higher than expected in this case, due to noise issues in the condensed electronics which
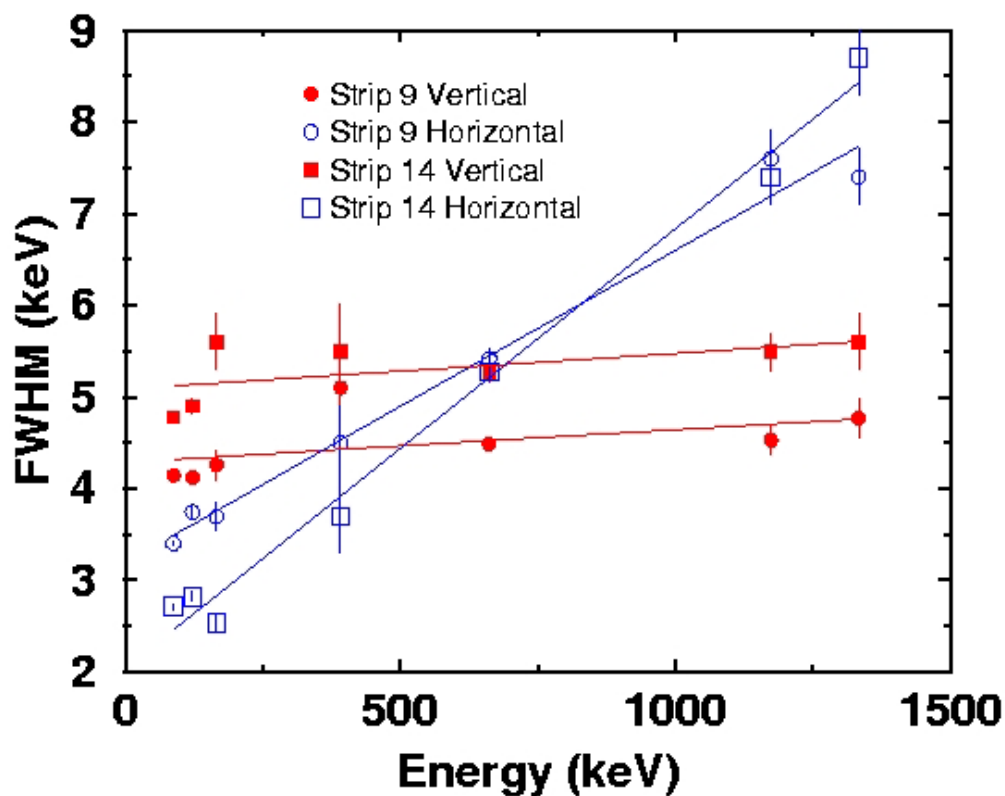
Fig. I-86. Variation of resolution with energy for some example strips on the lithium (horizontal) and boron (vertical) sides of the crystal.

are under investigation. The resolution of the boron strips measured using a simple single channel MCA was typically 2.3-keV FWHM at 122 keV. The behavior of the lithium strips is very different and exhibits a very strong variation with γ-ray energy, typical of that expected in a detector with strong fluctuations in the charge collection efficiency. In the case of strip detectors, it is not surprising to see an asymmetry in the properties of the two electrodes which is possible due to the small physical size of the electrodes. The induced signal in any particular electrode is small unless charge is very close to it; the signal generated in an electrode on one side of the detector is, therefore, dominated by the charges drifting towards that electrode. The variation of resolution with energy suggests that the electron collection by the lithium side suffers poorer efficiency than the collection

of the holes by the boron electrodes. A comparison of spectra taken with illumination from the front and from the back appears to rule out bulk trapping, and the effect may be associated with the saw cuts on the lithium side.

Investigations were made of multiple strip events in the detector. A cross-talk effect was observed when reconstructing the full energy from the sum of energies in events involving two adjacent strips, which is not present in the case of two non-adjacent electrodes (see Fig. I-87). There is a noticeable shift in gain in the case of adjacent double-strip events when compared to single-strip or non-adjacent double-strip events of the order of a few percent of the photopeak energy. This effect appears to arise from a capacitive coupling between adjacent strips.
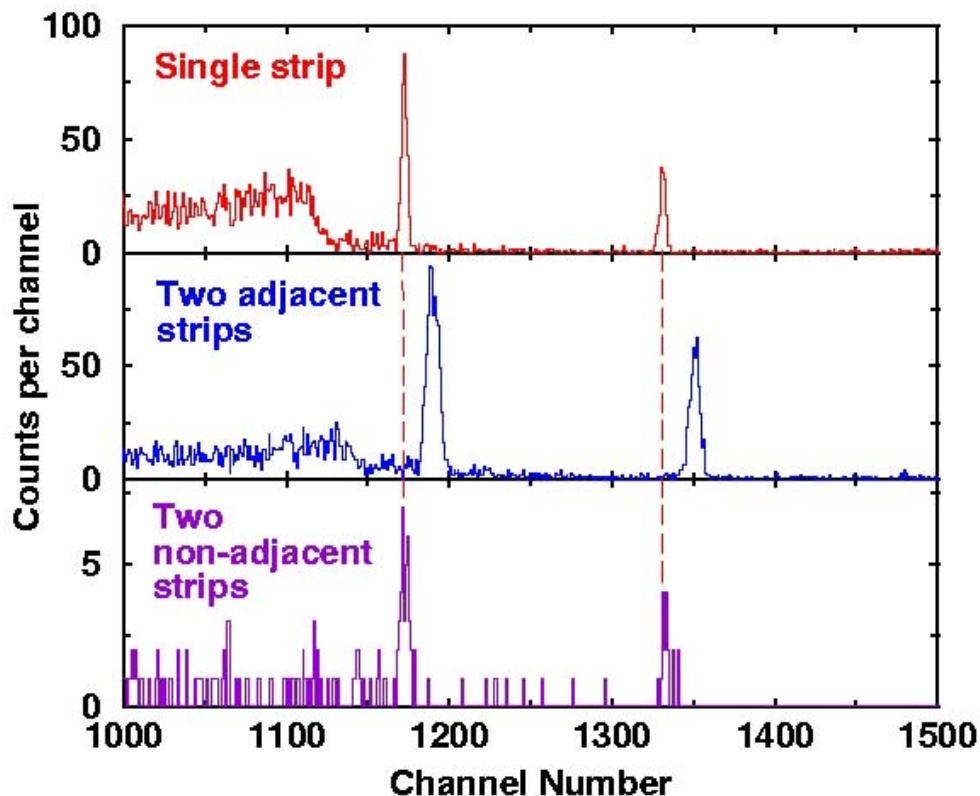
Fig. I-87. Illustration of the gain shifts between single-pixel events (top), two-pixel events with neighboring strips (middle) and two-pixel events with non-adjacent strips (bottom).

Illumination of the detector using calibrated sources from a distance of 10.35 cm from the center of the crystal results in an absolute efficiency of 2.19(4)% at 121 keV, which compares well with that expected from a Monte Carlo simulation of the detector.

A fourth generation planar strip detector was recently delivered which was designed to incorporate good resolution features onto one side of the detector which uses cold FETs. The properties of this detector are currently being evaluated.

_____

*On sabbatical leave from University of Manchester, United Kingdom.

g.13.   Position Interpolation in a Germanium Planar Detector Using Digital Pulse Processing (C. J. Lister, J. Ammann,* and S. M. Fischer*)

We have begun to investigate gamma ray "tracking" by using digital pulse processing. It is clear that both depth and lateral information can be easily obtained for planer germanium detectors. Using a bank of LeCroy digital storage oscilloscopes, triggered by events of interest selected by external electronics, we were able to capture images of charge deposition, and the induced charges produced as the charge migrates across the

crystal. Analysis of the relative intensity of image charges offers a rather straightforward way of obtaining sub-strip lateral position. Figure I-88 shows a typical image. Figure I-89 shows an analysis of several hundred images to obtain the lateral position sensitivity. The overall resolution is ~2 mm FWHM, though the resolution is depth-dependent, being better for very shallow or very deep interactions.

_____

*DePaul University.
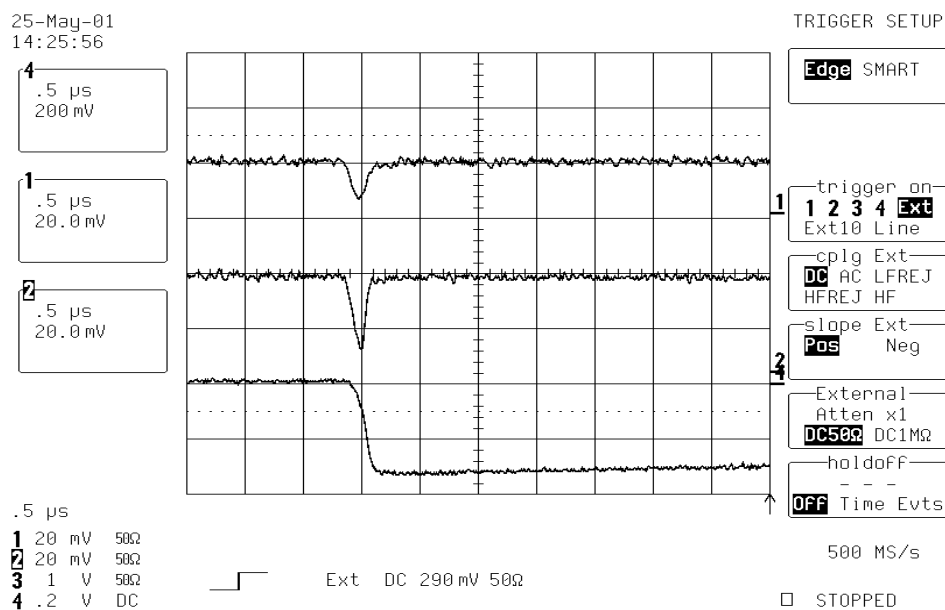
Fig. I-88. Digital recording of preamplifier pulses collected when all the charge from a 1.33 MeV gamma-ray is deposited under a single strip of the HpGeDSSD (bottom trace). The induced image charges can clearly be seen on the neighboring strips (top traces). The image shows an interaction with was slightly offset to one side of the strip, so the image charges have different intensity.
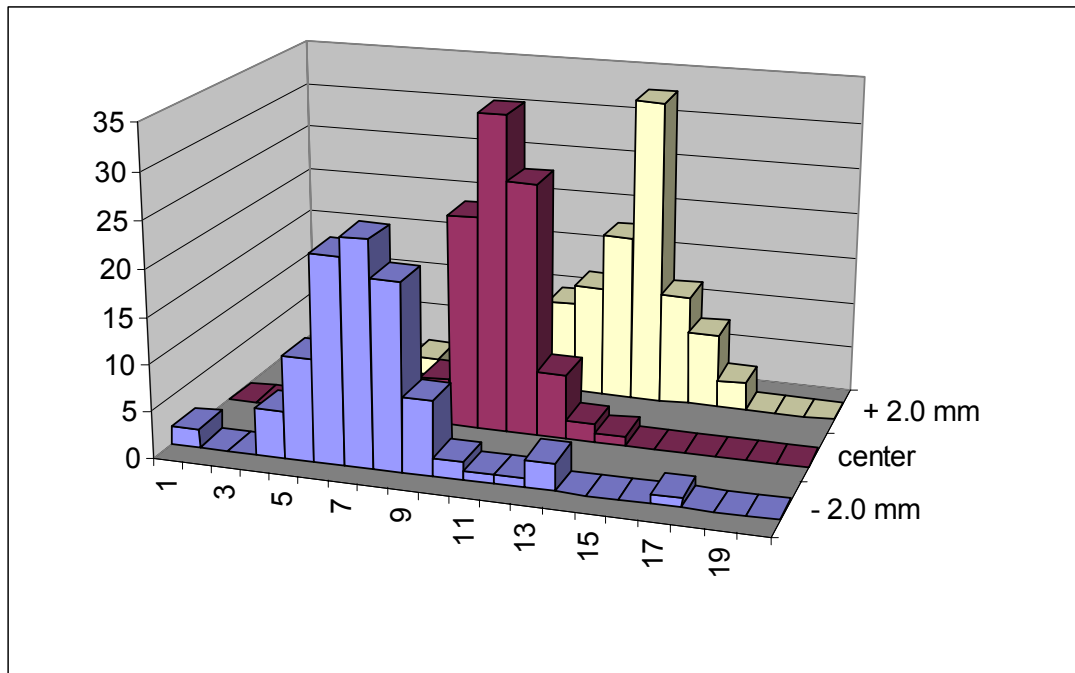
Fig. I-89. A distribution of calculated interaction positions measured for gamma-rays injected under a single strip, and inferred from the charge induced on the neighboring strips. The source was a ^{54}Mn line source, collimated to <0.25 mm, which emits 835 keV photons. It was positioned with a computer controlled motor drive in the center of a 5 mm strip and then offset by 2 mm towards either edge of the strip.

g.14. Accuracy of Gamma Ray Tracking as a Function of Detector Noise (T. L. Khoo, C. J. Lister, E. F. Moore, and S. Grullon*)

A useful application of gamma-ray tracking is to determine the direction of a photon incident on a detector and, thereby, to enhance gamma rays from a source at a specific location and suppress those from random directions. This feature can make it possible to investigate gamma radiation from a very weak source (common if the activity is very far from stability), which might otherwise be swarmed by background from, say, the room. As a start of a project to quantitatively ascertain the enhancement in sensitivity through gamma ray tracking, we used a Monte Carlo method to construct events from the source and from

random directions. The Compton interactions in a Ge detector were then analyzed, assuming that the photons originated from the source, to construct the energy spectrum. Gamma rays from the direction of the "source" were correctly identified, whereas those from random directions could be rejected. In the limit of zero noise, tracking can be correctly accomplished with close to unit efficiency. However, the success rate decreases as the detector noise increases, e.g. with a noise equivalent to 2.3 keV FWHM the correctly identified fraction dropped to ~80%.

_____

*Summer student, Florida International University.

g.15.   Use of HpGeDSSDs for Imaging and Material Analysis (C. J. Lister, D. Nisius,*
         and S. M. Fischer†)

As part of a NASA SBIR project, we are involved in exploiting our position sensitive planar detectors (HpGeDSSDs) to image small objects and deduce their material composition through differential x-ray absorption.   The NASA solicitation is to develop techniques to eventually search for fossils on Mars. In the short term it is to develop technologies that can produce real-time x-ray images.

For the Phase 1 test, a strong (50 mCi) ^{109}Cd source was used to produce a pencil beam of x-rays (22,24 keV) and 88 keV nuclear gamma rays. The divergent beam was focused on our 92 mm × 92 mm position sensitive LEPS detector placed ~2 m away.   The system had spatial resolution of ~700 µm. Small objects could be mounted on a goniometer and raised into the beam. The attenuation of radiation could then be determined, which depends on the thickness and elemental composition of the object.   The object could then be rotated in the beam, allowing data to be acquired which could produce a 3-D image.

_____

*BioImaging Research Inc., †DePaul University.

Figure I-90(a,b) shows a photograph of the experimental arrangement to produce an absorption image of a NASA sample consisting of a 7 mm × 3 mm quartz disk with two 1 mm holes, one filled with paraffin and one with graphite. The image is shown in Fig. I-91, where the overall absorption of x-rays by the disk is clear, as are the two holes which exhibit different degrees of absorption.

This project successfully completed Phase 1 and was funded for a Phase 2 SBIR. To improve the spatial resolution, a CdZnTe strip detector system is being built, which should have similar characteristics, but finer pitch strips that should give an order of magnitude position resolution improvement at the cost of about a factor four in energy resolution.   CdZnTe detectors operate at room temperature, so are more practical for the eventual Mars mission.

(a)   (b)

Fig. I-90. (a) left. A photograph of the experimental setup showing the source block and detector. (b) An enlargement of the quartz sample under study.
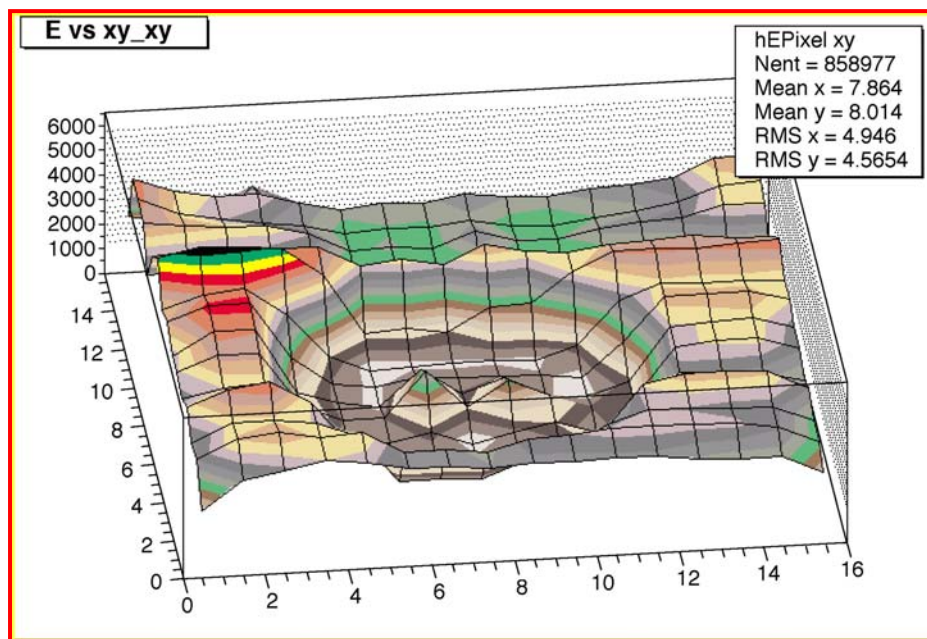
Fig. I-91. A two-dimensional absorption image of a 7 mm quartz disk with recessed paraffin and graphite inclusions. The position resolution is better than 700 μm.

g.16. Compton Polarization Measurements with a Double-Sided Germanium Strip Detector (N. J. Hammond, C. J. Lister, S. J. Freeman, S. M. Fischer, G. Mukherjee, R. V. F. Janssens, E. F. Moore, K. Teh, D. G. Jenkins, and G. D. Jones*)

We employed a double-sided germanium strip detector (GeDSSD) to measure the Compton polarization of low-energy gamma rays. Conventional gamma-ray polarimeters, using coaxial germanium detectors, are ineffective at such energies due to the increased probability of photoelectric absorption and the subsequent decrease in the photon mean free path. The strip detector used for this study possesses an effective pixel size of 25 mm^2 with a total active surface area of 640 cm^2 and therefore allows the identification of Compton-scattered events with much smaller path lengths. A novel technique for measuring the polarization sensitivity at low energy was proposed by Jones,[1] whereby alpha decay is used to fully align excited states in their m = 0 substates which then decay via pure dipole or quadrupole transitions of high, or even full ($|P| = 1$), linear polarization. We conducted a test to measure the efficacy of this technique and also to commission a new data acquisition system, Scarlet, which was used to stream data to the ROOT front-end analysis package. Using a ^{228}Th source and a single Si detector positioned as shown in Fig. I-92, we were able to identify both "vertically" and "horizontally" scattered E2 gamma rays following second generation alpha decays to the first excited state in ^{220}Rn. An example gamma-ray spectrum gated by such alphas is shown in Fig. I-93.

To make a definitive measurement we propose to use an additional Si detector in a position perpendicular to the first as displayed in Fig. I-92. This arrangement not only allows a doubling of the count rate but also facilitates the rotation of the target-Si detector system through pi radians which will be crucial to reduce systematic errors arising from differences in the efficiency of measuring horizontal and vertically scattered photons. A new target chamber, which houses both Si detectors and the source material was built to this effect. We are in the process of procuring a ^{227}Th source for the measurement which should additionally allow us to resolve spin ambiguities in the level structure of ^{219}Rn. We expect to begin collecting data in spring 2003.

_____

*University of Liverpool, United Kingdom.
[1]G. D. Jones, Nucl. Instrum. Methods **A491**, 452 (2002).
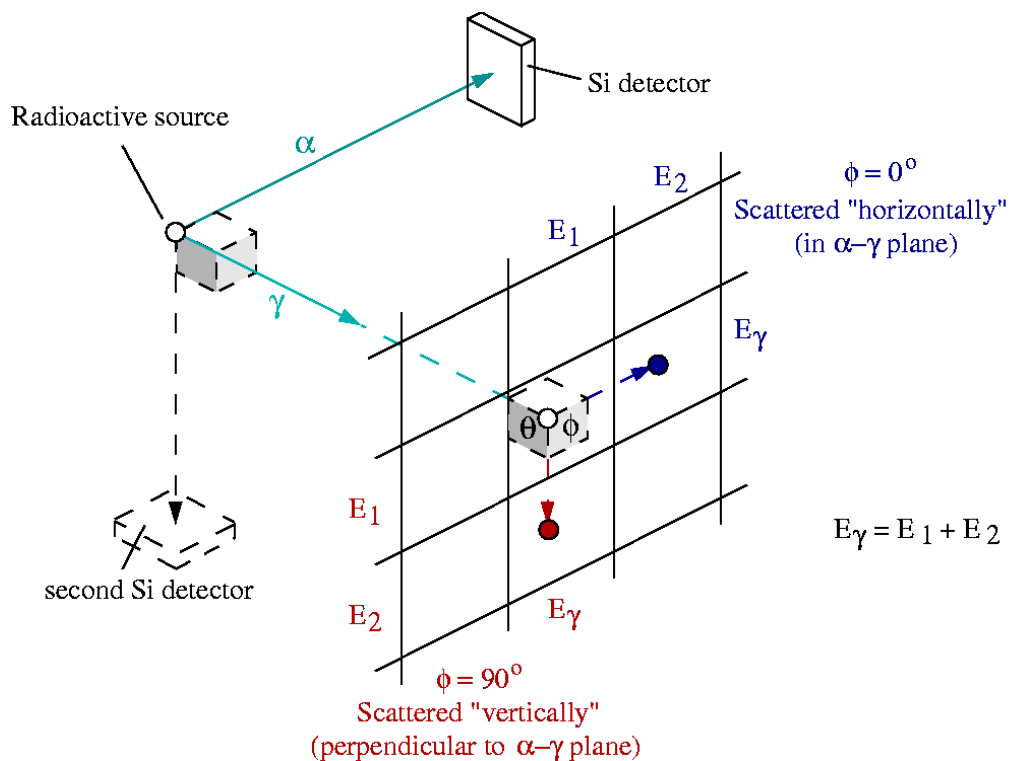
Fig. I-92. Schematic representation of set-up, with silicon detectors mounted at 90° to allow two simultaneous measurements of γ-ray polarization and remove many systematic uncertainties.
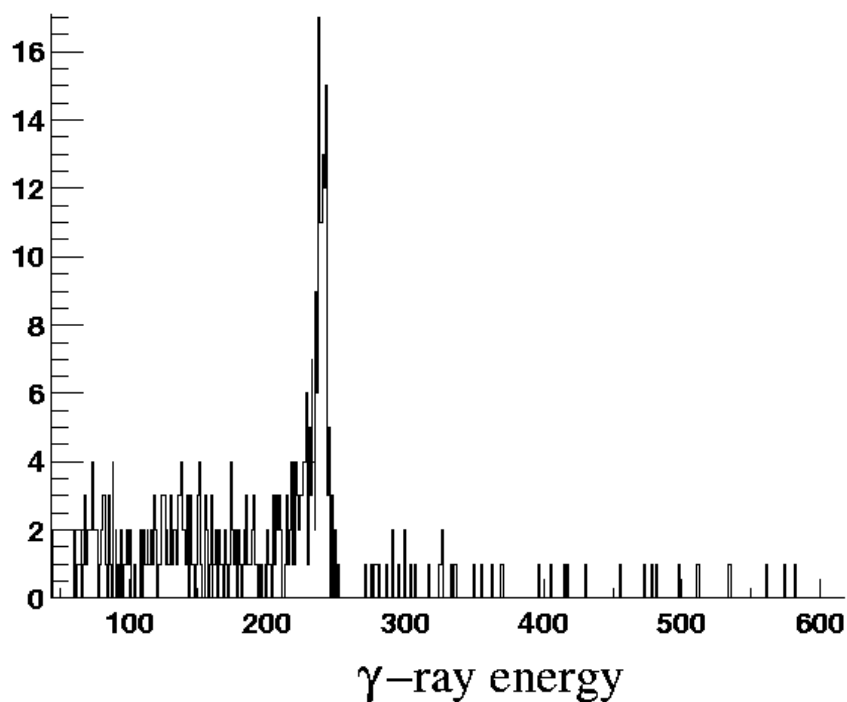
Fig. I-93. A typical γ-ray spectrum showing the 241 keV γ-ray following the 5449 keV α-decay of ^{224}Ra. The asymmetry of scattering of these γ-rays yields the polarization of the radiation.

g.17. Doppler Reconstruction of Gamma-Rays from Fast Moving Sources Using the "Mark 3" HpGeDSSD (C. J. Lister, N. Hammond, R. V. F. Janssens, M. P. Carpenter, K. Teh, S. J. Freeman,* and S. M. Fischer†)

Considerable progress is being made in making high purity germanium detectors that are position sensitive. One approach is to use large area planar wafers of germanium and fabricate orthogonal strip electrodes in order to achieve position sensitivity. The technical developments in these detectors are discussed in section g.12.

One application of detectors of this type is to achieve superior Doppler reconstruction from fast moving sources. We are looking at a useful "benchmark" test with which to evaluate position sensitive counters. The $^{12}C(^{136}Xe,4n)^{144}Sm$ reaction at 595 MeV seems to be ideal. It involves simple and robust beam and target, the targets can be fabricated very thin, the recoil velocity is high, $\beta = 8.7\%$, the reaction is dominated by a single channel which has a high production cross section of ~400 mb, and gamma rays covering a wide range of energies are produced.

Figure I-94 shows our latest spectrum. It consists of events firing a single strip on the front and a single strip on the back of the detector, so reflects the simplest data where only one interaction point is involved. The 5-mm strip pitch allows good angle determination and thus reasonable Doppler reconstruction, about 8-keV fwhm at 600 keV. At present, we are examining the "multi-hit events" to find how many can be reliably reconstructed. We are also studying the pulse risetimes in order to extract depth information, which can, in principle, further refine the hit-angle estimate.

Several areas of development emerge as important factors for further improvements. The intrinsic detector resolution can be improved. In April 2003 the "Mark 4" detector will be delivered with cold-FET preamps. Factory tests show the new counter has 1.1 keV resolution at 122 keV, a factor 2 better that the "Mark 3".

The electronic noise of the shaping amplifiers and ADC's needs improvement in order to preserve the detectors intrinsic energy resolution characteristics. At present, the high density 16-channel amplifiers appear to cause significant degradation of energy resolution, >0.5 keV, when compared to data collected with a single amplifier and MCA.

The mechanical alignment of detector and target become critical. Also, it becomes more important to align both the direction of the beam and the exact beamspot size and position.

The longitudinal velocity of residues needs to be determined on an event-by-event basis. This can best be achieved using the Fragment Mass Analyzer (FMA) to detect residues and measure their time-of-flight in the 8.2 m isochronous spectrometer. The intrinsic recoil cone due to evaporation is small, but the residue direction can also be established using two position-sensitive counters at the focal plane.

_____

*Sabbatical Visitor from the University of Manchester, United Kingdom, †DePaul University.
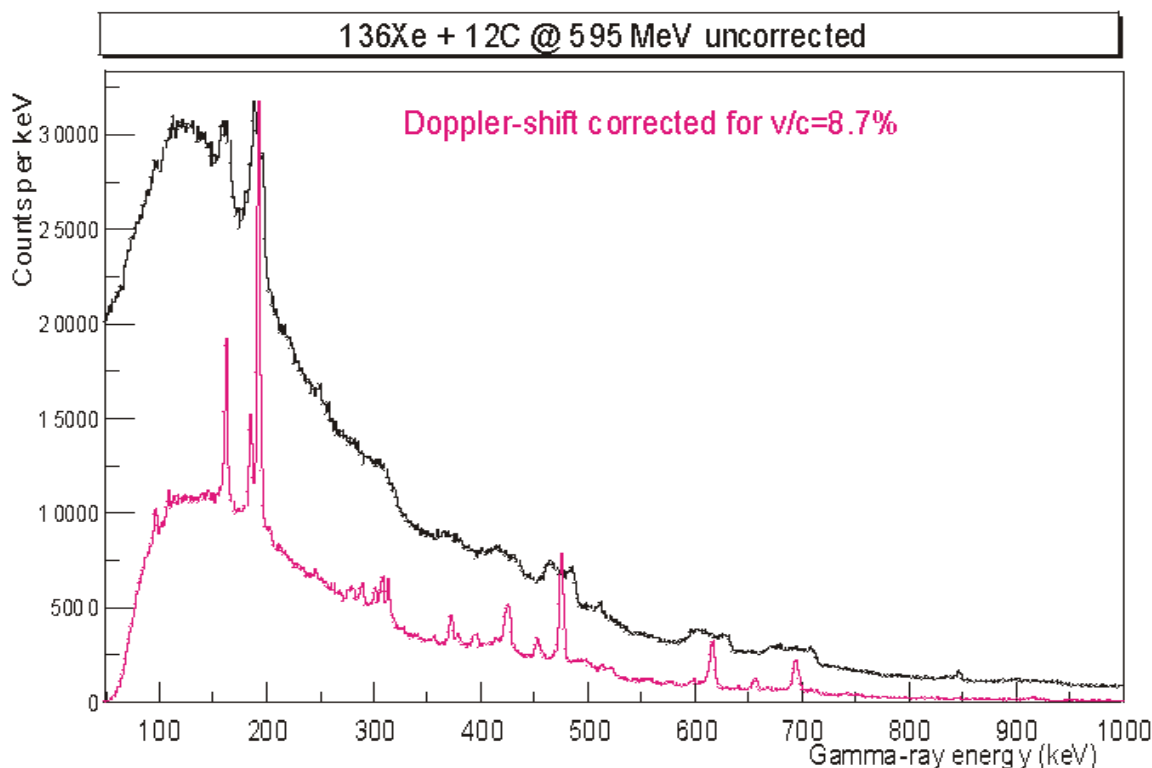
Fig. I-94. The effect of pixel-by-pixel Doppler correction. The raw data (black) reflects the energies of gamma-rays observed hitting the 92 × 92 mm detector that is mounted 100 mm from the target. The red curve is the subset of "single pixel" events (~20%) that have been corrected for the known kinematics of the reaction and using the measured hit position.

g.18.   Development of the X-Array, an Efficient Focal Plane Gamma Ray Spectrometer (C. J. Lister, M. P. Carpenter, R. V. F. Janssens, T. L. Khoo, T. Lauritsen, and E. F. Moore)

The X-Array spectrometer is a detector optimized for efficiently measuring electromagnetic radiation following proton, alpha, beta or isomeric decays. The array is designed for "offline" use, at the FMA focal plane, or at a remote tape station. For this application the design criteria are quite different from "in-beam" spectrometers like Gammasphere. Above all it needs very high efficiency for a broad range of gamma ray energies, from 10's keV to 10 MeV. It can be much more physically compact than "in-beam" systems, as multiplicities are low and there are no Doppler corrections to be made.

We made many MCNP Monte Carlo simulations of various designs, and selected a five-sided, double layer box which will surround the FMA focal plane. The first layer of detectors are made of large area position

sensitive LEPS detectors, which are being developed by our group in collaboration with Ortec (see section g.12.). The second layer of counters will be large volume germanium "clover" detectors, for enhancing the high energy efficiency and for suppressing backgrounds.

We started the procurement for the five large "clover" gamma-ray counters. After lengthy discussion with manufacturers concerning costs and performance, a non-segmented clover built from germanium crystals >60 mm in diameter was chosen. The specification was written and we are awaiting bids for the first two detectors. We hope to be able to instrument a "two-sided" box during this year to start exploring the many physics opportunities.

g.19. Gamma-Ray Tracking Coordinating Committee (T. L. Khoo, C. Baktash,* D. Cline (chair),† R. Kroeger,‡ A. Macchiavelli,§ M. Riley,¶ M. Thoennessen,‖ and K. Vetter**)

The Gamma-Ray Tracking Coordinating Committee [GRTCC] was appointed, on January 21, 2002, by the Directors of the Nuclear Science Divisions at the Argonne National Laboratory, Lawrence Berkeley National Laboratory, and Oak Ridge National Laboratory, at the request of the DOE Division of Nuclear Physics, to promote the development of γ-ray tracking detector technology in nuclear structure research. The goal was to help organize the γ-ray tracking community to provide widespread support and to provide an effective plan for the future. The initial charge, made to this Committee was to take a broad role in the development of γ-ray tracking detectors in this country. In particular there are three elements of the charge that should be addressed in a timely manner.

- Develop the various physics justifications for γ-ray tracking and establish the performance goals that are required in each area.

- Formulate a national R&D plan for γ-ray tracking detectors.

- Examine the currents efforts in γ-ray tracking that are underway in the United States and provide the Department of Energy with advice about how they should proceed.

The recommendations of the Committee were based on requested written answers to questions that were posed to the major γ-ray tracking detector projects, GRETA, GARBO, and MSU, the Gamma-Ray Tracking Fact Finding Meeting held at Argonne March 29-30, 2002 and extensive discussions by the Committee. The attendees to the fact-finding meeting included active participants developing the projects mentioned above, the European AGATA project, the NRL Astrophysics Tracking Group, the GRETA Steering Committee, and representatives of the Gammasphere User Group. The current and planned efforts in γ-ray tracking were discussed frankly and openly leading to unanimous support for a set of important and unambiguous conclusions. Based on the conclusions derived at the Argonne meeting, the other information provided, and discussion, the Coordinating Committee made the following recommendations (excerpted from the full report of the Committee):

1. A 4π Gamma-Ray tracking facility is an important new initiative within the 2002 NSAC Long Range Plan. This committee unanimously recommends a shell of closely packed coaxial Ge-detectors as outlined in the GRETA conceptual design for this 4π γ-ray tracking facility. We strongly recommend that DOE support this effort.

2. R&D necessary to demonstrate the full functionality of this detector was identified and has to be addressed at the highest priority. We note that a substantial fraction of this R&D effort is manpower that must be supported.

3. The R&D phase, the subsequent final design, and the construction of GRETA should continue to be a community effort; in particular, it should involve significant participation by the low energy nuclear physics national laboratories and universities.

4. Tracking with planar detectors is of interest to the nuclear science community and has a wide range of applications outside of nuclear physics. R&D efforts in this direction should be supported as part of the drive to develop tracking, as most of the electronics and software challenges are common to all tracking detectors.

5. Gammasphere continues to be the premier national γ-ray facility until GRETA becomes operational. This research facility must be supported to sustain the vitality of the field.

The Committee also made the following two observations regarding implementation of R&D for γ-ray tracking detectors:

(a) The current situation of a sole vendor for GRETA detector modules could have a significant impact on both the cost and delivery schedule for construction of GRETA. Development of a second vendor should have a high priority.

(b) Gamma-ray tracking, for all practical purposes, is an entirely new technique in γ ray detection, which has applications for homeland security in the detection of nuclear materials, with an emphasis on imaging and sensitivity, e.g. to image radioactivity

in dirty bombs. It also has applications in diverse areas of science such as astrophysics, and diagnostic medical uses.

The full report of the committee may be found at: www.pas.rochester.edu/~cline/full-report-19July.pdf.

_____

g.20.   Participation in GRETA and GRETINA Gamma Ray Tracking Projects
(C. J. Lister, M. P. Carpenter, R. V. F. Janssens, and T. L. Khoo)

The Heavy Ion group continued to be involved in the development of GRETA, a 4-π gamma-ray tracking detector. This concept is being developed at Lawrence Berkeley National Laboratory as a possible replacement for Gammasphere and a key device for exploiting radioactive beams at the Rare Isotope Accelerator, RIA. C. J. Lister is on the steering committee, and the other staff members in working groups. In the short-term, plans are being put into place to construct GRETINA, a ¼ of the full shell. We are interested in various physics and technical aspects of this project. One area of interest is signal digitization and deconvolution, an area that is important both for GRETA and for gamma ray tracking in HpGeDSSD planar wafers. We expect to formalize our long-term involvement in this project during the early part of 2003.

H. ATLAS USER PROGRAM

E. F. Moore

During the fiscal year 2002, ATLAS hosted strong "campaigns" involving radioactive beams, the CPT, the super-heavy element program, as well the AMS program. Some of these programs were driven by outside Users, and in all programs, there was considerable outside User involvement   Over 95% of all experiments performed in fiscal year 2002 included one or more outside Users and roughly 50% of the approved experiments had an outside User as the Principal Investigator. Frank Moore continued to be available in a user liaison capacity to handle the scheduling of ATLAS experiments, provide assistance in experiment proposal submission matters, and help facilitate the effective performance of research at ATLAS by outside scientists. In addition, a large portion of the heavy-ion in-house scientific staff and members of the technical support staff spent time in experiment setup, preparation, and assistance for the many different experiments performed at ATLAS.

A total of 123 Users from 47 different institutions were present at ATLAS for experiments in FY 2002. The pie chart below shows the distribution of the institutions represented by ATLAS Users and the number of Users of each type. Of the 41 Users from U.S. National Laboratories, 32 are from Argonne (27 from the Physics Division, 5 from other divisions). There were 32 students at ATLAS for experiments this FY, of which 11 were based at Argonne long-term. The names and institutions of all outside Users who were present at ATLAS in FY 2002 are listed below in section (b).
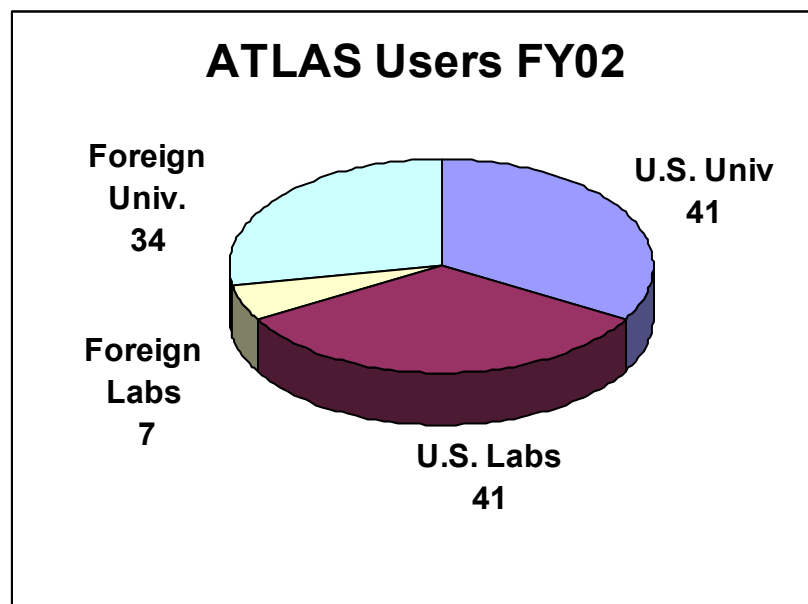
The Program Advisory Committee met twice during the 2002 fiscal year, on October 5, 2001 and May 3, 2002, to recommend experiments for beam time allocation at ATLAS.   In FY 2002 the Program Advisory Committee members were:

October 5, 2001

James Beene	Oak Ridge National Laboratory
Jolie Cizewski	Rutgers University
Stuart Freedman	University of California
David Morrissey	Michigan State University
Lee Riedinger (*chair*)	University of Tennessee
Robert Tribble	Texas A&M University
Alan Wuosmaa	Argonne National Laboratory

May 3, 2002

Art Champagne   University of North Carolina, Chapel Hill
James Beene   Oak Ridge National Laboratory
Jolie Cizewski   Rutgers University
Stuart Freedman   University of California
Augusto Macchiavelli   Lawrence Berkeley National Laboratory
David Morrissey   Michigan State University
Alan Wuosmaa   Western Michigan University

The PAC reviewed 30 proposals for 170 days of requested running time at the October meeting, and 29 proposals for 137 days at the May meeting. Due to the reduction of available beam time with 5-day/week operation for the entire FY, the PAC was asked to prioritize experiments into two categories: those that must be run at any cost (*priority I*), and those that should be granted beam time if at all possible (*priority II*). Of the submitted proposals for the two meetings, the Program Advisory Committee recommended priority I acceptance of 35 proposals for a total of 152 days of running time, and priority II acceptance of 12 proposals for 59 additional days of beam time.

The fall meeting of the American Physical Society, Division of Nuclear Physics was held in East Lansing, MI, from October 9-12, 2002. The U.S. national nuclear laboratories with low-energy heavy-ion facilities; ATLAS at Argonne, HRIBF at Oak Ridge, the 88" cyclotron at Lawrence Berkeley National Laboratory, and the NSCL at Michigan State University held a joint Users Meeting. The Chair of the ATLAS Users Group Executive Committee, Prof. Jolie Cizewski (U. Rutgers), introduced the ATLAS user program, and Frank Moore, Cary Davids, and Guy Savard presented an overview of the ATLAS facility and some elements of the current physics program. Mike Carpenter discussed preparations for the return of Gammasphere to ATLAS in FY 2003. There were approximately 100 scientists in attendance at the meeting.

In FY 2002 the ATLAS Executive Committee consisted of Jolie Cizewski (Rutgers University) as Chairperson, Michael Wiescher (University of Notre Dame), Partha Chowdhury (University Massachusetts, Lowell), and Gene Sprouse (SUNY Stony Brook).

a. Experiments Involving Outside Users

All experiments in which outside users directly participated during FY 2002 are listed below. The spokesperson for each experiment is given in square brackets after the title, and the collaborators who were present for the experiment are given with their home institution (as of the end of the FY) below each entry.

1.   Test of New FMA Focal Plane Microchannel Plate Detector [Lister]
        G. Mukherjee, University of Massachusetts, Lowell; S. Freeman, University of Manchester; J. Amann,
        S. Fischer, De Paul University; N. Hammond, R. Janssens, K. Lister, E. Moore, S. Sinha, Argonne
        National Lab.

2.   Study of the ^{8}B Neutrino Spectrum Through the ^{8}B(β^+)^{8}Be(2α) Decay Chain-II [Freedman]
        S. Freedman, University of California; W. Winter, Lawrence Berkeley National Lab.; J. Greene,
        D. Henderson, R. Janssens, C. Jiang, E. Moore, R. Pardo, T. Pennington, K. Rehm, G. Savard,
        J. Schiffer, G. Zinkann, Argonne National Lab.

3.   Measurement of the ^{17}F Breakup Cross Section at the Barrier [Romoli]
        F. Soramel, Università di Udine; M. Mazzocco, University of Padova; M. La Commara, E. Vardaci,
        University of Naples; A. Guglielmetti, University of Milano; J. Liang, Oak Ridge National Laboratory;
        L. Stroe, Lab. Nazionali di Legnaro; M. Romoli, I.N.F.N. Sezione di Napoli; M. Di Pietro,
        M. Pierroutsakou, I.N.F.N.; A. Heinz, GSI, Darmstadt; J. Greene, D. Henderson, C. Jiang, E. Moore,
        R. Pardo, K. Rehm, A. Wuosmaa, Argonne National Lab.

4. Measurement of Helium-3 to Helium-4 Ratios in Isotopically Purified Helium [Doyle]
     J. Caggiano, Yale University; P. Huffman, National Institute of Standards & Technology; D. McKinsey,
     Harvard University; A. Heinz, GSI, Darmstadt; P. Collon, R. Scott, Columbia University; R. Janssens,
     C. Jiang, D. Moehs, R. Pardo, K. Rehm, J. Schiffer, R. Vondrasek, Argonne National Lab.

5. Test of the RIA Gas Cell Prototype [Savard]
     J. Caggiano, Yale University; J. Clark, K. Sharma, J. Vaz, University of Manitoba; W. Trimble,
     University of Chicago; C. Boudreau, McGill University; A. Heinz, GSI, Darmstadt; B. Blank, J. Greene,
     D. Henderson, A. Levand, E. Moore, R. Pardo, K. Rehm, G. Savard, J. Schwartz, D. Seweryniak,
     J. Wang, Argonne National Lab.

6. Studies of Sub-ms Proton and α Emitters [Seweryniak]
     A. Woehr, University of Maryland; A. Heinz, GSI, Darmstadt; M. Carpenter, C. Davids, D. Seweryniak,
     Argonne National Lab.

7. Preparations Towards a Search for Super-Heavy Elements at ATLAS: PHASE I [Heinz]
     A.Woehr, University of Maryland; M. Smith, TRIUMF; A. Heinz, GSI, Darmstadt; P. Collon, Columbia
     University; I. Ahmad, B. Back, M. Carpenter, R. Janssens, C. Jiang, T. Khoo, F. Kondev,
      T. Lauritsen, K. Lister, E. Moore, G. Savard, J. Schiffer, D. Seweryniak, Argonne National Lab.

8. Establishing the Deformation of ^{140}Dy From Measurement of the Delayed Decay of the $K^{\pi} = 8^{-}$ Isomeric
State
     [Cullen]
     C. Wheldon, University of Surrey; D. Cullen, A. Fletcher, S. Freeman, L. Pattison, J. Smith, University
     of Manchester; A. Bruce, University of Brighton; M. Carpenter, R. Janssens, K. Lister, D. Seweryniak,
     Argonne National Lab.

9. Patterning of Columnar Defects with LiGA and Heavy Ion Lithography in High Temperature
Superconductors
     [Kwok]
     L. Undreiu, Western Michigan University; W. Kwok, G. Karapetrov, Argonne National Lab.

10. The ^{56}Ni(^{3}He,p) Reaction and the Question of T = 0, T = 1 Pairing in N = Z Nuclei [Macchiavelli]
     G. Mukherjee, University of Massachusetts, Lowell; P. Fallon, A. Macchiavelli, Lawrence Berkeley
     National Lab.; A. Heinz, GSI, Darmstadt; C. Jiang, R. Pardo, K. Rehm, J. Schiffer, Argonne National
     Lab.

11. High-K Isomers in ^{254}No by Electron and γ Spectroscopy [Khoo]
     P. Butler, G. Jones, University of Liverpool; M. Smith, TRIUMF; J. Cizewski, Rutgers University;
     A.Heinz, GSI, Darmstadt; I. Ahmad, M. Carpenter, C. Davids, R. Janssens, T. Khoo, T. Lauritsen,
     K. Lister, D. Seweryniak, Argonne National Lab.

12. Tests of a New Scattering Chamber at the FMA [Heinz]
     J. Shergur, A. Woehr, University of Maryland; K. Abu Saleem, Illinois Institute of Technology;
     A.Heinz, GSI, Darmstadt; R. Scott, Columbia University; I. Ahmad, M. Carpenter, J. Greene,
     D. Henderson, R. Janssens, C. Jiang, T. Khoo, F. Kondev, T. Lauritsen, K. Lister, E. Moore, R. Pardo,
     T. Pennington, G. Savard, J. Schiffer, D. Seweryniak, R. Vondrasek, Argonne National Lab.

13. Study of the ^{8}B Neutrino Spectrum Through the ^{8}B(β^{+})^{8}Be(2α) Decay Chain-III [Freedman]
     G. Mukherjee, University of Massachusetts, Lowell; S. Freedman, University of California; W. Winter,
     Lawrence Berkeley National Lab.; M. Paul, Hebrew University of Jerusalem; A. Heinz, GSI, Darmstadt;
     J. Greene, D. Henderson, R. Janssens, C. Jiang, E. Moore, R. Pardo, T. Pennington, K. Rehm,
     J. Schiffer, D. Seweryniak, G. Zinkann, Argonne National Lab.

14. Proton Decay of High-Z Nuclei [Davids]
    G. Mukherjee, University of Massachusetts, Lowell; J. Shergur, W. Walters, A. Woehr, University of
    Maryland; S. Robinson, University of Manchester; A. Mahmud, P. Munro, P. Woods, University of
    Edinburgh; A. Heinz, GSI, Darmstadt; A. Sonzogni, Brookhaven National Laboratory; C. Davids,
    D. Seweryniak, Argonne National Lab.

15. Continuation of the Mass Measurement Program Along the N=Z Line with the CPT Mass Spectrometer
    [Savard]
    L. Blomeley, J. Clark, M. Froese, K. Sharma, J. Vaz, University of Manitoba; D. Lascar, University of
    Chicago; J. Hardy, Texas A & M University; C. Boudreau, T. Cocolios, J. Crawford, S. Gulick, McGill
    University; A. Heinz, GSI, Darmstadt; A. Frankel, Cornell University; G. Savard, D. Seweryniak,
    J. Wang, Z. Zhou, Argonne National Lab.

16. Proton Decay of ^{121}Pr and ^{125}Pm [Davids]
    G. Mukherjee, University of Massachusetts, Lowell; J. Shergur, A. Woehr, University of Maryland;
    P. Munro, A. Robinson, P. Woods, University of Edinburgh; A. Heinz, GSI, Darmstadt; C. Davids,
    D. Seweryniak, Argonne National Lab.

17. Nucleosynthesis Chronometers ^{182}Hf, ^{244}Pu: Detection by Accelerator Mass Spectrometry [Paul]
    G. Mukherjee, University of Massachusetts, Lowell; M. Paul, Hebrew University of Jerusalem;
    A. Heinz, GSI, Darmstadt; R. Scott, Columbia University; C. Davids, R. Janssens, C. Jiang, F. Kondev,
    R. Pardo, K. Rehm, D. Seweryniak, R. Vondrasek, Argonne National Lab.

18. Commissioning of the Split Anode for the First Electric Dipole of the FMA [Davids]
    A. Robinson, University of Edinburgh; C. Davids, D. Henderson, T. Pennington, D. Seweryniak,
    Argonne National Lab.

19. Test of Fast Shaping Amplifiers for the Double-Sided Silicon Strip Detector [Davids]
    G. Mukherjee, University of Massachusetts, Lowell; J. Shergur, A. Woehr, University of Maryland;
    P. Munro, P. Woods, University of Edinburgh; A. Heinz, GSI, Darmstadt; C. Davids, D. Seweryniak,
    S. Sinha, P. Wilt, Argonne National Lab.

20. Survival Probability of Excited Hs Nuclei [Loveland]
    R. Charity, S. Komarov, Washington University; K. Aleklett, C. Rouki, Uppsala University;
    W. Loveland, D. Peterson, R. Yanez, Oregon State University

21. Dependence of the Level-Density Parameter on the Neutron-Proton Asymmetry [Charity]
    R. Charity, S. Komarov, D. Sarantites, L. Sobotka, Washington University; W. Loveland, Oregon State
    University; A. Caraley, Indiana University Cyclotron Facility

22. Coulomb Excitation of ^{128,130,132,134,136}Xe [Mueller]
    J. Enders, A Gade, T. Glasmacher, Z. Hu, K. Miller, W. Mueller, H. Olliver, B. Perry, Michigan State
    University; M. Carpenter, D. Henderson, R. Janssens, E. Moore, T. Pennington, Argonne National Lab.

23. Heavy Recoil Ion Test of an Upgraded MWPC for Nano- to Pico-Barn Cross-Section Experiments
    [Pennington]
    G. Mukherjee, University of Massachusetts, Lowell; J. Shergur, University of Maryland; B. Truett,
    Purdue University, Calumet; C. Davids, D. Henderson, K. Lister, T. Pennington, D. Seweryniak,
    Argonne National Lab.

24. AMS for ^{39}Ar: First Application of Dating Ocean Water [Collon]
    W. Kutschera, Universität Wien; R. Golser, University of Vienna; M. Paul, Hebrew University of
    Jerusalem; A. Heinz, GSI, Darmstadt; P. Collon, R. Scott, Columbia University; I. Ahmad, C. Jiang,
    R. Pardo, K. Rehm, R. Vondrasek, G. Zinkann, Argonne National Lab.

25. Development of a ^{37}K Beam for a Measurement of the ^{34}Ar$(\alpha,p)^{37}$K Reaction [Rehm]
    G. Mukherjee, University of Massachusetts, Lowell; L. Jisonna, R. Segel, Northwestern University;
    A.Heinz, GSI, Darmstadt; J. Greene, D. Henderson, R. Janssens, C. Jiang, E. Moore, R. Pardo,
    T. Pennington, K. Rehm, J. Schiffer, S. Sinha, Argonne National Lab.

26. Study of the Branching Ratio of the 4.033 MeV 3/2$^+$ State in ^{19}Ne-II [Rehm]
    R. Siemssen, University of Groningen; L. Jisonna, R. Segel, Northwestern University; M. Paul, Hebrew
    University of Jerusalem; A. Heinz, GSI, Darmstadt; J. Greene, D. Henderson, R. Janssens, C. Jiang,
    R. Pardo, K. Rehm, J. Schiffer, A. Wuosmaa, Argonne National Lab.

27. Effects of Ion Irradiation in Superconducting MgB$_2$ Single Crystals [Karapetrov]
    M. Hughes, University of California, San Francisco; G. Karapetrov, W. Kwok, Argonne National Lab.

28. Search for ^{105}Te and the Fine Structure in the α-Decay of ^{111}Xe [Seweryniak]
    G. Mukherjee, University of Massachusetts, Lowell; J. Shergur, University of Maryland; A. Robinson,
    University of Edinburgh; M. Lipoglavsek, M. Vencelj, Jozef Stefan Institute; A. Heinz, GSI, Darmstadt;
    D. Seweryniak, Argonne National Lab.

29. Continuation of the Mass Measurement Program Along the N=Z Line With the CPT Mass Spectrometer:
    Completion of the Mass 68 Measurement [Savard]
    L. Blomeley, J. Clark, M. Froese, K. Sharma, J. Vaz, University of Manitoba; D. Lascar, W. Trimble,
    University of Chicago; T. Cocolios, J. Crawford, McGill University; A. Heinz, GSI, Darmstadt;
    B. Blank, A. Levand, G. Savard, D. Seweryniak, J. Wang, Z. Zhou, Argonne National Lab.

30. The ^{56}Ni(^{3}He,p) Reaction and the Question of T=0, T=1 Pairing in N=Z Nuclei [Macchiavelli]
    G. Mukherjee, University of Massachusetts, Lowell; J. Cizewski, Rutgers University; M. Cromaz,
    A.Goergen, I. Lee, A. Macchiavelli, Lawrence Berkeley National Lab.; M. Paul, Hebrew University of
    Jerusalem; A. Heinz, GSI, Darmstadt; I. Ahmad, C. Davids, J. Greene, D. Henderson, R. Janssens,
    C. Jiang, E. Moore, R. Pardo, T. Pennington, K. Rehm, J. Schiffer, D. Seweryniak, S. Sinha, Argonne
    National Lab.

31. Fast Proton Decay of Odd-Odd ^{150}Lu [Davids]
    G. Mukherjee, University of Massachusetts, Lowell; A. Robinson, P. Woods, University of Edinburgh;
    B. Blank, C. Davids, D. Seweryniak, S. Sinha, Argonne National Lab.

32. Proposal to Measure the Total Radiative Capture Cross Section for the ^{12}C + ^{12}C System [Jenkins]
    B. Fulton, University of York; F. Haas, Université Louis Pasteur; G. Mukherjee, University of
    Massachusetts, Lowell; S. Freeman, University of Manchester; D. Jenkins, University of Liverpool;
    M. Carpenter, N. Hammond, R. Janssens, K. Lister, D. Seweryniak, Argonne National Lab.

33. Identification of Low-Lying, Low-Spin States in ^{74}Rb and ^{78}Y [Fischer]
    G. Mukherjee, University of Massachusetts, Lowell; S. Fischer, De Paul University; M. Carpenter,
    N. Hammond, R. Janssens, K. Lister, E. Moore, Argonne National Lab.

34. Spins of Excited States in ^{9}Li and the Nuclear Three-Body Force [Wuosmaa]
    A. Wuosmaa, Western Michigan University; A. Heinz, GSI, Darmstadt; J. Greene, R. Pardo, K. Rehm,
    S. Sinha, Argonne National Lab.

35. Radiative Capture and Fusion Dynamics in the Cold Fusion ^{90}Zr + ^{92}Mo Reaction [Carpenter]
    G. Mukherjee, University of Massachusetts, Lowell; D. Jenkins, University of Liverpool; A. Heinz, GSI,
    Darmstadt; I. Ahmad, M. Carpenter, C. Davids, N. Hammond, D. Henderson, R. Janssens, T. Khoo,
    F. Kondev, T. Lauritsen, K. Lister, E. Moore, T. Pennington, D. Seweryniak, S. Sinha, Argonne
    National Lab.

36. Silver Ion Implantation in Silicon Carbide [MacLean]
     H. MacLean, Massachusetts Institute of Technology; R. Scott, R. Pardo, R. Vondrasek, Argonne
     National Lab.

b.   Outside Users of ATLAS During the Period October 1, 2001 - September 30, 2002

This list includes all outside Users who were an experiment spokesperson (a), alternate spokesperson (b), student
(*), or collaborator actually present at ATLAS for an experiment. An additional 22 Users listed as collaborators
on the various experiment proposals were not at ATLAS in person, and thus are not represented in the list below.

1.   Brookhaven National Laboratory
             A. Sonzogni

2.   Columbia University
        a   P. Collon

3.   Cornell University
        *   A. Frankel

4.   De Paul University
        *   J. Amann
        a   S. Fischer

5.   GSI, Darmstadt
        ab   A. Heinz

6.   Harvard University
        a   J. Doyle
        *   D. McKinsey

7.   Hebrew University of Jerusalem
        a   M. Paul

8.   I.N.F.N.
             M. Di Pietro

9.   I.N.F.N. Sezione di Napoli
        a   M. Romoli
             M. La Commara

10. Illinois Institute of Technology
        *   K. Abu Saleem

11. Indiana University Cyclotron Facility
             A. Caraley

12. Jozef Stefan Institute
             M. Lipoglavsek
        *   M. Vencelj

13. Lab. Nazionali di Legnaro
             L. Stroe

14. Lawrence Berkeley National Lab.
             M. Cromaz
             P. Fallon
             A. Goergen
             I. Lee
        a   A. Macchiavelli
        *   W. Winter

15. Massachusetts Inst. of Technology
        b   T. Antaya
        a   H. MacLean

16. McGill University
        *   C. Boudreau
        *   T. Cocolios
             J. Crawford
             S. Gulick

17. Michigan State University
             J. Enders
             A. Gade
        b   T. Glasmacher
             Z. Hu
        *   K. Miller
        a   W. Mueller
        *   H. Olliver
        *   B. Perry

18. Nat'l. Inst. Of Standards & Tech.
             P. Huffman

19. Northwestern University
        *   L. Jisonna
             R. Segel

20. Oak Ridge National Laboratory
             J. Liang

21. Oregon State University
        a   W. Loveland
        b   D. Peterson
             R. Yanez

22. Purdue University, Calumet
      *   B. Truett

23. Rutgers University
           J. Cizewski

24. TRIUMF
           M. Smith

25. Texas A & M University
           J. Hardy

26. Université Louis Pasteur
           F. Haas

27. University of Brighton
           A. Bruce

28. University of California
      a   S. Freedman

29. University of California, San Francisco
      *   M. Hughes

30. University of Chicago
      *   D. Lascar
      *   W. Trimble

31. University of Edinburgh
      *   A. Mahmud
      *   P. Munro
      *   A. Robinson
      b   P. Woods

32. University of Groningen
           R. Siemssen

33. University of Liverpool
           P. Butler
      a   D. Jenkins
           G. Jones

34. University of Manchester
      a   D. Cullen
      *   A. Fletcher
           S. Freeman
      *   L. Pattison
      *   S. Robinson
           J. Smith

35. University of Manitoba
      *   L. Blomeley
      b*   J. Clark
      *   M. Froese
           K. Sharma
      *   J. Vaz

36. University of Maryland
      *   J. Shergur
      b   W. Walters
           A. Woehr

37. University of Massachusetts, Lowell
           G. Mukherjee

38. University of Milano
           A. Guglielmetti

39. University of Naples
           E. Vardaci

40. University of Padova
      *   M. Mazzocco

41. University of Surrey
      *   C. Wheldon

42. University of Vienna
           R. Golser

43. University of York
           B. Fulton

44. Universität Wien
      b   W. Kutschera

45. Università di Udine
           F. Soramel

46. Uppsala University
           K. Aleklett
      *   C. Rouki

47. Washington University
      a   R. Charity
      *   S. Komarov
           D. Sarantites
      b   L. Sobotka

48. Western Michigan University
      *   L. Undreiu
      a   A. Wuosmaa

49. Yale University
           J. Caggiano

II. OPERATION AND DEVELOPMENT OF ATLAS

OVERVIEW

Highlights of the operation of the Argonne Tandem Linear Accelerator System (ATLAS), a DOE national user facility, and related accelerator physics R&D projects are described in this chapter. ATLAS is funded for basic research in nuclear physics but also provides beams for other areas of research and development, including material science, and fusion research. In addition ATLAS has a rich program in developing the tools of accelerator mass spectroscopy (AMS) applied to wide ranging research programs such as oceanography, nuclear physics, astrophysics and geology. Over half of the beam time is allocated to experiments for which the spokesperson is an outside user. Recent ATLAS operating performance and related development projects are described in the next section. ATLAS personnel are also involved in developing technology in support of a future advanced facility, based on ATLAS technologies, for beams of short-lived nuclei. Projects related to the Rare Isotope Accelerator (RIA) Facility are described in the third section below.

Due to budgetary constraints, the ATLAS operating schedule was reduced in June 2001 from a 7 day-per-week schedule to a running schedule averaging 5 ⅓ days per week. With this reduced operating schedule ATLAS provided over 4400 hours of beam for research and provided thirty-seven different isotopic beams. Statistics about beam hours and users are given in Table II-1. Improvements in the funding are anticipated, which will allow resumption of 7-day operation in the second half of FY2003 coinciding with the reinstallation of Gammasphere at ATLAS.

ATLAS provides a range of radioactive species with intensities in the range 3×10^6 particles per second. This year 7.4% of all beam-time went to radioactive beams. Beams of long-lived species ($T_{1/2} > 2$ hours) produced at other facilities and placed in the ATLAS tandem ion source and beams of short-lived species produced in-flight by inverse-kinematics reactions have been developed at ATLAS. See the Heavy-Ion Research section for a summary of recent physics results from experiments using radioactive beams.

Table II-1. Summary of ATLAS experiments and user statistics.

	FY2002 (actual)	FY2003* (extrap.)	FY2004 (pred.)	FY2005 (pred.)
Beam Use for Research (hr)				
Nuclear Physics	3896	4550	5240	5200
Atomic Physics	0	0	00	0
Accelerator R & D	105	150	180	200
Accelerator Mass Spectroscopy	325	400	400	400
Other	90	100	100	100
Total	4416	5200	5920	5900
Number of Experiments Receiving Beam	37	45	53	53
Number of Scientists Participating in Research	123	160	200	200
Institutions Represented				
Universities (U.S.A.)	20	19	19	19
DOE National Laboratories	5	5	5	5
Other	21	27	27	27
Usage of Beam Time (%)				
In-House Staff	57	35	25	25
Universities (U.S.A.)	28	38	45	45
Other DOE National Laboratories	7	12	15	15
Other Institutions	8	15	15	15
Total	100	100	100	100

*Assumes 5-days/week operations, started June 1, 2001, continues through FY2002 and 7-day/week operation resumes in FY2003.

A. OPERATION OF THE ACCELERATOR

(R. C. Pardo, D. Barnett, J. Bogaty, A. Deriy, G. Gribbon, R. Jenkins, A. Krupa, E. Lindert, A. McCormick, S. McDonald, F. H. Munson, Jr., D. R. Phillips, D. Quock, A. Ruthenberg, R. H. Scott, S. Sharamentov, J. R. Specht, P. Strickhorn, R. C. Vondrasek, L. Weber, and G. P. Zinkann)

a.1. Operations Summary

ATLAS provided a total of 36 different isotopes for research in FY2002. The distribution of species is shown in Figure II-1. There continues to be a strong trend toward increased variety in requested beam species over past years and this year represents another new record for ATLAS in the number of isotopes provided, even during a period of reduced operating hours. Even so, ^{58}Ni continued to be the most popular beam, commanding over 25% of all beam time. Beams heavier than nickel were provided 18.9% of the time.

This year the tandem injector provided a little less than 20% of the beams for ATLAS research. This was due in large part to the seriously deteriorated condition of the tandem. At this time the corona voltage grading system is unable to operate at terminal voltages greater

than 6.5 MV. The tandem continues to be an important part of the ATLAS facility, both for operational flexibility with lighter beams and especially for its role in the long-lived radioactive beam program that continues to be an important research program. Therefore we have committed to a major upgrade of the tandem injector by replacing the corona system with an

all-resistor voltage grading system. Other improvements that are part of the project include a new terminal communication system, foil changer readout and reactivation of the terminal electrostatic quadrupole/steerer system. The schedule is to begin disassembly of the tandem corona system in June 2003 and return the tandem to operation in September 2003.
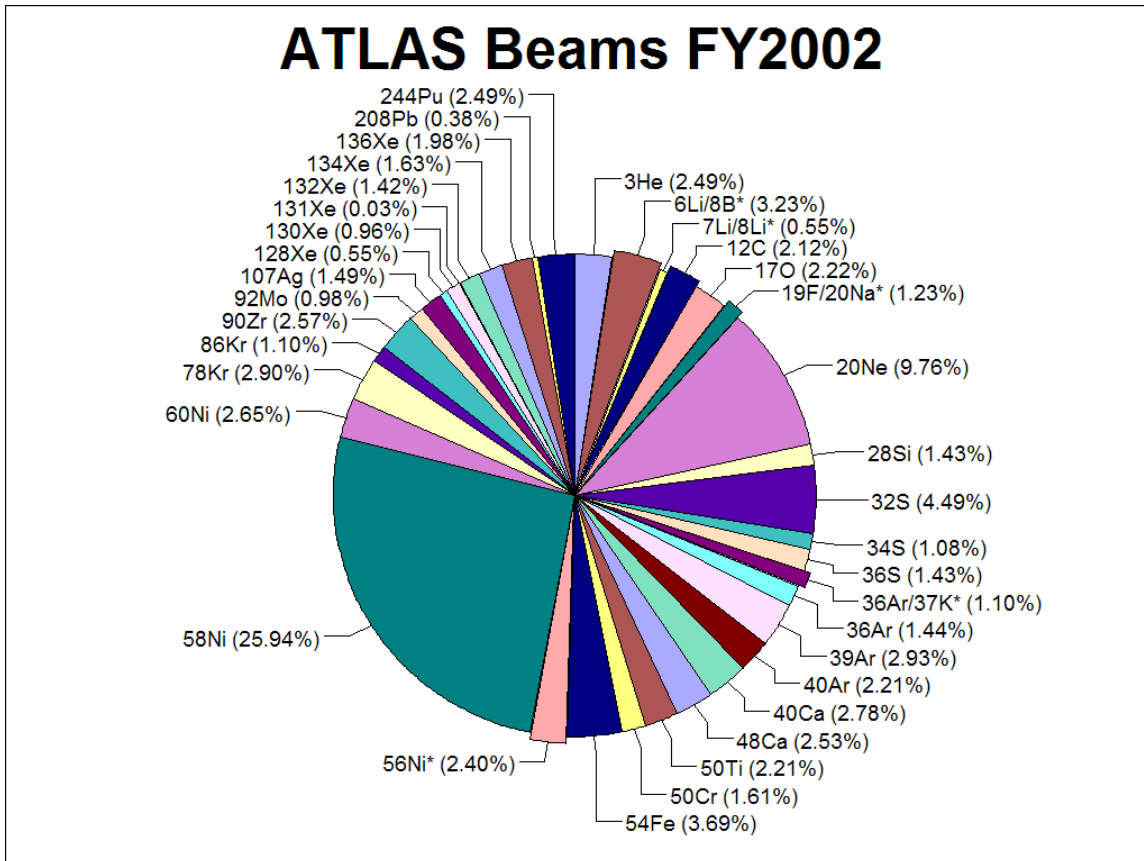
Fig. II-1. Distribution of beam time by isotope provided by ATLAS in FY2002. A total of 36 different isotopes were provided to the research program. Radioactive beams comprised 7.4% of all beam time in FY2002.

On the administrative side of operations, the facility's Safety Analysis Document (SAD) was rewritten and brought up to date. As part of the process, the facility's Safety Envelope and Operations Envelope were revised. These revisions provide us with some additional flexibility in handling higher current beams

as needed in a variety of ongoing research programs such as in-flight radioactive beam production and the search for superheavy elements. The revised SAD has been reviewed and recommended for approval by a local ad-hoc committee and has been submitted to the DOE for acceptance of the revised Safety Envelope.

B. DEVELOPMENTS RELATED TO ATLAS

b.1.   Status of the ECR Ion Sources (R. C. Vondrasek, R. H. Scott, and R. C. Pardo)

The ECR ion sources provided 27 different isotopes for the experimental program during FY2002, accounting for 82% of the beams produced at ATLAS. The increased reliance upon the ECR sources for beam production has been the impetus behind a program of upgrading the support systems of the ion sources. In addition to this work, refinement of existing techniques for material introduction into the ion source has continued.

Two development projects from last year have paid their dividends this year. The two-frequency heating implemented on ECR2 has produced a ^{238}U beam at intensities and charge states not before achieved at ATLAS. The peak usable charge state increased to 37+ with 3.0 eμA of beam. This allowed the beam to be accelerated to the coulomb barrier without the need of further stripping. In addition, the maximum intensity achieved was increased to 21.0 eμA in the 28+ charge state.

The second project was the utilization of a quartz liner on ECR2 during AMS experiments investigating ^{39}Ar. Even with the damaged hexapole bar reported last year still in place a running mode was found that allowed the first ocean samples to be measured. The quartz liner produced a reduction factor of 120 in the background ^{39}K contaminant.

The improved geometry of ECR1, realized through the rebuild in 2001, has allowed the source to operate at ever increasing magnetic field levels. This necessitated improvements in the source water-cooling system. The first step in this process was the replacement of the rotary water pump with a multi-stage centrifugal pump that delivers higher pressure and flow. In addition, the pump is constructed of materials which are highly resistant to the deionized water required by the system. This change has increased the cooling capacity of the system, but work continues on the primary side of the system to allow even more heat to be extracted.

As part of the ECR1 rebuild, the stainless steel plasma chamber was replaced with one constructed of aluminum. The change in the geometry of the chamber produced a mismatch of the RF into the chamber resulting in higher than normal reflected powers. To remedy this situation the klystron frequency was manually tuned from 10.500 GHz to 10.441 GHz producing a better match into the chamber. As a result, reflected RF power decreased from 25% of the total

forward power to < 2.0% resulting in improved source stability.

On ECR2 a dry forepump has been installed to alleviate the problem of oil contamination in the ion source system. This change from an oil to a dry forepump has reduced the carbon contamination in the source from a typical ^{12}C^{4+} background intensity of ~30 eμA to ~3.0 eμA. The reduction in carbon background has improved the source charge state performance.

As was reported last year, the ECR2 hexapole magnetic field has been slowly degrading. This degradation was initially brought on by a loss of cooling to the hexapole in 1997 and then worsened by the continued heating due to the increased plasma loss in the degraded areas. Rather than repair individual magnet bars, the decision was made to replace the entire hexapole assembly. The new hexapole will be constructed of higher grade permanent magnet material and will have a slightly different geometry. These changes will result in a 10.6% increase in the radial confining field produced by the hexapole.

A general improvement made on both sources was the installation of gas handling systems. These systems allow for a speedier change from one sample gas to another as well as a reduction in contaminants. Dry pumps are utilized to evacuate the system, and the boil-off nitrogen from the cryogenic system provides the back-fill gas.

Solid material introduction continues to be the main focus of development activities. Several new techniques have been developed for the introduction of minute quantities of sample material (~4.0 mg) as well as an increased efficiency in the sputtering process.

To improve the sputtering efficiency, the location of the sample material was shifted from the front of the target to the side. Due to the magnetic and electric field lines in the region of the sputtering process, material on the side of the sample is preferentially sputtered. This process was exploited during a ^{180}Hf AMS run when "side sputter" samples were utilized in order to reduce any possible contamination from the sputter holder itself. The geometry of the sample holder was also altered to better direct the field lines to the region where the sample material was located. Both of these changes improved the efficiency with which the sample material

was consumed by the source and helped to minimize the degradation of the sample holder.

High temperature ovens continue to be a focus for the ECR group. In the previous status report it was commented on that higher purity alumina was going to be utilized for oven construction in order to increase their operating temperature. An improvement was seen due to the new material but was not of the order to allow reliable oven operation at the temperatures required for the production of a high intensity titanium beam – which is the present goal.

b.2.   ATLAS ECR Source High-Voltage Monitoring and Control (J. M. Bogaty)

All ion species are injected into ATLAS PII Linac at the same velocity, 0.0085c. Velocity matching of our two ECR ion sources is very important so as to allow beam tunes performed with one source to be used with the other source.   To minimize retuning time and deliver the best beam quality, the replacement ion source must quickly be set up for the same total acceleration voltage.   This requires precise absolute measurement of extractor and platform voltage for both ion sources.

We presently measure and display ECR source extractor and platform voltages with 12 bit (0.024%) ADC's. Overall accuracy is certainly less than this because our commercial high voltage power supplies use standard analog amplifiers to process voltage divider signals.

Independent, high-quality commercial voltage dividers have been installed to monitor extractor voltage at both ion sources.   The dividers are sensed by precision instrumentation amplifiers developed at ATLAS. Particular attention was paid to closely matching the calibration of both ion source extractor voltage monitors. Our precision instrumentation amplifier and new high voltage dividers provide a relative measurement accuracy of 30ppm between ECRI and ECRII. Accuracy is preserved by replacing the 12 bit ADC's with 16 bit ADC's.   Similar electronic techniques have been employed to monitor platform acceleration voltages for ECRI and ECR II.

b.3.   Vibration Damper for an I-3 Interdigital Resonator (G. Zinkann, S. Sharamentov, and M. Kelly)

The last in a series of three very-low-velocity interdigital resonators was fitted with a vibration damper. The installation was completed on resonator R113, a β=0.016c cavity.   Presently in the PII section of ATLAS there are now dampers installed in a β=0.008c cavity and two β=0.016c cavities.

The construction of the last damper was modified in order to reduce the cost as compared to the previous two dampers. The tapered cylinder on the first two dampers was machined out of a solid 3"X 26" cylinder of stainless steel.   The new damper cylinder was formed from 0.125" stainless sheet. This modification lowered the construction cost by approximately $4,000.

The amount of power need for the fast tuner control is directly proportional to the fast tuner window.   The average tuning window of the fast tuners prior to installing the vibration dampers was 389 Hz. After installing the damper on the first β=.016c cavity, we were able to reduce the fast tuner window by 35%. The operation experience demonstrated that this reduction was conservative.   Under normal operating conditions, it is possible to reduce the average tuning window by as much as 50%. This would result in a 50% reduction in the power dissipated into the liquid nitrogen that cools the fast tuner system.

A new frequency vibration monitor chassis was constructed and employed in the analysis of the new damper installation.

The results for the last damper that was installed on the β=.016c resonator is shown in the Figs. II-2 and II-3.
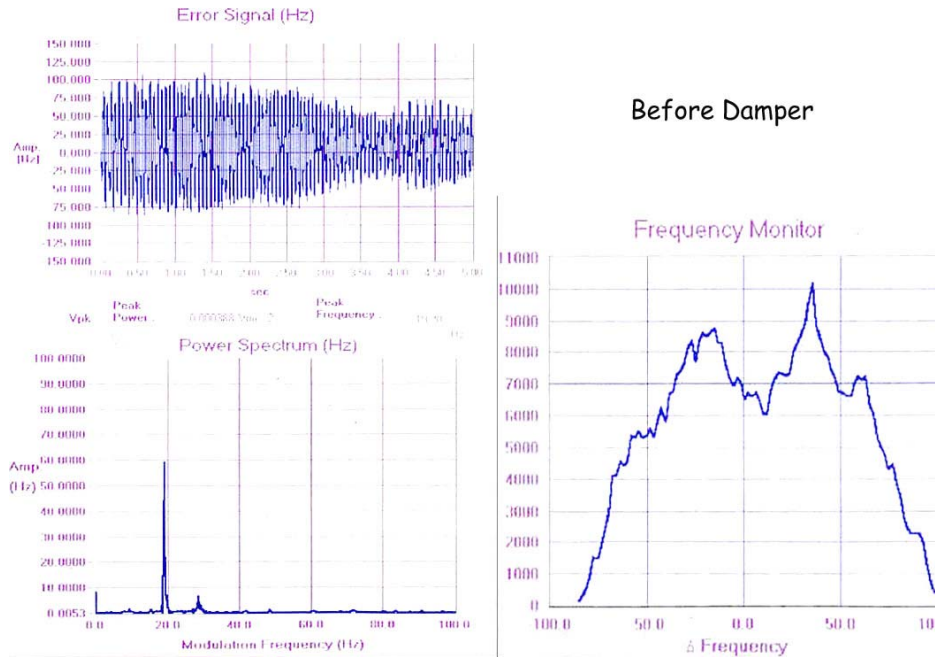
Fig. II-2. The lower right hand graph shows the distribution of the frequency deviations from the master oscillator frequency before the damper installation on R113, β=0.016c.
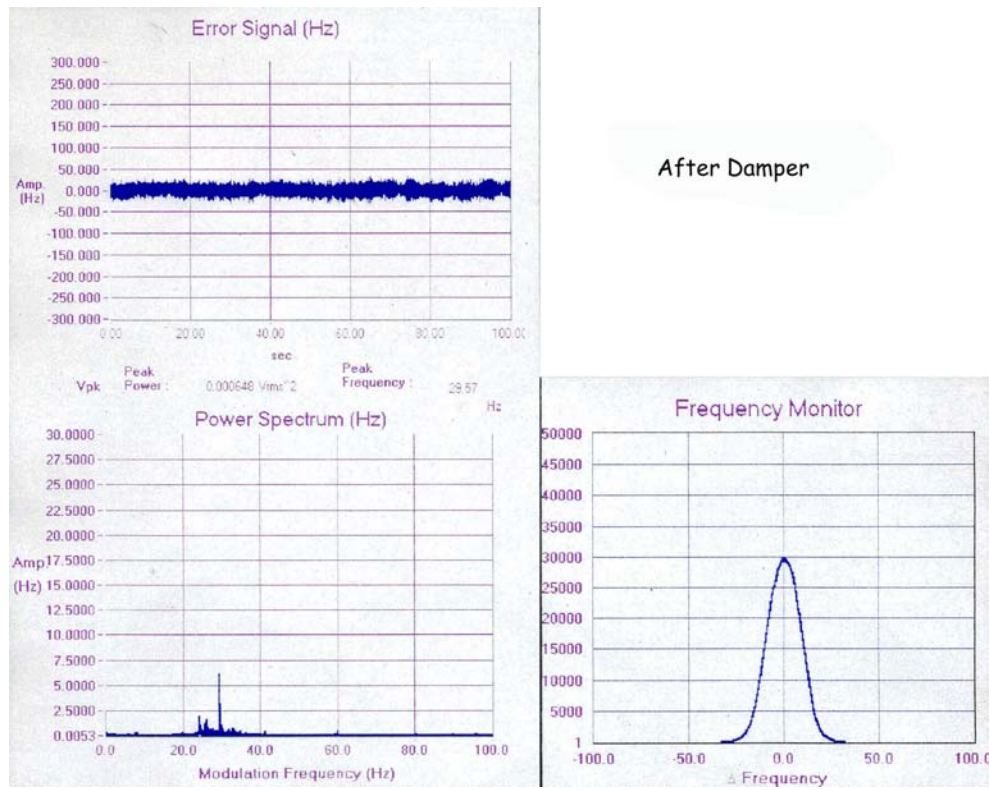
Fig. II-3. The lower right hand graph shows the distribution of the frequency deviations from the master oscillator frequency after the damper installation on R113, β=0.016c.

b.4.   Superconducting Resonator as a Beam-Induced Signal Pickup (S. Sharamentov, P. Ostroumov, B. Clifft, R. Pardo, G. Zinkann, and D. Quock)

The first demonstration of using a downstream resonator as a beam-induced RF field detector was presented in the 2001 Physics Division Annual Report. To test this concept, one of the 48 MHz RF control modules was modified and a new version of a 360^0 linear phase shifter was built to implement a *continuous phase rotation* scheme. This module along with the linear phase shifter was used for the extraction of beam-induced phase information from the pickup resonator's composite RF field. Using this hardware, a series of reference tunes were done. All of the superconducting resonators in α-cryostat were tuned for a range of ion beam species with a charge-to-mass ratio from 0.15 to 0.375. Subsequent ATLAS accelerator runs with various beam species using this library of reference tunes showed that the quality of the tunes was extremely good.

The first version of the application software, which can be used for automated beam phase measurements, was also developed. We plan to test this software after all of the α-cryostat RF control modules are modified.

b.5.   Bunch Shape Measurements in ATLAS (P. N. Ostroumov, N. E. Vinogradov, R. C. Pardo, S. I. Sharamentov, and G. P. Zinkann)

A device for the measurement of cw heavy-ion bunch time profile (or bunch shape) with resolution ~20 psec was built and installed at ATLAS in the beginning of 2002. The Bunch Shape Monitor (BSM) is based on the detection of secondary electrons produced by a primary beam hitting a tungsten wire. The bunch shape of the primary beam is transformed to a spatial distribution of low energy secondary electrons through transverse RF modulation. The modulation is achieved with a 97 MHz RF sweeper. The distribution of the secondary electrons is detected by a chevron microchannel plate detector (MCP) coupled to a phosphor screen. The signal image on the screen is measured by using a CCD camera connected to the PC.

During the last year, the BSM has been modified to provide user-friendly operation. The hardware modifications were related to the reconstruction of the HV power supply of the MCP and phosphor screen. A 90% transmission grid was installed upstream of the MCP to stop parasitic low energy secondary electrons. The BSM software based on LabView was modified for remote control and improvement of the data presentation. Complete operation of the BSM can be done from the ATLAS control room.

The BSM has been used for the measurements of various ion beam properties. As was found, the background signal observed during the first stage of BSM commissioning was originated by the primary beam halo hitting some parts of the wire holder. A careful vertical tuning completely eliminates any background signal. Figure II-4 shows typical bunch shapes for three different ion beams. Some measurements were done at a beam intensity of ~1 pnA (see Fig. II-4b). The BSM was applied for the longitudinal emittance measurements. For these measurements the very last Booster cavity was set in the bunching mode and its RF field level was varied while the bunch time profile was measured. Rms beam size was evaluated from the bunch time profile and used for a fitting procedure on the basis of beam dynamics simulation code TRACK. As a result of this procedure the graphs shown in Figure II-5 were calculated.

For some ATLAS runs a detection of the beam energy jitter is necessary and the BSM can be effectively used for this purpose and provide a resolution $\frac{\Delta W}{W} \cong 5 \cdot 10^{-4}$. The BSM is a powerful device for the measurement of longitudinal beam parameters and should be extensively used in the future RIA facility.

a)   **b)**   **c)**
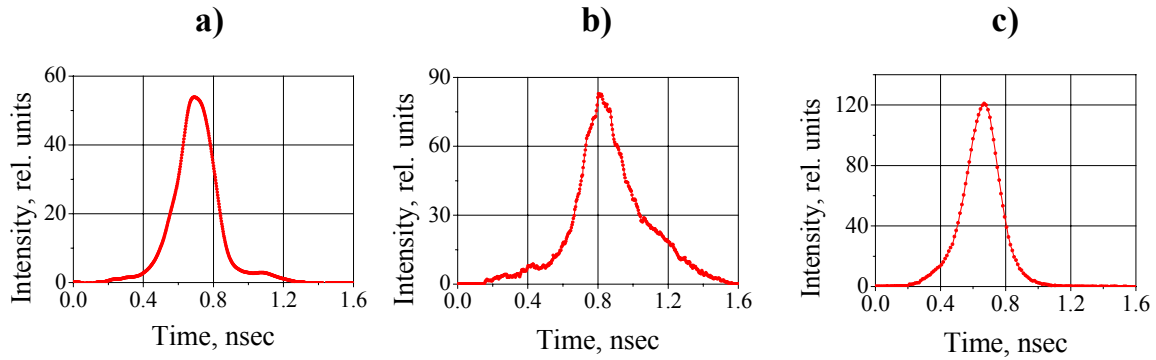
Fig. II-4. Typical bunch shapes. a) 397 MeV $^{58}Ni^{15+}$ beam, FWHM=344 psec; b) 153 MeV $^{16}O^{8+}$ beam, FWHM=315 psec; c) 185 MeV $^{54}Fe^{16+}$ beam, FWHM=215 psec.

a) 5RMS=2.8π keV/u-nsec   **b) 5RMS=3.0π keV/u-nsec**
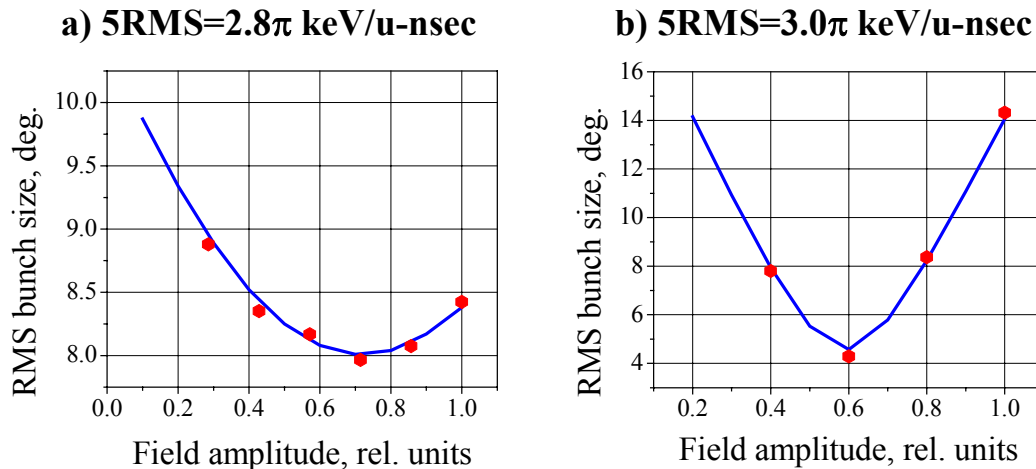
Fig. II-5. Rms bunch size as a function of the RF field amplitude in the buncher. Dots are measurements; solid curves are fitted by the TRACK code. a) 153 MeV $^{16}O^{8+}$ beam; b) 185 MeV $^{54}Fe^{16+}$ beam.

b.6.   Resonator Microphonics Monitor (S. Sharamentov and G. Zinkann)

A Frequency Vibration Monitor (FVM) chassis was built for conducting two different types of frequency stability measurement. The first type of measurement is a measurement of the mechanical stability of a super conducting resonator (SCR). For this mode, the SCR works in a phase locked loop (PLL), and the instantaneous frequency difference between a cavity feedback signal and a high-stability reference signal generator are monitored. The second type of measurement is a direct frequency deviation measurement between a test signal (for example, ATLAS master generator RF signal) and a reference RF signal. FVM utilizes the Cavity Resonance Monitor principle proposed by J. Delayen.[1] It has a frequency range from 6 MHz to 400 MHz, which covers all ATLAS and RIA RF frequencies. The sensitivity of the FVM is about 10 mV/Hz, typically.

[1]G. Davis, J. Delayen, M. Drury, T. Hiatt, C. Hovater, T. Powers, J. Preble, Proceedings of the 2001 Particle Accelerator Conference, Chicago, IL, 2001, edited by Peter Lucas (IEEE, Piscataway, NJ, 2001, p. 1152.

b.7.   **Resonator High Pressure Rinse** (G. Zinkann, M. Kelly, and R. Jenkins.)

We have continued with the High Pressure Rinse (HPR) program described in last year's annual report. Six cavities in F cryostat and four cavities in B cryostat have been rinsed. The results for the most recently rinsed cavities are shown in Figures II-6 and II-7.

The first cryostat that was rinsed in August 2001 has degraded slightly in performance. The field levels in Figure II-8 show the operating levels before the HPR, immediately after the HPR and now (March 2003).

Using the current operating field levels for C cryostat, the average operating field levels for all of the resonators that have been rinsed to date went from 2.50 MV/m before the HPR, to 3.28MV/m after the HPR.
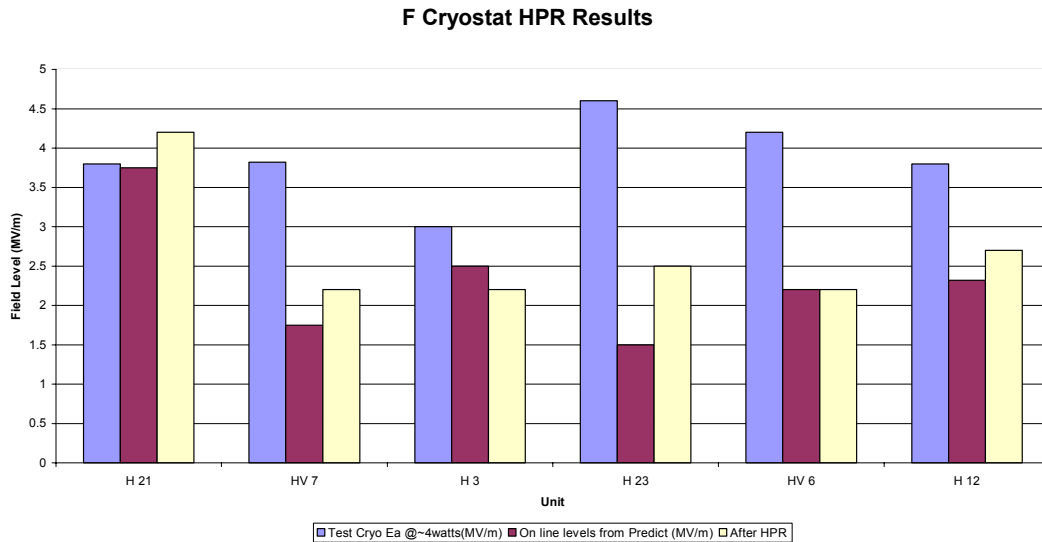
Fig. II-6. The HPR results for the six split-ring cavities in F cryostat.
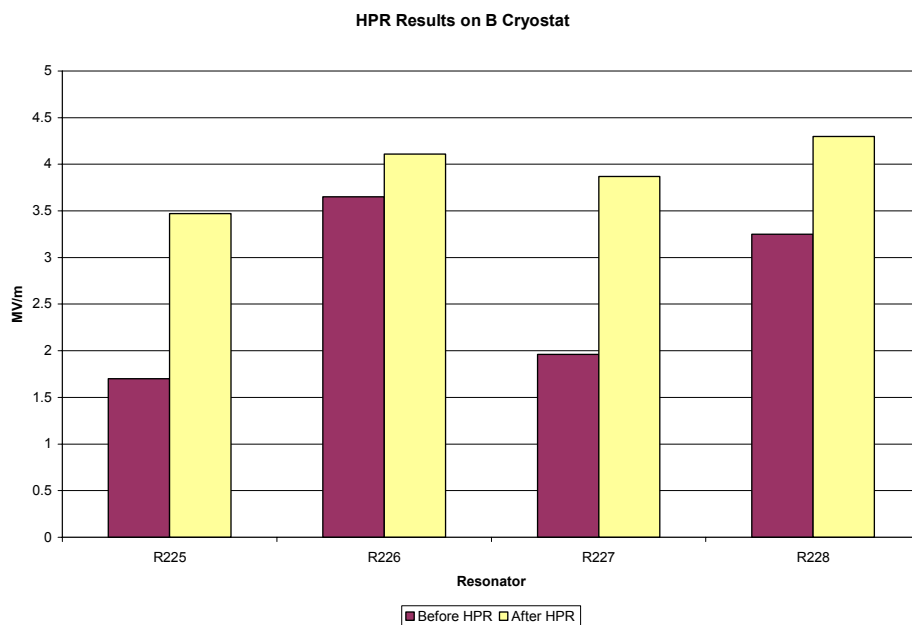
Fig. II-7. The HPR results on four cavities that were rinsed in B cryostat.

C Cryostat HPR Results
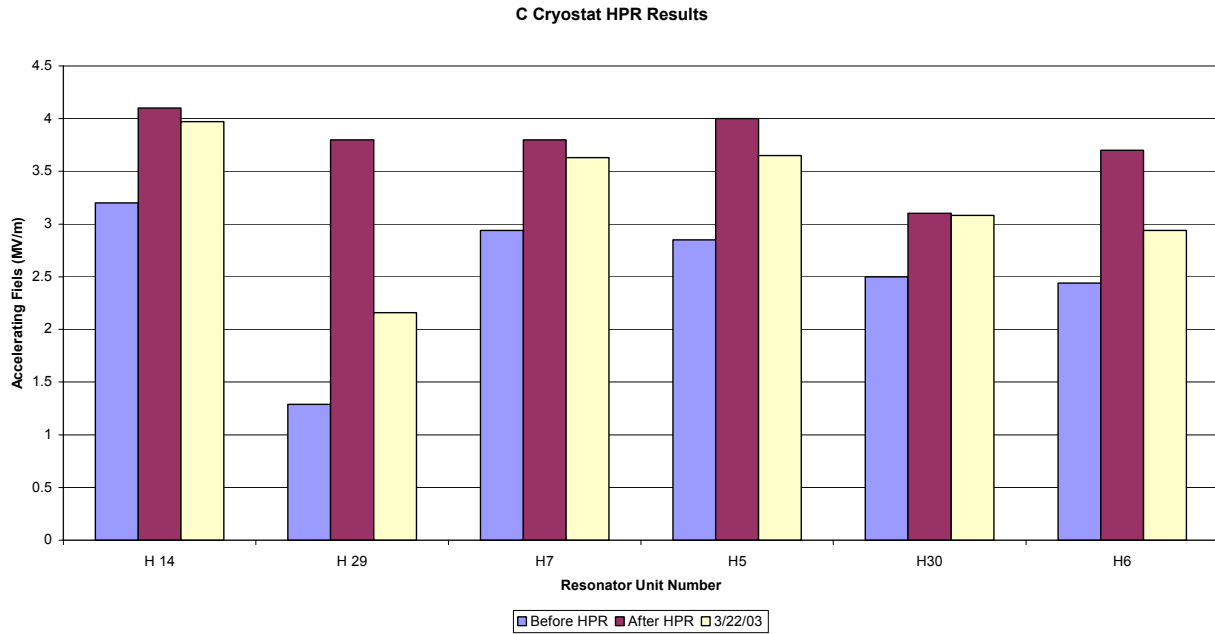
Fig. II-8. The operating field levels in C cryostat before the HPR (blue), immediately after the HPR (red) and about one and a half yeas after the HPR (tan).

b.8.   ATLAS Control System (F. H. Munson, D. Quock, and R. Enshiwat)

It is important for computer systems involved with the ATLAS control system to keep pace with commercial software upgrades and versions. The real-time portion of the ATLAS control system is based on the commercial product Vsystem marketed by Vista Control Systems. A Beta release of the newest Vsystem version (version 4.3) has been provided by the manufacturer. This version has been installed on an off-line system, and is being tested as a precursor to a future on-line installation.

Remote access to the ATLAS control system by authorized personnel is crucial for supporting operations. In the past this access has been provided by a telephone modem. With the heightened level of computer security, the laboratory has discouraged the use of telephone modems. To address this issue a new system has been installed that provides VPN (Virtual Private Network) and NAT (Network Address Translation) capabilities. These capabilities allow password protected remote access to the ATLAS control system through a secure channel, and the telephone modem has been disabled.

Several new or upgraded processes have been implemented. A new process that provides a graphical interface for controlling and monitoring a series of vacuum gauges that are associated with the ATLAS cryogenic subsystem has been made available. A new process has been installed that digitizes beam profile waveforms, and graphically reproduces the waveforms at the operator's console with the capability of archiving the data in a relational database. A new process has been made available that automatically reads a pre-determined set of Faraday cup currents with an option for archiving the data in a relational database. A new process has been implemented that enhances the capabilities of resonator module testing and data recording, which provides multiple options for data reporting and storage. The "Mass Scan" process has been updated. This new version allows the user to start multiple instances of the process, running each instance simultaneously and separately for each ion source at ATLAS. Finally, a new version of the process that measures TOF (time-of-flight) beam energies has been created. The new version makes it possible to read TOF energies in both the ATLAS exit area and Target Area 2 by detecting which target area is in use in order to use the correct detector pair combinations.

b.9.   ATLAS Cryogenic System (J. R. Specht, S. W. MacDonald, and R. C. Jenkins)

A computerized vacuum readout and control system was installed and commissioned. This system monitors all LHe and LN$_2$ distribution line vacuums via the ATLAS Vista control system. The Vista system also provides control of the vacuum gauges.

The installation of a new superconducting solenoid magnet was completed.   This system required the installation of new LN$_2$ and LHe filling systems. This magnet is used to focus radioactive beams for the experimental program.

The planning and engineering necessary for installing a surplus model 2800 LHe refrigerator obtained from LLNL was started. This 300 watt refrigerator would replace our existing 150 watt model 1600. Besides providing additional cooling, vacuum breaks would be added to the distribution system allowing increased cryogenic operating and maintenance flexibility.

Two additional He compressors were added to the existing ATLAS compressor system. These units were obtained from LLNL.   They will provide standby capability in the event of failure of any of our eight previously installed compressors. In addition they will provide the additional capacity needed when the LLNL 2800 is installed.

b.10. Selectable Power Supply and Magnet (P. Strickhorn, B. Clifft, and S. Sharamentov)

ATLAS emergency maintenance relies heavily on exact replacement spares that may be quickly swapped with a failed unit to restore operation quickly. For major magnet power supplies this philosophy is difficult to implement, but has been possible for some of our most important magnets. The ability to select between two (2) magnet power supplies and two (2) magnets (22º magnet and Michigan magnet) provides for a quick change over to an existing backup supply in case the original supply fails. This permanently wired switchover system reduces switching time between large power supplies to approximately 15 minutes versus up to 2 hours during off-shift hours. It also enhances personnel safety, since the system is hard wired, and eliminates the potential of working hot or incorrect termination when connecting the current leads.

This system consists of two power supplies, two DPDT switches, two magnets (22º magnet and Michigan magnet) and an interlock chassis. The interlock chassis is a latching interlock system and monitors which power supply and magnet are selected, display the status of each device selected along with its corresponding water flow and temperature switches, and provides an interface into the ATLAS control system.

III. R & D RELATED TO A FUTURE RARE ISOTOPE ACCELERATOR FACILITY

OVERVIEW

The Rare Isotope Accelerator (RIA), a next-generation facility for basic research in nuclear physics, is a high priority for construction in the United States by the Department of Energy. The overall concept for RIA was developed during 1999 by the ISOL Task Force, a sub-committee of the Nuclear Science Advisory Committee (NSAC). A preliminary cost analysis of the RIA project was developed jointly by Argonne National Laboratory and the National Superconducting Cyclotron Laboratory of Michigan State University. The costs were reviewed by another sub-committee of NSAC in January 2001. It is possible the Conceptual Design of RIA could begin in 2004 following the DOE Critical Decision 0 which is the Mission Need Statement for RIA. In the meantime, to prepare for construction on this time scale it is essential to continue a vigorous R&D program for RIA. This section is a progress report on the RIA R&D efforts at Argonne.

The RIA R&D topics addressed at Argonne during the year 2002 fall under four main categories: RIA Beam Dynamics, Superconducting Linac Technology, and Rare Isotope Production, Separation and Diagnostics, sections A-C below.

We continued to develop and improve the baseline design for the RIA proposal. Highlights of developments during 2002 include:

- Extensive refinements of the beam dynamics simulations and improvements to the lattice of the RIA Driver Linac including the development of an alternative baseline design using triple-spoke resonators in place of the reduced-beta elliptical resonators.
- Completion of the design and initiation of the construction of the three types of SC drift-tube resonators required for the mid-velocity regime of the RIA Driver Linac.
- Completion of a preliminary engineering design for a 57.5-MHz CW room-temperature RFQ for the front end of the RIA Driver Linac.
- Construction of a half-scale cold model of the proposed hybrid RFQ for the RIA Post Accelerator.
- Completion and initial testing of the prototype windowless liquid lithium fragmentation target.
- Development of a general 3-D Monte Carlo model for the simulation of the effusion process for radioactive isotopes from complex ISOL target/ion source configurations.

A. RIA BEAM DYNAMICS

a.1.   Beam Dynamics Studies Related To The RIA Project (P. N. Ostroumov,
V. N. Aseev, K. W. Shepard)

Beam dynamics studies were focused on the development of an end-to-end simulation code both for driver linac and post-accelerator. In addition, the overall linac design has been continuously improved by optimization of the accelerator systems.

Development of simulation code TRACK
It is important to have beam dynamics simulation code both for the cost-effective design of the RIA linacs and detailed calculations of beam parameters in the facility. The TRACK code was substantially modified during past year. Presently the code is capable of end-to-end simulations both for the driver linac and post-accelerator. The code has the following features:
- Multiparticle simulation of multiple component ion beams in six-dimensional phase space;
- 3D electromagnetic fields in rectangular mesh from the electromagnetic code Microwave Studio can be inserted into the TRACK;
- Integration of equations of motion by 4th order Runge-Kutta method;
- Fringing fields of magnets and multipoles are defined using the method of Enge coefficients;
- Realistic field distribution in solenoids;
- Misalignments of focusing elements and random errors of the electromagnetic fields are included;
- Space charge of multiple component ion beams is included;
- Regeneration of the particle distribution after the passage through stripping foils and films on the base of the SRIM code;

Currently TRACK can calculate charged-particle trajectories through the following elements:
- Any type of accelerating resonator with realistic 3D fields;
- Bending magnets with fringing fields;
- Multipoles (quadrupoles, sextupoles, …) with fringing fields;
- Solenoids with realistic field distribtions;
- RFQs;
- Multi-harmonic bunchers;
- Axial-symmetric electrostatic lenses;
- Change of electric potential (entrance/exit of a HV deck);
- Beam steering elements;
- Beam collimators;
- Stripper foils.

Front End of the driver linac
Detailed simulation of two-charge-state heavy ion beams in the Front End of the driver linac was performed. Beam distribution after the RFQ was obtained by simulation of a large number of particles ($\sim 10^5$) through the LEBT and RFQ. A strong coupling of the longitudinal and transverse motions in the beginning of the RFQ takes place. Due to the low velocity of particles in the heavy-ion RFQs the Hamiltonian of longitudinal motion depends on the amplitude of the transverse oscillations. The RFQ parameters were chosen to accept the central dense area of the initial energy-phase distribution into the separatrix corresponding to a particle moving on the axis. However, there are particles with large transverse amplitudes. These particles are captured for acceleration and have large amplitudes of longitudinal oscillations and form a halo in the longitudinal phase space. The total longitudinal emittance can significantly exceed the emittance of the central part containing 80 – 85% of particles. An obvious way to weaken the coupling between the transverse and longitudinal motions is to increase the injection energy and operate at lower frequency. Our present design addresses these issues by using 100-keV source voltage and 57.5-MHz injection frequency. The particle distribution simulated to the exit of the RFQ is used for the further beam dynamics studies in the superconducting section of the driver linac.

Electromagnetic fields of low-β SC resonators

The simulation of beam dynamics in the presence of all components of both electric and magnetic field is essential in superconducting quarter-wave resonators (SC QWR). The driver linac will use ~80 QWRs operating at 57.5 MHz and 115 MHz. Electrodynamics studies of the field distributions in the beam-cavity interaction area indicate appreciable dipole components of both electric and magnetic fields, especially for higher-frequency cavities. There is, however, another problem in QWR drift-tube design caused by quadrupole terms in the transverse Lorentz force which can cause appreciable emittance growth when the linac lattice includes transverse focusing by SC solenoids. Solenoidal focussing provides a compact lattice and maximizes transverse acceptance while maintaining low longitudinal emittance. Early SC resonator designs for accelerating heavy-ions included large diameter drift tubes to provide axial symmetry of the electric field in the beam aperture. Some recent QWR designs

eliminate the drift tube, perforating the cylindrical central stems. The reduced cylindrical symmetry around the beam axis introduces an appreciable quadrupole component of transverse rf field. Detailed analysis shows that the transverse effect of electric field in the accelerating gap can be represented as a sum of axially symmetric and quadrupole lenses. Rf field properties of several geometries of QWR and Half Wave Resonators (HWR) and the impact of field asymmetries on beam quality were studied by computer simulations of beam dynamics in realistic three-dimensional electromagnetic fields. Beam parameters were analyzed for several typical examples of accelerating-focusing lattice. We found that beam steering due to the dipole component of the rf field and emittance growth due to the quadrupole field component in the aperture can be largely avoided by the appropriate design of the SC resonators.

Focusing lattice design in sc linacs

In SC linacs, focusing elements alternate with accelerating cavities. In the design of the periodic focusing lattice of the SC linac, several important issues should be taken into account. Standard criteria such as stability of the transverse motion and maximum possible acceptance certainly should be applied. In SC linacs, due to the high accelerating gradients available from SC cavities and the relatively long focusing periods, strong interactions between transverse and longitudinal motion may occur. Long focusing periods containing several cavities per period decrease the cost of the accelerator. However, in some lattice designs, the transverse-longitudinal coupling can excite a parametric resonance of transverse oscillations. The condition for parametric resonances of transverse motion is fulfilled if the frequency of transverse oscillations is equal to a half-integer number of the frequency of longitudinal oscillations. This type of resonance condition can be a limiting factor to the total

voltage provided by a SC cavity, especially in the low-velocity section of SC linacs.

In the design of SC linacs, parametric resonances in transverse motion must be identified and avoided. The transverse emittance growth of the beam is more pronounced for larger longitudinal emittances. The parametric resonance can result in the formation of beam halo in transverse phase space if appropriate measures are not applied. In the RIA driver linac baseline design, a transverse phase advance in the range 60°-80° is recommended for the DTL. A transverse phase advance close to 90° is preferable in the elliptical cavity section. The results are valid for the selected lengths of the focusing periods of the RIA driver linac. Similar analysis techniques should be applied for different structures of the focusing period in SC linacs.

Stripper sections

In order to avoid beam losses in the high-energy section of the Driver Linac, the low-intensity unwanted charge states must be carefully separated and dumped. As long as the driver linac is designed for acceleration of multi-q beams, the beam transport system following the stripping foil must provide simultaneous matching of selected charge states to the six-dimensional acceptance

of the following SRF linac. This magnetic transport system (MTS) requires dipole magnets and a rebuncher in order to provide a proper transformation of the 6-dimensional beam emittance. The system has a dispersive area, effectively operating as a spectrometer. In the region of maximum dispersion, the unwanted charge states are removed by horizontal beam

collimation. We designed such systems for both stripping areas. We studied higher-order effects on the multi-q effective emittance in the MTS. Four sextupoles located in dispersive areas of the MTS were implemented in order to correct higher-order effects. The code COSY was applied for higher-order optimization of the MTS. To minimize the transverse emittance growth the beam is focused to the spot of 2-mm diameter at the location of the stripper. Final verification and optimisation has been carried out by the help of TRACK code. Careful optimization allows us to avoid any emittance growth of the multi-q beam transporting through the MTS.

Design of the high-β section of the driver linac using triple-spoke cavities

Spoke-loaded cavities offer several advantages compared with the higher frequency elliptical cavities that were proposed for this range of particle velocities. For example, the triple-spoke cavities can provide operation at 4.5 K, broader 'velocity acceptance' of the transit-time factor (TTF), more accelerating voltage per cavity, and, in the RIA application, provide 'beam-loss-free' acceleration. A detailed comparative study of the beam dynamics in the elliptical cavity linac (ECL) operating at 805 MHz and in the triple-spoke cavity linac (TSCL) operating at 345 MHz for the application in high-β section of the RIA driver linac was carried out. In the case of ECL the frequency jump results in lower longitudinal acceptance as an consequence of abrupt reduction of the phase width of the stable area in longitudinal phase space. In addition, due to the narrow 'velocity acceptance', the energy acceptance of the separatrix is low as well. Figure III-1 shows longitudinal acceptances for ECL and TSCL at the injection energy 81 MeV/u for $^{238}U^{89+}$ ion beam. Beam dynamics simulation included a careful design of the accelerating-focusing lattice of both ECL and TSCL linacs, the effect of carbon stripper with the thickness of 15 mg/cm^2 on the particle distribution and random errors of accelerating fields. The simulations show that the TSCL linac has a wide margin in energy acceptance to avoid any particle losses in the high-β section of the driver linac.
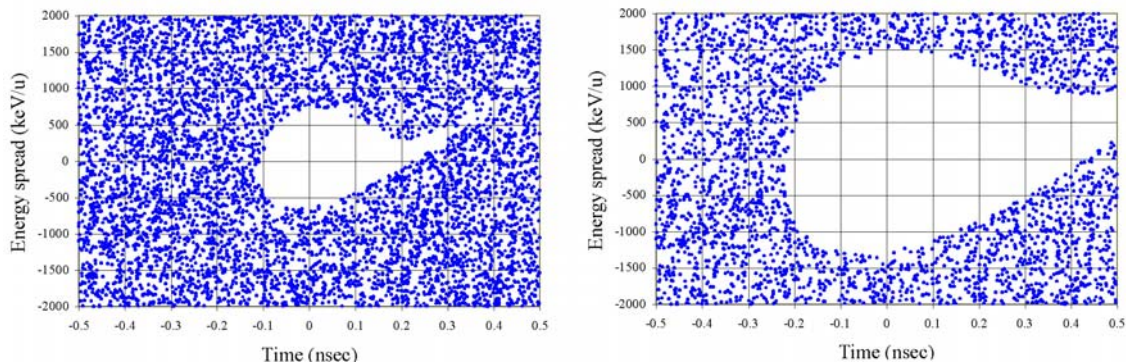
Figure III-1. Longitudinal acceptance of 805-MHz ECL (left) and 345-MHz (right) TSCL linacs shown in the same scale.

Beam dynamics in the post-accelerator

The section of the Radioactive Ion Beam (RIB) linac after the carbon stripper was conceptually designed for the acceleration of multiple-charge-state beams to enhance the available beam intensities for experiments. As was shown, a wide range of the charge spread Δq/q, about 20%, can be accepted and accelerated in the ATLAS accelerator. For the future RIB acceleration in ATLAS, we restricted the possible range of Δq/q to ≤11% in order to avoid emittance halo in the phase space. As a consequence of multiple-charge-state acceleration the total stripping efficiency is significantly higher than for the single charge-state beams, as can be seen in Fig. III-2. The RIB linac of the RIA Facility will produce beam intensities more than an order of magnitude higher than post-accelerators based on an ECR charge breeder. However, the transverse and longitudinal emittances of multi-q beams will be larger by a factor of ~3 as shown by beam measurements in ATLAS. ATLAS will require modifications of the bend regions for the effective acceleration of multi-q radioactive beams.
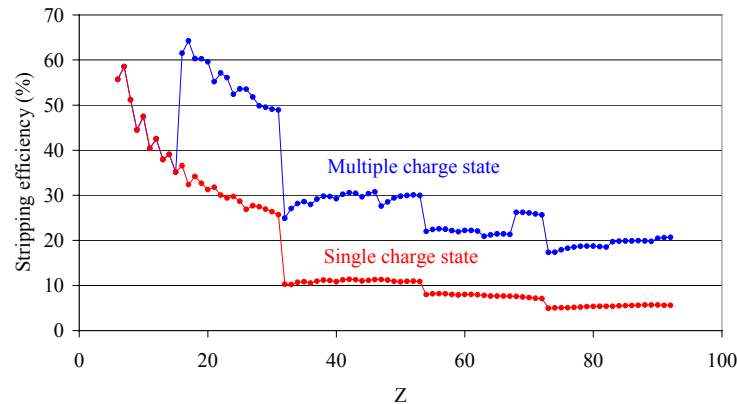
Figure III-2. RIB linac overall stripping efficiency in the regime of single and multiple charge state beam acceleration.

a.2.   **Beam DynamIcs Optimization in the Driver Linac: Current Developments**
         (E. Lessner and P. Ostroumov)

Use of multiple-charge states impose strict requirements on the steering procedure to avoid effective emittance growth. A program of detailed beam dynamics studies was initiated to simplify the accelerator design, enhance its performance, and develop specifications for the engineering design of the accelerator systems. As part of the program, two research items are being investigated:

- Development of a new fitting code based on realistic field distributions in solenoid magnets.
- Development of steering methods and algorithms with realistic solenoid- field distributions. Refinement of steering methods that utilize combined-field solenoids including dipole coils.

1.   Beam matching in the focusing lattice must be done with realistic field distributions in the solenoids Existing fitting codes do not include realistic field distributions in solenoids. Preliminary calculations of the matched beam parameters are based on fitting codes like TRACE. This code is based on transport matrices and assumes "rectangular" distribution of the magnetic field in solenoids. The simulation code TRACK can represent solenoids as a "matrix" or can integrate particle motion through the solenoid using realistic field distributions. We found significant differences between the TRACE fitting and TRACK in the low-energy section. We are developing a fitting code that includes 3D field distributions. One of the new optimization code features is the calculation of the defocusing effects for every cell of the SC RF cavities, especially important in the low-energy section of the linac.

2.   Frequent steering correction of multiple-charge-state beams is extremely important to avoid effective emittance growth. Several correction schemes are being studied. One scheme is the standard correction technique whereby the trajectory is minimized at the Beam Position Monitors (BPM). Another algorithm is based on the beam-based alignment technique whereby trajectory information from two or more different focusing configurations is used to correct component misalignments. Previously, we had proposed to develop combined-field solenoids that incorporate dipole steering coils. Preliminary studies showed that the steering coils do not produce non-linear effects on the beam. Additional studies will be done to design a correction algorithm that takes into account the actual beam rotation in the solenoid, which couples the horizontal and vertical beam motions, and to develop effective steering procedures of multiple-charge-state beams in the transverse phase space.

a.3.   Effects of Single Errors on the Prestripper Lontgitudinal Emmittance
(E. Lessner and P. Ostroumov)

A comprehensive study of partial effects of accelerating field random errors on the longitudinal beam parameters in the prestripper was performed using the code "elegant" *as an independent evaluation* ofthe prestripper linac beam dynamics simulations performed with the code TRACKL.   "elegant"[1] wasoriginally written to simulate electrons and was modified for simulation of two-charge state ion beams. In order to emulate heavy-ion dynamics, the electromagnetic fields and magnet component stranagths were mapaped such that:

$$E_e/(q_{HI}E_{HI}) = -m_e/(A_{HI} \text{ a.m.u.}),$$

where E_e and E_{HI} stand for the electron- and ion- field strengths, respectively; m_e is the electron mass, and A_{HI} is the ion atomic mass. Since space charge effects are negligible in the prestripper linac, simulation of a two-charge-state beam can be done sequentially, each equivalent electron bunch accelerated by fields whose strengths are given by the above mapping. The simulation results were then transformed back to heavy-ion parameters.

Table III-1. 4rms emittance at the end of the prestripper linac under single random errors.

[1]Phase Error (degrees)	4 RMS Emittance (π keV/u-ns) Calculated Average over 200 Seeds	4RMS Emittance (π keV/u-ns) Calculated Average over 200 Seeds
0.3	2.17	2.23
0.6	2.36	2.51
0.9	2.70	2.93
Field Strength Error)%)		
0.3	2.18	2.22
0.6	2.34	2.47
0.9	2.66	2.87

---

[1]M. Borland, "elegant: A Flexible SDDS-Compliant Code for Accelerator Simulation," APS-LS-287, http://www.aps.anl.gov/techpub/Isnotes/Is287.pdf

Random rf phase errors and field strength errors for the two-charge state 28^+ and 29^+ of uranium beam were simulated at three error levels and for 200 distinct seeds. Table I shows the 4rms emittance at the end of the prestripper linac resulting from each error type. Figures.III-3 and III-4 show the accumulated longitudinal emittance versus error strengths, and the histogram of the emittance growth factor for 0.9% rms field strength error, respectively.
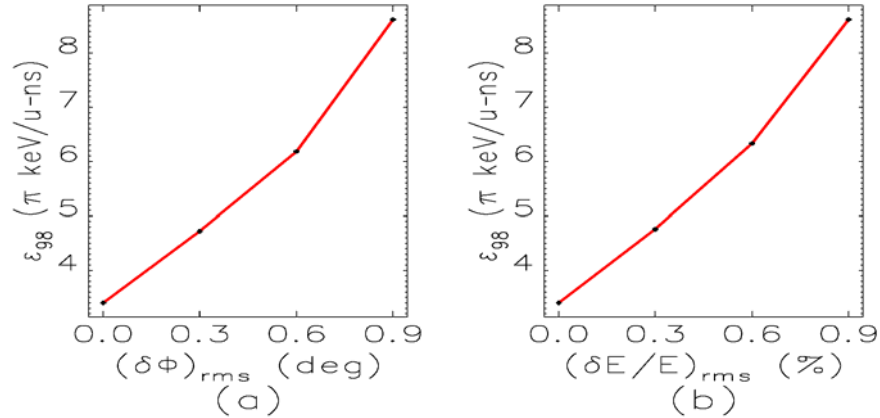
Figure III-3. Accumulated longitudinal emittance versus rf phase fluctuations (a) and accelerating field strength fluctuations (b). ε_{98} represents the superposition of the phase space areas at the exit of the prestripper linac, from which the distributions with the four largest areas were eliminated. The ε_{98} emittance, resulting from phase or field errors at the largest level, is of the order of 9 keV/u-nsec.

There were no particle losses at 0.9 ° rms phase error or at 0.9% rms strength error. The final distributions were well within the longitudinal acceptance of the low-β SRF linac.
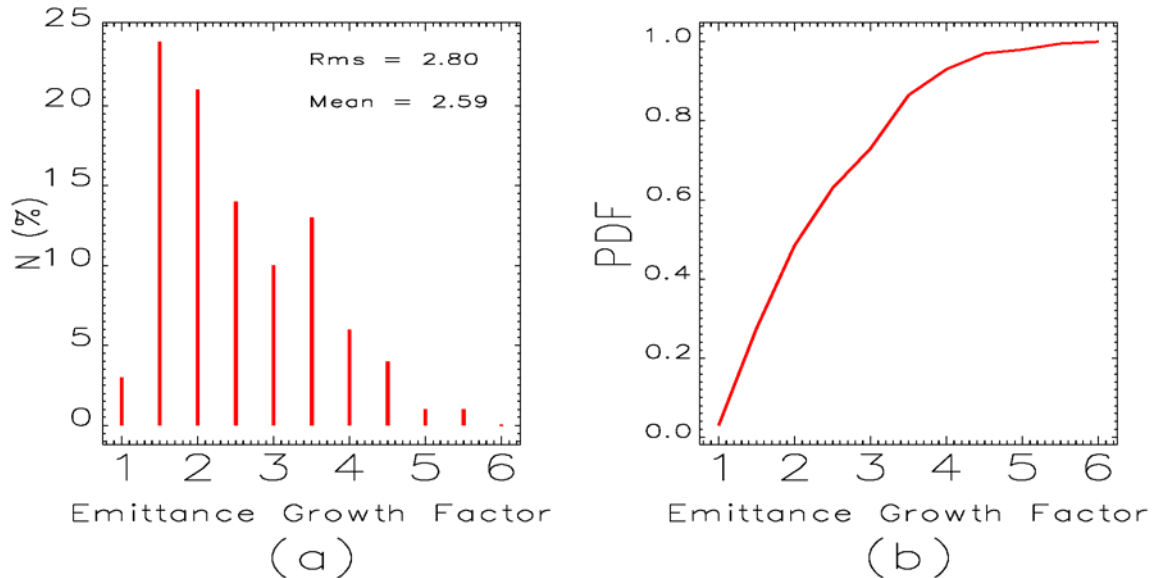
Figure III-4. Histogram (a) over 200 simulations of the emittance growth factor, defined as the ratio of the initial and final emittances for the 200 simulations, for 0.9% rms field strength errors, and the corresponding probability function (b). The frequencies are expressed in terms of the percentages of simulations resulting in the emittance values indicated. As can be seen, there is 98% probability that the emittance growth factor be less than 6.4.

a.4. A New Generation of Superconducting Solenoids for Heavy-ion Linac Applications (P.N. Ostroumov, S. H. Kim[*], E. S. Lessner, K. W. Shepard, R. E. Laxdal,[†] and R. Wheatley[‡])

For low- to medium-energy beams, drift spaces between accelerator components can cause effective emittance growth. An assembly of steering coils mounted on focusing solenoids is proposed that reduces drift spaces between resonators. Preliminary design studies were conducted on a 9-Tesla magnet (see Fig. III-5) to determine the feasibility of achieving high field, low fringe field, and integral dipole field, into one compact package. The assembly, including terminals, switches, and protection circuit, are designed to fit inside a 25-cm diameter helium reservoir and its overall length is 28 cm.

The bucking coils are sufficiently strong to minimize the stray field at distances greater then the physical length of the solenoid. The coils produce a low field region of less than 0.1 Tesla between 15 and 18 cm from the magnet centre. The geometrical configuration of the steering coil (see Fig. III-6) can be saddle-shaped, racetrack or circular (ring-shaped).
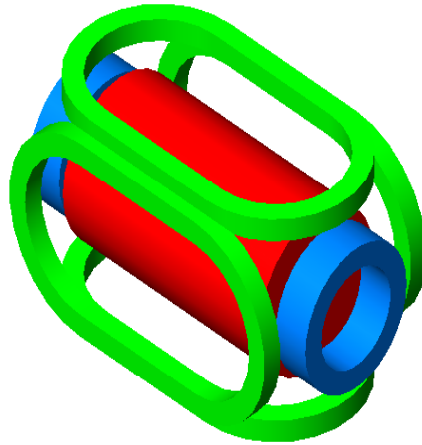
Figure III-5. Magnet assembly, showing solenoid, bucking coils, and racetrack steering dipole coils. The dipole coils generate 0.2 Tesla on the horizontal and vertical axes.

Parameters for the Racetrack Coil

Straight Section (cm)	12
Total Length (cm)	28
Coil Diameter and Vertical Separation (cm)	14.8
Central Magnetic Field (T)	0.2 @ 31.7 kA
Field Integral on the Beam Axis (T-mm)	47.2
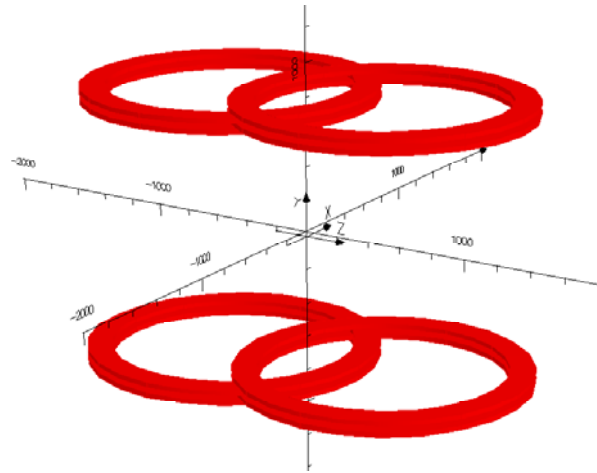
Figure III-6: Optional four-ring coil configuration with a radius of 7.7 cm and an overlap of 5.4 cm.

The steering coils can introduce non-linear effects on the beam dynamics. Numerical simulations were performed with the tracking code TRACK to determine the beam response to the realistic (3-D) magnetic field distributions including the steering coils. The steering algorithm corrects the horizontal and vertical beam slopes, x'_0 and y'_0, but not the beam displacements. For slope correction, both the horizontal and vertical slopes, as well as the beam-centre displacements, must be measured at the entrance of the solenoid/dipole assembly, due to the beam axial rotation in the solenoid (see Fig. III-7). The steering-field strength is set to the strength necessary to correct the beam slope calculated at the end of the solenoid with the dipole current turned off. Results are from simulations on the first part of the medium-β section of the SC driver linac, downstream of the first stripper.
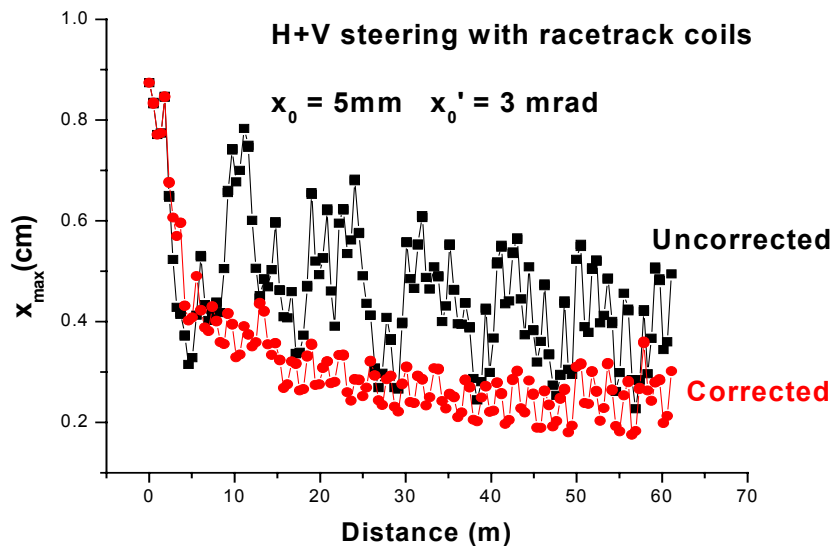
Figure III-7. Horizontal envelope for the five-charge-state uranium beam, before and after steering correction. 20,000 macro particles were used in the simulations.

∗XFD, ANL
†TRIUMF, Vancouver, B.C. V6T 2A3, Canada
‡American Magnetics Inc., Oak Ridge, TN 37831-250

Summary of the Normalized Transverse Emittance in the Horizontal Plane at the Entrance and Exit of the Lattice

Beam	One-charge-state		Five-charge-state	
Emittance (cm-mrad)	4-rms	Total	4-rms	Total
No Error (a) (b)	0.0593 0.0599	0.1145 0.1161	0.0593 0.0601	0.1145 0.1332
Uncorrected Error	0.0593 0.0597	0.1145 0.1175	0.0593 0.3633	0.1145 0.6906
Corrected Error	0.0593 0.0597	0.1145 0.1161	0.0593 0.0761	0.1145 0.2077

Initial Value   (b) Final   Value

The emittance growth for the corrected five-charge-state beam comes from the multiplicity of charge states (see Fig. III-8). The steering coils do not produce non-linear effects on the beam. The beam distortions are negligible and well within the large lattice aperture of 3.0 cm.   Further studies will include the solenoid-induced coupling in the steering algorithm.
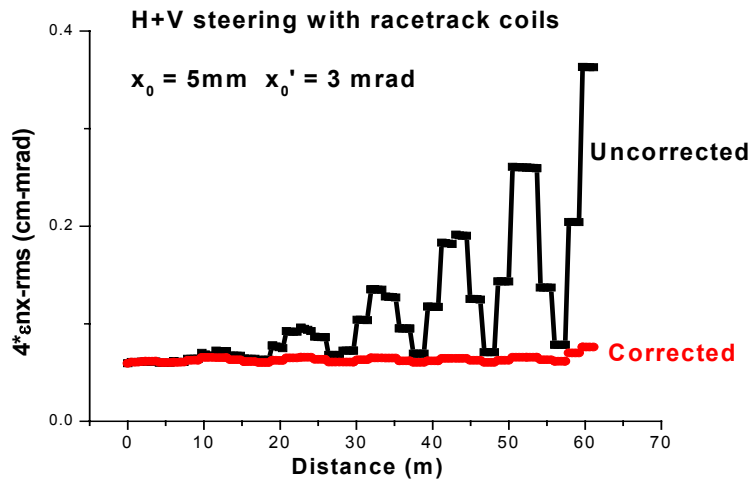
Figure III-8. 4-εn-rms emittance for the five-charge-state uranium beam. After correction, the emittance is reduced by a factor of three.

B. HEAVY-ION LINAC TECHNOLOGY

b.1. Prototype Quarter-Wave and Half-Wave Drift-Tube Resonators (K. W. Shepard, M. Kelly, J. Fuerst, and M. Kedzie)

Prototype construction was started for two types of drift-tube cavity which will be initially used to upgrade the existing ATLAS linac. The cavities are a 109-MHz QWR cavity and a 170-MHz half-wave resonant cavity which together can provide useful acceleration over a velocity range of 0.12 < v/c < 0.5. Figure III-9 shows cutaway views of the two cavities, which are approximately one meter in vertical extent. Both cavities are contained in an integral, stainless-steel helium vessel. Construction of both cavities is expected to be complete in FY2003.
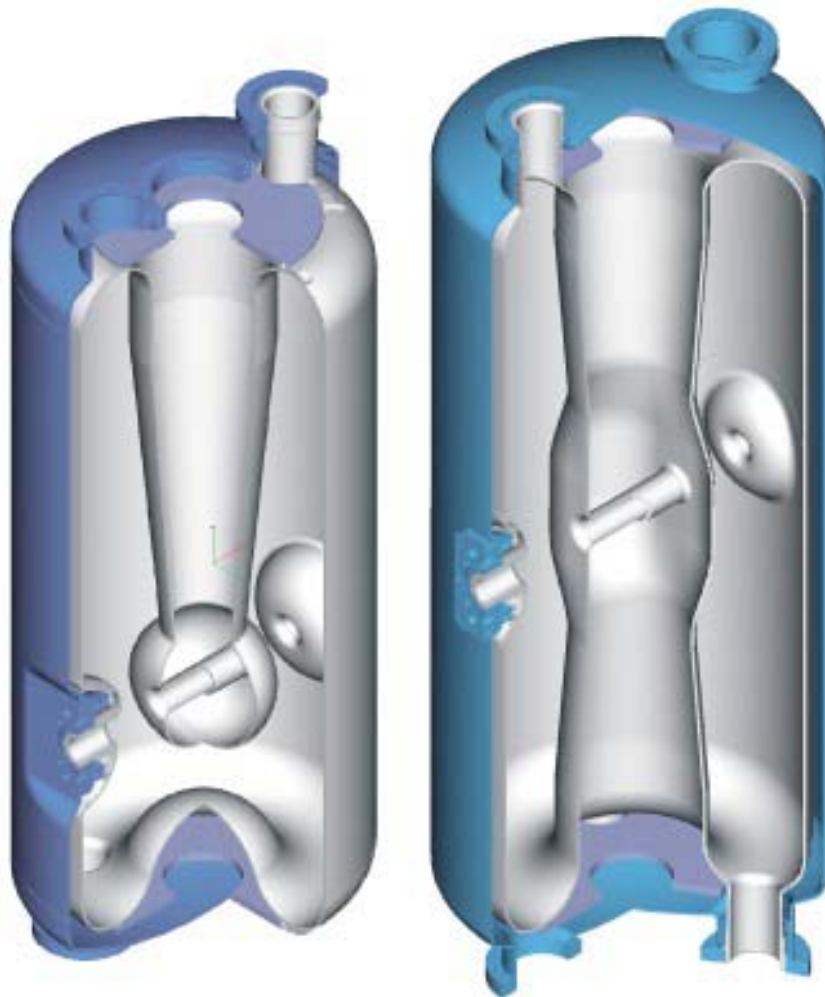
Figure III-9. Cutaway views of the quarter-wave and half-wave cavities showing both the niobium cavity shell and the integral stainless-steel outer helium vessel.

b.2. Prototype Cryomodule for Drift-Tube Resonators (K. W. Shepard, M. Kelly, J. Fuerst, and M. Kedzie)

Design of a prototype cryomodule for the above cavities is well-advanced.   The cryomodule will provide separate vacuum systems for cavity (beam) and cryogenic vacuum.   This will enable clean-room assembly of cavities, beam-line elements, and rf couplers, as detailed in Figure III-10. The end walls of the vacuum vessel are chamfered in the middle to allow room-temperature, low-particulate beam-line vacuum valves which seal and isolate the cavity-string assembly, to insert through the cryomodule vacuum wall.
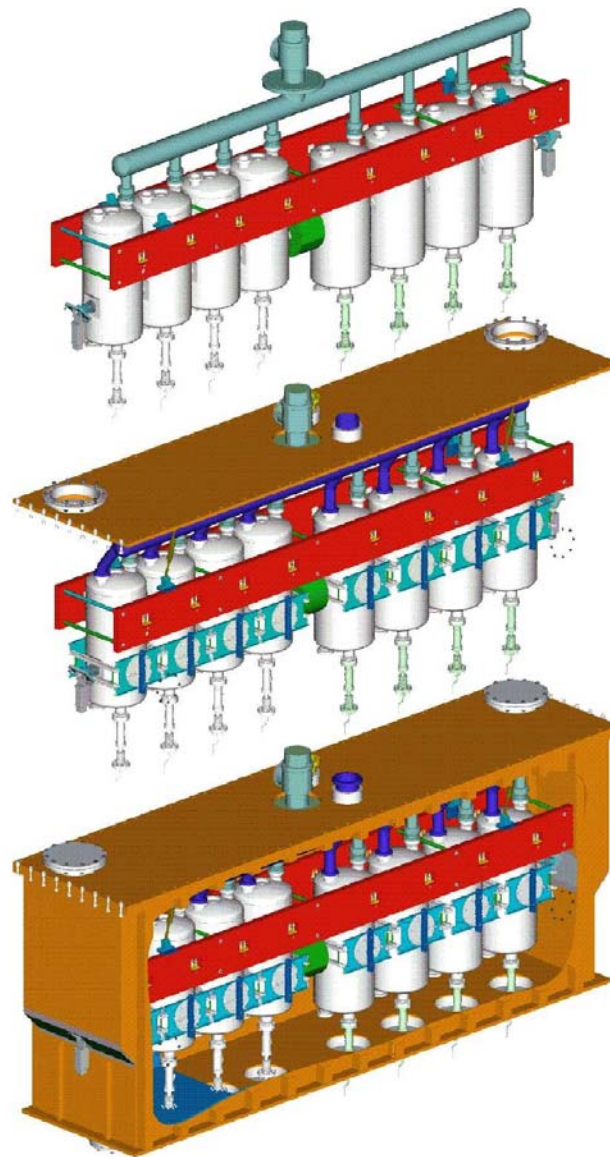
Figure III-10. Cryomodule assembly sequence. (Top) clean-room assembly of cavity string includes cavity and beam line vacuum and couplers. (Middle) Top flange assembly includes cryogenic systems. (Bottom) Completed cryomodule.

b.3. Prototype Double-Spoke Resonator (K. W. Shepard, M. Kelly, J. Fuerst, and M. Kedzie)

Construction of a prototype 2-spoke loaded 345-MHz superconducting cavity is nearing completion. The 3-cm aperture cavity, shown in Fig. III-11, has a useful stance of a multi-cell spoke cavity, and continues the development of spoke cavities that began with 350-MHz single-spoke cavities.of =0.29 and =0.4

successfully tested at ANL previously. The niobium elements of the cavity assembly are shown in Fig III-12, just prior to the closure welds that join the end-caps to the central, spoke-loaded section. Electromagnetic parameters for the two-spoke cavity are listed in Table III-2.
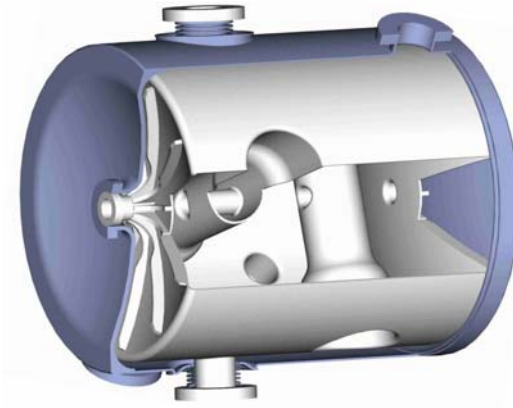
Figure III-11. Cut away view of a 345-MHz two-cell spoke cavity. The niobium housing diameter is 48 cm and the active length is 39 cm.
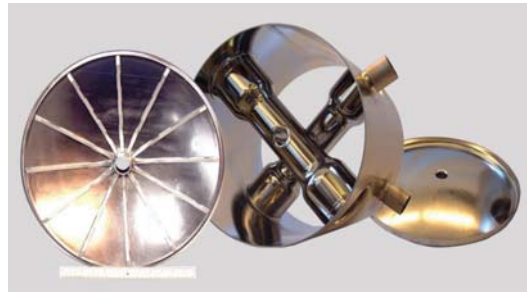
Figure III-12. Three pieces of the two-cell spoke cavity after receiving a heavy electropolish.

Table III-2. RF parameters for the β=0.4 two-cell spoke-loaded cavity.

frequency	347.072 MHz
Active Length =	-
$\beta_{Geom} =$	0.393
$QR_S =$	71
$U_o^* =$	151 mJ
$E^*_{peak} =$	3.47 MV/m
$B^*_{peak} =$	69 G

b.4. Hybrid RFQ Cold Model (P. N. Ostroumov, A. Barcikowski, B. Rusthoven, S. Sharma, N. E. Vinogradov, and G. Zinkann)

The Hybrid Radio Frequency Quadrupole (H-RFQ) is an accelerating structure designed to accelerate low-velocity heavy ions with a q/A ratio = 1/240. The unique design of this low-frequency (12.125MHz), low-velocity accelerating structure enables it to be used as an efficient front end injector for a RIB linac. The H-RFQ structure consists of 3 sections of drift tubes and 2 RFQ sections. In the drift tubes sections the beam is accelerated and defocused transversely. Transverse focusing is provided by the RFQ sections. Each of the RFQ sections consists of two sets of non-modulated vanes with a length βλ separated by a drift space βλ/2. The appropriate focusing strength is achieved by adjusting the distance between the vanes. Using the combination of the drift tube and RFQ structures, a factor of two higher output beam energy, as compared to a regular RFQ accelerator, is achieved.

A half-scale (24.25MHz) aluminum cold model of the Hybrid RFQ was designed, built and tested. The goals were to determine the final resonator dimensions, accelerating and focusing field distribution, quality factor and coupling to the external power supply. First, a numerical simulation of the cold model's electrodynamic parameters was done using MWS code. The numerical simulation of this complicated structure had some difficulties. The size of the drift tube gaps and the RFQ vane spacing is very small compared to the overall dimensions of the cavity. This difference required a very large number of mesh cells for the simulation which resulted in unacceptable calculation time and the solution was non-convergent. To rectify this, some simplification of the shape of the structure had to be implemented. Even for $\sim 2 \cdot 10^6$ mesh points, just a few cells for each drift tube and only one cell for each RFQ gap were simulated. The result is an estimate rather than a precise calculation of the electrodynamic parameters. With this estimate frequency error in the simulation was expected. The frequency tuners which are used in the real model were not considered in the MWS model due to the same problem. Therefore, the designed resonator dimensions needed experimental testing and the aluminum cold model of the H-RFQ (Fig. III-13) was built.

The experimental investigation of the 24.25 MHz H-RFQ cold model was carried out using both an HP Network Analyzer and standard bead-pull technique using a phase-lock-loop. The first measurements of the electrodynamics parameters of the cavity revealed three important shortcomings of the cold model. These are: the measured quality factor turned out to be 3.5 times lower than the calculated value, the frequency was approximately 2 MHz high, and there was a tilt in the field amplitude distribution of the third drift tube section. The Q error can be explained by a poor rf contact between the vertical stems and the moveable plates of the frequency tuners. The low precision of the MWS simulation was considered as the reason for the other drawbacks.

The sliding rf contacts of the model were provided by a special spring rf gasket. The gasket material was purchased at Bal Seal Engineering. We observed that the Q of the cavity varied by factors of two when these sliding tuners were adjusted. It was realized that the contacts were at fault. A stronger spring material from the same firm was used to improve the rf contact. In conjunction with the stronger gasket material, special conductive silver grease, supplied by Tecknit, was employed. After these modifications were made, the measured quality factor was stable and was about 70% of the calculated value. Table III-3 summarizes this result.

To improve the resonant frequency, the dimensions of the H-RFQ model were changed. Cylindrical insertions to lengthen the vertical stubs of the cavity were designed and installed to lower the eigenfrequency. After this modification the resonant frequency was close to the expected value as is seen from Table III-3.

To improve the final problem of the field distribution tilt (Fig. III-14), capacitive tuners were installed at the required locations. These tuners removed the field tilt in the end of the third drift tube section.

The main goals for the near future are to make the field distribution uniform all along the structure axis and to measure the transverse field distribution in the focusing RFQ sections.

Table III-3. Resonator parameters.

	MWS simulations	Before cavity modification	After cavity modification
Quality factor	4701	1350 - 2300	3360
Resonant frequency	24.65 MHz	26.5 MHz	24.25 MHz

Cylindrical insertions
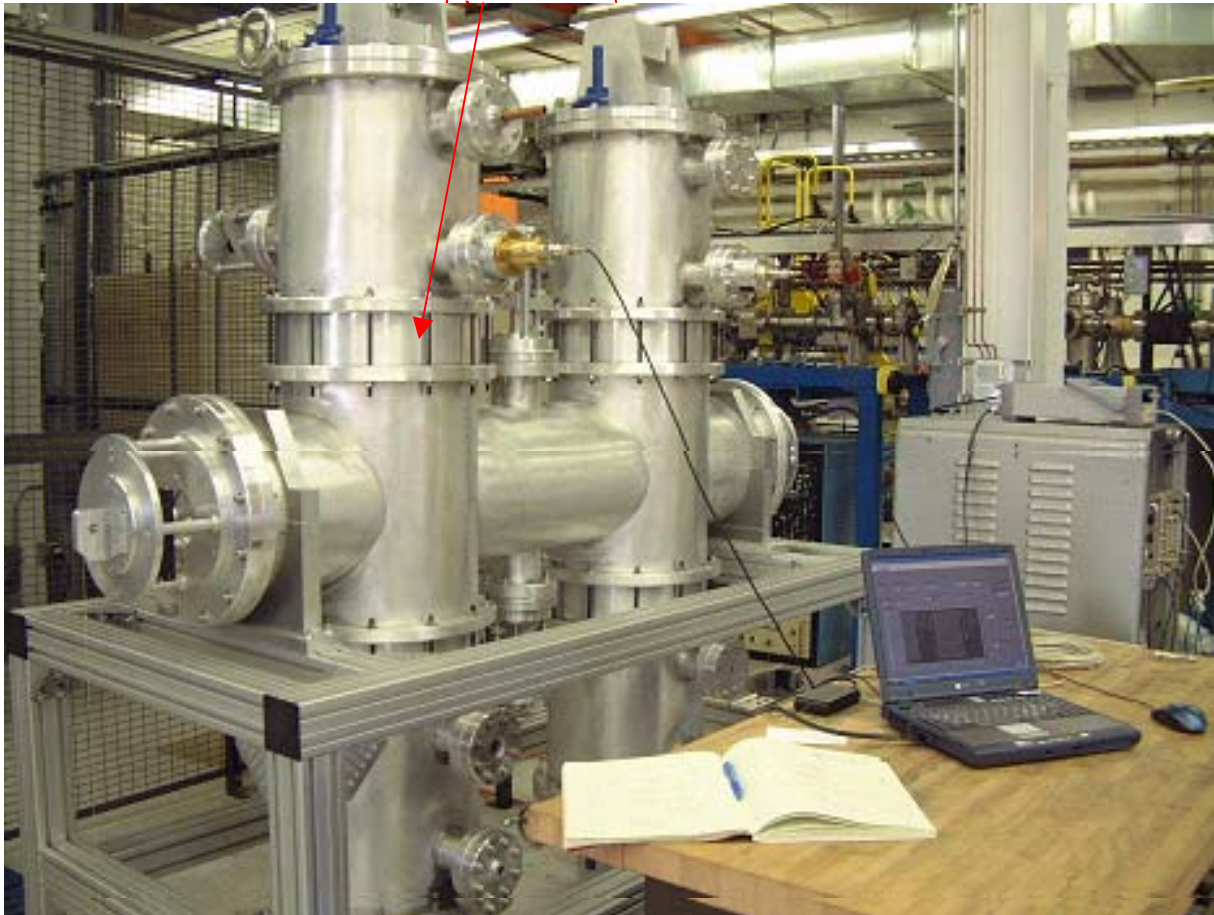
Figure III-13. The Hybrid RFQ half-scale aluminum cold model.
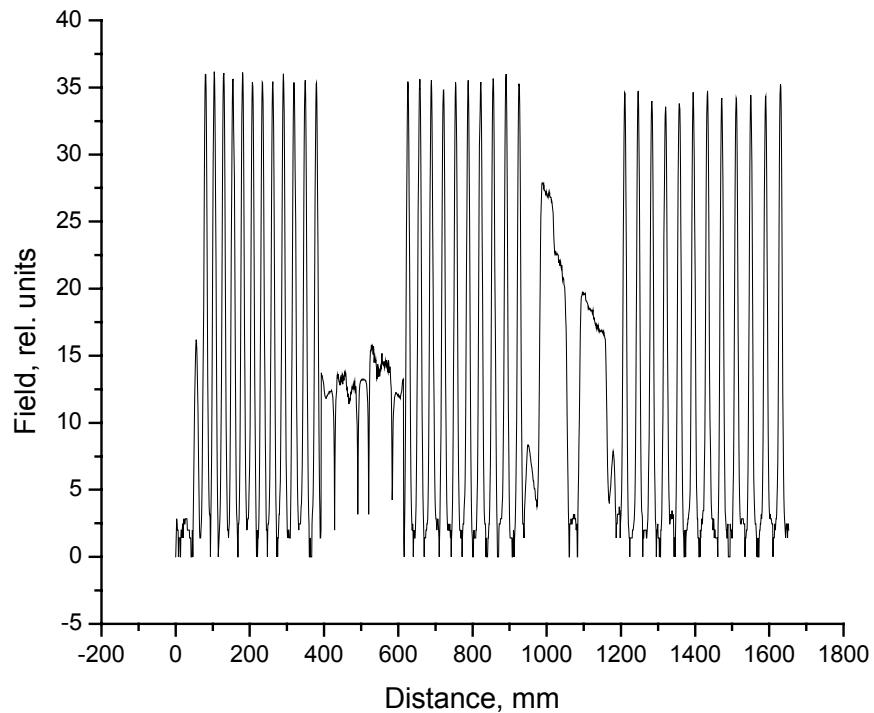
Figure III-14. Bead-pull measurements of the electric field distribution along the structure.

b.5.   Engineering Design of 57.5 MHZ CW RFQ for the RIA Driver Linac
(P. N. Ostroumov, A. Barcikowski, F. DePaola, A. A. Kolomiets, J. W. Rathke,[*]
E. Rotela, B. Rusthoven, S. Sharma, D. L. Schrage,[†] and T.J. Schultheiss[†]

A Continuous Wave (CW) Radio Frequency Quadrupole (RFQ) accelerator is being designed for the Rare Isotope Accelerator (RIA) Driver Linac. This device is required to accelerate a wide variety of ion species as well as perform simultaneous acceleration of multiple charge states. As such, the structure must operate over a wide range of RF power dissipation from ~0.65 kW to 48 kW. The physics design of this pseudo split-coaxial RF structure was established earlier. The design addresses the requirements for efficient cooling throughout the structure, precise alignment, reliable RF contacts, and fine tuning capability. The RF, thermal and structural analyses werecompleted in response to these requirements. An RF analysis was used to determine the heat loss distribution on the cavity's internal surfaces. The heat loads were then transferred to a thermal model of a single segment and scaled to

match total heat loss obtained from the code CST Microwave Studio. The thermal model includes the cavity vanes, walls and all cooling channels. To determine the coolant temperature rise, one-dimensional pipe flow elements were used. These elements account for fluid heat transport and heat transfer coefficients. The model was then used to minimize coolant flow by connecting the shell coolant channels in series. Temperature distributions were used as input to the structural model to determine stress levels and vane displacements. Different power levels were assessed as well as the thermal and structural response to vane-shell coolant temperature differences, which may be used to tune the resonant frequency. Results of these analyses show that the thermal and structural design of this RFQ is very robust.

[*]*Advanced Energy Systems, Inc. 27E Industrial Blvd., Medford, NY 11763.*
[†]*Los Alamos National Laboratory, M/S H817, Los Alamos, NM 87545*

A typical segment with cutaway sections to show the cooling passages is shown in Fig. III-15. Several different approaches to fabrication of the RIA RFQ were discussed during the conceptual design phase. Ultimately we have chosen a fully brazed assembly using step brazing to fabricate the vanes and quadrant details and finally a complete segment with end flanges. This approach borrows heavily from the techniques used successfully on the LEDA RFQ at Los Alamos. The RFQ is designed as a 100% OFE copper structure with SST end flanges. For the simplicity of machining, fixtures and post-brazed handling for the vanes will be made from Glidcop. Six longitudinal segments will be mechanically assembled to form the complete 4-meter RFQ structure.

The aluminum cold model of the RFQ segment was designed and constructed. This model is necessary to verify final internal dimensions of the RFQ prior to the fabrication of full cooper structure, testing of machining and final assembly tolerances. An aluminum vane was used for the test of gravity force effect on the horizontal vane profile. Precise measurements for the gravity deflections of the vane show acceptable deviations of the vane's profile. The final assembly of the aluminum model is in progress. An aluminum vane photograph is shown in Fig. III-16.

A full power engineering prototype of a single segment of the 57.5 MHz RFQ is being developed. The main reasons to proceed with fabrication and testing of the engineering model are: a) the transverse dimensions of the RFQ are significantly larger than those in 4-vane high-frequency RFQs built using the brazing technique; b) due to the large cut-out in the vane, it is prudent to demonstrate mechanical stability during high temperature brazing. Once the fabrication is complete, testing of the RFQ prototype over the wide range of input power is necessary. Successful testing of the RFQ over the wide range of rf power level will simplify the design and minimize the cost of the RIA Driver Front End: the same RFQ will be able to accelerate full range of ions from proton to uranium. Currently we perform pre-tests of major brazed junctions of the RFQ engineering prototype. Figure III-16 shows the OFE copper vane prepared for the brazing.
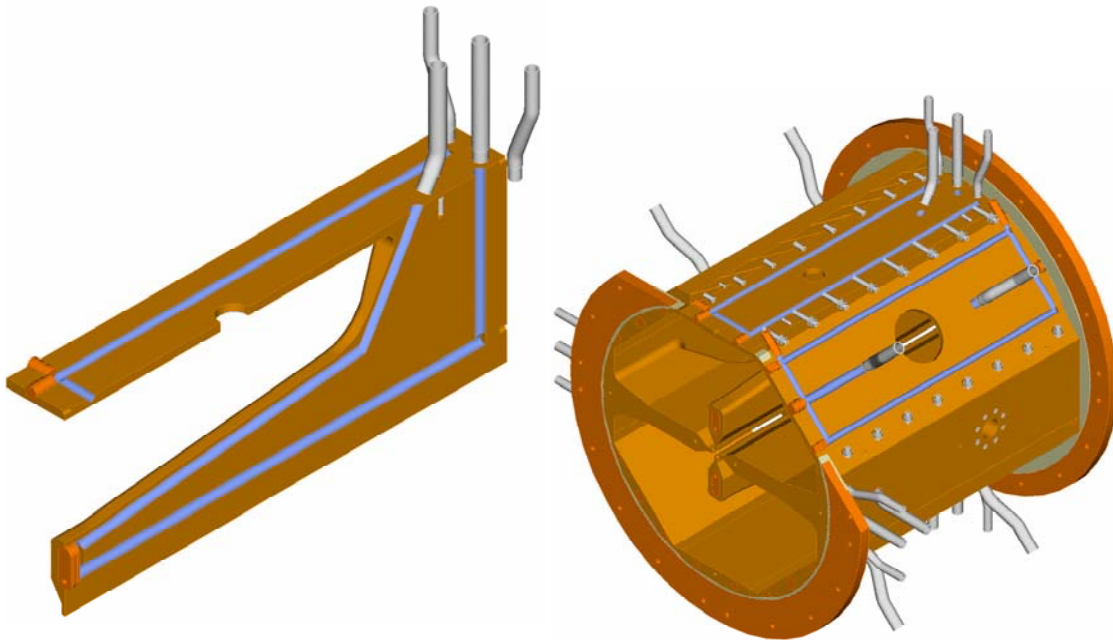
Figure III-15. Segment details with cooling channels. The vane assembly is shown separately on the left.
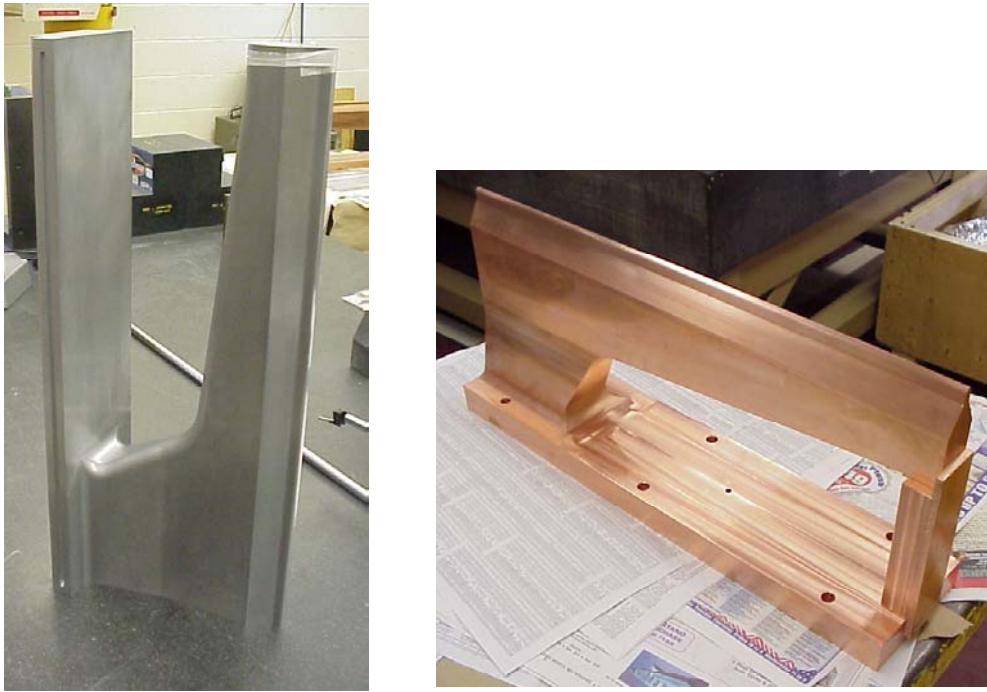
Figure III-16. Photographs of the aluminum (on the left) and copper (on the right) vanes.

C. RARE ISOTOPE PRODUCTION, SEPARATION, AND DIAGNOSTICS

c.1.   Development of Windowless Liquid Lithium Targets for Fragmentation and Fission of 400-KW Uranium Beams (J. A. Nolen, C. B. Reed[*], A. Hassanein[†], V. J. Novick[*], P. Plotkin[*], and J. R. Specht

Introduction

This section summarizes the on-going development of windowless liquid lithium targets being carried out for the RIA project. The goal of this work is to develop a fragmentation target that can easily work with uranium beams at least up to 100 kW and preferably up to 400 kW, the design limit of RIA. A schematic layout of the proposed concept is shown in Fig. III-17 and the performance goals for the target are listed in Table III-4. The beam-spot width is limited to 1 mm due to the optical requirements of the fragment separator. The target thickness is set by matching the energy loss of the beam with the acceptance of the fragment separator.

Thermal calculations for the full power RIA target

For a 400 MeV per nucleon uranium beam at a power of 400 kW the power density in lithium is 4 MW/cm^3, as indicated in Table III-5. For a graphite or beryllium target this would be about 15 MW/cm^3 due to their higher densities. With the lithium flowing at 20 m/s the power density is reduced by a factor of 20,000 keeping the maximum temperature below 300 C and the vapor pressure of the lithium at the hot spot below 10^{-6} T. For a nozzle cross section 1.5-cm wide by 3-cm long the total volume flow rate would be 9 liters/s and the average temperature rise would be 6 C.

Pressure/flow requirements and pump design for a prototype target

As a first step towards the design and construction of the full-sized windowless liquid-lithium target for RIA, a scaled-down prototype has been designed and is currently under construction. The prototype will have a thickness in the range of 1-2 cm and have a flow rate of 5-10 m/s.

_____
*Nuclear Engineering Division
†Energy Technology Division, Argonne.
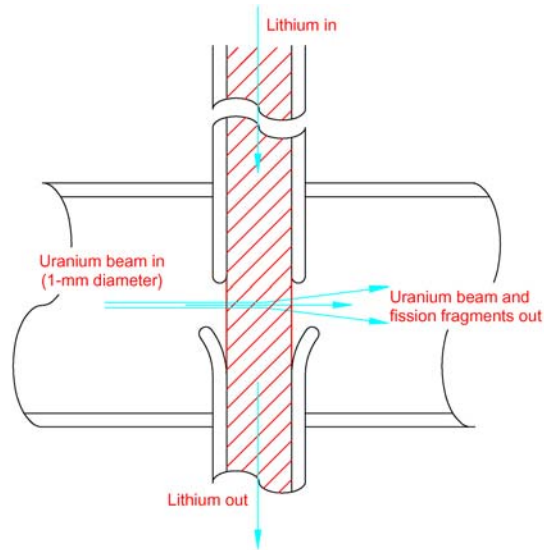
Figure III-17. Schematic layout of the concept of a windowless liquid lithium target for in-flight fission or fragmentation of heavy ions up to uranium, designed to work with beam power as high as 400 kW.

Table III-4. Target requirements for uranium beam.

Beam energy:	400 MeV/u
Beam power:	400 kW
Beam diameter:	1 mm
Target thickness:	1.5 g/cm^2

Table III-5. Thermal properties of the target.

Beam energy deposited:	120 kW
Power density at no flow:	4 MW/cm^3
Power density at 20 m/s:	200 W/ cm^3
Hot-spot temperature:	300 C
Maximum lithium vapor pressure	10^{-6} T

Goals of this prototype project are to evaluate the lithium flow properties for a variety of nozzle types and to check the performance of our permanent magnet liquid metal pump designs. A drawing of the first nozzle to be tried is shown in Fig. III-18. It is rectangular at the output end to increase the target thickness while minimizing the lithium volume flow-rate required.

A DC, permanent magnet Lorenz-force type of pump was chosen for this liquid-lithium loop. It is a larger version of the pump designed for the hybrid beryllium/lithium target described previously.   To achieve the higher volume flow rate at the correspondingly larger pressure drop required for the windowless target a rectangular pump duct is being used. A sketch of the pump duct and its corresponding equivalent electrical circuit is shown in Figure III-19. A photograph of the pump duct is shown in Figure III-20. The stainless steel duct was fabricated via a wire electric-discharge-machining process from a solid metal block to avoid possible problems with cracking and corrosion in weldments that have been experienced previously in pumps with cold-worked ducts.

Figure III-18. A section view of the tapered nozzle to be used in the prototype liquid-lithium target. It is rectangular, 10 mm by 5 mm, on the output and circular, 22 mm in diameter, on the input.
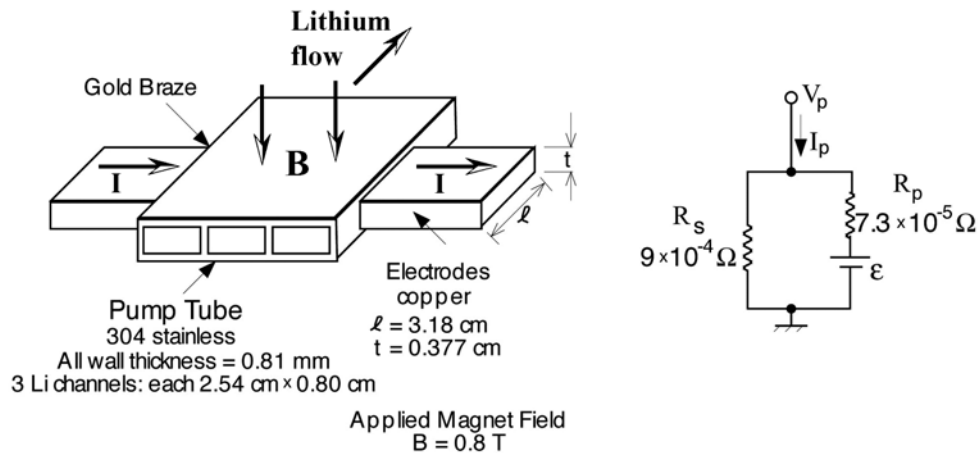
Figure III-19. Sketch of the DC permanent magnet pump concept and the equivalent electrical circuit of the pump duct.

Figure. III-20. Photograph of the pump duct and current electrodes for the prototype target.

The pump duct and plumbing of the liquid lithium loop are designed such that the pressure drops on these components are small relative to that at the pump nozzle. For the pump duct dimensions shown in Figure III-18 and nominally 5-cm piping, the pressure overall pressure drop of the system is calculated to be 30,000 Pa at 10 m/s nozzle velocity. With 0.75 T magnetic field the required pump current is 391 amperes at 71 mV. The total pump power is 28 watts, with 53% of this going into pumping lithium and the rest dissipated in the pump duct resistance.

Mechanical layout

A mechanical drawing of the liquid lithium loop is shown in Figure III-21. The lithium flows from the nozzle which is just above the center line of a standard 15-cm conflate vacuum cross.   There are clamp-on heaters and thermal insulation added to what is shown in the drawing.   A photograph of the partially assembled system is shown in Figure III-22.
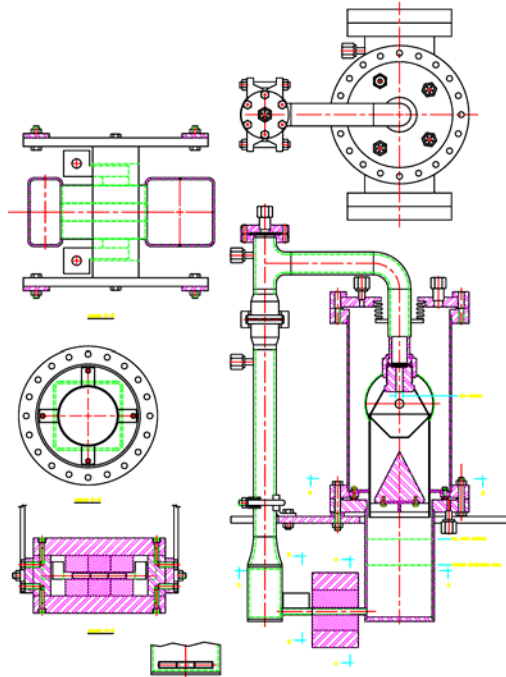
Figure III-21. Mechanical drawing of the liquid lithium target loop. The overall height of the loop is 0.6 m. A section view of the permanent magnet pump is shown at the lower left.
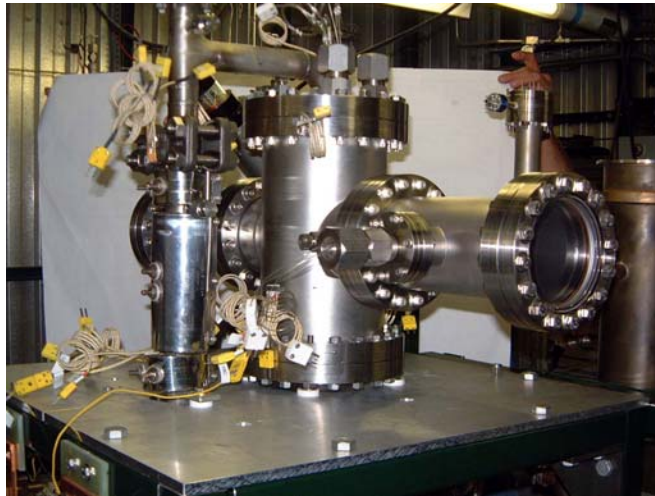
Figure III-22. A photograph of the partially assembly target system.

Safety issues and procedures

A general discussion of the safety procedures that are used for working with alkali-metal systems was given in Ref. 1. Specific procedures were written for the safe operation of the present system for initial testing within the existing liquid lithium laboratory at Argonne. These include a general safety document, a document of procedures for initial commissioning and operation of the loop, and a procedure to be followed for loading of the lithium into the pump loop.

Construction and testing

The mechanical and electrical components of this prototype system were fabricated and/or procured, the vacuum system leak checked after assembly, and the heaters and their controllers installed and debugged prior to loading the lithium. Approximately 760 g of lithium were loaded under an argon atmosphere and the assembly initially operated at atmospheric pressure with argon before commissioning under vacuum. Three runs were completed by the end of FY02 and 12 runs were completed by the end of CY02. The test runs provided evaluation of the pump design and flow characteristics relative to the design parameters, as well as the observation of the uniformity and stability of the lithium jet as a function of flow velocity. Alternative nozzle designs were also evaluated. Smooth, steady jet flow was observed for all anticipated nozzle velocities, up to roughly 10 m/s of lithium jet velocity, which corresponds to approximately 900 A of pump current. Next year's goal is to demonstrate operation of the system on-line at high beam power in a 40 kW beam on target dynamitron test rig at ANL.

The full-scale RIA liquid-lithium target requires scaling this prototype up by a factor of 3 in thickness and a factor of 2 in velocity. After the addition of a heat exchanger, the only additional sub-system to be incorporated for long-term operation at high intensity will be one for impurity control. Impurity control traps, both hot and cold, were developed as part of the inertial fusion materials irradiation developments. These methods were shown to provide for control of radioactive impurities such as tritium and ^{7}Be, as well as, carbon, nitrogen, and oxygen.

---

[1]J. A. Nolen, C. B. Reed, A. Hassanein, and I. C. Gomes, Nucl. Phys. **A701**, 312c-322c (2002).

c.2.   Simulations of Effusion from ISOL Target/Ion Source Systems (B. Mustapha and J. A. Nolen)

In a previous work,[1] we reported on the implementation of a Monte-Carlo calculation to simulate the release process of radioactive isotopes from ISOL-Targets. In this calculation, the effusion process is simulated using the tool-kit Geant-4[2] by tracking the particles through the target until released from the ion source. The diffusion is treated analytically using the solution of Fick's diffusion equation[3] for the considered form of the target material: foils, fibers or grains. We have also shown that it is possible to characterize the release process and extract its important parameters, the diffusion coefficient (D) and the sticking time per collision (τ_s), by fitting the simulated release curve to the experimental one measured with a given target geometry for a given isotope. The extracted information can then be used to improve the efficiency of existing targets and design new geometries more suitable to produce beams of rare isotopes.

In the same study, the simulation of the whole release process (diffusion, effusion and decay) of ^{8}Li from the RIST target[4] tested online at ISOLDE-CERN has revealed that the diffusion coefficient D can be determined only if the diffusion process is faster than the decay of the considered isotope. To determine D when the decay is faster than the diffusion (case of ^{8}Li), we could use the value measured for the closest stable isotope (^{7}Li).

To better characterize the diffusion and effusion processes and avoid the uncertainty coming from the undertermination of D, we propose here to deconvolute the two processes and study them separately. This will allow the unambiguous extraction of the release parameters from the appropriate measurements: τ_s from effusion measurements and D from diffusion measurements. It will also provide an independent benchmark of the effusion and diffusion parts of the calculation.

In this report, we focus on the study of the effusion part of the release process. The only parameter in this case is the sticking time τ_s. Furthermore, if we consider non-sticky particles (τ_s =0), noble gases for example, there will be no parameters at all and the problem is fully determined for a given geometry. Using effusion measurements for non-sticky particles, we can perform a direct and independent benchmarck of the effusion part of the calculation. The calculation will provide us with information like the total path length and number of collsions for a given geometry which could later be used to measure the sticking time of other particles.

We report here on the simulation of three Target/Ion Source systems used at Oak Ridge National Laboratory[5,6] to measure effusion times of different rare gases. Both low- and high-conductivity systems were used in these measurements. In the next section, the principle and the conditions of these measurements will be presented. In the next section, the results of the simulation of the low-conductivity systems will be presented and compared with the corresponding data. Some checks of the simulation using data for simple geometry components and using the conductance approach will be presented and discussed in the following section, followed by a comparison between the low- and high-conductivity systems based on the simulation. Our concluding remarks will be given in the last section.

Effusion measurements at ORNL

In these measurements, the considered gas is admitted to the system at a controlled rate through a needle-valve (see Figure III-23a) until a steady flow is reached. Then, a fast valve system closes the inlet in about 0.1 ms and the decay rate of the ion source current is measured, see Figure III-23b. The characteristic effusion time, τ_e, is determined by fitting the decay curve using an exponential form: \alpha exp(-t/ τ_e).
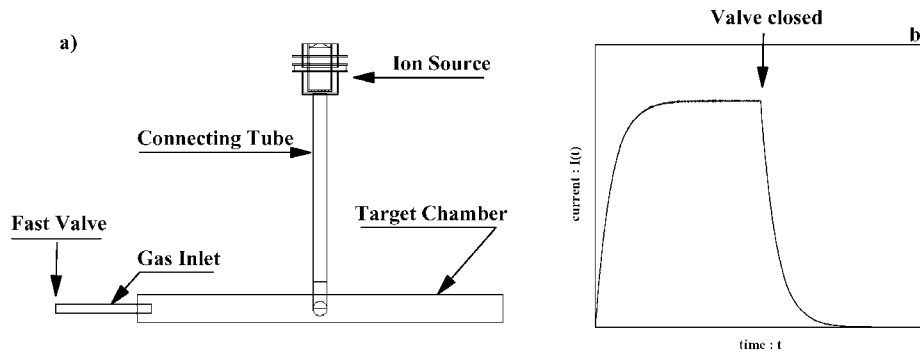
Figure III-23. Principle of ORNL measurements : a) A typical geometry used to measure effusion times (1st low-conductance system) showing all geometry components including the Gas Inlet/Valve system. b) A typical measured release curve showing the steady flow while the valve is open (the plateau) and the exponential decrease after the valve is closed.

The measurements were performed for different noble gases: He, Ne, Ar, Kr and Xe at different temperatures: 1073-1473 K. Two kinds of geometries were used: low- and high-conductivity systems. The low-conductivity geometry is characterised by small section tubes connecting the target chamber to the ionsource (see Figure III-24a). In the high-conductivity geometry, a more open connection is used (seeFigure III-24b).

For each geometry, the data were taken for both an empty target chamber and one filled with a Reticulated Vitreous Carbon Foam (RVCF) matrix. The simulation is performed only for the case of empty target chambers.

Simulation of low-conductivity systems

There are two low-conductivity systems for which effusion times were measured. They differ by the size of the target chamber. In the first (Figure III-23a), the target chamber was a 1.5 cm diameter and 19.3 cm long tube. In the second (Figure III-24a), a larger tube was used: 2.4 cm diameter with the same length. In both cases the target was connected to the ion source using an elbow (0.87 cm diamter, 3.5 cm total axis length) and a tube (0.87 cm diameter and 10 cm long).

The simulation of the first system (Figure III-23a) showed that particles travel on average 125 m before leaving through the ion source and collide about 11000 times with the internal surfaces of the system. The effusion time calculated for ^{4}He at 1473 K is 44.9 ms which is about twice the measured value ($\sim$ 23 ms). Trying to understand the extra delay in the simulation, we simulated the case without the ion source in order to estimate its contribution to the delay, the results are summarised in Table III-6.

Table III-6. Results of the simulation as the average number of surface collisions and total path length of particles for the first low-conductivity system (Figure III-23a) with and without the ion source. The calculated delay times for ^{4}He at 1473 K are compared to the measured value in the bottom line.

	W/ Ion Source	No Ion Source	Experiment
<N. collisions>	10987	4466	-
<Path length> (m)	125.3	90.3	-
τ (ms)	44.9	19.1	23.0

We notice that by removing the ion source, the simulation is faster than the data which seems to be consistent with the data because the ion source will introduce an additional delay anyway. The question now is: what is the real delay introduced by the ion source? Since we don't simulate the ionization process in the calculation, it is possible that we predict more delay than the experiment where particles could be extracted faster once ionised in the ion source. A possible precise measurement of the delay, introduced by the ion source, could be carried out by using a simple tube connected to the ion source instead of to the whole system.

The simulation of the second low-conductivity system (Figure III-24a) showed that on average particles travel about 300 m and collide about 15000 times before leaving the system. For ^{4}He at 1473 K, the calculated effusion time is 105.6 ms which is about 3 times the experimental value (~ 38 ms). And more surprisingly, even after removing the ion source the simulation predict more delay than the experiment, see Table III-7. This is of course inconsistent with the data and with the first geometry, because the argument of the accelerating effect of the ion source can't explain this discrepancy.
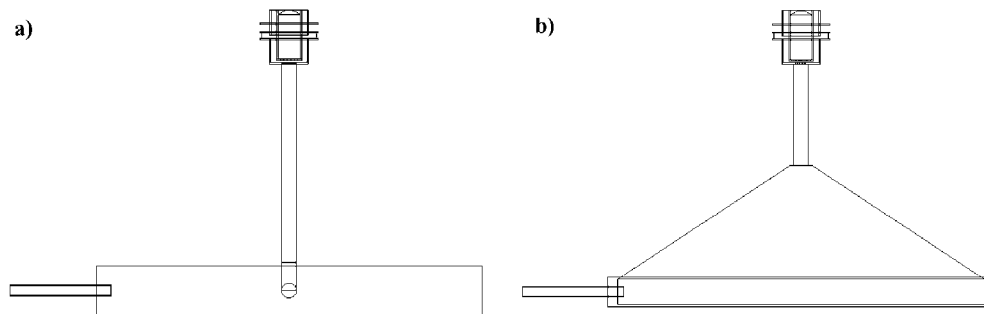
Figure III-24. Low- and high-conductivity systems : a) Geometry of a low-conductivity system (2nd low-conductivity system). b) Geometry of the high-conductivity system.

Table III-7. Results of the simulation as the average number of surface collisions and total path length of particles for the second low-conductivity system (Figure III-24a) with and without the ion source. The calculated delay times for ^{4}He at 1473 K are compared to the measured value in the bottom line.

	W/ Ion Source	No Ion Source	Experiment
<N. collisions>	15550	6540	-
<Path length>(m)	294.7	130.6	-
τ (ms)	105.6	46.8	38.1

The present conclusion is that the quantitative increase in the delay time calculated for the larger tube is in the right direction, but it is larger than seen experimentally. In order to find the source of this discrepancy, we performed some independent checks of the simulation. Tests using basic geometry components were carried out and confronted to experimental data. They are discussed in more detail in the next section.

Tests of the simulation

In 1960, Levenson et al.[7] reported on measurements of transmission probability of particles through simple shapes: tubes, elbows, etc. The measurements were performed by admitting a gas into one end of the considered shape and measuring the pressure at entrances and exits. The transmission probabilities from one end to another were then determined using the pressure difference.

After adapting the calculation to give the transmission probability, the simulation was performed for the tube and elbow shapes, the basic components of ORNL's systems. Tubes and elbows with different length-to-radius ratios (L/R) were considered. In the case of elbows, L is the total axis length.

Comparisons to the data are shown in Figure III-25a for tubes and Figure III-25b for elbows. We notice that the simulation agrees very well with the data within error bars. This test provides an important validation of the Monte Carlo simulations.
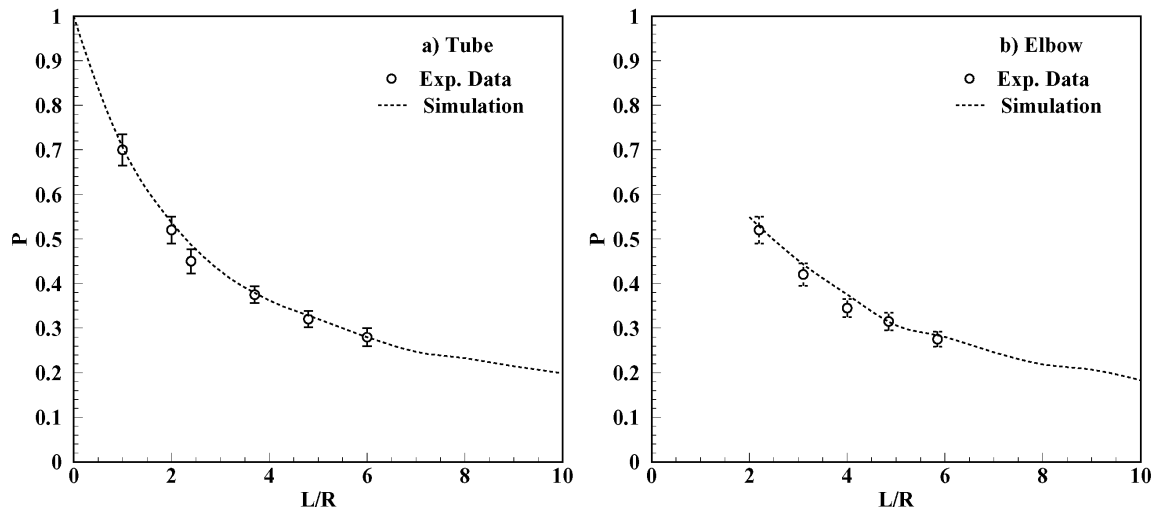
Figure III-25. Test of simulation using experimental data : a) case of a tube and b) case of an elbow. Open circles with error bars are data from[7] and dashed line is the result of the simulation.

This first test dealt only with transmission probabilities of particles through basic shapes and did not test the delay time predicted by the simulation. In order to check the timing from the calculation, we used the conductance approach well known in vacuum technology.

The problem of unsteady molecular flow through a long tube could be resolved by analogy to the one-dimension heat-conduction problem.[8]   Consider the case of N_0 particles trapped between the two ends of a long tube (L >> R). At t = 0, one end of the tube is opened and particles start leaving the tube. This is of course a non steady flow of particles because the number of particles leaving the tube is varying in time until no particle is left inside the tube.

Based on the above analogy, the number of particles leaving the tube at a time t is given by :

$$N(t) = N_0 \times \frac{8}{\pi^2 \tau_0} \sum_{n=0}^{\infty} \exp(-(2n+1)^2 \frac{t}{\tau_0})$$

τ_0 is the characteristic delay time (effusion time) given by the following expression :

$$\tau_0 = \frac{4}{\pi^2} \frac{V}{C}$$

where $V = \pi R^2 L$ is the volume of the tube,

$C = \frac{2}{3}\pi\frac{R^3}{L}v$ is the conductance of the tube

assuming L >> R. $v = \sqrt{\frac{8kT}{\pi M}}$ is the average Maxwell velocity for a particle of mass M at a temperature T.

The simulation was run for $N_0 = 10^5$ particles using a 1 cm diameter and 100 cm long tube ($V = 78.5$ cm^3). The conductance calculated for ^{4}He at 1473 K is C = 730.8 cm^3/s resulting in a delay time $\tau_0 = 43.5$ ms. The value determined from the simulation is 42.8 ms, in a good agreement with the conductance approach.

The comparison of the simulated N(t) with the conductance formula is shown in Figure III-26. A very good agreement is seen except at longer times where the end effect of the tube manifest itself by liberating all particles at a finite time.
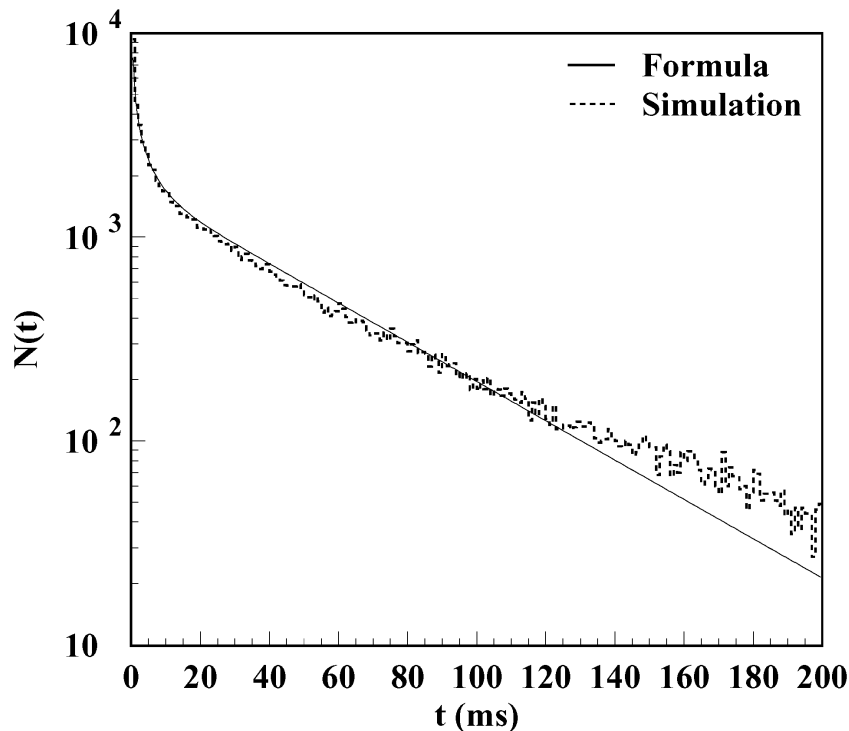
Figure III-26. *Comparison of the simulation with the conductance approach for a long tube.*

The simulation gives a delay time in good agreement with the conductance approach for a simple tube. We will now generalize this approach to the more complicated geometry of the low-conductivity systems used in ORNL's measurements.[5]

Because the geometry of the low-conductivity systems is essentially simple tubes with different lengths and sections connected to each other, it is possible to treat it like the serial coupling of these same tubes. In this case, the conductance C of the whole system could be obtained by :

$$\frac{1}{C} = \frac{1}{C_1} + \frac{1}{C_2} + \frac{1}{C_3} + ...$$

where 1,2,3,... denote the tubes. The total volume of the system is simply the sum of volumes $V + V_1 + V_2 + V_3 + ...$ The characteristic delay time in the system could be determined using the same expression for τ_0.

Applied to the two low-conductivity systems, this approach gave the results shown in Table III-8.

Table III-8. Comparison of the simulation with the conductance approach for the two low-conductivity systems.

	V (cm^3)	C (cm^3)	Conductance τ_0 (ms)	Simulation τ_0 (ms)	Experiment τ_0 (ms)
1st system	40.3	803.4	20.3	19.1	23.0
2nd system	97.0	856.9	45.9	46.8	38.1

We notice a good agreement between the simulation and the conductance approach for both geometries. Note that in Table III-8 neither the Monte Carlo simulation nor the conductance calculation include any delay from the ion source.

Comparison of low- and high-conductivity systems

The simulation of the high-conductivity system (Figure III-24b) showed that on average, particles travel about 355 m and collide about 22000 times inside the system including the ion source. The delay time calculated for ^{4}He at 1473 K is 127.3 ms which is more than 3 times the experimental value: 34.8 ms, see Table III-9. Simulating the case without the ion source gives a delay time of 33.5 ms which is smaller than the measured value. This result is consistent with the first low-conductivity geometry because the difference with the data could be explained by an eventual effect of the ion source.

The high-conductivity system was designed with more open geometry in the purpose of a faster release, but the experiment showed that the first low-conductivity system is faster. In order to understand the reason for that, we will use the conductance approach which gives almost the same results as the simulation.

Table III-9. Results of the simulation as the average number of surface collisions and total path legnth of particles for the high-conductivity system (Figure III-24.b) with and without the ion source. The calculated delay times for ^{4}He at 1473 K are compared to the measured value in the bottom line.

	W/Ion Source	No Ion Source	Experiment
<N. collisions>	221.55	5784	-
<Path length> (m)	355.5	93.5	-
τ (ms)	127.3	33.5	34.8

In the conductance approach, the delay time τ_0 is proportional to the ratio volume-to-conductance (V/C) of the system. So, in order to compare the conductance of two systems, we should consider the same volume V. In this case, the faster system is the one with the higher conductance C.   Comparing the high-conductivity system with a low-conductivity system having the same volume showed that the high-conductivity system is about 2 times faster than the low-conductivity one (71.1 ms for the low-conductivity case vs. 33.5 ms for the high-conductivity case). This confirms that using a more open geometry helps make the release faster. (Again the delay times are calculated without including the ion source.) However, the geometry of Figure III-23a is faster than that of the more open geometry of Figure III-24b, because it is dominated by the smaller overall geometry.

Concluding remarks

Monte-Carlo simulations of the low- and high-conductivity Target/Ion Source systems, recently tested at Oak Ridge National Laboratory, were performed. Compared to the experimental data, the simulation predicts more delay for all the systems. The simulation of the first low-conductivity and the high-conductivity systems without the ion source seems to give closer results to the data. However, the discrepancy seen for the second low-conductivity geometry can not be explained by an eventual effect of the ion source. On the other hand, the simulation seems to agree well with data measured for simple geometries and with the results obtained using the conductance approach well known in vacuum technology. The same conductance approach showed that the comparison of the low- and high-conductivity systems should be done for systems with the same total volume. In this case, the high-conductivity system is faster confirming the advantage of using more open geometries if the total volume is not increased.

At this stage, we consider that the simulation is partially validated. However, other verfications are needed. In collaboration with the ORNL's group, we propose special measurements to study the effect of the ion source. This could be done by replacing the target by a simple tube directly connected to the ion source. It will also be important to perform other measurements to confirm the data obtained for the second low-conductivity system.

_____

[1]B. Mustapha and J.A. Nolen, Proceedings of the 14th International Conference On Electromagnetic Isotope Separators And Techniques Related To Their Applications, May 6-10, 2002, Vectoria, Canada, to be published in Nucl. Instr. and Meth. B.
[2]Geant4 home page : http://geant4.web.cern.ch/geant4/.
[3]"The mathematics of diffusion" by John Crank, Clarendon Press, Oxford, 1975.
[4]C. J. Densham et al, Nucl. Instr. and Meth. B 126 (1997) 154.
[5]J.C. Bilheux, G.D. Alton et al, Proceedings of the Particle Accelerator Conference, June 18-22, 2001, Chicago, Illinois.
[6]J.C. Bilheux, G.D. Alton et al, Proceedings of the International Conference on the Application of Accelerators in Research and Industry, Nov.12-17, 2002, Denton, Texas, to be published by AIP.
[7]L.L. Levenson et al, Proceedings of the 7th National Symposium on Vacuum Technology Transactions, American Vacuum Society, Oct. 12-14, 1960, Cleveland, Ohio.
[8]"Foundations of Vacuum Science and Technology", edited by J. M. Lafferty, John Wiley & Sons, 1998.

Once the simulation is validated using the experimental data from noble gases, the calculated total path length and number of collisions will be fully determined for a given geometry. This information could then be used to extract the sticking time of more reactive species in future measurements. Combined with the future diffusion measurements at the UNISOR facility at Oak Ridge, a complete release study of an important range of rare isotopes will be possible.

c.3.   Calculated Intensity of Secondary High-Energy Neutron Beams from Uranium and Deuteron Beams at RIA (B. Mustapha, J. A. Nolen and B. B. Back)

Neutron sources and beams are of great interest for both fundamental research and applications in other fields like material sciences and biological sciences. At the proposed Rare Isotope Accelerator (RIA), spallation and fission of high-energy (up to 400 MeV/n) heavy-ion beams will be used to produce secondary beams of exotic and rare isotopes. Along with these nuclei, many neutrons will also be produced. Knowing the intensity and the characteristics of such secondary neutron beams is important for possible applications. It is also important for radiation shielding purposes to know the energy and angle spectra of these neutrons.

We report here on the calculation of the flux of high-energy neutrons produced by the in-flight spallation-fission reaction of a 400 MeV/n ^{238}U beam in a liquid ^{7}Li target. The calculation was performed using a Monte-Carlo code based on the two-step model of Serber[1] for the spallation reaction: an Intra-Nuclear Cascade (INC) step[2] followed by an Evaporation or Desexcitation step.[3] More details on the calculation are presented in the next section. The results in the form of neutron's energy and angle distributions as well as the corresponding flux are presented in the following section. A comparison with the deuteron break-up reaction (a well-known source of neutrons) at the same energy on the same target is discussed in the final section.

Description of the calculation

In order to simulate the inverse kinematics reaction: 400 MeV/n ^{238}U + ^{7}Li target, the calculation was performed first for the direct kinematics: 400 MeV/n ^{7}Li + ^{238}U target, using an INC + Evaporation-Fission codes. Then a Lorentz transformation is used to obtain the result for the inverse kinematics case. No particle transport is considered in this calculation, which means that we are assuming that the target is extremely thin, i.e. neither the beam energy-loss nor the secondary reactions in the target are included. In order to consider these effects, we should run the calculation for different incident nuclei, fragments of the beam, at different energies, down to the beam energy after the target. We will discuss later how the beam energy-loss and the secondary reactions in the target affect the production of neutrons and their energy-angle distributions. In this section, the model on which the INC + Evaporation-Fission calculation is presented and the codes used will be described.

The spallation reaction is well described by the two-step model of Serber.[1] A first step, where the incident particle (usually a nucleon or light nucleus) penetrates the larger target nucleus inducing a cascade of inter-nucleon interactions, is called the intra-nuclear cascade. During this step some energetic particles are ejected, mostly nucleons, and an excited fragment called prefragment is left behind. The second step corresponds to the deexcitation of the prefragment by emitting slower particles or by fission in the concerned mass region. This step is called deexcitation or evaporation-fission. An intermediate step called preequilibrium[4] could also take place to bring the prefragment from its locally excited state to its thermal equilibrium and during which some intermediate-energy nucleons and light nuclei could be emitted. The preequilibrium step is not considered in this calculation.

For the intra-nuclear cascade step the code ISABEL of Yariv and Frankel,[2] which could be used to simulate nucleus-nucleus collisions, was used for the direct-kinematics reaction ^{7}Li (400 MeV/n) + ^{238}U . The second step was simulated using the deexcitation code ABLA of Schmidt et al.[3] The code ABLA includes

deexcitation by particle emission known as evaporation and by fission. After fission, the fission fragments could also evaporate particles. The emission of neutrons, protons and alpha particles is considered. No

other composite particle emission is included. The results obtained for the direct kinematics are then transformed to the inverse kinematics case (RIA case) using the corresponding Lorentz transformation.

Results

After transforming to the inverse kinematics case, we obtained the result for the reaction 400 MeV/n ^{238}U + ^{7}Li. The result corresponds to a run of 10^5 interactions, in which about 2.7×10^6 neutrons are produced, 27 neutrons per reaction in average. Considering the reaction cross section ($\sim$ 5 barn), 11 neutrons are produced per incident ^{238}U nucleus on a 1 g/cm^2 ^{7}Li target. Considering a beam intensity of 1 pµA (100 kW beam power), 7.25×10^{13} neutrons are produced per second over all energies and angles.

The angular distribution shows that most of the neutrons are emitted into forward angles smaller than 7 deg, as Figure III-27(left) shows. The energy spectrum

shows an important peak centered around the beam energy (400 MeV) with a $\sim$ 300 MeV width, see Figure III-27(right) showing the energy spectra for different angle intervals. This peak contains mainly the neutrons produced by the evaporation step. In the center of mass, the evaporation neutrons are isotropic and their energy peaks at $\sim$ 1-2 MeV. When transformed to the laboratory frame, these neutrons become forward-peaked with energies about the beam energy per nucleon (400 MeV). We notice also the absence of this energy peak at large angles. These neutrons are mainly produced in the intra-nuclear cascade step.
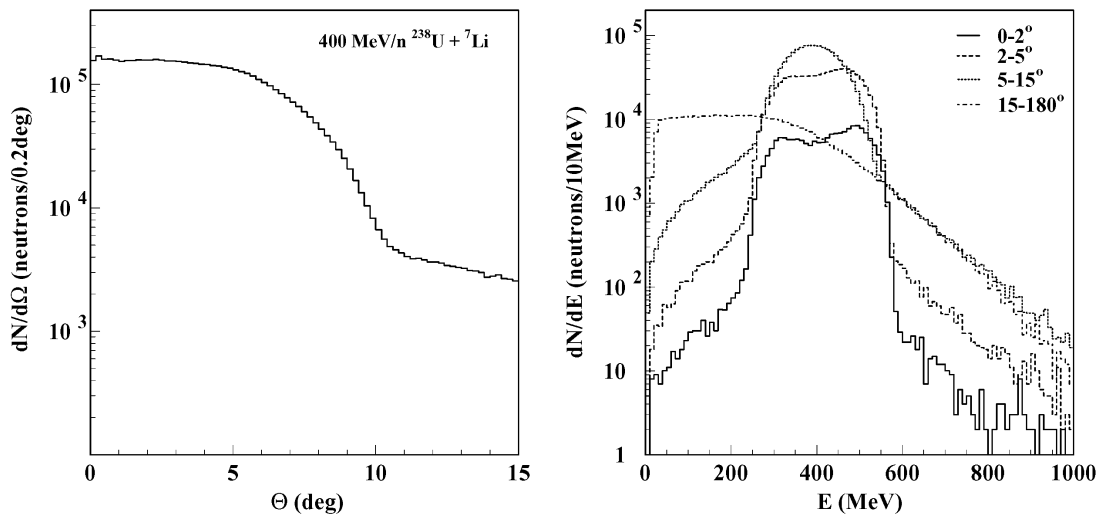
Figure III-27. Left- Angular distribution of neutrons from 10^5 spallation reaction of 400 MeV/n ^{238}U on a ^{7}Li target. Right- Energy spectrum for different angular intervals.

The peak asymmetry seen for θ < 5° is due to the fact that forward-emitted neutrons in the center of mass (higher energy in the Laboratory) are more likely to be within small Laboratory angles than the backward emitted ones. It is clear that neutrons in the energy peak are forward emitted in the laboratory frame and that those in the tail are emitted into large angles.

In order to consider the target thickness and study the effect of the beam energy loss on the neutron spectra, the 1 g/cm^2 target was considered as a set of 10 equal layers and by calculating the beam energy-loss using the code described in Ref. 5, we determined the incident energy on each layer. The beam loses about 9 MeV in each layer. The calculation was then performed at 10 different beam energies (from 400 to about 300 MeV/n)

on a 10 times thinner target 0.1 g/cm^2. The result showed that the neutron energy peak is slightly shifted towards lower energies. The angular distribution showed the same behavior but neutrons are slightly less forward focused. A reduction of about 5% in the total number of neutrons was also noticed. This effect is considered in the calculation of the neutron flux below.

Another important aspect of thick targets is secondary reactions. The effect of these secondary reactions was not considered in this calculation. However, we expect that secondary reactions will produce lighter final fragments that is usually due to the emission of more particles especially neutrons. Therefore, more neutrons will be produced, with energies lower than the primary

neutrons energies. In this calculation we considered only neutrons produced in primary reactions, which gives a lower limit of the neutron flux.

From the angular distribution of Figure III-27(right) we can determine the corresponding neutron flux. For a 1 pµA - 400 MeV/n ^{238}U beam incident on a 1 g/cm^2 liquid lithium target, the central neutron flux exceeds 10^{11} neutrons/cm^2/s at 1 m downstream of the target and it is about 10^9 neutrons/cm^2/s in the central 1 m^2 at 10 meter, see Figure III-28(left). This is a very high flux for neutrons of such high energy ~ 400 MeV), see Figure III-28(right). The energy width of the forward peak is about 300 MeV.
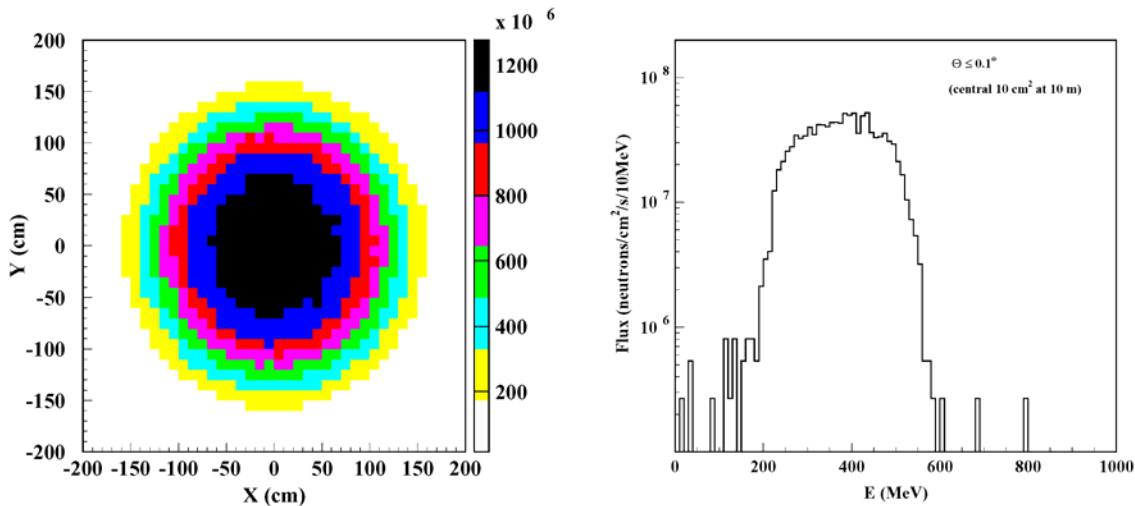
Figure III-28. Left- Neutron flux (neutrons/cm^2/s) at 10 m from the target. Right- Projection in energy of neutrons emitted at an angle θ < 0.1^o corresponding to the central 10 cm^2 at 10 m from the target.

Comparison to the deuteron breakup

Another important source of neutrons is the deuteron break-up reaction. In this section we calculate the energy-angle distribution of neutrons produced by deuteron breakup. For this purpose, we performed a calculation using the code LAHET[6] of the reaction of an 800 MeV (400 MeV/n) deuteron beam on a 5 g/cm^2 liquid-lithium target. The code LAHET considers the transport of particles in thick targets. 10^6 events were processed. The deuteron break-up cross section at this energy is about 200 mb, deduced from the measurement of ~ 1 GeV deuteron beam on a Be target.[7]

The angular distribution, presented in the left part of Figure III-29, shows that deuteron break-up neutrons are more forward focused than those from uranium reactions. This can be understood by looking at the right part of Figure III-29 showing the energy spectra for different angle intervals. The neutrons that are more forward focused, θ < 5°, have energies very close to the beam energy per nucleon. These neutrons were spectators in the reaction and have kept the direction and velocity of the beam, unlike the evaporation neutrons from uranium (forming the energy peak in the uranium case) that are isotropically emitted in the center of mass and focused by effect of the boost to the laboratory frame.
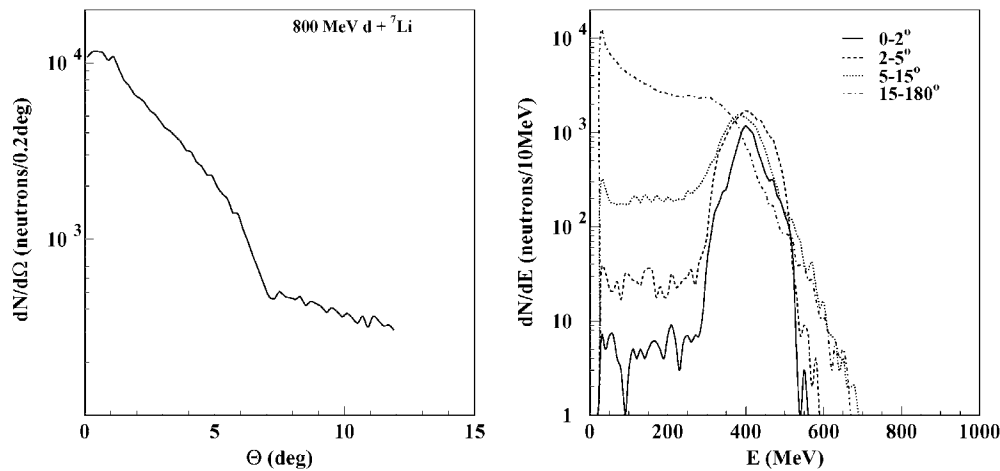
Figure III-29. Left- Angular distribution of neutrons from 10^6 deuterons at 800 MeV on a ^{7}Li target. Right- Energy spectrum for different angular bins.

The angular distribution shows that for an equivalent beam power, 100 kW, an 800 MeV deuteron beam on 1 g/cm^2 liquid ^{7}Li target produce half the neutron flux produced in the spallation of a 400 MeV/n uranium beam on the same target. But the energy distribution shows that forward neutrons from the deuteron break-up reaction have a better defined energy within a narrow peak centered about the beam energy per nucleon (400 MeV). Forward neutrons from the spallation reaction are more spread-out in energy as shown in Figure III-30. Therefore, more neutrons can be produced by using a thicker target in the case of deuteron break-up without significantly altering their energy-spectrum. However, this is not true for the case of spallation. Figure III-30 compares the energy spectra of forward neutrons produced in the deuteron break-up in a 5 g/cm^2 ^{7}Li target and the spallation of ^{238}U on a 1g/cm^2 ^{7}Li target. In this case, the neutron flux from deuteron break-up is twice the one produced by spallation-fission of uranium. At zero degrees it is about 3×10^9 n/cm^2/s corresponding to a neutron energy peak at 400 MeV

[1]R. Serber, Phys. Rev. 72 (1947) 1114.
[2]Y. Yariv and Z. Fraenkel, Phys. Rev. C 20 (1979) 2227.
[3]J.J. Gaimard and K.-H. Schmidt, Nucl. Phys. A 531 (1991) 709.
[4]J.J. Griffin, Phys. Rev. Lett. 17 (1966) 478.
[5]C. Scheidenberger et al, Nucl. Inst. Meth. B 90 (1998) 441.
[6]R.E. Prael and M.B. Chadwick, LANL Report NM-87545, 1997.
[7]J.F. Lecolley et al, Eur. Phys. J. A 5 (1999) 321.
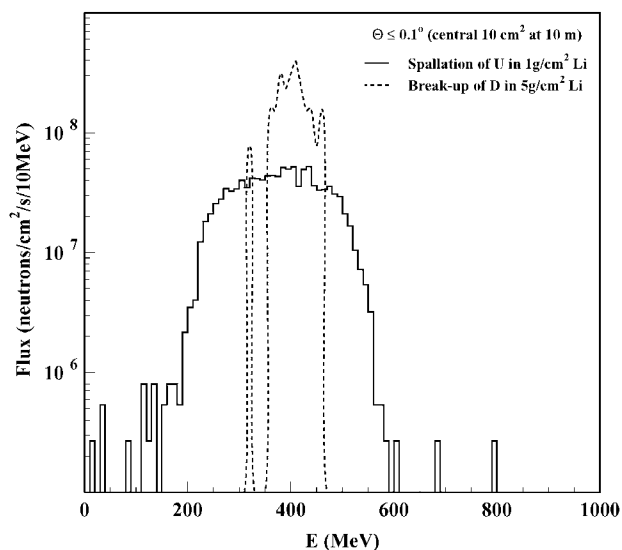
Figure III-30. Comparison for the same beam power (100 kW) of the neutron flux as a function of energy from ^{238}U spallation and Deuteron break-up on a liquid ^{7}Li target. The flux is calculated for the central 10 cm^2 at 10 m downstream of the target.

c.4.   Construction and First Tests of the Full-Scale RIA Gas Catcher Prototype
(G. Savard, T. Coccolios, A. Frankel, B. Blank, J. P. Greene, A. Heinz, A Levand, D. Seweryniak, W. Trimble, B.J. Zabransky, Z. Zhou, J. Clark[*], C. Boudreau[†], F. Buchinger[†], J.E. Crawford[†], S. Gulick[†], J.K.P. Lee[*], M. Maier[‡], K.S. Sharma*, J. Vaz[*], J.C. Wang[*], and the S258 Collaboration)

The ability to slow down and cool fast recoils from fragmentation or in-flight fission reactions with high efficiency is an essential component of the RIA concept. It is particularly important to produce reaccelerated beams of refractory and reactive elements. Standard ISOL techniques have difficulties with such elements while traditional IGISOL approaches do not provide enough stopping volume to efficiently accomplish this task. A new approach based on a large gas catcher system was developed to fulfill this task, a prototype built and an initial on-line test performed this year.

The design of the RIA gas catcher prototype was based on a smaller gas catcher, with a 7.6 cm inside diameter and a 25 cm length, which is working effectively at the front end of the Canadian Penning Trap (CPT) experiment at Argonne[1] where it cools both neutron-rich and proton-rich radioactive beams for high-efficiency injection into the CPT ion traps. The design of the smaller CPT gas catcher was essentially scaled up to obtain the first RIA prototype gas catcher ("the

big cell") designed to handle the range straggling of high-energy heavy-ion recoils and the angular straggling introduced by the final degrader and the window. Degraders in front of the entrance window remove all but roughly the last few MeVs energy per nucleon. Inside the catcher, the remaining energy is absorbed by ionizing room-temperature high-purity He at roughly 1/5 bar. Near-complete stopping of these ions is possible in .5 atm-m of He; the gas catcher aims to extract these ions efficiently.

These demands in stopping power determine the size of the big cell, a cylindrical gas volume 1.2 m long and 25 cm in diameter mated to a conical extraction cone. The construction of this large catcher was completed in the summer of 2002. 49 ring-shaped electrodes in the cylinder and 277 plates in the cone (see Figure III-31) provide DC bias for transport and extraction, and RF bias for focusing. Tuned circuits were constructed to provide the RF and DC fields to the cone and cylinder electrodes (Figure III-32). The catcher and the electronic circuits to apply the DC gradients and RF

fields were then installed inside a Faraday cage for high voltage safety.

Ions stopped in the gas catcher are pulled towards the cone, focused in the cone and extracted at the tip of the cone by gas flow through a 1.4 mm conical nozzle into an RFQ ion guide. The buffer gas is removed from the RFQ chamber by an Osaka TC440C helical groove pump with a Welch 1398 backing pump. DC electric fields extract the ions from the ion guide through a second nozzle into a vacuum system consisting of a time-of-flight line leading to a Si detector for activity measurement and a MCP detector for ion detection.

_____
[*]Department of Physics and Astronomy, University of Manitoba, Winnipeg MB R3T 2N2
[†]Department of Physics, McGill University, Montreal, PQ H3A 2T8
[‡]GSI, D-64291 Darmstadt, Germany
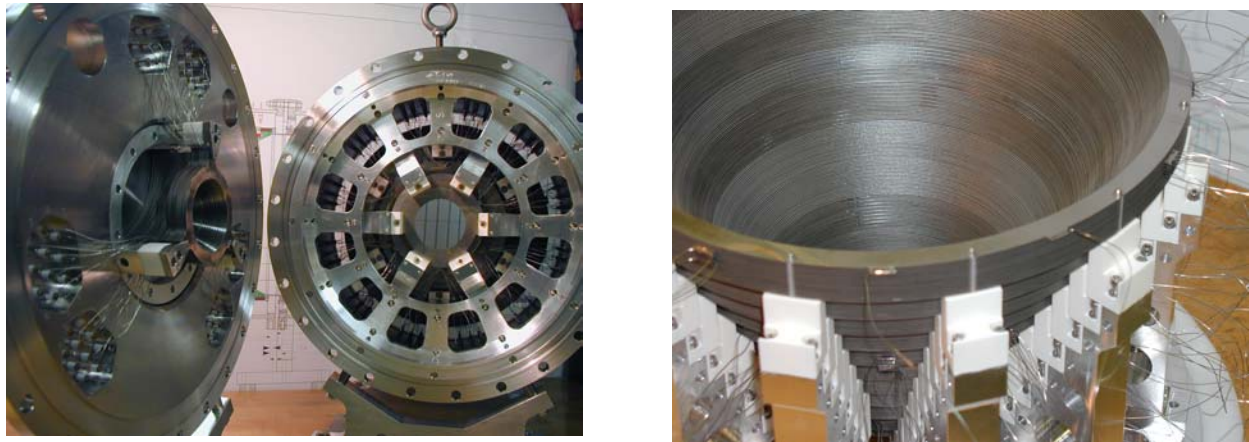
Figure III-31. View of the 2 completed sections of the conical extraction region with its 277 electrodes providing both DC gradient and a strong RF field close to the cone that repels the recoil ions.

Figure III-32. View of the capacitors and resistors connected to the internal electrodes to feed the DC and RF fields and that form part of the tank tuned circuits.

The large catcher volume results in longer extraction paths compared to the CPT gas catcher, placing even tighter requirements on the purity of the buffer gas. The much increased surface area puts severe constraints on the outgassing rate from the surfaces. The components of the gas catcher were cleaned to UHV standards and the entire cell is comprised of bakeable metal and ceramic. The fully instrumented large gas catcher was moved to the area II experimental area at ATLAS (see Figure III-33) for initial tests. The cell was first tested offline with a 5μCi ^{252}Cf fission source and degraders mounted inside the chamber in October 2002. The device was initially debugged and tested with activity from this source.
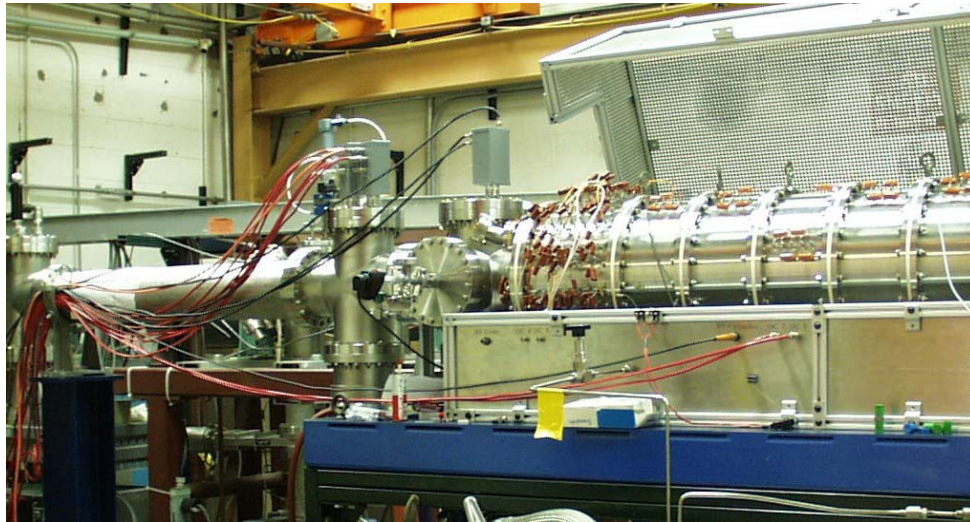
Figure III-33. RIA gas catcher prototype installed in the experimental area II at ATLAS. On the right we see the gas catcher inside the Faraday cage with the extraction section leading to the sections of RFQ. On the right we have the drift time-of-flight section leading to the detector system.

The gas catcher was then moved from target Area II and installed in the ATLAS general-purpose beamline. The catcher was attached to the ATLAS beamline by a ceramic insulator to allow high-voltage biasing of the cylinder itself and its vacuum separated from the beamline vacuum by an all-metal large-area 77cm^2 reinforced Havar window. In December 2002, the first on-line test of the full-scale prototype cell was performed by stopping and extracting a radioactive ^{25}Al beam provided by ATLAS through in-flight collection and separation of reaction products from a ^{2}H (^{24}Mg, ^{25}Al) reaction on a cooled deuterium gas target. The collection efficiency of the catcher was measured as a function of the pressure and applied electric fields. The big catcher showed roughly 25% extraction efficiency for ^{25}Al at the maximum fields reached in this first test.

The on-line testing will continue in 2003 with numerous improvements including further development of the detection system to improve the mass identification of the extracted activity and better control of the radioactive beams injected from the ATLAS accelerator into the gas catcher. Off-line tests of the gas cell with a ^{252}Cf fission source between on-line tests will also continue, as are tests of the mass distributions of the extracted fission fragment species under different configurations of applied electric field and degraders. Since the gas pressure and the electric field determine the mean extraction time, the losses in the cell due to interactions with contaminants in the gas can be investigated. The performance of the catcher cell is limited by the strength of the achievable electric fields in the gas and by the accumulation of charge in the volume of the cell; efforts to quantify both of these limitations are underway. After completing testing at

ATLAS energies, the prototype will be moved to GSI's FRS where beam time has been approved for tests of the cell's performance at full RIA fragment energies.

_____

[1]G Savard et al, "Development and operation of gas catchers to thermalize fusion-evaporation and fragmentation products," NIM A 492 (2002) 57

c.5. Assessment of E-Beam as a Monitoring Tool for Lithium Film Thickness
(Itacil Gomes and J. A. Nolen)

Calculations were performed to asses the potential application of a low energy (20-50 KeV) electron beam as a diagnostic tool to monitoring thin lithium film used as electron strippers for heavy-ion accelerators. The distribution of the electron scattered by the lithium is a function of the thickness of the lithium film. In this concept the low energy electron beam will not interfere with the interactions between heavy ions and lithium film and will have a negligible effect in the energy deposition in the lithium. The e-beam will be directed at an angle to the heavy ion beam and a collecting plate will be placed perpendicular to the e-beam direction at a distance that does not interfere with other accelerator structures (in the calculations a 30-cm distance was assumed).

Calculations were performed for lithium film thicknesses of 9, 10, 11, and 12 μm and electron beam energies of 20, 30, 40, and 50 KeV. It was observed that the lowest electron beam energy analyzed (20 KeV) was the one to provide the highest potential for discriminating the variation of thickness of the lithium film. Figure III-34 shows a plot of the fraction of electrons collected in a plate placed at 30 cm from the lithium film as a function of the radius of the plate. As can be noticed for a plate with 30 cm of radius the fraction of electrons collected in the plate varies from 52.1% for the 12-μm thick film to 68.4% for the 9-μm thick lithium film. There are larger percentage changes in charge fraction collected for the smaller diameter plates. These differences allow us to infer that a simple circuit to measure the charge of electrons collected by a plate would have enough discrimination potential to be a valuable on-line real-time diagnostic tool for the thickness of the lithium film. This work should continue to include different e-beam energies and lithium film thicknesses.

Figure III-34. *Fraction of electrons collected in a plate placed at 30-cm from the lithium film as a function of the plate radius for a 20-KeV electron beam impinging on a thin-film of flowing lithium.*

c.6.   Calculations of the Heat Deposition Profiles in a Lithium Jet by Electron Beams
(Itacil C. Gomes and J. A. Nolen)

The MCNPX[1] Monte Carlo transport code was used to simulate the interaction of electron beams with the lithium jet. The energy deposition profile inside the jet was scored in small volumes and input in the graphic program Origin[2] for displaying the information. The assumed lithium jet thickness was 1 cm and the e-beam energies 1, 3, and 5 MeV. The geometry was divided in 3300 meshes with 0.1 mm increments in the radial direction and 0.3 mm increments in the axial direction. The objective of the calculations was to verify if a uniform energy deposition profile across the lithium jet could be achieved to simulate the uranium beam energy deposition (in a fragmentation target of RIA) as it crosses the lithium jet.

Figures III-35, III-36, and III-37 display the energy deposition (MeV/cm^3-beam particle) in the lithium jet for the 1, 3 and 5-MeV electron beam cases, respectively.   Figure III-35 shows that the 1-MeV electron beam loses most of its energy at half-way inside the target (at roughly 5mm) where the energy deposition is already reduced by more than one order of magnitude. The maximum energy deposition is about 103 MeV/cm^3 at positions close to the entrance of the beam into the jet. The calculated total energy deposited into the jet per incident electron is 0.997MeV, meaning that basically all energy carried by the beam is deposited into the jet. Figure III-36 shows that the 3-MeV electron beam is not "stopped" inside the lithium jet and it is still depositing 5-MeV/cm^3 at the beam center line after 1-cm of lithium. The maximum energy deposition is about 95 MeV/cm^3 at positions close to the entrance of the beam into the jet. The calculated total energy deposited into the jet per incident electron is 0.823 MeV, meaning that 17.7% of the energy carried by the beam is deposited elsewhere. This represents that for a 40 kW electron beam, about 33 kW will be deposited into the lithium.

Figure III-35. Energy deposition profile in MeV/cm^3 along the thickness of the beam for a 1MeV electron beam incident on a fast-flowing lithium jet.
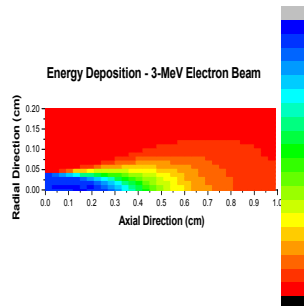
Figure III-36. Energy deposition (MeV/cm^3) profile for a 3-MeV electron beam incident on a fast-flowing lithium jet.
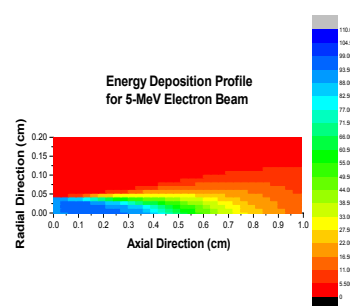
Figure III-37. Energy deposition (MeV/cm^3) profile for a 5-MeV electron beam incident on a fast-flowing lithium jet.

Figure III-37 shows that the 5-MeV electron beam is not "stopped" inside the lithium jet; it is still depositing 14-MeV/cm^3 in the center line of the beam after 1-cm of lithium. The maximum energy deposition is about 96 MeV/cm^3 at positions close to the entrance of the beam into the jet. The calculated total energy deposited into the jet per incident electron is 0.804 MeV, meaning that for a 40 kW electron beam, about 32 kW will be deposited into the jet. The maximum energy deposition of about 100 MeV/cm^3 is similar to that expected for a uranium beam hitting the lithium jet in the fragmentation target design.

Conclusions

The calculations indicated that there is no real gain in increasing the energy of the beam; the amount of energy deposited remains about the same. The energy deposition of the 1-MeV electron beam is much more concentrated in the first millimeters than in the other cases. The amount of energy escaping from the lithium jet is much larger in the high energy cases. The 1-MeV electron beam may present the best approach to simulate the energy deposition, due to its compactness in terms of energy deposition profile and the advantage of having the beam stopped inside the lithium jet. Also, the 1-MeV electron beam presents the highest overall energy deposition. The 3- and 5-MeV cases have a more concentrated energy deposition in the direction of the beam, and less scattering.

_____

[1]Laurie Waters, editor, "MCNPX User's Manual – Version 2.3.0", April 2002, LA-UR-02-2607.
[2]Origin – Microcal Software Inc. One Roundhouse Plaza, Northhampton, MA 01060 USA

IV. MEDIUM-ENERGY NUCLEAR PHYSICS RESEARCH

OVERVIEW

The overall goals of the Medium-Energy Physics research program in the Argonne Physics Division are to test our understanding of the structure of hadrons and the structure of nuclei, and to develop and exploit new technologies for high-impact applications in nuclear physics as well as other national priorities. In order to test our understanding of the structure of hadrons and the structure of nuclei within the framework of quantum chromodynamics, the medium-energy research program emphasizes the study of nucleons and nuclei on a relatively short distance scale. Because the electromagnetic interaction provides an accurate, well-understood probe of these phenomena, primary emphasis is placed on experiments involving electron scattering, real photons and Drell-Yan processes. The electron beams of the Thomas Jefferson National Accelerator Facility (TJNAF) are ideally suited for studies of nuclei at hadronic scales and represent one center of the experimental program. Staff members led in the construction of experimental facilities, serve as spokespersons or co-spokespersons for 16 experiments and are actively involved in several others. The group constructed the broad-purpose Short Orbit Spectrometer which forms half of the coincidence spectrometer pair that is the base experimental equipment in Hall C. We continue to improve the understanding of the spectrometer optics and acceptance. We will have a major role in re-establishing the SOS in Hall C this Spring for a series of five upcoming experiments. Argonne led the first experiment to be carried out at TJNAF in FY1996 and has completed eleven other experiments.

Recently, staff members have focused increasingly on studies of the nucleon. In FY2002 measurements were made on the ratio of the electromagnetic elastic form factors of the proton using a modified Rosenbluth method. These results will provide an important check of the polarization-transfer results that disagree so markedly from data recorded previously with the traditional Rosenbluth method. In FY2000, the exclusive cross sections from charged photopion production on the neutron and proton were measured up to a photon energy of 5.6 GeV as a test

of "transition region" models which describe the transition from hadronic degrees of freedom to quark-gluon degrees of freedom. Surprisingly, the results are consistent with predictions of pQCD even at these relatively low energies. Early in FY2003 measurements of polarization were performed for two-body photodisintegration of the deuteron at high energy. Measurements of kaon production on light nuclei provide important information on the basic strangeness production mechanisms and the poorly known low energy hyperon-nucleon interaction. A new initiative to search for color transparency in rho production in nuclei was approved by the JLab Program Advisory Committee and is scheduled to begin in July, 2003 in Hall B at JLab. This work represents an important extension of Argonne's earlier rho electro-production studies at HERMES.

HERMES, a broadly based North American-European collaboration is studying the spin structure of the nucleon using internal polarized targets in the HERA storage ring at DESY. Deep inelastic scattering has been measured with polarized electrons on polarized hydrogen, deuterium and ^{3}He. Argonne has concentrated on the hadron particle identification of HERMES, a unique capability compared to other spin structure experiments. In 1999 and under Argonne leadership, the dual-radiator ring imaging Cerenkov counter (RICH) was brought into operation at the design specifications to provide complete hadron identification in the experiment. The RICH has been operating routinely since its installation. This has allowed HERMES to make decisive measurements of the flavor dependence of the spin distributions. Subsequently, HERMES has performed a five-component decomposition of the proton's spin structure function and the first measurement of the x-dependence of the strange sea polarization. In addition, HERMES provided the first direct indication of a positive gluon spin contribution to the nucleon. Recent HERMES rho electro-production data were consistent with the concept of color transparency. A follow-up experiment will be performed in Hall B at JLab to confirm or deny this finding. Recently, HERMES has provided the first measurement of the b_1 structure function of the deuteron. During 2001, HERMES installed a transversely polarized target and is poised to provide the first measurements of the transversity structure function of the proton.

Measurements of high mass virtual photon production in high-energy proton-induced reactions have determined the flavor dependence of the sea of antiquarks in the nucleon. These measurements give insight into the origin of the nucleon sea. In the same experiment, the high-x absolute Drell-Yan cross sections were measured. These results demonstrate that modern high-x parton distributions are significantly in error. In FY01, a new initiative was approved by the FNAL PAC to continue these measurements with much higher luminosity at the FNAL Main Injector. These Drell-Yan experiments not only provide the best means to measure anti-quark distributions in the nucleon and nuclei, but represent an outstanding opportunity to perform these measurements at an ideal proton beam energy of 120 GeV.

The technology of laser atom traps provides a unique environment for the study of nuclear and atomic systems and represents a powerful new method that is opening up exciting new opportunities in a variety of fields, including nuclear physics. The group has developed a high-efficiency, high-sensitivity magneto-optical trap for rare, unstable isotopes of krypton. The group has collected and purified ancient ground water from the Nubian aquifer in Egypt. Cross checks with low-level counting techniques for ^{85}Kr have validated the new technique. For the first time, the group has trapped a single atom of ^{41}Ca from purified urine samples from patients who have ingested a ^{41}Ca tracer. This is a necessary first step to develop a new method for measuring rates of bone loss in humans. Recently, an optical trap was constructed and tested for the purpose of measuring the charge radius of ^{6}He at ATLAS. This trap will be moved and re-established in the BGO area at ATLAS in preparation for the experiment.

A new initiative to search for an electric dipole moment (EDM) of ^{225}Ra was begun during the past year.   The ultimate goal is to search for a non-zero EDM for ^{225}Ra and improve the sensitivity for nuclear EDM searches by approximately two orders of magnitude. This test of time-reversal symmetry represents an outstanding opportunity to search for new physics beyond the Standard Model. A new optical trapping laboratory for radium is being established for this experiment. In addition, an exploratory study is underway to determine the feasibility of measuring $\sin^2\theta_W$ in parity violating deep inelastic electron scattering from deuterium at either Jefferson Lab or SLAC.

A. NUCLEON PROPERTIES

a.1.   New Measurement of (G_E/G_M) for the Proton (J. Arrington, D. F. Geesaman, K. Hafidi, R. J. Holt, H. E. Jackson, D. H. Potterveld, P. E. Reimer, E. C. Schulte, K. Wijesooriya, B. Zeidman, and the E01-001 collaboration)

The structure of the proton is a matter of universal interest in nuclear and particle physics. Charge and current distributions are obtained through measurements of the electric and magnetic form factors, $G_E(Q^2)$ and $G_M(Q^2)$. These form factors can be separated by measuring elastic electron-proton scattering at two or more values of the virtual photon polarization parameter ε (*i.e.* by performing a Rosenbluth separation). Several such measurements have been made, and global fits to these measurements[1] showed that the ratio of G_E to G_M was consistent with unity, indicating equal distributions of charge and magnetization within the proton. Recent measurements at Jefferson Laboratory[2] used a recoil polarization measurement to extract G_E/G_M at large values of Q^2. They found that the ratio of $\mu_p G_E/G_M$ was unity at low Q^2, but fell linearly with increasing Q^2, reaching a value of 0.3 at $Q^2 = 5.5$ GeV^2 (see Fig IV-1).

It was initially suggested that the Rosenbluth data were unreliable at large Q^2 based on the inconsistency of form factors extracted from various Rosenbluth separations. A re-examination of the cross section measurements shows that the inconsistency is a result of the incomplete treatment (or lack of treatment) of normalization uncertainties when data from different experiments are combined to extract the form factors. When the normalization uncertainties are properly included, or when the form factors are extracted from a single data set, the results are not inconsistent. In addition, we performed a global reanalysis of the world's e-p cross section data, and find that the discrepancy is not the result of errors in a single data set, nor can it be explained by 'reasonable' adjustments of the experimental normalization factors.[3] In order to be confident in our knowledge of the proton form factors, we must determine not only which result is correct, but also why these two techniques disagree. A systematic problem with either set of measurements

would most likely affect other measurements which use the same techniques.

Experiment E01-001[4] was performed at Jefferson Lab in May 2002. Data were taken to allow a Rosenbluth extraction of G_E/G_M in the range where the previous data disagree with the recoil polarization measurements. The goal is to have a single data set that will provide a high-precision measurement of the ratio, with careful tests of the systematic uncertainties. In addition to careful monitoring of potential uncertainties, this measurement used a different experimental technique which significantly decreased our sensitivity to the systematics that have limited previous measurements.

The main difference in this measurement is that we detected the struck proton, rather than the scattered electron. Detecting the proton means that there is no ε-dependence to the momentum of the detected particle, much less rate-dependence, and significantly less sensitivity to uncertainties in the beam energy or scattering angles. Finally, the radiative corrections are smaller, and have less ε dependence.

The other unusual feature of this measurement is that while we perform a Rosenbluth extraction at high-Q^2 in one spectrometer, we will make a simultaneous measurement at low Q^2. Because the value of G_E/G_M at low Q^2 is relatively well known, and because the kinematics chosen make the low Q^2 measurement insensitive to the photon polarization ($\Delta\varepsilon$ is kept small), we can use the low Q^2 point as a pseudo-luminosity monitor to correct for any error in the beam charge and target thickness measurements.

_____
[1]R. C. Walker *et al.*, Phys. Rev. D **49**, 5671 (1994).
[2]M. K. Jones *et al.*, Phys. Rev. Lett. 84, 1398 (2000); O. Gayou *et al.*, Phys. Rev. C **64**, 038292 (2001); O. Gayou *et al.*, Phys. Rev. Lett. **88**, 092301 (2002).
[3]J. Arrington, preprint, hep-ph/0209243.
[4]Jefferson Lab Experiment E01-001, 'New Measurement of (G_E/G_M) for the Proton', J. Arrington and R. E. Segel, spokespersons.

Figure IV-1 shows the existing Rosenbluth and recoil polarization results, along with projected uncertainties for E01-001 for two cases: $\mu_p G_E/G_M = 1$, and $\mu_p G_E/G_M$ consistent with the polarization measurements. If the results agree with previous Rosenbluth extractions, then it will still be unclear which technique is correct, but we will rule out several of the most likely causes for systematic errors in the previous Rosenbluth

extractions. If we agree with the polarization transfer measurements, we will be sure of the $\mu_p G_E/G_M$ results extracted by this technique, and will have identified the likely causes for the discrepancy with the standard Rosenbluth measurements. The analysis of the data is currently underway at Argonne, and we expect preliminary results in 2003.
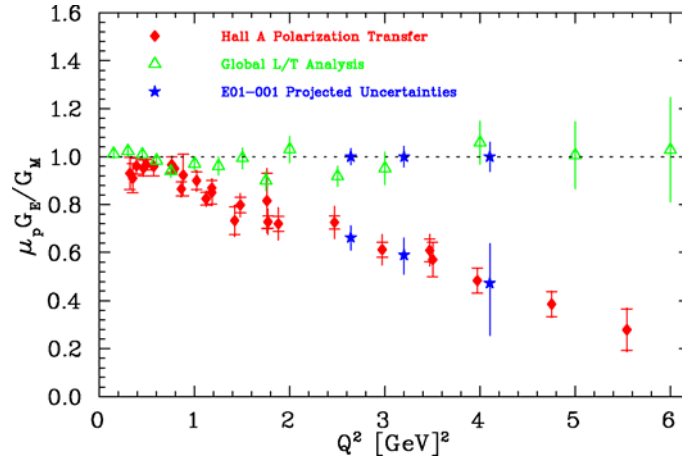
Fig. IV-1. Existing measurements of $\mu_p G_E/G_M$ along with projected uncertainties for this experiment. Uncertainties are shown for results consistent with form factor scaling, and for results consistent with the polarization transfer results.

a.2.   Separated and Unseparated Structure Functions in the Nucleon Resonance Region
   (J. Arrington, D. F. Geesaman, R. J. Holt, T. G. O'Neill, D. H. Potterveld, and the
   E99-119, E00-002, and E00-116 collaborations)

A great deal of our understanding of the quark sub-structure of the nucleon comes from inclusive electron scattering. Reliable *global* descriptions of inclusive electroproduction data are necessary for electron-nucleon scattering model development, accurate radiative correction calculations, and the extraction of form factors, structure functions, and parton distribution functions from inclusive electron scattering experiments. However, most measurements have focused on the deep inelastic region. High precision cross section measurements in the resonance region, combined with a separation of the longitudinal σ_L and transverse σ_T components, will substantially improve the global description of electroproduction at moderate to high Q^2 and large Bjorken-x. While the ratio R = σ_L/σ_T has been measured up to high Q^2 for elastic and deep inelastic scattering, there exist few measurements of R in the resonance region at moderate or high

momentum transfers. The current uncertainty in R in the resonance region is greater than 100%. Experiment E94-110[1] ran in 1999 in Hall C at Jefferson Lab, and made a precision measurement of R in the resonance region, up to $Q^2 = 4.5$ GeV^2.

Previous JLab measurements of inclusive scattering in the resonance region, measuring just the F_2 structure function, have been analyzed in terms of Local Duality. It was observed that the resonance region data, when averaged over the Nachtmann variable, ξ, reproduced the structure function as measured in the deep inelastic region[2]. This duality of the DIS and resonance structure function held to better than 10%, down to $Q^2 = 0.5$ GeV/c^2. It was also observed that at low ξ, the resonance region structure function deviated from the DIS value, and showed a valence-like behavior[3], going to zero as ξ decreased. While this duality has been

observed for hydrogen, deuterium, and nuclear targets for F_2, no such data existed for the F_1 structure function in the resonance region. The new results from E94-110 yield a high-precision measurement of R in the resonance region, and also show that duality holds in both the F_2 and F_1 structure functions (see Fig. IV-2). In addition, the data show for the first time longitudinal contributions to the resonance electroproduction. These data will allow improved extractions of the transition form factors from inclusive measurements, which usually involves assuming that the resonance production occurs only in the transverse channel.

Future experiments, three of which are scheduled to run in 2003, will further extend these duality measurements. There is an approved experiment to extend duality studies of F_2 on hydrogen and deuterium to $Q^2 = 7.5$ GeV^2, another to make measurements at low x and Q^2 to study the valence-like nature of the resonance region structure function, and a measurement of duality in semi-inclusive pion production ('tagged' electron scattering). In addition, there is an approved experiment to perform a similar Rosenbluth separation in the resonance region for deuterium.

---

[1]JLab experiment E94-110, 'Measurement of R=σ_L/σ_T in the Nucleon Resonance Region', C. E. Keppel, spokesperson.
[2]I. Niculescu *et al.*, Phys. Rev. Lett. **85**, 1182 (2000).
[3]I. Niculescu *et al.*, Phys. Rev. Lett. **85**, 1186 (2000).
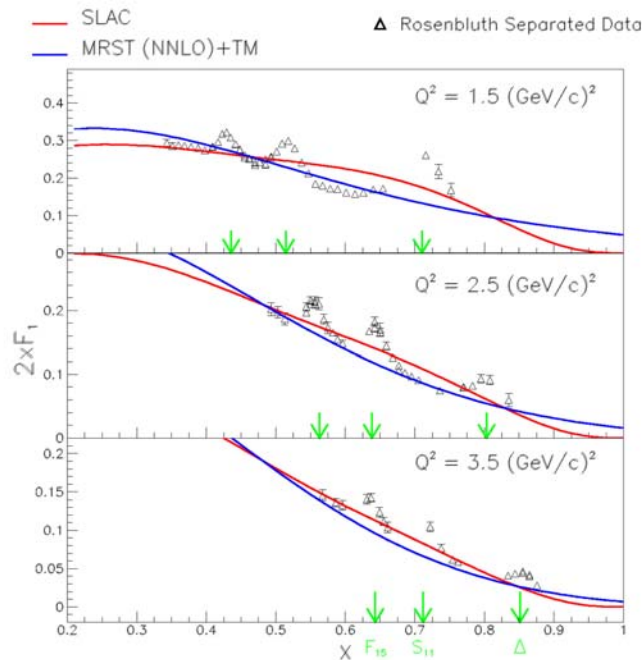
Fig. IV-2. The separated structure function, 2xF$_1$, as a function of x for three Q^2 bins, compared to a SLAC parameterization for DIS and a NNLO calculation using MRST parton distribution functions and target mass corrections.

a.3.   Charged Pion Photoproduction From the Nucleon (R. J. Holt, J. Arrington, K. Bailey, P. E. Reimer, F. Dohrmann, K. Hafidi, T. O'Connor, E. C. Schulte, K. Wijesooriya, and JLab E94-104 Collaboration)

The goal of experiment E94-104 is to measure the cross sections for the $\gamma n \to \pi^- p$ and the $\gamma p \to \pi^+ n$ reactions for photon energies up to 5.5 GeV and at several reaction angles. The experiment was completed and the data are nearing the final analyses. From these data, the π^-/π^+ ratio can be formed and compared with existing models. One of the most celebrated models of the

transition region from hadronic degrees of freedom to the quark-gluon degrees of freedom is represented by a one-hard gluon exchange diagram. This model gives a definite prediction[1] for the ratio:

$$\frac{d\sigma(\gamma n \to \pi^- p)}{d\sigma(\gamma p \to \pi^+ n)} = \left(\frac{ue_d + se_u}{ue_u + se_d}\right)^2$$

where the e_i are the charges of the quarks, and s and u are the usual Mandelstam variables. The data at $\theta_{cm} = 90^0$ are shown in Fig IV-3. The cross sections for both the reactions are consistent with the constituent counting rules at the highest energies, while the ratio at

the highest energies is consistent with the pQCD prediction. The results are in remarkable agreement with pQCD; however, data should be taken at higher energies to confirm this trend. The results also indicate a rather broad, resonance-like structure near s = 5 GeV^2, which should be further investigated with complete angular distribution and polarization measurements. The data at other angles are presently undergoing analysis.

[1]H. Huang and P. Kroll, Eur. Phys. J. **C17**, 423 (2000).
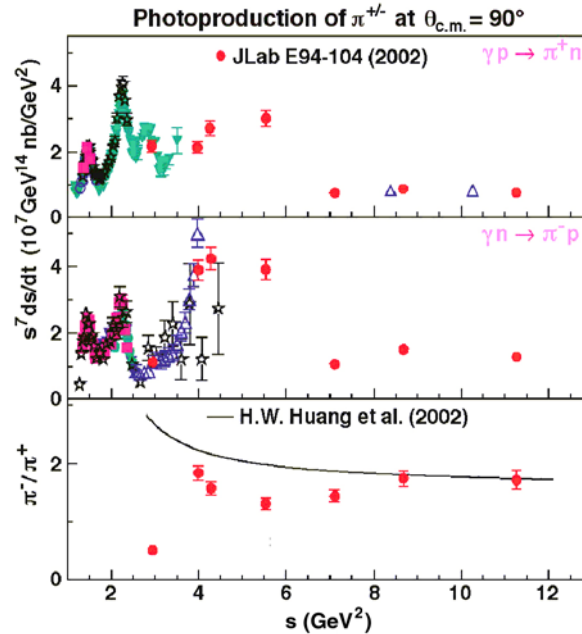
Fig. IV-3. *The two upper panels display the quantities $s^7 d\sigma/dt$ as a function of s for the $\gamma p \to \pi^+ n$ and the $\gamma n \to \pi^- p$ reactions, respectively. The ratio of these two cross sections is shown in the lower panel along with the pQCD prediction of Huang and Kroll.*

a.4. Search for QCD Oscillations in the $\gamma N \to \pi N$ Reactions (R. J. Holt, J. Arrington, D. F. Geesaman, H. E. Jackson, P. E. Reimer, K. Hafidi, E. C. Schulte, K. Wijesooriya, and JLab E02-010 Collaboration)

A proposal to search for QCD oscillations in exclusive charged photopion reactions was approved by the Jefferson Laboratory Program Advisory Committee. The goal of the experiment is to search in photopion reactions for the oscillatory effect observed in exclusive high-energy proton-proton elastic scattering. In p-p elastic scattering the cross section was found to oscillate about the $1/s^{10}$ dependence expected from the constituent counting rules. This oscillatory behavior has been ascribed[1] to a short distance (hard-scattering) amplitude which interferes with a long-distance

amplitude (Landshoff). This process is analogous to coulomb-nuclear interference observed in low energy charged particle scattering; however, the QCD oscillations arise from soft gluon radiation rather than from photon radiation as in the QED case. This interference also can give rise to polarizations observed in high energy exclusive hadron-hadron scattering processes. In the proposed experiment, the cross sections will be measured in a fine energy scan up to the highest energy available at Jefferson Lab.

[1]S. J. Brodsky, C. E. Carlson, and H. Lipkin, Phys. Rev. D **20**, 2278 (1979); J. P. Ralston and B. Pire, Phys. Rev. Lett. **65**, 2343 (1990).

B. SUBNUCLEONIC EFFECTS IN NUCLEI

b.1. Proton Polarization Angular Distribution in Deuteron Photodisintegration
(R. J. Holt, J. Arrington, K. Hafidi, P. E. Reimer, E. C. Schulte, K. Wijesooriya, and JLab E00-007 Collaboration)

The overall goal of experiment E00-007 is to determine the mechanism that governs photoreactions in the GeV energy region. Our previous measurements[1] of induced polarization in deuteron photodisintegration produced surprising results at photon energies between 1 and 2 GeV. First these results disagreed markedly with previous experiments and secondly there was a remarkable disagreement with the meson-exchange model. The induced polarizations above 1 GeV and at $\theta_{cm} = 90^0$ were near zero, consistent with hadron helicity conservation.; however, it might be expected that the results could have been accidentally zero because of a $\sin(n\theta)$ dependence where n happens to be even. Thus, the goal of this experiment was to determine the angular dependence of the polarization. The experiment was completed in October 2002 and data were taken at five center-of-mass angles: 37^0, 53^0, 70^0, 90^0 and 110^0. The induced polarizations as well as polarization transfers were measured. Presently, the data are undergoing analysis.

_____
[1]K. Wijesooriyia et. al., Phys. Rev. Lett. **86**, 2975 (2001).

b.2. Measurement of the Transparency Ratio for the A(γ,π⁻p) Reaction in Helium and Deuterium (R. J. Holt, J. Arrington, K. Bailey, P. E. Reimer, F. Dohrmann, K. Hafidi, T. O'Connor, E. C. Schulte, K. Wijesooriya, and JLab E94-104 Collaboration)

The transparency for the ^{4}He(γ,π⁻p) reaction compared with the D(γ,π⁻p)p reaction was measured as a function of photon energy in Hall A at Jefferson Laboratory. The fundamental process $\gamma n \rightarrow \pi^- p$ exhibits a scaling behavior consistent with the constituent counting rules above a photon energy of 2.5 GeV. Thus, one can use this reaction in the nuclear medium to determine whether the onset of color transparency has been observed. The pion is expected[1] to exhibit the phenomenon of color transparency more readily than the proton since the pion has only two constituent partons. The data are presently being analyzed.

_____
[1]B. Blättel et al, Phys. Rev. Lett. **70**, 896 (1993).

b.3. Measurements of the Nuclear Dependence of R = σ_L/σ_T at Low Q² (J. Arrington, D. F. Geesaman, T. G. O'Neill, D. H. Potterveld, and the E99-118 Collaboration)

Inclusive electron scattering is a well understood probe of the partonic structure of nucleons and nuclei. Deep inelastic scattering has been used to make precise measurements of nuclear structure functions over a wide range in x and Q^2. The ratio R = σ_L/σ_T has been measured reasonably well in deep inelastic scattering at moderate and high Q^2 using hydrogen and deuterium targets. However, R is still one of the most poorly understood quantities measured in deep inelastic scattering and few measurements exist at low Q^2 or for nuclear targets. Existing data rule out significant nuclear effects in R only at moderate to large values of Q^2.

Jefferson Lab Experiment E99-119 is a direct measurement of R at low x and low Q^2. The experiment was performed in July of 2000 and data was taken for hydrogen, deuterium, and heavier nuclei. The data are largely analyzed, but the cross section extraction at extremely small values of x and Q^2 involve large radiative corrections. While the radiative corrections will limit the region for which R can be extracted, these data are ideal for testing the radiative correction procedures in these extreme kinematics, and in particular the corrections coming from the nuclear elastic contributions.

b.4.   Electroproduction of Kaons and Light Hypernuclei (J. Arrington, K. Bailey, F. Dohrmann, D. F. Geesaman, K. Hafidi, B. Mueller, T. G. O'Neill, D. H. Potterveld, P. Reimer, B. Zeidman, and the E91-016 Collaboration)

Jefferson Lab experiment E91-016, "Electroproduction of Kaons and Light Hypernuclei is a study of the production of Kaons on targets of H, D, ^{3}He, and ^{4}He at an incident electron energy of 3.245 GeV and $Q^2 \approx 0.37$ GeV^2. For H and D targets, additional data were obtained at an energy of 2.445 GeV and $Q^2 \approx 0.5$ GeV^2. The scattered electrons and emergent kaon were detected in coincidence with the use of the HMS and SOS spectrometers in Hall C. Particle identification utilizing time-of-flight techniques together with Aerogel Cerenkov detectors provided clean missing-mass spectra and allowed subtraction of random backgrounds. In addition to obtaining spectra, angular distributions were measured at forward angles with respect to the virtual photons.

The fundamental interaction being studied is the $N(e,e'K^+)Y$ where Y is either Λ or Σ and N is a nucleon, either free or bound in a nucleus. For H, the final state can only be a Λ or Σ^0, with a missing mass spectrum consisting of two sharp peaks. For heavier targets, however, not only can Σ^- be produced on the neutron, but the relative motion of the bound nucleons results in quasi-free broadening of the peaks. Since there is no known bound state in the mass 2 hyper-nuclear system, only quasi-free production is observed. For the heavier targets, ^{3,4}He, both Fermi broadening and a rapidly increasing number of final state configurations makes it more difficult to separate the various contributions Because of the small mass difference between Σ^0 and Σ^-, distinguishing between these contributions is not possible without assuming that the Λ/Σ^0 ratio is the same as that for the free proton. Subtraction of the normalized Σ^0 contribution yields a value for Σ^- production on the neutron. The ratio of cross sections, Σ^0/Σ^-, suggests s-channel dominance for the $D(e,e'K^+)$ reaction in the present kinematic regime.

The analyses of the data for ^{4}He provide unambiguous evidence for the formation of the bound hypernucleus hyper-^{4}H; the first observation of electroproduction of a hyper-nuclear bound state. From other reactions, a 1^+ excited state bound by ~ 1 MeV is known to exist in this nucleus; the 0^+ ground state is bound by 2.04 MeV. For ^{3}He, the evidence for the electroproduction of the hypertriton, *i.e.* the p-nΛ state bound by ~ 130 keV, is less convincing. While barely discernible near zero degrees, because of kinematic effects, the bound state becomes more evident away from zero degrees.

Extraction of cross sections for specific channels becomes more difficult with increasing mass because of the rapidly growing number of possible final configurations. However, the various models that have been utilized for the helium isotopes yield simulations that are in reasonable agreement with the shapes of the spectra. Since it is not possible to distinguish between Σ^0 and Σ^- production, the analyses assume the Λ/Σ^0 ratio data for H obtained at the same laboratory settings as input to extract the Σ^- yields. Further analyses of these results are in progress.

In addition, the excellent particle identification allowed an ancillary study of the electroproduction of ω mesons on the proton. The relatively large cross section for this process, combined with kinematic focusing of the residual protons, provided high yields and excellent statistical accuracy over a wide range of c.m. angles. A representative missing mass spectrum is shown in Fig. IV-4. The data result in new insights into the fundamental production mechanisms.

E91-016 was a high-statistics study of Kaon electroproduction on the light nuclei ^{2}H, ^{3}He, and ^{4}He. During the course of the experiment, extensive data were obtained for the H target as well as additional calibration data for C and Al. These latter data have been analyzed to ascertain the general mass dependence of the cross section for Kaon electroproduction. E91-016 has provided all or a substantial fraction of the thesis data for five students from Hampton University, University of Pennsylvania, and Temple University.
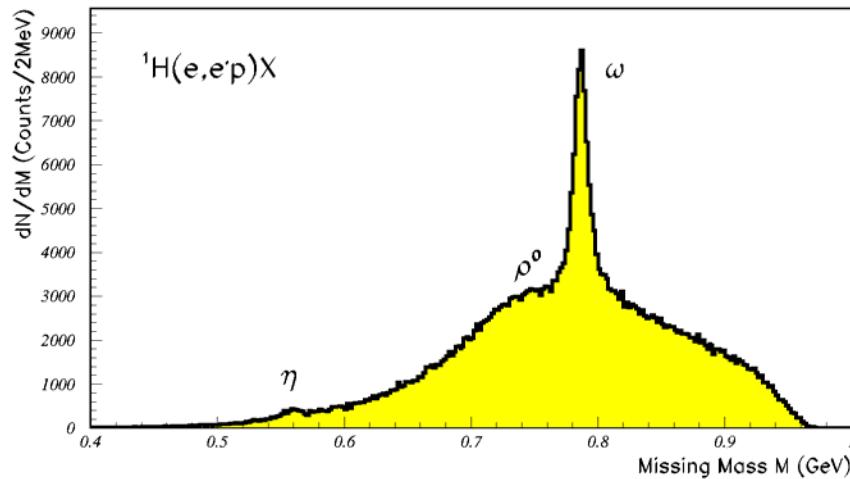
Fig. IV-.4. Missing mass spectrum for light vector meson electroproduction, showing signals from η, ρ^0, and ω production.

b.5.   Measurement of the EMC Effect in Very Light Nuclei (J. Arrington, F. Dohrmann,
D. Gaskell, D. F. Geesaman, K. Hafidi, R. J. Holt, H. E. Jackson, D. H. Potterveld,
P. E. Reimer, B. Zeidman, and the E00-101 collaboration)

In nuclei, the quark momentum distribution varies with the density of the nucleus. The structure function is suppressed in heavy nuclei at large values of x (corresponding to large quark momenta), and enhanced at low x values. Measurements to date indicate that the overall form of this modification is the same for all nuclei, but the magnitude of the enhancement and suppression is larger for heavier nuclei. Many attempts have been made to explain the EMC effect, but none of the proposed models can fully reproduce the observed modifications, and there is still no consensus on which effect or combination (if any) explain the data.

Experiment E00-101[1] will measure the EMC effect for ^{3}He and ^{4}He. The current data cannot distinguish different models of the density dependence of the effect. Because ^{4}He has an anomalously large density for a light nucleus, it is the most sensitive test to determine if the EMC effect scales with A or with nuclear density. More importantly, these measurements of the EMC effect can be compared to exact few body calculations. If the EMC effect is caused by few

nucleon interactions, the universal shape observed in heavy nuclei may be a result of a saturation of the effect, and the shape may be different in few-body nuclei. While the existing data on heavy nuclei all show the same x-dependence, there are calculations that predict significantly different dependences for very light nuclei. By making precise measurements in light nuclei, we will be able to distinguish between different models of the EMC effect based on their predictions for few-body nuclei.

Finally, a measurement of $A \leq 4$ nuclei will help constrain models of the EMC effect in deuterium. Models of nuclear effects in deuterium and ^{3}He must be used to extract information on neutron structure, and a high precision measurement including ^{1}H, ^{2}H, ^{3}He, and ^{4}He will give a single set of data that can be used to evaluate these models in several light nuclei. This will help to quantify the model dependence of the neutron structure functions inferred from measurements on ^{2}H and ^{3}He.

---

[1]Jefferson Lab Experiment E00-101, 'A Precise Measurement of the Nuclear Dependence of Structure Functions in Light Nuclei', J. Arrington, spokesperson.

b.6.   Measurement of High Momentum Nucleons in Nuclei and Short Range Correlations
(J. Arrington, D. F. Geesaman, K. Hafidi, R. J. Holt, H. E. Jackson, P. E. Reimer,
E. C. Schulte, and the E02-019 collaboration)

Inclusive scattering from nuclei at low energy transfer (corresponding to $x > 1$) is dominated by quasielastic scattering from nucleons within the nucleus. As the energy transfer is decreased, the scattering probes nucleons of increasing momentum and we can map out the distribution of high momentum nucleons in nuclei. Experiment E89-008[1] measured inclusive scattering for deuterium, carbon, iron, and gold at $x > 1$ using 4 GeV electrons at Jefferson Lab. These data can be used to constrain the high momentum components of nuclear spectral functions. In addition, as the high momentum nucleons are dominantly generated by short range correlations (SRCs), these data allows us to examine the strength of two-nucleon correlations in heavy nuclei.

Experiment E02-019[2] will extend these measurements to higher values of x and Q^2 using the 6 GeV electron beam at JLab. In addition to measuring scattering from deuterium and heavy nuclei, data will be taken on ^{3}He and ^{4}He. The higher Q^2 values in this experiment should simplify the extraction of the high momentum components, as effects such as final state interactions should be reduced as Q^2 is increased. Measurements with few-body nuclei (^{2}H, ^{3}He, and ^{4}He) allow contact with theoretical calculations via essentially "exact" calculations for few-body systems. This can be used to study in detail contributions to the interaction beyond the impulse approximation (*e.g.* final state interactions). Data on heavy nuclei can then be used to constrain the high momentum components of their spectral functions, as well as allowing an extrapolation to nuclear matter.

The extension to higher energies will provide us will significantly greater sensitivity to the high momentum components of the nuclear wave function, probing nucleons with momenta in excess of 1000 MeV/c. This will improve our ability to study the structure of nucleon correlations in nuclei. Direct comparisons of heavy nuclei to deuterium at large x will allow us to map out the strength of two-nucleon correlations in both light and heavy nuclei. These data will also be significantly more sensitive to the presence of multi-nucleon correlations. Just as the ratio of heavy nuclei to deuterium at $x > 1.5$ shows that the distribution in heavy nuclei is dominated by two-nucleon correlations, a similar ratio of heavy nuclei to ^{3}He at $x > 2.5$ may provide the first experimental signature of three-nucleon correlations. Multi-nucleon correlations will also modify the Q^2-dependence of the ratio to deuterium, due to the QCD-evolution of the structure function. Any additional strength at $x > 2$ coming from multi-nucleon correlations in heavy nuclei will be evolved down to lower x values as Q^2 increases, leading to an increase in the ratio to deuterium. Figure IV-5 shows calculations of this ratio with and without the presence of multi-nucleon correlations. E02-019 will reach $Q^2 \approx 8$ GeV^2 for $x \approx 1.7$, where the multi-nucleon correlation model predicts a factor of two increase in this ratio. This will be an important first step in the study of multi-nucleon correlations.

In addition to probing nucleon distributions and short range correlations, these data fill in a significant void in our knowledge of the nuclear structure function. Little data exist for nuclei at large x, yet such data are important in the study of scaling and duality, higher twist effects, and nuclear dependence of the structure function. In addition, while the $x > 1$ structure function is often neglected, it must be included in studies of the energy-momentum sum rule or analysis of the QCD moments. While E02-019 will focus on the study of the high momentum nucleons in nuclei, it provides the data necessary for a variety of studies.

---

[1]J. Arrington *et al*., Phys. Rev. Lett. **82**, 2056 (1999).
[2]Jefferson Lab Experiment E02-019, 'Inclusive Scattering from Nuclei at $x > 1$ and High Q2 with a 6 GeV Beam', J. Arrington, D. B. Day, A. Lung, and B. W. Filippone spokespersons.
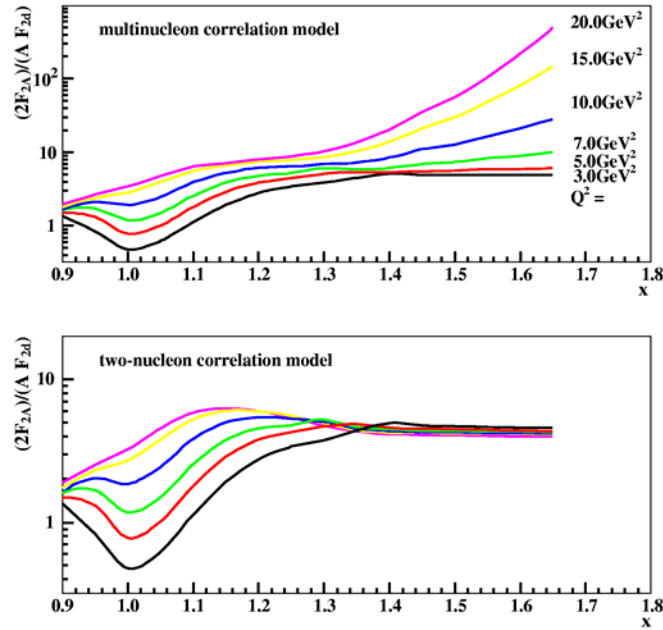
Fig. IV-5. Calculation of the ratio of structure function of Iron to Deuterium for x > 1 in the two-nucleon correlation model and the multi-nucleon correlation model.

C. QUARK STRUCTURE OF MATTER

c.1.   The Structure Function of the Pion (R. J. Holt, P. E. Reimer, and K. Wijesooriya)

The light mesons have a central role in nucleon and in nuclear structure. The masses of the lightest hadrons, the mesons, are believed to arise from chiral symmetry breaking.   The pion, being the lightest meson, is particularly interesting not only because of its importance in effective theories, but also because of its importance in explaining the quark sea in the nucleon and the nuclear force in nuclei.   Most of our information about the pion structure function in the valence region originates from π p Drell-Yan scattering on a W target. The analysis of the Drell-Yan data was questioned[1] recently, and now studies of this analysis are underway. The Drell-Yan data[2] were re-analyzed with the following improvements: next-to-leading order analysis, modern nucleon structure functions and modern nuclear effects, and a less-restrictive formula for the pion structure function. The results of this re-analysis are undergoing checks now to ensure reliability.

Studies were completed to examine the feasibility of making measurements at Jefferson Lab using an 11-GeV incident electron beam. With the relatively high luminosity which can be achieved at an upgraded Jefferson Lab, the pion structure can be measured, over a limited range in x. Additional investigations are being made of this reaction using a future electron-ion collider.[3]

_____
[1]M. B. Hecht *et a*l., Phys. Rev. C **63**, 025213 (2001).
[2]J. S. Conway *et a*l., Phys. Rev. D **39**, 92 (1989).
[3]R. J. Holt and P. E. Reimer, Proc. of the Second Workshop on the Polarized Electron Ion Collider, MIT (2000).

c.2. Measurements of Spin-Structure Functions and Semi-Inclusive Asymmetries for the Nucleon at HERA (H. E. Jackson, A. El Alaoui, K. G. Bailey, T. P. O'Connor, K. Hafidi, D. H. Potterveld, P. Reimer, Y. Sanjiev, and the HERMES Collaboration)

HERMES, HERA measurement of spin, is an international collaboration of 31 institutions formed to address a basic question of hadronic structure. How do the spins of its constituent quarks combine with the spin of the glue and the angular momentum of the partons to give the proton its spin of ½? The HERMES experiment uses polarized internal targets in the HERA 30 GeV lepton storage ring at the DESY laboratory, in Hamburg Germany. By emphasizing semi-inclusive deep inelastic scattering (SIDIS) in which a hadron is observed in coincidence with the scattered lepton, HERMES brings a new dimension to studies of spin structure. The collaboration has collected and analyzed millions of deep-inelastic scattering events using longitudinally polarized electrons and positrons incident on longitudinally polarized internal gas targets of ^{1}H, ^{2}H, and ^{3}He, as well as thicker unpolarized gas targets. Measurements have been extended to a new domain during the past year with the installation and commissioning of a target with polarization transverse to the beam polarization. The scope of the HERMES program has evolved far beyond the original focus on the spin structure of the nucleon and now encompasses a broad range of subjects in polarized and unpolarized physics, but with the common goal of providing fundamental insights into the structure of the nucleon and how it is affected by the nuclear medium.

The study of the spin structure of the nucleon continues to be of highest priority. Spin asymmetries have been measured using polarized targets of hydrogen, deuterium, and ^{3}He. Analysis of the inclusive and semi-inclusive deep-inelastic scattering data from these unique undiluted targets has resulted in the world's most precise determination to date of the separate contributions of the up, down and sea quarks to the nucleon spin. Preliminary results from the most recent analyses have probed for the first time directly the polarization of the strange sea as well as the flavor asymmetry of the light sea polarization. While inclusive measurements have become a calibration benchmark for SIDIS studies, even here new physics continues to emerge. For the first time, the tensor polarized structure function for the deuteron has been measured using the HERMES polarized target. The result shows the promise of a new probe of nuclear effects at the partonic level. The observation of a single-spin asymmetry in the azimuthal distribution of positive pions detected in coincidence with the deep-inelastic scattering of positrons from a *longitudinally*

polarized proton target has been a development of major interest.

The theoretical interpretation of this result is under vigorous discussion. One possible explanation involves a particular chiral-odd fragmentation function that could make feasible at HERMES the first measurement of transversity, the only remaining unmeasured and one of the three most fundamental (leading twist) flavor-sets of parton distribution functions. Current measurements with a transversely polarized proton target will provide a clear test of the validity of this explanation as opposed to an alternative possible reaction mechanism, the Sivers effect, which involves totally different physics. Recent measurement of a lepton-beam spin asymmetry in the azimuthal distribution of detected photons in Deeply Virtual Compton Scattering (DVCS) has provoked wide interest. Interference with the indistinguishable but well-understood Bethe-Heitler process fortuitously gives rise to a rich variety of such asymmetries, which will continue to emerge from HERMES data. DVCS is considered to be the most reliable of the various hard exclusive processes that constrain the generalized or 'skewed' parton distributions, which are now the subject of intense theoretical development as, *e.g*., they embody information about *orbital* angular momenta of partons. This type of measurement has been extended to exclusive and semi-inclusive electroproduction of pions and kaons where HERMES is releasing regularly new data showing for the first time substantial single-spin azimuthal asymmetries.

The ability to run with high density unpolarized targets provides HERMES with a tool reaching far beyond spin structure studies. The large momentum and solid angle acceptance of the HERMES spectrometer open a broad range of physics topics to exploration, and have resulted in a tool for the general study of photon-hadron interactions. Using its unique capabilities, in recent years HERMES has performed a measurement of the flavor asymmetry between up and down quarks in the nucleon sea, studies of fragmentation of up and down quarks to pions, measurement of the DIS and resonance contributions to the generalized Gerasimov-Drell-Hearn integral for both the proton and neutron, a measurement of the spin transfer from virtual photons to Λ^0 hyperons, and measurements of the effect of the nuclear environment. In the past year, a demonstration of the effects of color transparency in the production of rho mesons has been published, and the study of parton

propagation in nuclei has been extended to heavy nuclear targets. Recent developments and new results pertaining to these physics topics are discussed in more detail below.

The spectrometer and associated equipment continue to perform at design capability. As time and resources permit, systems are continually upgraded and new capabilities are added. The data acquisition software has been completely revamped to run under linux. The RICH particle identification system provides hadron separation over almost the full HERMES acceptance. A new transversly polarized target has been installed for operations during the 2002-2004 running period.

Installation of a system of silicon strip detectors for enhanced detection of Lambda decay products is almost complete. Design work is in progress for a large acceptance recoil detector array to be used to enhance solid angle acceptance and missing mass resolution in planned measurements of DVCS. These continuing investments in enhanced capability ensure that HERMES will continue to produce results at the forefront of the field. HERMES has a broad physics program and has had scientific impact on an number of fundamental questions about the strong interaction. HERMES is playing an important role in the worldwide experimental investigation of QCD.

c.3. Flavor Decomposition of the Sea Quark Helicity Distributions in the Nucleon from Semi-Inclusive Deep-Inelastic Scattering (K. Hafidi, A. El Alaoui, K. G. Bailey, T. P. O'Connor, H. E. Jackson, D. H. Potterveld, P.E. Reimer, and the HERMES Collaboration)

The last decade has seen a remarkable progress in measuring the polarized quark distribution using inclusive Deep Inelastic Scattering (DIS). However, the information available from DIS has inherent limitations, as the cross sections are sensitive to only the square of the charge of the quark absorbing the exchanged virtual photon. Therefore sea quarks can not be distinguished from valence quarks. In addition the precision and kinematic coverage of the DIS measurements is still rather limited. Consequently, present Next to Leading Order (NLO) analyses also use information from hyperon β-decay to constrain the problem via the additional assumption of SU(3) flavor symmetry among baryons, which is known to be inexact. The results from QCD NLO analyses indicated that the quark spin account for a relatively small fraction of the total nucleon spin, of order of 20-40% (the value depends on the NLO factorization scheme used in the analysis). Further, the strange sea would seem to have a negative polarization of order of -10% which is very sensitive to SU(3) symmetry breaking effect.

Semi-inclusive measurements represent an alternative approach that avoids this assumption about SU(3) symmetry and allows direct measurements of the quark helicity distributions and in the particular of the sea quarks. In these measurements, a hadron is detected in coincidence with the scattered beam lepton. Through the fragmentation functions, a probabilistic relation exits between the flavor of the struck quark and the flavor content of the hadrons generated in the final state. By measuring the spin asymmetry for hadrons of various types, one may separate the polarized parton distributions by flavor.

Measurements of scattering asymmetries with identified pions and kaons from a deuterium target in combination with identified pions from hydrogen target and with inclusive data result in the first five flavor extraction of quark polarizations, *i.e.* Δu, Δd, $\Delta\bar{u}$, $\Delta\bar{d}$, and Δs from semi inclusive data, with the only assumption that s and $\bar{s}$ have the same polarization. Factorization into parton distributions and fragmentation functions is assumed in the relation between the measured asymmetries and quark polarizations. The resulting coefficients or "purities" include effects of experimental acceptance, and are determined with a Monte Carlo generator and CTEQ low Q^2 parton distributions.

Figure IV-6a shows the results compared to two LO QCD fits[1] to previously published inclusive data. These fits not only assume SU(3) flavor symmetry to incorporate hyperon β-decay data, but also here invoke symmetry among the sea distributions in order to present them separately. The extracted helicity distributions of u(x) and d(x) are consistent with previous (semi) inclusive results.[2] The sea distributions, extracted separately here for the first time, are consistent with zero and with each other. There is no indication of the negative polarization of the strange sea that appears in the analysis of only inclusive data assuming SU(3) symmetry applied to hyperon β-decay data. Another interesting feature of the results, is shown in Fig. IV-6b, there is no evidence of a large a positive flavor asymmetry between $\bar{u}(x)$ and $\bar{d}(x)$ in

the light quark sea that was predicted by a theoretical calculation based on the chiral quark soliton model.[3] In contrast to this possible discrepancy, this model does successfully explain the previously observed substantial value for the unpolarized flavor asymmetry between $\bar{u}(x)$ and $\bar{d}(x)$.[4]

In conclusion, a leading order extraction from new semi inclusive DIS data has produced separated helicity distributions for five flavors: Δu, Δd, $\Delta \bar{u}$, $\Delta \bar{d}$, and $\Delta s \equiv \Delta \bar{s}$. There is no evidence for either a negative strange sea polarization or for a flavor asymmetry in the helicity distributions of the light sea.

[1] M. Glück *et al.*, Phys. Rev. D **63**, 094005 (2001); J. Blümlein and H. Bötcher *et al.*, Nucl. Phys. **B636**, 225 (2002).
[2] B. Adeva *et al.*, Phys. Lett. **B420**, 180 (1998); K. Ackerstaff *et al.*, Phys. Lett. **B464**, 123 (1999).
[3] B. Dressler *et al.*, EPJC **14**, 147 (2000).
[4] B. Dressler *et al.*, hep-ph/9809487.
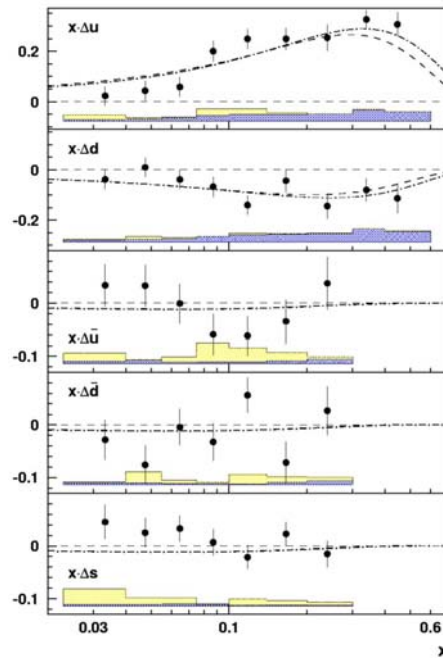
Fig. IV-6a. Quark helicity distributions at $\langle Q^2 \rangle = 2.5$ GeV^2 as a function of Bjorken x.
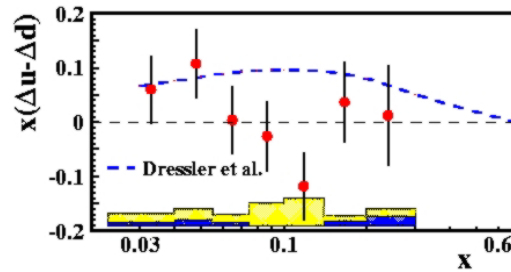
Fig. IV-6b. The light quark sea flavor asymmetry $\Delta\bar{u} - \Delta\bar{d}$ in the helicity distributions, at $\langle Q^2 \rangle = 2.5$ GeV^2.

c.4. Study of Factorization and Flavor Content of the Nucleon in Unpolarized Semi Inclusive Deep Inelastic Scattering at HERMES (K. Hafidi, A. El Alaoui, K. G. Bailey, T. P. O'Connor, H. E. Jackson, D. H. Potterveld, P. E. Reimer, and the HERMES Collaboration)

Semi Inclusive Deep Inelastic Scattering (SIDIS) has been used extensively in recent years as an important testing ground for QCD. Indeed, SIDIS offers a great opportunity for studying the spin and the flavor content of the nucleon. However, using SIDIS relies on the factorization assumption between the hard scattering process and the hadronization of the struck quark.

Although at high energy the scattering and production mechanisms factorize, it remains unclear to what extent factorization applies at lower energies. HERMES has shown that within the experimental precision, which was dominated by statistical accuracy, factorization works reasonably well at the HERMES kinematic conditions.[1] By accumulating an order of magnitude more statistics, it is now possible to perform a more precise test of factorization.

In this analysis, all HERMES unpolarized and averaged polarized hydrogen and deuterium data have been used. The ratios $(\bar{d} - \bar{u})/(u - d)$ and d_v/u_v will be determined from the analysis of charged pion yields. The kinematic range is $0.02 < x < 0.4$ with the average Q^2 of 2.5 GeV^2. The flavor asymmetry $(\bar{d} - \bar{u})/(u - d)$ was determined for fixed x-bins as a function of z, where z is the fraction of photon energy carried by the detected hadron. A flat z-dependence would be the proof of factorization. As shown in Fig.IV-7, the projected statistical precision of the ongoing analysis represents a considerable improvement of our ability to check factorization.

_____
[1]K. Ackerstaff *et al.,* Phys. Rev. Lett. **81**, 5519 (1998).
[2]E. A. Hawker *et al*., Phys. Rev. Lett. **80**, 3715 (1998); R. S. Towell *et al.,* Phys. Rev. D **64**, 052002 (2001).
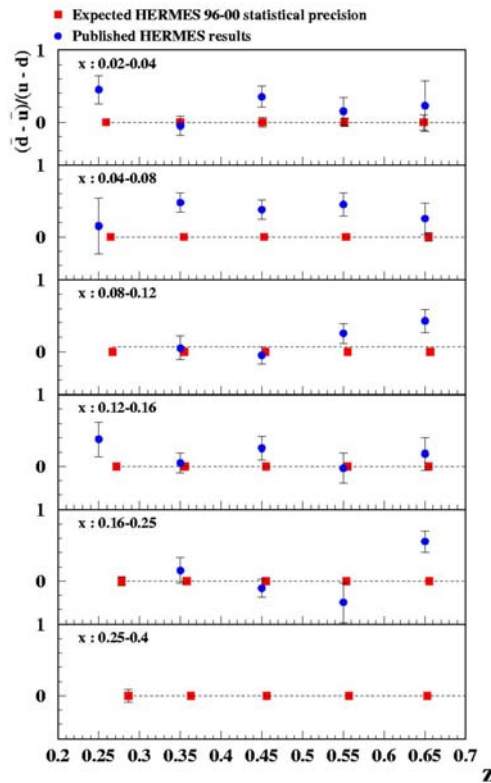
Fig. IV-7. The projected $(\bar{d} - \bar{u})/(u - d)$ as a function of z in different bins of x, compared with previously-published results.

The extraction of the sea flavor asymmetry and also the valence quark distribution in the proton will be performed. The measurement of the ratio $\bar{d}/\bar{u}$ from Fermilab Drell-Yan experiment[2] E866 seems to indicate that at x ~ 0.3, the ratio begins to become smaller than unity which means that the sea asymmetry reverses from an excess of $\bar{d}$ at low x to an excess of $\bar{u}$ at high x. HERMES data can access the relatively high x region up to x ~ 0.4. Measuring d_v/u_v will provide an additional test of factorization by comparing HERMES results with a QCD fit of other high energy data. In conclusion, with the ongoing analysis, we will be able to quantify with high precision the validity of the factorization assumption. We will also extract the flavor asymmetry ratio $(\bar{d} - \bar{u})/(u - d)$ and the valence content of the proton d_v/u_v using π^+/π^- yield ratios on hydrogen and deuterium.

c.5.   Azimuthal Asymmetries and Transversity (H. E. Jackson, A. El Alaoui, K. G. Bailey, T. P. O'Connor, K. Hafidi, D. H. Potterveld, P. Reimer, Y. Sanjiev, and the HERMES Collaboration)

Recent measurements of single-spin azimuthal asymmetries by HERMES have been recognized as a potentially powerful source of information about the spin structure of the nucleon,[1] complementary to inclusive deep-inelastic scattering. Significant azimuthal target-spin asymmetries in electroproduction of charged and neutral pions on a longitudinally polarized hydrogen target has been published.[2,3] It has been suggested that these single-spin asymmetries may provide information on the transversity distribution, which describes the probability to find a quark with its spin parallel or antiparallel to the spin of the nucleon that is polarized transversely to its infinite momentum. Transversity is a chiral-odd distribution function, which implies that it is not observable in an inclusive measurement. Therefore, a second chiral-odd object must be involved in the process to conserve chirality. In semi-inclusive scattering this has been postulated to be a chiral odd fragmentation function, the Collins function. The HERMES results on target single-spin asymmetries have elicited a number of phenomenological studies to evaluate these asymmetries in the framework of the Collins mechanism. Theoretical predictions have also been made for single-spin asymmetries in DIS off the nucleons in a deuterium target.

HERMES has made the first observation of target-spin azimuthal asymmetries for semi-inclusive pion and kaon production on a longitudinally polarized deuterium target. The data were recorded during the 1998, 1999, and 2000 running period of the HERMES experiment. The measured asymmetries show no dependence on polarity of the beam charge. The requirements imposed on the kinematics of the scattered lepton are 1 GeV^2 < Q^2 < 15 GeV^2, W > 2 GeV, 0.023 < x < 0.4 and y < 0.85. Contributions from target fragmentation are suppressed by requiring z > 0.2 and exclusive meson production is suppressed by requiring the cut z < 0.7. The asymmetries appear in the distribution of the hadrons in the azimuthal angle ϕ around the virtual photon direction, relative to the lepton scattering plane. In Fig. IV-8, the azimuthal asymmetries are displayed as a function of ϕ , integrated over the experimental acceptance. The corresponding analyzing powers in the sin ϕ moment of the cross section are 0.012 ± 0.002(stat) ± 0.002(syst.) for positive pions, 0.006 ± 0.003(stat) ± 0.002(syst.) for negative pions, 0.021 ± 0.005(stat) ± 0.003(syst) for neutral pions, and 0.013 ± 0.006(stat) ± 0.003(syst) for positive kaons. These findings can be well described by model calculations where the asymmetries are interpreted in the context of transversity. The observed asymmetries for positive pions and kaons are consistent with the assumption of u-quark dominance in the quark distribution and fragmentation process.

[1]P. J. Mulders and R. D. Tangermann, Nucl. Phys. B **461**, 197 (1996).
[2]HERMES collaboration, A. Airapetian *et al*., Phys. Rev. Lett. **84**, 4047 (2000).
[3]HERMES collaboration, A. Airapetian *et al*., Phys. Rev. **64**, 097101 (2001).
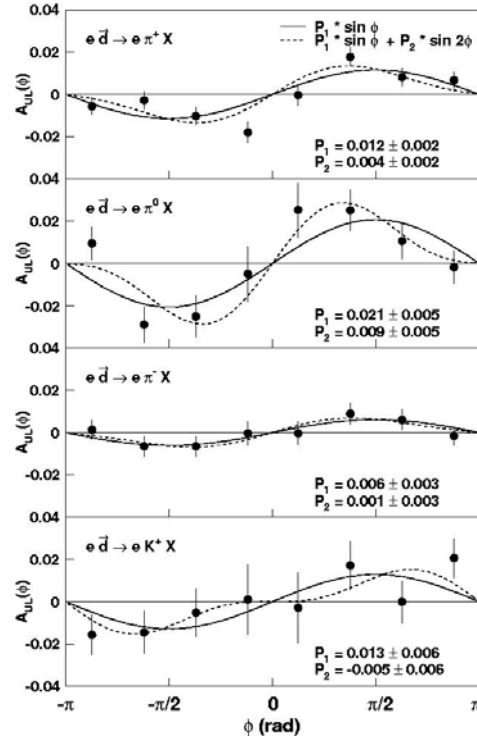
Fig. IV-8. Target spin asymmetries $A_{UL}(\phi)$ for electroproduction of π^+, π^0, π^- and K^+ mesons. Fits of the form $P_0 + P_1 \sin \phi$ (solid line) and $P_0 + P_1 \sin \phi + P_2 \sin 2\phi$ (dashed line) are also displayed in the figure. The error bars give the statistical uncertainties of the measurements. The values of the coefficients P_0 are all compatible with zero and the coefficients P_1 and P_2 for the various hadrons and their statistical uncertainties are listed in each panel.

c.6.   Evidence for Quark-Hadron Duality in the Proton Spin Asymmetry A_1
  (H. E. Jackson, A. El Alaloui, K. G. Bailey, T. P. O'Connor, K. Hafidi, D. H. Potterveld,
  P. Reimer, and the HERMES Collaboration)

The interaction between baryons and between baryons and leptons can generally be described by two complementary approaches: with quark-gluon degrees of freedom at high energy, where the quarks are asymptotically free, and in terms of hadronic degrees of freedom at low energy, where effects of confinement are large. In some specific cases, where the description in terms of hadrons is expected to apply most naturally, the quark-gluon description can be successfully used. Such cases are examples of so-called quark-hadron duality. Bloom and Gilman[1] first noted this relationship between phenomena in the nucleon resonance region and in deep inelastic scattering (DIS). Specifically, they observed that the cross section for electro-production of nucleon resonances, if averaged over a large enough range of invariant mass W of the initial photon-nucleon system, exhibited the same

behavior as the cross section observed in the DIS region. In other words, the curve measured as a function of the Bjorken scaling variable $x = Q^2/2m\nu$ in DIS processes at high Q^2 and high ν, approximately approaches the averaged curve measured in the resonance region at lower ν and Q^2 (here - Q^2 is the transferred four-momentum squared, M is the proton mass and ν the energy of the exchanged virtual photon in the target rest frame). The spin-dependent lepton–nucleon scattering data taken by HERMES have been used to investigate the validity of the concept of quark-duality for the spin asymmetry A_1. Longitudinally polarized positrons were scattered off a longitudinally polarized hydrogen target for values of Q^2 between 1.2 and 12 GeV^2 and values of W^2 between 1 and 4 GeV^2.

_____
[1]E. D. Bloom and F. J. Gilman, Phys. Rev. **D4**, 2901 (1971).
[2]A. Airapetian *et al.,* Phys. Rev. Lett. **90**, 052501 (2003).

The average double-spin asymmetry in the nucleon resonance region is found to agree[2] with that measured in DIS at the same values of the Bjorken scaling variable x. This finding implies that the description of A_1 in terms of quark degrees of freedom is valid in the nucleon resonance region for values of Q^2 above 1.6 GeV^2.

c.7. Search for the Onset of Color Transparency: The JLab E02-110 Experiment
(K. Hafidi, B. Mustapha, J. Arrington, A. El Alaoui, D. F. Geesaman, R. J. Holt, D. H. Potterveld, P. E. Reimer, E. C. Schulte, X. Zheng, and the Hall B Collaboration)

According to QCD, pointlike colorless systems, such as those produced in exclusive processes at high Q^2 have a vanishingly small transverse size. Therefore, they are expected to travel through nuclear matter experiencing very little attenuation. This phenomenon is known as color transparency (CT). An analogous mechanism is well known in QED: the interaction cross section of an electric dipole is proportional to its square size. As a result the cross section vanishes for objects with very small electric dipole moments. Since color is the charge of QCD, and by analogy to QED, the cross section of a color-neutral dipole, as formed by a pair of oppositely colored quarks for instance, is also predicted to vanish for small sized hadrons. Color transparency cannot be explained in the hadronic picture of nuclear matter (Glauber theory) and calls upon the quark's degrees of freedom. Earlier measurements were mainly focused on quasi-elastic hadronic $(p,2p)$[1] and leptonic $(e,e'p)$[2] scattering off nuclear targets. None of these experiments were able to produce evidence for CT up to $Q^2 \sim 8$ GeV^2. The strongest evidence for CT so far comes from Fermilab experiment E791 on the A-dependence of coherent diffractive dissociation of 500 GeV/c pions into di-jets.[3] A recent measurement performed by the HERMES collaboration using exclusive ρ^0 electroproduction off nitrogen adds further evidence for the existence of CT. [4]

The main goal of E02-110 experiment[5] is to look for the onset of CT in the incoherent diffractive ρ^0 electro and photoproduction on deuterium, carbon and copper. In this process (see Fig. IV-9a), the virtual photon fluctuates into $q\bar{q}$ pair which travels through the nuclear medium evolving from its small initial state with a transverse size proportional to $1/Q$, to a "*normal size*" vector meson detected in the final state. Therefore, by increasing the value of Q^2 one can squeeze the size of the produced $q\bar{q}$ wave packet. The photon fluctuation can propagate over a distance which is known as the coherence length ℓ_c. The coherence length can be estimated relying on the uncertainty principle and Lorentz time dilatation as $\ell_c = 2\nu/(Q^2 + M_{q\bar{q}}^2)$, where ν is the energy of the virtual photon and $M_{q\bar{q}}$ is the mass of the $q\bar{q}$ pair dominated by the ρ^0 mass in the case of exclusive ρ^0 electroproduction. What is measured in the reaction is how transparent the nucleus appears to "*small size*" ρ^0 by taking the ratio of the nuclear per-nucleon (σ_A/A) to the free nucleon (σ_N) cross sections, which is called nuclear transparency $T_A = \dfrac{\sigma_A}{A\sigma_N}$. Consequently, the signature of CT is an increase in the nuclear transparency T_A with increasing hardness (Q^2) of the reaction. Recent theoretical calculations by Kopeliovich *et al.*[6] predicted an increase of more than 40% at $Q^2 \sim 4$ GeV^2.

However, one should be careful about other effects that can imitate this signal. Indeed, measurements by HERMES have shown that T_A increases when ℓ_c varies from long to short compared to the size of the nucleus. This so-called coherence length effect can mock the signal of CT and should be under control to avoid mixing it with CT effect.

[1]A. S. Carroll *et al.*, Phys. Rev. Lett. **61**, 1698 (1988); Y. Mardor *et al.*, Phys. Rev. Lett. **81**, 5085 (1998); A. Leksanov *et al*. Phys. Rev. Lett. **87**, 212301 (2001).
[2]N. C. R. Makins *et al.*, Phys. Rev. Lett. **72**, 1986 (1994); T. G. O'Neill *et al.*, Phys. Lett. **B351,** 87 (1995); D. Abbott *et al.*, Phys. Rev. Lett. **80**, 5072 (1998); K. Garrow *et al.*, Phys. Rev. C **66**, 044613 (2002).
[3]E. M. Aitala *et al*., Phys. Rev. Lett. **86**, 4773 (2001).
[4]A. Airapetian *et al*., Phys. Rev. Lett. **90**, 052501 (2003).
[5]Jefferson Lab Experiment E02-110, "Q2 Dependence of Nuclear Transparency for Incoherent ρ^0 electroproduction", K. Hafidi, B. Mustapha and M. Holtrop spokespersons.
[6]B. Kopeliovich *et al.,* Phys. Rev. C **65**, 035201 (2002).

Therefore, the E02-110 experiment will measure the Q^2 dependence of the transparency T_A at fixed coherence length ℓ_c.   Figure.IV-9b shows the projected uncertainties for complementary ℓ_c values to map the whole Q^2 region up to 4 GeV^2. These measurements will benefit from the high luminosity beam available at JLab and the large acceptance spectrometer (CLAS) in Hall B.
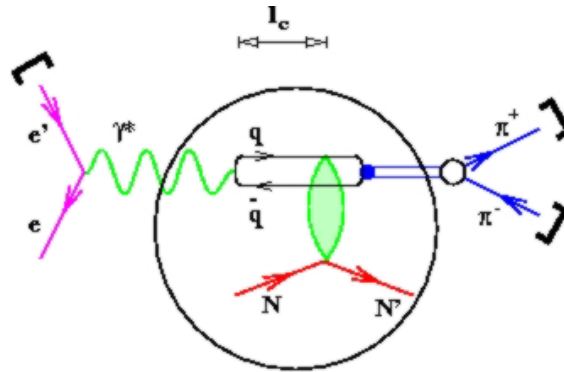
Fig. IV-9a. Exclusive leptoproduction of the ρ^0 meson.
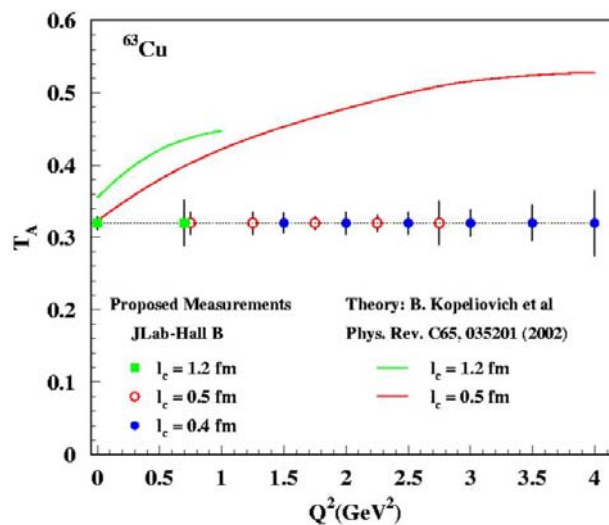
Fig. IV-9b. Theoretical predictions and expected statistical accuracy

c.8.   The Q^2 Dependence of Nuclear Transparency for Exclusive ρ^0 Production
   (K. Hafidi, A. El Alaoui, K. G. Bailey, T. P. O'Connor, H. E. Jackson, D. H. Potterveld, P. E. Reimer, and the HERMES Collaboration)

One of the fundamental predictions of QCD is the existence of a phenomenon called Color Transparency (CT).   With the same goal and spirit of the measurements in the previous report,* HERMES measured the nuclear transparency for exclusive ρ^0 electroproduction on hydrogen and nitrogen and for fixed coherence length values ℓ_c covering the region from 1.3 to 2.5 fm. Presenting the data in a way which keeps ℓ_c constant represents a simple prescription to eliminate the Coherence Length (CL) effect from the Q^2 dependence of the nuclear transparency. A value for T_A has been extracted for each (ℓ_c,Q^2) sub-bin for ρ^0 production (as illustrated in Fig. IV-10 for coherent production on nitrogen). The data have been fitted with a common Q^2 slope (p_1), which has been extracted assuming $T_A = p_0 + p_1 \cdot Q^2$. Combining both coherent

and incoherent production, the value of the Q^2 slope was found to be positive and equal to (0.074 ± 0.021) GeV^{-2} .[1] This result represents a more than a 3σ signal of Color Transparency, and is in good agreement with the theoretical predictions.[2] It represents one of the very few measurements that can claim to provide evidence of Color Transparency.

_____

[1]A. Airapetian *et al.,* Phys. Rev. Lett. **90**, 052501 (2003).
[2]B. Kopeliovich *et al*., Phys. Rev. C **65**, 035201 (2002) 035201.
***Footnote**: see previous report on "Search for the Onset of Color Transparency: The JLab E02-110 Experiment".
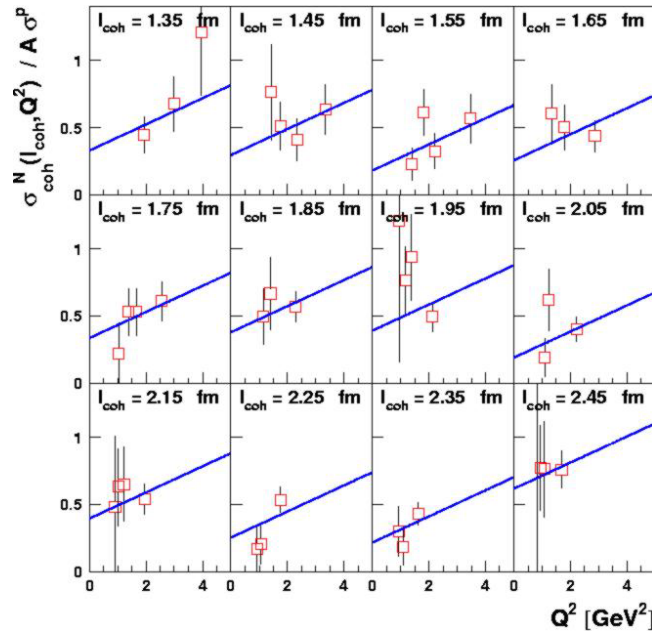
Fig. IV-10. Nuclear transparency as a function of Q^2 in fixed ℓ_c bins for coherent ρ^0 electroproduction on nitrogen.

c.9. The Q^2 Dependence of the Generalized Gerasimov-Drell-Hearn Integral for the Deuteron, Proton, and Neutron (H. E. Jackson, A. El Alaloui, K. G. Bailey, T. P. O'Connor, K. Hafidi, D. H. Potterveld, P. Reimer, and the HERMES Collaboration)

The Gerasimov-Drell-Hearn (GDH) sum rule connects the anomalous contribution to the magnetic moment of the target nucleus with an energy-weighted integral of the difference of the helicity-dependent photoabsorption cross sections. Originally conceived for real photons, the GDH integral can be generalized to the case of photons with virtuality Q^2. For spin ½ targets such as the nucleon, it then represents the non-perturbative limit of the first moment Γ_1 of the spin structure function $g_1(x,Q^2)$ in deep inelastic scattering (DIS). The data collected by HERMES with a deuterium target have been analyzed together with a re-analysis of previous measurements on the proton. These data provide an unprecedented and complete measurement of the generalized GDH integral for photon-virtuality ranging over $1.2 < Q^2 < 12.0$ GeV^2

and for photon-nucleon invariant mass squared W^2 ranging over $1 < W^2 < 45$ GeV^2, thus covering simultaneously the nucleon-resonance and the deep inelastic scattering regions. These data allow the study of the Q^2 dependence of the full integral, which is sensitive to both the Q^2–evolution of the resonance form factors and contributions of higher twist. The contribution of the nucleon-resonance region is seen to decrease rapidly with increasing Q^2. As expected, at higher Q^2 the data are found to be in agreement with previous measurements of the first moment of g_1. From data on the deuteron and proton, the GDH integral for the neutron has been derived and the proton-neutron difference evaluated. This difference is found to satisfy the fundamental Bjorken sum rule at $Q^2 = 5$ GeV^2

c.10.   First Measurement of the Deuteron Tensor Polarized Structure Function b_1
(H. E. Jackson, A. El Alaoui, K. G. Bailey, T. P. O'Connor, K. Hafidi, D. H. Potterveld, P. E. Reimer, Y. Sanjiev, and the HERMES Collaboration)

The deep inelastic scattering (DIS) of leptons by nucleons is characterized by four fundamental structure functions, F_1, F_2, g_1, and g_2. The latter two require polarized beams and targets in order to be measured, and the study of g_1 has been a primary goal for HERMES. When a deuteron is the scatterer, there are four additional fundamental structure functions,[1] b_{1-4}, that arise because the deuteron has spin 1, but which have never before been measured. The first, b_1, is of considerable interest. It is sensitive to differences in the quark momentum distribution between the 0 helicity (q^0) and the spin-averaged ±1 helicity ($q^+ + q^-$) states of the hadron. Of leading twist, b_1 should be identically zero for a simple composition of nucleons in the s state. However, a non-zero b_1 is possible through nuclear effects such as binding, the d state of the deuteron, and shadowing effects such as coherent double scattering.[2,3] If non-zero, it should properly be taken into account when extracting the neutron structure functions from deuterium data (hitherto it has been ignored.) Moreover, a non-zero value could indicate that the

quark sea becomes tensor polarized in the deuteron, which is unexpected in the naïve quark parton model.

HERMES has measured b_1 for the first time, using the same gaseous, tensor-polarized deuterium target developed for its nucleon structure function measurements[4]. An atomic beam source injected deuterium atoms of specific nuclear polarization states into a windowless storage cell in the HERA positron ring, and scattered particles were detected and identified in the HERMES detector. The tensor asymmetry of the DIS cross section, A_{zz}, is given by: $A_{zz} = [(\sigma^+ + \sigma^-) - 2\sigma^0]/(3\sigma_uT) \approx -2b_1/(3F_1)$, where σ^0, σ^+, and σ^- are the cross sections measured in the zero helicity and ±1 helicity target states, σ_u is the unpolarized cross section, and T is the degree of tensor polarization in the target. The measured tensor asymmetry and inferred b_1 are shown as a function of the Bjorken variable x in Fig. IV-11.

_____

[1]P. Hoodbhoy *et al*., Nucl. Phys. B **312,** 571 (1989).
[2]J. Edelmann *et al*., Phys. Rev. C **57,** 3392 (1998).
[3]K. Bora and R.L. Jaffe, Phys. Rev. D **57,** 6906 (1998).
[4]K. Ackersdtaff *et al*., Nucl. Instr. Meth. A **417,** 230 (1998).
[5]F. E. Close *et al.,* Phys. Rev. D **42**, 2377 (1990).
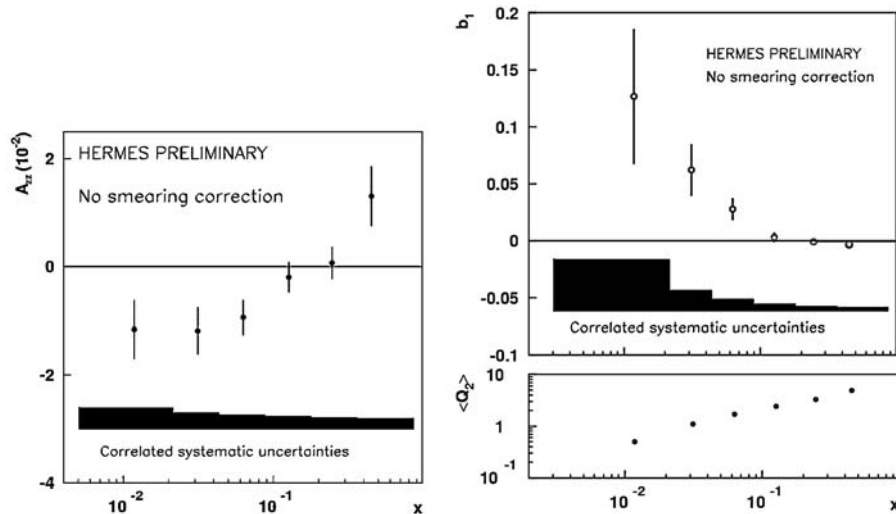
Fig. IV-11. Preliminary HERMES results for the tensor asymmetry A_{zz} (left plot) and b_1 (right plot) as a function of Bjorken x. The error bars are statistical only, and the shaded bands show the estimated systematic uncertainties. The Q^2 range of the measurements is shown in the lower panel on the right, in GeV^2.

A_{zz} is found to be less than 0.02 over the measured range, and therefore its neglect in extracting g_1 from HERMES deuterium data is estimated to cause less than a 1% error.   The data indicate that b_1 is small but different from zero, with a rise at low x that is qualitatively consistent with models of coherent double scattering, suggesting a significant tensor polarization of the sea quarks that would violate the Close-Kumano sum rule.[5] Further calculations of b_1 by the theoretical community are eagerly anticipated.

c.11. Measurements with Unpolarized Targets: Hadron Formation (H. E. Jackson, A. El Alaoui, K. G. Bailey, T. P. O'Connor, K. Hafidi, D. H. Potterveld, P. E. Reimer, Y. Sanjiev, and the HERMES Collaboration)

HERMES has an active program of measurements with unpolarized nuclear targets. By comparing the same interaction on different nuclear targets, HERMES is able to measure the effects of the nuclear medium on the interaction and subsequent hadronization of the quarks from the interaction. HERMES has measured the pion, kaon and (anti)proton fragmentation functions, and their attenuation in a nuclear environment. By embedding the fragmentation process in the nuclear medium, one can study the time propagation of the hadron formation process. In HERMES this attenuation is measured by the hadron multiplicity ratio, which is the ratio of the number of hadrons produced in a DIS event for on nuclear target to that from a deuterium target. The multiplicity ratio is measured as a function of the energy transferred to the struck quark, ν, and hadron energy fraction, $z = E_h/\nu$ (where E_h is the hadron's energy).

Hadron attenuation can be related to the formation length (or time) of the hadron. Such data can also be used to derive empirical values for the hadron formation time and the energy loss of a quark propagating in the medium. These quantities are of considerable theoretical and experimental interest, since these concepts also apply to the Drell-Yan process and heavy-ion collisions. HERMES data have been interpreted[1] in terms of final state interactions. This medium modification of the fragmentation of the propagating parton results from induced gluon radiation due to multiple parton scattering, and gives rise to additional terms in the QCD evolution equations that soften the fragmentation functions. As shown in Fig. IV-12, this treatment provides an excellent description of the HERMES results.   From these data, this treatment gives a quark energy loss of $dE/dx \approx 0.5$ GeV/fm in cold nuclear matter.

---

[1]E. Wang, and X.-N. Wang, Phys. Rev. Lett. **89** 162301 (2002).
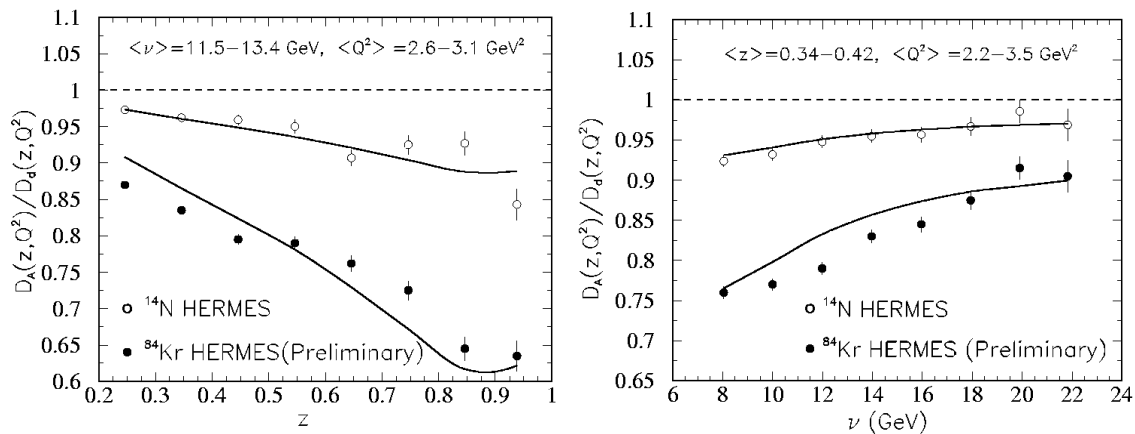
Fig. IV-12. At the left is the predicted nuclear modification of jet fragmentation functions (curves) compared to HERMES data on the ratios of hadron distributions between nuclear and deuterium targets in DIS. At the right is the energy dependence of this predicted nuclear modification (curves) compared to the HERMES data.

c.12.   A Dual Radiator Ring-Imaging Cerenkov Counter for HERMES (H. E. Jackson, A. El Alaloui, K. G. Bailey, T. P. O'Connor, K. Hafidi, D. H. Potterveld, P. Reimer, and the HERMES Collaboration)

A dual radiator Ring Imaging Cerenkov (RICH) detector for the identification of hadrons has been in routine operation[1] as part of the HERMES spectrometer since 1998. Its design and construction which involved eight collaborating institutions was led by the Argonne group.   The pattern recognition software for identification of the different hadrons in the RICH is based on two different methods: an indirect ray tracing method (IRT) and a direct ray tracing method(DRT). Both methods are combined in a likelihood analysis which selects the most probable particle type. The IRT and DRT exist in parallel; a decision network chooses the optimal method depending on event topology. The IRT method has been demonstrated to give reliable results, and has been the basis of all data analysis carried out to date. Features of the performance of the DRT method are not understood. Over most of the

range of momenta, contrary to expectation, DRT identification efficiencies are substantially lower than those of IRT.   Work continues to understand this behavior, to test and to tune the DRT method. With the demonstration of reliable operation of DRT, a final training of the decision network will be performed in order to implement its use in providing the highest efficiencies for reliable particle identification.   The particle samples obtained with these procedures will be characterized by efficiencies for correct identification of specific particle type and contamination of samples from mis-identification.   Unfolding procedures have been developed for correcting for these effects. Current efforts are focused on developing analysis routines for propagating systematic errors in the parameters used in the unfolding procedure.

---

[1]N. Akopov *et al.*, Nucl. Instr. Meth. **A479**, 511 (2002).

c.13.   Measurement of the Antiquark Flavor Asymmetry of the Proton Sea Using Drell-Yan Scattering (P. E. Reimer, D. F. Geesaman, S. B. Kaufman, and the FNAL E866/NuSea collaboration)

While it is not required by any fundamental symmetry, it has—until recently—been widely assumed that the distributions of anti-down, $\bar{d}$, and anti-up, $\bar{u}$, quarks in the proton were identical.   This was based on the assumption that the proton's sea arose perturbatively from gluons splitting into quark-antiquark pairs. Since the mass difference between the up and down quarks is small, equal numbers of up and down pairs would result. A ratio of $\bar{d}/\bar{u}$ which is not unity is then a clear sign of nonperturbative origins to the quark-antiquark sea of the proton.

To explore the difference between $\bar{d}$ and $\bar{u}$, Fermilab E866/NuSea measured the ratio $\bar{d}/\bar{u}$ as a function of the momentum carried by the struck quark, x. This was accomplished using the Drell-Yan mechanism, in which

a quark (or antiquark) in the proton beam annihilates with an antiquark (or quark) in the target. The resulting annihilation produces a virtual photon that decays into a pair of leptons, which are seen in the detector. From the ratio of hydrogen to deuterium Drell-Yan cross sections, the ratio $\bar{d}/\bar{u}$ and difference $\bar{d} - \bar{u}$ were extracted and unexpectedly large *x*-dependent flavor asymmetry in the proton's sea was revealed.   The differences seen in Fig. IV-13 are non-perturbative in nature, and several approaches have been suggested that could produce this difference.   These are represented by the curves in Fig. IV-13.   These approaches include meson cloud models of the nucleon,[1] chiral quark models in which the mesons couple directly to the constituent quarks[2] and instanton models.[3]

---

[1]J. C. Peng *et al.*, Phys. Rev. D **58**, 092004 (1998); N. Nikoleav *et al.*, Phys. Rev. D **60**, 014004 (1999).
[2]A. Szczurek *et al.*, J. Phys. G **22**, 1741 (1996); P.V. Pobylitsa *et al.*, Phys. Rev. D **59**, 034024 (1999).
[3]A. E. Dorokhov and N. I. Kochelev, Phys. Lett. B, 335 (1991); Phys. Lett. B **304** 167 (1993).
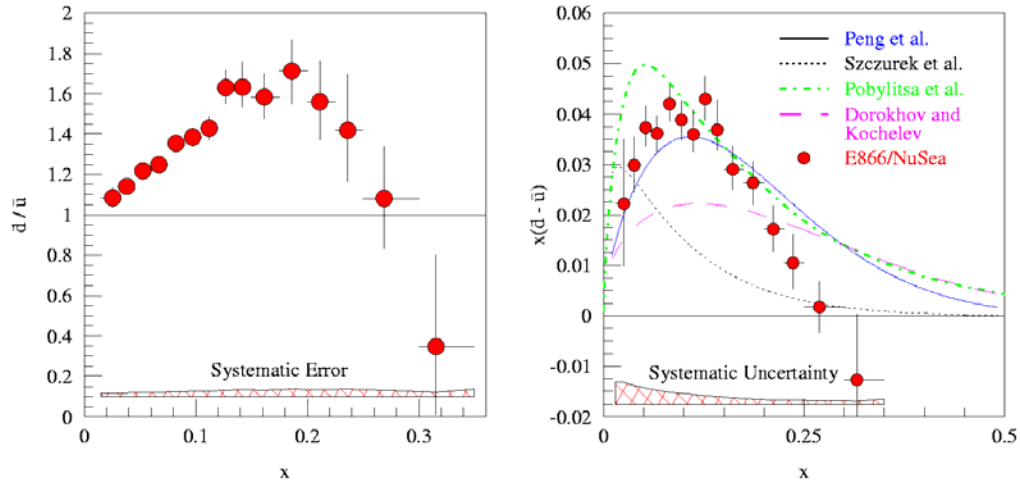
Fig. IV-13. The ratio of $\overline{d}/\overline{u}$ (left) and $x\left(\overline{d} - \overline{u}\right)$ (right) as a function of x, the fraction of the proton's momenta carried by the struck quark. The curves in the right graph represent different model calculations as descried in the text.

c.14. Measurement of the Absolute Drell-Yan Cross Section on Hydrogen and Deuterium (P. E. Reimer, D. F. Geesaman, S. B. Kaufman, and the FNAL E866/NuSea Collaboration)

Very little is known about the regime in which only one parton carries much of proton's momentum—different theoretical treatments prescribe different behaviors as x $\rightarrow$ 1 and very little data are available to serve as a guide. Drell-Yan absolute cross sections are sensitive to the high-x behavior of the *beam's* quarks and the intermediate-*x* behavior of the target antiquarks. E866 has measured the absolute cross sections for *proton-* *proton* and *proton-deuterium* Drell-Yan. The Drell-Yan cross section is dominated by the beam proton distribution of 4u(x)+d(x) as x $\rightarrow$ 1. The absolute cross sections, relative to a next-to-leading order (NLO) calculation are shown in Fig. IV-14. As can be seen in the figure, the quark distribution used in the calculation *overpredict* the data significantly at large-*x*.
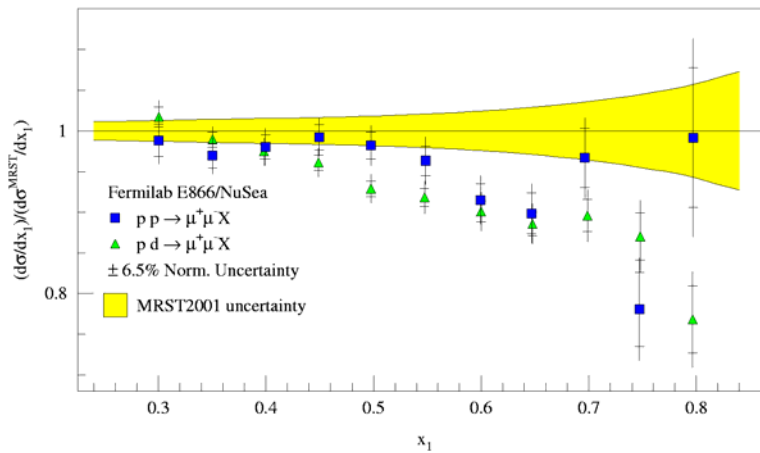
Fig. IV-14. The ratio of Drell-Yan cross section measured by Fermilab   E866/NuSea for proton-deuterium (triangles) and proton-proton (squares) to calculated NLO cross section based on the MRST2001 parton distributions. The yellow band represents the uncertainty given by MRST2001 on 4u(x)+d(x).

c.15.   Production of Υ and J/ψ from 800-GeV Protons Incident on Hydrogen and Deuterium (P. E. Reimer, D. F. Geesaman, S. B. Kaufman, and the FNAL E866/NuSea Collaboration)

The Υ and J/ψ mesons are produced when partons from the beam and target interact to form a virtual gluon, which then hadronizes into a heavy meson resonance. The virtual gluon may be generated by the annihilation of either a quark-antiquark pair or a pair of gluons (also called gluon-gluon fusion). Hence resonance production is sensitive to both the quark and gluon distributions with the target and beam. The J/ψ is believed to be produced primarily through gluon-gluon fusion, while Υ production is thought to proceed via both gluon-gluon fusion and quark-antiquark annihilation. Because the gluon distribution for the proton and neutron are similar, the per nucleon J/ψ cross section should be the same for both hydrogen and deuterium. For the Υ, on the other hand, the ratio of deuterium to hydrogen cross sections is expected to be larger than unity for the values of fractional momenta, x, probed by FNAL E866/NuSea, since $\bar{u}_n \rangle \bar{u}_p$ in this region, which allows for more $u_{beam} \rangle \bar{u}_{target}$ annihilations with deuterium.

The FNAL E866/NuSea hydrogen and deuterium data contain 30 thousand Υ and 1 million J/ψ events. The production cross sections for these mesons have been extracted and can be compared to predictions based on models and parton distributions available in the literature. Color evaporation model calculations have been performed for both Υ and J/ψ production from hydrogen and deuterium. Although it is an extremely simple model, the color evaporation model does reproduce the observed x-Feynman shape of the cross section. The measured cross section ratios for both the J/ψ and the Υ are near unity as shown in Fig.IV-15. In the case of the J/ψ, this is not surprising, since J/ψ production is expected to proceed through gluon fusion. In the case of the Υ, however, the value near unity is in disagreement with color evaporation model calculations. This deviation may indicate that the parton distribution functions underestimate the hard gluon (x $\approx$ 0.25) distribution in the proton.
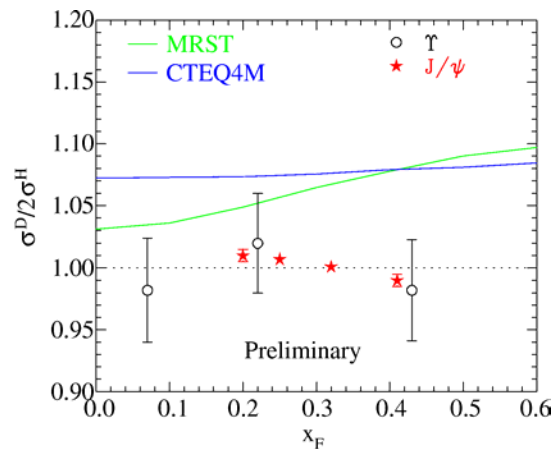
Fig. IV-15. The data points show the ratio of cross section for J/ψ and Υ production from deuterium to hydrogen. The curves represent color evaporation model calculations for this ratio for Υ production using two different parameterizations of the nucleon parton distributions. (J/ψ production is expected to have a ratio near 1.)

c.16. Drell-Yan Measurements with 120-GeV Protons, FNAL E906 (P. E. Reimer, D. F. Geesaman, J. Arrington, K. Hafidi, R. J. Holt, D. H. Potterveld, and the FNAL E906 Collaboration)

The Drell-Yan measurements of Fermilab E866/NuSea have provided new insight into the antiquark sea in the proton and nuclear dependence phenomena. FNAL E906 has been approved by Fermilab to extend Drell-Yan measurements to larger values of x (the fraction of the proton's momenta carried by the struck quark) using the new 120 GeV Main Injector at Fermilab.

The proton and the neutron are composite objects, made of quarks, antiquarks and gluons, collectively known as partons. While many of the properties of the proton may be attributed to its three valence quarks, it is, in fact, much more complicated, with over 50% of its momentum being carried by the its sea quarks and gluons. To understand the structure of the proton, it is necessary to understand the sea quarks, their origins and their interactions with the gluons that bind the proton together. E906 is specifically designed to probe the sea quarks of the proton. Vacuum polarization accounts for the creation of a flavor symmetric sea. Previous E866 Drell-Yan data, however, exhibit a large

asymmetry between $\bar{d}$ and $\bar{u}$ for x < 0.25 clearly indicating a non-perturbative origin to the sea. Above x > 0.28, however, the existing data, albeit with poor statistical uncertainty, indicate the ratio $\bar{d}/\bar{u}$ returns to unity. This result dramatically changed the sea quark parton distribution fits and was completely unpredicted by meson cloud and other non-perturbative models. The return of $\bar{d}/\bar{u}$ to unity clearly signals a change in the mechanism by which the sea is generated. Fermilab E906 will determine $\bar{d}/\bar{u}$ and $\bar{d}-\bar{u}$ for $0.1 \leq x \leq 0.45$, encompassing the non-perturbative region and extending well into the region where the sea appears to return to symmetry, allowing for the study of the relative importance of the perturbative and non-perturbative sea. The current parton distributions now reproduce the previous Drell-Yan data for 0.28 < x <0.3, but allow $\bar{d}/\bar{u}$ <1 as *x* increases above 0.3. This is not expected in either meson or perturbative models and is simply indicative of the complete lack of data. E906 will provide this data, as shown in Fig. IV-16.
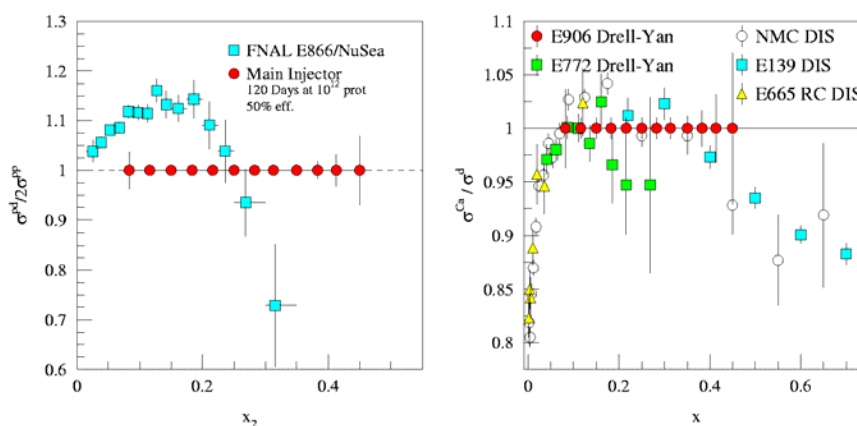
Fig. IV-16. The statistical uncertainty of E906's measurement of the ratio of hydrogen to deuterium cross sections (arbitrarily plotted at 1) compared with the E866 measurements of the same quantity (left). The statistical uncertainty of E906's measurement of the ratio of deuterium to calcium cross sections (arbitrarily plotted at 1) compared with previous Drell-Yan and deep inelastic scattering (DIS) measurements (right).

Very little is known about the regime in which only one parton carries much of proton's momentum—different theoretical treatments prescribe different behaviors as x → 1 and very little data is available to serve as a guide. Through the partons in the beam proton, Fermilab E906 will access these distributions. The Drell-Yan cross section is dominated by the distribution of 4u(x)+d(x) as x → 1. E906 will extend the data provided by

Fermilab E866 to higher *x* and provide much more precise *proton* data than is currently available.

Models based on the hypothesis that nuclear binding in governed by the exchange of mesons have been used to quite successfully describe the nuclear force. Given the success of these models, it is natural to look for direct experimental evidence for the presence of these mesons

in nuclei. Thus far, however, no direct evidence has been found. If present, these mesons will lead to an enhancement of antiquarks in the nucleus, and Drell-Yan is ideally suited to measure this enhancement. Fermilab E906 will collect data using nuclear targets, in addition to hydrogen and deuterium to look for these effects.

From deep inelastic scattering (DIS) experiments, we know that the quark level structure of a nucleon with in a nucleus *is* different from that of a free nucleon. In the range $0.10 < x < 0.25$, a surplus of quarks (approximately 2-4%) in nuclei, known as antishadowing, is clearly observed in DIS data. To understand these phenomena, it is important to determine if it is a general property of the quark and antiquark distributions, or just a property of the valence or sea quarks. Drell-Yan, with its ability to measure sea-only quark effects, is the ideal reaction in which to measure this. Early Drell-Yan data indicate that this surplus might not be present, but with poor statistical uncertainty (3-5%). Fermilab E906's measurements will clearly determine if there is antishadowing in the sea, with statistical uncertainties of less than 1% throughout this region (see Fig. IV-16).

Using the same nuclear target data, Fermilab E906 will also study the propagation of colored partons in strongly interacting, cold nuclear matter. By comparing the Drell-Yan yields from different nuclear targets and looking for apparent shifts in the beam parton's momentum distributions between nuclei, E906 will be able to measure the beam parton's energy loss. Previous Drell-Yan studies have placed upper limits on parton energy loss. With increased sensitivity from the 120 GeV beam and better statistical accuracy, Fermilab E906 will turn these upper limits into measurements. These measurements will aid in the understanding of jet suppression data from RHIC.

FNAL E906 is able to make these improvements over previous measurements because of the lower beam energy available at the Fermilab Main Injector. For fixed x_{beam} and x_{target} the cross section scales as the inverse of the beam energy. Thus a factor of seven more events for the same integrated luminosity can be achieved. At the same time, the primary background to the measurement, muons from J/ψ decays, decreases with increasing beam energy, allowing for an increase in instantaneous luminosity by another factor of seven. These two factors combine to provide roughly 50 times more events for the same beam time.

FNAL E906 has been approved by the Fermilab PAC and will most likely begin collecting data in late 2008. In the mean time, a number of new detector elements must be constructed, the most significant of which is a new large dipole magnet to focus the Drell-Yan muons.

D. ATOMIC TRAP TRACE ANALYSIS

d.1. ATTA for Practical ^{81}Kr and ^{85}Kr Analysis (K. Bailey, X. Du, Z.-T. Lu, P. Mueller, T. P. O'Connor, Z. El Alfy,* B. El-Kaliouby,† B. E. Lehmann,‡ R. Lorenzo,‡ R. Purtschert,‡ N. C. Sturchio,§ M. Sultan,¶ and L. Young‖)

We are developing the Atom Trap Trace Analysis (ATTA) method for the analysis of two long-lived krypton isotopes, ^{81}Kr ($t_{1/2} = 2.3 \times 10^5$ years) and ^{85}Kr ($t_{1/2} = 10.8$ years). ^{81}Kr analyses can be used to determine the ages of ancient ice and groundwater in the range of 5×10^4 to 1×10^6 years; ^{85}Kr analyses can serve as a means to help verify compliance with the Nuclear Non-Proliferation Treaty.

In ATTA, atoms of the desired isotope are selectively captured into a Magneto-Optical Trap (MOT) and detected by observing the fluorescence of trapped atoms. While the principle of ATTA was demonstrated in 1999, the counting efficiency of the method realized at the time was too low for any practical applications. Since then, we have focused our effort on both improving the efficiency and the operational reliability in order to develop a system for practical use. 1) The linear correlation between the results of ATTA and low level counting (LLC) demonstrated the validity of quantitative ATTA analyses; 2) this also provides a new measurement on the atmospheric abundance of ^{81}Kr (Fig. IV-17). Based on the slope of the correlation line and the assumption that ATTA counts ^{81}Kr and ^{85}Kr with equal efficiency, we can derive that the ^{81}Kr/Kr ratio is $(1.1 \pm 0.1) \times 10^{-12}$ in modern atmosphere. This value disagrees with the earlier measurements by 3-5 standard deviations. We plan to calibrate the ATTA efficiency of ^{81}Kr independent of ^{85}Kr in the near future.

With this successful demonstration, we are poised to use ATTA for its first application: to date the ancient groundwater of the Nubian Aquifer, Egypt. In 2002, a geological expedition formed by this collaboration explored the Western Desert of Egypt and extracted gas samples at six deep groundwater sites in the region. The samples have now been reduced to nearly pure Kr by the Bern group, and will soon be analyzed using ATTA at Argonne.

_____
*Egyptian Geological Survey and Mining Authority, Cairo, †Ain Shams University, Cairo, Egypt, ‡University of Bern, Switzerland, §University of Illinois at Chicago, ¶SUNY, Buffalo, ‖Chemistry Div., ANL

$Y=a*X+b$
$a=0.265+-0.017$
$b=-0.100+-0.324$
reduced Chi-squared 0.53
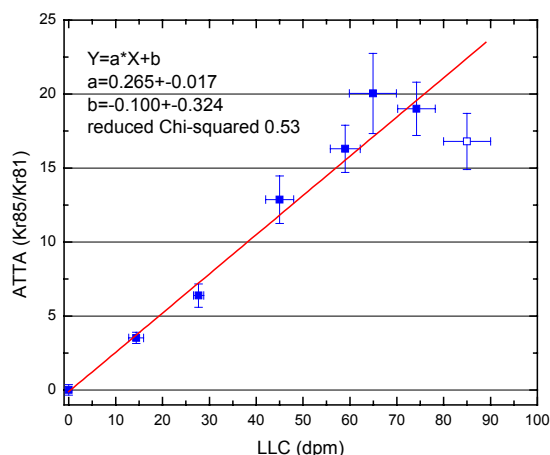
Fig. IV-17. Comparison between ATTA and LLC. In ATTA, both ^{81}Kr and ^{85}Kr atoms are counted, and the ratio of the atom counts represent the ratio of isotopic abundances. In LLC, only the decay of ^{85}Kr are counted, and the unit is decays per minute (dpm) per cm^3 of Kr at STP. The data point shown in open square represents a sample that had been severely contaminated with air in the sample preparation stage, and is not included in the fit.

d.2. ^{41}Ca Analysis for Biomedical Applications (K. Bailey, J. P. Greene, Z.-T. Lu, I. D. Moore, P. Mueller, T. P. O'Connor, L. Young,* C. Geppert,† and K. D. A. Wendt†)

We are developing an instrument for the trace analyses of ^{41}Ca based upon the Atom Trap Trace Analysis (ATTA) method. Since calcium is one of the most abundant elements in human bones and tissues, and ^{41}Ca is a long-lived isotope with very low radioactivity, ^{41}Ca as an artificial tracer is likely to find applications in bio-medicine. At present, ^{41}Ca is being studied as a tracer both in the biomedical research of bone metabolism and in the medical diagnosis of osteoporosis.

We have developed a calcium atom trap and succeeded in detecting individual ^{41}Ca atoms at the isotopic abundance level of $10^{-9} – 10^{-8}$ in biomedical samples. These samples, extracted from urine of subjects who had ingested ^{41}Ca, were provided by the Osteodiet Project, a European collaboration of physicists and medical scientists, with the aim of studying dietary strategies for osteoporosis prevention.

_____
* Chemistry Division, ANL, †Institut fur Physik, Johannas Gutenberg-Universitat Mainz, Mainz, Germany
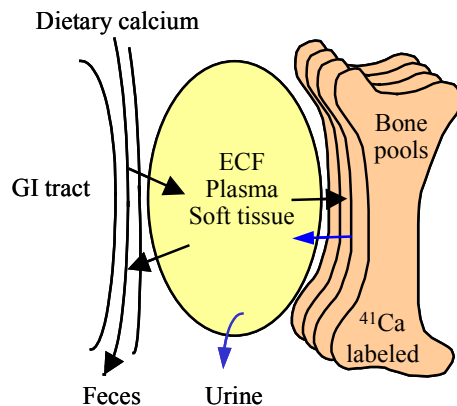
Fig. IV-18. Diagram of calcium flow in human body. ^{41}Ca is an ideal tracer for studying calcium transport in bio-systems and for measuring bone-loss rates.

d.3.   Measuring the Charge Radius of ^{6}He (K. Bailey, J. Greene, R. J. Holt, D. Henderson, R. V. F. Janssen, C.-L. Jiang, Z.-T. Lu, I. D. Moore, P. Mueller, T. P. O'Connor, R. C. Pardo, G. T. Pennington, K. E. Rehm, J. P. Schiffer, L.-B. Wang, G. Drake,* and M. Paul†)

This collaboration aims to determine the charge radius of ^{6}He by measuring the atomic isotope shift of the 2^3S_1-3^3P_2 transition between ^{4}He and ^{6}He in the metastable 2^3S_1 level. Since ^{6}He atoms are short-lived and are available only in small numbers, we plan to produce the ^{6}He atoms at the ATLAS accelerator facility, capture individual ^{6}He atoms with a laser trap, and perform precision laser spectroscopy on the trapped atoms.

In the past year, we have developed a fast and efficient helium atom trap system. By measuring the fluorescence of trapped ^{4}He atoms, we determined that, at the ^{4}He injection rate of 2×10^{15} s^{-1}, the trap can capture ^{4}He atoms at the rate of 2×10^6 s^{-1} with an efficiency of 10^{-9}. We expect that, by adding a fast gas recirculation step, the efficiency will be further improved another order of magnitude. While there are several helium trap systems already operating in

laboratories around the world, our system is unique in its design aimed for capturing short-lived helium isotopes and differ from all the existing systems in two significant ways: it takes a much shorter time (~ 0.1 s) to transfer an injected atom into the trap, and its capture efficiency is higher than conventional systems by approximately two orders of magnitude. At present, the trapping laser system at 1083 nm is complete, the spectroscopy laser system at 389 nm is under development.

Tests performed in 2001 indicate that ^{6}He atoms can be produced and extracted at ATLAS at the rate of 3×10^6 s^{-1}. Combining the expected efficiency and production rate, we expect to capture ^{6}He in the trap at the rate of 100 per hour, which is quite sufficient for the isotope shift measurement. At present, a laser area is being prepared at the experimental area of ATLAS.

_____
*University of Windsor, Canada, †Hebrew University, Israel.

d.4.   Search for Anomalously Heavy Isotopes of Helium in the Earth's Atmosphere
(R. J. Holt, Z.-T. Lu, P. Mueller, T. P. O'Connor, J. P. Schiffer, and L.-B. Wang)

Our knowledge of the stable particles that may exist in nature is defined by the limits set by measurements. There remain possibilities for 'superheavy' particles in the mass range of $10 - 10^5$ amu (atomic mass unit). There have also been suggestions that there may be very tightly bound stable states of hadronic matter. A more recent motivation for experimental searches is the possible existence of strange quark matter ('strangelets' with approximately equal numbers of up, down and strange quarks). A particularly favorable case is presented by particles of charge +2e, in other words helium-like particles. Normal helium is severely depleted in the terrestrial environment because of its light mass. A heavy (mass > 20 amu) and doubly-charged particle would then be helium-like but behave as other noble gases and remain in the atmosphere. The concentration of noble-gas-like atoms in the atmosphere and the subsequent very large depletion of the known light ^{3,4}He isotopes from the atmosphere allow significantly enhanced limits to be set.

In this work, we used a laser spectroscopy technique and took advantage of the isotope shift due to the higher mass of the heavy nucleus. The signature of an anomalously heavy isotope of helium atoms would be a resonance absorption signal occurring at a laser frequency away from the resonance of the abundant isotopes. We performed the search by probing the 1s2s $^3S_1 \rightarrow$ 1s2p $^3P_2$ transition at 1083 nm in helium atoms collected from the atmosphere. For the search the laser frequency was slowly scanned in the range of 20 – 109 GHz above the transition frequency of ^{4}He, which corresponds to a search in the mass range of 5 amu – infinity. We find at the 95% confidence level that there is no anomalous peak with an amplitude larger than 7.9 $\times 10^{-2}$ times the ^{3}He (isotopic abundance = 1.4 ppm) amplitude anywhere in the entire frequency range.

It is believed that the sun and the planets formed from the same starting material, and that this original composition is preserved in the sun. Based on the well-documented deficiency factors of noble gas elements, and assuming that the deficiency factors for the anomalous helium follow the same mass dependence, we can set limits on their abundance in the solar system (Fig. IV-19). Compared with the previous searches of such particles with mass spectrometry, this work significantly extends our knowledge over a wider range of mass and with much improved limits.
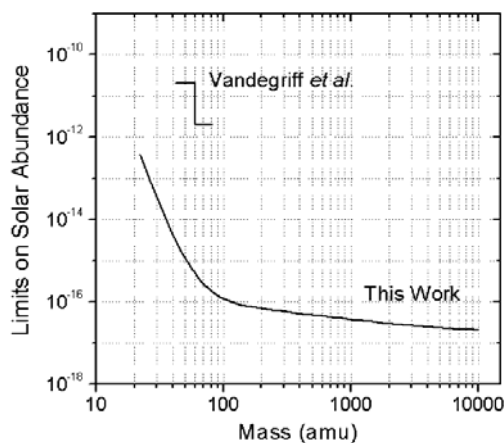
Fig. IV-19. Limits on the abundance of anomalous He-like particles in the solar system. The limits set by a previous mass-spectrometry-based search conducted by Vandegriff et al. cover the range of 42 – 82 amu. The limits set by our laser-spectroscopy-based search cover the range of 20 – 10,000 amu.

E. TESTS OF FUNDAMENTAL SYMMETRIES

e.1. Optical Trapping of Radium and the Electric Dipole Moment
(I. Ahmad, R. J. Holt, Z.-T. Lu, and E. C. Schulte)

We propose to investigate the feasibility of laser trapping and cooling of radium-225 (^{225}Ra) atoms. The realization of this proposal would enable us to measure the electric dipole moment (EDM) of ^{225}Ra and test the fundamental time-reversal symmetry (T-symmetry). The violation of time-reversal symmetry is among the most fundamental issues in physics. It is strongly believed that the underlying mechanism of the violation of T-symmetry holds the key to new physics beyond the Standard Model.

^{225}Ra is an especially good case for the search of the EDM because it has a relatively long lifetime ($t_{1/2}$ = 14.9 d), has spin ½ which eliminates systematic effects due to electric quadrupole coupling, is available in relatively large quantities from the decay of the long-lived ^{229}Th ($t_{1/2}$ = 7300 yr), and has a well-established octupole nature. The octupole deformation increases the enhancement of the atomic EDM by increasing the Schiff moment collectively and by the parity doubling of the energy level. For example, the sensitivity to T-odd, P-odd effects in ^{225}Ra is expected to be a factor of 375 larger than in ^{199}Hg, which has been used by previous searches to set the lowest limit (< 2 x 10^{-28} e cm) so far on the atomic EDM. Work on this project is at the initial stage.

e.2. Measurement of $\sin^2\theta_W$ through Parity Violation in Deep Inelastic Scattering on Deuterium (P. E. Reimer, J. R. Arrington, K. Hafidi, R. J. Holt, H. E. Jackson, D. H. Potterveld, E. C. Schulte, and X. Zheng)

One of the basic parameters of the Standard Model is $\sin^2\theta_W$, which represents the relative coupling strength of the weak and electromagnetic forces. The value of this parameter is predicted to vary (or run) as a function of the energy at which it is probed, Q^2 and measurement of this "running" provide strict tests of the Standard Model. At an energy equivalent to the mass of the Z-boson $(Q^2 = M_z^2)$, $\sin^2\theta_W$ is very well known, but away from this Q^2, there are very few other measurements. Interest in measurements of $\sin^2\theta_W$ has burgeoned because of recently reported results from the NuTeV collaboration at Fermilab, which found a *three standard deviation* difference with the Standard Model in their neutrino-iron measurement of $\sin^2\theta_W$ at $Q^2 \approx 20$ GeV^2. The asymmetry from parity violation in electron-deuterium deep inelastic scattering (DIS) is proportional to $\sin^2\theta_W$, and relatively large ($A_d \approx 10^{-4} Q^2$), making it quite accessible experimentally. Historically, DIS parity violation from a deuterium target was first observed by Prescott *et al.* in the mid-1970's and was used to establish the Weinberg-Salam model. Investigations are underway to repeat this experiment, focusing on facilities at an upgraded 12 GeV Jefferson Laboratory (and possibly at SLAC). In a relatively short experiment, a DIS parity violation experiment could achieve the statistical sensitivity needed to investigate the NuTeV result, and using a deuterium target, it should not suffer from the uncertainties in nuclear effects and nuclear parton distributions unlike the NuTeV iron measurement.

V.   THEORETICAL PHYSICS

OVERVIEW

Our research addresses important problems in theoretical nuclear physics involving the structure and dynamics of hadrons and nuclei. There is strong emphasis on comparison with data from Argonne's ATLAS facility, from JLab, and from other laboratories around the world, and predicting phenomena observable with a rare isotope accelerator. Our work includes the modeling and application of quantum chromodynamics (QCD) to light- and heavy-hadron structure at zero temperature and density, and at the extremes of temperature and density appropriate to the early universe, neutron stars, and RHIC experiments. We develop reaction theories to use in exploring hadron structure using the data from meson and nucleon-resonance production experiments at JLab, MIT-Bates and Mainz. We construct realistic two- and three-nucleon potentials that give accurate fits to nucleon-nucleon elastic scattering data and properties of light nuclei, and use them in detailed many-body calculations of light and near closed-shell nuclei, nuclear matter and neutron stars, and in a variety of astrophysically important electroweak reactions. Our nuclear structure and reaction studies include coupled-channels calculations of heavy-ion reactions near the Coulomb barrier, and calculations of observables in breakup reactions of nuclei far from stability. We also study high-spin deformation and the structure of the heaviest elements at the mean-field level, and work toward an understanding of the interplay between collective modes at the many-body level. Additional research is pursued in atomic physics, neutron physics, quantum computing, and fundamental quantum mechanics. Several of our projects involve major numerical simulations using the massively parallel computer systems at Argonne and NERSC.

A. NUCLEAR DYNAMICS WITH SUBNUCLEONIC DEGREES OF FREEDOM

The objective of this research program is to investigate the role of: quark-gluon degrees of freedom in hadron structure and interactions, and in nuclear dynamics; the development and application of reaction theories for use in exploring hadron structure using the data from meson and nucleon-resonance production experiments at modern experimental facilities; and to investigate relations of Poincaré covariant dynamics specified by mass operators to complementary dynamics specified by Green functions.

At the level of quark-gluon degrees of freedom, the Dyson-Schwinger equations (DSEs) provide a Poincaré covariant, nonperturbative method for studying QCD in the continuum. The existence of symmetry preserving truncations enables the simultaneous exploration of phenomena such as: confinement, dynamical chiral symmetry breaking, and bound state structure and interactions. In addition the DSEs provide a generating tool for perturbation theory and hence yield model-independent results for the ultraviolet behavior of strong interaction observables. This means that model studies facilitate the use of physical processes to constrain the long-range behavior of the quark-quark interaction in QCD, which is poorly understood and whose elucidation is a key goal of modern experimental programs. The last year saw numerous successful applications. For example, we showed that a Ward-Takahashi identity preserving Bethe-Salpeter kernel can always be calculated explicitly from a dressed-quark-gluon vertex whose diagrammatic content is enumerable and that this kernel is nonplanar in all but the simplest case. In doing so we made clear that this simplest case, the rainbow-ladder truncation, is the first term in a systematic and nonperturbative scheme, and thereby explained its quantitative success. Moreover, in a direct application of nonequilibrium quantum mean field theory we demonstrated that a 9-TW-peak x-ray free electron laser could produce a plasma of electron-positron pairs directly from the QED vacuum.

At the level of meson and baryon degrees of freedom, we are continuing our effort to develop dynamical models for interpreting the data of few-GeV hadron reactions in terms of the quark-gluon substructure of nucleon resonances (N^*) as predicted by various QCD-based hadron models. In the past year we have extended our dynamical model for pion electroproduction in the Δ region to also investigate neutrino induced reactions. It is found that the axial N-Δ transitions also contain large pion cloud contributions and the existing neutrino induced pion production data are consistent with the constituent quark model. For investigating higher mass N^* resonances, we developed a unitary coupled-channel $\pi\pi N$ model. In our investigation of vector meson photoproduction, we showed that coupled-channel effects are essential in identifying the nucleon resonances using spin observables. Finally, we investigated the quark-exchange mechanisms of deuteron photodisintegration at 2-6 GeV, with the aim of exploring the transition from a hadronic picture to a quark-gluon picture of nuclear dynamics.

Relativistic quantum dynamics requires a unitary representation of space-time symmetries (Poincaré group) and localization of states, such that states localized in relatively space-like regions are causally independent. Recent mathematical developments indicate how manifolds of localized states can be defined strictly within the framework of relativistic quantum mechanics without reference to infinite systems.

a.1. Quantum Effects with an X-ray Free Electron Laser (C. D. Roberts, S. M. Schmidt,* and D.V. Vinnik†)

A quantum kinetic equation coupled with Maxwell's equation was used to estimate the laser power required at an X-ray free-electron laser (XFEL) facility to expose intrinsically quantum effects in the process of QED vacuum decay via spontaneous pair production. We found that a 9-TW-peak XFEL laser with photon energy of 8.3 keV could be sufficient to initiate particle accumulation and the consequent formation of a plasma of spontaneously produced pairs (Fig. V-1). In that plasma, the evolution of the particle number will exhibit non-Markovian aspects of the strong-field pair production process, and the internal currents will generate an electric field whose interference with that of the laser leads to plasma oscillations. An article describing this work was published.[1]

[1]C. D. Roberts, S. M. Schmidt and D. V. Vinnik, Phys. Rev. Lett. **89**, 153901 (2002).
*University of Tuebingen, Germany, †Helmholtz-Gemeinschaft, Germany.
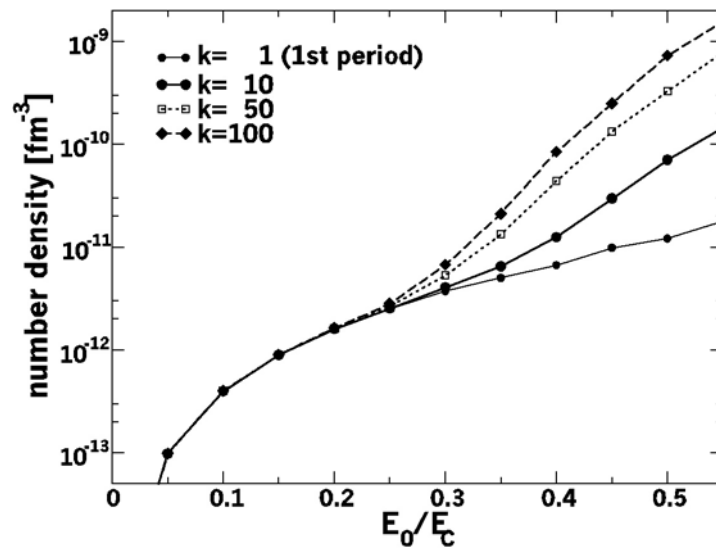
Fig. V-1. Peak particle number density in the laser spot volume versus laser field strength, measured in terms of the critical field: $eE_{cr} = mc^2$. (k counts the number of elapsed laser periods.) There is a striking qualitative change at $E_0 \approx 0.25\ E_{cr}$, which marks the onset of particle accumulation; viz., beyond this point the number of particles in the spot volume increases materially over the lifetime of the lasing pulse.

a.2. Nucleon Mass and Pion Loops (M. B. Hecht, C. D. Roberts, M. Oettel,* A. W. Thomas,* S. M. Schmidt,† and P. C. Tandy‡)

We solved Poincaré covariant Faddeev equations for the nucleon and delta to illustrate that an internally consistent description in terms of confined-quark and non-pointlike confined-diquark-correlations can readily be obtained. Subsequently, we calculated the πN-loop induced self-energy corrections to the nucleon's mass and showed them to be independent of whether a pseudoscalar or pseudovector coupling is used. Applying phenomenological constraints, we argued that this self-energy correction reduces the nucleon's mass by up to several hundred MeV. However, we demonstrated that this effect does not qualitatively alter the picture, suggested by the Faddeev equation, that baryons are quark-diquark composites, although neglecting the π-loops leads to a quantitative overestimate of the nucleon's axial-vector diquark component. An article describing this work was published.[1]

*CSSM, University of Adelaide, Australia, †University of Tübingen, Germany, ‡Kent State University.
[1]M. B. Hecht, C. D. Roberts, S. M. Schmidt, P. C. Tandy and A. W. Thomas, Phys. Rev. C **65**, 055204 (2002).

a.3.   Bethe-Salpeter Equation and a Nonperturbative Quark-Gluon Vertex
(C. D. Roberts, A. Bender,* W. Detmold,* and A. W. Thomas*)

A Ward-Takahashi identity preserving Bethe-Salpeter kernel can always be calculated explicitly from a dressed-quark-gluon vertex whose diagrammatic content is enumerable. We illustrated that fact using a vertex obtained via the complete resummation of dressed-gluon ladders. While this vertex is planar, the vertex-consistent kernel is nonplanar and that is true for any dressed vertex. In an exemplifying model, the rainbow-ladder truncation of the gap and Bethe-Salpeter equations yielded many results; e.g., π- and ρ-meson masses, that are changed little by including higher-order corrections. Moreover, we saw that the bulk of the ρ-π mass splitting is present in the chiral limit and that its value is not materially influenced by improving the kernel. These results demonstrate that the mass difference is driven by the DCSB mechanism and is not the result of a carefully contrived chromo-hyperfine interaction. In addition, it was apparent that repulsion generated by nonplanar diagrams in the vertex-consistent Bethe-Salpeter kernel for quark-quark scattering is sufficient to guarantee that diquark bound-states do not exist. This analysis confirms the importance of preserving symmetries in studies of QCD's bound states. An article describing this work was published.[1]

_____
*CSSM, University of Adelaide, Australia.
[1]A. Bender, W. Detmold, C.D. Roberts and A.W. Thomas, Phys. Rev. C **65** (2002) 065203.

a.4.   Dyson-Schwinger Equations: A Tool for Hadron Physics (C. D. Roberts and
P. Maris*)

Dyson-Schwinger equations furnish a Poincaré covariant framework within which to study hadrons. However, their application has long been plagued by concerns over the need to employ a truncation scheme in order to arrive at a tractable problem. It was recently shown that there exists at least one systematic, nonperturbative, symmetry-preserving DSE truncation procedure; and this has enabled the proof of exact, model-independent results. For example, the gap equation reveals that dynamical chiral symmetry breaking is tied to the long-range behavior of the strong interaction, which is thereby constrained by observables, and the pion is precisely understood, and seen to exist simultaneously as a Goldstone mode and a bound state of strongly dressed quarks. The rainbow-ladder truncation is the leading-order term in the systematic scheme. That realization has enabled the systematic error associated with this simplest truncation to be quantified, and that explains and underpins a one-parameter model efficacious in describing an extensive body of mesonic phenomena. Incipient applications to baryons have brought successes and encountered challenges familiar from early studies of mesons, and promise a covariant field theory upon which to base an understanding of contemporary large momentum transfer data. This body of work reveals that the momentum-dependent *dressing* of the propagators of QCD's elementary excitations is a fundamental feature of strong QCD that is observable in hadron physics. We completed an extensive review, explaining these foundations and reviewing many applications, which was accepted for publication.

_____
*North Carolina State University.

a.5.   Facets of Confinement and Dynamical Chiral Symmetry Breaking
(C. D. Roberts, P. Maris,* A. Raya,† and S. M. Schmidt‡)

The gap equation is a cornerstone in understanding dynamical chiral symmetry breaking and, perhaps, confinement too.   The existence of a symmetry-preserving truncation enables proofs of important results and also a gap-equation-based analysis of contemporary lattice data on quark and gluon propagators. The available lattice data is for quenched QCD and this exploratory study suggests that physical observables are materially underestimated in the quenched theory: the pion decay constant by as much as a factor of two.   In addition it re-emphasizes that multiplicative renormalizability can provide very useful constraints on the gap equation's kernel. An article describing this research was submitted for publication.

*North Carolina State University, †Universidad Michoacana de San Nicolás de Hidalgo, Mexico, ‡Helmholtz-Gemeinschaft, Germany.

a.6.   Concerning the Quark Condensate (C. D. Roberts, K. Langfeld,*
R. Pullirsch,† H. Markum,† and S. M. Schmidt‡)

We verified that the gauge-invariant trace of the massive dressed-quark propagator possesses a spectral representation, with a non-negative spectral density $\rho(\lambda)$, when considered as a function of the current-quark mass. This is key to establishing that the OPE condensate, which sets the ultraviolet scale for the momentum-dependence of the trace of the dressed-quark propagator, does indeed measure the density of far-infrared eigenvalues of the gauge-averaged massless Dirac operator, à la the Banks-Casher relation. This relation is intuitively appealing because a measurable accumulation of eigenvalues of the massless Dirac operator at zero-virtuality expresses a mass gap in its spectrum. In our continuum analysis we found that one requires $am \le (a\Lambda_{QCD})^3$ if $\rho(\lambda) = 0$ is to provide a veracious estimate of the OPE condensate. The residue at the lowest-mass pole in the flavor-nonsinglet pseudoscalar vacuum polarization provides a measure of the OPE condensate that is accurate for larger current-quark masses. An article describing this work was accepted for publication.

*University of Tübingen, Germany, †Technical University of Vienna, Austria, ‡Helmholtz-Gemeinschaft, Germany.

a.7.   Analysis of a Quenched Lattice-QCD Dressed-Quark Propagator
(C. D. Roberts, M. S. Bhagwat,* M. A. Pichowsky,* and P. C. Tandy*)

We studied quenched-QCD using a rainbow-ladder truncation of the Dyson-Schwinger equations and demonstrated that existing results from lattice simulations for the dressed-gluon and –quark Schwinger functions can be correlated via a gap equation. As usual, the ultraviolet behavior of this equation's effective interaction is fully determined by perturbative QCD. For the infrared, we employed a simple Ansatz whose parameters were fixed in a least squares fit of the gap equation's solutions to lattice data on the dressed-quark mass function at available current-quark masses. With our best-fit parameters the mass functions obtained from the gap equation were indistinguishable from the lattice results (Fig. V-2). To correlate the lattice's dressed-gluon and dressed-quark Schwinger functions it was necessary for the kernel to exhibit infrared enhancement over and above that observed in the dressed-gluon function alone. In our model we ascribed that to an enhancement of the quark-gluon vertex. The gap equation provides a solution for the dressed-quark Schwinger function at arbitrarily small current-quark masses and, in particular, in the chiral limit: no extrapolation is involved.   It may therefore be used as a tool with which to estimate the chiral limit behavior of the lattice propagator.   In addition, knowing the gap equation's kernel, it is straightforward to construct symmetry-preserving Bethe-Salpeter equations whose bound state solutions describe mesons.   This enabled an analysis which indicates that chiral and physical pion observables are significantly smaller in the quenched theory than in full QCD. An article describing this work was submitted for publication.

*Kent State University.
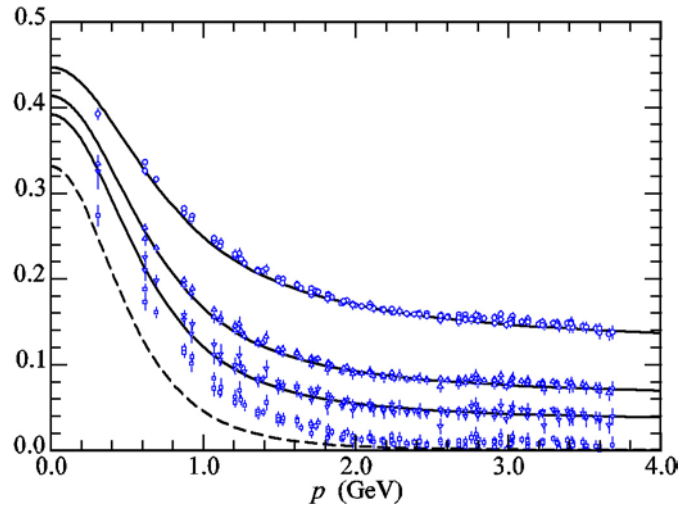
Fig. V-2. Data, upper three sets, lattice results for the quark mass function (in GeV); lower points (circles), linear extrapolation of lattice results to the chiral limit; i.e., am = 0. Solid curves, our best-fit-interaction gap equation solutions for the mass function; dashed-curve, solution of the gap equation obtained in the chiral limit. There is a marked discrepancy between our chiral limit result, which is calculated directly, and the linear extrapolation of lattice data.

a.8.   Comparison of Point-Form Quantum Mechanics and Quantum Field Theory (F. Coester, A. Krassnigg, and C. D. Roberts)

We will explore the extent to which a relationship exists between bound state studies in relativistic quantum field theory and in relativistic quantum mechanics. Dyson-Schwinger equations provide a Poincaré covariant framework for continuum bound state studies in quantum field theory. In relativistic quantum mechanics, we adopt the point form because it, too, is manifestly covariant. In quantum mechanics one studies a mass operator and its eigenvalues. A key question is whether a mass operator and Hilbert space exist that can describe features equivalent to those obtained in quantum field theory. To be concrete, we will first compare results obtained for vector mesons in the two approaches, seeking to identify elements of qualitative equivalence and differences that may indicate model-dependent artifacts. An extension to axial-vector mesons will follow. These states are particularly sensitive to long-range features of QCD's interaction; viz., aspects of confinement. A study of pion properties is expected to be crucial. The dichotomous nature of the pion, as both a Goldstone mode and bound state of massive constituents, is likely to make a valid description in quantum mechanics impossible.

a.9.   Axial-Vector Diquarks in the Baryon (A. Krassnigg and C. D. Roberts)

It was shown that a product Ansatz for the nucleon's Faddeev amplitude using only a scalar-diquark can provide a good description of leptonic and nonleptonic couplings and form factors, with some notable exceptions; e.g., the neutron's charge radius and axial vector coupling. Properly incorporating the lower component of the nucleon's spinor helps somewhat in addressing these exceptions. However, discrepancies remain, and we anticipate that their amelioration requires the inclusion of axial-vector diquark correlations and a pion cloud. We plan to explore this, and quantify the effects of these contributions on $G^p_E(q^2)/G^p_M(q^2)$ and the N $\rightarrow$ Δ transition form factor, current data on both of which we believe are dominated by nonperturbative dynamics.

a.10. Valence-Quark Distributions in the Nucleon (A. Krassnigg and C. D. Roberts)

The pion provides the simplest theoretical subject for a calculation of the valence quark distribution function. However, pion targets are not readily available for experiment and the most reliable measurements of quark distribution functions were performed on nucleon targets. We intend to extend the approach developed for the pion so as to employ it in a calculation of the nucleon's valence quark distribution. In the first studies, the target nucleon will be represented by a quark-plus-scalar-diquark product Ansatz for its Faddeev amplitude. This promises to provide the first Poincaré covariant calculation of the nucleon's valence quark distribution function. Improving the nucleon model via the inclusion of axial-vector diquark correlations and a pion cloud will enable the drawing of a connection between deep inelastic scattering measurements and the "soft physics" wrapped up in nucleon structure. For example, it will provide a means of testing the validity and importance of diquark clustering in the nucleon, and the relation between the d/u-ratio at large-x and confinement, as it is exhibited in the momentum-space extent of the Faddeev amplitude.

a.11. J/ψ Suppression as a Signal of Quark Gluon Plasma Formation
   (C. D. Roberts, D. B. Blaschke,* and Yu. L. Kalinovsky†)

We developed a successful approach to describing heavy-meson observables at zero temperature. That enables a reliable extrapolation into the domain of nonzero temperature, which is relevant to the RHIC program. The suppression of the J/ψ production cross section is touted as a unique signal of quark gluon plasma formation, and such suppression was observed at CERN. We propose to study J/ψ production in the expectation that additional insight will follow from the Dyson-Schwinger equations' capacity to unify nonperturbative aspects of light- and heavy-meson observables via a microscopic description using QCD's elementary excitations. Our initial focus is the T-dependence of J/ψ break-up by hadronic comovers; *i.e.,* the substructure induced T-dependence of those interactions with other mesons in the medium that dissociates the J/ψ. These processes are likely to be affected by the dramatic T-dependence of the dressed-light-quark mass function in the neighborhood of the QGP phase boundary and a possible T-dependent reduction in the mass of the open-charm final states. Our goal is to elucidate the mechanisms involved and the fidelity of J/ψ suppression as a signal of quark gluon plasma formation.

_____
*University of Rostock, Germany, †LCTA, JINR, Dubna, Russia.

a.12. Particle Ratios at RHIC and Chemical Freeze-Out (S. Schramm,
   D. Zschiesche,* H. Stöcker,* and J. Schaffner-Bielich†)

We investigated hadronic particle production in ultrarelativistic heavy-ion collisions at RHIC. Thermodynamical equilibrium calculations of particle production in high energy particle- and nuclear collisions have been carried out for a long time. Experimental data for hadron abundances and ratios have been obtained in heavy-ion collisions at the SIS, AGS, SPS and more recently at the RHIC facility.

The plethora of data revived interest in extracting a common temperature and chemical potential for the chemical freeze-out point that determines the particle ratios using a thermal equilibrium model analysis. The experimentally determined hadron ratios can be fitted quite well with simple non-interacting gas models, if a sudden breakup of a thermalized source is assumed and the subsequent feeding of the various channels from strongly decaying higher resonances is taken into account. From the χ^2 freeze-out fits one has constructed a quite narrow band of freeze-out values in the T-μ_B plane. The extracted freeze-out parameters are close to the assumed phase transition curve for SPS and RHIC energies. However, if the system passes through the vicinity of the phase transition (or through the crossover range) as suggested by the data for T and μ_B, one cannot neglect the very in-medium effects that are responsible for the phase transition in the first place. Thus, non-interacting gas models, as they completely neglect any kind of possible in-medium modification, can only yield limited insight. Therefore, we based our studies on a relativistic self-consistent hadronic 3-flavor model. One can view the model as a thermodynamically consistent effective theory or as a toy model that includes the restoration of chiral symmetry at high temperatures or densities. In either case the model incorporates temperature and density dependent hadronic masses and effective chemical potentials.

Depending on the chosen parameters and degrees of freedom, different scenarios for the chiral phase change are predicted by the model: strong or weak first order phase transition or a crossover. The transitions take place around T_c = 155 MeV, in qualitative agreement with lattice predictions for the critical temperature for the onset of a deconfined and chirally restored phase.

A whole range of particle ratios are calculated in the SU(3) model and compared with the RHIC data for Au + Au at √130 AGeV. In addition a comparison with non-interacting gas calculations was performed.

Since different parameterizations of the model show qualitatively different phase transition scenarios, we investigate whether the particle production, *i.e.* the chemistry of the system, is sensitive to the phase transition behavior. Since we have shown that the current data are described by all three different phase transition scenarios (strong first order, weak first order or smooth crossover) and the ideal gas model, we can so far neither favor nor rule out any one scenario. (See Fig. V-3).

In all interacting models the effective masses at freeze-out are shifted by up to 15% from their vacuum values. The fit values for the chemical freeze-out temperature and chemical potential depend on the order of the phase transition. The crossover case yields temperatures that are shifted by 15 MeV as compared to the non-interacting gas model while the model calculations with a first order phase transition show more than 30 MeV lower temperatures.

Strikingly, the fitted freeze-out points are located very close to the phase transition boundary in the first-order phase transition scenarios, but T is always smaller than T_c. This suggests that at RHIC the system emerges after passing through the chiral phase transition. This of course is only true if a first order phase transition does actually occur in QCD at small chemical potentials and high T. Furthermore, from our studies it becomes clear that a "freezing" of the relative abundances of various hadrons in the symmetric phase (at $T > T_c$) is definitely excluded.

_____
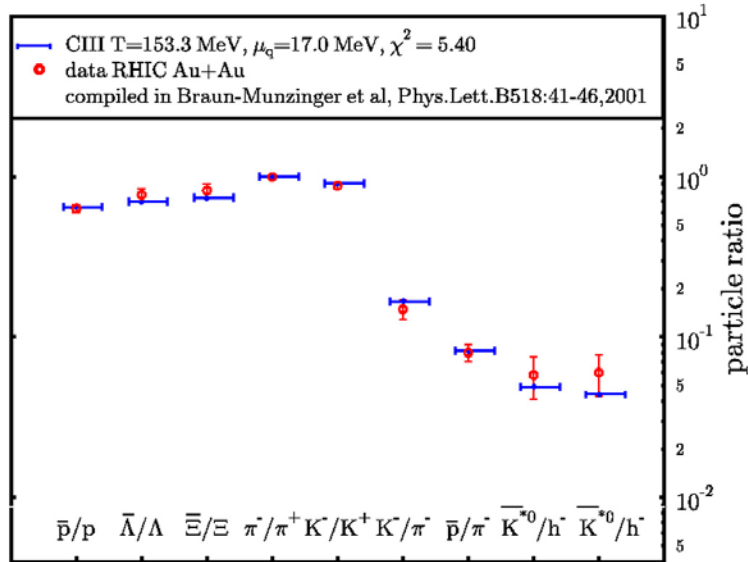
Fig. V-3. Hadronic particle ratios calculated with two different parameterizations[1] compared to experimental data obtained at RHIC.

a.13.   HBT Analysis of Relativistic Heavy Ion Collisions (S. Schramm, D. Zschiesche,* and H. Stöcker*)

Bose-Einstein correlations in multi-particle production processes can provide important information on the space-time dynamics of fundamental interactions. Therefore correlations of identical pions produced in high-energy collisions of heavy ions could yield some insight into the characteristics of a hypothetical phase transition that might occur during the highly excited stage of the heavy-ion collision.

In particular, a potential first-order phase transition leads to a prolonged time of hadronization as compared to a smooth cross-over or a hadron gas with no symmetry restoration at all, and accordingly such a phase transition has been related to large Hanbury-Brown-Twiss (HBT) radii deduced from the 2-pion correlations. A coexistence phase of hadrons and quark gluon plasma droplets reduces the "explosivity" of the high-density matter before hadronization, prolonging the emission duration of pions.

The correlations should then depend on the hadronization, the critical temperature T_c and the latent heat of the transition. Calculations assuming a first-order phase transition are usually performed with an equation of state that is constructed by matching the bag model with an ideal hadron gas model, for which the latent heat of the transition is large. Consequently, also the predicted HBT radii are large. We studied the impact of a weaker first-order transition with relatively small latent heat and considered its influence on the space-time characteristics of the expansion and on HBT radii. As a limiting case we calculated the dynamics of the system for a smooth crossover transition at high temperatures.

Similar scenarios were investigated before, but without explicit reference to chiral symmetry restoration and dynamically changing hadron masses. To investigate the space-time dynamics and the influences of different types of phase transitions we performed a hydrodynamic simulation using various equations-of-state obtained from a chiral model. The hydrodynamical equations describe the collective evolution of the system, while the chiral model supplies the underlying equation of state. As the hot and dense central region of the heavy-ion collision expands in the longitudinal and transverse directions, the effective

hadron masses approach their vacuum values. The initial excitation energy of the system is converted into collective flow and massive hadrons.

By considering various equations of state in the simulation one can get more information on how to discriminate between the different phase transition scenarios from observable correlations. The model used in this calculation contains only hadronic degrees of freedom, which limits the investigation to the chiral phase transition but not the deconfinement phase transition to a state of quarks and gluons. Still, the main effect as far as the collective expansion of the system is concerned originates from the difference in the latent heat for the transition, irrespective of its specific microscopic origin.

Within this approach we determined the HBT-radii relevant to experiments at CERN and RHIC and compared the results to NA49- and STAR data, respectively. One can clearly observe that a small latent heat, meaning a weak first-order phase transition or even a smooth cross over, leads to distinctly large radii in the HBT analysis for the side-direction R_{side} (signaling a rapid evolution of the system during the transition from light hadrons or quarks to the chirally broken phase and to small radii in out-direction R_{out}), which are closest to the data in almost all cases. (See Fig.V-4).

However, a quantitative description of the data, both at SPS energy as well as at RHIC energy, is not reached within the present hydrodynamical approach using the various SU(3) chiral EoS.

It was argued that the decay of a droplet of chirally symmetric matter from a region of negative pressure may yield small HBT radii, as well as a smaller ratio R_{out}/R_{side}. We are currently investigating this possibility.

More realistic freeze-out descriptions may improve the results. However, it appears probable that a quasi-adiabatic first-order phase transition with large latent heat, for which a hydrodynamical description should be adequate, cannot describe the pion HBT data from either SPS or RHIC experiments.

---

*University of Frankfurt.
[1]D. Zschiesche, S. Schramm, H. Stöcker, W. Greiner, Phys.Rev. C **65**, 064902 (2002).
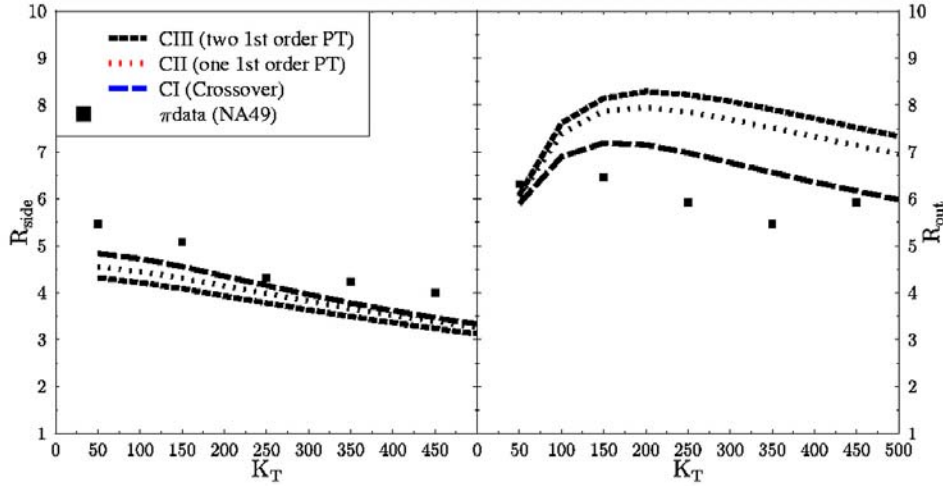
Fig. V-4. The figure shows the resulting HBT radii in the side-direction R_{side} and in the out-direction R_{out} relative to the scattering plane for central Pb + Pb collisions at SPS energy compared to data from the NA49 collaboration.[1] The general result suggests a better fit to the data assuming weak phase transitions.

a.14. Dyson Approach to Nonequilibrium Field Theory (B. Mihaila, F. Cooper,* and J. F. Dawson†)

Classical field theory: We study the domain of validity of a Schwinger-Dyson approach to non-equilibrium dynamics when $\langle\phi(x)\rangle \neq 0$. We perform exact numerical simulations of the one- and two-point functions of a single component $\lambda\phi^4$ field theory in 1 + 1 dimensions in the classical field theory case.[1] We compare these results to two self-consistent truncations of the Schwinger-Dyson equations which ignore three-point vertex function corrections. The first approximation, which we called the bare vertex approximation (BVA), sets the three-point function to one. It gives a promising description for $\langle\phi(x)\rangle \neq \phi(t)$. The second approximation, which ignores higher in $1/N$ corrections to the two-particle irreducible (2PI) generating functional is not as accurate for $\phi(t)$ for the case $N = 1$. Both approximations have serious deficiencies in describing the two-point function when $\phi(0) \gtrsim 0.4$.

Quantum field theory: We perform a detailed numerical investigation of the dynamics of a single component "explicitly broken symmetry" $\lambda\phi^4$ field theory in 1 + 1 dimensions,[2] using a Schwinger-Dyson equation truncation scheme based on ignoring vertex corrections (BVA). We assume here that the initial state is described by a Gaussian density matrix peaked around some non-zero value of $\langle\phi(0)\rangle$, and characterized by a single-particle Bose-Einstein distribution function at a given temperature. We compute the evolution of the system using three different approximations: Hartree, BVA and a related 2PI-1/N expansion, as a function of coupling strength and initial temperature. In the Hartree approximation, the static phase diagram shows that there is a first-order phase transition for this system. As we change the initial starting temperature of the system, we find that the BVA relaxes to a new final temperature and exhibits behavior consistent with a second-order phase transition. We find that the average fields equilibrate for arbitrary initial conditions in the BVA, unlike the behavior exhibited by the Hartree approximation, and we illustrate how $\langle\phi(t)\rangle$ and $\langle\chi(t)\rangle$ depend on the initial temperature and on the coupling constant. The Fourier transform of the two-point functions at late times can be fit by a Bose-Einstein distribution function whose temperature is independent of momentum. We interpret this as evidence for thermalization.

_____
*Los Alamos National Laboratory, †University of New Hampshire.
[1]F. Cooper, J. Dawson, and B. Mihaila, Phys. Rev. D **67**, 51901(R) (2003).
[2]F. Cooper, J. Dawson, and B. Mihaila, Phys. Rev. D **67**, 56003 (2003.

a.15. Continuum Versus Periodic Lattice Monte Carlo Approach to Classical Field
Theory (B. Mihaila and J. F. Dawson*)

We discuss two Monte Carlo approaches of obtaining the dynamical evolution of a classical ϕ^4 field theory system,[1] one based on a standard periodic lattice formulation in coordinate space, the other in momentum space. Both methods require the assumption of periodic boundary conditions, but the different levels at which this assumption is made allows the momentum-space approach to avoid certain artifacts of the lattice-based method. In particular, the intrinsic mismatch in initial conditions at finite cutoff values, results in different values of the "thermalized" field, at large times. The discrepancy is worse for smaller values of the cutoff, but the two approaches converge to the same result in the continuum limit. The mismatch in initial conditions is due to the fact that by using a finite-difference approximation for the spatial derivative operator together with the assumption of periodic boundary conditions on the lattice, we have, in fact introduced an approximation of the dispersion relation, which is now viewed as an expansion in the lattice spacing a. In order to improve the quality of the spatial derivative approximation in the lattice case, one would normally have to take the limit when the lattice spacing a goes to zero. We are, however, prevented from doing that, since the choice of the momentum cutoff Λ also determines the choice of the lattice spacing $a = \pi/\Lambda$. Consequently, we cannot improve the agreement of the lattice dispersion relation with the continuum for a given momentum-space cutoff. The momentum-space approach does not exhibit this limitation.

_____
*University of New Hampshire.
[1]B. Mihaila and J. Dawson, Phys. Rev. D **65**, 71501(R) (2002).

a.16. Parallel Algorithm with Spectral Convergence for Nonlinear Integro-
Differential Equations (B. Mihaila and R. E. Shaw*)

We discuss a numerical algorithm[1] for solving nonlinear integro-differential equations, and illustrate our findings for the particular case of Volterra type equations. The algorithm combines a perturbation approach meant to render a linearized version of the problem and a spectral method where unknown functions are expanded in terms of Chebyshev polynomials (El-gendi's method). From a computational point of view, each iteration involves two stages, namely initializing the relevant matrices and solving a linear system of equations. Both stages can be rendered parallel in a suitable manner, and the efficiency of the code increases when applied to complicated multi-step, multi-dimensional problems. This approach is shown to be suitable for the calculation of two-point Green functions required in next-to-leading-order studies of time-dependent quantum field theory.

_____
*University of New Brunswick, Canada.
[1]B. Mihaila and R. E. Shaw, J. Phys. A: Math. Gen. **35**, 5315 (2002).

a.17. Dynamical Model of Weak Pion Production Reactions (T.-S. H. Lee,
Toru Sato,* and D. Uno*)

The dynamical model of pion electroproduction developed in an Argonne-Osaka University collaboration[1] has been extended to investigate the weak pion production reactions. With the Conserved Vector Current (CVC) hypothesis, the weak vector currents are constructed from electromagnetic currents by isospin rotations. Guided by the effective chiral Lagrangian method and using the unitary transformation method developed previously, the weak axial vector currents for π production are constructed with no adjustable parameters. In particular, the N-Δ transitions at $Q^2 = 0$ are calculated from the constituent quark model and their Q^2-dependence is assumed to be identical to that determined in the study of pion electroproduction. The main feature of our approach is to renormalize these bare N-Δ form factors with the dynamical pion cloud effects originating from the non-resonant π production mechanisms. The predicted cross sections of neutrino-induced pion production reactions, $N(\nu_\mu,\mu^-\pi)N$, are in good agreement with the existing data. This is illustrated in Figs.V-5a and V-5b. We show that the renormalized (dressed) axial N-Δ
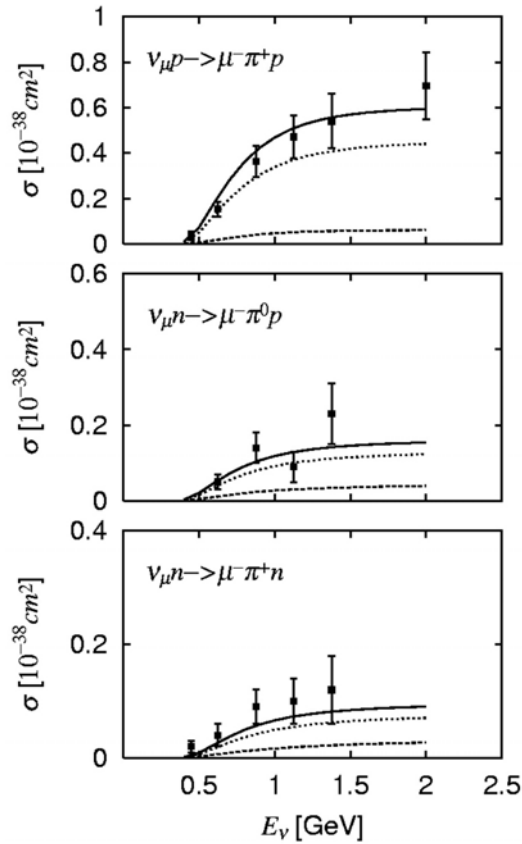
Fig. V-5a. Total cross sections of $N(\nu,\mu\bar{}\ \pi^+)N$ reactions. The solid curves are from full calculations. The dashed curves are from turning off pion cloud effects on N-Δ transitions. The dotted curves are the contributions from the non-resonant amplitude.
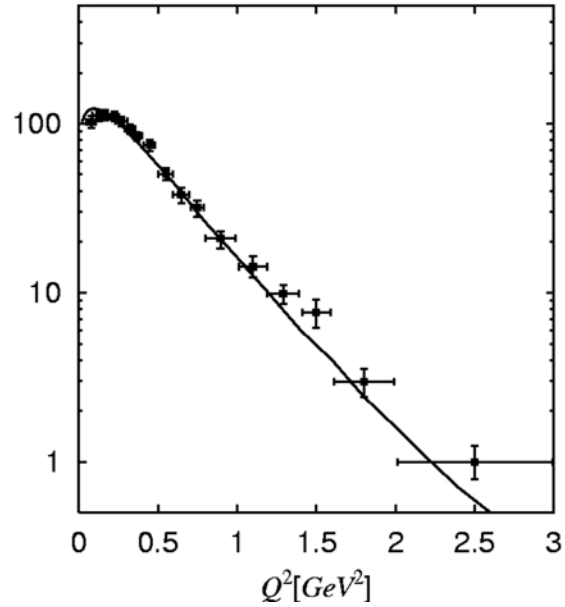
Fig. V-5b. The differential cross sections $d\sigma/dQ^2$ of $p(\nu,\mu\bar{}\ \pi^+)$ reaction.

form factor contains large dynamical pion cloud effects, and these renormalization effects are crucial in getting agreement with the data. We conclude that the N-Δ transitions predicted by the constituent quark model are consistent with the existing neutrino-induced pion production data in the Δ region, contrary to previous observations. This is consistent with our previous findings in the study of pion electroproduction reactions. However, more extensive and precise data of neutrino-induced pion production reactions are needed to further test our model and to pin down the Q^2-dependence of the axial vector N-Δ transition form factor.

_____
*Osaka University, Japan.
[1]Toru Sato and T-S. H. Lee, Phys. Rev. C **63**, 055201 (2001).

a.18.   One-loop Corrections to Vector Meson Photoproduction Near Threshold
   (T.-S. H. Lee and Y. Oh*)

One-loop corrections to ω photoproduction near threshold were investigated by using the approximation that all relevant transition amplitudes are calculated from the tree diagrams of effective Lagrangians. With the parameters constrained by the data of $\gamma N \to \pi N$, $\gamma N \to \rho N$, and $\pi N \to \omega N$ reactions, it is found that one-loop effects due to the intermediate πN and ρN states can significantly change the differential cross sections and spin observables. This is illustrated in Fig. V-6. The results from this investigation suggest strongly that the coupled-channel effects should be taken into account in extracting reliable resonance parameters from vector meson photoproduction data in the resonance region. A paper describing our results was published.[1] We have extended our approach to also investigate ρ and ϕ photoproduction reactions and found that the one-loop 2-π exchange mechanisms can replace the conventional, phenomenological σ-exchange in explaining existing data.

_____
*Yonsi University, Seoul, Korea.
[1]Yongseok Oh and T.-S. H. Lee, Phys. Rev. C **66**, 045201 (2002).
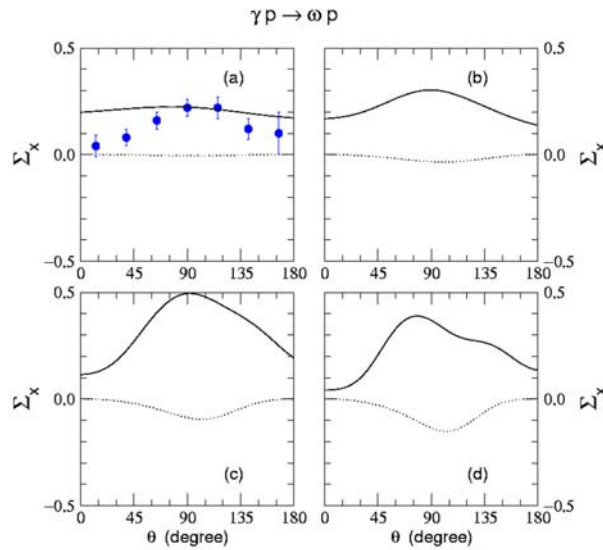
Fig. V-6. Single photon asymmetry Σ_x for $\gamma p \to \omega p$ at E_γ = 1.125 GeV (a), 1.23 GeV (b), 1.45 GeV (c), and 1.68 GeV (d). The dotted curves are from neglecting one-loop corrections.

a.19.   Effective Lagrangian Approach to ω Photoproduction Near Threshold
   (T.-S. H. Lee and Alexander I. Titov*)

We apply the effective Lagrangian approach to investigate the role of nucleon resonances in ω-meson photoproduction at energies near threshold.   The nonresonant amplitudes are taken from previous investigations at higher energies and consist of the pseudoscalar meson exchange and nucleon Born terms. The resonant amplitudes are calculated from effective Lagrangians with the N* → γN and N* → ωN coupling constants fixed by empirical helicity amplitudes and the vector meson dominance model.   The contributions from nucleon resonances are found to be significant in changing the differential cross sections in a wide interval of t and various spin observables. In particular, we suggest that a crucial test of our predictions can be made by measuring single- and double-spin asymmetries.   A paper describing our results was published.[1]

_____
*JAERI, Tokai, Japan.
[1]Alexander I. Titov and T.-S. H. Lee, Phys. Rev. C **66**, 015204 (2002).

a.20   Coherent φ and ω Meson Photoproduction from Deuterium and Nondiffractive Channels (T.-S. H. Lee, A. I. Titov,* and M. Fujiwara†)

For coherent photoproduction of φ and ω mesons from deuterium at forward angles, the isovector π-exchange amplitude is strongly suppressed.   We show a possibility to study the nondiffractive channels associated with   unnatural parity exchange in φ photoproduction and with baryon resonance excitations in ω photoproduction by measuring the spin observables.   A paper describing our result was published.[1]

_____
*JINR, Dubna, Russia, †Osaka University, Japan.
[1]A. I. Titov, M. Fujiwara, and T.-S. H. Lee, Phys. Rev. C **66**, 022202(R) (2002).

a.21.   η Meson Production in NN Collisions (T.-S. H. Lee, K. Nakayama,* and J. Speth†)

η meson production in both proton-proton and proton-neutron collisions is investigated within a relativistic meson exchange model of hadronic interactions. It is found that the available cross section data can be described equally well by either the vector or pseudoscalar meson exchange mechanism for exciting the $S_{11}(1535)$ resonance. It is shown that the analyzing power data can potentially be very useful in distinguishing these two scenarios for the excitation of the $S_{11}(1535)$ resonance. A paper describing our results was published.[1]

_____
*University of Georgia, †Forschungszentrum-Jülich, Germany.
[1]T.-S. H. Lee, K. Nakayama, and J. Speth, Phys. Rev. C **65**, 045210 (2002).

a.22.   Study of Nucleon Resonances with Double Polarization Observables in Pion Photoproduction (T.-S. H. Lee, D. Dutta,* and H. Gao*)

Motivated by new experimental opportunities at Jefferson Lab, the role of nucleon resonances in the double polarization observables of pion photo-production is investigated. As an example, we show that the not-well-determined two-star resonance $N_{3/2}^-(1960)$ can be examined by performing experiments on beam-recoil polarization at large angles. A paper describing our results was published.[1]

_____
*Massachusetts Institute of Technology.
[1]T.-S. H. Lee, D. Dutta, and H. Gao, Phys. Rev. C **65**, 044619 (2002).

a.23   Spin Effects and Baryon Resonance Dynamics in φ-Meson Photoproduction at Few GeV (T.-S. H. Lee and A. I. Titov*)

The diffractive φ-meson photoproduction amplitude is dominated by Pomeron exchange but also contains terms that govern the spin-spin and spin-orbit interactions. We show that these terms are responsible for the spin-flip transitions at forward photoproduction angles and appear in the angular distributions of φ → K^+K^- decay in reactions with unpolarized and polarized photon beams. At large momentum transfers, the main contribution to the φ-meson photoproduction is found to be due to the excitation of nucleon resonances. Combined analysis of ω and φ photoproduction indicates strong OZI-rule violation in φNN* couplings. We also show that the spin observables are sensitive to the dynamics of φ-meson photoproduction at large angles and could help distinguish different theoretical models of nucleon resonances. Predictions for spin effects in φ-meson photoproduction are presented for future experimental tests. A paper describing our results was submitted for publication.

_____
*Japan Atomic Energy Research Institute, Tokai.

a.24.   Unitary ππN Model for Investigating N* Resonances (T.-S. H. Lee, A. Matsuyama,* and T. Sato†)

In the second and third resonance regions, the πN and γN reactions involve three-body ππN channel in addition to various stable two-body channels such as ηN, ωN, and KΛ. To interpret the data in these energy regions correctly in terms of N* excitations predicted by various hadron models, it is essential to account for the ππN unitarity cut in any coupled-channel approach. We achieved this by developing a unitary coupled-channel ππN dynamical model with interactions derived by using the unitary transformation method.

The numerical techniques needed for solving the resulting coupled integral equations were developed. In a model calculation including πN, πΔ, and ρN channels, we show that the ππN unitary condition has very large effects on πN reaction cross sections. We are now carrying out realistic calculations with N* in the S_{11} channel, aimed at exploring whether the empirical πN and γN amplitudes in this partial wave are consistent with the constituent quark model predictions.

_____

*Shizuoka University, Japan, †Osaka University, Japan.

a.25.   Quark-exchange Mechanism of γd → np Reaction at 2-6 GeV (T.-S. H. Lee and B. Julia-Diaz*)

Within the constituent quark model, we examine the extent to which deuteron photodisintegration at 2-6 GeV can be described by the quark-exchange mechanism. The main feature of our approach is an exact loop-integration over the exchanged quark propagator. With the parameters constrained by *np* scattering data up to 12 GeV, the calculated differential cross sections disagree with the data in both magnitude and energy-dependence. The results can be improved greatly if we use a smaller size parameter for quark wave functions. We find that the on-shell

approximation used by others in previous investigations of the quark-exchange mechanism is not valid. This is illustrated in Fig. V-7. We also find that the predicted cross sections are sensitive to the mass parameters in the quark and gluon propagators. It is important to account for the momentum-dependence of these parameters in this energy region where the transition from the hadronic picture to the quark-gluon picture is taking place. A paper describing our results is being prepared for publication.

_____

*University of Salamanca, Spain.
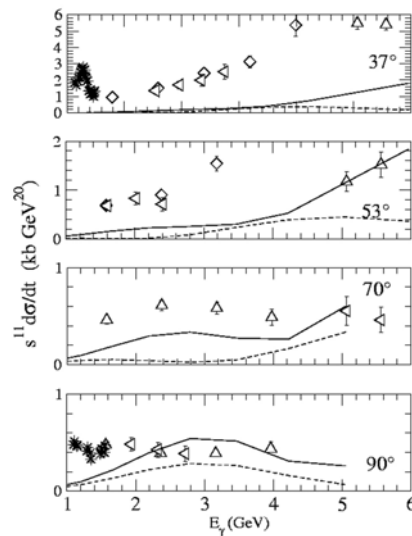
Fig. V-7. The γd → np differential cross sections. The solid curves are from exact loop integration, while the dashed curves are from taking the on-shell approximation used in previous investigations.

a.26. Locality in Relativistic Quantum Mechanics[1] (F. Coester)

The fundamental requirements of relativistic quantum theory are: 1) Implementation of relativistic space-time symmetry, realized by unitary representations of the Poincaré group, and 2) Einstein causality, which requires an appropriate definition of states localized in finite space-time regions. Implementation of the locality requirements is discussed extensively in the literature in the context of the algebraic formulation of quantum field theories. The basic ingredients are operator algebras, nets of localized sub-algebras with the covariance, union, intersection and inclusion properties of the associated space-time regions. "Essentially localized" state vectors are obtained by application of local operators to the vacuum state. Essential features of this framework are infinitely many degrees of freedom and inequivalent Hilbert-space representations of the states depending on the dynamics. Finite systems necessarily appear as subsystems of infinite systems.[1] In relativistic quantum mechanics the emphasis was on the implementation of the Poincaré symmetry by unitary representations of the Poincaré group on the Hilbert space of states, which is a finite tensor product of irreducible representations (single-particle states), or a finite direct sum of such spaces. The Poincaré generators can be expressed as functions of kinematic operators and the mass operator which specifies the dynamics. The choice of the kinematic operators determines the form of kinematics, that is a subset of generators which are independent of the mass operator. Einstein causality is realized asymptotically by the properties of cluster separability. Recent mathematical developments indicate how manifolds of localized states can be defined strictly within the framework of relativistic quantum mechanics without reference to infinite systems. This construction involves the domains of unbounded operators defined as functions of the Poincaré generators.

---

[1]F. Coester, Few Body Systems Suppl. **14** (2003).

a.27. Current Density Operators in Relativistic Quantum Mechanics[1] (F. Coester)

Relativistic quantum mechanics is a mathematically well-defined framework for the description of few nucleons, few hadrons and/or few constituent quarks for a limited range of the total mass spectrum. The Hilbert space of states consists of irreducible representation spaces of the Poincaré group (single-particle states), finite tensor products of single particle states, and finite direct sums of such tensor products, which is the same for interacting and noninteracting systems. The dynamics is specified by a unitary representation of the Poincaré group which may be identical to the representation of noninteracting constituents for a kinematic subgroup. The "form of kinematics" depends on the choice of that subgroup. Within this framework the dynamics generates fully covariant conserved currents from current density operators that are covariant under the kinematic subgroup. The choice of the form of kinematics implies important qualitative differences, which can be illustrated by simple toy models.

---

[1]F. Coester, Few-Body Systems Suppl., to be published.

B. NUCLEAR FORCES AND NUCLEAR SYSTEMS

The goal of this program is to achieve a description of nuclear systems ranging in size from the deuteron and triton to nuclear matter and neutron stars using a single parameterization of the nuclear forces. Aspects of our program include both the construction of two- and three-nucleon potentials and the development of many-body techniques for computing nuclear properties with these interactions. Detailed quantitative, computationally-intensive studies are essential parts of this program.

Quantum Monte Carlo (QMC) calculations of light ($A \leq 10$) nuclei with realistic interactions have been the main focus of our recent efforts. Our nonrelativistic Hamiltonian contains the accurate Argonne v_{18} two-nucleon (*NN*) potential, which includes charge-independence breaking terms, and either the venerable Urbana IX three-nucleon (*NNN*) potential, or one of several new Illinois *NNN* models. The QMC calculations include both variational (VMC) and Green's function (GFMC) methods. We begin with the construction of variational trial functions based on sums of single-particle determinants with the correct total quantum numbers, and then act on them with products of two- and three-body correlation operators. Energy expectation values are evaluated with Metropolis Monte Carlo integration and parameters in the trial functions are varied to minimize the energy. These optimized variational wave functions can then be used to study other nuclear properties. They also serve as a starting point for the GFMC calculations, which systematically remove higher excited-state components from the trial wave functions by propagation in imaginary time.

We are currently studying all $A \leq 10$ nuclei with experimentally known bound state or resonance energies, including ≈ 60 excited states. These are the first calculations treating $A \geq 6$ nuclei directly with realistic *NN* and *NNN* interactions. In GFMC calculations, with the new Illinois *NNN* models, we can reproduce most of the experimental ground- and excited-state energies within 0.7 MeV. In the last year we found that GFMC propagation started with orthogonalized VMC wave functions for several states of the same J^π preserves the orthogonality to a very good approximation. This enabled the calculation of many more states for $A \leq 10$, in previous years only some 30 states were done. We also made a study of the sensitivity of the binding energies to various features of the *NN* potential. We find that a complicated potential, including tensor and spin-orbit terms, is needed to reproduce such critical experimental features as the non-existence of bound 5- and 8-body nuclei. In another study we showed that modern nuclear Hamiltonians cannot produce a bound tetraneutron, despite a recent claimed experimental observation. Finally, we are also studying the properties of neutron drops with the goal of providing additional constraints for the construction of Skyrme interactions that are used in the modeling of neutron-rich nuclei in neutron star crusts.

Efforts using the coupled cluster [exp(S)] method also continued last year. The coupled cluster method is being used to study nuclei in the ^{12}C-^{16}O range, using the same realistic Hamiltonian as the quantum Monte Carlo calculations. Comparisons of GFMC and exp(S) results are being made for ^{4}He and neutron drops. We are also able to compare both methods with results of traditional shell model calculations. Lastly, studies of hypernuclei are also continuing, particularly the charge-symmetry-breaking of ΛN interactions.

b.1.   Quantum Monte Carlo Calculations of Light p-shell Nuclei (S. C. Pieper, R. B. Wiringa, J. Carlson,* V. R. Pandharipande,† and K. Varga‡)

Since the early 1990s, we have been studying the ground and low-lying excited states of light p-shell nuclei as A-body problems with realistic nucleon-nucleon (NN) and three-nucleon (NNN) interactions using advanced quantum Monte Carlo (QMC) methods. Our preferred Hamiltonians contain the Argonne v_{18} NN potential (AV18), which gives an excellent fit to elastic NN scattering data and the deuteron energy and Illinois NNN potentials, which we have fit to binding energies of $A \le 8$ nuclei. The QMC methods include both variational Monte Carlo (VMC), which gives an initial approximate solution to the many-body Shrödinger equation, and the Green's function Monte Carlo (GFMC), which systematically improves on the VMC starting point and produces binding energies that are accurate to within 2%. In recent years we concentrated on $A = 9,10$ nuclei, and we are now making preliminary calculations of ^{12}C.

The VMC calculations begin with the construction of an antisymmetric Jastrow trial wave function that includes single-particle orbits coupled to the desired JM values of the state of interest as well as pair and triplet spatial correlations. It is then acted on by a symmetrized product of two-body spin, isospin, tensor, and spin-orbit correlation operators, induced by the NN potential, and three-body correlation operators for the NNN potential. The wave functions are diagonalized in the small basis of different Jastrow spatial symmetry components to project out higher excited states with the same quantum numbers.

In the GFMC calculations, we operate on a version of the VMC trial function with the imaginary time propagator, $\exp[-(H'-E_0)\tau]$, where H' is a simplified Hamiltonian, E_0 is an estimate of the eigenvalue, and τ is the imaginary time. The excited-state components of the trial function will then be damped out for large τ, leaving the exact lowest eigenfunction with the quantum numbers of the input variational wave function. The expectation value of H is computed for a sequence of increasing values of τ to determine the convergence. Our H' contains a simplified, reprojected eight-operator version of the NN potential, AV8′, and the full NNN potential. The small correction, H-H', is computed perturbatively. The many-body propagator is written as a symmetrized product of exact two-body propagators, with the NNN potential treated in lowest order.

In previous years we made significant improvements in the GFMC algorithms, especially in solving the fermion sign problem for nuclear systems. The method and program now seems stable but with the availability of increased computer time we are making more extensive tests. The computer resources (both CPU time and memory) required for these calculations increase exponentially with the number of nucleons. Therefore, progress to bigger nuclei usually requires a new generation of computers.

Our recent QMC work is described in the following subsections.

_____
*Los Alamos National Laboratory, †University of Illinois, Urbana, ‡Oak Ridge National Laboratory.

b.2.   Recent Progress in Quantum Monte Carlo Calculations (S. C. Pieper, R. B. Wiringa, and J. Carlson*)

This year, we finished and published an extensive set of calculations of natural-parity states in $A = 9,10$ nuclei.[1] These calculations used essentially complete p-shell basis sets for the Jastrow wave functions; in several cases this lowered our earlier (unpublished) energies by 1-2 MeV. The present state of our calculations, including newer results discussed below, is shown in Fig. V-8. There is generally good agreement of the results using the Illinois-2 NNN potential and the importance of a NNN potential is clearly shown.

Since then we have made use of large blocks of early-user time on the second phase of the NERSC Seaborg and on Argonne's new Jazz computer to make extensive tests of the reliability of the GFMC for $A = 8$-10. Specifically, we studied our use of an approximate propagator for the three-body potential. This approximation was developed and reported a number of years ago for lighter nuclei with the Urbana-IX NNN potential; in those cases it gave better than 1% accuracy. It appears that in larger nuclei with the Illinois potentials it can be less accurate, with errors up to 2%. This is unfortunate, because the three-body

propagator uses an increasing fraction of the total computational time as *A* increases. The most accurate propagator that we have takes twice as long as the approximate one. We are continuing to study this and make other tests of the reliability of GFMC for *A* = 8-10.

GFMC starts with a trial wave function of certain quantum numbers and propagates to the lowest-energy state that is not orthogonal to the starting wave function. In the process of constructing the starting wave function (previous section), a small diagonalization produces several orthogonal wave functions with the same quantum numbers. We found that GFMC propagation seems to maintain this orthogonality; the propagation results in stable excited-state energies and the propagated wave functions remain almost orthogonal to the other starting wave functions (we cannot compute the overlap of two different GFMC propagations at present). Thus we can now compute many second and higher states of the

same quantum numbers in a given nucleus; so far, as shown in Fig. V-8, we are obtaining mostly good agreement with known experimental energies for these states. This work is also continuing.

Finally, we made use of the new Jazz computer at Argonne to make our first, preliminary, calculations of ^{12}C. These were first made with just the AV8' and AV18 *NN* potentials and then one calculation (40,000 2.4GHz Pentium-4 processor hours) was made using AV18 plus the Illinois-2 *NNN* potential. The starting wave function had just the ^{1}S[444] symmetry and so is certainly inadequate. Since then we expanded the program to also include a $(p_{3/2})^8$ basis state; this lowers the starting energy by only 1.2 MeV, but we do not know what effect it will have on the GFMC propagation. These preliminary calculations are also using the approximate three-body propagator discussed above. Thus more extensive calculations (requiring much more computer time) will be needed before a definitive result can be obtained.

_____

*Los Alamos National Laboratory.
[1]S. C. Pieper, K. Varga, and R. B. Wiringa, Phys. Rev. C **66**, 044310/1-14 (2002).
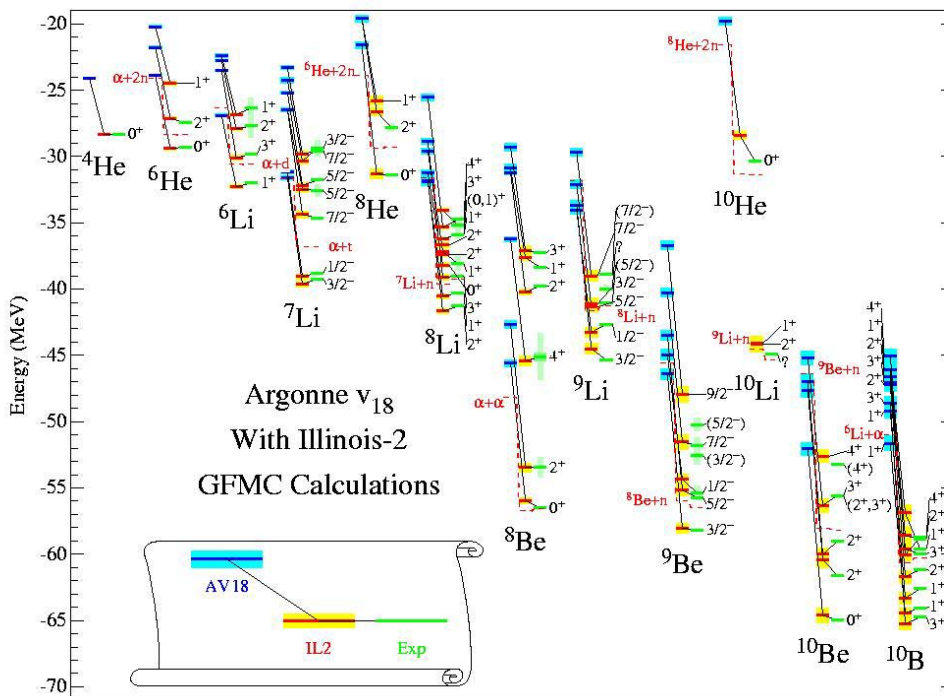
Fig.V-8. GFMC energies for A = 4-10 nuclei using the AV18 NN potential by itself and with the Illinois-2 NNN potential, compared to experiment.

b.3.   Evolution of Nuclear Structure with Nuclear Forces (R. B. Wiringa and S. C. Pieper)

One of the most intriguing features of light nuclei is the absence of stable five- and eight-body systems. This fact is of enormous importance for the chemical evolution of the universe, limiting big bang nucleosynthesis to elements no heavier than lithium, while giving stars like our sun a long lifetime during which biological evolution can take place. In this work we studied what aspects of nuclear forces are necessary to obtain observed nuclear spectra, *i.e.*, the binding and relative stability of light nuclei, including the crucial mass gaps at A = 5 and 8.

We know from our quantum Monte Carlo (QMC) studies of light nuclei that a realistic two-nucleon potential, like Argonne v_{18} (AV18), that accurately reproduces NN scattering data, is unable to reproduce nuclear binding energies precisely without the addition of a fairly sophisticated three-nucleon force, such as one of the Illinois models. Nevertheless, AV18 by itself does produce reasonable nuclear spectra, with ^{5}He unstable against breakup into ^{4}He + n and ^{8}Be unstable against breakup into ^{4}He + ^{4}He. It also gives a fairly good ordering of low-lying excited states, although some weakly bound nuclei, like ^{6}He and ^{8}He are not predicted to be stable.

We constructed a series of progressively simpler two-nucleon potentials to see what aspects of the nuclear force are crucial to these stability issues. The first simplification is AV8', a reprojected version of AV18 retaining central, spin, isospin, tensor, and spin-orbit forces, but dropping quadratic momentum-dependent and charge-independence-breaking terms. AV8' reproduces the charge-independent average of S- and P-wave phase shifts and the deuteron properties of AV18

using eight operators instead of eighteen. QMC calculations of the light nuclei show that the spectra from AV8' are shifted to slightly greater binding than AV18, but overall are very similar.

We dropped the spin-orbit terms and readjusted the remaining six operators (to preserve the deuteron binding) to create an AV6' model. This model still fits S-wave phases well, but no longer reproduces $^3P_{0,1,2}$ partial waves. It does have mass gaps at A = 5 and 8, but the intervening ^{6,7}Li nuclei are not clearly stable. Eliminating tensor terms, and again adjusting the remaining four operators (to preserve deuteron binding), we produced an AV4' model. This force gives ^{8}Be more than twice as bound as ^{4}He, so the A = 8 mass gap has disappeared, although A = 5 nuclei are still unstable. Finally, we eliminate additional operators, producing AV2' and AV1' models, which retain the features of a repulsive core and intermediate-range attraction. However, these models provide no saturation in the light p-shell nuclei, predicting ever-increasing binding as nucleons are added. The purely central AV1' model would predict that the most stable nuclei up to A = 10 are the series of helium isotopes.

We conclude from this study that the A = 5 and 8 mass gaps require a combination of spin-isospin exchange forces and tensor forces, and that stability of the intervening A = 6,7 nuclei probably also requires spin-orbit forces. Thus the nature of the universe we live in is crucially dependent on the complicated nature of the *NN* interaction that we actually observe in the laboratory. This work was published as a Physical Review Letter[1] and featured online in Physical Review Focus.

_____
[1]R. B. Wiringa and S. C. Pieper, Phys. Rev. Lett. **89**, 182501, 1-4 (2002).

b.4.   Can Modern Nuclear Hamiltonians Tolerate a Bound Tetraneutron? (S. C. Pieper)

A recent experimental paper reported the apparent observation of bound tetraneutrons. This inspired a number of approximate calculations by several authors, using simplified forces, of the energy of ^{4}n; the conclusions were that ^{4}n is unbound. I have completed more reliable calculations, using GFMC with the AV18 + Illinois-2 Hamiltonian, of ^{4}n. These show that for such a realistic force ^{4}n is not bound, but might have a (probably very broad) resonance at +2 MeV. I also

made calculations using some of the simplified models (Volkov potentials) that other authors had used approximately. My results are that the Volkov potentials (which are known to have a bound dineutron) result in ^{4}n with negative energies, although the ^{4}n energy is still above the energy for breakup into two dineutrons; the previous results had not indicated the possibility of such a low energy.

A number of modifications of the AV18 + Illinois-2 Hamiltonian were made to force ^{4}n to have a energy of about -0.5 MeV. The resulting Hamiltonians were then used to compute the energies of other light nuclei. Some of the results are shown in Fig. V-9. In all cases the modifications result in dramatic disagreements with other experimental energies. For example, if the binding of the ^{4}n is achieved by modifying the $^1S_0$ part of AV18 (the only channel that will achieve such binding), then the dineutron becomes bound by about the same amount so that, in fact, the ^{4}n can still break into two dineutrons. This results in a large change in the experimentally well determined $^1S_0$ phase shifts. Furthermore, ^{3}H becomes overbound by 50% and other light nuclei also become very overbound.

It was suggested that three- or four-neutron potentials could bind ^{4}n; such potentials would not affect any two-nucleon properties. By making the potentials act only in isospin 3/2 or 2 channels, effects on some nuclei (like ^{3}H or ^{4}He) can also be avoided. However, it turns out that the potentials must be made quite strong to produce a minimally bound ^{4}n. As is shown in Fig.V-9, this results in large changes to the binding energies of any nucleus in which the potential can have non-zero expectation value; in particular the most bound $A = 6, 8$ systems are pure neutron systems! Thus it appears that should the experimental claim of a bound ^{4}n be confirmed, our current very successful understanding of nuclear forces would have to be severely modified. This work was submitted for publication.
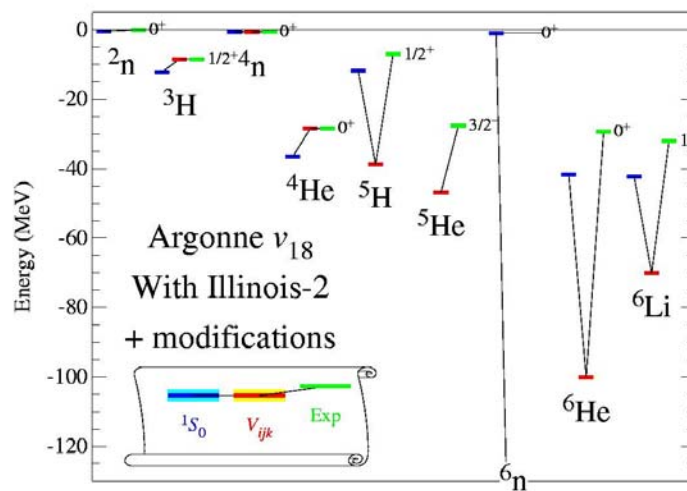
Fig. V-9. Comparison with experiment of energies of light nuclei using modified Hamiltonians. Left (blue) bars obtained by modifying the $^1S_0$ part of AV18, middle (red) bars obtained with an additional T = 3/2 NNN potential; both changes were chosen to give a ^{4}n with about -0.5 MeV energy.

b.5.   Pairing and Spin-orbit Splitting in Neutron Drops (S. C. Pieper and V. R. Pandharipande*)

Systems of neutrons interacting with realistic forces are unbound. However, bound systems may be made by adding an artificial external well to the Hamiltonian. These may then be used to study spin-orbit splitting and pairing energies in neutron-rich systems and to possibly provide "experimental" energies to help constrain Skyrme models for large neutron-rich nuclei. A number of years ago we published results for 7 and 8 neutrons interacting via AV18 + Urbana IX in an external well and the corresponding 6-neutron system was also published.

We are now studying from 1 to 10 neutrons, all in the same well, interacting with several Hamiltonians. Some preliminary results are shown in Fig. V-10. The well is the same one that was used before and is strong enough to bind one or two neutrons (*s*-shell) but not to bind a *p*-wave neutron. Thus the binding of 3-8 neutrons arises only from the combined effects of the nuclear Hamiltonian and the external well. The 9-neutron system is not bound (the ^{9}n($\frac{1}{2}^+$) energy is slightly above the ^{8}n energy); calculations have not yet

been made for ^{10}n. One can see that the spin-orbit splitting gradually increases as the p-shell is filled (from 3 to 7 neutrons) and then becomes dramatically

smaller for the d-shell in 9 neutrons. The staggering of the ^{2,3,4}n, ^{4,5,6}n, and ^{6,7,8}n energies shows the pairing energies. This work is continuing.

_____
*University of Illinois, Urbana-Champaign.
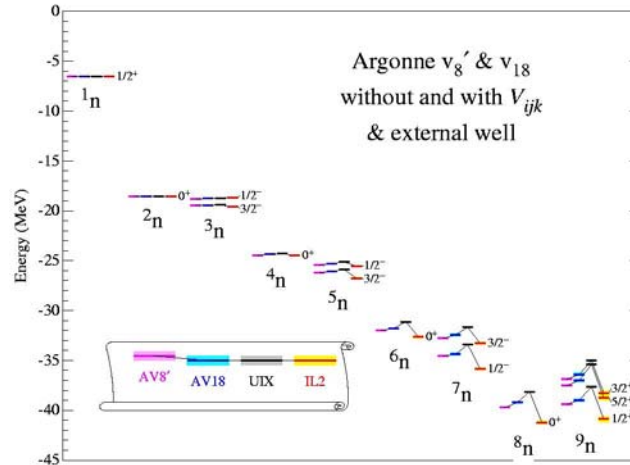
Fig. V-10. Energies of neutron systems interacting with the indicated Hamiltonians and an artificial external Woods Saxon well (V=20 MeV, R=3.0 fm, a=0.65 fm).

b.6.   Quadratic Momentum Dependence in the Nucleon-Nucleon Interaction
(R. B. Wiringa, A. Arriaga,* and V. R. Pandharipande†)

Modern nucleon-nucleon (NN) interactions all start with eight basic operators, including central, spin-spin, tensor, and spin-orbit terms, and each of these times isospin-isospin. With these operators it is possible to fit S- and P-wave phase shift data and deuteron properties reasonably well, as evidenced by the AV8' potential model. However, to fit higher partial waves, $e.g.$, the difference between $^1S_0$ and $^1D_2$ partial waves, it is necessary to add operators with a quadratic momentum dependence (QMD). An example is the use of four L^2 and two $(L \cdot S)^2$ operators in the AV18 potential.

There are other possible choices for the QMD terms, $e.g.$, p^2 instead of L^2 operators, and different kinds of quadratic spin-orbit terms. One advantage of the AV18 operators is that the potential is local, since L^2 commutes with functions of radial coordinates. However, potentials based on field-theoretic models of meson-exchange are more likely to have p^2 terms, as in the Bonn, Nijmegen, and Paris potentials. The p^2 operator does not commute with functions of r and consequently such models are nonlocal, and somewhat

harder to evaluate in our quantum Monte Carlo many-body calculations. Nevertheless, there is evidence that such nonlocal potentials can provide somewhat more attraction in light nuclei, such as ^{3}H and ^{4}He.

We are studying the effect of such nonlocality in the NN potential model by making a phase-equivalent variant of AV18 where L^2 operators were converted to p^2 operators. The magnitude of these terms is constrained by the need to fit higher partial waves. Initial VMC results suggest that the nonlocal variant, which we call AV18pq, is indeed slightly more attractive in the light nuclei: 140 keV in ^{3}H and 420 keV in ^{4}He. However, these nuclei are still underbound compared to experiment, calling for the addition of a three-nucleon (NNN) potential. When the Urbana IX (UIX) NNN potential is added, the extra attraction of the nonlocal potential is greatly reduced; in fact the AV18/UIX and AV18pq/UIX Hamiltonians give identical binding energies for ^{4}He. Thus it appears that this kind of nonlocality has little practical effect on ground state energies.

_____
*University of Lisbon, Portugal, †University of Illinois at Urbana-Champaign.

b.7.   The Three-Body Interaction in Mean-Field Calculations (T. Duguet, R. B. Wiringa, and S. C. Pieper)

Three-body forces were proven crucial to obtain good saturation properties in nuclear matter, to describe spectroscopic properties of light nuclei in *ab-initio* calculations, and to the treatment of nucleon-induced deuteron break-up or nucleon-deuteron elastic scattering. However, self-consistent mean-field calculations of (heavier) finite nuclei include the effect of three-body forces only in a very schematic way. As a result, we would like to propose a three-body interaction based on realistic three-body forces derived from meson-exchange field theory to be used in self-consistent mean-field methods. The challenge is to obtain a form which is simple enough to be tractable but which does not give up the essential physics contained in each channel of the interaction. For instance, one has to reconcile the crucial binding effect of the three-body force in light nuclei with its saturation character at the normal density of nuclear matter. Our experience from the calculations of light nuclei with realistic forces will be of great help for this purpose.

b.8.   Coupled-Cluster Expansion Approach to Nuclear Structure (B. Mihaila and J. Heisenberg*)

We continued our project on developing a realistic description of the ground-state of closed-shell nuclei in the p-shell (^{12}C and ^{16}O). These calculations use the coupled-cluster expansion (CCE), together with a realistic nuclear interaction and currents. Just as the GFMC method, the CCE approach is an exact approach to solving the nuclear many-body problem. The present calculations are done in configuration space, and suffer from limitations due to the intrinsic cutoffs one has to impose when defining the model space. The single-particle states are expanded out in an harmonic oscillator basis, and satisfy the same type of boundary conditions for both the hole and particle states. In effect we discretize the continuum part of the one-body mean-field Hamiltonian used to define the single-particle spectrum. This results in the necessity of a large configuration space and subsequent significant storage problems and lengthy execution time.

A new approach to solving the CCE equations is underway with a study of the nuclear matter problem. In the nuclear matter case we are dealing with the diametrically opposite case of a purely continuum system. In this work we are also pursuing a different approach to solving the CCE equations, in which one avoids the direct calculation of the two-, three- (*etc*.) particle-hole excitations altogether, and rather concentrates on calculating expectation values in a formalism reminiscent of GFMC for finite nuclei. The new approach is well-suited for implementation on massively parallel multiprocessor machines. We believe that the experience acquired in this process will provide significant insight into new ways of approaching the CCE equations for finite systems.

_____

*University of New Hampshire.

C. NUCLEAR STRUCTURE AND HEAVY-ION REACTIONS

This research focuses on nuclear structure in unusual regimes: nuclei far from stability, and superdeformed nuclei at high spin. We also study heavy-ion reactions near the Coulomb barrier. Much of this work is closely tied to experiments performed at ATLAS and at radioactive beam facilities.

Our studies of drip-line nuclei focus on breakup reactions, induced by the Coulomb and nuclear fields from a target nucleus. A critical issue is to develop a realistic description of the breakup mechanisms as a necessary tool for extracting nuclear structure properties of drip-line nuclei. We applied our numerical technique of calculating the time-evolution of the two-body wave function for the relative motion of a halo nucleon and a core nucleus, in the time-dependent fields from a target nucleus. Our results are used to test the validity of simpler reaction models and to analyze related experiments.

Our numerical studies of the Coulomb dissociation of proton halo nuclei on high-Z targets show that the conventional first-order perturbation theory for distant collisions is a poor approximation at low energy. The leading order correction is a dynamic polarization effect, which reduces the dissociation probability. A further complication for loosely bound nuclei such as ^{8}B is the influence of close collisions, where projectile and target have a non-zero overlap during the collision. Our calculations are consistent with low energy measurements of the one-proton removal from ^{8}B and ^{17}F.

We applied our coupled-channels technique to study heavy-ion fusion reactions. The primary goal is to develop a good understanding of the energy dependence of the fusion cross section, in particular at extreme sub-barrier energies, where measurements are difficult so one has to rely on extrapolations.

Some nuclear structure problems, with which we are involved, are superdeformation, heavy and superheavy elements, proton radioactivity, the neutron deficient Pb region and neutron-proton pairing near the N = Z line. To study these problems we make use of (1) the Strutinsky method as well as (2) self-consistent mean field (SCMF) calculations using the Gogny interaction, and (3) many-body (MB) wave functions.

In nuclides with roughly equal number of protons and neutrons, T = 1 and T = 0 n-p pairing will play an important role, in addition to the usual like-nucleon T=1 pairing. To adequately treat and understand these effects, it is necessary to go beyond the quasiparticle approximation and to study not only those nuclei that are exactly on the N = Z line. The rare isotope accelerator (RIA) will provide considerable spectroscopic information on nuclides near the N = Z line. We extended our many-body code to include neutron-proton pairing interactions. We found that there is a new quantum number for characterizing collective states; *i.e.*, the number parity of the T = 0 and T = 1 n-p pairs. In addition to the collective states, there are states in which some levels are 'blocked', *i.e.* have an odd number of nucleons in the level. All states in odd mass nuclei fall into this category. Also, the ground states of odd-odd nuclei are more likely to be of this type as the neutron excess increases. We extended our method to include states of this type and studied the structure of low-lying states in odd-odd nuclei. Our studies of superdeformation

at both low and high spins address the issue of possible new regions of superdeformation and hyperdeformation. Special emphasis is placed on the study of fission barriers at high spin as this is crucial for the possible production of very extended nuclei.

c.1.   Dynamic Polarization in the Coulomb Dissociation of ^{8}B (H. Esbensen and G. F. Bertsch*)

We calculated the dissociation of ^{8}B to all orders in the Coulomb field from high-Z targets.[1] The motivation is to test the validity of first-order perturbation theory, and to determine the magnitude of the dynamic polarization effect, which we observed in previous calculations of the Coulomb dissociation of ^{17}F at low beam energies.[2] The ground state of ^{8}B is modeled as a two-body system, consisting of a proton and a ^{7}Be core and bound as a p-wave in a Wood-Saxon well. The relative motion of projectile and target is described by a classical Coulomb trajectory. The time evolution of the ^{8}B two-body system in the Coulomb field from a target nucleus is obtained by solving the time-dependent Schrödinger equation numerically.

The leading order correction to first-order perturbation theory is of order Z^3 in the target charge Z. It is caused by a dynamic polarization where the wave function of the proton-core system has time to adjust itself during the collision with the target. Corrections that are odd in Z can be isolated from the numerical calculations simply by repeating them with a negative target charge. Denoting the two Coulomb dissociation probabilities by $P^{(+)}$ and $P^{(-)}$, for a positive and negative target charge, respectively, one can then define the charge asymmetry ratio

$$B = \left[P^{(+)} - P^{(-)} \right] / \left[P^{(+)} + P^{(-)} \right].$$

One can parameterize the charge asymmetry ratio to leading order in Z as

$$B = \frac{CZe^2}{E_{beam}\sqrt{b^2 + a^2}} \left(\frac{40}{E_{beam}} \right)^\nu,$$

as function of beam energy (per nucleon) and impact barameter b. The coefficients we obtain for ^{8}B are $C = -1.25$, $a = 37$ fm, and v = 0.07. The dynamic polarization can cause a substantial reduction in the dissociation probability. The reduction is up to 30% in the example illustrated below.

The conventional first-order Coulomb dissociation is based on Coulomb form factors that are strictly correct only for distant collisions, i.e., when projectile and target do not overlap during the collision. This is a very good approximation for stable nuclei but it becomes questionable for weakly bound halo states that have a large spatial extent. We find that the reduction due to close collisions sets in at impact parameters less than 25 fm in the case of ^{8}B on a nickel target. Moreover, this reduction is weakly-dependent of beam energy.

The combined effect of close collisions and dynamic polarization explains quite well lthe (^{8}B, ^{7}Be) breakup cross section that was measured at 3.2 MeV/u on a nickel target. The comparison with the data is shown in Fig. V-11. The top curve (a) is the result of the conventional first-order Coulomb dissociation for distant collisions. The dashed curve (b) is the first-order result one obtains by treating close collisions correctly. The dotted curve (c) is the full dynamical calculation of the Coulomb dissociation. The reduction of this curve compared to curve (b) is mainly due to the dynamic polarization. Finally, curve (d) is the total (^{8}B, ^{7}Be) cross section, obtained by also including the nuclear proton-target interaction in the calculation. The effect of a Coulomb-nuclear interference in the diffraction dissociation is surprisingly weak. The main reason that curve (d) is above curve (c) at large angles is the contribution from stripping. This work was published.[1]

_____
*Institute for Nuclear Theory, University of Washington.
[1]H. Esbensen and G. F. Bertsch, Phys. Rev. C **66**, 044609 (2002).
[2]H. Esbensen and G. F. Bertsch, Nucl. Phys. **A706**, 383 (2002).
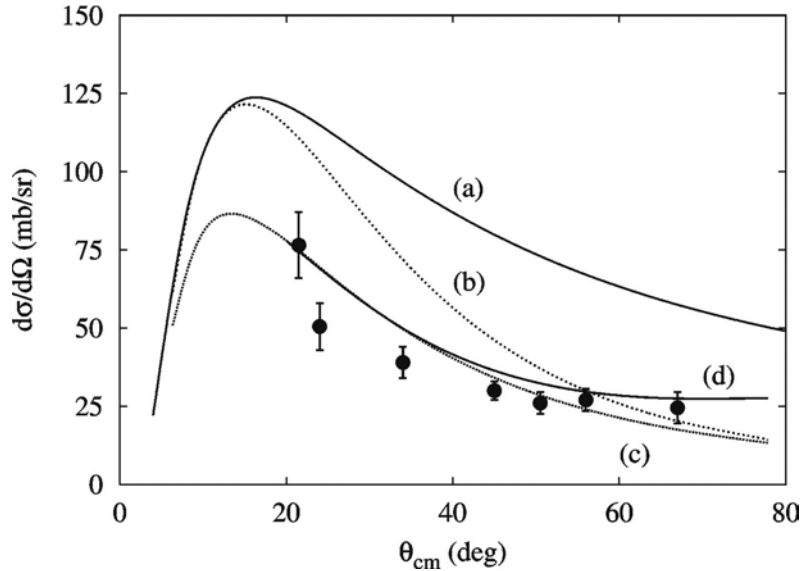
*Fig. V-11. (^{8}B,^{7}Be) breakup at 26 MeV on a Ni target. The data are from V. Guimaraes et al., Phys. Rev. Lett. **84**, 1862 (2000).*

c.2.   Interplay of E1 and E2 Transitions in Multi-phonon Coulomb Excitation
(H. Esbensen and A. Volya)

The dynamic polarization effect, which we observed in numerical studies of the Coulomb dissociation of ^{17}F and ^{8}B, is of general interest because it occurs in other fields of physics. In atomic physics, for example, it leads to a difference in the stopping powers of protons and anti-protons. It is caused by the interplay of dipole (E1) and quadrupole (E2) transitions in higher-order processes.

The simplest system that can be used to illustrate the dynamic polarization is a three-dimensional harmonic oscillator that is perturbed by a time-dependent dipole and quadrupole Coulomb field from a heavy ion. In an effort to get more insight, we decided to study this system in more detail.[2] The excitation of harmonic oscillators by external, time-dependent fields that are linear and quadratic in the oscillator coordinates (or momenta) represents the most general quantum mechanical problem for which the dynamics is completely classical. In fact, by employing classical dynamics and Wigner transformations, which relate the classical phase space distribution and the quantum mechanical density matrix, it is possible to generate the excitation probabilities of interest, as discussed in Ref. 3.

We adopted a different approach in, Ref. 2, namely, to calculate the time evolution of the creation and annihilation operators in the Heisenberg representation. The transformation that relates these operators before and after the interaction is an example of a generalized Bogoliubov transformation. Thus we obtained an exact analytic expression for the total excitation probability in terms of a complex three-dimensional vector and a symmetric three-by-three matrix. These 9 complex amplitudes are determined by classical equations of motion. The vector is related to a displacement in the classical phase space; it is mainly generated by the E1 field but it also has contributions from the E2 field. In fact, it is the interplay between these two fields in the displacement vector that is responsible for the dynamical polarization. The three-by-three matrix, on the other hand, is generated entirely by the E2 field. In quantum optics, it is referred to as squeezing.[3]

The total excitation probability of an oscillator, perturbed by the Coulomb dipole and quadrupole fields from a heavy nucleus at a fixed impact parameter $b = 4$, is illustrated in Fig. V-12, as a function of velocity (in oscillator units).   The parameters were chosen to simulate the excitation of ^{17}F on a nickel target. The solid curve in the middle is the result in first-order perturbation theory. The top and bottom curves are the exact results to all orders in the dipole and quadrupole fields, for an attractive and a repulsive interaction, respectively.   The reduction/enhancement of the

probability for repulsive/attractive interactions compared to the first-order result is consistent with the findings for the Coulomb dissociation of [17]F in Ref. 1.

The simplicity of the analytic expression we have obtained for the total excitation probability allows us to discuss a quantum perturbation expansion in terms of iterative solutions for the 9 classical, complex amplitudes mentioned above. Thus we could easily extract the dynamic polarization effect as an

interference between the dominant first-order dipole and a second order dipole-quadrupole amplitude. We have also discussed the influence of quadrupole transitions on the two-phonon dipole excitation. Most importantly, and in contrast to previous discussions of the dynamic polarization effect, our formulation provides the exact answer to all orders in the dipole and quadrupole fields. This work was published.[2] A further discussion of related phenomena in other branches of physics was accepted for publication.[3]

---

[1]H. Esbensen and G. F. Bertsch, Nucl. Phys. **A706**, 383 (2002).
[2]Alexander Volya and H. Esbensen, Phys. Rev. C **66**, 044604 (2002).
[3]Alexander Volya and H. Esbensen, J. Opt. B (in press 2003).
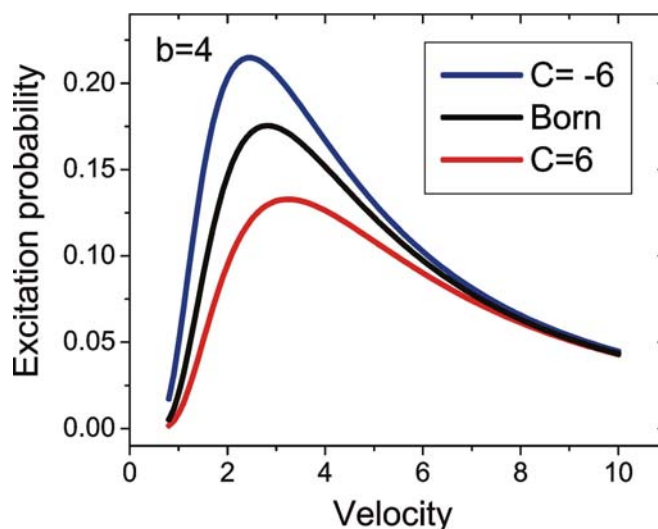
Fig. V-12. Total Coulomb excitation probability for repulsive (lowest curve) and attractive (highest curve) Coulomb interaction with a Ni target. The middle curve is the first-order result.

c.3.   [17]F Breakup Reactions on Pb near the Coulomb Barrier (H. Esbensen, F. Liang,* and others*)

We applied our numerical methods[1] to calculating [17]F → [16]O + proton two-body breakup on a Pb target at low energies. This is done by solving the time-dependent Schrödinger equation for the [16]O+p two-body system in the Coulomb and nuclear fields from the target nucleus. The time-dependence of the fields is generated by assuming that the relative motion of projectile and target follows a classical Coulomb trajectory. The two-body Hamiltonian, which is based on a simple Woods-Saxon well, was adjusted to give the correct separation energy of [17]F and also a reasonable value of the S-factor for radiative proton capture on [16]O.

The results were compared to measurements at low energy on a Pb target. The first set of measurements

was performed at 170 MeV and included singles events of oxygen fragments, and also events of oxygen fragments in coincidence with a proton.[2] The coincidence yield was surprisingly small in comparison to Coulomb dissociation. However, the measurement was performed at a large scattering angle, where nuclear interactions and a strong absorption set in. Including the proton-target nuclear interaction and also the effect of absorption of the [16]O fragment on the target, we obtained reasonable agreement with the measured proton-oxygen coincidences.

The angular distribution of oxygen fragments has a strong peak at grazing angles. The yield is much higher than the calculated cross section for proton transfer to

bound states in Bi. The total breakup cross section that we obtain in our two-body model of ^{17}F is in much better agreement with the data. It is dominated by proton stripping, which in the calculation is generated as an absorption by the imaginary proton-target interaction. The diffraction dissociation, where both the proton and the ^{16}O core fragment appear in the continuum after the collision, is a much smaller component at grazing angles, but it becomes the dominant component at forward angles. This work was published.[3]

The measurement of the angular distribution of oxygen fragments was repeated at 98 and 120 MeV.[3]   One motivation for performing such measurements is to get

data that can put constraints on speculations about the influence of breakup reactions on the yield of fusion. Unfortunately, our two-body model cannot predict the fusion because the relative motion of projectile and target is treated classically, and it is an input to the calculation. The model can only predict the breakup yield. An example at 120 MeV is shown in Fig. V-13. The measured elastic scattering (top part) is used to calibrate the absorption of the oxygen fragment; this absorption determines the falloff at large angles. The observed peak of oxygen fragments (bottom part) is reproduced quite well by the calculation (the solid curve), which again is dominated by stripping (the dotted curve). This work was accepted for publication.[3]

_____
*Oak Ridge National Laboratory.
[1]H. Esbensen and G. F. Bertsch, Nucl. Phys. **A706**, 383 (2002).
[2]J. F. Liang *et al.*, Phys. Rev. C **65**, 051603 (2002).
[3]J. F. Liang *et al.*, Phys. Rev. C (in press 2003).
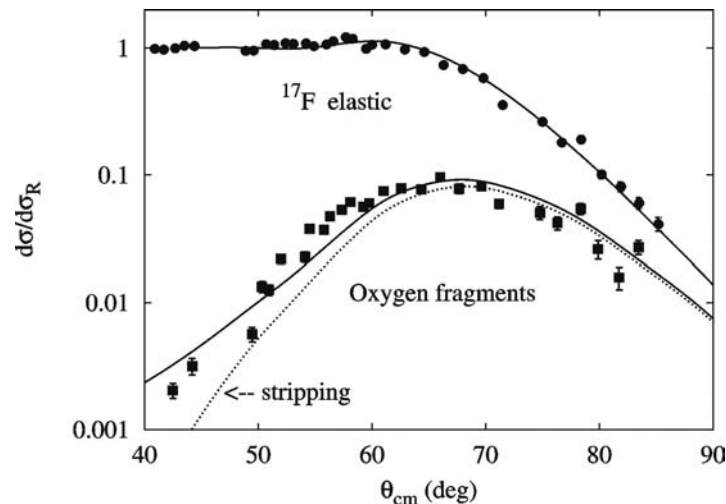
Fig. V-13. Elastic scattering and breakup of ^{17}F on a Pb target at 120 MeV.

c.4.   Energy Dependence of $^{27}Al + {}^{A}Ge$ Fusion at Sub-barrier Energies
   (H. Esbensen and C. L. Jiang)

Theoretical and experimental studies of heavy-ion fusion have, in the past, focused on the energy dependence of cross sections near and slightly below the Coulomb barrier. One way to amplify certain features of the data is to extract the so-called barrier distribution, which is defined as the second derivative of cross section times energy, $B = d^2/dE^2(E\sigma_f)$. The goal has been to explain this distribution in terms of the structure of the reacting nuclei.

Not much attention was devoted to the energy dependence of cross sections far below the Coulomb barrier. In fact, many models assume that $E\sigma_f$ has a simple exponential dependence, as given by the Hill-Wheeler formula. Recently we pointed out[1] that the fusion cross sections for several systems exhibit a much steeper falloff at energies far below the Coulomb barrier. This feature is emphasized in the so-called logarithmic slope, $L(E) = d/dE[log(E\sigma_f)]$. For several heavy-ion systems it appears that the value of $L(E)$

continues to grow steeply with decreasing energy, even far below the Coulomb barrier. Coupled-channels calculations, on the other hand, do not reproduce this behavior.

Here we chose to illustrate the low-energy behavior of $L(E)$ by analyzing the rather accurate fusion data for ^{27}Al + ^{76}Ge that were reported in Ref. 2. Values of $L(E)$ extracted from the measurement are shown in the Fig. V-14. The solid curve is the result of coupled-channels calculations that fit the measured fusion cross section quite accurately (with a $\chi^2 = 1.8$). The dotted curve in the middle shows the result of the one-dimensional barrier penetration, with a Coulomb barrier of 53.3 MeV. It increases steeply with decreasing energy in the vicinity of the Coulomb barrier but the rise levels off far below the barrier. The coupled-channels calculation has a similar behavior but is shifted a few MeV toward lower energies. In fact, the transition from the steep to the slower rise occurs at an energy where the barrier distribution $B(E)$ goes to zero.

The modest rise in the calculated values of $L(E)$ far below the lowest barrier is similar to what one obtains by assuming a constant S-factor. Thus with $E\sigma_f = S$

exp(-2$\pi\eta$), where S is a constant S-factor and $\eta = Z_1Z_2e^2/(\hbar v)$ is the Sommerfeld parameter, one obtains $L(E) = \pi\eta/E$. This quantity is shown by the top dotted curve in Fig. V-14. It represents, in some sense, an extreme value of $L(E)$ because a constant S-factor implies an s-wave penetration of the Coulomb potential all the way to $r = 0$. It is therefore surprising that values of $L(E)$ extracted from some measurements can exceed the curve for constant S-factor.

The agreement between the coupled-channels calculation and measurements is very good in the case considered here. However, one cannot exclude the possibility that $L(E)$ would steadily increase if measurements were performed at even lower energies, just as has been observed for other systems.[1] The general trend of the coupled channels calculations we have performed, on the other hand, is similar to that shown in the figure, namely, that the steepness of $L(E)$ levels off below the lowest barrier. The analysis of fusion for other ^{27}Al + ^{4}Ge systems is in progress.

_____

[1]C. L. Jiang *et al*., Phys. Rev. Lett. **89**, 052701 (2002).
[2]E. F. Aguilera *et al*., Phys. Rev. C **41**, 910 (1990).
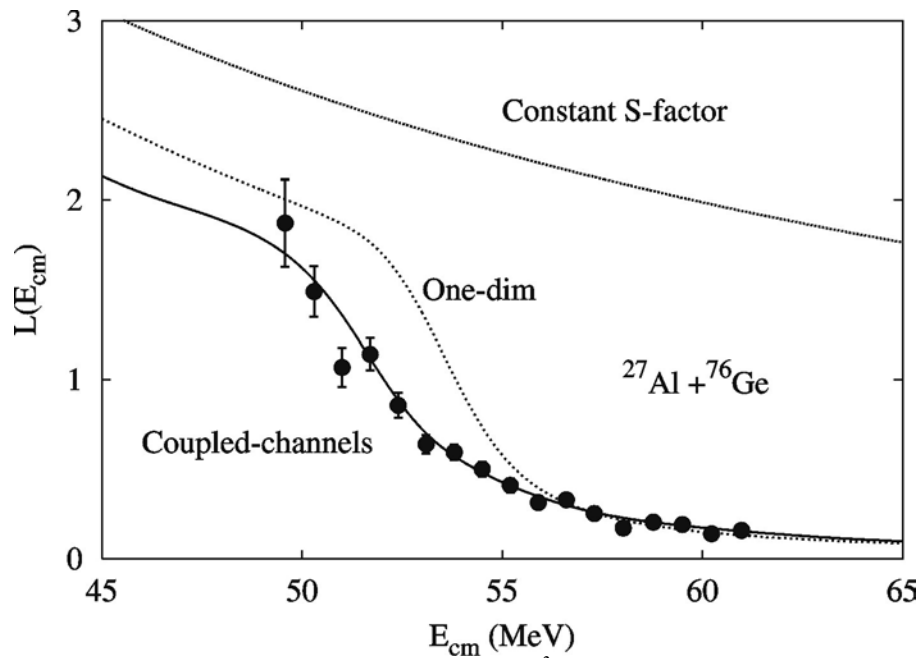
Fig. V-14. Logarithmic slope of measured fusion cross sections[2] are compared to coupled-channels calculations, one-dimensional barrier penetration, and to values for a constant S-factor.

c.5.   Mean Field and Many Body Wave Functions (R. R. Chasman)

We are continuing the development of a program for calculating many-body variational wave functions that puts pairing and particle-hole two-body interactions on an equal footing. The complexity of the wave functions depends only on the number of levels included in the valence space. In these wave functions, we conserve particle number and parity strictly; projecting states of good particle number and parity before carrying out the variational calculations. We also extended the program to calculate the spectroscopic factors involved in proton decay. This is useful for studies of nuclides near the proton drip line.

By using residual interaction strengths (*e.g.*, the quadrupole interaction strength or pairing interaction strength) as generator coordinates, one gets many different wave functions; each having a different expectation value for the relevant interaction mode. Such wave functions are particularly useful when one is dealing with a situation in which a configuration interaction treatment is needed. Because the same basis states are used in the construction of all the many-body wave functions, it is possible to easily calculate overlaps and interaction matrix elements for the many-body wave functions obtained from different values of the generator coordinates (which are not in general orthogonal).   The valence space can contain a very large number of single-particle basis states, when there are constants of motion that can be used to break the levels up into sub-groups. To increase this size, we have parallelized our code to run on the SP computer system, and we are modifying the code to deal with octupole correlations in heavy nuclei.

Recently, our major effort was to extend our many-body code to include neutron-proton pairing interactions, in both the $T = 0$ and $T = 1$ modes. This involved putting neutrons and protons in the same subgroup. In dealing with blocked levels, in the case of a simultaneous treatment of $T = 1$ and $T = 0$ interactions, the variational amplitudes are complex. We extended the code to deal with these complex amplitudes.

c.6.   Neutron-Proton Pairing (R. R. Chasman)

We extended[1] our many-body method to include n-p pairing, with full projection of neutron and proton particle number before doing a variational calculation. We also found that there is a new quantum number that holds exactly for collective states; *i.e.* those states in which no levels are blocked.   This new quantum number (Q) is the number parity of the $T = 0$ and $T = 1$ n-p pairs. Fixing the number parity of one n-p mode fixes the other, when the number of neutrons and protons is fixed. This number parity is closely related to the isospin quantum number.   The collective states are the ground states for $N = Z$ nuclides. We project Q - before doing a variational calculation.   By doing calculations that conserve Q, we find a remarkable multiplicity of degenerate levels in odd-odd nuclides, with $N = Z$ (2m). Such multiplets are at or near ground for m = 1 or 2.   The form of our variational wave function includes an explicit amplitude for 'alpha like' correlations in each level as well as the usual amplitudes for n-n, p-p and n-p pairs.

In odd-odd $N = Z$ nuclei,[2] the ground state is a doublet, consisting of a $Q = 0$ and $Q = 1$ state, when the $T = 0$ and $T = 1$ pairing strengths are equal. The splitting of this ground state doublet affords some information about the relative strengths of the $T = 0$ and $T = 1$ pairing strengths. In Fig. V-15b we plotted the splitting of these two states as a function of the $T = 0$ pairing strength, while keeping the $T = 1$ pairing strength fixed. Results are displayed for two choices of energy level spacing, 1) equally spaced levels, and 2) a level system in which the five levels closest to the Fermi level are bunched together. Because the pairing correlations are stronger in the bunched level system, the splittings are larger.

[1]R. R. Chasman, Phys. Lett. B **524**, 81 (2002).
[2]R. R. Chasman, Phys. Lett. B **553**, 204 (2003).
[3]D. G. Jenkins *et al*., Phys. Rev. C **65**, 064307 (2002).

In addition to the collective states discussed above, there are configurations in which one or more levels are blocked. These configurations constitute the ground states of all odd-mass nuclides and are likely to be the ground state or close in energy to the ground state of odd-odd nuclei with increasing neutron excess. For these blocked levels, the amplitudes are complex. We extended our treatment of n-p pairing to include configurations with blocked levels. In Fig. V-15a, we display the level spectra in the two model odd-odd systems used in the splitting calculation discussed above. The notable feature here is the remarkable increase in level density near the ground state with increasing neutron number. This feature was noted[3] in an analysis of levels of odd-odd nuclei.
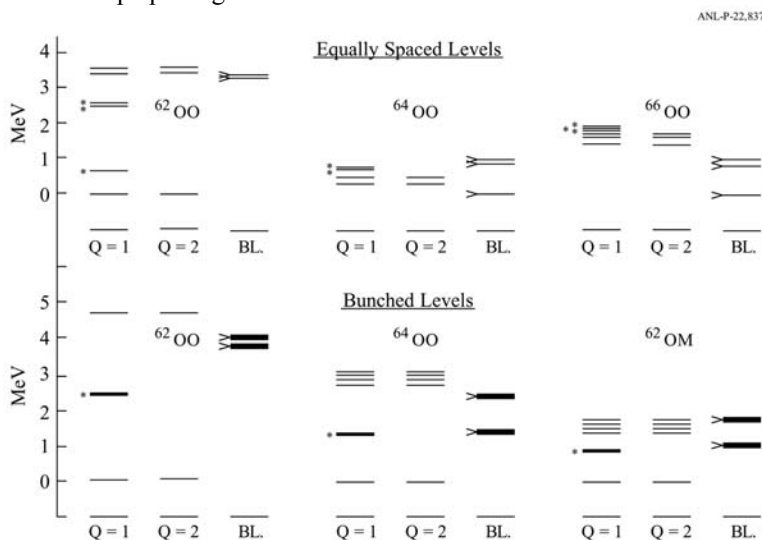
Fig. V-15a. Low-lying states in odd-odd nuclei near N = Z. BL (blocked) indicates configurations in which two levels have odd number parity and for which Q is no longer a good quantum number. The thick lines in the BL column in the bunched level scheme indicate a degeneracy of ten. The arrowhead on the left of all blocked levels indicates an additional factor of two in the number of levels coming from the two values of Ω with $\Omega = \Omega_1 \pm \Omega_2$. The Ω-blocked levels in the Q = 1 column are marked with an asterisk. The thick lines with asterisks in the bunched levels for Q = 1 have a degeneracy of five.
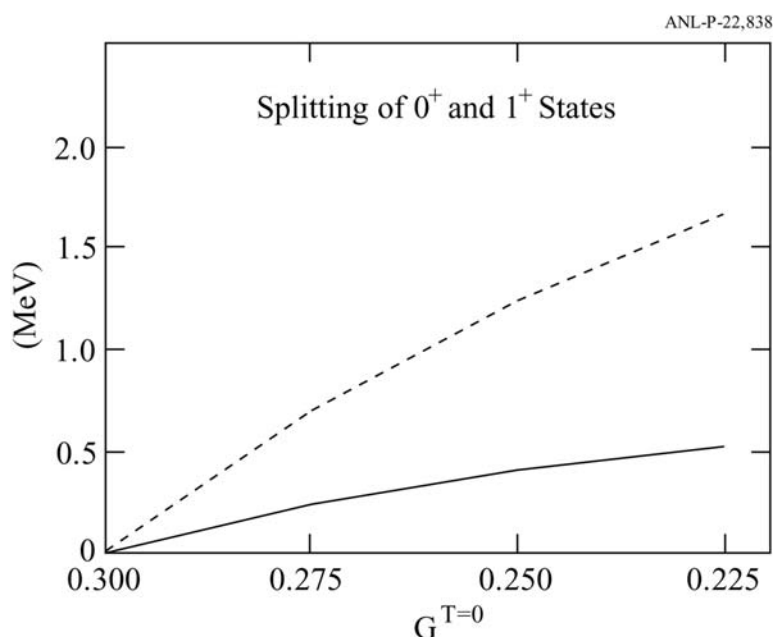
Fig. V-15b. Excitation energy of Q = 2 state in ^{62}OO as a function of $G^{T=0}$. $G^{T=1}$ has the value of 0.3 MeV. The dashed line gives the splitting for the bunched levels and the solid line is used for the equally spaced levels.

c.7. Octupole Correlations in Light Actinides (R. R. Chasman)

The difficulty in dealing with octupole correlations in the light actinides is that the effects are not sufficiently large to give rise to a well defined deformation. A many-body wave function is needed to deal effectively with these correlations. We started to apply our many-body approach to a re-examination of this region. In our early work, which was the first to predict parity doublets in the odd-mass nuclides of this region, we were limited to subgroups of at most five Nilsson orbitals. Advances in our code, and the use of parallel processing, make it feasible to deal with subgroups consisting of as many as eight Nilsson orbitals. One application of this calculation will be a study of the structure of the $\frac{1}{2}^{\pm}$ parity doublet in ^{225}Ra, that is being studied to put new upper limits on the dipole moment of the neutron.

c.8. Studies of Nuclear Energy Surfaces (R. R. Chasman, J. L. Egido,* and L. M. Robledo*)

This collaborative research program[1,2,3] focuses on the study of nuclear energy surfaces, with an emphasis on very deformed shapes using several complementary methods: 1) the Strutinsky method, 2) Hartree-Fock-Bogoliubov (HFB) calculations using the Gogny interaction, and 3) Many-Body (MB) variational wave functions that we described above. Our strategy is to identify phenomena and nuclides of interest using the Strutinsky method and to study the most interesting cases with the HFB and many-body (MB) approaches. The two latter approaches include many-body effects and describe these features more accurately.

The great advantage of the Strutinsky method is that one can study the energy surfaces of many nuclides ($\sim$300) with a single set of calculations. Although the HFB and MB calculations are quite time consuming relative to the Strutinsky calculations, they have many advantages. For the studies of Pb, they have the advantage that configuration interaction effects can easily be incorporated in the calculations. In this way, we deal directly with the issue of ensuring the orthogonality of states that have the same spins and parities. We recently examined the effects of angular momentum projection on the low-lying spectra of the even Pb isotopes in the HFB calculations. We find that angular momentum projection does not substantially bring down the energy of the oblate 0^+ state.

---

*Universidad Autonoma de Madrid.
[1]R. R. Chasman and L. M. Robledo, Phys. Lett. **B351**, 18 (1995).
[2]J. L. Egido, L. M. Robledo, and R. R. Chasman, Phys. Lett. **B393**, 13 (1997).
[3]R. R. Chasman, J. L. Egido, and L. M. Robledo, Phys. Lett. **B513**, 513 (2001).

c.9. Order Generated by Random Many-Body Dynamics (A. Volya and V. Zelevinsky)

We demonstrate a coexistence of quantum chaos and order in strongly interacting mesoscopic systems. In this study[1,2] we consider a simple shell-model system of one single-particle *j*-level that can host 2j + 1 identical fermions. The system is driven by random two-body interactions that preserve rotational symmetry. It was shown previously that the ground state spin has an unexpectedly large probability to be $J_0 = 0$.[3] The statistical model[4] predicts the probabilities of $J_0 = 0$ and $J = J_{max}$ (maximum spin possible) to be significantly enhanced. For the maximum spin this probability, however, is suppressed by the fact that the corresponding state is unique and does not obey statistical regularities. Now we consider excited states of random realizations with $J_0 = 0$ that dominate the statistics. We first chose those 5 to 15% of realizations where the ground state has $J_0 = 0$ while the first excited state has $J_1 = 2$. For these realizations we compare the values of the quadrupole moment of the $J_1 = 2$ state and the quadrupole transition strength, B(E2), from this state to the ground state. The resulting normalized histogram for the ratio $Q^2/B(E2)$ is shown in Fig. V-16. The dashed line indicates the value of this ratio for the rigid rotor. It is clear from the figure that selected systems, governed by interactions of random nature, exhibit collective properties of regular deformation.

This work shows collective features emerging in a finite many-body system with random dynamics. To trace the origin of this collectivity, one has to go beyond the

standard statistical descriptions and include non-linear correlations that shape the many-body mean field. The observed empirical results that come along with random interactions but exhibit generic collective features

suggest that the robust realistic properties are not necessarily a result of a unique nature-chosen interaction, but rather a manifestation of kinematic rules and symmetries of a quantum mesoscopic system.

_____

*Michigan State University.

[1] A. Volya and V. Zelevinsky, Proc. of the Wigner Centennial Conf., Pécs, Hungary (2002), pp. 10.

[2] V. Zelevinsky and A. Volya, Proc. of the 7th International Spring Seminar on Nuclear Physics, ed. A. Covello (World Scientific, Singapore, 2002) p. 261.

[3] C. W. Johnson, G. F. Bertsch, and D. J. Dean, Phys. Rev. Lett. **80**, 2749 (1998).

[4] D. Mulhall, A. Volya and V. Zelevinsky, Phys. Rev. Lett. **85**, 4016 (2000).
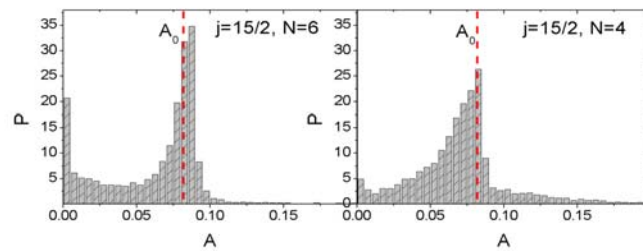
Fig. V-16. The normalized histograms display the distribution of the ratio $A = Q^2/B(E2)$ for all random realizations with $J_0 = 0$ and $J_1 = 2$, for the systems of $N = 4$ and $N = 6$ particles on a $j = 15/2$ orbital. The vertical dashed lines show the Alaga prediction for a rigid rotor.

c.10.   Non-Hermitian Effective Hamiltonian and Continuum Shell Model
(A. Volya and V. Zelevinsky*)

The intrinsic dynamics of a system with open decay channels is described by a non-Hermitian and energy-dependent effective Hamiltonian. We discuss ways of incorporating this approach into the shell model context. Although the main ideas of the approach are well known, right now, with the main interests of nuclear studies shifted away from the line of stability, it seems to be an appropriate moment to revive them and convert into a working tool for the solution of numerous practical problems of nuclear theory. The applications of the approach are not limited to nuclear physics; they were found useful in optics, see Ref. 1 and references therein, in atomic physics, condensed matter, physics of microwave cavities, theory of measurement and quantum computing.

We view the effective Hamiltonian as a sum of three terms,

$$\mathcal{H} = H^\circ + V - \frac{i}{2} W(E), \qquad (1)$$

where the intrinsic Hermitian part $H^\circ + V$ consists of independent particle energies, and the effective Hermitian interaction V is assumed to include renormalization terms generated by the virtual coupling through continuum.   The imaginary part $W(E)$ originates from the real processes of decay to channels that are open at a given energy. It is represented by the residues of the on-shell terms corresponding to the delta-functions coming from the energy conservation and causality requirements imposed on the energy denominators.

At this stage,[2] a phenomenological form of the effective Hamiltonian borrowed from a traditional shell model is extended with new energy-dependent non-Hermitian terms that are parameterized in a way properly representing the kinematics of reaction processes near thresholds. The main goal here is to develop and discuss methods for solving the many-body problem with the use of the effective Hamiltonian (1). Besides the fact that internal dynamics are represented by a non-

Hermitian Hamiltonian responsible for decays, the calculations require a correct account of threshold singularities in the amplitudes of the processes at low energies. We also emphasize the need for self-consistency of two types, (i) regular solution for the complex energies of quasistationary states governed by the energy-dependent Hamiltonian and (ii) the consistent determination of bound state energies, open channels and reaction thresholds for a chain of nuclides connected by those channels. The latter implies that the new continuum shell model, in contrast to its traditional analog, treats the whole range of nuclei, linked by reactions, in a single picture with a common effective interaction. Such a continuum treatment almost certainly requires new computational efforts and the method we employed, an hybrid of the exact solution for the pairing interaction with the interaction through the continuum seems to be a promising instrument for future development.

Table V-I. Seniority $s = 0$ and $s = 1$ states in oxygen isotopes. Energies and neutron decay widths are shown. Results are compared to the full shell model calculations and to known experimental data. Ground state energies relative to the ^{16}O core are given in bold. The rest of the energies are excitation energies in a given nucleus.

A	J	E	Γ	$E_{s.m.}$	$E_{exp.}$	$\Gamma_{exp.}$
		(MeV)	(keV)	(MeV)	(MeV)	(keV)
16	0	**0.00**	0	**0.00**	**0.00**	0
17	5/2	**-3.95**	0	**-3.95**	**-4.14**	0
17	1/2	0.78	0	0.78	0.87	0
17	3/2	5.59	96	5.59	5.08	96
18	0	**-12.17**	0	**-12.17**	**-12.19**	0
19	5/2	**-15.75**	0	**-16.06**	**-16.14**	0
19	1/2	1.33	0	1.47	1.47	0
19	3/2	5.22	101	5.53	6.12	0
20	0	**-23.41**	0	**-23.83**	**-23.75**	0
21	5/2	**-26.67**	0	**-27.47**	**-27.55**	0
21	1/2	1.38	0	1.33		
21	3/2	4.60	63	4.83		
22	3/2	**-33.94**	0	**-34.62**	**-34.40**	0
23	1/2	**-35.78**	0	**-37.07**	**-37.15**	0
23	5/2	2.12	0	2.72		
23	3/2	2.57	13	3.28		
24	0	**-40.54**	0	**-41.05**	**-40.85**	0
25	3/2	**-39.82**	14	**-40.28**		
25	1/2	2.37	0	2.36		
25	5/2	4.98	0	3.96		
26	0	**-42.04**	0	**-42.04**		
27	3/2	**-40.29**	339	**-40.29**		
27	1/2	3.42	59	3.42		
27	5/2	6.45	223	6.45		
28	0	**-41.26**	121	**-41.26**		

As one demonstration of the techniques developed, we present a realistic self-consistent shell model calculation for oxygen isotopes in the mass region A = 16 to 28, TableV-I. In this study we use a universal *sd*-shell model description with the semi-empirical effective interaction, restricted to pairing and monopole components. Despite these simplifications, the overall agreement with the observed data is good. In our view, however, the main merit of this calculation is in demonstrating the power of the method.

_____

*Michigan State University.
[1]A. Volya and V. Zelevinsky, Tech. Rep., ANL (2002); LANL preprint quant-ph/0303010.
[2]A. Volya and V. Zelevinsky, ANL preprint PHY-10327-TH-2002; LANL preprint nucl.th/0211039.

c.11. Two-Dimensional Calculations of Nuclei in a Chiral Model (S. Schramm)

From the point of view of nuclear structure there has been significant progress in describing finite nuclei using relativistic meson field models. Those calculations are quite successful in describing nuclear properties over a wide range of mass numbers.

It is possible to obtain sensible behavior of excited matter, a good description of nuclear saturation as well as of nuclei and hypernuclei with a single model and a single set of parameters. I based the investigation on a hadronic model with chirally symmetric interactions incorporating flavor-SU(3) symmetry to calculate nuclear properties within this approach. I determined a new improved set of model parameters generated by a fit to properties of a set of spherical nuclei. The results showed that the quality of the description of nuclear properties is about at the same level of accuracy and even slightly exceeds the one of the currently used most successful dedicated relativistic nuclear structure approaches. For the first time in this context the isospin-triplet meson was taken into account, which naturally occurs within the SU(3) scheme in its coupling to the baryons as well as in the nonlinear meson-meson interactions.

I investigated deformed nuclei in a 2-dimensional nuclear calculation and found good results for nuclear quadrupole deformations in comparison with available data. A study of possible superheavy elements did not show any distinct magic numbers for neutrons as well as for proton numbers that could be deduced from the gap energies as shown in Fig. V-17. Currently I am extending the investigation by considering a number of improvements. This includes a projection onto good particle numbers as well as, in case of the deformed calculations, a projection onto good angular momentum. Also first three-dimensional studies were performed and a calculation including configuration mixing is underway.

_____

[1]S. Schramm, Phys. Rev. C **66**, 064310 (2002).
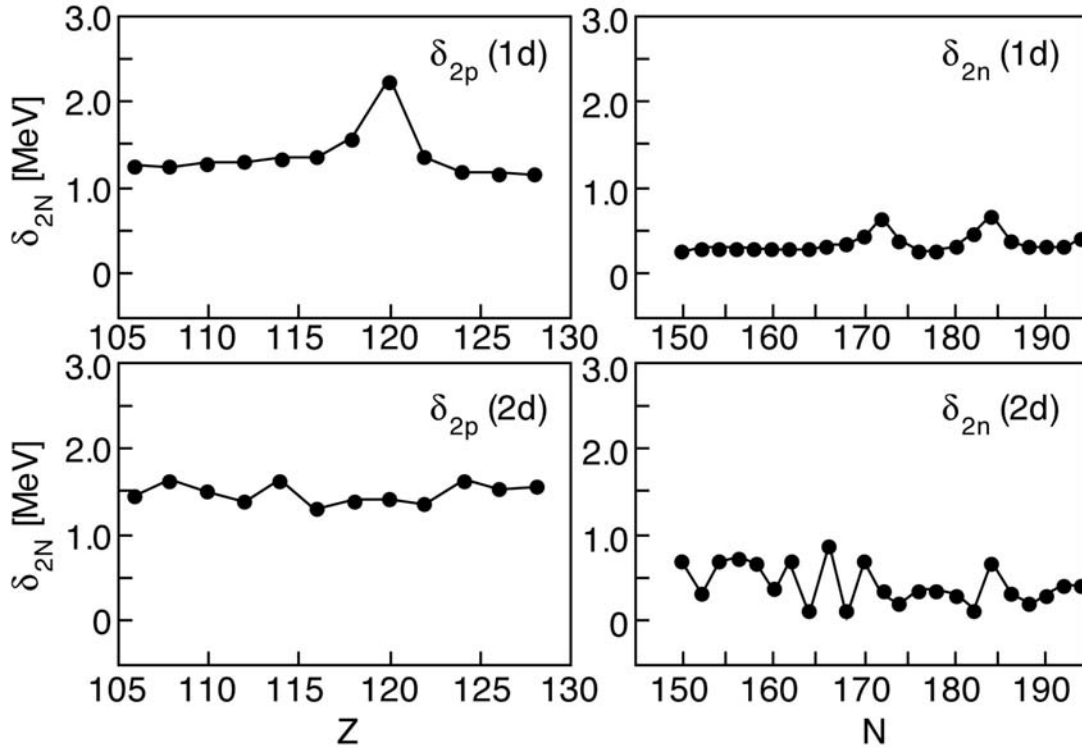
Fig. V-17. The figure shows the two-nucleon gaps δ_{2p} (left panels) and δ_{2n} (right panels) in units of MeV. Results for superheavy nuclei are shown. The upper panels show the results of a calculation assuming spherical symmetry. The lower panels display the results from a 2-dimensional calculation assuming axial symmetry.[1]

c.12.   **Rotating Neutron and Hyperstars** (S. Schramm and D. Zschiesche*)

Neutron star properties can give important clues for understanding the isospin dependence of nuclear forces. The most directly observable property of a neutron star is its rotational frequency, through its pulsar radio signals emitted from the magnetic poles of the star. It is crucial to relate star properties with other isospin-sensitive observables like neutron distribution radii in neutron-rich nuclei or multi-fragmentation in heavy-ion collisions with different N/Z nuclei.

This is the motivation for developing and applying a hadronic model with a broad applicability including the regime of infinite nuclear matter, finite nuclei and chiral symmetry restoration to relate predictions in the various areas. As at high densities it is favorable to populate hyperonic states in addition to nucleons inside of the star, the model is based on SU(3) in flavor space.

We extended our calculations of static neutron stars and hyperstars to study the properties of rotating neutron (hyper-) stars. To this end we extend the theoretical treatment of static systems based on the solution of the Tolman- Oppenheimer-Volkov equations for the star

structure by following the formalism developed by Hartle and Thorne to treat the general relativistic equations for the structure of rotating stars. In order to solve those equations we first determined the equation of state and its hyperonic matter contributions, and then integrated the differential equations for the metric tensor inside of the star, which determines its structure and shape.

As shown in Fig. V-18 the resulting star shapes show a significant eccentricity for rapidly rotating stars (comparable to that of superdeformed nuclei), which also effects a deformation of its hypermatter distribution in the interior of the star. The moment of inertia shows a strong dependence on the rotational frequency. This needs to be taken into account for determining the spinning-down behavior of the pulsar.

We did not find a back-bending of the inertia with decreasing rotational frequency as was suggested by other authors. For such a back-bending effect to occur, the interior of the star has to go through major structural changes during the spin-down as is the case for the

analogous phenomenon in rapidly rotating nuclei due to pairing breakup. In the present calculation the slow transition of the hadronic model towards chiral restoration at high densities and low temperatures prohibits any major observable effects. However, we found possible transitions of rapidly rotating pure neutron stars that convert to hyperstars during the slowdown of the pulsar.

The calculations showed that, owing to rotation, the maximum star mass can be increased from 1.64 to 1.94 solar masses compared to the case of a static star.[1] This value still shows a clear reduction from projections of star calculations without hyperons which typically show mass limits beyond 2 solar masses. With more observational data being collected it would be interesting to see whether a relation between masses and pulsar frequencies can be established.

With regard to maximum star masses a discussion of the possible effects of populating higher baryonic resonances in the neutron star should be performed. Those additional degrees of freedom might change the high-density behavior of the system significantly, generating a different structure of the time-evolution of the rotating star. Such a calculation might set tight constraints on the theoretical descriptions of hadronic resonances and their couplings to other fields by studying their effect on neutron star properties, especially on the star's mass. We are currently investigating this point.

_____

*University of Frankfurt.
[1]S. Schramm and D. Zschiesche, J. Phys. G: Nucl. Part. Phys. **29**, 531 (2003).
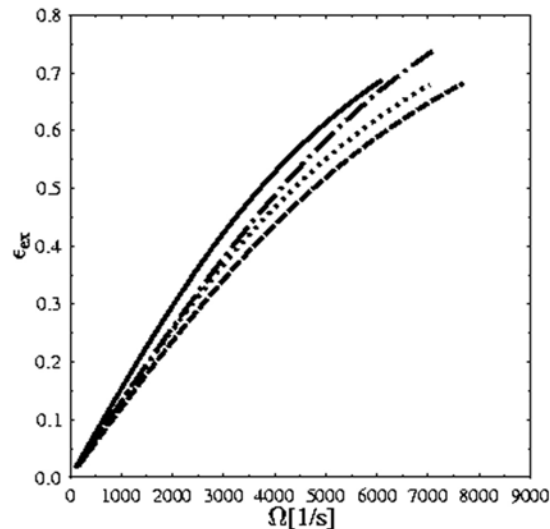
Fig. V-18. The figure shows the eccentricity of the deformed rotating neutron star as function of rotational frequency $\Omega = 2\pi\nu$ for different masses for the static neutron star.[1]

c.13. The Effective Interaction in Nuclei for Calculations Beyond the Mean-Field
(T. Duguet, M. Bender,* H. Heenen,* P. Bonche,† and J. Meyer‡)

We extended the standard Goldstone-Brueckner perturbation theory to motivate methods beyond the mean-field, such as the Generator Coordinate Method or the Projected Mean-field Method, from a perturbative point of view for the first time. We derived the effective interaction removing the hard-core of the bare nucleon-nucleon force accordingly. Simplifying this effective vertex, we proposed an extended version for the Skyrme interaction, which is valid for configuration mixing calculations.

We started to perform calculations beyond the mean-field level to validate this extended Skyrme model quantitatively. Here, it is interesting to concentrate on exotic properties of nuclei, where correlations associated with the restoration of symmetries broken at the mean-field level and large amplitude vibrations are crucial to reproduce the data. As a first topic, we are studying shape coexistence in neutron-deficient lead, mercury and polonium isotopes by configuration mixing of symmetry-restored HFB wave functions. The main issue is to understand the interplay of the

interaction properties to describe shape isomerism correctly in the whole mass region. In particular, we intend to illustrate the importance of the density dependence of the interaction. At the same time, we will learn about other properties of the interaction such as its surface tension, its pairing channel, and the single-particle spectra it generates. Indeed, the quantitative description of shape isomerism results from

the delicate combination of all these characteristics. To go one step further, we need to probe the effective interaction in different mass regions and for different nuclear properties. To do so, we started calculations beyond the mean-field to study shape isomerism in tin isotopes and shell quenching towards the drip-lines in lighter nuclei.

*Universite Libre de Bruxelles, Belgium, †CEA/Saclay, France, ‡IPNL/CNRS-IN2P3, France.

c.14. Probing the Gateway to Superheavy Nuclei in Cranked Relativistic Hartree-Bogoliubov Theory (A. V. Afanasjev, T. L. Khoo, I. Ahmad, S. Frauendorf,* and G. A. Lalazissis†)

The cranked relativistic Hartree-Bogoliubov theory (CRHB), including approximate particle number projection through the Lipkin-Nogami method and the Gogny force in the particle-particle pairing channel, was employed in a systematic study of the nuclei around ^{254}No. The deformation, rotational response, pair correlations, quasiparticle spectra, nucleon separation energies and shell structure of these nuclei were extensively studied with different RMF forces.

While the deformation properties are well reproduced, the calculations reveal that an accurate description of other observables requires better model forces both in the particle-hole and particle-particle channels. The calculated moments of inertia show only small sensitivity to the RMF force and thus to the details of the single-particle structure. In contrast to previous studies, where the moments of inertia in lighter systems are well reproduced, good agreement in the heaviest nuclei can only be obtained with a decrease ($\approx 12\%$) of the strength of the D1S Gogny force in the pairing channel.

The CRHB theory was extended for a detailed description of quasi-particle states in odd and odd-odd nuclei. For the first time, the blocking procedure in such nuclei was performed fully self-consistently, with effects of the breaking of time-reversal symmetry (nuclear magnetism) taken into account. Analysis of quasi-particle spectra in odd ^{249,251}Cf and ^{249}Bk nuclei with the NL1 and NL3 forces suggests that the energies

of most spherical orbitals, from which active deformed states of these nuclei emerge, are described with an accuracy of better than 0.5 MeV. However, for a few subshells the discrepancies reach 1.0 MeV. As the RMF forces were only fitted to bulk properties of spherical nuclei without considering single-particle energies, this level of agreement is impressive. However, in very heavy systems, where the level density is high, the accuracy is not sufficient for reliable predictions of the location of deformed shell gaps, which are small (≈ 1 MeV).

The results of our analysis have implications for the study of superheavy nuclei. The NL-SH and NL-RA1 forces do not provide satisfactory descriptions of the single-particle energies: the deviations between experiment and theory in the $A \sim 250$ mass region reach 2 MeV for some spherical subshells. Hence their application to superheavy nuclei is not recommended. The extrapolation of the results for quasiparticle states obtained in the $A \sim 250$ mass region suggests that the NL1, NL3 and NL-Z forces provide reasonable descriptions of most of the states in the vicinity of the $Z = 120$ and $N = 172$ spherical shell gaps. However, it is not possible to estimate the accuracy of the description of some low-j states, such as $\nu 3d_{3/2}$, $\nu 4s_{3/2}$ and $\pi 3p_{3/2}$, $\pi 3p_{1/2}$, which are located near these gaps. Thus the particle numbers corresponding to magic gaps in superheavy nuclei remains an open question. An article describing this research was published.[1]

*University of Notre Dame, †Aristotle University, Thessaloniki, Greece.
[1]A.V. Afanasjev et al., Phys. Rev. C 67, 024309 (2003)

D. ATOMIC THEORY AND FUNDAMENTAL QUANTUM MECHANICS

In addition to research on hadronic and nuclear physics, we also conduct research in atomic physics, neutron physics, and quantum computing.

Work in atomic physics includes the studies of interactions of electrons or high-energy photons with matter, in support of experiments performed at Argonne's Advanced Photon Source (APS). Theoretical studies are being conducted on the physics of the photoeffect and Compton scattering by bound electrons, focusing on topics selected in view of basic importance, timeliness, and potential in applications. Data on crystalline silicon for the interactions of photons over the entire spectral range were comprehensively analyzed with the use of dispersion relations and sum rules, and results are being prepared for publication. Cross sections for triple ionization of atomic lithium by electron impact, measured by Argonne colleagues, were theoretically interpreted.

Theoretical work in support of a new experiment to measure the neutron electric-dipole moment continues. The principal current focus is on a preliminary proof-of-principle experiment to measure the neutron magnetic-dipole moment in the same way. In addition, an analysis of the basis of the spin-statistics theorem in nonrelativistic quantum mechanics has shown that spin-zero particles must obey boson statistics without the assumptions of quantum field theory. Continuing work seeks to discover what additional assumptions are needed to extend that result to non-zero spins.

Work in areas related to quantum computing continued by completing an investigation of cyclic networks of quantum gates. The work was the research component of a Ph. D. thesis given by the University of Michigan to a graduate student working at Argonne.

In addition, work was completed on a framework for developing a coherent theory of mathematics and physics together. This research was partly based on the universal applicability of quantum mechanics, and the requirements that: such a theory be maximally valid and strong, and describe its own validity and strength to the maximum extent possible. This work and other studies of the necessary physical nature of language were the bases for initiating research on resource limited theories and their extensions as an approach to a theory of everything. The ideas developed are based on a well known but unappreciated relation between the size of the physical system investigated, the indirectness of the reality status of system properties being investigated, and physical resources needed for the investigations.

d.1.   Interactions of Photons with Matter (M. Inokuti and D. Y. Smith*)

In support of experiments in atomic and condensed-matter physics with the use of synchrotron radiation, theoretical studies are being conducted on the physics of photo-absorption and Compton scattering, focusing on topics selected in view of basic importance, timeliness, and potential applications.

One theme of long-term studies has been the use of

dispersion relations and sum rules for indices of response of matter over the entire range of photon energies. A comprehensive analysis of optical data on silicon is nearly complete, and is being prepared for publication. A novel method for characterizing the refractive index of a substance in a region of near transparency was formulated and applied to silicate glasses.[1]

_____
*University of Vermont.
[1]D. Y. Smith, M. Inokuti, and W. Karstens, Radiat. Effects Defects Solids **157**, 823 (2002).

d.2.   Interactions of Charged Particles with Matter (M. Inokuti)

Stopping power, the total yield of ionization, and its statistical fluctuations are examples of quantities describing the penetration of charged particles through matter and are important to applications such as the detection of particles and the analysis of their charges and kinetic energies. The understanding of those quantities in terms of individual collisions and associated cross sections remains a major challenge and is the goal of our continuing effort.

For instance, the cross section for triple ionization of

the lithium atom by electron impact, recently measured by Argonne colleagues, was interpreted.[1]

An essay[2] on the role of physics in radiation sciences was written in commemoration of the 50th Anniversary of the Radiation Research Society. Extensive work for the International Commission on Radiation Units and Measurements (ICRU) continues on the editing of its reports and on physical data such as stopping powers and various interaction cross sections.

_____
[1]M.-T. Huang, W. W. Wong, M. Inokuti, S. H. Southworth, and L. Young, Phys. Rev. Lett., in press.
[2]M. Inokuti and S. M. Seltzer, Radiat. Res. **158**, 3 (2002).

d.3.   Spin and Statistics in Nonrelativistic Quantum Mechanics: The Spin-Zero Case (Murray Peshkin)

I completed a proof from stated assumptions of ordinary nonrelativistic quantum mechanics based on the Schrödinger equation that identical spinless particles with no degrees of freedom other than the spatial ones must obey symmetric statistics. The key assumption is one introduced earlier by Leinaas and Myrheim, that the configuration space for two particles must consist of the unordered pairs $\{r_1, r_2\}$. That assumption is the mathematical implementation of the physical principle that the dynamical variables in the theory should be in one-to-one relation with the physically measurable quantities.   Then   the indistinguishability of the two particles is reflected by the wave function for spin-zero particles depending upon the unordered pairs, for which $\{r_2, r_1\} = \{r_1, r_2\}$. Leinaas and Myrheim were able to show that this assumption and its generalization to non-zero spins

limit the possible statistics to fully symmetric or fully antisymmetric, eliminating intermediate statistics. Berry and Robbins later extended the work of Leinaas and Myrheim, giving a precise mathematical treatment of the problem for all spins and relating the statistics to the topology of the configuration space, but they too were unable to eliminate the "wrong" statistics for any spin. I was able to eliminate antisymmetric statistics for identical spin-zero particles by using an additional assumption, that the wave functions must be continuous because of the second derivatives in the Hamiltonian. Ongoing research seeks to relate these considerations to the proofs from quantum field theory, which appear superficially to have an entirely different physical basis. I am also attempting to generalize the nonrelativistic proof to include nonzero spins.

d.4. The Representation of Numbers in Quantum Mechanics (P. Benioff)

Work on quantum mechanical representations of natural numbers, integers, and rational numbers was published.[1] The representations were based on the use of creation and annihilation operators for bosons and fermions to represent numbers in a k-ary basis as states of quantum systems. Products of the same operators were used to represent various arithmetic operations on the states representing numbers. The importance of the requirement of efficient implementability for physical models of the axioms was emphasized. This condition requires the use of successor operations for each value of j, corresponding to addition of k^{j-1} if $j > 0$ and (for rational numbers) k^j if $j < 0$. It follows from the efficient implementability of these successors, which are used in all computers, that implementation of the addition and multiplication operators, which are defined in terms of iterations of the successors, should be efficient. Implementation of definitions of the addition and multiplication operators based on the successor for $j = 1$ only, which is the only successor defined in the usual axioms of arithmetic, are not efficient.

_____
[1]P. Benioff, Algorithmica. **34**, 529-559 (2002).

d.5. Towards a Coherent Theory of Mathematics and Physics (P. Benioff)

Work was completed on a description of a framework for developing a coherent theory of mathematics and physics together.[1] The two main requirements that such a theory must satisfy are that it is valid and sufficiently strong, and it must maximally describe its own validity and sufficient strength. The mathematical logical definition of validity is used. This says that a theory is valid if all theorems of the theory are true in any domain of the theory. Other aspects of a coherent theory include universal applicability, the relation to the anthropic principle, and possible uniqueness. The requirement that the coherent theory maximally describe its own validity and completeness follows from universal applicability in that intelligent systems, and experimental and computational equipment are all included in the domain of the theory. It follows that the dynamical process of validation of the theory is in the theory domain, so the theory must describe in some sense its own validation. The uniqueness possibility would hold if the two basic requirements were so restrictive that only one theory can satisfy them. The work suggests that the basic properties of the physical and mathematical universes are entwined with and emerge with a coherent theory. Support for this includes the indirect reality status of properties of very small or very large far away systems compared to moderate sized nearby systems. Discussion of the necessary physical nature of language includes physical models of language and a proof that the meaning content of expressions of any axiomatizable theory seems to be independent of the algorithmic complexity of the theory. Gödel maps seem to be less useful for a coherent theory than for purely mathematical theories because all symbols and words of any language must have representations as states of physical systems. These states are already in the domain of a coherent theory.

_____
[1]P. Benioff, Foundations of Physics, **32**, 989-1029, (2002).

d.6. Language is Physical (P. Benioff)

Work was completed on some aspects of the physical nature of language.[1] In particular, physical models of language must exist that are efficiently implementable. The existence requirement is essential because without physical models no communication or thinking would be possible. Efficient implementability for creating and reading language expressions is discussed and illustrated with a quantum mechanical model. Physical states of systems that represent language expressions can have meaning, either as an informal language or as a formal language associated with mathematical or physical theories. Any universally applicable physical theory, or coherent theory of physics and mathematics together, includes in its domain physical models of expressions for both the informal language used to discuss the theory and the expressions of the theory itself. It follows that some formulas in the formal theory express some of their own physical properties.

_____
[1]Prepared from notes for talk at 1st Feynman Festival, Univ. Maryland, Aug., 2002 (to appear in Quantum Information Processing).

The inclusion of intelligent systems in the domain of the theory means that the theory, *e.g.* quantum mechanics, must describe, in some sense, its own validation. Maps of language expressions into physical states are discussed. A spin projection example is considered, as are conditions under which such a map is a Gödel map.

d.7.   Resource-Limited Theories and their Extensions: A Possible Approach to a Theory of Everything (P. Benioff)

Work was begun on resource-limited theories and their extensions as a possible approach to a coherent theory of physics and mathematics or, for short, a theory of everything. The work, which is based on earlier research,[1] starts with the idea that the extension of physical and mathematical theories to include the amount of space, time, momentum, and energy resources required to determine properties of systems may influence what is true in physics and mathematics at a foundational level. One proceeds by associating to each amount, r, of resources a domain, D_r, a theory, T_r, and a language, L_r. D_r is limited in that all statements in D_r require at most r resources to verify or refute. T_r is limited in that any theorem of T_r must be provable using at most r resources. Also any theorem of T_r must be true in D_r. L_r is limited in that all expressions in L_r require at most r resources to create, display, and maintain. Consequences of these resource limitations are being investigated with a goal of further characterizing the theories and describing the use of resources by observers to develop theories of physics and mathematics.

---

[1]P. Benioff, Foundations of Physics **32**, 989-1029, (2002); Quantum Information Processing, (quant-ph 0210211).

d.8.   Cyclic Networks of Quantum Gates (Paul Benioff and Peter Cabauy*)

Work was completed on initial steps in an analysis of cyclic networks of quantum gates. These networks include feedback loops as well as external lines. All one and two qubit networks with one and two loops were investigated as well as two qubit networks with a third qubit on an external line. The analysis included a group theory classification of the networks, a study of their dynamics, and perturbation effects induced by the third, external qubit. Some ideas on the use of cyclic networks in quantum algorithms, quantum memories, and quantum sensors were discussed. This work provided the bulk of a Ph. D. Thesis awarded to Peter Cabauy from the University of Michigan in the fall of 2002. A paper was submitted to Physical Review A.

---

*ANL and University of Michigan.

E. OTHER ACTIVITIES

e.1.   Hadron Structure and GeV Electroweak Interactions (T.-S. H. Lee)

In the past few years, a large amount of high precision data on the nucleon's electromagnetic reactions in the few-GeV energy region was accumulated in experiments at several laboratories around the world. Furthermore, there is a possibility that high quality neutrino scattering data in the same energy region could soon become available at Fermi Laboratory and also at several neutrino facilities currently under construction. These developments provide tremendous opportunities for understanding non-perturbative aspects of hadron structure. To aid in exploiting these opportunities, the Theory Group hosted a workshop in the week of July 29 – August 2, 2002, whose goal was to focus attention on the theoretical challenges that the data presents, and encourage and facilitate collaborative research. There were twenty invited talks on subjects ranging from nucleon structure and nucleon resonances, through simulations of lattice QCD and models of electroweak reactions; and there was also ample time for discussions between the forty participants drawn from around the world. Articles stimulated by discussions at the Workshop have begun to appear.

e.2.   15th Annual Midwest Theory Get-Together (C. D. Roberts)

The Theory Group hosted the fifteenth Annual Midwest Theory Get-Together on October 25-26, 2002. Nuclear theorists from eight Midwest universities, FNAL and ANL met to learn about the research goals and foci of different individuals and groups throughout the region. While the organizational duties rotate amongst the participants, Argonne is the regular host site because of its meeting facilities and central location. The organizers for 2002 were Timothy Londergan and Adam Szczepaniak of Indiana University in Bloomington. The meeting provides a good chance for students to broaden their outlook and get some practical speaking experience in a friendly atmosphere. The format is informal, with an agenda of talks being volunteered at the beginning of the meeting. In 2002 we had thirty-four registered participants: faculty, postdocs and students. Over the Friday afternoon and Saturday morning approximately twenty-five presentations were made, covering topics such as: relativistic heavy ion collisions; no-core shell model; nuclear pairing; nucleon matter; quantum Monte-Carlo methods; wavelet methods for few body physics; effective field theories; hadron physics; and QCD. No one left unhappy.

OTHER EDUCATIONAL ACTIVITIES IN THE PHYSICS DIVISION

a. Enhancement of Minority Involvement in DOE Nuclear Physics Programs
(B. Zeidman)

The ANL Physics Division, through its Minority Program, continues to attract highly qualified students who apply for participation in the programs of the Physics Division and other ANL divisions. The program is directed toward identification of physics departments with relatively strong programs and faculty interested in stimulating their students to pursue research, particularly in summer programs. Returning, as well as new, minority physics majors participated in the ANL Summer Program during 2002. More than a dozen former participants are currently enrolled in programs leading to doctorates in physics. Two students who performed Ph.D. thesis research in the Physics Division received their degrees this past year.

The program is an ongoing effort based upon personal interactions with a substantial number of qualified minority students and faculty. During visits to the Physics Departments of HBCU colleges (Historically Black Colleges and Universities) and other institutions with large minority populations, lectures are presented and there are discussions of activities in physics at ANL and other laboratories, graduate programs, etc. Other activities include attendance at meetings of minority organizations, appointment as Adjunct Professor at Hampton University, and serving on the Advisory Boards of the Centers of Excellence at both Hampton University and Morehouse College.

b. Nuclear Physics Award for Faculty in Undergraduate Institutions
(B. Zeidman)

The goal of the 'Faculty Program', is to enhance undergraduate science education through faculty awards for minority and HBCU faculty that will allow them to directly participate in the ANL Physics Division research program and increase the number of undergraduates involved in research. A participant has obtained independent funding for continuing research collaboration with ANL that involves several undergraduate students. Several minority faculty members and students who have been involved in research collaboration with the Physics Division for the past few years will return this year. In order to maximize the scope of the program, existing educational programs are being utilized to supplement support for some of the participants and more formal collaborative arrangements are being discussed.

c. Scientific Support of SciTech Museum Exhibits and Outreach Programs
   (D. Henderson)

SciTech (Science and Technology Interactive Center) is a hands-on science museum located in Aurora, Illinois, near Argonne. With the help of volunteers and institutional support from Argonne, Fermilab, and several technological companies, SciTech has become an acknowledged leader in developing exhibits to teach modern science in a museum context.
D. Henderson of the Physics Division serves voluntarily as an exhibit developer on a regular basis. Several other staff members volunteer from time to time. The Physics Division collaborates with SciTech in developing exhibits for the museum and for use in Argonne's public educational activities. These efforts involve no significant programmatic costs.

Mr. Henderson has been awarded, by Kane County, a certificate of appreciation for his volunteer efforts at Scitech.

STAFF MEMBERS OF THE PHYSICS DIVISION

Listed below are the staff of the Physics Division for the year ending December 31, 2002.
The program headings indicate only the individual's current primary activity.

SCIENTIFIC STAFF

EXPERIMENTAL NUCLEAR PHYSICS STAFF

Regular Staff

      Irshad Ahmad, Ph.D., University of California, 1966
      John Arrington Ph.D., California Institute of Technology, 1998
      Birger B. Back, Ph.D., University of Copenhagen, 1974
      Michael P. Carpenter, Ph.D., University of Tennessee, 1987
      Yanglai Cho, Ph.D., Carnegie-Mellon University, 1966
  * Cary N. Davids, Ph.D., California Institute of Technology, 1967
      Susan Fischer, Ph.D., University of Notre Dame, 1994
  † Donald F. Geesaman, Ph.D., State University of N.Y., Stony Brook, 1976
      Kawtar Hafidi, Ph.D., University of Paris South XI, 1999
  ‡ Walter F. Henning, Ph.D., Technical University of Munich, 1968
      Roy J. Holt, Ph.D., Yale University, 1972
  § Harold E. Jackson, Jr., Ph.D., Cornell University, 1959
  ¶ Robert V.F. Janssens, Ph.D. Univ. Catholique de Louvain, Belgium, 1978
      Cheng-lie Jiang, Ph.D. China Institute of Atomic Energy, 1960
      Michael P. Kelly, Ph.D., University of Washington, 1999
      Teng Lek Khoo, Ph.D., McMaster University, 1972
      Torben Lauritsen, Ph.D., State University of New York, 1990
      Eliane Lessner, Ph.D., Syracuse University, 1975
      Christopher J. Lister, Ph.D., University of Liverpool, 1977
      Zheng-tian Lu, Ph.D., University of California, Berkeley, 1994
      Eugene Moore, Ph.D., Florida State University, 1988
** Jerry A. Nolen, Jr., Ph.D., Princeton University, 1965
      Peter N. Ostroumov, Ph.D. Moscow Engineering and Physical Institute, 1982
      Richard C. Pardo, Ph.D., University of Texas, 1976
      David H. Potterveld, Ph.D., Caltech, 1988
      Karl Ernst Rehm, Ph.D., Technical University, Munich, 1973
      Paul Reimer, Ph.D. University of Illinois, 1996
†† Guy Savard, Ph.D., McGill University, 1988
†† John P. Schiffer, Ph.D., Yale University, 1954
      Dariusz Seweryniak, Ph.D., Uppsala University, 1994
      Kenneth W. Shepard, Ph.D., Stanford University, 1970
      Kenneth Teh, Ph.D., Vanderbilt University, 1988
‡‡Alan H. Wuosmaa, Ph.D., University of Pennsylvania, 1989

_____

   * Adjunct Professor, Vanderbilt University.
   † Director of the Physics Division.
   ‡ On leave of absence at GSI, Darmstadt.
   § Associate Director of the Physics Division.
   ¶ Associate Director of the Physics Division. Adjunct Professor, Michigan State University and Adjoint
      Professor, Vanderbilt University.
 ** Director of the ATLAS Facility. Adjunct Professor, Michigan State University.
 †† Joint appointment with the University of Chicago.
 ‡‡ Left the Physics Division in August 2002.

Special Appointments

   * R. Russell Betts, Ph.D., University of Pennsylvania, 1972
      Lowell M. Bollinger, Ph.D., Cornell University, 1951
      William J. Childs, Ph.D., University of Michigan, 1956
      Donald S. Gemmell, Ph.D., Australian National University, 1960
      F. Paul Mooring, Ph.D., University of Wisconsin, 1951
   † Michael Paul, Ph.D., Hebrew University of Jerusalem, 1973
      Gilbert J. Perlow, Ph.D., University of Chicago, 1940
      G. Roy Ringo, Ph.D., University of Chicago, 1940
      Ralph E. Segel, Ph.D., Johns Hopkins University, 1955
      George E. Thomas, B.A., Illinois Wesleyan, 1943
   § Ben Zeidman, Ph.D. Washington University, 1957

THEORETICAL NUCLEAR PHYSICS STAFF

Regular Staff

      Richard R. Chasman, Ph.D., University of California, 1959
      Henning Esbensen, Ph.D., University of Aarhus, 1977
   ¶ Tsung-Shung Harry Lee, Ph.D., University of Pittsburgh, 1973
      Steven C. Pieper, Ph.D., University of Illinois, 1970
      Craig D. Roberts, Ph.D., Flinders University of South Australia, 1989
      Robert B. Wiringa, Ph.D., University of Illinois, 1978

Special Appointments

      Paul Benioff, Ph.D., University of California, 1959
      Arnold R. Bodmer, Ph.D., Manchester University, 1953
      Fritz Coester, Ph.D., University of Zurich, 1944
      Mitio Inokuti, Ph.D., University of Tokyo, 1962
      Dieter Kurath, Ph.D., University of Chicago, 1951
      Robert D. Lawson, Ph.D. Stanford University, 1953
   ‖ Vijay Pandharipande, Ph.D., University of Bombay, 1969
      Murray Peshkin, Ph.D., Cornell University, 1951

_____

   * Special Term Appointee from the University of Illinois-Chicago.
   † Special Term Appointee from the Hebrew University of Jerusalem.
   § Special Term Appointee. Adjunct Professor, Hampton University.
   ¶ Adjunct Professor, University of Pittsburgh.
   ‖ Special Term Appointee from the University of Illinois, Urbana.

TEMPORARY APPOINTMENTS

Postdoctoral Appointees

Thomas Duguet (from CEA, Saclay, France):
   Theoretical studies.
   (November 2002-   )

* Kawtar Hafidi (from CEN, Saclay, France):
   Medium-energy physics.
   (November 1999-February 2002))

Neil J. Hammond (from University of Liverpool):
   Research at ATLAS.
   (July 2002-   )

† Andreas Heinz (from GSI, Darmstadt, Germany):
   Heavy-ion research at ATLAS.
   (February 1999-September 2002)

David Jenkins (University of York, UK):
   Heavy-ion research at ATLAS.
   (January 2000--   )

* Michael Kelly (from University of Washington, Seattle, WA):
   Heavy-ion research at ATLAS.
   (June 1999-February 2002)

Bogdan Mihaila (from University of New Hampshire, Durham, NH):
   Theoretical studies.
   (October 2000--December 2002)

Ian Moore (Shuster Laboratory, UK):
   Medium-energy physics.
   (November 2001--   )

Gopal Mukherjee (from University of Massachusetts, Lowell, MA):
   Heavy-ion research at ATLAS.
   (October 2001--   )

Brahim Mustapha (from University of Paris, France):
   ATLAS operations and development.
   (May 2000--   )

Elaine Schulte (from University of Illinois-Urbana):
   Medium-energy physics studies.
   (February 2002-   )

_____
*   Joined regular staff in February 2002.
†   Enrico Fermi Scholar.

Shrabani Sinha (from India Institute of Technology, Bombay):
    Research at ATLAS.
    (June 2002-   )

Alexander Volya (from Michigan State University, E. Lansing, MI):
    Theoretical physics studies.
    (January 2002 -   )

Nikolai Vinogradov (from Moscow Engineering Physical Institute, Russia):
    ATLAS operation and development.
    (November 2001--   )

Krishni Wijesooria (from Jefferson Laboratory, Newport News, VA):
    Medium-energy physics.
    (October 2000—December 2002)

Zhen Zhou (from University of Giessen, Germany):
    Research at ATLAS.
    (February 2002-   )

TECHNICAL AND ENGINEERING STAFF
(and areas of activity)

Kevin G. Bailey (B.S. University of Nebraska, 1989).
    Technical assistance, medium-energy physics.

John M. Bogaty (A.A.S. DeVry, 1961).
    Electrical systems, ATLAS operation and development.

Benny E. Clifft (A.S.E.E., DeVry, 1959).
    Electrical systems, ATLAS operation and development.

*   Joseph Falout (B.S.M.E. University of Illinois, 1970).
    Experimental equipment design.

Joel Fuerst (MSME, Northwestern University, 1990).
    Cryogenic development at ATLAS.

John P. Greene (M.S. DePaul University, 1982).
    Target preparation.

*   Ray E. Harden (A.A.S. Milwaukee School of Engineering, 1957).
    ATLAS operator

*   Dale J. Henderson (B.S. Elmhurst College, 1951).
    Detector development, technical assistance, heavy-ion physics.

James M. Joswick (A.A.S. Milwaukee School of Engineering, 1964).
    ATLAS experimental equipment maintenance, technical assistance, heavy-ion physics.

Mark Kedzie
    ATLAS experimental equipment development.

*   Raymond B. Kickert
    ATLAS experimental equipment maintenance, technical assistance, heavy-ion physics.

_____
*   Special Term Appointee.

Anthony Levand (BSME, University of Illinois, 1986).
Design control at ATLAS.

* Paul Markovich (B.S. Purdue University, 1972).
Surface chemistry, ATLAS development and operation.

Thomas P. Mullen (B.S. Marquette University, 1966).
Division ESH/QA engineer.

Floyd Munson, Jr. (A.A.S. DeVry, 1966, B.S. Lewis University, 1993).
Control system for ATLAS.

Bruce G. Nardi (A.A.S. Morton Jr. College, 1967; A.A.S. DeVry, 1969).
Electronics design and maintenance.

Tom O'Connor (M.S. DePaul University, 1995).
Technical assistance, medium-energy physics.

Tad Pennington (M.S. University of Missouri, 1989; M.S. University of Alabama, 1998)
Detector development, technical assistance, heavy-ion physics.

Deborah Quock (M.S. Rice University, 1985)
Technical assistance, ATLAS control system.

Sergey Sharamentov (MS, Moscow Engineering Physical Institute, 1976).
Electrical systems, ATLAS operation and development.

James R. Specht (A.A.S. DeVry, 1964).
Cryogenics engineer. ATLAS development and operation.

Philip Strickhorn (B.S. DeVry, 1990).
Electrical and technical assistance with ATLAS operations.

Richard Vondrasek (B.S. University of Chicago, 1990).
ATLAS operator.

Philip R. Wilt (Johnstown Technical School 1973).
Electronics design and maintenance.

Bruce J. Zabransky (M.S. University of Illinois, Chicago, 1973).
Mechanical Engineer.

Gary P. Zinkann (B.S. DeVry, 1975).
ATLAS operations supervisor.

ADMINISTRATIVE STAFF

† Allan Bernstein, M.B.A., Rosary College, 1986
† James E. Nelson, B.A., University of Illinois, 1975
* Karen J. Thayer

---

* Special Term Appointee.
† Assistant Director of the Physics Division.

VISITORS AND STUDENTS

Long-Term Visitors (at Argonne more than 4 months)

Anatolijs Afanasjevs (from University of Notre Dame, IN):
Theoretical physics studies.
(July 2001—June 2002)

El Alaoui Moulay Ahmed (from Laboratory for Theoretical Physics, Morocco):
Medium-energy physics.
(February 2001--   )

Vladislav Asseev (from Institute for Nuclear Research of Russian Academy of Sciences, Russia)
Accelerator development.
(April-October 2002)

Bertram Blank (from University of Bordeaux, France):
Research at ATLAS
(August 2002--   )

Jason Clark (from University of Manitoba, Canada):
Heavy-ion research at ATLAS.
(May 1999-   )

Sean Freeman (from University of Manchester, U.K.):
Research at ATLAS.
(October 2002--   )

Itacil Gomes (from Technology Division, Argonne National Laboratory)
Linac development.
(September 2000--   )

Burt Holzmann (from University of Chicago, Chicago, IL):
Heavy-ion research at ATLAS.
(October 2001--   )

Michael Kroupa (from Monmouth College, Monmouth, IL):
Theoretical physics studies.
(July 2002--   )

Walter Kutschera (from University of Vienna, Austria):
Research at ATLAS.
(August 2002--   )

Ioana Mihaila (from Coastal Carolina University, Conway, SC):
Theoretical physics studies.
(November 2001--   )

Peter Mueller (from Johannes Gutenberg University, Mainz, Germany):
Medium-energy physics.
(November 2001--   )

Iouri Sanjiev (from St. Petersburg Nucl. Phys. Institute, Gatchina, Leningrad, Russis):
Medium energy studies.
(November 2000--   )

Stefan W. Schramm (from University of Frankfurt, Germany):
Theoretical physics studies.
(November 2001--   )

Jason Shergur (from University of Maryland, College Pk., MD):
Research at ATLAS.
(January 2002--   )

* David Smith (from University of Vermont, Burlington, VT):
Theoretical physics studies.
(February 2002--   )

Jicheng Wang (from University of Manitoba, Canada):
Heavy-ion research at ATLAS.
(January 2001--   )

Andreas Woehr (from University of Maryland, College Park, MD):
Heavy-ion research at ATLAS.
(January 2001--   )

Short-Term Visitors (at ANL for less than 4 months at a time)

* Nour-eddi Berrah (from Western Michigan University, Kalamazoo, MI):
Atomic physics research.
(October 1991--   )

Chantal Boudreau (from McGill University, Montreal, Quebec):
Heavy-ion research at ATLAS.
(May 2000—April 2001; September 2001—March 2002)

Thomas Dombeck (from University of Chicago, Chicago, IL):
Heavy-ion research.
(January 2000--   )

* Christopher Fasano (from Monmouth College, Monmouth, IL):
Theoretical studies.
(February 1999-   )

† Susan Fischer (from DePaul University, Chicago, IL):
Heavy-ion research at ATLAS.
(October 1998—January 2002)

Michael Froese (from University of Manitoba, Canada):
Heavy-ion research at ATLAS.
(May 2001--   )

David J. Hofman (from University of Illinois, Chicago, IL):
Heavy-ion research at ATLAS.
(September 2000--   )

* Judith Katzy (from University of Illinois, Chicago, IL):
Heavy-ion research at ATLAS.
(February 1998--   )

_____
*   Guest Faculty Research Participant.
†   Joined regular staff January 2002.

Andre Kolomiets (from ITEP, Russia):
   Accelerator development.
   (July-October 2000; November 2000—May 2002)

*   Donald McLeod (from University of Illinois, Chicago, IL):
   Heavy-ion research at ATLAS.
   (June 1994--   )

Rachid Nouicer (from University of Chicago, Chicago, IL):
   Heavy-ion research at ATLAS.
   (April 1998--   )

Agnes Pailloux (from University of Strassbourg, France):
   Medium-energy physics studies.
   (March-June 2002)

*   Eugene Shiles (Retired Professor)
   Theoretical physics studies.
   (August 2002)

Peter Winter (from Rheinische-Friedrich Wilhelms Universitat, Bonn, Germany):
   Medium-energy physics studies.
   (July-October 2002)

Resident Graduate Students

Peter Cabauy (from University of Michigan, Ann Arbor, MI):
   Theoretical studies.
   (February-September 2000; January 2001—June 2002)

Mauricio Portillo (from Michigan State University, E. Lansing, MI):
   Accelerator development.
   (September 1995—May 2002)

Issam Qattan (from Northwestern University, Evanston, IL):
   Medium-energy physics.
   (August 2001--   )

†   Elaine Schulte (from University of Illinois, Urbana, IL):
   Medium-energy studies.
   (August 2000—February 2002)

Guest Graduate Students

Khalefeh Abu Saleem (from Illinois Institute of Technology, Chicago, IL):
   Heavy-ion research at ATLAS.
   (June 1999-   )

Xu Du (from Northwestern University, Evanston, IL):
   Medium-energy physics.
   (June 1999-   )

_____
*   Guest Faculty Research Participant.
†   Postdoctoral Appointee as of February 2002.

Andrew Geraci (from University of Chicago, Chicago, IL):
   Accelerator development.
   (December 1999-   )

Louis Jisonna (from Northwestern Universiity, Evanston, IL):
   Heavy-ion research at ATLAS.
   (June 2000--   )

Issam Qattan (Northwestern University, Evanston, IL):
   Medium-energy physics studies.
   (September 2001--   )

Christian Trempe (from McGill University, Montreal, QC):
   Heavy-ion research at ATLAS.
   (May-August 2000)

Li-Bang Wang (from University of Illinois, Urbana, IL):
   Medium-energy studies.
   (September 2001--   )

Undergraduate Students

Krystal Bavlsik (Nazareth Academy)
Laura Blomley (University of Manitoba)
Matthew Brolley (North Central College)
Thomas Cecil (Murray State University)
Thomas Cocolios (McGill University)
Ryan Enshiwat (University of Manitoba)
Michael Froese (University of Manitoba)
Sean Grullon (Florida International University, Miami)
James Jenkins (DePaul University)
William Karstens (St. Michael's College)
Nikola Kunovski (North Central College)
Daniel Lascar (University of Chicago)
Luke Luginbuhl (Illinois Central College)
Janelle Neubauer (North Central College)
Daniel Peterson (University of Notre Dame)
Marty Pickens (Monmouth College)
Peter Probst (University of Illinois-Chicago)
Patrick Salcido (Richard J. Daley College)
Barbara Truett (Purdue University, Calumet)
Jennifer Welsh (University of Illinois-Urbana)

2002 Pre-College Students

Michelle Alvarado (Hoffman Estates High School)
Todd Strobel (Carl Sandburg High School, Orland Park, IL)

PUBLICATIONS DURING 2002

HEAVY-ION NUCLEAR PHYSICS RESEARCH

Energy Dependence of Particle Multiplicities in Central Au + Au Collisions
  B. B. Back et al. (PHOBOS Collaboration)
    Phys. Rev. Lett. **88**, 022302/1-4 (2002)

Direct Decay from the Superdeformed Band to the Yrast Line in $^{152}_{66}\text{Dy}_{86}$

  T. Lauritsen, M. P. Carpenter, T. Døssing, P. Fallon, B. Herskind, R. V. F. Janssens,
  D. G. Jenkins, T. L. Khoo, F. G. Kondev, A. Lopez-Martens, A. O. Macchiavelli, D. Ward,
  K. S. Abu Saleem, I. Ahmad, R. Clark, M. Cromaz, J. P. Greene, F. Hannachi, A. M. Heinz,
  A. Korichi, G. Lane, C. J. Lister, P. Reiter, D. Seweryniak, S. Siem, R. C. Vondrasek, and
  I. Wiedenhöver
    Phys. Rev. Lett. **88**, 042501/1-4 (2002)

Melting of Crystalline Confined Plasmas
  J. P. Schiffer
    Phys. Rev. Lett. **88**, 205003/1-4 (2002)

Prompt Proton Decay Scheme of ^{59}Cu
  D. Rudolph, C. Andreoiu, C. Fahlander, R. J. Charity, M. Devlin, D. G. Sarantites,
  L. G. Sobotka, D. P. Balamuth, J. Eberth, A. Galindo-Uribarri, P. A. Hausladen,
  D. Seweryniak, and Th. Steinhardt
    Phys. Rev. Lett. **89**, 022501/1-4 (2002)

Unexpected Behavior of Heavy-Ion Fusion Cross Sections at Extreme Sub-Barrier Energies
  C. L. Jiang, H. Esbensen, K. E. Rehm, B. B. Back, R. V. F. Janssens, J. A. Caggiano,
  P. Collon, J. Greene, A. M. Heinz, D. J. Henderson, I. Nishinaka, T. O. Pennington, and
  D. Seweryniak
    Phys. Rev. Lett. **89**, 052701/1-4 (2002)

Large Angle Elastic Alpha Scattering on a $N = Z$ Nucleus Above $A = \boldsymbol{40}$
  K. E. Rehm, C. L. Jiang, I. Ahmad, J. Caggiano, P. Collon, J. P. Greene, D. Henderson,
  A. Heinz, R. V. F. Janssens, R. C. Pardo, T. Pennington, J. P. Schiffer, R. H. Siemssen,
  A. H. Wuosmaa, M. Paul, and P. Mohr
    Phys. Rev. Lett. **89**, 132501/1-4 (2002)

Pseudorapidity and Centrality Dependence of the Collective Flow of Charged Particles in
Au + Au Collisions at $\sqrt{s_{NN}} = 130$ GeV
  B. B. Back *et al.*
    Phys. Rev. Lett. **89**, 222301/1-4 (2002)

Octupole Vibration in Superdeformed $^{152}_{66}$Dy$_{86}$

T. Lauritsen, R. V. F. Janssens, M. P. Carpenter, T. Døssing, P. Fallon, B. Herskind,
D. G. Jenkins, T. L. Khoo, F. G. Kondev, A. Lopez-Martens, A. 0. Macchiavelli, D. Ward,
K. S. Abu Saleem, I. Ahmad, R. M. Clark, M. Cromaz, T. Døssing, A. M. Heinz, A. Korichi,
G. Lane, C. J. Lister, and D. Seweryniak
   Phys. Rev. Lett. **89**, 282501/1-4 (2002)

Isovector Pairing in Odd-Odd $N = Z$ ^{50}Mn

C. D. O'Leary, M. A. Bentley, S. M. Lenzi, G. Martínez-Pinedo, D. D. Warner, A. M. Bruce,
J. A. Cameron, M. P. Carpenter, C. N. Davids, P. Fallon, L. Frankland, W. Gelletly,
R. V. F. Janssens, D. T. Joss, C. J. Lister, P. H. Regan, P. Reiter, B. Rubio, D. Seweryniak,
C. E. Svensson, S. M. Vincent, and S. J. Williams
   Phys. Lett. **B525**, 49-55 (2002)

First Observation of Excited Structures in Neutron-Deficient ^{179}Hg: Evidence for Multiple
Shape Coexistence

F. G. Kondev, M. P. Carpenter, R. V. F. Janssens, C. J. Lister, K. Abu Saleem, I. Ahmad,
H. Amro, J. Caggiano, C. N. Davids, A. Heinz, B. Herskind, T. L. Khoo, T. Lauritsen,
W. C. Ma, J. J. Ressler, W. Reviol, L. L. Riedinger, D. G. Sarantites, D. Seweryniak, S. Siem,
A. A. Sonzogni, P. G. Varmette, and I. Wiedenhöver
   Phys. Lett. **B528**, 221-227 (2002)

Identification of Excited States in ^{140}Dy

D. M. Cullen, M. P. Carpenter, C. N. Davids, A. M. Fletcher, S. J. Freeman, R. V. F. Janssens,
F. G. Kondev, C. J. Lister, L. K. Pattison, D. Seweryniak, J. F. Smith, A. M. Bruce, K. Abu
Saleem, I. Ahmad, A. Heinz, T. L. Khoo, E. F. Moore, G. Mukherjee, C. Wheldon, and
A. Woehr
   Phys. Lett. **B529**, 42-49 (2002)

Structure of ^{52,54}Ti and Shell Closures in Neutron-Rich Nuclei Above ^{38}Ca

R. V. F. Janssens, B. Fornal, P. F. Mantica, B. A. Brown, R. Broda, P. Bhattacharyya,
M. P. Carpenter, M. Cinausero, P. J. Daly, A. D. Davies, T. Glasmacher, Z. W. Grabowski,
D. E. Groh, M. Honma, F. G. Kondev, W. Krblas, T. Lauritsen, S. N. Liddick, S. Lunardi,
N. Marginean, T. Mizusaki, D. J. Morrissey, A. C. Morton, W. F. Mueller, T. Otsuka,
T. Pawlat, D. Seweryniak, H. Schatz, A. Stolz, S. L. Tabor, C. A. Ur, G. Viesti,
I. Wiedenhöver, and J. Wrzesiński
   Phys. Lett. **B546,** 55-62 (2002)

Spectroscopy of Transfermium Nuclei: $^{252}_{102}$No
  R.-D. Herzberg, N. Amzal, F. Becker, P. A. Butler, A. J. C. Chewter, J. F. C. Cocks.
  O. Dorvaux, K. Eskola, J. Gerl, P. T. Greenlees, N. J. Hammond, K. Hauschild, K. Helariutta,
  F. Heβberger, M. Houry, G. D. Jones, P. M. Jones, R. Julin, S. Juutinen, H. Kankaanpää,
  H. Kettunen, T. L. Khoo, W. Korten, P. Kuusiniemi, Y. Le Coz, M. Leino, C. J. Lister,
  R. Lucas, M. Muikku, P. Nieminen, R. D. Page, P. Rahkila, P. Reiter, Ch. Schlegel,
  C. Scholey, O. Stezowski, Ch. Theisen, W. H. Trazaska, J. Uusitalo, and H. J. Wollersheim
     Phys. Rev. C **65**, 014303/1-7 (2002)

Observation of Rotational Bands in the Neutron-Rich ^{107}Ru Nucleus
  S. J. Zhu, J. H. Hamilton, A. V. Ramayya, J. K. Hwang, C. Y. Gan, X. Q. Zhang, C. J. Beyer,
  J. Kormicki, M. Sakhaee, L. M. Yang, L. Y. Zhu, R. Q. Xu, Z. Zhang, Z. Jiang, W. C. Ma,
  E. F. Jones, P. M. Gore, J. D. Cole, M. W. Drigert, I. Y. Lee, J. O. Rasmussen, T. N. Ginter,
  Y. X. Luo, S. C. Wu, C. Folden, P. Fallon, P. Zielinski, K. E. Gregorich, A. 0. Macchiavelli,
  S. J. Asztalos, G. M. Ter-Akopian, Yu. Ts. Oganessian, M. A. Stoyer, J. P. Greene,
  R. V. F. Janssens, and I. Ahmad
     Phys. Rev. C **65**, 014307/1-6 (2002)

Excitations of Two- and Three-Valence-Proton Nuclei ^{107}Te and ^{135}I
  S. K. Saha, C. Constantinescu, P. J. Daly, P. Bhattacharyya, C. T. Zhang, Z. W. Grabowski,
  B. Fornal, R. Broda, I. Ahmad, D. Seweryniak, I. Wiedenhöver, M. P. Carpenter,
  R. V. F. Janssens, T. L. Khoo, T. Lauritsen, C. J. Lister, and P. Reiter
     Phys. Rev. C **65**, 017302/1-4 (2002)

^{100}Sn Core Excitations in ^{102}In
  M. Lipoglavšek, C. Baktash, M. P. Carpenter, D. J. Dean, T. Engeland, C. Fahlander,
  M. Hjorth-Jensen, R. V. F. Janssens, A. Likar, J. Nyberg, E. Osnes, S. D. Paul, A. Piechaczek,
  D. C. Radford, D. Rudolph, D. Seweryniak, D. G. Sarantites, M. Vencelj, and C.-H. Yu
     Phys. Rev. C **65**, 021302(R)/1-5 (2002)

Rotational Structures in ^{129}Nd and Signature Splitting Systematics of the $\nu h_{11/2}$ Bands in
A ~130 Nuclei
  O. Zeidan, D. J. Hartley, L. L. Reidinger, M. Danchev, W. Reviol, W. D. Weintraub,
  Jing-ye Zhang, A. Galindo-Uribarri, C. J. Gross, S. D. Paul, C. Baktash, M. Lipoglavsek,
  D. C. Radford, C. H. Yu, D. G. Sarantites, M. Devlin, M. P. Carpenter, R. V. F. Janssens,
  D. Seweryniak, and E. Padilla
     Phys. Rev. C **65**, 024303/1-15 (2002)

First Observation of Excited States in ^{139}I
  W. Urban, T. Rzaca-Urban, A. Korgul, J. L. Durell, M. J. Leddy, M. A. Jones, W. R. Phillips,
  A. G. Smith, B. J. Varley, I. Ahmad, L. R. Morss, and N. Schulz
     Phys. Rev. C **65**, 024307/1-4 (2002)

Angular Correlation, Spin Alignment, and Resonance Behavior in ^{12}C + ^{12}C Inelastic Scattering
   A. H. Wuosmaa, D. J. Hofmann, B. B. Back, D. J. Blumenthal, S. Fischer, D. J. Henderson,
   R. V. F. Janssens, C. J. Lister, V. Nanal, D. Nisius, M. D. Rhein, and P. R. Wilt
      Phys. Rev. C **65**, 024609/1-11 (2002)

Centrality Dependence of Charged Particle Multiplicity at Midrapidity in Au + Au Collisions at
$\sqrt{s_{NN}}$ = 130 GeV
   B. B. Back *et al.* (PHOBOS Collaboration)
      Phys. Rev. C **65**, 031901(R)/1-4 (2002)

Highly Deformed Band Structure in ^{57}Co
   W. Reviol, D. G. Sarantites, R. J. Charity, V. Tomov, J. Dobaczewski, D. Rudolph,
   R. M. Clark, M. Cromaz, P. Fallon, A. 0. Macchiavelli, M. P. Carpenter, and D. Seweryniak
      Phys. Rev. C **65**, 034309/1-10 (2002)

Competition Between Terminating and Collective Structures Above Spin 40 $\hbar$ in ^{154}Dy
   W. C. Ma, R. V. F. Janssens, T. L. Khoo, I. Ragnarsson, M. A. Riley, M. P. Carpenter,
   J. R. Terry, J. P. Zhang, I. Ahmad, P. Bhattacharyya, P. J. Daly, S. M. Fischer, J. H. Hamilton,
   T. Lauritsen, D. T. Nisius, A. V. Ramayya, R. K. Vadapalli, P. G. Varmette, J. W. Watson,
   C. T. Zhang, and S. J. Zhu
      Phys. Rev. C **65**, 034312/1-8 (2002)

β-Decay Studies of $^{135-137}$Sn Using Selective Resonance Laser Ionization Techniques
   J. Shergur, B. A. Brown, V. Fedoseyev, U. Köster, K.-L. Kratz, D. Seweryniak, W. B. Walters,
   A. Wöhr, D. Fedorov, M. Hannawald, M. Hjorth-Jensen, V. Mishin, B. Pfeiffer, J. J. Ressler,
   H. O. U. Fynbo, P. Hoff, H. Mach, T. Nilsson, K. Wilhelmsen-Rolander, H. Simon,
   A. Bickley, and the ISOLDE Collaboration
      Phys. Rev. C **65**, 034313/1-9 (2002)

Structure of High-Spin States in ^{91}Sr and ^{92}Sr
   E. A. Stefanova, M. Danchev, R. Schwengner, D. L. Balabanski, M. P. Carpenter,
   M. Djongolov, S. M. Fischer, D. J. Hartley, R. V. F. Janssens, W. F. Mueller, D. Nisius,
   W. Reviol, L. L. Riedinger, and O. Zeidan
      Phys. Rev. C **65**, 034323/1-10 (2002)

Widths of Astrophysically Important Resonances in ^{18}Ne
   B. Harss, C. L. Jiang, K. E. Rehm, J. P. Schiffer, J. Caggiano, P. Collon, J. P. Greene,
   D. Henderson, A. Heinz, R. V. F. Janssens, J. Nolen, R. C. Pardo, T. Pennington,
   R. H. Siemssen, A. A. Sonzogni, J. Uusitalo, I. Wiedenhöver, M. Paul, T. F. Wang, F. Borasi,
   R. E. Segel, J. C. Blackmon, M. Smith, A. Chen, and P. Parker
      Phys. Rev. C **65**, 035803/1-9 (2002)

Toward Complete Spectroscopy of ^{128}Pr and Rotational Structures in ^{126}Pr
  D. J. Hartley, L. L. Riedinger, M. Danchev, W. Reviol, O. Zeidan, Jing-ye Zhang, A. Galindo-
  Uribarri, C. J. Gross, C. Baktash, M. Lipoglavsek, S. D. Paul, D. C. Radford, C.-H. Yu,
  D. G. Sarantites, M. Devlin, M. P. Carpenter, R. V. F. Janssens, D. Seweryniak, and E. Padilla
    Phys. Rev. C **65**, 044329/1-22 (2002)

β Decay Studies of ^{109,107}Sb
  J. J. Ressler, W. B. Walters, D. S. Brenner, C. N. Davids, A. Heinz, G.-L. Poli, J. Shergur, and
  D. Seweryniak
    Phys. Rev. C **65**, 044330/1-12 (2002)

Testing Mean-Field Models Near the $N = Z$ Line: γ-Ray Spectroscopy of the $T_z = \frac{1}{2}$ Nucleus ^{73}Kr
  N. S. Kelsall, S. M. Fischer, D. P. Balamuth, G. C. Ball, M. P. Carpenter, R. M. Clark,
  J. Durell, P. Fallon, S. J. Freeman, P. A. Hausladen, R. V. F. Janssens, D. G. Jenkins,
  M. Leddy, C. J. Lister, A. 0. Macchiavelli, D. G. Sarantites, D. C. Schmidt, D. Seweryniak,
  C. E. Svensson, B. J. Varley, S. Vincent, R. Wadsworth, A. N. Wilson, A. V. Afanasjev,
  S. Frauendorf, I. Ragnarsson, and R. Wyss
    Phys. Rev. C **65**, 044331/1-13 (2002)

Excited States of the Proton Emitter ^{105}Sb
  M. Lipoglavšek, C. Baktash, M. P. Carpenter, D. J. Dean, T. Engeland, C. Fahlander,
  M. Hjorth-Jensen, R. V. F. Janssens, A. Likar, J. Nyberg, E. Osnes, S. D. Paul, A. Piechaczek,
  D. C. Radford, D. Rudolph, D. Seweryniak, D. G. Sarantites, M. Vencelj, and C. H. Yu
    Phys. Rev. C **65**, 051307(R)/1-4 (2002)

Core-Excited Smoothly Terminating Band in ^{114}Xe
  E. S. Paul, A. J. Boston, H. J. Chantler, J. P. Nolan, M. P. Carpenter, R. V. F. Janssens,
  F. G. Kondev, D. Seweryniak, C. J. Chiara, D. B. Fossan, T. Koike, K. Starosta,
  D. R. LaFosse, A. M. Fletcher, J. C. Lisle, D. Patel, J. F. Smith, W. Reviol, D. G. Sarantites,
  R. Wadsworth, A. N. Wilson, and I. Ragnarsson
    Phys. Rev. C **65**, 051308(R)/1-4 (2002)

Identification of New States in ^{26}Si Using the ^{29}Si(^{3}He,^{6}He)^{26}Si Reaction and Consequences for
the ^{25}Al $(p,\gamma)^{26}$Si Reaction Rate in Explosive Hydrogen Burning Environments
  J. A. Caggiano, W. Bradfield-Smith, R. Lewis, P. D. Parker, D. W. Visser, J. P. Greene,
  K. E. Rehm, D. W. Bardayan, and A. E. Champagne
    Phys. Rev. C **65**, 055801/1-6 (2002)

Centrality Dependence of the Charged Particle Multiplicity Near Midrapidity in Au + Au
Collisions at $\sqrt{s_{NN}} = 130$ and 200 GeV
  B. B. Back *et al.* (PHOBOS Collaboration)
    Phys. Rev. C **65**, 061901(R)/1-4 (2002)

$T = 0$ and $T = 1$ States in the Odd-Odd $N = Z$ Nucleus, $^{70}_{35}Br_{35}$

  D. G. Jenkins, N. S. Kelsall, C. J. Lister, D. P. Balamuth, M. P. Carpenter, T. A. Sienko,
  S. M. Fischer, R. M. Clark, P. Fallon, A. Görgen, A. 0. Macchiavelli, C. E. Svensson,
  R. Wadsworth, W. Reviol, D. G. Sarantites, G. C. Ball, J. Rikovska Stone, O. Juillet,
  P. Van Isacker, A. V. Afanasjev, and S. Frauendorf
    Phys. Rev. C **65**, 064307/1-16 (2002)

Breakup Time Scale Studied in the 8 GeV/$c\pi$ + ^{197}Au Reaction
  L. Pienkowski, K. Kwiatkowski, T. Lefort, W.-c. Hsi, L. Beaulieu, V. E. Viola, A. Botvina,
  R. G. Korteling, R. Laforest, E. Martin, E. Ramakrishnan, D. Rowland, A. Ruangma,
  E. Winchester, S. J. Yennello, B. Back, H. Breuer, S. Gushue, and L. P. Remsberg
    Phys. Rev. C **65**, 064606/1-8 (2002)

Confirmation of Triple Shape Coexistence in ^{107}Hg: Focal Plane Spectroscopy of the α Decay of ^{183}Pb
  D. G. Jenkins, A. N. Andreyev, R. D. Page, M. P. Carpenter, R. V. F. Janssens, C. J. Lister,
  F. G. Kondev, T. Enqvist, P. T. Greenlees, P. M. Jones, R. Julin, S. Juutinen, H. Kettunen,
  P. Kuusiniemi, M. Leino, A.-P. Leppännen, P. Nieminen, J. Pakarinen, P. Rahkila, J. Uusitalo,
  C. D. O'Leary, P. Raddon, A. Simons, R. Wadsworth, and D. T. Joss
    Phys. Rev. C **66**, 011301(R)/1-5 (2002)

Breakup of the Doubly Magic ^{100}Sn Core
  M. Lipoglavšek, C. Baktash, J. Blomqvist, M. P. Carpenter, D. J. Dean, T. Engeland,
  C. Fahlander, H. Hjorth-Jensen, R. V. F. Janssens, A. Likar, J. Nyberg, E. Osnes, S. D. Paul,
  A. Piechaczek, D. C. Radford, D. Rudolph, D. Seweryniak, D. G. Sarantites, M. Vencelj, and
  C.-H. Yu
    Phys. Rev. C **66**, 011302(R)/1-5 (2002)

Signature Inversion in Doubly Odd ^{124}La
  H. J. Chantler, E. S. Paul, A. J. Boston, M. P. Carpenter, R. Charity, C. J. Chiara,
  P. T. W. Choy, C. N. Davids, M. Devlin, A. M. Fletcher, D. B. Fossan, D. G. Jenkins,
  N. S. Kelsall, T. Koike, D. R. LaFosse, P. J. Nolan, D. G. Sarantites, D. Seweryniak,
  J. F. Smith, K. Starosta, R. Wadsworth, and A. N. Wilson
    Phys. Rev. C **66**, 014311/1-16 (2002)

Excitation Energies in ^{22}Mg from the ^{25}Mg(^{3}He,^{6}He)^{22}Mg Reaction
  J. A. Caggiano, W. Bradfield-Smith, J. P. Greene, R. Lewis, P. D. Parker, K. E. Rehm,
  and D. W. Visser
    Phys. Rev. C **66**, 015804/1-5 (2002)

Observation of Excited States in the Near-Drip-Line Nucleus ^{125}Pr
  A. N. Wilson, D. R. LaFosse, J. F. Smith, C. J. Chiara, A. J. Boston, M. P. Carpenter,
  H. J. Chantler, R. Charity, P. T. W. Choy, M. Devlin, A. M. Fletcher, D. B. Fossan,
  R. V. F. Janssens, D. G. Jenkins, N. S. Kelsall, F. G. Kondev, T. Koike, E. S. Paul,
  D. G. Sarantites, D. Seweryniak, K. Starosta, and R. Wadsworth
    Phys. Rev. C **66**, 021305(R)/1-5 (2002)

First Observation of ^{109}Te β^+ and Electron Capture Decay to Levels of ^{109}Sb
   J. J. Ressler, W. B. Walters, C. N. Davids, D. J. Dean, A. Heinz, M. Hjorth-Jensen,
   D. Seweryniak, and J. Shergur
     Phys. Rev. C **66**, 024308/1-7 (2002)

Evidence for a $1g_{9/2}$ Rotational Band in ^{51}Mn
   J. Ekman, D. Rudolph, C. Fahlander, I. Ragnarsson, C. Andreoiu, M. A. Bentley,
   M. P. Carpenter, R. J. Charity, R. M. Clark, M. Cromaz, P. Fallon, E. Ideguchi,
   A. 0. Macchiavelli, M. N. Mineva, W. Reviol, D. G. Sarantites, D. Seweryniak, V. Tomov,
   and S. J. Williams
     Phys. Rev. C **66**, 051301(R)/1-5 (2002)

Population of the 168-keV ($g_{7/2}$) Excited State in ^{103}Sn in the α Decay of ^{107}Te
   D. Seweryniak, W. B. Walters, A. Woehr, M. Lipoglavsek, J. Shergur, C. N. Davids, A. Heinz,
   and J. J. Ressler
     Phys. Rev. C **66**, 051307(R)/1-4 (2002)

Proton Emission in Au + Au Collisions at 6, 8, 10.8 GeV/Nucleon
   B. B. Back, R. R. Betts, J. Chang, W. C. Chang, C. Y. Chi, Y. Y. Chu, J. B. Cumming,
   J. C. Dunlop, W. Eldredge, S. Y. Fung, R. Ganz, E. Garcia, A. Gillitzer, G. Heintzelman,
   W. F. Henning, D. J. Hofman, B. Holzman, J. H. Kang, E. J. Kim, S. Y. Kim, Y. Kwon,
   D. McLeod, A. C. Mignerey, M. Moulson, V. Nanal, C. A. Ogilvie, R. Pak, A. Ruangma,
   D. E. Russ, R. K. Seto, P. J. Stanskas, G. S. F. Stephans, H. Q. Wang, F. L. H. Wolfs,
   A. H. Wuosmaa, H. Xiang, G. H. Xu, H. B. Yao, and C. M. Zou (E917 Collaboration)
     Phys. Rev. C **66**, 054901/1-10 (2002)

Rotational Band Structures in $N = 89$ ^{153}Gd
   T. B. Brown, M. A. Riley, D. Campbell, D. J. Hartley, F. G. Kondev, J. Pfohl,
   R. V. F. Janssens, S. M. Fischer, D. Nisius, P. Fallon, W. C. Ma, J. Simpson, and
   J. F. Sharpey-Schafer
     Phys. Rev. C **66**, 064320/1-13 (2002)

The 3rd International Conference on Exotic Nuclei and Atomic Masses (ENAM2001)
   C. N. Davids
     Nuclear Physics News **12**, 14-15 (2002)

A New Technique for Measuring g Factors of Excited States in Fission Fragments Using Large
Arrays of Ge Detectors
   D. Patel, A. G. Smith, G. S. Simpson, R. M. Wall, J. F. Smith, 0. J. Onakanmi, I. Ahmad,
   J. P. Greene, M. P. Carpenter, T. Lauritsen, C. J. Lister, R. V. F. Janssens, F. G. Kondev,
   D. Seweryniak, B. J. P. Gall, 0. Dorveaux, and B. Roux
     J. Phys. G **28**, 649-663 (2002)

High-Resolution In-Beam Particle Spectroscopy - New Results on Prompt Proton Emission from
^{58}Cu
  D. Rudolph, D. G. Sarantites, C. Andreoiu, C. Fahlander, D. P. Balamuth, R. J. Charity,
  M. Devlin, J. Eberth, A. Galindo-Uribarri, P. A. Hausladen, D. Seweryniak, L. G. Sobotka,
  and Th. Steinhardt
      Eur. Phys. J. A **14**, 137-146 (2002)

Evolution of Shapes in ^{59}Cu
  C. Andreoiu, D. Rudolph, I. Ragnarsson, C. Fahlander, R. A. E. Austin, M. P. Carpenter,
  R. M. Clark, J. Ekman, R. V. F. Janssens, T. L. Khoo, F. G. Kondev, T. Lauritsen,
  T. Rodinger, D. G. Sarantites, D. Seweryniak, T. Steinhardt, C. E. Svensson, O. Thelen,
  and J. C. Waddington
      Eur. Phys. J. A **14**, 317-348 (2002)

The Neutron and Proton Two-Particle Nucleus ^{134}Sb: New Low-Spin States Observed in the
Decay of ^{134}Sn and an Estimate of the Energy of the 7^- Isomer
  A. Korgul, H. Mach, B. Fogelberg, W. Urban, W. Kurcewicz, T. Rzaca-Urban, P. Hoff,
  H. Gausemel, J. Galy, J. L. Durell, W. R. Phillips, A. G. Smith, B. J. Varley, N. Schulz,
  I. Ahmad, L. R. Morss, M. Górska, V. 1. Isakov, K. I. Erokhina, J. Blomqvist, F. Andreozzi,
  F. Coraggio, A. Covello, and A. Gargano
      Eur. Phys. J. A **15**, 181-184 (2002)

First Results from the PHOBOS Experiment at RHIC
  Gunther Roland (for the PHOBOS Collaboration)
      Proceedings of the 15th International Conference on Ultra-Relativistic Nucleus-Nucleus
      Collisions (QM 2001), Long Island, NY, January 15-20, 2001; Nucl. Phys. **A698,** 54c-63c
      (2002)

$dN_{ch}/d\eta$ Distributions from PHOBOS
  A. H. Wuosmaa (for the PHOBOS Collaboration)
      Proceedings of the 15th International Conference on Ultra-Relativistic Nucleus-Nucleus
      Collisions (QM 2001), Long Island, NY, January 15-20, 2001; Nucl. Phys. **A698,** 88c-93c
      (2002)

The PHOBOS Detector at RHIC
  Robert Pak (for the PHOBOS Collaboration)
      Proceedings of the 15th International Conference on Ultra-Relativistic Nucleus-Nucleus
      Collisions (QM 2001), Long Island, NY, January 15-20, 2001; Nucl. Phys. **A698,** 416c-419c
      (2002)

Determination of the Collision Geometry and Measurement of the Centrality Dependence of
$dN/d\eta$ at Midrapidity
  Judith M. Katzy (for the PHOBOS Collaboration)
      Proceedings of the 15th International Conference on Ultrarelativistic Nucleus-Nucleus
      Collisions (QM 2001), Long Island, NY, January 15-20, 2001; Nucl. Phys. **A698,** 555c-558c
      (2002)

Charged Particle Flow Measurement for $|\eta| < 5.3$ with the PHOBOS Detector
  Inkyu Park (for the PHOBOS Collaboration)
    Proceedings of the 15th International Conference on Ultra-Relativistic Nucleus-Nucleus
    Collisions (QM 2001), Long Island, NY, January 15-20, 2001; Nucl. Phys. **A698,** 564c-570c
    (2002)

First Results from the PHOBOS Spectrometer
  Nigel George (for the PHOBOS Collaboration)
    Proceedings of the 15th International Conference on Ultra-Relativistic Nucleus-Nucleus
    Collisions (QM 2001), Long Island, NY, January 15-20, 2001; Nucl. Phys. **A698,** 655c-658c
    (2002)

A Kinematically Complete Measurement of the Coulomb Dissociation of ^{8}B
  B. Davids, D. W. Anthony, T. Aumann, Sam M. Austin, T. Baumann, D. Bazin,
  R. R. C. Clement, P. A. Lofy, T. Nakamura, B. M. Sherrill, J. Yurkon, C. N. Davids,
  and H. Esbensen
    Proceedings of the 5th International Conference on Radioactive Nuclear Beams (RNB-5),
    Divonne, France, April 3-8, 2000; Nucl. Phys. **A701,** 14c-17c (2002)

Performance of the PHOBOS Silicon Sensors
  M. P. Decowski, B. B. Back, M. D. Baker, D. S. Barton, R. R. Betts, R. Bindel,
  A. Budzanowski, W. Busza, A. Carroll, E. Garcia, N. George, K. Gulbrandsen, S. Gushue,
  C. Halliwell, J. Hamblen, G. A. Heintzelman, C. Henderson, R. Holyńiski, D. J. Hofman,
  B. Holzman, E. Johnson, J. L. Kane, J. Katzy, N. Khan, W. Kucewicz, P. Kulinich, W. T. Lin,
  S. Manly, D. McLeod, J. Michalowski, A. C. Mignerey, J. Mülmenstädt, R. Nouicer,
  A. Olszewski, R. Pak, 1. C. Park, H. Pernegger, C. Reed, L. P. Remsberg, M. Reuter,
  C. Roland, G. Roland, L. Rosenberg, P. Sarin, P. Sawicki, W. Skulski, S. G. Steadman,
  G. S. F. Stephans, P. Steinberg, M. Stodulski, A. Sukhanov, J.-L. Tang, R. Teng, A. Trzupek,
  C. Vale, G. J. van Nieuwenhuizen, R. Verdier, B. Wadsworth, F. L. H. Wolfs, B. Wosiek,
  K. Woźniak, A. H. Wuosmaa, and B. Wyslouch
    Proceedings of the 9th International Vienna Conference on Instrumentation, Vienna, Austria,
    February 19-23, 2001; Nucl. Instrum. Methods **A478,** 299-302 (2002)

Preparation of Isotopic Ruthenium Targets Using an Ion Beam Sputtering Source
  John P. Greene
    Proceedings of the 20th World Conference of the International Nuclear Target Development
    Society (INTDS), Antwerp, Belgium, October 2-6, 2000; Nucl. Instrum. Methods **A480,**
    119-123 (2002)

Results from the PHOBOS Experiment at RHIC
  B. B. Back (for the PHOBOS Collaboration)
    Proceedings of the 17th Winter Workshop on Nuclear Dynamics, Park City, UT, March 10-
    17, 2001; Acta Phys. Hung. **15**, 225-235 (2002)

Structure and Spectroscopy of Transcurium Nuclei
  I. Ahmad
    Proceedings of the 2nd International Symposium on Advanced Science Research
    (ASR2001), Tokai, Ibaraki, Japan, November, 13-15, 2001; Journal of Nuclear and
    Radiochemical Sciences **3**, 179-182 (2002)

Specific Heat and Latent Heat in Finite and Infinite One-Component Plasmas
  J. P. Schiffer
    Proceedings of the 2001 Workshop on Non-Neutral Plasmas, San Diego, CA, July 30-
    August 2, 2001, AIP Conference Proceedings **606**, 127-134 (2002)

Possible Triaxial Superdeformation in ^{174}Hf
  D. J. Hartley, M. Djongolov, L. L. Riedinger, F. G. Kondev, R. V. F. Janssens, K. Abu
  Saleem, I. Ahmad, D. L. Balabanski, M. P. Carpenter, P. Chowdhury, D. M. Cullen,
  M. Danchev, G. D. Dracoulis, H. El-Masri, J. Goon, A. Heinz, R. A. Kaye, T. L. Khoo,
  T. Lauritsen, C. J. Lister, E. F. Moore, M. A. Riley, D. Seweryniak, I. Shestakova, G. Sletten,
  P. M. Walker, C. Wheldon, I. Wiedenhöver, O. Zeidan, and Jing-ye Zhang
    Proceedings of the International Conference on Nuclear Structure, Grand Teton National
    Park, WY, May 22-25, 2002, eds. Ani Aprahamian, Jolie A. Cizewski, Stuart Pittel, and N.
    Victor Zamfir, AIP Conference Proceedings **638**, 119-123 (2002)

Octupole Effects at Super and Normal Deformation
  R. V. F. Janssens
    Proceedings of the International Conference on Nuclear Structure, Grand Teton National
    Park, WY, May 22-25, 2002, eds. Ani Aprahamian, Jolie A. Cizewski, Stuart Pittel,
    and N. Victor Zamfir,
      AIP Conference Proceedings **638**, 205-212 (2002)

Recoil Separators
  Cary N. Davids
    14th International Conference on Electromagnetic Isotope Separators and Techniques
    Related to Their Applications (EMIS-14), Victoria, B.C., Canada, May 6-10, 2002, Book of
    Abstracts, p. 7 (2002)

Improvements in the Injection System of the Canadian Penning Trap Mass Spectrometer
  J. Clark, R. C. Barber, K. S. Sharma, J. Vaz, J. C. Wang, C. Boudreau, F. Buchinger,
  J. E. Crawford, S. Gulick, J. K. P. Lee, R. B. Moore, J. C. Hardy, J. A. Caggiano, A. Heinz,
  G. Savard, D. Seweryniak, and G. Sprouse
    14th International Conference on Electromagnetic Isotope Separators and Techniques
    Related to Their Applications (EMIS-14), Victoria, B.C., Canada, May 6-10, 2002, Book of
    Abstracts, p. 117 (2002)

Counting ^{44}Ti Nuclei from the ^{40}Ca$(\alpha,\gamma)^{44}$Ti Reaction
  M. Paul, C. Feldstein, I. Ahmad, D. Berkovits, C. Bordeanu, J. Caggiano, J. Goerres,
  J. Greene, M. Hass, A. Heinz, D. Henderson, S. K. Hui, R. V. F. Janssens, C. L. Jiang,
  S. Jiang, R. C. Pardo, T. Pennington, K. E. Rehm, G. Savard, G. Verri, R. Vondrasek,
  I. Wiedenhöver, and M. Wiescher
    7th International Symposium on Nuclei in the Cosmos VII, Fuji-Yoshida, Japan, July 8-12,
    2002, Book of Abstracts, p. 43 (2002)

High Energy Photons from Very Symmetric Reactions: The Giant Dipole Resonance in the
Highly Rotating ^{179}Au Nucleus
  F. Camera, A. Bracco, F. Della Vedova, S. Leoni, S. Mantovani, B. Million, M. Pignanelli,
  O. Wieland, M. Carpenter, V. Nanal, D. Hofman, B. B. Back, F. G. Kondev, T. L. Khoo,
  C. J. Lister, A. M. Heinz, R. V. F. Janssens, D. Jenkins, T. Lauritsen, E. F. Moore,
  D. Seweryniak, M. Thoenessen, R. Varner, I. Dioszegi, and A. Lopez-Martens
    Conference on Frontiers of Nuclear Structure, Berkeley, CA, July 29-August 2, 2002,
    LBNL-50598 Abs., Book of Abstracts, p. 5 (2002)

Shape Co-Existence at the Outer Edges of Stability
  M. P. Carpenter, F. G. Kondev, R. V. F. Janssens, K. Abu Saleem, I. Ahmad, M. Alcorta,
  H. Amro, J. Caggiano, J. A. Cizewski, M. Danchev, C. N. Davids, D. J. Hartley, A. Heinz,
  B. Herskind, D. G. Jenkins, T. L. Khoo, T. Lauritsen, C. J. Lister, W. C. Ma, G. L. Poli,
  P. Reiter, J. Ressler, W. Reviol, L. L. Riedinger, D. G. Sarantites, D. Seweryniak, S. Siem,
  M. B. Smith, A. A. Sonzogni, P. G. Varmette, and I. Wiedenhöver
    Conference on Frontiers of Nuclear Structure, Berkeley, CA, July 29-August 2, 2002,
    LBNL-50598 Abs., Book of Abstracts, p. 6 (2002)

Very Extended Shapes in ^{108}Cd
  A. Görgen, R. M. Clark, P. Fallon, M. Cromaz, M. A. Deleplanque, R. M. Diamond,
  G. J. Lane, I. Y. Lee, A. O. Macchiavelli, R. G. Ramos, F. S. Stephens, C. E. Svensson,
  K. Vetter, D. Ward, M. P. Carpenter, R. V. F. Janssens, and R. Wadsworth
    Conference on Frontiers of Nuclear Structure, Berkeley, CA, July 29-August 2, 2002,
    LBNL-50598 Abs., Book of Abstracts, p. 19 (2002)

Insights into the Origin of Nuclear Molecules from Studies of the Heavy Ion Radiative Capture
Reaction
  D. G. Jenkins, C. J. Lister, B. Truett, R. V. F. Janssens, T. L. Khoo, A. Wuosmaa,
  B. R. Fulton, J. Pearson, M. Freer, R. M. Clark, P. Fallon, A. Görgen, and A. O. Macchiavelli
    Conference on Frontiers of Nuclear Structure, Berkeley, CA, July 29-August 2, 2002,
    LBNL-50598 Abs., Book of Abstracts, p. 27 (2002)

Narrow Spreading Widths of Excited Bands in a Superdeformed Well
  A. Lopez-Martens, T. L. Khoo, I. Calderin, T. Dossing, B. Herskind, T. Lauritsen, M. Matsuo,
  K. Yoshida, D. Ackermann, S. Asztalos, D. J. Blumenthal, I. Ahmad, H. Amro,
  M. P. Carpenter, R. M. Clark, M. A. Deleplanque, R. M. Diamond, P. Fallon, S. M. Fischer,
  G. Hackman, F. Hannachi, R. V. F. Janssens, A. Korichi, R. Krücken, I. Y. Lee,
  A. O. Macchiavelli, R. W. MacLeod, D. Nisius, G. D. Schmid, F. S. Stephens, and K. Vetter
    Conference on Frontiers of Nuclear Structure, Berkeley, CA, July 29-August 2, 2002,
    LBNL-50598 Abs., Book of Abstracts, p. 29 (2002)

Linking of Yrast and Excite Superdeformed Bands in $^{152}_{66}$Dy$_{86}$

  T. Lauritsen, M. P. Carpenter, T. Dossing, P. Fallon, B. Herskind, R. V. F. Janssens,
  D. G. Jenkins, T. L. Khoo, F. G. Kondev, A. Lopez-Martens, A. O. Macchiavelli, D. Ward,
  K. S. Abu Saleem, I. Ahmad, R. Clark, M. Cromaz, J. P. Greene, F. Hannachi, A. M. Heinz,
  A. Korichi, G. Lane, C. J. Lister, P. Reiter, D. Seweryniak, S. Siem, R. C. Vondrasek,
  and I. Wiedenhöver
    Conference on Frontiers of Nuclear Structure, Berkeley, CA, July 29-August 2, 2002,
    LBNL-50598 Abs., Book of Abstracts, p. 33 (2002)

Low Level Density in Odd-Odd N = Z in the A ~ 70 Region
  C. J. Lister, D. G. Jenkins, S. M. Fischer, D. P. Balamuth, and J. Rikovska Stone
    Conference on Frontiers of Nuclear Structure, Berkeley, CA, July 29-August 2, 2002,
    LBNL-50598 Abs., Book of Abstracts, p. 35 (2002)

Possible Triaxial Superdeformed Bands in ^{174}Hf
  M. Djongolov, D. J. Hartley, L. L. Riedinger, F. G. Kondev, R. V. F. Janssens, E. F. Moore,
  K. Abu Saleem, I. Ahmad, D. L. Balabanski, M. P. Carpenter, P. Chowdhury, D. M. Cullen,
  M. Danchev, G. D. Dracoulis, H. El-Masri, J. Goon, A. Heinz, R. A. Kaye, T. L. Khoo,
  T. Lauritsen, C. J. Lister, M. A Riley, D. Seweryniak, I. Shestakova, G. Sletten, P. M. Walker,
  C. Wheldon, I. Wiedhoever, and 0. Zeidan
    Conference on Frontiers of Nuclear Structure, Berkeley, CA, July 29-August 2, 2002,
    LBNL-50598 Abs., Book of Abstracts, p. 48 (2002)

Proton Decay Studies at ATLAS
  C. N. Davids, D. Seweryniak, P. J. Woods, T. Davinson, A. Heinz, H. Mahmud, P. Munro,
  J. J. Ressler, J. Shergur, W. B. Walters, and A. Woehr
    Conference on Frontiers of Nuclear Structure, Berkeley, CA, July 29-August 2, 2002,
    LBNL-50598 Abs., Book of Abstracts, p. 51 (2002)

Limits of the Energy-Spin Phase Space Beyond the Proton Drip Line: Entry Distributions of Pt
and Au Isobars
  M. B. Smith, J. A. Cizewski, M. P. Carpenter, F. G. Kondev, T. L. Khoo, T. Lauritsen,
  R. V. F. Janssens, K. Abu Saleem, I. Ahmad, H. Amro, M. Danchev, C. N. Davids,
  D. J. Hartley, A. Heinz, C. J. Lister, W. C. Ma, G. L. Poli, J. J. Ressler, W. Reviol,
  L. L. Riedinger, D. Seweryniak, and I. Wiedenhöver
    Conference on Frontiers of Nuclear Structure, Berkeley, CA, July 29-August 2, 2002,
    LBNL-50598 Abs., Book of Abstracts, p. 54 (2002)

High Spin Studies of N ~ Z Nuclei in the Mass 70 Region
  N. S. Kelsall, C. E. Svensson, S. Fischer, D. E. Appelbe, R. A. E. Austin, D. P. Balamuth,
  G. C. Ball, J. A. Cameron, M. P. Carpenter, R. M. Clark, M. Cromaz, M. A. Deleplanque,
  R. M. Diamond, J. L. Durell, P. Fallon, S. J. Freeman, P. A. Hausladen, D. F. Hodgson,
  R. V. F. Janssens, D. G. Jenkins, G. J. Lane, M. J. Leddy, C. J. Lister, A. O. Macchiavelli,
  C. D. O'Leary, D. G. Sarantites, F. S. Stephens, D. C. Schmidt, D. Seweryniak, B. J. Varley,
  S. Vincent, K. Vetter, J. C. Waddington, R. Wadsworth, D. Ward, A. N. Wilson,
  A. V. Afanasjev, S. Frauendorf, I. Ragnarsson, and R. Wyss
    Conference on Frontiers of Nuclear Structure, Berkeley, CA, July 29-August 2, 2002,
    LBNL-50598 Abs., Book of Abstracts, p. 62 (2002)

Coulomb Excitation and Few Nucleon Transfer Reactions with ^{209}Bi Beams on ^{237}Np and
^{241}Am Targets
  K. Abu Saleem, R. V. F. Janssens, M. P. Carpenter, F. G. Kondev, I. Wiedenhöver,
  G. Hackman, I. Ahmad, J. P. Greene, J. Caggiano, P. Chowdhury, D. Cline, A. Heinz,
  T. L. Khoo, T. Lauritsen, C. J. Lister, A. O. Macchiavelli, D. Seweryniak, and A. Sonzogni
    Conference on Frontiers of Nuclear Structure, Berkeley, CA, July 29-August 2, 2002,
    LBNL-50598 Abs., Book of Abstracts, p. 65 (2002)

High Spin States in ^{38}Ar
  R. A. E. Austin, D. E. Appelbe, G. C. Ball, M. P. Carpenter, R. M. Clark, M. Cromaz,
  R. V. F. Janssens, A. O. Macchiavelli, D. Rudolph, D. G. Sarantites, C. E. Svensson,
  and J. C. Waddington
    Conference on Frontiers of Nuclear Structure, Berkeley, CA, July 29-August 2, 2002,
    LBNL-50598 Abs., Book of Abstracts, p. 68 (2002)

Dramatic Structure Changes Along the Yrast Line in ^{160}Yb
  D. B. Campbell, M. A. Riley, J. Simpson, A. Pipidis, C. Chandler, J. Lisle, M. A. Bentley,
  F. G. Kondev, L. L. Riedinger, D. E. Hartley, P. Fallon, R. Clark, D. C. Radford,
  I. Ragnarsson, and A. Afanasjev
    Conference on Frontiers of Nuclear Structure, Berkeley, CA, July 29-August 2, 2002,
    LBNL-50598 Abs., Book of Abstracts, p. 75 (2002)

Signature Inversion in Doubly Odd ^{124}La
  H. J. Chantler, E. S. Paul, A. J. Boston, M. P. Carpenter, R. Charity, C. J. Chiara,
  P. T. W. Choy, C. N. Davids, M. Devlin, A. M. Fletcher, D. B. Fossan, D. G. Jenkins,
  N. S. Kelsall, T. Koike, D. R. LaFosse, P. J. Nolan, D. G. Sarantites, D. Seweryniak,
  J. F. Smith, K. Starosta, R. Wadsworth, and A. N. Wilson
    Conference on Frontiers of Nuclear Structure, Berkeley, CA, July 29-August 2, 2002,
    LBNL-50598 Abs., Book of Abstracts, p. 81 (2002)

Measurement of B(M1)-Values in the Band Crossing Region of Shears Band 1 in ^{197}Pb and
Their Interpretation in the Semi-Classical Model
   J. R. Cooper, R. Krucken, C. W. Beausang, J. R. Novak, P. von Brentano, A. Dewald,
   G. Kemper, T. Klug, M. P. Carpenter, R. V. F. Janssens, T. Lauritsen, I. Wiedenhöver,
   R. M. Clark, and A. 0. Macchiavelli
      Conference on Frontiers of Nuclear Structure, Berkeley, CA, July 29-August 2, 2002,
      LBNL-50598 Abs., Book of Abstracts, p. 82 (2002)

Identification of Excited States in ^{140}Dy
   D. M. Cullen, M. P. Carpenter, C. N. Davids, A. M. Fletcher, S. J. Freeman, R. V. F. Janssens,
   F. G. Kondev, C. J. Lister, L. K. Pattison, D. Seweryniak, J. F. Smith, A. M. Bruce, K. Abu
   Saleem, I. Ahmad, A. Heinz, T. L. Khoo, E. F. Moore, G. Mukherjee, C. Wheldon, and
   A. Woehr
      Conference on Frontiers of Nuclear Structure, Berkeley, CA, July 29-August 2, 2002,
      LBNL-50598 Abs., Book of Abstracts, p. 85 (2002)

Are *np*-Pairs Playing a Role in the *A = 46*, *T = 1* Triplet?
   P. E. Garrett, W. E. Ormand, R. W. Bauer, J. A. Becker, L. A. Bernstein, D. Appelbe,
   J. A. Cameron, M. P. Carpenter, R. V. F. Janssens, C. J. Lister, D. Seweryniak, D. D. Warner,
   and E. Tavukcu
      Conference on Frontiers of Nuclear Structure, Berkeley, CA, July 29-August 2, 2002,
      LBNL-50598 Abs., Book of Abstracts, p. 91 (2002)

A Search for Multi-Quasiparticle Isomers in Odd-Mass Nuclei Near A ~130
   F. G. Kondev, D. J. Hartley, G. D. Dracoulis, R. A. Bark, A. P. Byrne, M. P. Carpenter,
   J. C. Hazel, R. V. F. Janssens, T. Kibedi, G. J. Lane, L. L. Riedinger, and A. N. Wilson
      Conference on Frontiers of Nuclear Structure, Berkeley, CA, July 29-August 2, 2002,
      LBNL-50598 Abs., Book of Abstracts, p. 100 (2002)

Ne, Na and Al Burning in Astrophysically Important (p,γ) Reactions
   C. J. Lister, D. G. Jenkins, B. Truett, B. R. Fulton, J. Pearson, M. P. Carpenter, G. Mukherjee,
   K. E. Rehm, A. H. Wuosmaa, R. A. Kaye, M. Freer, A. 0. Macchiavelli, P. Fallon, and
   A. Gorgen
      Conference on Frontiers of Nuclear Structure, Berkeley, CA, July 29-August 2, 2002,
      LBNL-50598 Abs., Book of Abstracts, p. 107 (2002)

Coulomb Excitation of Stable Even-Even Xenon Nuclei from *A* = 124 to 134
   W. F. Mueller, M. P. Carpenter, J. A. Church, D. C. Dinca, A. Gade, T. Glasmacher,
   D. T. Henderson, Z. Hu, R. V. F. Janssens, C. J. Lister, P. A. Lofy, K. L. Miller, E. F. Moore,
   H. Olliver, T. O. Pennington, B. C. Perry, B. T. Roeder, and I. Wiedenhöver
      Conference on Frontiers of Nuclear Structure, Berkeley, CA, July 29-August 2, 2002,
      LBNL-50598 Abs., Book of Abstracts, p. 114 (2002)

Decay of a High-K Isomer in ^{254}No by γ and Electron Spectroscopy
  G. Mukherjee, T. L. Khoo, D. Seweryniak, I. Ahmad, A. Aprahamian, P. Boutachkov,
  P. A. Butler, M. P. Carpenter, P. Chowdhury, J. A. Cizewski, C. N. Davids, A. Heinz,
  R. Herzberg, R. V. F. Janssens, G. Jones, R. Julin, F. G. Kondev, T. Lauritsen, M. Leino,
  C. J. Lister, E. Ngijoi-yogo, P. Reiter, M. Shawcross, M. B. Smith, A. Teymurazyan,
  J. Uusitalo, and A. Woehr
    Conference on Frontiers of Nuclear Structure, Berkeley, CA, July 29-August 2, 2002,
    LBNL-50598 Abs., Book of Abstracts, p. 115 (2002)

Identification of the $K^\pi = 25^+$ Structure in ^{182}Os
  L. K. Pattison, D. M. Cullen, J. F. Smith, A. M. Fletcher, P. M. Walker, H. M. El-Masri,
  Zs. Podolyák, R. J. Wood, C. Scholey, C. Wheldon, G. Mukherjee, D. Balabanski,
  M. Djongolov, Th. Dalsgaard, H. Thisgaard, G. Sletten, F. Kondev, D. Jenkins,
  G. D. Dracoulis, G. J. Lane, I.-Y. Lee, A. O. Macchiavelli, S. Frauendorf, and D. Almehed
    Conference on Frontiers of Nuclear Structure, Berkeley, CA, July 29-August 2, 2002,
    LBNL-50598 Abs., Book of Abstracts, p. 125 (2002)

High Spin States in ^{114}Xe: Building a Bridge Between the Mass 110 and 130 Regions
  E. S. Paul, A. J. Boston, J. P. Carpenter, H. J. Chantler, C. J. Chiara, A. M. Fletcher,
  D. B. Fossan, R. V. F. Janssens, T. Koike, F. G. Kondev, D. R. LaFosse, J. C. Lisle,
  P. J. Nolan, D. Patel, W. Reviol, D. G. Sarantites, D. Seweryniak, J. F. Smith, K. Starosta,
  R. Wadsworth, A. N. Wilson, and I. Ragnarsson
    Conference on Frontiers of Nuclear Structure, Berkeley, CA, July 29-August 2, 2002,
    LBNL-50598 Abs., Book of Abstracts, p. 126 (2002)

Mirror Symmetry in $^{53}_{27}\text{Co}_{26}$ and $^{53}_{27}\text{Fe}_{27}$
  S. J. Williams, M. A. Bentley, J. Ekman, D. T. Joss, C. D. O'Leary, D. Rudolph,
  D. D. Warner, C. Andriou, A. M. Bruce, J. A. Cameron, M. P. Carpenter, R. M. Clark,
  C. Fahlander, P. Fallon, L. Frankland, W. Gelletly, E. Ideguchi, C. J. Lister,
  A. 0. Macchiavelli, G. Martínez-Pinedo, M. N. Mineva, A. Poves, P. H. Regan, P. Reiter,
  W. Reviol, B. Rubio, J. Sanchez-Solano, D. G. Sarantites, D. Seweryniak, C. Svensson,
  and S. M. Vincent
    Conference on Frontiers of Nuclear Structure, Berkeley, CA, July 29-August 2, 2002,
    LBNL-50598 Abs., Book of Abstracts, p. 143 (2002)

Candidate Chiral Bands in the Odd-A Nucleus ^{135}Nd
  S. Zhu, U. Garg, B. K. Nayak, S. Frauendorf, S. S. Ghugre, N. S. Pattabhiraman, D. B. Fossan,
  K. Starosta, C. Vaman, A. 0. Macchiavelli, R. V. F. Janssens, and R. S. Chakrawarthy
    Conference on Frontiers of Nuclear Structure, Berkeley, CA, July 29-August 2, 2002,
    LBNL-50598 Abs., Book of Abstracts, p. 148 (2002)

New Theoretical Results on the Proton Decay of Deformed and Near-Spherical Nuclei
    Cary N. Davids and Henning Esbensen
        Proceedings of the Conference on Exotic Nuclei at the Proton Drip Line, Camerino, Italy,
        September 25-28, 2001, eds. C. M. Petrache and G. Lo Bianco, pp. 101-111 (2002)

Identification of Excited States in ^{140}Dy
    M. P. Carpenter, C. N. Davids, R. V. F. Janssens, F. G. Kondev, C. J. Lister, D. Seweryniak,
    K. Abu Saleem, I. Ahmad, A. Heinz, T. L. Khoo, E. F. Moore, D. M. Cullen, A. M. Fletcher,
    S. J. Freeman, L. K. Pattison, J. F. Smith, A. M. Bruce, G. Mukherjee, C. Wheldon, and
    A. Woehr
        April 2002 Meeting of the American Physical Society, Albuquerque, NM, April 20-23,
        2002; Bull. Am. Phys. Soc. **47**, 70 (2002)

High-K Bands at High Spin in ^{174}Hf
    D. J. Hartley, L. L. Riedinger, M. Djongolov, D. Balabanski, M. Danchev, J. Goon, O. Zeidan,
    F. G. Kondev, R. V. F. Janssens, K. Abu Saleem, I. Ahmad, M. P. Carpenter, A. Heinz,
    T. L. Khoo, T. Lauritsen, C. J. Lister, D. Seweryniak, I. Wiedenhöver, G. D. Dracoulis,
    P. Chowdhury, I. Shestakova, D. M. Cullen, C. Wheldon, P. M. Walker, H. El-Masri,
    M. A. Riley, R. A. Kaye, and G. Sletten
        April 2002 Meeting of the American Physical Society, Albuquerque, NM, April 20-23,
        2002; Bull. Am. Phys. Soc. **47**, 71 (2002)

Triaxial Superdeformed Bands in ^{174}Hf
    M. Djongolov, D. J. Hartley, L. L. Riedinger, D. L. Balabanski, M. Danchev, J. Goon,
    O. Zeidan, F. G. Kondev, R. V. F. Janssens, K. Abu Saleem, I. Ahmad, M. P. Carpenter,
    A. Heinz, T. L. Khoo, T. Lauritsen, C. J. Lister, D. Seweryniak, I. Wiedenhöver,
    P. Chowdhury, I. Shestakova, D. M. Cullen, C. Wheldon, G. D. Dracoulis, H. El-Masri,
    P. M. Walker, R. A. Kaye, M. A. Riley, and G. Sletten
        April 2002 Meeting of the American Physical Society, Albuquerque, NM, April 20-23,
        2002; Bull. Am. Phys. Soc. **47**, 71 (2002)

Evidence of Fine Structure a Peaks in ^{174,176}Au
    J. Tm. Goon, D. J. Hartley, M. Danchev, L. L. Riedinger, O. Zeidan, F. G. Kondev,
    M. P. Carpenter, R. V. F. Janssens, K. H. Abu Saleem, I. Ahmad, C. N. Davids, A. Heinz,
    T. L. Khoo, T. Lauritsen, C. J. Lister, G. L. Poli, J. Ressler, D. Seweryniak, I. Wiedenhöver,
    W. C. Ma, H. Amro, W. Reviol, J. A. Cizewski, and M. Smith
        April 2002 Meeting of the American Physical Society, Albuquerque, NM, April 20-23,
        2002; Bull. Am. Phys. Soc. **47**, 71 (2002)

Production and Decay of ^{257}Rf
    A. Heinz, R. V. F. Janssens, D. Seweryniak, K. Abu Saleem, B. Back, M. P. Carpenter,
    C. N. Davids, J. P. Greene, D. J. Henderson, C.-L. Jiang, T. L. Khoo, F. G. Kondev,
    T. Lauritsen, C. J. Lister, E. F. Moore, R. C. Pardo, T. Pennington, G. Savard, J. P. Schiffer,
    A. Woehr, J. Shergur, P. Collon, and M. B. Smith
        April 2002 Meeting of the American Physical Society, Albuquerque, NM, April 20-23,
        2002; Bull. Am. Phys. Soc. **47**, 72 (2002)

High Spin States in ^{237}Np and ^{241}Am
   K. Abu Saleem, R. V. F. Janssens, F. G. Kondev, I. Ahmad, J. Caggiano, M. P. Carpenter,
   J. P. Greene, A. Heinz, T. L. Khoo, T. Lauritsen, C. J. Lister, D. Seweryniak, I. Wiedenhöver,
   G. Hackman, P. Chowdhury, D. Cline, C. Wun, M. Devlin, N. Fotiades, E. H. Seabury,
   and A. O. Macchiavelli
      April 2002 Meeting of the American Physical Society, Albuquerque, NM, April 20-23,
      2002; Bull. Am. Phys. Soc. **47**, 72 (2002)

Excited Rotational! Structure with a Very Extended Shape in ^{108}Cd
   A. Görgen, R. M. Clark, P. Fallon, M. Cromaz, M. A. Deleplanque, R. M. Diamond,
   G. J. Lane, I. Y. Lee, A. O. Macchiavelli, R. G. Ramos, F. S. Stephens, C. E. Svensson,
   K. Vetter, D. Ward, M. P. Carpenter, R. V. F. Janssens, and R. Wadsworth
      April 2002 Meting of the American Physical Society, Albuquerque, NM, April 20-23, 2002;
      Bull. Am. Phys. Soc. **47**, 73 (2002)

Neutron-Proton Correlations in A ~ 80, N ~ Z Nuclei
   S. M. Fischer
      April 2002 Meting of the American Physical Society, Albuquerque, NM, April 20-23, 2002;
      Bull. Am. Phys. Soc. **47**, 117 (2002)

Mass Measurement of ^{68}Se Using the Beta End-Point Method
   Mark Shawcross, Arthur Teymurazyan, Ani Aprahamian, Plamen Boutachkov, Irena Zartova,
   Jose L. Galache, Joachim Goerres, Michael Wiescher, Darek Seweryniak, Andreas Woehr,
   Robert Janssens, Cary Davids, Andreas Heinz, Daeg Brenner, and Susan M. Fischer
      April 2002 Meting of the American Physical Society, Albuquerque, NM, April 20-23, 2002;
      Bull. Am. Phys. Soc. **47**, 118 (2002)

Deformed Structures in the Vicinity of $^{40}_{20}$Ca$_{20}$

   C. J. Chiara, E. Ideguchi, M. Devlin, F. Lerma, W. Reviol, S. K. Ryu, D. G. Sarantites,
   J. N. Wilson, C. Baktash, A. Galindo-Uribarri, D. Rudolph, D. R. Lafosse, M. P. Carpenter,
   R. V. F. Janssens, T. Lauritsen, C. J. Lister, P. Reiter, D. Seweryniak, P. Fallon, A. Görgen,
   and A. O. Macchiavelli
      April 2002 Meeting of the American Physical Society, Albuquerque, NM, April 20-23,
      2002; Bull. Am. Phys. Soc. **47**, 118 (2002)

Spectroscopy of the $N = Z$ Nucleus ^{46}V
   P. E. Garrett, W. E. Ormand, R. W. Bauer, J. A. Becker, L. A. Bernstein, D. Appelbe,
   J. A. Cameron, M. Carpenter, R. V. F. Janssens, C. J. Lister, D. Seweryniak, D. D. Warner,
   and E. Tavukcu
      April 2002 Meeting of the American Physical Society, Albuquerque, NM, April 20-23,
      2002; Bull. Am. Phys. Soc. **47**, 119 (2002)

Measurement of the ^{8}B Neutrino Spectrum with a New Technique
   W. T. Winter, K. E. Rehm, C. L. Jiang, I. Ahmad, S. J. Freedman, J. Greene, A. Heinz,
   D. Henderson, R. V. F. Janssens, E. F. Moore, G. Mukherjee, R. C. Pardo, M. Paul,
   T. Pennington, G. Savard, J. P. Schiffer, D. Seweryniak, and G. Zinkann
      April 2002 Meeting of the American Physical Society, Albuquerque, NM, April 20-23,
      2002; Bull. Am. Phys. Soc. **47**, 151 (2002)

Pushing Towards the Sensitivity Limits of Gammasphere
   C. J. (Kim) Lister
      2002 Fall Meeting of the Division of Nuclear Physics of the American Physical Society, East
      Lansing, MI, October 9-12, 2002; Bull. Am. Phys. Soc. **47**, 11 (2002)

Precision Mass Measurements Along the rp- and r-Process Paths
   Guy Savard
      2002 Fall Meeting of the Division of Nuclear Physics of the American Physical Society, East
      Lansing, MI, October 9-12, 2002; Bull. Am. Phys. Soc. **47**, 12 (2002)

Collectivity in the Neutron-Rich Nuclei ^{34}Mg ^{35,36}Al, and ^{37}Si
   J. A. Church, C. M. Campbell, D.-C. Dinca, J. Enders, T. Glasmacher, Z. Hu, K. L. Miller,
   W. F. Mueller, H. Olliver, B. C. Perry, M. Steiner, and A. Stolz
      2002 Fall Meeting of the Division of Nuclear Physics of the American Physical Society, East
      Lansing, MI, October 9-12, 2002; Bull. Am. Phys. Soc. **47**, 23 (2002)

Observation of a Sharp Band Crossing in ^{68}Se
   S. M. Fischer, C. J. Lister, and D. P. Balamuth
      2002 Fall Meeting of the Division of Nuclear Physics of the American Physical Society, East
      Lansing, MI, October 9-12, 2002; Bull. Am. Phys. Soc. **47**, 65 (2002)

First Observation of ^{109}Te β^+ and EC Decay to Levels in ^{109}Sb
   Jason Shergur, Jo Ressler, William Walters, Cary Davids, David Dean, Andreas Heinz,
   Morten Hjorth-Jensen, and Dariusz Seweryniak
      2002 Fall Meeting of the Division of Nuclear Physics of the American Physical Society, East
      Lansing, MI, October 9-12, 2002; Bull. Am. Phys. Soc. **47**, 66 (2002)

The Branching Ratio $\Gamma_\alpha/\Gamma\gamma$ of the 4.033 MeV State in ^{19}
   K. E. Rehm, A. H. Wuosmaa, C. L. Jiang, J. Greene, A. Heinz, D. Henderson,
   R. V. F. Janssens, E. F. Moore, G. Mukherjee, R. C. Pardo, T. Pennington, J. P. Schiffer,
   R. H. Siemssen, L. Jisonna, R. E. Segel, and M. Paul
      2002 Fall Meeting of the Division of Nuclear Physics of the American Physical Society, East
      Lansing, MI, October 9-12, 2002; Bull. Am. Phys. Soc. **47**, 67 (2002)

Multi-Particle-Gamma-Ray Angular Correlation Measurements in ^{12}C + ^{12}C Inelastic Scattering
   A. H. Wuosmaa, J. Caggiano, M. P. Carpenter, A. Heinz, R. V. F. Janssens, F. G. Kondev,
   T. Lauritsen, C. J. Lister, I. Wiedenhöver, D. G. Sarantitis, M. Devlin, and L. Sobotka
      2002 Fall Meeting of the Division of Nuclear Physics of the American Physical Society, East
      Lansing, MI, October 9-12, 2002; Bull. Am. Phys. Soc. **47**, 78 (2002)

Structure of ^{52,54}Ti and Shell Closures in Neutron-Rich Nuclei Above ^{48}Ca
  R. V. F. Janssens, B. Fornal, P. F. Mantica, B. A. Brown, M. P. Carpenter, F. G. Kondev,
  T. Lauritsen, D. Seweryniak, I. Wiedenhoever, R. Broda, W. Krolas, T. Pawlat, J. Wrzesinksi,
  A. D. Davies, T. Glasmacher, D. E. Groh, S. N. Liddick, D. J. Morrissey, A. C. Morton,
  W. F. Mueller, H. Schatz, A. Stolz, P. Bhattacharyya, P. J. Daly, Z. W. Grabowski,
  M. Cinausero, N. Marginean, S. Lunardi, C. A. Ur, G. Viesti, M. Honma, T. Mizusaki,
  T. Otsuka, and S. L. Tabor
    2002 Fall Meeting of the Division of Nuclear Physics of the American Physical Society, East
    Lansing, MI, October 9-12, 2002; Bull. Am. Phys. Soc. **47**, 78 (2002)

Shape Co-Existence in ^{174}Pt
  J. Tm. Goon, D. J. Hartley, M. Danchev, L. L. Riedinger, O. Zeidan, F. G Kondev,
  M. P. Carpenter, R. V. F. Janssens, K. H. Abu Saleem, I. Ahmad, C. N. Davids, A. Heinz,
  T. L. Khoo, T. Lauritsen, C. J. Lister, G. L. Poli, J. Ressler, D. Seweryniak, I. Wiedenhover,
  W. C. Ma, H. Amro, W. Reviol, J. A. Cizewski, and M. Smith
    2002 Fall Meeting of the Division of Nuclear Physics of the American Physical Society,
    East Lansing, MI, October 9-12, 2002; Bull. Am. Phys. Soc. **47**, 79 (2002)

Coulomb Excitation of Even-Even Xenon Nuclei from A = 124 to 134
  W. F. Mueller, J. A. Church, D. C. Dinca, A. Gade, T. Glasmacher, Z. Hu, P. A. Lofy,
  K. L. Miller, H. Olliver, B. C. Perry, B. T. Roeder, I. Wiedenhoever, M. P. Carpenter,
  D. T. Henderson, R. V. F. Janssens, C. J. Lister, E. F. Moore, and T. O, Pennington
    2002 Fall Meeting of the Division of Nuclear Physics of the American Physical Society, East
    Lansing, MI, October 9-12, 2002; Bull. Am. Phys. Soc. **47**, 80 (2002)

Possible Smooth Band Termination in ^{123}LA
  H. I. Park, D. J. Hartley, L. L. Riedinger, O. Zeidan, Jing-Ye Zhang, A. Galindo-Uribarri,
  M. P. Carpenter, R. V. F. Janssens, D. Seweryniak, M. Devlin, W. Reviol, D. G. Sarantites,
  B. G. Dong, and I. Ragnarsson
    2002 Fall Meeting of the Division of Nuclear Physics of the American Physical Society, East
    Lansing, MI, October 9-12, 2002; Bull. Am. Phys. Soc. **47**, 80 (2002)

Decay of the r-Process Waiting-Point Nuclide ^{130}Cd to Levels of ^{130}In
  K.-L. Kratz, I. Dillmann, O. Arndt, M. Hannawald, B. Pfeiffer, A. Ostrowski, A. M. El-Taher,
  A. Wöhr, J. Shergur, W. B. Waiters U. Köster, V. Fedoseyev, H. Ravn, D. Seweryniak,
  P. Hoff, B. A. Brown, and T. Isoldecoll
    2002 Fall Meeting of the Division of Nuclear Physics of the American Physical Society, East
    Lansing, MI, October 9-12, 2002; Bull. Am. Phys. Soc. **47**, 81 (2002)

New Isomer in ^{217}Th Using RDT
  G. Mukherjee, T. L. Khoo, D. Seweryniak, I. Ahmad, M. P. Carpenter, C. N. Davids,
  A. Heinz, R. V. F. Janssens, F. G. Kondev, T. Lauritsen, C. J. Lister, A. Woehr,
  P. Chowdhury, E. Ngijoi-Yogo, A. Aprahamian, P. Boutachkov, M. Shawcross,
  A. Teymurazyan, P. A. Butler, R. Herzberg, G. Jones, J. A. Cizewski, M. B. Smith, R. Julin,
  M. Leino, J. Uusitalo, and P. Reiter
    2002 Fall Meeting of the Division of Nuclear Physics of the American Physical Society, East
    Lansing, MI, October 9-12, 2002; Bull. Am. Phys. Soc. **47**, 82 (2002)

Decay of a 2-qp Isomer in ^{254}No
  G. Mukherjee, T. L. Khoo, D. Seweryniak, I. Ahmad, M. P. Carpenter, C. N. Davids,
  A. Heinz, R. V. F. Janssens, F. G. Kondev, T. Lauritsen, C. J. Lister, A. Woehr,
  P. Chowdhury, E. Ngijoi-Yogo, A. Aprahamian, P. Boutachkov, M. Shawcross,
  A. Teymurazyan, P. A. Butler, R. Herzberg, G. Jones, J. A. Cizewski, M. B. Smith, R. Julin,
  M. Leino, J. Uusitalo, and P. Reiter
    2002 Fall Meeting of the Division of Nuclear Physics of the American Physical Society, East
    Lansing, MI, October 9-12, 2002; Bull. Am. Phys. Soc. **47**, 82 (2002)

Precise Mass Measurement of Neutron-Rich Nuclei from Fission Fragments of ^{252}Cf
  J. C. Wang, J. Clark, K. S. Sharma, J. Vaz, J. P. Greene, A. Heinz, G. Savard, D. Seweryniak,
  Z. Zhou, F. Buchinger, J. E. Crawford, S. Gulick, and J. K. P. Lee
    2002 Fall Meeting of the Division of Nuclear Physics of the American Physical Society, East
    Lansing, MI, October 9-12, 2002; Bull. Am. Phys. Soc. **47**, 82 (2002)

Observation of the GDR in Highly Excited ^{224}Th
  J. Seitz, T. Baumann, K. Eisenman, P. Heckman, M. Thoennesen, R. L. Varner, D. J. Hofman,
  V. Nanal, I. Dioszegi, B. B. Back, M. P. Carpenter, M. P. Kelly, T. L. Khoo, T. Pennington,
  and R. H. Siemssen
    2002 Fall Meeting of the Division of Nuclear Physics of the American Physical Society, East
    Lansing, MI, October 9-12, 2002; Bull. Am. Phys. Soc. **47**, 83 (2002)

Measurement of the ^{8}B Neutrino Spectrum
  W. T. Winter, I. Ahmad, S. J. Freedman, J. Greene, A. Heinz, D. Henderson, R. V. F. Janssens,
  C. L. Jiang, E. F. Moore, G. Mukherjee, R. C. Pardo, M. Paul, T. Pennington, K. E. Rehm,
  G. Savard, J. P. Schiffer, D. Seweryniak, and G. Zinkann
    2002 Fall Meeting of the Division of Nuclear Physics of the American Physical Society, East
    Lansing, MI, October 9-12, 2002; Bull. Am. Phys. Soc. **47**, 84 (2002)

Unexpected Behavior of Heavy-Ion Fusion Cross Sections at Extreme Sub-Barrier Energies
  C. L. Jiang, H. Esbensen, K. E. Rehm, B. B. Back, R. V. F. Janssens, J. A. Caggiano,
  P. Collon, J. Greene, A. M. Heinz, D. J. Henderson, I. Nishinaka, T. O. Pennington,
  and D. Seweryniak
    2002 Fall Meeting of the Division of Nuclear Physics of the American Physical Society, East
    Lansing, MI, October 9-12, 2002; Bull. Am. Phys. Soc. **47**, 92 (2002)

Study of Effect of the Breakup on the Fusion Cross Section of the System ^{6,7}Li + ^{59}Co
  F. A. Souza, M. G. Munhoz, A. Szanto de Toledo, E. E. Alonso, J. Takahashi, E. M. Szanto,
  N. Aissaoui, R. Liguori Neto, N. Carlin, S. J. Sanders, C. Beck, M. Rousseau, P. Bednarczyk,
  S. Courtin, F. Haas, F. Hoellinger, N. Kintz, O. Stezowski, S. Szilner, A. Hachem, E. Martin,
  R. V. F. Janssens, and A. Wuosmaa
     2002 Fall Meeting of the Division of Nuclear Physics of the American Physical Society, East
     Lansing, MI, October 9-12, 2002; Bull. Am. Phys. Soc. **47**, 92 (2002)

Low-K Rotational Structures in ^{174}Hf
  M. K. Djongolov, D. J. Hartley, D. L. Balabanski, M. Danchev, J. Tm. Goon, L. L. Riedinger,
  O. Zeidan, E. F. Moore, R. V. F. Janssens, F. G. Kondev, T. Lauritsen, M. P. Carpenter,
  C. J. Lister, K. Abu Saleem, I. Ahmad, A. Heinz, T. L. Khoo, D. Seweryniak, I. Wiedenhöver,
  M. A. Riley, P. Chowdhury, I. Shestakova, R. Kaye, H. El-Masri, P. M. Walker,
  G. D. Dracoulis, G. Sletten, D. M. Cullen, and C. Wheldon
     2002 Fall Meeting of the Division of Nuclear Physics of the American Physical Society, East
     Lansing, MI, October 9-12, 2002; Bull. Am. Phys. Soc. **47**, 94 (2002)

Coulomb Excitation and Few Nucleon Transfer Reactions with ^{209}Bi Beams on ^{237}Np and
^{241}Am Targets
  K. Abu Saleem, R. V. F. Janssens, M. P. Carpenter, F. G. Kondev, I. Ahmad, J. P. Greene,
  J. Caggiano, A. Heinz, T. L. Khoo, T. Lauritsen, C. J. Lister, D. Seweryniak, A. Sonzogni,
  I. Wiedenhöver, G. Hackman, P. Chowdhury, D. Cline, C. Wu, A. O. Machiavelli, M. Devlin,
  N. Fotiades, and E. H. Seabury
     2002 Fall Meeting of the Division of Nuclear Physics of the American Physical Society, East
     Lansing, MI, October 9-12, 2002; Bull. Am. Phys. Soc. **47**, 94 (2002)

Observation of Candidate Chiral Bands in the Odd-A Nucleus ^{135}Nd
  S. Zhu, U. Garg, B. K. Nayak, S. Frauendorf, S. S. Ghugre, N. S. Pattabhiraman, D. B. Fossan,
  K. Starosta, T. Koike, C. Vaman, A. O. Macchiavelli, R. V. F. Janssens, and
  R. S. Chakrawarthy
     2002 Fall Meeting of the Division of Nuclear Physics of the American Physical Society, East
     Lansing, MI, October 9-12, 2002; Bull. Am. Phys. Soc. **47**, 94 (2002)

Extending the Region of Triaxial Superdeformation: Candidate TSD Bands in ^{174}Hf
  D. J. Hartley, M. Djongolov, L. L. Riedinger, D. L. Balabanski, M. Danchev, J. Goon,
  O. Zeidan, Jing-Ye Zhang, F. G. Kondev, R. V. F. Janssens, K. Abu Saleem, I. Ahmad,
  M. P. Carpenter, A. Heinz, T. L. Khoo, T. Lauritsen, C. J. Lister, E. F. Moore, D. Seweryniak,
  I. Wiedenhöver, M. A. Riley, D. M. Cullen, C. Wheldon, P. Chowdhury, I. Shestakova,
  G. D. Dracoulis, H. El-Masri, P. M. Walker, R. Kaye, and G. Sletten
     2002 Fall Meeting of the Division of Nuclear Physics of the American Physical Society, East
     Lansing, MI, October 9-12, 2002; Bull. Am. Phys. Soc. **47**, 95 (2002)

A Recoil Separator for Research in Superheavy Element Chemistry
  C. N. Davids
     2002 Fall Meeting of the Division of Nuclear Physics of the American Physical Society, East
     Lansing, MI, October 9-12, 2002; Bull. Am. Phys. Soc. **47**, 98 (2002)

OPERATION AND DEVELOPMENT OF ATLAS
and
R & D RELATED TO A FUTURE RARE ISOTOPE ACCELERATOR FACILITY

Low Cost Upgrade of 6.4 GHz ECRIS and Recent Results with 14 GHz ECRIS at JYFL
  H. Koivisto, P. Heikkinen, E. Liukkonen, J. Ärje, and R. Vondrasek
    Proceedings of the 9th International Conference on Ion Sources (ISCIS'O1), Oakland, CA,
    September 3-7, 2001; Rev. Sci. Instrum. **73**, 534-536 (2002)

Techniques for the Measurement of Ionization Times in ECR Ion Sources Using a Fast Sputter
Sample and Fast Gas Valve
  R. C. Vondrasek, R. H. Scott, R. C. Pardo, and D. Edgell
    Proceedings of the 9th International Conference on Ion Sources (ISCIS'01), Oakland, CA,
    September 3-7, 2001; Rev. Sci. Instrum. **73**, 548-551 (2002)

Completion of the ATLAS ECR-I Ion Source Upgrade Project
  D. P. Moehs, R. Vondrasek, R. H. Scott, R. C. Pardo, and J. M. Montgomery
    Proceedings of the 9th International Conference on Ion Sources (ISCIS'01), Oakland, CA,
    September 3-7, 2001; Rev. Sci. Instrum. **73**, 576-579 (2002)

Argon Ionization Cross Sections for Charge State Distribution Modeling in Electron Cyclotron
Resonance Ion Source
  I. N. Bogatu, D. H. Edgell, J. S. Kim, R. C. Pardo, and R. Vondrasek
    Proceedings of the 9th International Conference on Ion Sources (ISCIS'01), Oakland, CA,
    September 3-7, 2001; Rev. Sci. Instrum. **73**, 638-640 (2002)

Electron Cyclotron Resonance Ion Source One-Dimensional Fluid Modeling
  Dana H. Edgell, Jin-Soo Kim, Ioan N. Bogatu, Richard C. Pardo, and Richard C. Vondrasek
    Proceedings of the 9th International Conference on Ion Sources (ISCIS'01), Oakland, CA,
    September 3-7, 2001; Rev. Sci. Instrum. **73**, 641-643 (2002)

Modified Electron Cyclotron Resonance Source Design for ^{3}He Accelerator Mass Spectroscopy
(Abstract)
  R. C. Pardo, D. P. Moehs, R. H. Scott, and R. C. Vondrasek
    Proceedings of the 9th International Conference on Ion Sources (ISCIS'01), Oakland, CA,
    September 3-7, 2001; Rev. Sci. Instrum. **73**, 887 (2002)

Yield Calculations for a Facility for Short-Lived Nuclear Beams
  C. L. Jiang, B. B. Back, 1. Gomes, A. M. Heinz, J. Nolen, K. E. Rehm, G. Savard,
  and J. P. Schiffer
    Nucl. Instrum. Methods **A492,** 57-73 (2002)

Production of Neutron-Rich Isotopes by One- and Two-Step Processes in ISOL Targets
  M. Portillo, J. Nolen, I. Gomes, V. N. Panteleev, D. V. Fedorov, A. E. Barzakh,
  V. I. Beznosjuk, F. V. Moroz, S. Yu. Orlov, and Yu. M. Volkov
    Nucl. Instrum. Methods **B194,** 193-206 (2002)

High-Order Maps with Acceleration for Optimization of Electrostatic and Radio-Frequency Ion-Optical Elements
  Andrew A. Geraci, Teresa A. Barlow, Mauricio Portillo, Jerry A. Nolen, Kenneth W. Shepard,
  Kyoko Makino, and Martin Berz
    Rev. Sci. Instrum. **73**, 3174-3180 (2002)

ISOL Beams from Fragmentation: the Best of Both Worlds
  G. Savard, J. Schwartz, J. Caggiano, J. P. Greene, A. Heinz, M. Maier, D. Seweryniak,
  and B. J. Zabransky
    Proceedings of the 5th International Conference on Radioactive Nuclear Beams (RNB-5),
    Divonne, France, April 3-8, 2000; Nucl. Phys. **A701,** 292c-295c (2002)

Liquid-Lithium Cooling for 100-kW ISOL and Fragmentation Targets
  J. A. Nolen, C. B. Reed, A. Hassanein, and I. C. Gomes
    Proceedings of the 5th International Conference on Radioactive Nuclear Beams (RNB-5),
    Divonne, France, April 3-8, 2000; Nucl. Phys. **A701,** 312c-322c (2002)

Prospects for Exotic Beam Facilities in North America
  J. A. Nolen
    Proceedings of the International Symposium on Perspectives in Physics with Radioactive
    Isotope Beams 2000 (RIB00), Hayama, Kanagawa, Japan, November 13-16, 2000; Eur.
    Phys. J. A **13**, 255-261 (2002)

Development of Windowless Liquid Lithium Targets for Fragmentation and Fission of 400-kW
Uranium Beams
  J. A. Nolen, C. B. Reed, A. Hassanein, V. J. Novick, P. Plotkin, and J. R. Specht
    14th International Conference on Electromagnetic Isotope Separators and Techniques
    Related to Their Applications (EMIS-14), Victoria, B.C., Canada, May 6-10, 2002, Book of
    Abstracts, p. 17 (2002)

An Adjustable Thickness Li/Be Target for Fragmentation of 3-kW Heavy Ion Beams
  J. A. Nolen, C. B. Reed, A. Hassanein, V. J. Novick, P. Plotkin, J. R. Specht, D. J. Morrissey,
  J. H. Ottarson, and B. M. Sherrill
    14th International Conference on Electromagnetic Isotope Separators and Techniques
    Related to Their Applications (EMIS-14), Victoria, B.C., Canada, May 6-10, 2002, Book of
    Abstracts, p. 18 (2002)

A Post Accelerator for the U. S. Rare Isotope Accelerator Facility
  P. N. Ostroumov, M. P. Kelly, A. A. Kolomiets, J. A. Nolen, M. Portillo, and K. W. Shepard
    14th International Conference on Electromagnetic Isotope Separators and Techniques
    Related to Their Applications (EMIS-14), Victoria, B.C., Canada, May 6-10, 2002, Book of
    Abstracts, p. 31 (2002)

Development and Operation of Gas Catchers to Thermalize Fusion-Evaporation and
Fragmentation Products
    Guy Savard, A. Heinz, J. P. Greene, D. Seweryniak, B. J. Zabransky, Z. Zhou, J. Clark,
    K. S. Sharma, J. Vaz, J. C. Wang, C. Boudreau, and the 5258 Collaboration
        14th International Conference on Electromagnetic Isotope Separators and Techniques
        Related to Their Applications (EMIS-14), Victoria, B.C., Canada, May 6-10, 2002, Book of
        Abstracts, p. 46 (2002)

Status of the R&D for the Rare Isotope Accelerator Project
    Guy Savard
        14th International Conference on Electromagnetic Isotope Separators and Techniques
        Related to Their Applications (EMIS-14), Victoria, B.C., Canada, May 6-10, 2002, Book of
        Abstracts, p. 78 (2002)

Energy and Range Focusing of In-Flight Separated Exotic Nuclei
    C. Scheidenberger, H. Geissel, M. Maier, G. Münzenberg, G. Savard, V. Shishkin, H. Weick,
    M. Winkler, F. Attallah, K.-H.Behr, S. Eliseev, M. Hausmann, M. Hellström, E. Daza,
    B. Kindler, Y. Litvinov, B. Lommel, G. Marx, M. Matos, N. Nankov, T. Ohtsubo,
    K. Sümmerer, Z.-Y. Sun, and Z. Zhou
        14th International Conference on Electromagnetic Isotope Separators and Techniques
        Related to Their Applications (EMIS-14), Victoria, B.C., Canada, May 6-10, 2002, Book of
        Abstracts, p. 80 (2002)

Optimization of ISOL Targets Based on Monte-Carlo Simulation of Ion Release Curves
    B. Mustapha and J. A. Nolen
        14th International Conference on Electromagnetic Isotope Separators and Techniques
        Related to Their Applications (EMIS-14), Victoria, B.C., Canada, May 6-10, 2002, Book of
        Abstracts, p. 96 (2002)

The Rare Isotope Accelerator Project
    Guy Savard
        Conference on Frontiers of Nuclear Structure, Berkeley, CA, July 29-August 2, 2002,
        LBNL-50598 Abs., Book of Abstracts, p. 50 (2002)

Bunch Shape Measurement of CW Heavy-Ion Beam
    N. Y. Vinogradov, P. Billquist, P. N. Ostroumov, R. C. Pardo, M. Portillo, S. I. Sharamentov,
    and G. P. Zinkann
        XXI International Linear Accelerator Conference (LINAC2002), Gyeongju, Korea, August
        19-23, 2002, Book of Abstracts, p. 61 (2002)

Design Features of High-Intensity Medium-Energy Superconducting Heavy-Ion Linac
    P. N. Ostroumov
        XXI International Linear Accelerator Conference (LINAC2002), Gyeongju, Korea, August
        19-23, 2002, Book of Abstracts, p. 62 (2002)

A New Generation of Superconducting Solenoids for Heavy-Ion Linac Application
   P. N. Ostroumov, K. W. Shepard, S. H. Kim, R. E. Laxdal, and R. Wheatley
      XXI International Linear Accelerator Conference (LINAC2002), Gyeongju, Korea, August
      19-23, 2002, Book of Abstracts, p. 116 (2002)

The U.S. RIA Project
   J. Nolen
      XXI International Linear Accelerator Conference (LINAC2002), Gyeongju, Korea, August
      19-23, 2002, Book of Abstracts, p. 54 (2002)

Preliminary Engineering Design of a 57.5 MHz CW RFQ for the RIA Driver Linac
   J. W. Rathke, T. J. Schultheiss, P. N. Ostroumov, A. A. Kolomiets, and D. L. Schrage
      XXI International Linear Accelerator Conference (LINAC2002), Gyeongju, Korea, August
      19-23, 2002, Book of Abstracts, p. 142 (2002)

RF, Thermal and Structural Analysis of the 57.5 MHz CW RFQ for the RIA Driver Linac
   T. J. Schultheiss, J. W. Rathke, P. N. Ostroumov, and A. A. Kolomiets
      XXI International Linear Accelerator Conference (LINAC2002), Gyeongju, Korea, August
      19-23, 2002, Book of Abstracts, p. 143 (2002)

Minimizing Transverse-Field Effects in Superconducting Quarter-Wave Cavities
   P. N. Ostroumov and K. W. Shepard
      XXI International Linear Accelerator Conference (LINAC2002), Gyeongju, Korea, August
      19-23, 2002, Book of Abstracts, p. 143 (2002)

A Prototype Superconducting 345 MHz Two-Cell Spoke Cavity
   K. W. Shepard, M. Kedzie, M. P. Kelly, J. Fuerst, and E. Peterson
      XXI International Linear Accelerator Conference (LINAC2002), Gyeongju, Korea, August
      19-23, 2002, Book of Abstracts, p. 144 (2002)

Superconducting Drift-Tube Cavity Development for the RIA Driver Linac
   K. W. Shepard, M. P. Kelly, and J. Fuerst
      XXI International Linear Accelerator Conference (LINAC2002), Gyeongju, Korea, August
      19-23, 2002, Book of Abstracts, p. 145 (2002)

MEDIUM-ENERGY NUCLEAR PHYSICS RESEARCH

Single-Spin Azimuthal Asymmetry in Exclusive Electroproduction of π^+ Mesons
   A. Airapetian *et al.* (HERMES Collaboration)
      Phys. Lett. **B535**, 85-92 (2002)

Measurement of Longitudinal and Transverse Cross Sections in the ^{3}He$(e,e'\pi^+)^3$H Reaction at
W = 1.6 GeV
   D. Gaskell **et al.**
      Phys. Rev. C **65**, 011001(R)/1-5 (2002)

Polarization Measurements in Neutral Pion Photoproduction
   K. Wijesooriya *et al.* (for the Jefferson Lab Hall A Collaboration)
      Phys. Rev. C **66**, 034614/1-14 (2002)

High Energy Angular Distribution Measurements of the Exclusive Deuteron Photodisintegration
Reaction
   E. C. Schulte *et al.* and the JLab Hall A Collaboration
      Phys. Rev. C **66**, 042201(R)/1-5 (2002)

Nuclear Transparency from Quasielastic $A(e,e'p)$ Reactions up to $Q^2 = 8.1$ (GeV/c)^2
   K. Garrow *et al.* (for the JLab E94-139 Collaboration)
      Phys. Rev. C **66**, 044613/1-10 (2002)

The HERMES Dual-Radiator Ring Imaging Cerenkov Detector
   N. Akopov *et al.* (the HERMES RICH Collaboration)
      Nucl. Instrum. Methods *A479*, 511-530 (2002)

HERMES and the Spin on the Proton
   H. E. Jackson (on behalf of the HERMES Collaboration)
      Int. J. Mod Phys. A **17**, 3551-3570 (2002)

PHY-10444-ME-2002
Transverse Spin: HERMES Results and Future Plans
   N. C. R. Makins, for the HERMES Collaboration
      Proceedings of the European Workshop on the QCD Structure of the Nucleon, Ferrara, Italy,
      April 3-6, 2002; Nucl. Phys. **A711,** 41c-49c (2002)

HERMES Results and Future on DVCS and DUES
   D. Hasch (on behalf of the HERMES Collaboration)
      Proceedings of the European Workshop on the QCD Structure of the Nucleon, Ferrara, Italy,
      April 3-6, 2002; Nucl. Phys. **A711**, 148c-153c (2002)

Beam-Charge Asymmetry Associated with DVCS at HERMES
  F. Ellinghaus (on behalf of the HERMES Collaboration)
    Proceedings of the European Workshop on the QCD Structure of the Nucleon, Ferrara, Italy,
    April 3-6, 2002; Nucl. Phys. **A711,** 171c-174c (2002)

Exclusive Vector Meson Production on Nuclei at HERMES
  A. B. Borissov, on behalf of the HERMES Collaboration
    Proceedings of the European Workshop on the QCD Structure of the Nucleon, Ferrara, Italy,
    April 3-6, 2002; Nucl. Phys. **A711,** 269c-273c (2002)

Measurement of Polarization Observables in Υ and φ Production with 800 GeV $p + Cu$ Collision
  P. E. Reimer *et al.* (FNAL E866 Collaboration)
    Proceedings of the International Nuclear Physics Conference on Nuclear Physics in the 21st
    Century (INPC 2001), Berkeley, CA, July 30-August 3, 2001, eds. E. Norman, L. Schroeder,
    and G. Wozniak, AIP Conference Proceedings **610**, 420-424 (2002)

Towards Measuring the Charge Radii of ^{6}He and ^{8}He
  P. Müller, L.-B. Wang, K. Bailey, X. Du, J. Greene, A. M. Heinz, R. J. Holt, D. Henderson,
  R. V. F. Janssens, C.-L. Jiang, C. Law, Z.-T. Lu, I. D. Moore, T. P. O'Connor, R. C. Pardo,
  T. Pennington, K. E. Rehm, J. P. Schiffer, M. Paul, and G. W. F. Drake
    14th International Conference on Electromagnetic Isotope Separators and Techniques
    Related to Their Applications (EMIS-14), Victoris, B.C., Canada, May 6-10, 2002, Book of
    Abstracts, p. 43 (2002)

Improvements on Detecting ^{81,85}Kr with ATTA
  P. Müller, X. Du, K. Bailey, Z.-T. Lu, I. D. Moore, T. P. O'Connor, and L. Young
    14th International Conference on Electromagnetic Isotope Separators and Techniques
    Related to Their Applications (EMIS-14), Victoria, B.C., Canada, May 6-10, 2002, Book of
    Abstracts, p. 44 (2002)

Ultrasensitive Isotope Trace Analysis of ^{41}Ca
  I. D. Moore, K. Bailey, Z.-T. Lu, P. Müller, T. P. O'Connor, and L. Young
    14th International Conference on Electromagnetic Isotope Separators and Techniques
    Related to Their Applications (EMIS-14), Victoria, B.C., Canada, May 6-10, 2002, Book of
    Abstracts, p. 146 (2002)

Single Spin Azimuthal Asymmetry Associated with Deeply Virtual Compton Scattering
  James Ely (for the HERMES Collaboration)
    April 2002 Meeting of the American Physical Society, Albuquerque, NM, April 20-23,
    2002; Bull. Am. Phys. Soc. 47, 92 (2002)

Flavor Decomposition of Polarized Quark Distributions in the Nucleon
  H. E. Jackson *et al.* (on behalf of the HERMES Collaboration)
    April 2002 Meeting of the American Physical Society, Albuquerque, NM, April 20-23,
    2002; Bull. Am. Phys. Soc. **47**, 197 (2002)

Polarization Measurements in π^0 Photoproduction
  K. Wijesooriya
    April 2002 Meeting of the American Physical Society, Albuquerque, NM, April 20-23,
    2002; Bull. Am. Phys. Soc. **47**, 216 (2002)

Do Ordinary Nuclei Contain Exotic States of Matter?
  John Arrington
    2002 Fall Meeting of the Division of Nuclear Physics of the American Physical Society, East
    Lansing, MI, October 9-12, 2002; Bull. Am. Phys. Soc. **47**, 17 (2002)

Angular Distribution Measurements of the $d(\gamma,p)n$ Differential Cross Section at Hign Energies
  E. C. Schulte *et al.* for the Hall A Collaboration at JLab
    2002 Fall Meeting of the Division of Nuclear Physics of the American Physical Society, East
    Lansing, MI, October 9-12, 2002; Bull. Am. Phys. Soc. **47**, 25 (2002)

Towards Measuring the Charge Radius of ^{6}He
  Li-Bang Wang, Peter Mueller, Kevin Bailey, John Greene, Andreas Heinz, Roy Holt,
  Dale Henderson, Robert Janssens, Cheng-Lie Jiang, Zheng-Tian Lu, Thomas O'Connor,
  Richard Pardo, Tad Penninngton, Karl Rehm, and John Schiffer
    2002 Fall Meeting of the Division of Nuclear Physics of the American Physical Society, East
    Lansing, MI, October 9-12, 2002; Bull. Am. Phys. Soc. **47**, 101 (2002)

THEORETICAL PHYSICS

Quantum Effects with an X-Ray Free Electron Laser
  C. D. Roberts, S. M. Schmidt, and D. V. Vinnik
    Phys. Rev. Lett. **89**, 153901/1-4 (2002)

Evolution of Nuclear Spectra with Nuclear Forces
  R. B. Wiringa and Steven C. Pieper
    Phys. Rev. Lett. **89**, 182501/1-4 (2002)

N-P Pairing in Nuclei
  R. R. Chasman
    Phys. Lett. **B524**, 81-86 (2002)

Weak Transitions in A = 6 and 7 Nuclei
  R. Schiavilla and R. B. Wiringa
    Phys. Rev. C **64**, 054302/1-13 (2002)

Multipole Expansion for Relativistic Coulomb Excitation
  H. Esbensen and C. A. Bertulani
    Phys. Rev. C **65**, 024605/1-7 (2002)

Nucleon Resonances with Double Polarization Observables of Pion Photoproduction
  D. Dutta, H. Gao, and T.-S. H. Lee
    Phys. Rev. C **65**, 044619/1-6 (2002)

η Meson Productions in NN Collisions
  K. Nakayama, J. Speth, and T.-S. H. Lee
    Phys. Rev. C **65**, 045210/1-12 (2002)

Elastic Scattering and Breakup of ^{17}F at 10 MeV/Nucleon
  J. F. Liang, J. R. Beene, H. Esbensen, A. Galindo-Uribarri, J. Gomez del Campo, C. J. Gross,
  M. L. Halbert, P. E. Mueller, D. Shapira, D. W. Stracener, I. J. Thompson, and :R. L. Varner
    Phys. Rev. C **65**, 051603(R)/1-5 (2002)

Nucleon Mass and Pion Loops
  M. B. Hecht, C. D. Roberts, M. Oettel, A. W. Thomas, S. M. Schmidt, and P. C. Tandy
    Phys. Rev. C **65**, 055204/1-17 (2002)

Bethe-Salpeter Equation and a Nonperturbative Quark-Gluon Vertex
  A. Bender, W. Detmold, A. W. Thomas, and C. D. Roberts
    Phys. Rev. C **65**, 065203/1-16 (2002)

Effective Lagrangian Approach to the ω Photoproduction Near Threshold
  Alexander I. Titov and T.-S. H. Lee
    Phys. Rev. C **66**, 015204/1-12 (2002)

Coherent ϕ and ω Meson Photoproduction from Deuteron and Nondiffractive Channels
  A. I. Titov, M. Fujiwara, and T.-S. H. Lee
    Phys. Rev. C **66**, 022202(R)/1-5 (2002)

Monte Carlo Integration in Glauber Model Analysis of Reactions of Halo Nuclei
  K. Varga, Steven C. Pieper, Y. Suzuki, and R. B. Wiringa
    Phys. Rev. C **66**, 034611/1-7 (2002)

Quantum Monte Carlo Calculations of A = 9, 10 Nuclei
  Steven C. Pieper, K. Varga, and R. B. Wiringa
    Phys. Rev. C **66**, 044310/1-14 (2002)

Role of E1-E2 Interplay in Multiphonon Coulomb Excitation
  Alexander Volya and Henning Esbensen
    Phys. Rev. C **66**, 044604/1-10 (2002)

Dynamic Polarization in the Coulomb Dissociation of ^{8}B
  H. Esbensen and G. F. Bertsch
    Phys. Rev. C 66**, 044609/1-4 (2002)

One-Loop Corrections to ω Photoproduction Near Threshold
  Yongseok Oh and T.-S. H. Lee
    Phys. Rev. C **66**, 045201/1-9 (2002)

Continuum Versus Periodic Lattice Monte Carlo Approach to Classical Field Theory
  Bogdan Mihaila and John F. Dawson
    Phys. Rev. D **65**, 071501/1-5 (2002)

Higher-Order Effects in the Two-Body Breakup of ^{17}F
  H. Esbensen and G. F. Bertsch
    Nucl. Phys. **A706,** 383-399 (2002)

Use of Mathematical Logical Concepts in Quantum Mechanics: An Example
  Paul Benioff
    J. Phys. A **34**, 5843-5857 (2002)

Numerical Approximations Using Chebyshev Polynomial Expansions: El-gendi's Method Revisited
  Bogdan Mihaila and Ioana Mihaila
    J. Phys. A **35**, 731-746 (2002)

Parallel Algorithm with Spectral Convergence for Nonlinear Integro-Differential Equations
  B. Mihaila and R. E. Shaw
    J. Phys. A **35**, 5315-5331 (2002)

Physics as an Element of Radiation Research
  Mitio Inokuti and Stephen M. Seltzer
    Radiation Research **158**, 3-12 (2002)

The Representation of Numbers in Quantum Mechanics
  Paul Benioff
    Algorithmica **34**, 529-559 (2002)

Pion-Nucleus Internations
  T.-S. H. Lee and R. P. Redwine
    Ann. Rev. Nucl. Part. Sci. **52**, 23-63 (2002)

Cauchy's Dispersion Equation Reconsidered: Dispersion in Silicate Glasses
  D. Y. Smith, Mitio Inokuti, and W. Karstens
    Radiation Effects and Defects in Solids **157**, 823-828 (2002)

Quantum Monte Carlo for Light Nuclei
  Steven C. Pieper
    Proceedings of the 5th International Conference on Radioactive Nuclear Beams (RNB-5),
    Divonne, France, April 3-8, 2000; Nucl. Phys. **A701,** 357c-362c (2002)

Goldstone Boson's Valence-Quark Distribution
  C. D. Roberts
    Proceedings of the 11th International Light-Cone Workshop on Light-Cone Physics:
    Particles and Strings, Trento, Italy, November 3-11, 2001; Nucl. Phys. **B108,** 227-233
    (2002)

Space Searches with a (quantum Robot
  Paul Benioff
    American Mathematical Society Annual Meeting, Washington, DC. January 17-21, 2000;
    Contemporary Mathematics **305**, 1-12 (2002)

Quantum Monte Carlo Calculations of Light Nuclei
  Steven C. Pieper
    Proceedings of the International Symposium on Perspectives in Physics with Radioactive
    Isotope Beams 2000 (RIB00), November 13-16, 2000, Kanagawa-Hayama, Japan; Eur.
    Phys. J. A **13**, 75-79 (2002)

Study of Hadron Quark-Substructure with GeV Electrons and Photons
  T.-S. H. Lee
    Proceedings of the International Workshop on Physics with GeV Electrons and Gamma-
    Rays, eds. T. Tamae, J. Kasagi, T. Terasawa, H. Yamazaki, Sendai, Japan, February 13-15,
    2001 (University Academy Press, Inc., Tokyo, Japan 2001) pp. 1-6

Rotating Nuclei in the Relativisitic Mean Field Theory: Microscopic Nature of Nuclear
Magnetism
  A. V. Afanasjev, S. G. Frauendorf, and P. Ring
    Proceedings of the NATO Advanced Research Workshop on The Nuclear Many-Body
    Problem 2001, Brijuni, Pula, Croatia, June 2-5, 2001, eds. W. Nazarewicz and D. Vretenar
    (Kluwer Academic Publishers 2002) pp. 103-110

Quantum Monte Carlo Calculations of P-Shell Nuclei
  Steven C. Pieper
    Proceedings of the NATO Advanced Research Workshop on the Nuclear Many-.Body
    Problem 2001, Brijuni, Pula, Croatia, June 2-5, 2001, eds. W. Nazarewicz and D. Vretenar
    (Kluwer Academic Publishers 2002) pp. 11-18

Modern Dyson-Schwinger Equation Studies
  M. B. Hecht and C. D. Roberts
    Proceedings of the 9th International Symposium on Meson-Nucleon Physics and the
    Structure of the Nucleon (MENU2001), Washington, DC, July 26-31, 2001; πN Newsletter
    16, 202-212 (2002)

Probing the Gateway to Superheavy Nuclei in Cranked Relativistic Hartree-Bogoliubov Theory
  A. V. Afanasjev, T. L. Khoo, S. Frauendorf, I. Ahmad, and G. A. Lalazissis
    Conference on Frontiers of Nuclear Structure, Berkeley, CA, July 29-August 2, 2002,
    LBNL-50598 Abs., Book of Abstracts, p. 1 (2002)

QMC Calculations of Light Nuclei
  Steven C. Pieper
    April 2002 Meeting of the American Physical Society, Albuquerque, NM, April 20-23,
    2002; Bull. Am. Phys. Soc. **47**, 91 (2002)

Evolution of Nuclear Spectra with Nuclear Forces
  R. B. Wiringa and Steven C. Pieper
    April 2002 Meeting of the American Physical Society, Albuquerque, NM, April 20-23,
    2002; Bull. Am. Phys. Soc. **47**, 165 (2002)

Nuclear Shell Model for States Embedded in the Continuum
  Alexander Volya and Vladimir Zelevinsky
    2002 Fall Meeting of the Division of Nuclear Physics of the American Physical Society, East
    Lansing, MI, October 9-12, 2002; Bull. Am. Phys. Soc. **47**, 35 (2002)

Quantum Monte Carlo Calcuations of A $\leq$ 10 Nuclei
  Steven C. Pieper and R. B. Wiringa
    2002 Fall Meeting of the Division of Nuclear Physics of the American Physical Society, East
    Lansing, MI, October 9-12, 2002; Bull. Am. Phys. Soc. **47**, 35 (2002)

Breakup of ^{17}F by ^{208}Pb Near the Coulomb Barrier
  J. F. Liang, J. R. Beene, A. Galindo-Uribarri, J. Gomez del Campo, C. J. Gross, P. A.
  Hausladen, Y. Larochelle, P. E. Mueller, D. Shapira, D. W. Stracener, R. L. Marner, Henning
  Esbensen, and J. D. Bierman
    2002 Fall Meeting of the Division of Nuclear Physics of the American Physical Society, East
    Lansing, MI, October 9-12, 2002; Bull. Am. Phys. Soc. **47**, 92 (2002)

Rare Isotope Accelerators
  Guy Savard
    April 2002 Meeting of the American Physical Society, Albuquerque, NM, April 20-23,
    2002; Bull. Am. Phys. Soc. **47**, 192 (2002)